Development of a Rapid Liquid Freezer

A thesis presented in partial fulfilment of the requirements for the degree of

Doctor of Philosophy

in

Food Technology

at Massey University, Manawatū,

New Zealand

Jolin Pierre Morel

2021

Acknowledgements

I am extremely grateful to my primary supervisor, Richard Archer, for all of his support, advice, suggestions, and help. Further thanks go to my co-supervisors, Jason Hindmarsh and Mohammed Farid, for their advice and support.

I would like to acknowledge the New Zealand Ministry of Business, Innovation and Employment for providing the funding for this work through the Food Industry Enabling Technologies programme.

I am deeply indebted for all the help, advice, and suggestions provided by my co-workers, Lindsay Robertson and Georg Ripberger, especially around equipment and experimental designs. Their experience and ideas were invaluable for the success of this project.

Thanks go to the all of technical staff in the School of Food and Advanced Technology, especially lab managers and workshop technicians who helped me throughout this project.

I would like to single out Craig Prichard for particular thanks. His help and his contacts within the NZ Sheep Dairy industry were extremely valuable. They helped me collect samples and understand the challenges and opportunities for Sheep Dairy in New Zealand. I would also like to thank his ewes for providing the raw material for several of my experiments.

I am grateful for all the camaraderie provided by the wider FIET community and the other post-grad students I have met during my studies. The assistance and support the FIET and post-grad communities have provided is deeply appreciated and they have always been a great sounding board for ideas.

Last, but certainly not least, I'd like to thank all my family and friends, especially my parents, and Hanna for all their love and support during my studies.

Thesis Abstract

Small sheep dairy farms often make insufficient volumes of milk for economic daily collection and are limited by transport distances to processors. A method of long-term on-farm storage of milk would enable the industry to grow. Freezing would allow extended milk storage on farms. But existing methods of freezing for on-farm applications have shortcomings around materials handling, labour requirements and product quality. The project reported in this thesis aimed to develop the engineering science behind an economically viable freezing method that would improve on current methods.

The first period of this project focused on two freezer designs which were thought to be promising: Rolling Droplet Freezing (RDF) and Falling-Film Flake freezing (FFF). RDF was selected as the initial focus of the research program and consisted of a system where droplets of milk would roll down an angled super-hydrophobic surface against a cold air flow and freeze. RDF was abandoned due to concerns about construction costs and operating reliability. In a condensing atmosphere, droplets rolling on superhydrophobic surfaces occasionally transitioned from a Cassie-Baxter wetting state to a Wenzel wetting state, which caused the droplets to stick.

FFF was then developed further. A pilot scale unit was designed and constructed, and preliminary pilot-scale trials that were conducted with pure water and ovine milk reconstituted from powder. The partition coefficient of FFF was measured as 0.946 at an operating temperature of -30°C. At higher operating temperatures the partition coefficient was reduced. Detaching frozen solids by applying a burst of heat to the freezer/ice interface was studied and this method of detachment was successful with pure water, but ineffective for ovine milk. The development of FFF was put on hold with the conception and development of the continuous tubular freezer.

Ice formed in a solution can show morphologies ranging from highly dendritic structures with entrapped solutes, which are homogenous on a gross scale, to large crystals of pure ice with solutes rejected and compressed into inter-crystalline spaces. To investigate which sheep milk components influence ice morphology at various freezing rates, whole milk was separated into skim milk and into a casein-free serum phase. A simulated sheep milk ultrafiltrate was also prepared. The morphology of the ice/sample interface was observed in a custom-built microscope stage at freezing front velocities from <0.5 μms^{-1} to 50 μms^{-1} with a spatial temperature gradient of 35-38 Kcm^{-1}. The morphology arising from extremely rapid freezing front velocities was investigated by supercooling slides on a temperature-controlled stage and observing the nucleation and recalescence of the samples.

The morphology of ice at the interface changed from a planar to columnar and then to dendritic as freezing front velocity increased, with the transitions from one morphology to another occurring at lower speeds in more complicated solutions. A map of freezing front behaviours was developed. The transition between interface morphologies was at different velocities and transition differed based upon the interface velocity. At lower interface velocities a columnar interface grew directly from a planar starting condition. At higher velocities an intermediate dendritic zone formed, which then settled into a columnar interface. The ice formed by rapid freezing from subcooled solutions was highly dendritic, with ice growth rates of approximately 21,000 μms^{-1}, which was close to the diffusion-limited ice growth rate in water of similar degrees of supercooling.

The morphology of frozen ovine milk was also studied by Cryogenic Scanning Electron Microscopy (Cryo-SEM): Milk was frozen by three different methods-slow quiescent freezing (SF), rapid directional freezing (DF), and droplet freezing in LN_2. Ice crystals rejected unfrozen

solids into the region between crystals in all samples, including those frozen by immersion into liquid nitrogen. There was a distinct difference in morphology between the SF and DF samples, with the bands of unfrozen solids being significantly smaller in DF samples, and the long axes of ice crystals were aligned with the direction of heat flow. SF samples lacked any particular ice growth direction, and ice crystals were orders of magnitude larger. Lactose crystallisation was observed in some SF samples but was not observed in any DF samples. Fat globules were engulfed in ice crystals in DF samples, but rejected in SF samples.

To study the effects of frozen storage temperature and time, samples of raw ovine milk were stored frozen at -10°C, -18°C and -28°C to -30°C for up to 8 weeks. Further samples were stored below -20°C for 6 months. After thawing at 20°C, samples were tested for a range of properties and serum samples were collected by separating the fat phase and micellar casein phase by centrifugation. A gel was observed in milk stored at -10°C for 4 weeks and 8 weeks but was not observed in milk stored at lower temperatures. The gel dispersed under heating and homogenisation. There was no change observed in the pH, or serum protein level of thawed samples after frozen storage at any temperature. The whiteness of the milk decreased during frozen storage and the yellowness increased. Both of these changes were reversed on homogenisation. The serum Ca^{2+} levels in milk stored at -10°C and -18°C dropped over the storage period, while no trend was seen in milk stored below -28°C, indicating that the migration of Ca^{2+} may play a role in the formation of gels after frozen storage. Milk that had been stored below -20°C for 6 months had a similar viscosity and appearance to fresh milk.

A possible mechanism for the formation of gels at -10°C, but not -18°C or -28°C lies in the altered solute environment, and the physical agglomeration of milk components in the spaces between ice crystals, driving the gelation of closely packed casein micelles, with Ca^{2+} stabilising this network. It is well established in literature that the viscosity of an unfrozen phase increases by several orders of magnitudes as it decreases in temperature and approaches a glassy state. This increased viscosity reduces protein mobility and solute diffusion, which reduces the rate of gel formation.

The tendency for frozen milk particles to bind together during frozen storage was evaluated. Frozen pellets of whole ovine milk were stored under weights at -10°C and -18°C and pellets of frozen concentrated milk stored at -18°C and -28°C. Ovine milk pellets bound together at -10°C but not -18°C, while concentrated milk bound together at -18°C, but not -28°C. This can be linked to the volume and viscosity of the unfrozen phase in these samples.

Differential scanning calorimetry was used to determine the fraction of freezable water frozen at any temperature. The melting onset temperature was observed, and this was used to determine the solids content maximally freeze concentrated solution ($X_s(T_m)$). $X_s(T_m)$=0.875 for whole ovine milk $X_s(T_m)$=0.85 for skim milk, and $X_s(T_m)$=0.81 for ovine milk serum. This was also determined for whole ovine milk by the magnitude of the overall latent heat release during melting, which gave a value for whole milk of $X_s(T_m)$=0.85±0.016. A partial phase diagram for ovine milk was generated from the data collected.

The insights generated from observing both the dendritic morphology of high velocity ice fronts and progressive freezing behaviour led to conceptualising a novel tubular freezer, subsequently constructed. It was hypothesised that reducing the volume or area of ice in contact with the freezer wall, due to the inclusion of unfrozen product, could reduce the adhesion strength between a frozen product and the freezer wall. By controlling the outlet temperature, the volume fraction of unfrozen product could be controlled. The adhesion strength could thereby be controlled, and a set of operating conditions could be found that would allow a mostly frozen product to be extruded as a solid from a cooled tube by a high-pressure pump. This was tested on a benchtop scale (up to 5mL/minute, with a freezer internal diameter of 4.2mm and cooled length of 500mm), with ovine milk, fruit juice, fruit pulp, concentrated coffee, bovine cream and

concentrated milks. The system successfully froze all samples. The operating pressure was found to increase with increased frozen fraction, and therefore with decreased operating temperature. The ice morphology of milk and juice frozen by this equipment was imaged by cryo-SEM and by optical microscopy. The ice crystals were radially aligned, increasing in size closer to the centre of the frozen product plug, which was expected due to the heat flows and the relationship between freezing front velocity and feature sizing. This positive preliminary result led to the construction of a larger scale prototype unit which consisted of a spiral tube with a length of 5000 mm, and an internal diameter of 10 mm. This was used successfully for a product flowrate of approximately 6 $kghr^{-1}$.

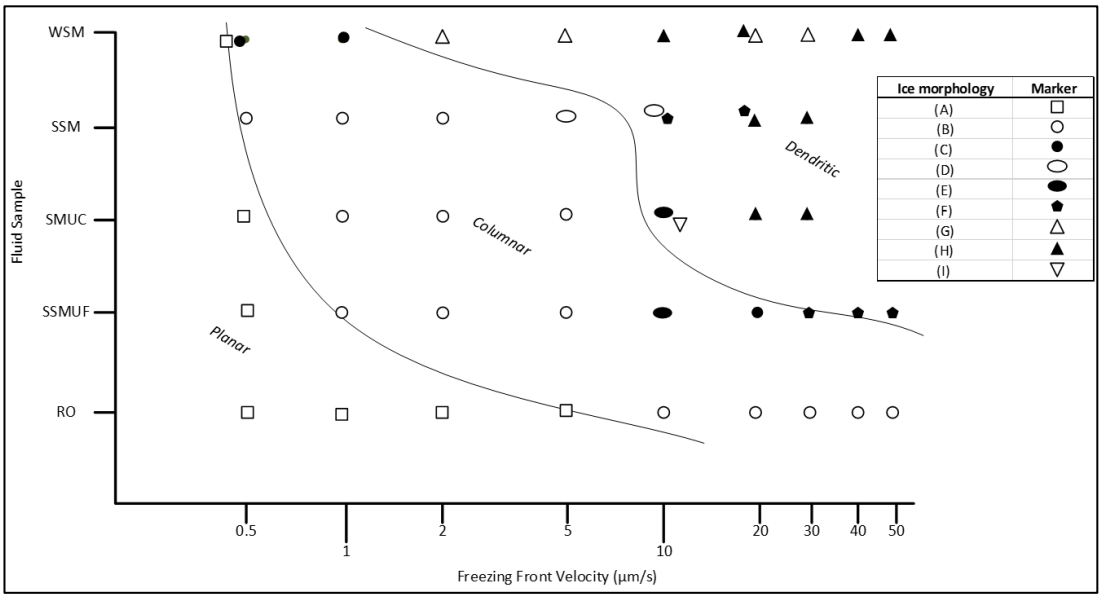

The figure above shows the map of morphologies seen in ice/fluid interfaces, as this interface advances at different speeds and in different ovine milk fractions. The figure to the right shows the morphologies corresponding to the symbols on the map above. These are reproduced from Chapter 4.

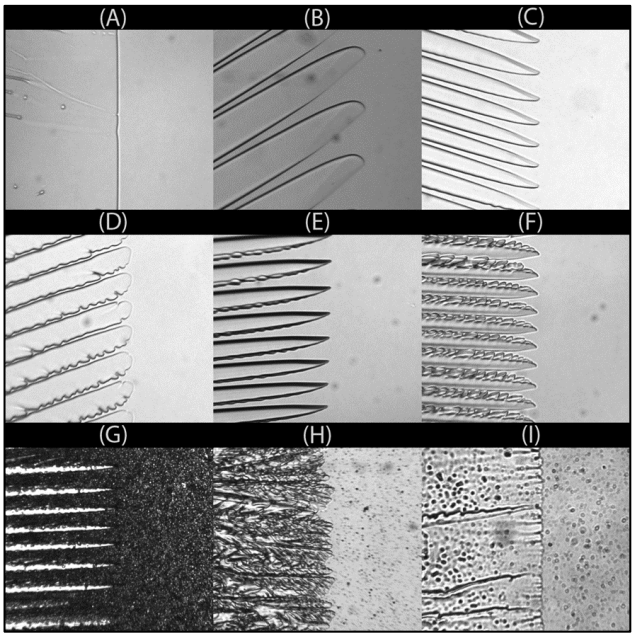

The figure below, reproduced from Chapter 6, shows a partial phase diagram of ovine milk as constructed from DSC measurements and calculation from observed transitions. The diagram shows the phases present as a function of temperature and solids concentration, phase transitions, and the maximally-freeze-concentrated solids concentration of ovine milk.

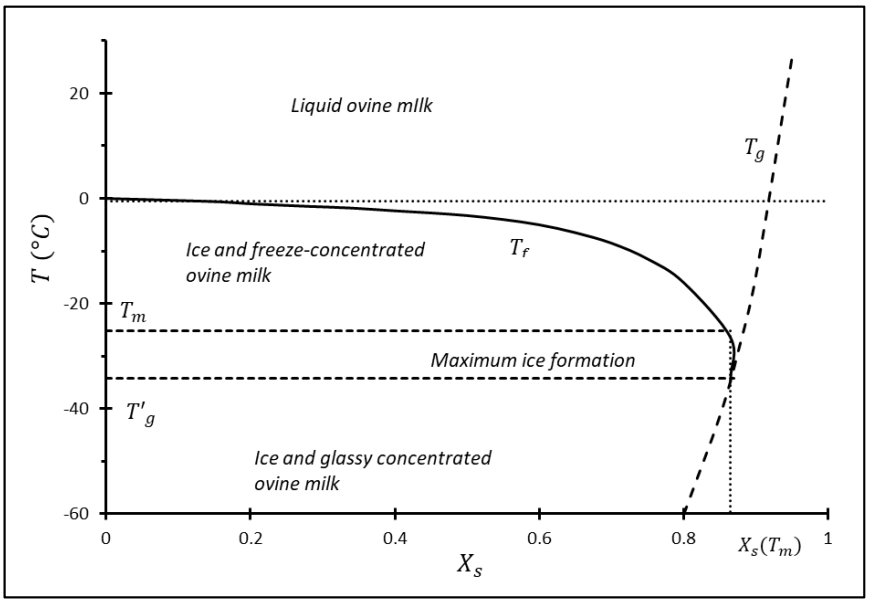

Table of Contents

List of Figures

Glossary of Selected Terms.

This glossary is intended to define several terms that are used in this thesis. It is not intended to be a comprehensive survey of all technical language used.

- **Adhesion strength.**
  The force per unit area required to detach a sample on a surface.
- **Apparent ice fraction.**
  The apparent fraction of the freezable water which has undergone a phase change at a given temperature, as inferred from DSC measurements.
- **Apparent unfrozen fraction.**
  The apparent fraction of the freezable water which has not undergone a phase change at a given temperature, as inferred from DSC measurements.
- **Apparent adhesion strength.**
  The apparent force per unit area required to detach a frozen plug adhered to the interior wall of the tubular freezer, as determined from operating pressure and total cooled interior area.
- **Characteristic distance.**
  The dimension which defines the scale of the physical process described. Typically calculated as the ratio of volume and surface area.
- **DSC.**
  Differential Scanning Calorimetry – an analytical technique that measures heat flows required to heat, cool, or maintain a temperature.
- **Eutectic point.**
  Formation of co-crystals of solute and solvent. The increased viscosity in food samples at the eutectic point means that nucleation is often kinetically limited, and this crystallisation does not occur.
- **Freezable water.**
  Freezable water is the fraction of total water in a sample that freezes between the onset of freezing at the initial freezing point, and the glass transition temperature. Water which remains unfrozen after the glass transition temperature is not bound in an energetic or thermodynamic sense, but rather is kinetically prevented from crystallising due the extreme viscosity of the glassy phase.
- **Freezing.**
  Freezing is the process by which water in an aqueous sample changes phase to ice.
- **Freezing Front**
  The location of the interface between unfrozen liquid and solid ice. In a dendritic or columnar interface the location of the freezing front is considered to be the location of the leading crystal tips.
- **Glass transition.**
  A kinetic transition characterised by a sudden increase in viscosity, as a sample transitions from a highly viscous, or viscoelastic fluid, to a non-crystalline solid.
- **Ice front velocity/ice growth rate/freezing front velocity.**
  The rate at which a growing interface between ice and unfrozen sample advances into the subcooled sample. Typically described in μms^{-1}.

- **Icephobic surface.**
  A surface typified by an ice adhesion strength between ice and the surface significantly lower than that between ice and an untreated substrate.
- **Initial freezing point/temperature.**
  The temperature at which a sample starts to freeze if no subcooling occurs.
- **Maximally freeze concentrated state.**
  The state at which the unfrozen phase will no longer concentrate as a result of ice crystal formation removing water from the phase. This occurs when the viscosity of the phase increases such that further crystal growth will not occur over the timeframe of the measurement.
- **Melting onset transition.**
  The transition at which ice crystal formation ceases during the cooling of a freezing sample. Further crystal formation will not occur within the measurement time period due to extreme viscosity of the unfrozen phase.
- **MPAES.**
  Microwave Plasma Atomic Emission Spectrometry– an analytical technique that measures the elemental composition of a sample using the intensity and wavelength of emitted light from a microwave excited plasma containing the sample to be analysed.
- **Nucleation.**
  The formation of a stable crystal nuclei in a system where the new phase is thermodynamically favoured. The first stage in several common phase transitions**.**
- **Subcooling.**
  Cooling a sample below its equilibrium freezing temperature without formation of ice crystal. A sample persists in a subcooled state until nucleation occurs.
- **Superhydrophobic surface.**
  A surface typified by a high contact angle between the surface and water, typically a surface is considered superhydrophobic if the contact angle is greater than 150°.
- **Volume fraction.**
  The fraction of a sample's volume in a given phase (solid/liquid. Frozen/unfrozen).

Chapter 1: Programme Background and Literature Review

1.1 Rationale for Project and Project Aims

The New Zealand Sheep Dairy Industry is small but has the potential to grow and be a significant export income earner for NZ, by sustainably producing a range of high value product. However, the small and geographically disperse nature of the industry has created logistical challenges that limit its growth.[1]

The ovine dairy industry (and other specialist dairy industries, such as cervine or caprine), does not have the transportation and processing infrastructure across New Zealand that the bovine industry has, and those processors who may be interesting in increasing manufacturing of ovine milk products may be located far from milk producers.

Therefore, farmers who would like to enter the industry are either limited by who they can sell their milk to, forced to process their own milk, or are unable to enter the market altogether. Furthermore, many farmers the Author has spoken to would like a storage-stable form of their product, which would allow them a stable income throughout the year.

This is further exacerbated by the small scale of production of ovine dairy farms, where individual ewes may produce 1.5-2 L/day at peak production[2]. For a farm of 200-300 ewes, which may be a typical size of a small to medium scale operation[1], this would mean a peak daily production of 600 L. NZ regulations require that milk be processed in NZ within 72 hours of milking [3], this means small volumes of milk must be transported regularly, at significant shipping cost.

The small daily volume of production also limits the processors willing to accept ovine milk, as typical processing volumes in the dairy industry are much larger than that achieved by ovine milk producers.

Clearly a method of storage is needed which will allow for the aggregation of significant volumes of milk before shipping and processing. What has been previously suggested is freezing on farm.

While freezing has attractions, and can allow for year round supply, which is desirable from a number of viewpoints, the slow bulk freezing methods previously suggested have downsides, ranging from degradation of quality [4, 5], to microbial growth during the thawing of large volumes of raw milk[6].

What is needed is a method for freezing volumes on farm, with minimal quality degradation, and in a form that allows for easy handling, storage and final processing. The on-farm freezer should also be affordable, environmentally sustainable, reliable, and require minimal labour to maintain or operate. If these criteria are met, then frozen milk may become a tradeable article of commerce in the same way liquid milk is today.

The Food Industry Enabling Technologies (FIET) programme, funded by the New Zealand Ministry of Business, Innovation and Employment (MBIE), established a research project to investigate the freezing phenomena in ovine milk and the changes occurring during frozen storage, and use this research to develop a novel and effective on-farm freezer. The freezer development was to use ovine milk as an exemplar product, however a solution that was applicable across the wider range of liquid foodstuff freezing, especially freezing of low viscosity, moderate total solids, liquid foodstuffs was desirable. Therefore, the freezer developed should be suitable for other high-value products.

1.2 Sheep Dairying

Sheep have been milked for millennia [7], primarily in regions surrounding the Mediterranean sea. In 2017, sheep milk accounted for approximately 1.26% of global milk production, with a global production of 10.4M tonnes of whole milk, from a global flock of 245M dairy sheep [8].

Sheep were first brought to New Zealand in 1773 by James Cook, and from the late 19th century to the 1980s meat and wool farming formed the backbone of New Zealand's economy[9]. In recent years the bovine dairy industry has become New Zealand's largest export earner[10]. However, with the recent instability in commodity prices, there has been a growth in interest in sheep dairying, which has the potential for higher returns than bovine dairy, and offers several revenue streams for the farmer (milk, meat and wool)[1].

New Zealand is ideally located to grow the sheep dairying industry. NZ has a temperate climate, land suitable for pastoral farming methods, a long history of sheep farming, a world-leading bovine dairy industry, and emerging markets in Asia. Some commenters have said that the sheep dairy industry in NZ has the potential to grow to grow to a billion dollar industry[1], becoming one of the 10 largest global producers of sheep milk. Recently the Ministry for Primary Industries (MPI) has announced a Primary Growth Partnership (PGP) in conjunction with Spring Sheep Dairy, making a combined $30 million investment in R&D aimed at growing the NZ sheep dairy industry[11].

1.3 Sheep Milk Composition

1.3.1 Gross Composition.

Sheep's milk is typically higher in total solids than the more common cow and goat milks, primarily in fats and protein, leading to a higher cheese yield, when compared on equivalent volumes of milk[7, 12]. The total solids composition of sheep milk generally varies from 17% to 21%, depending on breed, farming system, nutrition, and individual animal performance [4, 7, 13, 14].

Ovine milk typically forms a firmer curd on renneting when compared with caprine or bovine milk, as a result of this higher casein content [15].

1.3.2 Protein Composition

Sheep milk caseins have a Ca content of 3.7 g/100 g casein, higher than caprine milk (3.6) and bovine milk (2.9)[13].

The caseins are between 76% -83% of the total protein content of ovine milk [4].

1.3.3 Fat Composition

Ovine milk contains a lower proportion of short and medium-chain fatty acids than caprine milk [15]. These have been suggested [15]to be partially responsible for ovine milk having a milder taste when compared with caprine milk.

Ovine milk and caprine milk are higher in medium-chain triglycerides than bovine milk. These medium-chain triglycerides are easier to digest than longer chain fatty acids. [16].[17]

Ovine milk has been found to have a high CLA and omega 3 fatty acid content [17]

1.3.4 Salts and Sugars

The lactose content of sheep milk at ~4.9% on average, is similar to that of bovine milk[4], but lower on a dry matter basis (22%-27% vs. 33%-40%)[13], and ovine milk has a higher lactose: water ratio.

1.4 Sheep Milk Properties and Variation

1.4.1 Variation in Sheep Milk

The production volume of ovine milk, its quality and its composition can vary widely with breed, nutrition, days in lamb, parity, farming system, milking technique, and climate [18]

The initial freezing point of sheep milk from one farm was found to decrease over 7 months of milking from an average of -0.584°C to -0.724°C, with a whole season average of -0.617°C[19]. Another study found an average freezing point of -0.559°C with a range from -0.733°C to -0.360°C[20]

Daily milk production in specific milk breeds (Awassi and Assaf) has been found to peak in the first 4 weeks and decrease slowly until the end of lactation. In Israeli conditions, the average daily production from a flock was found to peak in June and reach a minimum in October [2]. Milk yield also increased with time postpartum before conception, and peaked at the second parity, decreasing with further parities[2]. Total milk yield also increases with the age of first lambing [21].

Specialist dairy breeds, particularly those like the Lacaune which have had significant improvement from breeding programmes [22], have higher total milk yields. These breeds include the East Friesian (up to 550 kg/season), Improved Awassi (530 kg/ season), Awassi (400 kg/ season), Assaf (333 kg/season) ,and the Lacaune (285 kg/ season) [23]. In New Zealand, the dairy sheep flock lacks the genetic performance seen elsewhere, and milk yields average approximately 200 kg/season [1, 24].

The total solids concentration of sheep milk is often inversely proportional to the total yield of milk produced[16].

1.4.2 Sheep Milk Properties

Ovine milk is more viscous than caprine or bovine milk, and is affected by composition, temperature, pH and age, with an average viscosity of 2.48 mPa.s [12]. The viscosity increases during cooling, partly due to an increase in the voluminosity of casein micelles, with a partial dissociation of β-casein from the micelle. The voluminosity of hydrated casein micelles is roughly 4 cm^3g^{-1} [25].

The fat globules in ovine milk have an average diameter of 3.3µm, smaller than caprine (3.5 µm) and bovine(4.6 µm) milks. [13]

The density of ovine milk is 1037 kgm^{-3}, which is similar to bovine and caprine milk[13].

1.5 Sheep Milk Products

Sheep's milk is mainly used to make yoghurts and cheeses, due to its high total solids content and its history in hot dry regions, where these products served as an effective way to preserve milk. Some examples of sheep cheeses include the famous Feta (Greece), Manchego (Spain), Pecorino(Italy), Ricotta (Italy), and Roquefort (France) cheeses [5, 7].

Less traditional products from sheep milk include fresh pasteurised milk[26], UHT and ESL milk[27], flavoured milk products[28], skim and whole milk powders[24], infant formulas, ice creams[26], sweets, probiotics[29] and even cosmetics and soaps[30].

1.6 Review of Freezing Physics

Ice is the solid phase of water, which is of critical importance to many industries, and plays a critical role in earth's climate. There are approximately 17 experimentally confirmed crystalline polymorphs of solid ice and at least 4 forms of amorphous ice, with more predicted by computational modelling[31]. Ice I_H is the form of ice exclusively encountered in daily life, and in

the food processing industry, as it exists at atmospheric pressure and at temperatures common to food processing [32].

Freezing is the exothermic liquid-solid phase transition experienced by water when it is cooled below its equilibrium freezing temperature, which is 0.00°C at atmospheric pressure[33]. Ice is a crystalline solid, so the process of freezing is a form of crystallisation. Under extreme conditions however, water can be vitrified forming an amorphous solid below ~130 K [34].

Crystallisation consists of two processes, nucleation followed by crystal growth from the melt. Incorporation of impurities into the crystal structure, or the crystal matrix may occur during the crystal growth phase. The size, morphology and distribution of the crystals is determined by the interaction of these two processes.

1.6.1 Nucleation

Nucleation is the creation of crystal nuclei from a supercooled or supersaturated liquid. For crystal growth to proceed, the nuclei have to be sufficiently large that further growth is thermodynamically favourable. The rate of creation of these nuclei is the nucleation rate[35].

There are two main forms of nucleation, primary and secondary nucleation. Primary nucleation is the spontaneous formation of nuclei either from the bulk, in homogeneous nucleation, or at a nucleation site, in heterogeneous nucleation. Secondary nucleation is the formation of new crystal nuclei by the break-up of previously formed crystal[36]s.

Primary homogenous nucleation of water requires a large driving force, in the form of supersaturation or supercooling to occur. Nucleation begins when small crystal-like molecular aggregates form. The classical theory of primary nucleation describes the work required to create a nucleus as having a surface term and a volume term[35]:

$$W = W_s + W_v \tag{1-1}$$

Where W_S is the work required to form a new surface interface, and W_v is the work required to create the new bulk phase. W_s is positive, whereas W_v is negative as the new bulk phase has a lower Gibbs free energy. The change in Gibbs free energy on the formation of a small particle in liquid can therefore be written as[37]:

$$\Delta G = \Delta G_s + \Delta G_v \tag{1-2}$$

The classical nucleation theory analysis assumes the nuclei are spherical, so this becomes[36]:

$$\Delta G = 4\pi r^2\sigma + \frac{4}{3}\pi r^3 \Delta G_u \tag{1-3}$$

$$\Delta G_u = -\frac{4\pi r^3}{3v} kT \ln \beta \tag{1-4}$$

Where r is the particle radius, ΔG_s is the surface free energy change, ΔG_v is the change in volume free energy and is negative, σ is the surface energy of the particle per unit are, $\Delta G_u$is the change in free energy per unit volume, and β is the ratio of the vapour pressure and the vapour pressure at equilibrium freezing temperature for the solute (The saturation ratio), and k is the Boltzmann constant[38].

This relationship is plotted in Figure 1-1 [39, 40]. If molecular clusters are below a critical radius r_c, further growth is energetically unfavourable and the clusters dissolve. Above this radius, further growth is energetically favourable and crystal nuclei are formed.

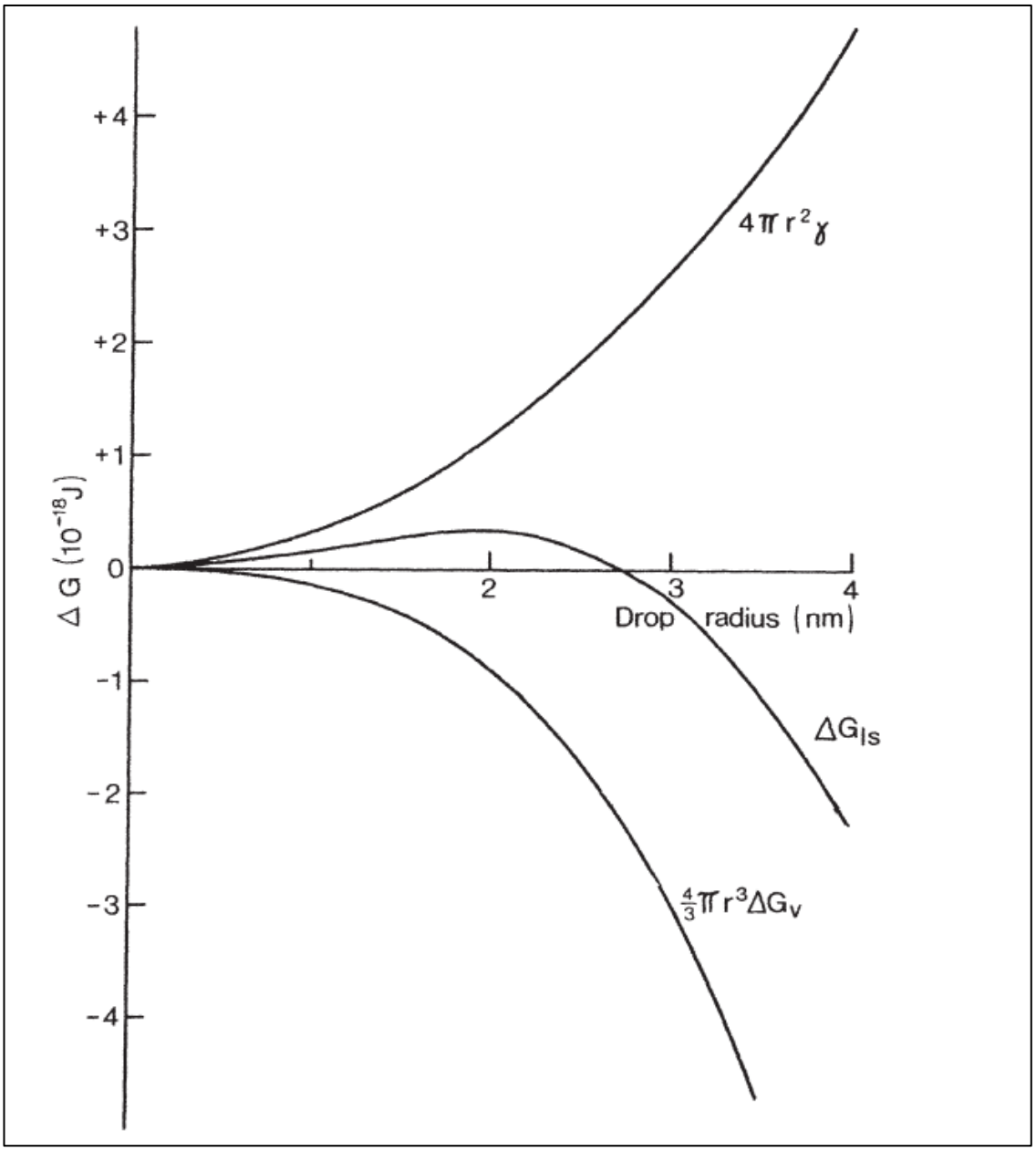

Figure 1-1: Thermodynamics of homogenous nucleation in water at -40°C. From [40]. The critical nucleus contains around 200 molecules and r_c=1.9 nm. The monotonically increasing curve represents the surface free energy term resulting from the formation of a solid/liquid interface. The monotonically decreasing curve represents the volumetric free energy change that occurs when a lower-energy solid is formed from a liquid. ΔG_{ls} is the total free energy change for the transition of the nucleus from liquid to solid.

These molecular clusters form as a result of spontaneous agglomeration of water molecules. These can be easily dispersed by thermal vibrations. At sufficient supercooling these clusters reach critical radius and grow into nuclei.

The radius of a critical nuclei is given by the following equation where Ω is the molar volume [41].

$$r_c = \frac{2\sigma}{\ln \beta} \cdot \frac{\Omega}{RT} \tag{1-5}$$

The critical energy barrier is given as [42], with v_{ice} being the volume of a water molecule in ice and :

$$\Delta G_c = \frac{16\pi\sigma^3 v_{ice}^2}{3k^2T^2 \ln \beta^2} \tag{1-6}$$

The homogenous nucleation rate J_{hom}at a given level of supercooling is a product of the number of clusters of critical radius in a volume, n_c , and the rate that new molecules move to these clusters from liquid phase.

The number of critical radius nuclei is derived from the population distribution of clusters, which is a Boltzmann distribution:

$$n_c \cong n_1 \exp\left(-\frac{\Delta G_c}{kT}\right) \tag{1-7}$$

Where n_1 is the number of monomolecules of water in a volume. The rate that the nucleus acquires new molecules is proportional to the number of monomolecules at the cluster surface and the frequency of their incorporation into a cluster. This frequency is described as follows, where $\nu_{molecule}$ is the vibrational frequency of a molecule at a given temperature, h is Planck's constant, and ΔF is the activation free energy change for diffusion into the nucleus:

$$\nu_{inc} = \nu_{molecule} \exp\left(-\frac{\Delta F}{kT}\right) \tag{1-8}$$

$$\nu_{molecule} \cong \frac{kT}{h} \tag{1-9}$$

Using these relationships, the homogenous nucleation rate can be calculated as shown in equation (1-11) , where $n_s$is the number density of molecules on the nuclear surface, V_w is the volume of water and $\mathcal{Z}$ is the Zeldovich factor (which corrects for the fact that some nuclei of critical radius dissolve, rather than grow further[43]) :

$$J_{hom} = n_s 4\pi (r_c)^2 \mathcal{Z} \cdot \nu_{inc} \cdot \frac{n_1}{Vw} \exp\left(-\frac{\Delta G_c}{kT}\right) \tag{1-10}$$

$$J_{hom} = n_s 4\pi (r_c)^2 \mathcal{Z} \left(\frac{kT}{h}\right) \exp\left(-\frac{\Delta F}{kT}\right) \cdot \frac{n_1}{Vw} \exp\left(-\frac{\Delta G_c}{kT}\right) \tag{1-11}$$

$$J_{hom} = A \cdot \exp \frac{16\pi\sigma^3 v^2}{3k^3T^3 \ln \beta^2} \tag{1-12}$$

As can be seen from the above relationships, J_{hom} is a product of a kinetic term (A) describing the incorporation of molecules to a nucleus, and a thermodynamic term describing the number of nuclei of a critical size at a given temperature. The rate of nucleation can be seen to be inversely proportional to the cube of the temperature of the system.

ΔF has a large influence on the nucleation rate, as can be seen from equation (1-11). ΔF is a function of the temperature of the system and the diffusivity of crystal species in the melt D [44]:

$$\Delta F = \frac{\delta \ln D(T)}{\delta T} kT^2 \quad (1\text{-}13)$$

The Stokes-Einstein equation shows that the diffusivity of a particle is inversely proportional to the dynamic viscosity of the fluid it is in: $D \propto \frac{1}{\eta}$ [45]. Therefore, in classical nucleation theory, the homogenous nucleation rate is decreased by an increase in viscosity, all other factors remaining constant.

As the nucleation rate describes a stochastic process, the probability of a given number of stable nuclei forming during a given time period can be described by a Poisson Distribution [46].

Heterogeneous nucleation occurs at the surface of a foreign particle or surface. Heterogeneous nucleation requires a lower degree of supercooling or supersaturation. The nucleus "wets" the foreign surface with a contact angle θ, similar to how a drop of water wets a surface. The effective surface energy of the nucleus is lower, and the free energy required for nucleation modified as follows[47]:

$$\Delta G_{heterogeneous} = \Delta G_{homogeneous} \cdot f(\theta) \quad (1\text{-}14)$$

$$f(\theta) = \frac{2 - 3\cos\theta + \cos^3\theta}{4} \quad (1\text{-}15)$$

Once a nucleus forms, a crystal of ice will grow in the supercooled water, releasing latent heat until the system reaches the equilibrium freezing temperature. This stage is known as recalescence.

1.6.1.1 Crystal Growth

Of the large variety of crystalline ice phases, the hexagonal ice I_H is the most commonly encountered. This crystalline form has a hexagonal crystal structure with 3 a-axes in one plane, and the c-axis normal to this plane [48]. The face perpendicular to the c-axis is called the basal face, while those faces 30° to a plane perpendicular to the a-axes are the primary prism faces. The faces perpendicular to the a-axis are the secondary prism faces. This is shown in Figure 1-2.

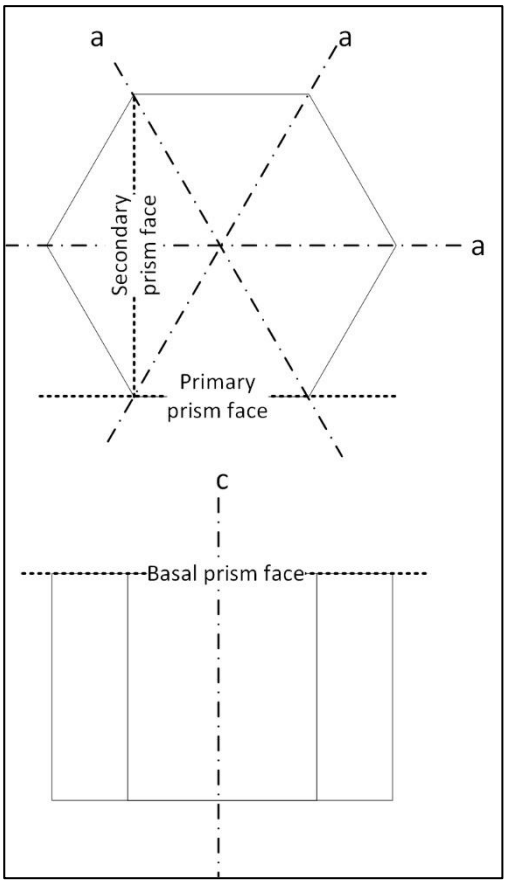

Figure 1-2: The crystal faces and axes of Ice 1_H. Top view and side view shown.

The growth rates of the crystal faces show distinct differences with temperature[49], which leads to ice crystals grown in isolation having varying morphology with temperature: Crystals grown at -2°C are planar, columnar at -5°C, planar at -15°C and columnar at -30°C [50]. In crystals grown at -5.5°C, the condensation coefficient (proportional to growth rate) for the basal plane was 10x of that for the prism faces[50].

The high level of supercooling possible before nucleation in pure water results in rapid initial crystal growth rates, which are controlled by the kinetics of the system and depart from those predicted by thermodynamic and diffusion based models [51]. This makes controlling the crystalline orientation experimentally difficult[52]. However, this has been overcome in studies growing single crystal boules using growth tubes to isolate the most stable growth face [52]. This work suggests that the secondary prism face is the most stable during growth in ice/water interfaces at 0°C. During growth of boules from polycrystalline seeds ice does not form a random lattice structure, rather the prism faces of the ice crystals dominate ice growth, with the c-axis being tilted away from the direction of ice growth [53]. This orientation is the result of the crystal growth rate and enthalpy differing between the basal and prism faces, leading to the prism faces being favoured over the basal faces [52-54].

1.6.2 Freezing in Pure Water and Solutions

The freezing point is a colligative property of a solution and is therefore affected by the molar concentration of solutes present.

A liquid will generally freeze when its chemical potential is larger than that of the solid at the same temperature:

$$\mu_{solid} \leq \mu_{liquid} \tag{1-16}$$

In an ideal solution, the chemical potential of component A can be calculated from its molar fraction x_A [55]:

$$\mu_A = \mu_A^0 + RT \ln x_A \tag{1-17}$$

The freezing condition becomes:

$$\mu_{A,solid} = \mu_{A,liquid} \tag{1-18}$$

By taking the constant pressure temperature derivative of the chemical potential:

$$\left[\frac{\delta}{\delta T}\left(\frac{\mu_A - \mu_A^0}{RT}\right)\right]_p = \left(\frac{\delta \ln x_A}{\delta T}\right)_p \tag{1-19}$$

$$-\frac{\mu_A - \mu_A^0}{RT^2} + \frac{1}{RT}\left[\left(\frac{\delta \mu_A}{\delta T}\right)_p - \left(\frac{\delta \mu_A^0}{\delta T}\right)_p\right] = \left(\frac{\delta \ln x_A}{\delta T}\right)_p \tag{1-20}$$

And given that:

$$\mu = H - TS \tag{1-21}$$

$$\left(\frac{\delta \mu}{\delta T}\right)_p = -S \tag{1-22}$$

$$-\frac{H_A - TS_A - H_A^0 + TS_A^0}{RT^2} + \frac{1}{RT}[-S_A + S_A^0] = \left(\frac{\delta \ln x_A}{\delta T}\right)_p \tag{1-23}$$

For water freezing, H_A^0 is the enthalpy of ice, and H_A is the enthalpy of liquid water, so:

$$H_A^0 - H_A = \Delta H_{fus} \tag{1-24}$$

The relationship then becomes:

$$\frac{\Delta H_{fus}}{RT^2} = \left(\frac{\delta \ln x_A}{\delta T}\right)_p \tag{1-25}$$

Integrating this from T^0, the equilibrium freezing temperature of pure water, to T, the freezing temperature of water in the solution, gives:

$$-\frac{\Delta H_{Fus}}{R}\left(\frac{1}{T} - \frac{1}{T^0}\right) = \ln x_A \tag{1-26}$$

$$\frac{1}{T} - \frac{1}{T^0} = \frac{T^0 - T}{TT^0} \cong \Delta T/(T^0)\text{^}2 \tag{1-27}$$

$$-\frac{\Delta H_{fus} \Delta T}{R(T^0)^2} = \ln x_A \tag{1-28}$$

For dilute solutions, where x_A is close to 1, $\ln x_A \approx -(1 - x_A) = -x_B$, where x_B is the molar fraction of the solute. This gives a linear relationship between x_B and ΔT.

As shown above, the freezing point depression of a solution is dependent on the molar concentration of the solute, so high molecular mass solute such as proteins have less effect on the equilibrium freezing temperature, compared to low molecular mass solutes such as salts or simple sugars [48].

In concentrated solutions this relationship no longer holds. Second-order polynomials have been used to describe the relationship between concentration and freezing point depression in food products [56]. More accurate semi-empirical models[57] or mechanistic models [58]for the relationship between solute concentration and freezing point depression have been developed.

Ice growing in a solution will cause the remaining unfrozen fraction X_{uf} to become more concentrated in solutes. As previously discussed, the freezing point of a solution decreases as the molar concentration of solutes increases. Therefore, the equilibrium freezing point of a solution will decrease as water is removed from the liquid phase. The temperature-time profiles of a solution and pure water during freezing in a confined volume are show in Figure 1-3.

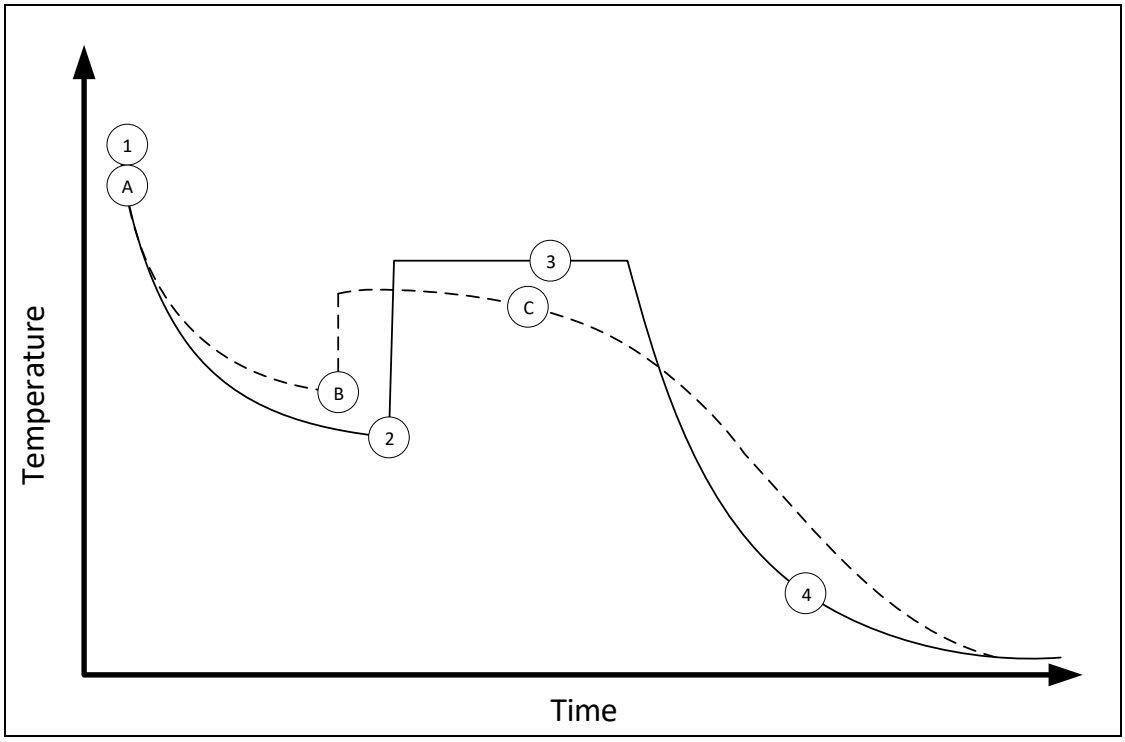

Figure 1-3: Temperature-time profiles during the freezing of pure water and a solution.

The two curves show the following stages of freezing a confined volume:

Freezing in pure water

1. Onset of cooling.
2. Nucleation and Recalescence.
3. Equilibrium Freezing.
4. Cooling of ice to final temperature.

Freezing in a solution.

A. Onset of cooling.
B. Nucleation and recalescence.
C. Freezing with a progressive concentration of solutes in the unfrozen phase, and progressive depression of freezing point.

The solution temperature after recalescence is lower than the equilibrium freezing temperature of the pure solvent, as recalescence removes a fraction of the water as ice and increases the concentration of solutes in the unfrozen phase. For low degrees of supercooling the fraction of ice removed can be estimated by equating the sensible heat removed during supercooling, and the latent heat released by nucleation and recalescence[59]:

$$X_{frozen,recalescence} \cdot \Delta H_{fus} = \Delta T_{supercooling} \cdot Cp \quad (1\text{-}29)$$

$$X_{frozen,recalescence} = \frac{\Delta T_{supercooling} \cdot Cp}{\Delta H_{fus}} \quad (1\text{-}30)$$

1.6.2.1 Freeze Concentration.

The freezing point depression of solutions can be exploited as a separation method, to increase the concentration of a solute, or to purify a solvent by removing impurities. This has been applied to fruit juices[60-64], milk products[65-69], coffee[70], and as a method of purifying water in desalination[71-73] and waste-water treatment[74].

Freeze concentration can be broadly divided into two main categories: Progressive and suspension[32]. Progressive freeze concentration operates by freezing ice onto a cooled surface and decanting the concentrated liquid that remains. This cooled surface may be a static tube in static or flowing fluid[73, 75], or a cooled surface over which a falling film flows [63, 69, 70, 76, 77].

Suspension freeze concentration operates by forming a large population of small crystals in a bulk solution, and then growing these crystals at a low ice growth rate, with the aim of forming highly spherical ice crystals with a low solute content. The ice crystals are then separated from the concentrated bulk solution and washed to recover solute. There are several embodiments of this form of freeze concentration, including multilayer stirred crystallisers with counter-current ice and feed flows [68], fluidised beds [66], or a system with a scraped surface heat exchanger for generating crystal nuclei, a crystallisation vessel for crystal growth, and a wash column for separating concentrate from ice crystals [78]. This last system is typical of commercially available systems [79]. The ice crystals formed by this method of freeze crystallisation are typically smooth disks, and are formed at low levels of supercooling[32].

The partition coefficient is a key parameter in understanding the behaviour and performance of freeze concentration systems, and is derived as follows, where c_s and c_l are the concentrations of solute in the solid matrix and liquid solvent respectively[62]:

$$K = \frac{c_s}{c_l} \quad (1\text{-}31)$$

Falling film freeze concentration uses ice growth rates of 0.01-1 μms^{-1} to separate ice and solutes [68, 78, 80]. A fluid runs over a cooled surface as a falling film and freezes onto the surface. The ice has a lower solids concentration than the liquid running off the surface, so the concentration in the liquid phase increases. Even slow freezing has a fairly high partition coefficient, with values of approximately 0.45 being recorded for freezing front velocities of 2 μms^{-1} [62]. Moreno et al [70] found partition coefficients close to 1 with 15 wt.% coffee at ice growth rates of 4 μms^{-1}.

Chen and Chen[62] developed a generalised semiempirical relationship describing the partition coefficient K for a progressive freeze concentration system, as a function of freezing point depression FPD, ice growth rate v_f, and superficial velocity of the fluid over the ice surface u_s:

$$K = a + bFPD + cFPD^2 + d\left(\frac{v_f}{u_s^{0.5}}\right) \quad (1\text{-}32)$$

The partition coefficient for concentrated milks increases with the solids concentration, as would be expected from the increased FPD. The partition coefficient of sucrose solutions has been found to decrease with increasing superficial fluid velocity[69].

The partition coefficient under flow conditions has been studied analytically, and used to derive models for the partition coefficient as a function of ice growth rate, mass transfer coefficient, solute concentration at the interface and the bulk concentration [81].

1.6.2.2 Changes in Ice Crystal Structure During Storage

Ostwald ripening is a process that can cause the size distribution of a population of ice crystals to change over time. The equilibrium freezing temperature of small ice crystals is depressed as the surface free energy for a given volume of crystals increases as the crystal size decreases, due to the increased surface area/volume ratio of small crystals. This depression can be calculated as follows, where T_f is the equilibrium freezing temperature for a crystal with an infinite radius of curvature, σ is the crystal areal surface energy (1.5-3.2x10^{-2}Jm^{-2} [82]), ρ_s is the crystal density, ΔH is the latent heat of freezing and $R_s$is the crystal radius[83].

$$\Delta T_f = \frac{2\sigma T_f}{\rho_s \Delta H R_s} \tag{1-33}$$

While the magnitude of this driving force is low (for a 10µm crystal ΔT_f is 0.0073°C [83]), it is nonetheless sufficient to lead to changes in the population size distribution of ice crystals over a storage period, with a shift to a larger mean particle size occurring.

Other forms of recrystallisation that can occur are isomass ripening and accretive recrystallisation. Isomass recrystallisation is the tendency of high surface area crystals to change shape to minimise the surface area, and hence surface energy, without changing mass. Accretive recrystallisation occurs when two crystals in contact with each other merge to form a single larger crystal[48].

1.6.3 Freezing in Colloids

Another process where the distribution of particles between an advancing ice front and a liquid phase is important is freeze casting. Freeze casting is used to create porous ceramic and nanoparticle structures through the formation of regularly structured ice crystals, and the rejection of particles into the inter-crystal spaces. The ice is removed by freeze drying, leaving a porous structure that can be sintered[84-86]. A similar process in the food field is freeze texturing, which is a method to produce structure in meat analogues, similar to the traditional Japanese method of producing frozen soybean curd called kori-tofu[32, 87]. An ice front moving parallel to the heat flux forms a network of needles or dendrites of ice in the protein, which persists as structured pores when the liquid is melted and removed.

1.6.3.1 Particle Interactions with Advancing Interfaces

Above a critical ice front velocity, particles suspended in a solvent are engulfed and trapped in the advancing ice front[88].The critical ice front velocity can be calculated by the following relationship [89], where $\Delta\sigma_0$ is the change is free energy of the particle, a_0 is the intermolecular distance of the fluid, η is the fluid viscosity, d is the thickness of the liquid film at the freezing front interface, R_p is the particle diameter and z is an exponent specific to the studied system.

$$v_c = \left(\frac{\Delta\sigma d}{3\eta R_p}\right)\left(\frac{a_o}{d}\right)^z \tag{1-34}$$

For specific systems this critical velocity can be expressed as a function of the particle diameter. There are two opposing forces acting on a particle just ahead of a freezing interface. There is a repulsive force that arises from the system's resistance to an increase in surface energy, and an attractive force resulting from viscous drag which pushes the particle towards the interface.[90]. A force balance between these two forces allows the critical velocity equation (1-34) to be derived.

The drag force F_d is a modified form of Stokes equation [91], where v is the freezing front velocity, and other symbols are the same as those in equation (1-34):

$$F_d = 6\pi\eta v R_p^2/d \tag{1-35}$$

From a thermodynamic perspective, a particle will only be trapped if the free energy of the system is minimised by the incorporation of the particle in the advancing interface, that is $\Delta\sigma_0$ <0:

$$\Delta\sigma_0 = \sigma_{ps} - (\sigma_{pl} + \sigma_{sl}) \tag{1-36}$$

Where σ_{ps} is the surface energy between the particle and the solid, $\sigma_{pl}$is the surface energy between the particle and the liquid, and σ_{sl} is the surface energy between the liquid and solid phases.[92].

This value for $\Delta\sigma_0$ can then be used to determine the force rejecting the solid from the front:

$$F_\sigma = 2\pi R_p \Delta\sigma_0 \left(\frac{a_0}{d}\right)^Z \tag{1-37}$$

When these two forces are balanced, one gets the critical velocity equation shown in (1-34) [91].

For 1µm spheres of polystyrene the critical velocity of ice growth has been calculated as approximately 30µms^{-1} [88].

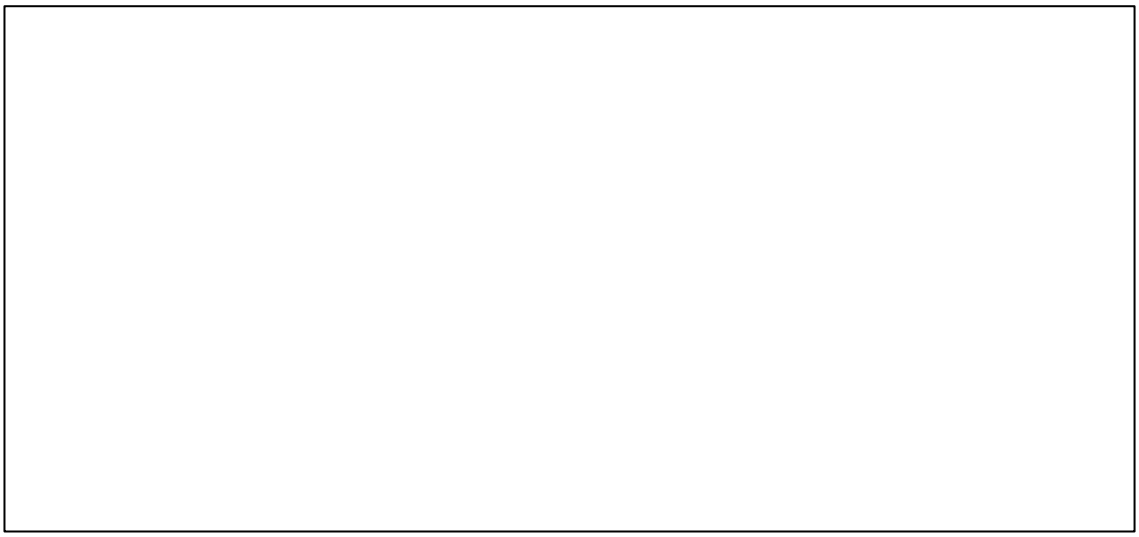

Figure 1-4: Trapping particles in an advancing freezing front. From Waschkies et al (2011) [88].

However, the above relationships are only valid for idealised systems and geometries. For complicated systems such as freezing in soils, and systems which involve particle-particle interactions and soft particles, the behaviour is much more complicated [93].

The advancing ice front can have its freezing temperature reduced as a result of two main factors, solvent constitutional supercooling (SCS), due to dissolved solutes in the solvent and their migration away from the interface, leading to freezing point depression ahead of the advancing interface and particulate constitutional supercooling (PCS) resulting from the thermodynamics of multiple particle interactions ahead of an advancing ice front[94]. This has been measured experimentally, and SCS was found to dominate for alumina and polystyrene suspensions in dilute HCl [95].

1.6.3.2 Freezing Front Instabilities and Morphology

It is well known that in many directional freezing or solidification systems a planar interface becomes unstable and transitions to a more complex interface; this is known as Mullins-Sekerka instability.[96]. This morphology is determined by the interaction between macroscopic driving forces, supersaturation or supercooling, and the microscopic properties of the interface, surface tension, interfacial energy and crystal growth kinetics.

Mullins and Sekerka found that infinitesimal perturbations at the interface of a growing spherical crystal can either decrease over time, or increase and lead to unstable growth if the perturbation is above a critical radius[97].This analysis was extended to planar surfaces with a sinusoidal perturbation of infinitesimal initial amplitude [98], which showed that if the perturbations grew, the interface would become unstable. In a unidirectionally advancing solidification interface in a pure melt in a 2-dimensional system, there is a degree of supercooling ahead of the interface caused by the balance between the crystal growth rate as a function of supersaturation and the thermal gradient of the system.

If a sharp perturbation exists, the thermal gradient and the growth rate at the perturbation are higher. This would make it favourable for an interface to break up into a number of perturbations. This is described in terms of heat removal, but the phenomenon is equally applicable to mass transport, and diffusion of crystal species to the growing interface.

However, a complicated interface with a number of perturbations would have a significantly larger interfacial area, and a larger interfacial energy, which is thermodynamically unfavourable. The increased curvature of the interface at perturbations also leads to an increase in the chemical potential of the perturbed region as a result of the Gibbs-Thomson effect. This decreases the chemical potential gradient between the melt and the solid and reduces the growth rate at the tips. The balance between the kinetic forces driving destabilisation of the interface and the thermodynamic forces promoting a flat interface is partly responsible for the variation in interface morphologies seen in advancing solidification interfaces.

In a suspension being directionally frozen the crystal network and, therefore the pore morphology of a freeze-dried product are strongly dependant on the solvent. Water based suspensions have typically lamellar pores, camphene-based suspension form dendritic pores and tert-butyl-alcohol based suspension result in prismatic pores [99].

However, water-based suspensions can also grow in a dendritic fashion [88, 89].The α-value of a solvent is calculated from the latent heat h_E at the equilibrium temperature T_E the gas constant R and a factor dependent on the crystallographic environment of the interface ξ.

$$\alpha = \frac{h_E \xi}{R T_E} \tag{1-38}$$

This value determines whether crystal growth occurs in a dendritic or faceted manner. Dendritic growth generally occurs when α<1[100]. The entropy of melting h_E/RT_E of water is approximately 2.6 [90, 101], yet it readily forms dendrites, as ξ has a typical maximum of 0.5-1 for the close packed crystal plane and less for others.

These phenomena in an idealised unidirectional solidification of a suspension of monodisperse hard particles, have been described mathematically, with an emphasis on particle size and particle fraction [102]. This framework has shown that under certain conditions suspensions of small particles can result in constitutional supercooling, which destabilises the interface. Larger particles can form stable porous media, where the water phase can become supercooled and nucleate. This framework provides a partial explanation for the range of freezing morphologies seen in soils, tissues and colloids [93, 102, 103].

For suspensions of monodisperse hard particles in water, mathematical analysis of the stability of the advancing ice interface has showed that an increase in particle size stabilises the advancing ice interface, and increases in the particle density destabilise the interface [104]. The stability equation is similar to that derived for dilute alloys [98, 104]. The increase in stability with particle size, is related to the surface energy at the interface, which scales with R_p^5. However, this analysis only considered particles at the nanoscale, with a constant partition coefficient. As the particle size increases, the diffusion coefficient of the particles also decreases, so they cannot be transported away from the interface as easily. This leads to particle engulfment and loss of stability at the interface.

Particles can also destabilise an interface by influencing the thermal gradient ahead of the interface [105]. As a particle with differing thermal conductivity to the melt in pushed ahead of the interface, it induces a change in the thermal profile ahead of the interface. An insulating particle can lead to a reversal in the thermal gradient as the gap between it and the interface decreases, and heat is rejected more easily through the solid phase.

1.6.3.3 Feature Spacing

The feature spacing in an advancing solidification front decreases with increasing freezing front velocity [88, 89, 99]. This is also observed in freeze-texture meat analogues [106].

The relationship between feature spacing λ and interface velocity v_f in freezing water-based colloids has been described as a power law $\lambda = A \cdot v_f^{-n}$ [88, 89, 99]. The prefactor A has been reported to increase with increased solid content [88]. The exponent n has been reported to show a dependence on particle size in alumina suspensions, with n decreasing as particle size decreases [89], varying from 0.67 to 1. Various other colloid freezing studies have reported n values from 0.33 to 0.7[99] .

1.6.4 Controlling the Onset of Nucleation

In many applications it is desirable to control the onset or degree of nucleation in crystalliser or freezer. There are several methods that can increase the rate of nucleation, however many of these are novel and are yet to be employed at a commercial scale.

1.6.4.1 Ice Nucleating Substances

There are several substances that effectively promote ice nucleation, either by providing sites for heterogenous nucleation, or having crystalline structures similar to ice, and thereby promoting nuclei growth [107, 108]. However, while these are of great interest in studies of atmospheric ice formation[109-112], they are not suitable for application in a food product, where hygiene and food safety are paramount, and therefore the addition of foreign substances is not ideal.

1.6.4.2 Ultrasound Assisted Nucleation

Ultrasonic assisted crystallisation is also known as sonocrystallisation and has been noted in many systems for around 70 years[113]. Ultrasound assisted freezing or nucleation has been investigated in apples [114], potatoes [115], sucrose solutions[113], and pharmaceutical proteins [116].

Ultrasound can induce nucleation and increases the reproducibility of when nucleation occurs. The degree of supersaturation required for nucleation is reduced by the application of ultrasound[117]. The exact mechanism that occurs during sonocrystallisation is not known [113, 117]. It has been suggested that similar mechanisms that cause increased nucleation in cavitating systems are also responsible for ultrasound assisted nucleation. These mechanisms are discussed further below.

1.6.4.3 Microwave Assisted Nucleation

Somewhat counter-intuitively, the application of microwave can assist in the nucleation and freezing of food products. Microwave assisted freezing has been trialled in pork[118] and other meats [119]. The ice crystal size in meat that had been frozen along with the application of microwave was found to be smaller than that frozen conventionally, and lower levels of tissue damage and supercooling were noticed. [118]. The mechanism behind this phenomenon is not well understood, but may be due to the interaction of microwaves and water molecules causing the water to aggregate intro "ice-like" molecular clusters, which leads to a higher nucleation rate.

1.6.4.4 Electric Field Assisted Nucleation

Both static and moving electrostatic fields, and applied electric charges can affect the nucleation rate and size of ice crystals in a frozen system [119]. In one study the temperature of homogenous nucleation in distilled water increased with increased electric field strength [120]. The effect of static electric fields on the freezing of pork meat has been studied, and has been found to reduce supercooling and the average size of ice crystals[121].

It has been suggested that the applied electrostatic field induces a dipole alignment in water molecules. These aligned water molecules form clusters more easily, which promotes the formation of ice nuclei, increases nucleation rate and reduces supercooling[122].

1.6.4.5 Cavitation Driven Nucleation

Cavitation is the formation of bubbles in a liquid due to low or negative pressure regions. When these bubbles collapse an extremely high pressure is generated in the centre of the collapsing region.

In a supercooled or supersaturated system cavitation causes an increase in nucleation rate. Cavitation also induces nucleation at lower degrees of supercooling/supersaturation than would be required for nucleation in a quiescent state.

The mechanism behind this phenomenon was uncertain for many years. It had been suggested that the evaporation at the bubble/liquid interface caused local cooling, increasing supercooling and increasing nucleation rates. Another suggestion was that the existence of a gas/liquid interface promoted heterogeneous nucleation. However, neither of these mechanisms was sufficient to explain the increase in nucleation rates seen in cavitating systems. An elegant experiment in the 1960's separated the effects of cavitation bubble formation and collapse[123]. It is now thought that the increase in pressure during cavity collapse pushes the water to temperature/pressure conditions where high pressure ice exists [124], and these germs then lead to further ice growth. This can be seen on the water phase diagram in Figure 1-12, where the temperature of the equilibrium liquid/solid phase change increases with pressure above 207 MPa. The pressures encountered at the centre of collapsing cavitation bubbles have been found to be on the order of several GPa [125], well above the pressures found in high pressure processing equipment, or achievable by conventional pumps.

1.7 Review of Existing Storage Work and Milk Gelation Mechanisms

Milk is an extremely perishable substance [126], due to the presence of significant nutritive value and favourable pH and osmolarity for the growth of spoilage organisms.

Milk is also a highly valuable source of nutrition and income and has been for centuries. As milk is produced for only a limited season and spoils rapidly, finding methods of preserving milk for transportation or consumption outside of the normal production season has been the primary driver for the development of dairy products. Butters, ghee, cheeses, yoghurts, fermented milk products, dried products, heat treated products, and extended shelf life dairy products are all the result of attempts to increase the shelf life of dairy products.

This problem is even more severe for sheep milk, as the small daily production volumes and rudimentary state of the NZ sheep dairy industry in many regions means that producers face a challenge in supplying fresh milk to processors. While the vast majority of cow dairy producers in the western world store fresh milk in chilled vats prior to processing, sheep dairy producers are often forced to store their milk as a frozen product until it can be processed into dairy products [6]. The process of freezing and thawing, and frozen storage has a wide range of effects on the physicochemical and microbiological properties of the milk.

1.7.1 Physico-Chemical Effects of Frozen Storage

The slow freezing of milk and its storage at higher temperatures (>-20°C) has been linked to decreases in total solids, fats and non-fat milk solids[127],development of rancid flavours[128], increased coagulation time and decreased curd firmness in cheese making[129], and losses in cheese yield and increased occurrence of rancid flavours in cheese[130] .

Freezing has also been shown to reduce the stability of milk-like soy beverages [131], and to cause agglomeration of previously stable colloidal dispersions[132].

Yoghurt manufactured from frozen RO concentrated whole sheep milk, stored at -20°C, has been reported to have similar quality to that made from fresh milk. However, yoghurt made from frozen RO concentrated skim milk has been found to have inferior quality when compared with that made from fresh milk[133]. The skim milk yoghurt formed a thick “cream layer” at the surface, displayed increased syneresis and had a grainy texture[133].

It has been found that storage temperature has a major effect on the recovery of milk components. Wendorff [5] stored milk in 13.5L buckets and 170mL containers, at -15°C and -27°C. The milk stored at -15°C showed higher levels of protein degradation; a higher level of Acid Degree Value, which has been correlated to increased levels of Free Fatty Acids (FFA)[134];and a lower bacterial count, which is most likely due to the growth of larger ice crystals in the higher temperature samples. In another study, Wendorff reported that 40% of the casein in milk was destabilised after 9 months storage at -15°C [130]. The figure below is reproduced from this study.

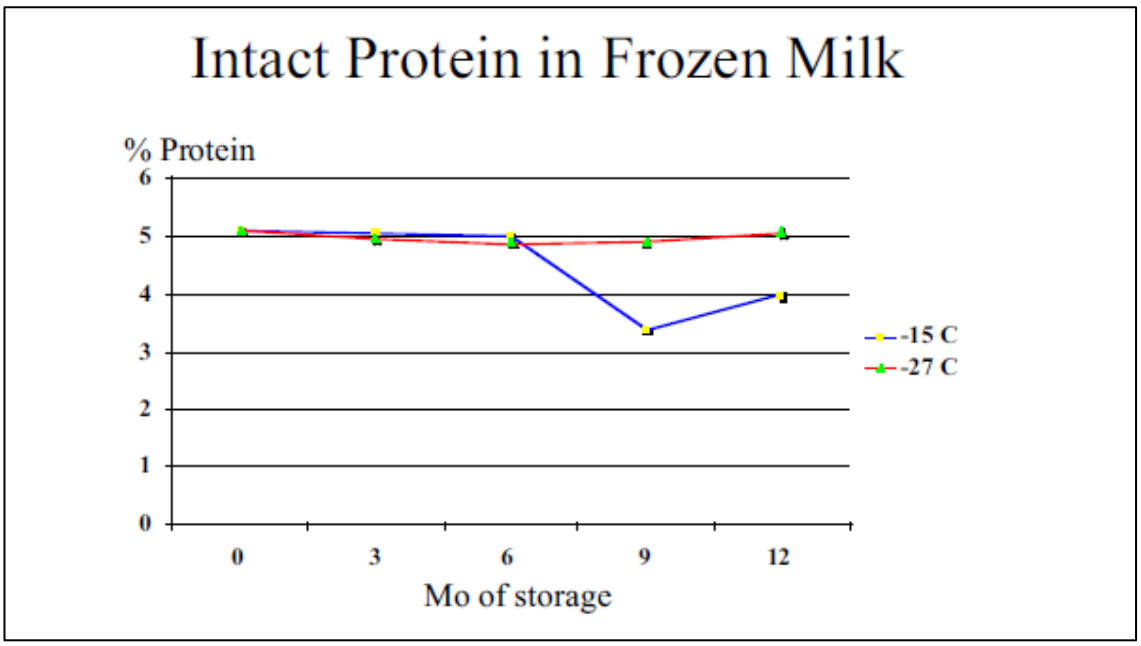

Figure 1-5: Intact Protein in frozen sheep milk after storage periods up to 12 months (Mo), from[130].

Separation of proteins and the formation of sediment has been reported in ewes milk stored at -12°C and -20°C [135].

Other studies have also found high levels of FFAs in milk stored at -12°C, when compared with milk stored at -20°C or -27°C. However, lipolytic enzymes retain activity better after storage at -27°C [127]. This also indicates that minor components such as enzymes may survive frozen storage better at lower temperatures [127] .

The digestibility of casein from milk frozen and stored at -9.5°C is reduced [128].

Between -10°C and -20°C, a significant fraction of the milk remains unfrozen. It has been suggested that protein flocculation occurs in the unfrozen phase[128] .

There have been a range of explanations proposed for the reduction of protein stability in frozen milk. These explanations focus on the salt balance within the unfrozen fraction of the milk, the crystallisation of lactose, and the growth of ice crystals.

It has been noted that in frozen UF concentrated milk samples that the protein stability is lowest at -12°C [136], and that this aligns with previous authors who had found that the temperature range above -20°C was least desirable for protein stability[5]. The concentrated milk (at solids concentrations up to 35%) was found to be more stable than un-concentrated milk, and lactose hydrolysis also increased protein stability. Protein stability in this study was noted to be lower in rapidly frozen samples. However, this was less evident when lactose was hydrolysed. As the samples were frozen to different final temperatures, then held at -8°C during the storage period, it was suggested that this difference in stability could be a result of the different temperature histories experienced by the rapid frozen samples leading to higher levels of lactose crystallisation[136]. The long storage at -8°C would have led to Oswald ripening and increased the ice crystal size, limiting the benefits of small ice crystals due to rapid freezing noted in other work.

When the milk is frozen, solids concentration in the unfrozen phase increases. This increase in concentration leads to an increase in lactose concentration and may lead to lactose crystallisation. Lactose becomes supersaturated in bovine milk during freezing at approximately -2°C[137]. As lactose crystallises, it crystallises as α-lactose monohydrate[138] and further removes water from the system, as well as the lactose cryo-protectant itself. Removal of lactose from the unfrozen portion also decreases its viscosity which kinetically favours micelle polymerization[139].

The T_g of a dairy system can be estimated from the Gordon-Taylor equation, where X_s is the weight fraction of the solute, T_{g_s} is the glass transition temperature of the anhydrous solute, X_w is the weight fraction of water, T_{g_w} is the glass transition temperature of water, and k is an empirical constant :

$$T_g = \frac{X_s T_{g_s} + k X_w T_{g_w}}{X_s + k X_w} \tag{1-39}$$

The glass transition of water varies slightly from reference to reference, being reported in dairy science literature as -135°C[140-142], -137°C[137], -138°C [143],-139°C[144]. This variation is not unexpected given the experimental difficulties inherent in forming glassy water, leading to a range of values being cited. A value of -137°C, above which an ultraviscous low-density-liquid is formed on heating is the currently favoured value[145]. Some of the values fitted to the Gordon-Taylor equation for dairy products are shown in the table below:

Table 1-1:Published values for the Gordon-Taylor equation for dairy products.

Solute	T_g(°C)	k	Reference
Bovine skim milk.	92	6.7	[140]
Bovine skim milk with hydrolysed lactose.	49	8.0	[140]
Bovine whole milk (32% fat).	92	-	[140]
Bovine whole milk.	100.6	8.57	[146]
Bovine skim Milk	101	6.5	[146]

As discussed in section 6.1 the homogenous crystallisation rate is reduced by increased viscosity. The viscosity of a supersaturated solution increases rapidly as it approaches , and this viscosity can be estimated from one of the two forms of the Williams-Landel-Ferry (WLF) equation [147], where a_T is the ratio of viscosities between the temperature T and the reference temperature ($a_t = \eta(T)/\eta(T_s)$), T_s is a reference temperature ideally at least 50°C above T_g, T_g is the glass transition temperature, and C_1 and C_2 are empirical coefficients specific to the system being investigated:

$$(a)\colon \log_{10} a_T = -\frac{C_1(T - T_S)}{C_2 + T - T_S} \quad or\ (b)\colon \log_{10} a_T = -\frac{17.44\left(T - T_g\right)}{51.6 + T - T_g} \tag{1-40}$$

The authors caution against using the generalised form of the equation shown in (1-40) (b) unless absolutely necessary due to the difficulties inherent in accurately determining T_g, and the universal form of the fitting coefficients[147].

Coefficients C_1 and C_2 for the WLF equation have been published for lactose, using recrystallisation rates to estimate viscosity near T_g [148], and these have been found to fit well to experimental data for amorphous lactose at values of $T - T_g$ from -2K to 7K [149]. In contrast to Koschak [136], other literature suggests that rapid freezing decreases lactose crystallisation [137]. It is my opinion that this second view is likely to be correct, as lactose remains highly supersaturated at all temperatures below -2°C and this level of supersaturation will be constant for all cooling rates, so long as crystallisation does not occur. A rapidly cooled sample will spend less time at temperatures significantly above T_g, where the viscosity according to the WLF equation is orders of magnitude lower, and the nucleation rates higher as suggested by Classical Nucleation Theory. A slowly cooled sample will spend more time at temperatures where the nucleation rate is higher than the final storage temperature, which will increase the probability of a stable lactose nucleus forming and crystallisation occurring.

The balance of calcium and phosphorus in the milk also affects the stability of frozen milk. The removal of soluble phosphorous changes the equilibrium between the colloidal and soluble salts, which destabilises the micelles in the unfrozen phase[136]. Studies on the changes in frozen bovine milk have found that there is a steady loss of soluble calcium during storage at -7°C, which reaches a new constant level after 120 days. Inorganic phosphate was found to drop during the first 60 days of frozen storage. This change was partially reversible after stirring for 48 hours at 5°C. The protein stability dropped at a similar rate to the Ca^{2+} concentration. Increases in viscosity were also partially reversible on storage [150]. The link between Ca^{2+} and micelle destabilisation has been noted by other authors who noted slight drops in soluble Ca^{2+} and moderate drops in soluble PO_4^{2+}during frozen storage[151]. The lower drop in soluble component when compared with Chen and Yamauchi's 1969 study[150], was linked to the slow (48hours) thawing, which allowed the salt system to revert to a more normal distribution [151].

Removal of Ca^{2+} from the system also leads to a destabilisation of the micelles[139]. However, removal of up to 30% of the Ca^{2+} from milk by ultrafiltration has been found to increase the protein stability of the frozen milk [136].

The freezing of milk leads to pH decreases in the unfrozen phases as salts concentrate in the unfrozen phase. Supersaturation can also occur which increases the concentration of salts further[152]. This also means that the pH profile in freezing milk may be affected by the speed of freezing. The magnitude of pH changes in milk indicate that phosphates come out of the colloidal phase into the soluble phase before being precipitated [152].The salt precipitation occurs at a similar rate to lactose crystallisation. This occurs to a greater extent in slowly frozen samples, as rapid freezing limits the time available for salt precipitation [153]. The total magnitude of pH change in frozen bovine milk is relatively small, with a drop in pH to roughly 6.1 to 6.2 on frozen storage at -10°C recorded [152]. The pH varied slightly during the first 20 days of frozen storage as various salts crystallised [152].

For long term storage, oxygen-proof packaging has been shown to reducing the development of rancid flavours in frozen milk[154] .

Physical aggregation is another phenomenon that affects the stability of the system. This has been identified as a factor in the destabilisation of calcium fortified soy beverages [131]. The rejection of solutes and particles had several interacting effects:

- Interactions between oil droplets were enhanced due to them being aggregated into a smaller volume.
- Ice formation could interfere with the interfacial protein films surrounding the oil droplets.
- Increased solute concentration leads to shielding of electrostatic repulsion between particles. When this was combined with physical aggregation, particle repulsion was overcome, and particles aggregated together.

Sugars were identified as having a cryo-protectant effect as they inhibited water crystallisation and increased the viscosity of the unfrozen phase, which decreased mass transfer limited processes [131].

Wendorff [5], lists and tested several possible pre-treatments that have been suggested to improve the protein stability in frozen milk:

1. Lactose hydrolysis
2. Pre-freezing heat treatment to resolubilise lactose.
3. Addition of sodium hexametaphosphate.

It was found that lactose hydrolysis and the addition of sodium hexametaphosphate improved the stability of milk frozen at -12°C for up to 12 months [5]. However, hexametaphosphate adds a salty flavour to milk, and may destabilise milk fats [128], so may be unsuitable as a method to improve stability for milk stored in freezers at ~-12°C.

Storage below -20°C is recommended, with stability decreasing at higher temperatures[136]. At temperatures of -27°C and below, the high viscosity of the unfrozen phase, and low kinetic energy of the milk components limits the crystallization of lactose and aggregation of protein.

Yoghurt of good quality can be made from milk stored below -20°C for up to 12 months[5, 135],however yoghurt from milk stored at -12°C, has been reported to have unacceptable quality [135].

Wendorff [5, 130] concludes that ovine milk should be frozen rapidly and stored at -27°C for maximum stability, and if milk is stored at -12°C, then it should not be stored for longer than 3 months.

Rapid freezing has also been recognised for a long time as a method of preserving the fat emulsion in milk, as it prevents fat separation and the growth of large destructive ice crystals [155].

Protein stability can be reduced by cold storage or freezing in several ways. The first is a thermodynamic process called cold unfolding. The Gibbs-Helmholtz equation describes the Gibbs free energy change on denaturation, and can be used to model the temperature variation of the thermodynamic stability of proteins [156]. $\Delta G_D(T)$is the Gibbs free energy change of denaturation at a temperature T. ΔG_Dfollows a skewed parabola with the protein stability decreasing both above and below the temperature of maximum stability. As a result, there are two temperatures outside of which $\Delta G_D(T)$ becomes negative, these are the cold unfolding temperature and the denaturation temperature, T_D. $\Delta H_D$is the enthalpy change on denaturation, and ΔC_P is the difference in heat capacity between the natural and denatured states.

$$\Delta G_D(T) = \Delta H_D\left(1 - \frac{T}{T_D}\right) + \Delta C_p\left[(T - T_D) - T\ln\left(\frac{T}{T_D}\right)\right] \quad (1\text{-}41)$$

β-lactoglobulin has been shown to undergo a reversible cold unfolding transition (this is distinct from the thermal denaturation that occurs at higher temperatures) [157] . The cold-unfolding temperature of β-lactoglobulin is decreased by increased concentration and by increasing sugar content, implying increased protein stability. The kinetics of this cold unfolding have been studied and found to be dependent on the viscosity of the system. In highly viscous solutions or glasses, the half-life of the cold unfolding process will be long, with a half-life of 2.5x10^4 years at T_g and 2.2 years in a sucrose solution at $T - T_g$=25°C [158].

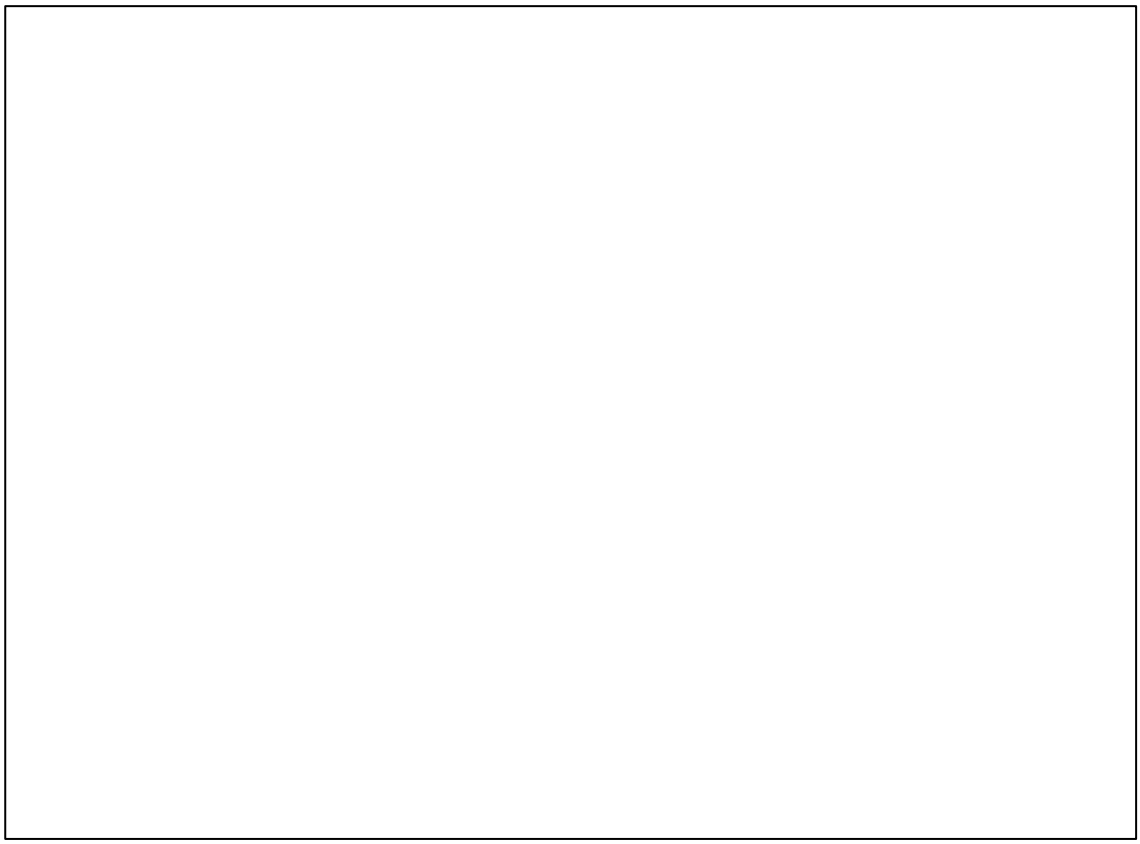

Figure 1-6: The Gibbs free energy of denaturation for staphylococcal nuclease as a function of pH and temperature, showing the parabolic form of the temperature relationship, with denaturation becoming thermodynamically favourable above the higher denaturation temperature and below the cold unfolding temperature. From [159].

1.7.2 Microbial Effects of Frozen Storage.

It is well known that psychrotrophic spoilage bacteria continue to grow during chilled storage of raw milk. In goat milk for example, these bacteria cause lipolysis which affects the quality of products made from this stored milk[160]. These psychrotrophs limit the overall time a raw milk can be stored unfrozen. Goat milk that has been stored in chilled bulk tanks for 48h shows higher levels of mesophilic aerobes, coliforms, *E. coli*, and psychrotrophic bacteria than milk directly after milking, or after 24h of storage[161].

In one study, sheep milk that has been frozen and stored at -25°C and thawed at 40°C had significantly reduced total bacterial counts after 2, 4, and 6 months of storage, with the only statistically significant drop occurring after 2 months of storage and the total bacterial count remaining stable after this period[154].

Recently work has been conducted in Brazil investigating the effect of frozen storage, and frozen form factor on microbial levels in sheep milk[6]. It was found that there was no significant increase in bacterial counts immediately post thawing, but certain combinations of storage container and thawing temperature had higher bacterial growth post thawing than others. It was found that milk frozen in 1 L bags and thawed at 7°C remained microbially acceptable, whereas milk frozen in 1 L bags or 5 L buckets and thawed at 25°C was unsuitable after a further day of storage. This was linked to the increased thawing time required in 5 L buckets and the increased thawing temperature promoting higher levels of microbial growth.

In the manufacture of yoghurts, slow freezing and thawing has been found to reduce the lag phase before culture growth[162], possibly as a result of physical damage from ice crystals exposing lipids to bacterial lipase activity. The overall fermentation profile of milk that was frozen, thawed and refrigerated for 24h before processing was similar to that of fresh milk.

Further changes in yoghurt properties when compared with fresh milk were found with milk that had been thawed immediately prior to processing, however these differences diminished when the thawed milk had been stored for 24h prior to processing.

1.7.3 Milk Gels

The formation of a milk gel is one of the key steps in forming many dairy products, such as yoghurt and cheeses, and is also linked to undesirable changes in some milk products, such as age-gelation in UHT milks[163].

Milk gels formed by the action of rennet or acidification are typically irreversible[164]. Renneting is a two-stage reaction which forms a protein gel network in milk. The first stage involves the enzymatic hydrolysis of κ-casein by chymosin, which reduces the net negative charge and steric repulsion of casein micelles. The second stage involves the agglomeration of these altered micelles and the formation of a coagulum or gel. The native structure of the casein micelles needs to be present, and Ca^{2+} species need to be in the liquid phase for aggregation to occur[165]. Aggregation is inhibited below 15°C, and below a minimum Ca^{2+} concentration, indicating that aggregation involves both hydrophobic and electrostatic interactions[164].

Yoghurt is a commonly encountered milk acid gel. The acidification is usually caused by bacterial cultures which convert lactose to lactic acid by fermentation [166]. Decreasing the pH of milk increases the voluminosity of casein micelles as CCP is solubilised, and when the isoelectric point (IEP) of casein is reached the micelles aggregate. At the IEP their charges are neutralised, which removes the electrostatic repulsion stabilising the suspension. In unheated milk the aggregated micelles show little cross-linking and the gel is lower strength than gels formed from heated and acidified milk, as interactions between β-lactoglobulin and κ-casein form filaments that cross-link the casein gel and reduce the number of dense clusters of casein micelles [166]. Acidified milk systems also do not aggregate at temperatures below <10°C, indicating that hydrophobic interactions are important in the formation of acid gels[167]

Casein micelles can also be destabilised by the addition of ethanol, which acts to collapse the hairy layer of protruding κ-casein, removing the steric stabilisation this layer provides. This is also affected by the ionic environment of the micelles, where the electrostatic repulsion must be lower than the hydrophobic aggregating forces [167].

Physical aggregation of casein micelles has been linked to the cold gelation of highly concentrated micellar casein concentrate (HC-MCC) and recombined concentrated milk (RCM)[168, 169]. These suspensions formed a thermally reversible gel on cooling as micelles physically aggregated in the limited volume available, and attractive forces at low temperatures overcome the thermal kinetic energy of the micelles. Outer tendrils of adjacent micelles overlap and penetrate into the hydration spheres of each other. The addition of a Ca^{2+} chelating agent disrupted the gel, suggesting that Ca^{2+} ions act to link neighbouring casein micelles by bridging negatively charged regions of the proteins. However, at higher micelle concentrations, chelation of Ca^{2+} ions was not sufficient to disrupt the gel, indicating that other bonding mechanisms are also present[169]. It is also suggested that that at cooler temperatures, reduced hydrophobic interactions result in protein strands in casein micelles being less tightly bound, allowing these strands to interact and form a gel network[168].

Figure 1-7: Mechanism of cold gelation in HC-MCC, taken from Lu et al ,2015[169].

Gels can also form in milk that has been sterilised by UHT processing by several mechanisms; proteolytic degradation by heat stable plasmin; proteolytic degradation by heat stable exogenous enzymes; and physico-chemical age gelation [163]. Gelation by indigenous plasmin typically occurs in direct-UHT milk when plasmin hydrolyses α and β caseins [170], forming fragments which interact by hydrophobic bonding and Ca^{2+} bridging to form a gel. Proteolytic degradation by exogenous enzymes occurs when heat stable proteases hydrolyse κ-casein proteins to form "para-κ-casein-like" peptides in the serum phase and on the micelles, and "glyco-macro-peptide-like" peptides in the serum[171]. These peptides interact with denatured whey proteins and casein micelles to form a gel on storage [163]. Physico-chemical gelation occurs when β-lactoglobulin denatures during UHT processing and formed a complex with κ-casein [163]. During storage this complex dissociates from the micelle into the serum forming a cross-linking gel network.

1.8 Review of Existing Freezing Methods

1.8.1 Possible Methods:

Freezing is a common method of preserving perishable foods[172, 173].A wide range of methods have been developed to freeze liquid foods, both for preservation and production of frozen desserts. These methods are evaluated here to gauge their suitability for use as an on-farm freezer for sheep milk.

In order to be suitable as an on-farm freezer the methods needs to meet the following criteria:

- Freezing speed: The time required to cool any given particle of milk to the final storage temperature. As discussed earlier in this chapter, several authors have linked rapid freezing to improved product quality.
- Form factor of the frozen product: The shape of the final frozen product. This affects the handling, storage and thawing behaviour and methods that are required.
- Complexity of the system: a process that needs to be implemented in an on-farm setting, should be as simple as possible to improve reliability and reduce maintenance costs, and should be intuitive to minimally trained operators.

- Ease of handling the frozen product: The frozen product should be simple to handle, transport and thaw at the volumes encountered in farm and processing environments, allowing it to become a standard item of commerce.
- Suitability of the method for small- and large-scale embodiments: The system should be suitable for the volumes of production encountered on-farm and require minimal infrastructure for installation. Suitability for large scale operations is ideal.
- Capital expenditure required: this should be minimised to ensure the method is financially feasible for farmers to adopt.
- Operator input, and oversight required for reliable operation: This should be minimised to aid adoption on farm. Automated systems can also improve product quality, safety and consistency by reducing the possibility of human errors.

1.8.2 Blast Freezing in Containers.

This method covers a range of embodiments, all of which share the same underlying principle, but differ in particulars.

The liquid to be frozen is packed into a sealed container, typically pails or bladders, and placed into a blast chiller, cooling tunnel or freezer, and held until the desired temperature is reached. The containers may be immersed in a coolant, or have a liquid coolant sprayed onto them to increase heat transfer rates. Circulation fans contribute to the cooling load in blast freezers, in some cases making up ca. 30% of the total cooling load.

The cooling time of these methods decreases as the characteristic distance L_C of the container, where $L_C = \frac{V_{container}}{A_{Surface}}$, decreases. Increasing the heat flux ϕ_q, by increasing surface heat transfer coefficient $h_{Surface}$ or the temperature difference ΔT, also decreases the cooling time[174], but to the effect of increasing $h_{Surface}$ declines as L_C increases.

The frozen containers are then stored in a cold store until thawed. Thawing may occur in the containers or bladders. Thawing time is determined by similar factors as the cooling time and can be significant for containers with large characteristic distances and small heat fluxes[175, 176].

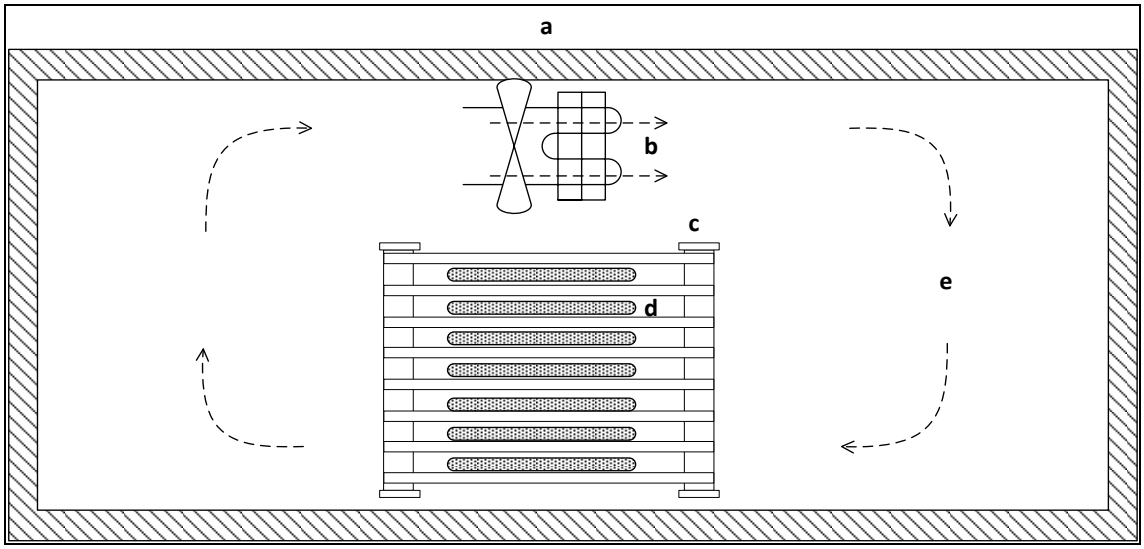

Figure 1-8: Freezing liquid products in bladders or containers. a) Insulated freezer walls; b) evaporator unit; c) freezer shelving; d) product in containers or bladders; e) cold air flow.

Capital cost for this method can be minimal for a basic installation consisting of a refrigerated room and food safe containers, however a significant amount of manual product handling is need during the container filling process and container storage steps. This can be reduced by

increased capital expenditure on automated product handling equipment, or by using large (1T) containers which has an adverse effect on freezing and thawing times. The freezing time determined[177]for a 1-dimensional slab of food in a -30°C blast freezer is shown below to illustrate the effect of changing $h_{surface}$ and L_C.

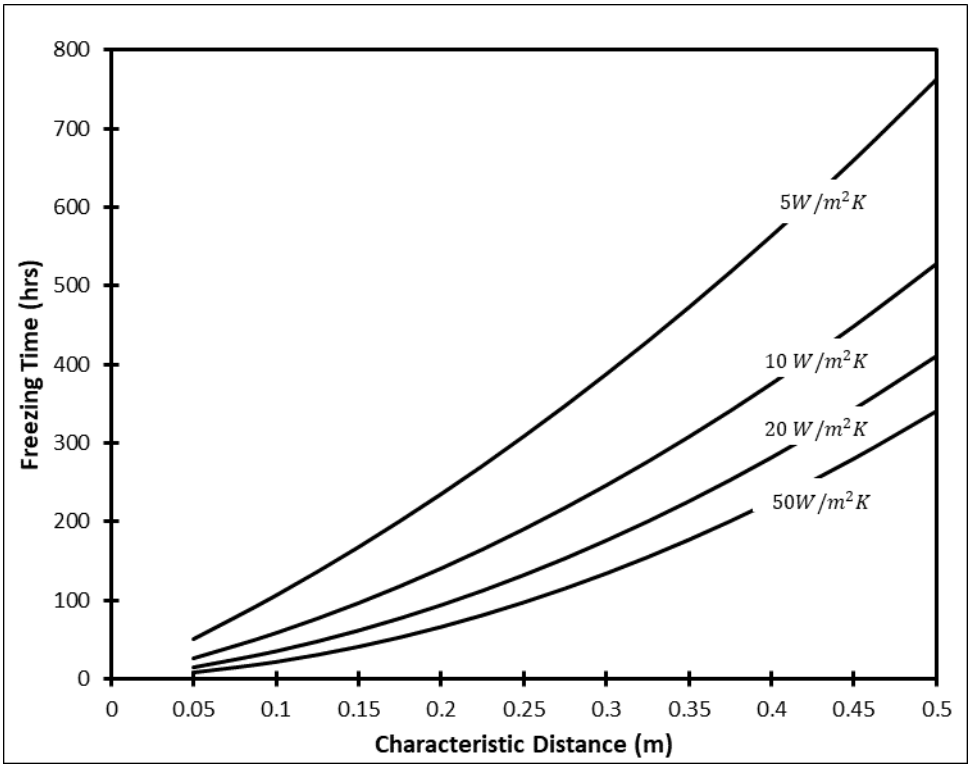

Figure 1-9: The freezing time of a 1D slab with thermal properties identical to water in a -30°C blast freezer.

These parameters, along with the thermal conductivity, are used to calculate the Biot number:

$$Bi = \frac{h_{surface} L_C}{k}$$

The Biot number is a dimensionless number that describes a body's ratio of internal and external resistance to heat transfer. When $Bi \ll 1$, there are minimal thermal gradients inside the body, while $Bi \gg 1$ indicates that the internal resistance to heat transfer is dominant, and there are significant thermal gradients inside the body.

1.8.3 Individually Quick Frozen Products

There are a range of methods to produce Individually Quick Frozen (IQF) products. Typically, droplets or thin layers of food to be frozen are deposited on a flexible belt. This belt travels through a cooled chamber and is frozen by the cold airflow over the product, or by a cryogen sprayed onto the product. This belt is often arranged in a vertical spiral to maximise the length of belt for a given floor space[178].

The form factor of the frozen product can be adjusted to suit the application. This technology is scalable from small sizes, to significant volumes, if sufficient floor space and energy is available on site.

The small characteristic distance of the product to be frozen can allow these freezers to rapid cool products to their final storage temperature if the coolant heat transfer coefficients are sufficiently high[179].

Due to the presence of a moving belt in the cooled zone, the refrigeration system must also remove the energy input from drive motors. Air circulation fans also contribute to the heat load which must be removed.

While the product quality produced, and scale of these freezers may be suitable for the on-farm freezer application, the capital cost, floor space requirement and complexity of the moving belt make this technology less desirable for an on-farm freezer.

1.8.4 Prilling Tower/ Direct Contact Refrigerant Immersion Freezer

Another method for the rapid freezing of liquids is to form droplets of liquids and drop them into a cold air stream or liquid refrigerant which cools the droplets and freezes them, while preventing agglomeration. This has been proposed in many different embodiments [180-182].

Dropping these liquid products into a cold airstream is typical of prilling towers, which are widely used in the fertiliser industry to make pelletised ammonium nitrate, urea and compound fertilisers. The height of the tower must be sufficient allow the particle to solidify enough to prevent breaking apart on impact. Those used in the fertiliser industry are typically over 50 m tall for 2 mm droplets[183]. Therefore, the capital costs for this method of freezing would be extreme and be unsuitable for on-farm use.

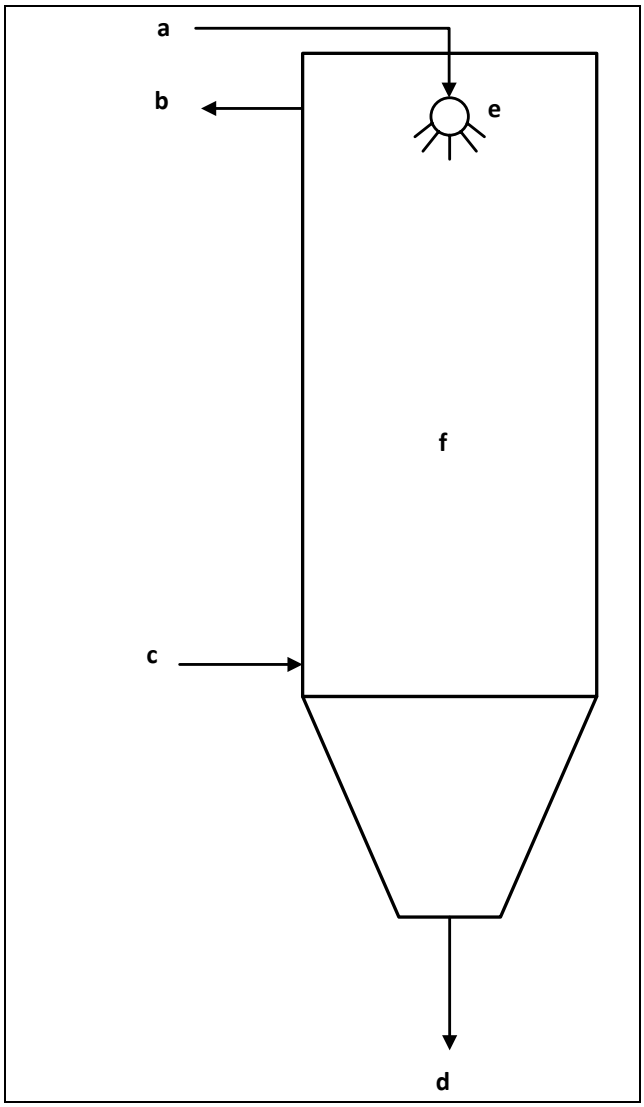

Figure 1-10: Prilling Tower: a) Liquid product feed; b) air exit; c) cold air inlet; d) frozen product outlet; e) liquid product atomiser; f) cooling chamber.

Dropping liquid into a liquid refrigerant, causing it to freeze into spherical particles, has been proposed in a variety of embodiments. However, this direct contact method requires a refrigerant that is food safe, and evaporates at a low temperature at atmospheric pressure. Refrigerants that evaporate at suitable temperatures at above or below atmospheric pressure, could be used, but would require the freezing to occur in a pressure vessel. The refrigerant must also be suitable for atmospheric release from an ozone depletion and greenhouse gas standpoint. As a result, liquid nitrogen (LN2) is the most commonly used refrigerant. Production of LN2 is an energy intensive process requiring approximately 1800-2600 $kJkg^{-1}$ [184, 185]. LN2 freezing typically requires 1-1.5 kg of LN2 for each kg of frozen product[172]. LN2 freezing therefore has a low energy efficiency, and production of LN2 occurs at centralised plants. A freezer using LN2 as a refrigerant would effectively require "double-shipping", transporting equal masses of refrigerant to, and product away from, a farm. This is unlikely to be economically viable.

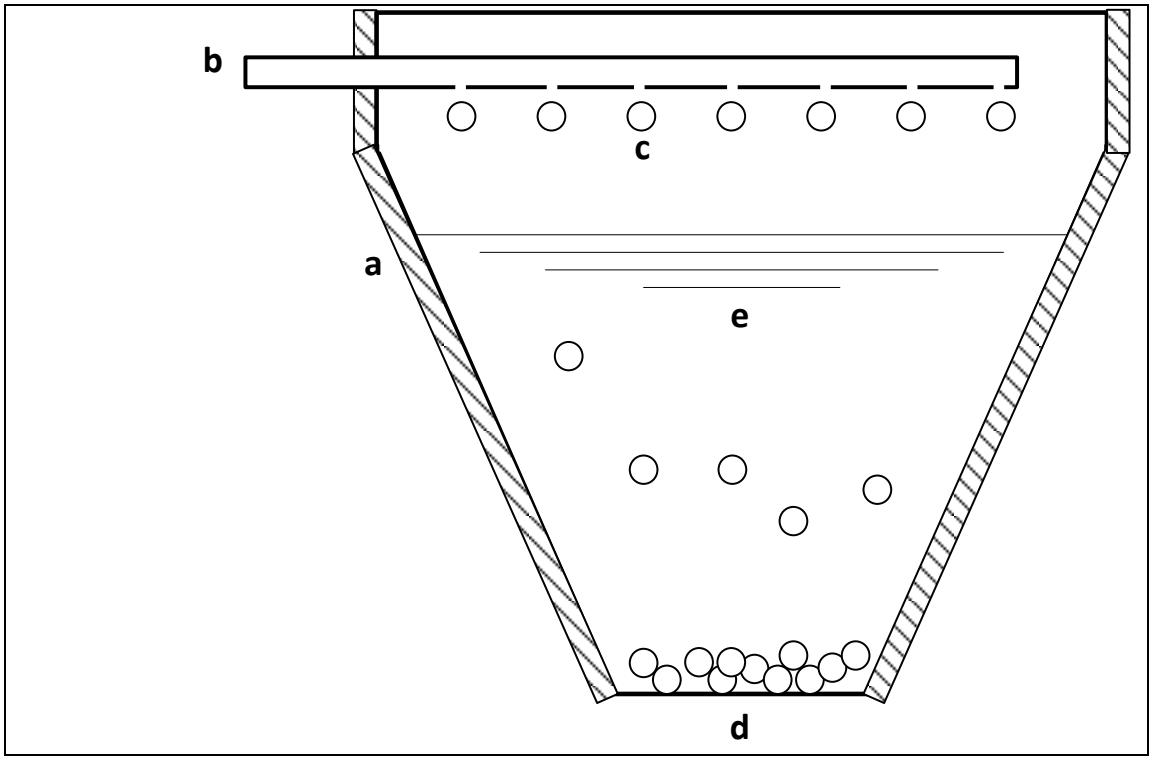

Figure 1-11: Freezing of liquid droplets by immersion in liquid refrigerant. a) Insulated process vessel; b) Liquid product distributor; c) droplets of liquid product; d) frozen product; e) liquid refrigerant.

The product form factor and quality from these methods is excellent, as small spherical particles can be easily handled as a bulk, and rapidly thawed due to the small characteristic distance.

These systems can be highly mechanised, to reduce the operation intervention required, however the system complexity makes them unaffordable and unsuitable for small farms.

1.8.5 High Pressure Freezing.

The equilibrium freezing temperature of water at atmospheric temperature is 0°C, however increasing the pressure of a system decreases this temperature[186]. The minimum freezing temperature of -22°C is reached at 207.5 MPa. The phase diagram of water is shown in Figure 1-12. This property of water can be exploited to increase nucleation by cooling a product below 0°Cat elevated pressures and then releasing the pressure[187]. This leads to significant supercooling and homogenous nucleation throughout the volume of product, and may be of use

for freezing products where a uniform ice crystal distribution is desired over a large volume. At a pressure of 900 MPa, ice VI can be formed at room temperature without any form of cooling[188], however research in this area is limited.

The products are typically placed inside pressure suitable containers and immersed in a fluid that transmits both pressure and heat, inside the high-pressure freezing apparatus.

The form factor of this process is variable, and changes from product to product, as such it is difficult to make any conclusions about the ease of handling and thawing of the frozen product.

This is a batch process, and operational and capital expenses are high. While the batch nature of the process means it's suitable for small volumes of products, the high capital and operational costs, and the complexity of the system makes it unsuitable for on farm application.

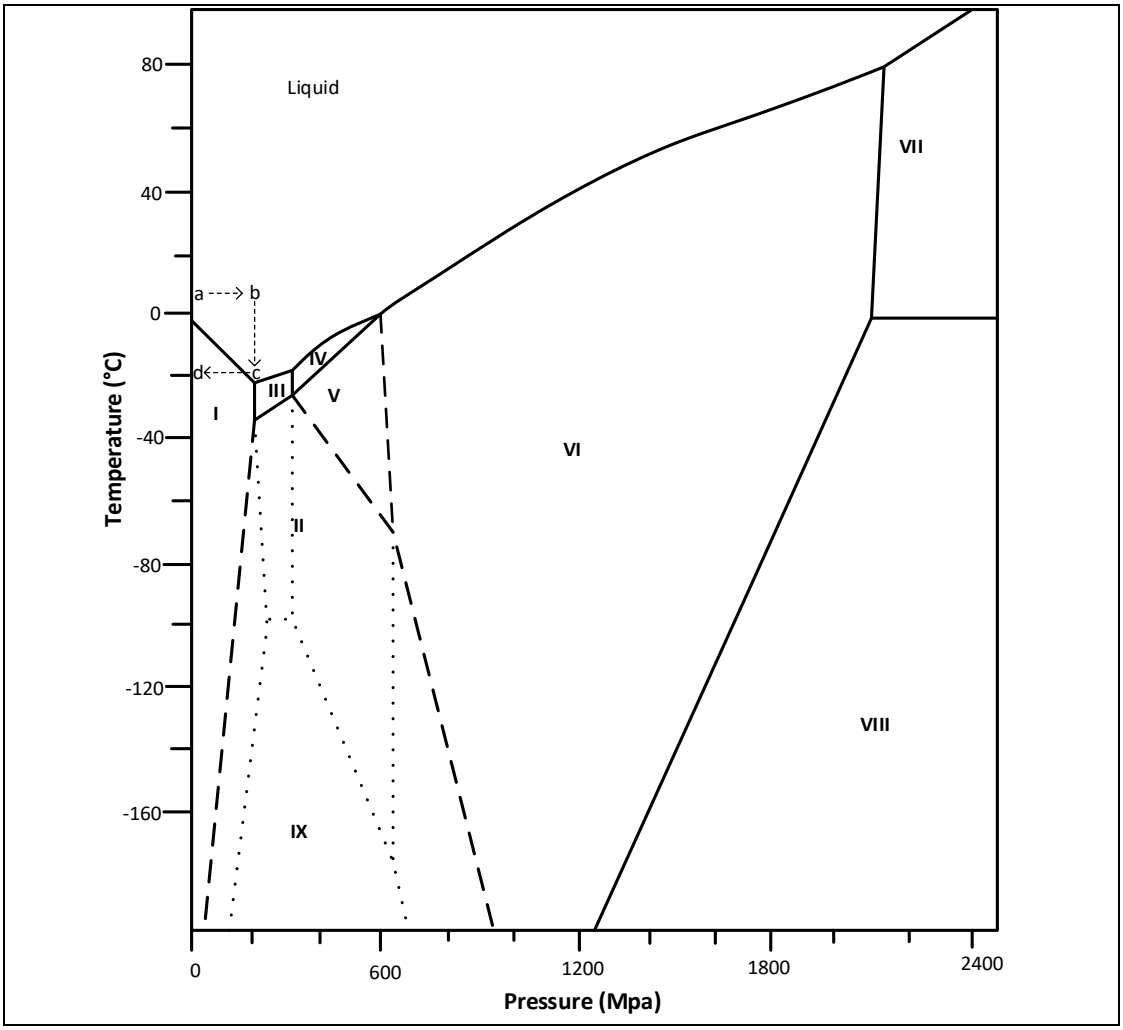

Figure 1-12: Equilibrium solid/liquid phase diagram of water. Redrawn from[186].The pressure and temperature changes exploited in high pressure freezing are shown in the sequence a →b→c→d.

1.8.6 Rolling Droplet Freezer.

Droplets of a liquid product to be frozen are rolled down an inclined plane with a super-hydrophobic surface against a cooled airflow. The droplets do not stick to the due to the small contact area between a droplet and a super-hydrophobic surface. The droplets are frozen into free-flowing spherical particles which can be easily handled, and rapidly thawed.

This concept of this technology was developed at Massey University, and preliminary experiments were conducted however these tests demonstrated that there was a tendency for

ice to adhere on SH surfaces in a condensing atmosphere, due to the transition from Cassie-Baxter to Wenzel wetting states. This behaviour has also been reported in the literature around super-hydrophobic and icephobic surfaces[189], especially for condensing atmospheres[190, 191] [192], and temperatures below -20 °C to -25°C[47].Ice adhesion could occur on the inclined surfaces, causing further build-up of ice, which would be difficult to detect during operation, and difficult to resolve without raising the temperature of the system above freezing.

The capital and operational costs of this method were anticipated to be affordable for an on-farm unit, and scaling to larger sizes was believed to be feasible.

This method was initially selected for further development, and will be discussed further in Chapter 3, however ultimately the ice adhesion risk was deemed too high, fabrication of critical components was found to be extremely difficult at the pilot scale, and another method of freezing was selected.

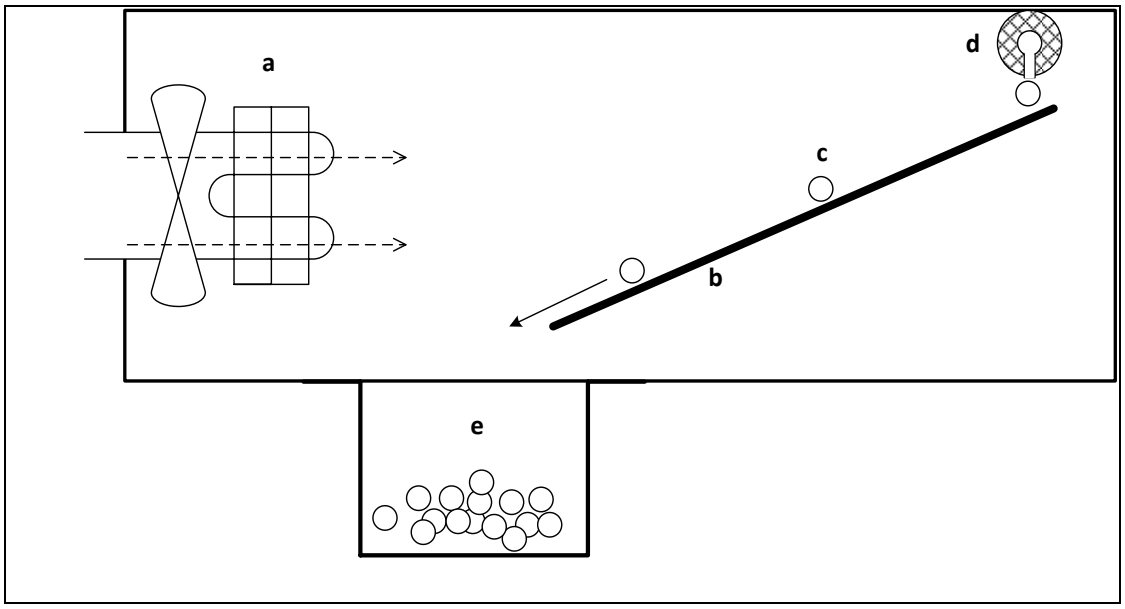

Figure 1-13: A schematic representation of the rolling droplet freezer. a) Air handling unit including refrigeration system; b) inclined super-hydrophobic surface; c) droplet of product; d) droplet generator; e) product storage bin.

1.8.7 Scraped Surface Heat Exchanger.

The liquid product is pumped into a scraped surface heat exchanger, where heat is removed, freezing a significant proportion of the liquid[193]. The scraped surface heat exchanger causes a significant level of secondary nucleation [194],leading to a large population of ice crystals, of a fairly uniform size [195].

The product is necessarily a slurry as a fully solidified product would not be pumpable, however the scraped surface heat exchanger removes the majority of the latent heat. Scraped surface heat exchangers are often combined with a belt-freezer to remove the remaining enthalpy and cool the product to a suitable storage temperature.

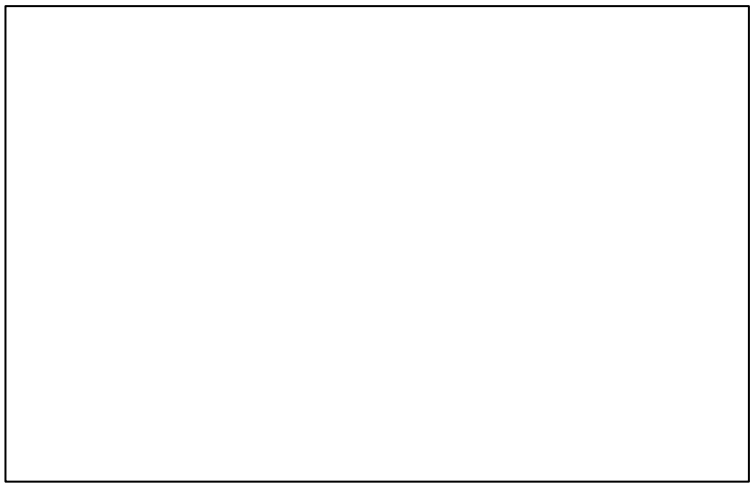

Figure 1-14: A schematic representation of a Scraped Surface Heat Exchanger. From[195].

1.8.8 Cooled Moulds/ Cooled Trays

This is a commonly used method for producing frozen products such as ice cubes or ice-creams[196]. Liquid product is poured into the moulds, or onto the trays, and heat is removed by coolant jackets or channels on the tray or mould. When the product is frozen, it is removed by inverting the mould, or deforming the mould in such a way as to release the product.

The form factor of this method can be varied substantially, so form factors that enable rapid thawing can be produced.

These freezers can be automated and are suitable for large scale applications. The basic principle is also effective at small scales, however at small scale the complexity of the systems required to handle product without operator intervention makes it less attractive than other freezers evaluated.

1.8.9 Direct Contact Refrigerant Mixer Freezer

A refrigerant is directly mixed with the product to be frozen and the mix is forced through a tube or chamber, which allows for sufficient residence time for complete freezing of the product. The refrigerant is separated from the product, and the frozen product is formed into the desired shape.

This method is suited to unattended operation, and scales well to larger scale. However, this direct contact method requires a refrigerant that meets the same requirements as the prilling tower refrigerants as described in section 1.8.4 . As a result, liquid nitrogen is the most commonly used refrigerant.

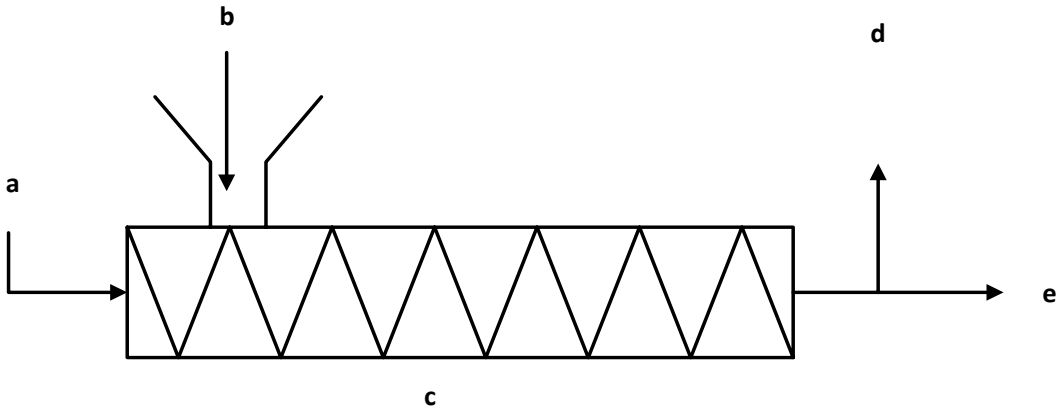

Figure 1-15: Freezing a liquid product by mixing with refrigerant. a) Liquid refrigerant inlet; b) liquid product inlet; c) mixing section; d) refrigerant boils off; e) frozen product outlet.

There are several different embodiments of this system described in patent literature [197, 198]The cost and complexity of handling liquid nitrogen makes this method unsuitable for on-farm freezers.

1.8.10 Falling Film Freezer

In a falling film system, a product to be frozen flows in a falling film over vertical plates, vertical tubes or vertical annuli. On the other side of the plate, or on the inside of the tubes/annuli, a coolant flows. This coolant can be a heat transfer fluid such as a propylene glycol solution, or a boiling refrigerant. The product freezes to the cooled surface and an ice layer grows. This layer grows to a desired thickness and the ice is the removed by the application of heat, which melts a thin layer of ice allowing the bulk of the ice to slough off under gravity.

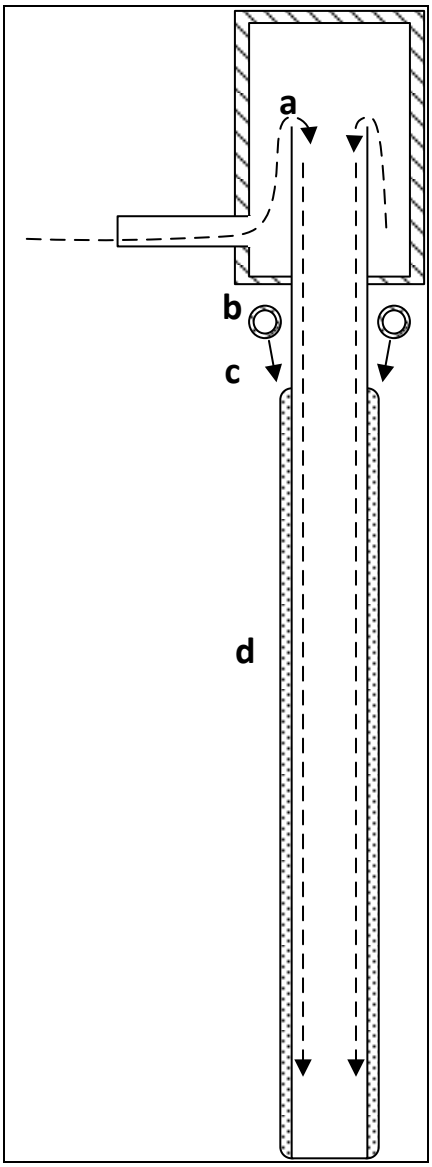

Figure 1-16: Falling film freezer. a) Coolant flow path; b) liquid product distributor; c) liquid product flow; d) product frozen to freezer wall.

Commercially available systems such as those provided by Berg Chilling Systems Inc. of Canada are capable of making 10-50 metric Tonnes per day of ice, which is easily handled and stored for extended periods[199]. Berg also claims that their product is suitable for freezing fruit juices of up to 22% total solids, which would normally be affected by freeze concentration, as well as blood plasmas, processed meats and concrete [200].

Solidification of falling films is also used for freeze concentration and melt purification[201], a process that differs in aim but has many similarities.

Static Crystallisation of falling films has been used to desalinate sea water [73], to concentrate orange juice[63], apple and pear juices[80], coffee[70] and milk, and to fractionate milk fat [69, 78, 202].

The frozen product produced is in the form of flakes, which can be easily handled as a bulk. The small characteristic distance of flakes also ensures that the frozen product can be rapidly thawed.

These systems operate at atmospheric pressure and have low to moderate complexity and therefore capital costs. They are also suitable for unattended operation and therefor are suitable for on-farm application.

The scaling principles are fairly simple, as increased capacity can be achieved by increasing the surface area of the freezer, along with a corresponding increase in chiller power.

This method was selected for further development, and the development work conducted on this will be discussed in Chapter 3

1.8.11 Frozen Product Extruder

The product to be frozen is forced by an augur through a cooled jacked, which removes the heat required to freeze the product. The frozen product is forced through dies to form it into the desired shape. This method is similar to that used in some commercial ice makers. This method has been suggested as a method for freezing concentrated milk [203].

The freezing speed is fairly rapid and produces frozen product with characteristic distances small enough to allow for rapid freezing.

This method is suited to unattended operation, and scales well to larger scale.

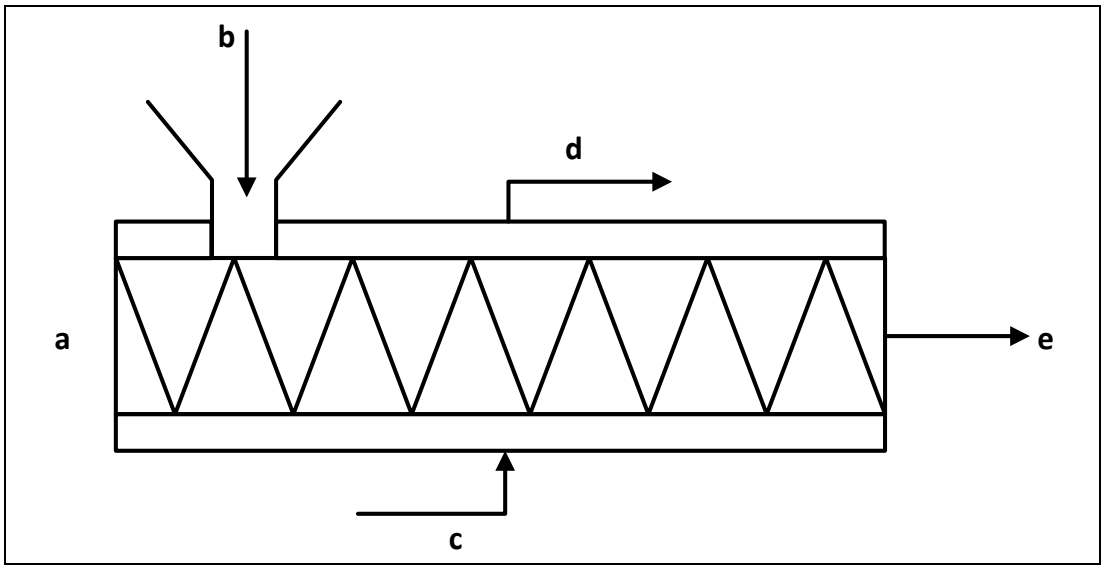

Figure 1-17: A frozen product extruder. a) Jacketed extruder vessel; b) liquid product inlet; c) coolant inlet; d) coolant outlet; e) frozen product exit.

1.8.12 Continuous Tubular Freezing

This method was recently developed at Massey University. The phenomenon of freezing point depression is exploited to freeze the majority of a liquid product, by forcing the product at high pressure through a jacketed tube. The coolant in the jacket removes the heat required to partially freeze the product and cool it to a temperature where it is mostly frozen, and appears as a slightly wet solid. The remaining unfrozen product is sufficient to lubricate the solid and prevent it from sticking to the tube wall.

The tube is of small diameter, so the characteristic distance is minimal, less than ~15 mm, and freezing is rapid. The frozen product emerges as a cylinder that can be forced against an anvil to break product into cylindrical pellets of approximately equal length

The system is simple and requires no moving parts with the exception of coolant and product pumps. The system can scale to moderate volumes easily. Increasing the tube diameter assists with scaling, as the force acting upon the end of the frozen plug at a given pressure increases with the square of the diameter, and the adhesion force preventing movement scales linearly

based on the tube perimeter, and therefore linearly with diameter. Scaling to larger volumes may require a tube bank configuration to be adopted to ensure sufficient throughput, while maintaining small characteristic distances.

The simple operating principle means that this method is suited for unattended operation and suitable for on farm use.

The capital expenditure will be low as no complicated geometries or specialised materials are required.

The ease of operation, low system complexity, low capital costs and suitability for small scales led to this method being selected for further development. This work will be discussed in chapter 6.

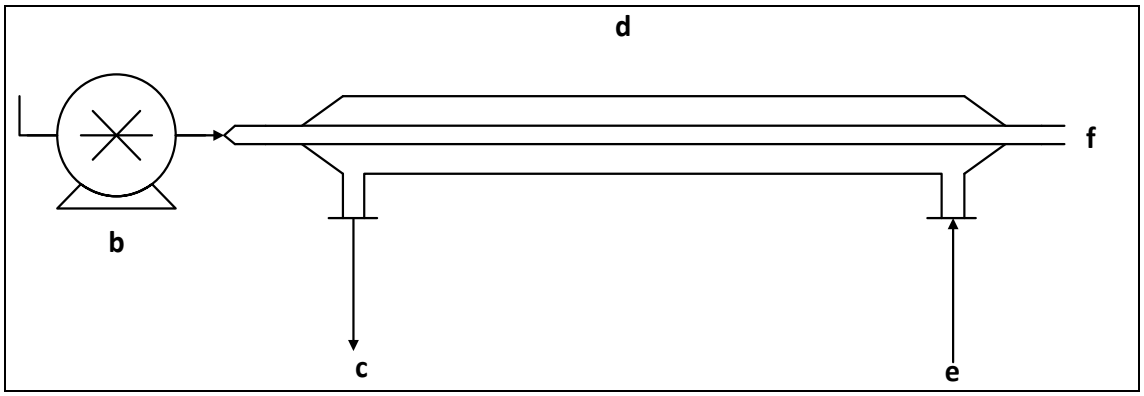

Figure 1-18: Tube freezer. a) Liquid product inlet; b) high pressure positive displacement pump; c) coolant outlet; d) jacketed tube; e) coolant inlet; f) frozen product outlet.

There are many other possible methods for freezing liquids. Only the methods described above were investigated closely.

1.8.13 Qualitative Comparison

Table 1-2:Qualitative comparison of freezing methods for liquid food-stuffs.

	Freezing Speed	***Form Factor***	***System Complexity.***	***Ease of Product Handling***	***Small Scale suitability***	***Large Scale Suitability***	***Capex***	***Operator input Requirement***
Blast Freezer and Bladders/containers	Low	Large Block	Low	Low	High	High	Moderate	Moderate/High
Prilling Tower/Droplets in refrigerant.	Very High	Spherical Pellets	Moderate/High	High	Very Low	Moderate	Very High	Low
High Pressure Freezer	High Nucleation rate	Variable	High	Moderate	Very Low	Low	High	High
Rolling Droplet	High	Spherical Pellets	Moderate	High	High	Moderate	Moderate	Low
Scraped Surface	Moderate/High	Formed Slurry/Pre-frozen bottle	High	Moderate	Low	High	High	Low
Cooled Moulds	Low	Blocks/Pellets	Moderate/High	Moderate	Moderate	High	Moderate	Low/Moderate
Cooled Trays	Moderate	Flat Sheets	Moderate	Moderate	Moderate	High	Moderate	Low/Moderate
Direct Refrigerant Contact.	Moderate/high	“Whipped” extrusion	High	High	Low/Moderate	Moderate/High	Moderate/High	Low
Falling Film	Moderate/high	Curved Flakes	Moderate	High	Moderate/High	Moderate	Low	Low/Moderate
Frozen Product Extruder	Moderate/high	Extruded cylinder	Moderate	High	Moderate	Moderate/High	Moderate	Low
Continuous Tubular Freezer	Moderate/High	Pellets	Low	High	Very High	Low/Moderate	Low	Low

1.9 Research Aims

In order to develop a reliable on-farm freezer, there were several research areas which needed to be investigated:

1. Measure properties of ovine milk of interest for the performance of an on-farm freezer.
2. Understand what changes occur in raw ovine milk during freezing and frozen storage, and the effect of freezing conditions and frozen storage temperature on these changes. The areas of interest would be the formation of large particles or gels and changes in the protein or calcium balances affecting this, and the processing suitability of milks after frozen storage, particularly for fresh products, homogenisation and heat treatment.
3. Understand the heat flows during the freezing process in ovine milk, track the state of water in ovine milk during the freezing process, and identify physical transitions such as glass transitions in ovine milk, with the aim of using this data for design of an on-farm freezer, and for understanding the storage stability of frozen ovine milk.
4. Understand the factors influencing the ice morphology of the frozen system, and how this affects the behaviour of the frozen milk, to guide operation of a freezer designed for ovine milk; and how the ice morphology can be controlled to achieve acceptable quality of frozen ovine milk.
5. Use the understanding gained of the freezing processes to select or develop a method for freezing ovine milk that would be robust, reliable and affordable and suitable for on-farm storage, and conduct trials of this method to assess its suitability for ovine milk.
6. Model the behaviour of the selected method to optimise for best performance in an on-farm application, or allow for further development of the freezing method.

These research areas are investigated in the following chapters:

Chapter 3 discusses the measurements of relevant properties of ovine milk that will be conducted, and outlines the research and development work that was conducted on two candidate freezing methods. These freezing methods were rolling-droplet freezing and falling-film flake freezing. Both methods were investigated in depth, and developed to differing extents. Rolling-droplet freezing was abandoned after preliminary single droplet trials, due to scale-up and reliability concerns. Falling-film flake freezing was trialled at the pilot scale, and then superseded by the continuous tubular freezing method discussed in chapters 7 and 8.

Chapter 4 covers the ice morphology of frozen ovine milk, and the effects of heat flow, freezing front velocity, and milk components on ice morphology.

Chapter 5 reports changes occurring during the frozen storage of ovine milk at various temperatures. The properties of freeze-thawed milk observed and discussed are in viscosity, colour, pH, particle size distribution, sediment formation, serum calcium levels, serum protein levels, heat stability and the effectiveness of high-pressure homogenisation at remedying the effects of frozen storage.

Chapter 6 reports and discusses a series of DSC studies of heat flows during the freezing and melting of ovine milk and ovine milk fractions, and the thermal transitions detected during melting studies. The relationship between temperature and unfrozen fraction is explored with these DSC measurements and a partial phase diagram for ovine milk is developed.

Chapters 7 and 8 describes the final method developed and selected for a rapid and reliable on-farm freezer: the continuous tubular freezing method. This method was developed from the knowledge of the effects of heat flow on ice morphology and the relationship between temperature and ice fraction. The freezing method involves forming a frozen plug in a cooled tube, with the adhesion of the frozen product putatively being reduced by trapped unfrozen

fractions at the product/wall interface, and the plug being continuously extruded due to the high pressure developed by the feed pump. These chapters discuss the principle of this freezer, lab-scale and pilot-scale trials, product trials and ice morphology in the frozen product, and models of the system behaviour.

Chapter 9 provides the conclusions of this work, and possible directions for further research and development work.

1.10 References.

[1] L. Griffiths, "Business Plan for the NZ Sheep Dairy Industry," 2015, Available: http://www.nuffield.org.nz/uploads/media/2014_Lucy_Griffiths__Cruickshank_.pdf.

[2] G. E. Pollott and E. Gootwine, "Reproductive Performance and Milk Production of Assaf Sheep in an Intensive Management System," *Journal of Dairy Science,* vol. 87, no. 11, pp. 3690-3703, 2004.

[3] *Animal Products Notice: Manufacture of Dairy Based Infant Formula Products and Formulated Supplementary Foods for Young Children,* M. f. P. Industries, 2017.

[4] M. Ramos and M. Juarez, "Milk | Sheep Milk," in *Encyclopedia of Dairy Sciences*, J. W. Fuquay, Ed. Second Edition ed., 2011.

[5] W. L. Wendorff, "Freezing Qualities of Raw Ovine Milk for Further Processing," *Journal of Dairy Science,* vol. 84, pp. E74-E78, 2001.

[6] A. A. L. Tribst, L. T. P. Falcade, and M. M. de Oliveira, "Strategies for raw sheep milk storage in smallholdings: Effect of freezing or long-term refrigerated storage on microbial growth," *J Dairy Sci,* 2019.

[7] G. F. W. Haenlein and W. L. Wendorff, "Sheep Milk," in *Handbook of Milk of Non-Bovine Mammals*, Y. W. Park, Ed.: Blackwell Publishers, 2006.

[8] "FAOSTAT Database," F. a. A. O. o. t. U. Nations, Ed., ed. Rome, Italy, 2017.

[9] R. P. Hugh Stringleman. (2015, 18 December 2016). *Sheep farming, Te Ara - the Encyclopedia of New Zealand*. Available: http://www.TeAra.govt.nz/en/sheep-farming

[10] N. Z. T. Enterprise. (2016, 18 December 2016). *Invest in New Zealand > Statistics*. Available: https://www.nzte.govt.nz/en/invest/statistics/

[11] MPI, "High value sheep milk PGP programme officially kicks off," ed: MPI 2016.

[12] Y. W. Park, "Rheological characteristics of goat and sheep milk," *Small Ruminant Research,* vol. 68, no. 1-2, pp. 73-87, 2007.

[13] Y. W. Park, M. Juárez, M. Ramos, and G. F. W. Haenlein, "Physico-chemical characteristics of goat and sheep milk," *Small Ruminant Research,* vol. 68, no. 1-2, pp. 88-113, 2007.

[14] L. Day, M. Broadhurst, and L. Samuelsson. (2016) New Zealand Sheep Milk-nutritional composition. *Food New Zealand*. 20,21.

[15] J. M. Jandal, "Comparative aspects of goat and sheep milk," *Small Ruminant Research,* vol. 22, no. 2, pp. 177-185, 1996.

[16] M. R. Sanz Sampelayo, Y. Chilliard, P. Schmidely, and J. Boza, "Influence of type of diet on the fat constituents of goat and sheep milk," *Small Ruminant Research,* vol. 68, no. 1-2, pp. 42-63, 2007.

[17] K. Raynal-Ljutovac, G. Lagriffoul, P. Paccard, I. Guillet, and Y. Chilliard, "Composition of goat and sheep milk products: An update," *Small Ruminant Research,* vol. 79, no. 1, pp. 57-72, 2008.

[18] R. Bencini and G. Pulina, "The quality of sheep milk: a review," *Australian Journal of Experimental Agriculture,* vol. 37, no. 4, p. 485, 1997.

[19] B. Janštová, P. Navrátilová, M. Králová, and L. Vorlová, "The freezing point of raw and heat treated sheep milk and its variation during lactation," *Acta Veterinaria Brno,* vol. 82, no. 2, pp. 187-190, 2013.

[20] O. Hanus *et al.*, "Relationship between freezing point and raw ewes' milk components as a possible tool for estimation of milk adulteration with added water," *Journal of Food and Nutrition Research,* vol. 54, no. 4, pp. 281-288, 2015.

[21] E. Gootwine and G. E. Pollott, "Factors affecting milk production in Improved Awassi dairy ewes," *Animal Science,* vol. 71, no. 03, pp. 607-615, 2016.

[22] F. Barillet, C. Marie, M. Jacquin, G. Lagriffoul, and J. M. Astruc, "The French Lacaune dairy sheep breed: use in France and abroad in the last 40 years," *Livestock Production Science,* vol. 71, no. 1, pp. 17-29, 2001.

[23] M. H. Fahmy and J. N. B. Shrestha, "Animals that Produce Dairy Foods | Sheep Breeds A2 - Fuquay, John W," in *Encyclopedia of Dairy Sciences (Second Edition)*San Diego: Academic Press, 2002, pp. 325-339.

[24] P. SW and P. C, "The sheep dairy industry in New Zealand: a review," presented at the Proceedings of the New Zealand Society of Animal Production, Dunedin, 2015.

[25] P. Walstra, *Dairy Technology*. Boca Raton: CRC Press, 1999.

[26] W. L. Wendorff and S. Kalit, "Processing of Sheep Milk," in *Handbook of Milk of Non-Bovine Mammals*, Y. W. Park, G. F. W. Haenlein, and W. L. Wendorff, Eds., 2017.

[27] Beurrespa. (2019, 6 March). *Sheep's Milk and Sheep's Milk products*. Available: http://www.beurrespa.es/en/oveja_en.html

[28] C. F. Balthazar *et al.*, "Novel milk-juice beverage with fermented sheep milk and strawberry (Fragaria x ananassa): Nutritional and functional characterization," *J Dairy Sci,* vol. 102, no. 12, pp. 10724-10736, 2019.

[29] C. F. Balthazar *et al.*, "Sheep Milk: Physicochemical Characteristics and Relevance for Functional Food Development," *Comprehensive Reviews in Food Science and Food Safety,* vol. 16, no. 2, pp. 247-262, 2017.

[30] Z. Z. Merino. (2019, 6 March). *Sheep's Milk Soap*. Available: https://www.zeezeemerino.co.nz/product/sheeps-milk-soap/

[31] C. G. Salzmann, "Advances in the experimental exploration of water's phase diagram," *J Chem Phys,* vol. 150, no. 6, p. 060901, 2019.

[32] G. Petzold and J. M. Aguilera, "Ice Morphology: Fundamentals and Technological Applications in Foods," *Food Biophysics,* vol. 4, no. 4, pp. 378-396, 2009.

[33] F. Franks, "Water: A Comprehensive Treatise." New York: Springer Science+ Business Media, 1982.

[34] P. G. Debenedetti, "Supercooled and glassy water," *Journal of Physics Condensed Matter,* Review vol. 15, no. 45, pp. R1669-R1726, 2003.

[35] H. Kiani and D.-W. Sun, "Water crystallization and its importance to freezing of foods: A review," *Trends in Food Science & Technology,* vol. 22, no. 8, pp. 407-426, 2011.

[36] J. W. Mullin, "Nucleation," in *Crystallization (Fourth Edition)*, J. W. Mullin, Ed. Oxford: Butterworth-Heinemann, 2001, pp. 181-215.

[37] H. Li, I. V. Roisman, and C. Tropea, "Influence of solidification on the impact of supercooled water drops onto cold surfaces," *Experiments in Fluids,* Article vol. 56, no. 6, 2015.

[38] B. J. Murray *et al.*, "Kinetics of the homogeneous freezing of water," *Phys Chem Chem Phys,* vol. 12, no. 35, pp. 10380-7, 2010.

[39] D. Erdemir, A. Y. Lee, and A. S. Myerson, "Nucleation of Crystals from Solution: Classical and Two-Step Models," *Accounts of Chemical Research,* vol. 42, no. 5, pp. 621-629, 2009.

[40] F. Franks, "The Properties of Aqueous Solutions at Subzero Temperatures," in *Water and Aqueous Solutions at Subzero Temperatures*, F. Franks, Ed. Boston, MA: Springer US, 1982, pp. 215-338.

[41] W. Beckmann, "Crystallization: Basic Concepts and Industrial Applications." Wiley-VCH, 2013.

[42] S. Karthika, T. K. Radhakrishnan, and P. Kalaichelvi, "A Review of Classical and Nonclassical Nucleation Theories," *Crystal Growth & Design,* vol. 16, no. 11, pp. 6663-6681, 2016.

[43] H. Vehkamäki, A. Määttänen, A. Lauri, I. Napari, and M. Kulmala, "Technical Note: The heterogeneous Zeldovich factor," *Atmos. Chem. Phys.,* vol. 7, no. 2, pp. 309-313, 2007.

[44] B. Zobrist, T. Koop, B. P. Luo, C. Marcolli, and T. Peter, "Heterogeneous Ice Nucleation Rate Coefficient of Water Droplets Coated by a Nonadecanol Monolayer," *The Journal of Physical Chemistry C,* vol. 111, no. 5, pp. 2149-2155, 2007.

[45] A. Einstein, "Über die von der molekularkinetischen Theorie der Wärme geforderte Bewegung von in ruhenden Flüssigkeiten suspendierten Teilchen," *Annalen der Physik,* vol. 322, no. 8, pp. 549-560, 1905.

[46] L. Goh *et al.*, "A Stochastic Model for Nucleation Kinetics Determination in Droplet-Based Microfluidic Systems," *Cryst Growth Des,* vol. 10, no. 6, pp. 2515-2521, 2010.

[47] V. Bahadur, L. Mishchenko, B. Hatton, J. A. Taylor, J. Aizenberg, and T. Krupenkin, "Predictive model for ice formation on superhydrophobic surfaces," *Langmuir,* vol. 27, no. 23, pp. 14143-50, 2011.

[48] K. L. K. Cook and R. W. Hartel, "Mechanisms of Ice Crystallization in Ice Cream Production," *Comprehensive Reviews in Food Science and Food Safety,* vol. 9, no. 2, pp. 213-222, 2010.

[49] K. Libbrecht, "Growth rates of the principal facets of ice between −10°C and −40°C," *Journal of Crystal Growth,* vol. 247, no. 3, pp. 530-540, 2003.

[50] K. G. Libbrecht and H. Yu, "Crystal growth in the presence of surface melting: supersaturation dependence of the growth of columnar ice crystals," *Journal of Crystal Growth,* vol. 222, no. 4, pp. 822-831, 2001.

[51] A. Criscione, D. Kintea, Ž. Tuković, S. Jakirlić, I. V. Roisman, and C. Tropea, "Crystallization of supercooled water: A level-set-based modeling of the dendrite tip velocity," *International Journal of Heat and Mass Transfer,* vol. 66, pp. 830-837, 2013.

[52] M. J. Shultz, P. J. Bisson, and A. Brumberg, "Best Face Forward: Crystal-Face Competition at the Ice–Water Interface," *The Journal of Physical Chemistry B,* vol. 118, no. 28, pp. 7972-7980, 2014.

[53] M. J. Shultz, A. Brumberg, P. J. Bisson, and R. Shultz, "Producing desired ice faces," *Proceedings of the National Academy of Sciences,* vol. 112, no. 45, p. E6096, 2015.

[54] M. J. Shultz, P. J. Bisson, and A. Brumberg, "Correction to “Best Face Forward: Crystal-Face Competition at the Ice–Water Interface”," *The Journal of Physical Chemistry B,* vol. 120, no. 39, pp. 10420-10420, 2016.

[55] F. C. Andrews, "Colligative Properties of Simple Solutions," *Science,* vol. 194, no. 4265, pp. 567-571, 1976.

[56] H. D. Chang and L. C. Tao, "Correlations of Enthalpies of Food Systems," *Journal of Food Science,* vol. 46, no. 5, pp. 1493-1497, 1981.

[57] C. S. Chen and N. Steven, "Prediction and Correlation of Freezing Point Depression of Aqueous Solutions," *Transactions of the ASAE,* vol. 30, no. 4, pp. 1176-1180, 1987.

[58] X. Ge and X. Wang, "Estimation of Freezing Point Depression, Boiling Point Elevation, and Vaporization Enthalpies of Electrolyte Solutions," *Industrial & Engineering Chemistry Research,* vol. 48, no. 10, pp. 5123-5123, 2009.

[59] X. D. Chen and P. Chen, "Freezing of aqueous solution in a simple apparatus designed for measuring freezing point," *Food Research International,* vol. 29, no. 8, pp. 723-729, 1996.

[60] J. M. Auleda, M. Raventós, and E. Hernández, "Calculation method for designing a multi-plate freeze-concentrator for concentration of fruit juices," *Journal of Food Engineering,* vol. 107, no. 1, pp. 27-35, 2011.

[61] L. Bayindirli, M. Ozilgen, and S. Ungan, "Mathematical-Analysis of Freeze Concentration of Apple Juice," *Journal of Food Engineering,* vol. 19, no. 1, pp. 95-107, 1993.

[62] P. Chen and X. D. Chen, "A generalized correlation of solute inclusion in ice formed from aqueous solutions and food liquids on sub-cooled surface," *Canadian Journal of Chemical Engineering,* Article vol. 78, no. 2, pp. 312-319, 2000.

[63] J. Sánchez, Y. Ruiz, M. Raventós, J. M. Auleda, and E. Hernández, "Progressive freeze concentration of orange juice in a pilot plant falling film," *Innovative Food Science & Emerging Technologies,* vol. 11, no. 4, pp. 644-651, 2010.

[64] T. Mahmutoğlu and A. Esin, "Distribution coefficients at the interface for carrot juice at slow freezing rates," *Journal of Food Engineering,* vol. 27, no. 3, pp. 291-295, 1996.

[65] Y. H. Chang and R. W. Hartel, "Flow properties of freeze-concentrated skim milk," *Journal of Food Engineering,* vol. 31, no. 3, pp. 375-386, 1997.
[66] B. Habib and M. Farid, "Freeze concentration of milk and saline solutions in a liquid–solid fluidized bed," *Chemical Engineering and Processing: Process Intensification,* vol. 46, no. 12, pp. 1400-1411, 2007.
[67] R. W. Hartel and L. A. Espinel, "Freeze Concentration of Skim Milk," *Journal of Food Engineering,* vol. 20, no. 2, pp. 101-120, 1993.
[68] Z. L. Zhang and R. W. Hartel, "A multilayer Freezer for freeze concentration of liquid milk," *Journal of Food Engineering,* vol. 29, no. 1, pp. 23-38, 1996.
[69] P. Chen, X. D. Chen, and K. W. Free, "An experimental study on the spatial uniformity of solute inclusion in ice formed from falling film flows on a sub-cooled surface," *Journal of Food Engineering,* vol. 39, no. 1, pp. 101-105, 1999.
[70] F. L. Moreno, M. Raventós, E. Hernández, and Y. Ruiz, "Behaviour of falling-film freeze concentration of coffee extract," *Journal of Food Engineering,* vol. 141, pp. 20-26, 2014.
[71] P. M. Williams, M. Ahmad, B. S. Connolly, and D. L. Oatley-Radcliffe, "Technology for freeze concentration in the desalination industry," *Desalination,* vol. 356, pp. 314-327, 2015.
[72] W. Cao, C. Beggs, and I. M. Mujtaba, "Theoretical approach of freeze seawater desalination on flake ice maker utilizing LNG cold energy," *Desalination,* vol. 355, pp. 22-32, 2015.
[73] A. Rich *et al.*, "Freezing desalination of sea water in a static layer crystallizer," *Desalination and Water Treatment,* vol. 13, no. 1-3, pp. 120-127, 2010.
[74] M. Wakisaka, Y. Shirai, and S. Sakashita, "Ice crystallization in a pilot-scale freeze wastewater treatment system," *Chemical Engineering and Processing: Process Intensification,* vol. 40, no. 3, pp. 201-208, 2001.
[75] O. Miyawaki, L. Liu, Y. Shirai, S. Sakashita, and K. Kagitani, "Tubular ice system for scale-up of progressive freeze-concentration," *Journal of Food Engineering,* vol. 69, no. 1, pp. 107-113, 2005.
[76] J. Sánchez, E. Hernández, J. M. Auleda, and M. Raventós, "Freeze concentration of whey in a falling-film based pilot plant: Process and characterization," *Journal of Food Engineering,* Article vol. 103, no. 2, pp. 147-155, 2011.
[77] R. Gulfo, J. M. Auleda, M. Raventós, and E. Hernández, "Calculation process for the recovery of solutes retained in the ice in a multi-plate freeze concentrator: Time and concentration," *Innovative Food Science & Emerging Technologies,* vol. 26, pp. 347-359, 2014.
[78] J. Sanchez, E. Hernandez, J. M. Auleda, and M. Raventos, "Review: freeze concentration technology applied to dairy products," *Food Sci Technol Int,* vol. 17, no. 1, pp. 5-13, Feb 2011.
[79] GEA. (2020, 13 January). *Crystallisation technology-Freeze concentration plants*. Available: https://www.gea.com/en/products/freezeconcentrationplants.jsp
[80] E. Hernández, M. Raventós, J. M. Auleda, and A. Ibarz, "Concentration of apple and pear juices in a multi-plate freeze concentrator," *Innovative Food Science & Emerging Technologies,* vol. 10, no. 3, pp. 348-355, 2009.
[81] X. D. Chen, W. D. Wu, and P. Chen, "An analytical relationship of concentration-dependent interfacial solute distribution coefficient for aqueous layer freeze concentration," *AIChE Journal,* Article vol. 61, no. 4, pp. 1334-1344, 2015.
[82] P. V. Hobbs, *Ice physics*. Clarendon Press, 1974.
[83] H. G. Schwartzberg, "Food Freeze Concentration," in *Biotechnology and Food Process Engineering*: Marcel Dekker, Inc., 1990, pp. 127-202.
[84] S. Smith and G. Pickrell, "Porous Material Fabrication using Ice Particles as a Pore Forming Agent," in *Advances in Synthesis, Processing, and Applications of Nanostructures*: John Wiley & Sons, Inc., 2012, pp. 121-127.

[85] W. Li, M. Anderson, K. Lu, and J. Y. Walz, "Fabrication of Porous Mullite by Freeze Casting and Sintering of Alumina-Silica Nanoparticles," in *Advances in Synthesis, Processing, and Applications of Nanostructures*: John Wiley & Sons, Inc., 2012, pp. 57-64.

[86] K. Lu, "Nanoparticle-Based Material Shaping," in *Nanoparticulate Materials*: John Wiley & Sons, Inc., 2012, pp. 263-328.

[87] M. Watanabe, "Freeze Texturing of Food Materials by Ice-nucleation with the Bacterium Erwinia ananas AU - Arai, Soichi," *Agricultural and Biological Chemistry,* vol. 50, no. 1, pp. 169-175, 1986.

[88] T. Waschkies, R. Oberacker, and M. J. Hoffmann, "Investigation of structure formation during freeze-casting from very slow to very fast solidification velocities," *Acta Materialia,* vol. 59, no. 13, pp. 5135-5145, 2011.

[89] S. Deville, E. Saiz, and A. P. Tomsia, "Ice-templated porous alumina structures," *Acta Materialia,* Article vol. 55, no. 6, pp. 1965-1974, 2007.

[90] U. G. Wegst, M. Schecter, A. E. Donius, and P. M. Hunger, "Biomaterials by freeze casting," *Philos Trans A Math Phys Eng Sci,* vol. 368, no. 1917, pp. 2099-121, 2010.

[91] C. Körber, "Phenomena at the advancing ice–liquid interface: solutes, particles and biological cells," *Quarterly Reviews of Biophysics,* vol. 21, no. 2, pp. 229-298, 1988.

[92] C. Körber, G. Rau, M. D. Cosman, and E. G. Cravalho, "Interaction of particles and a moving ice-liquid interface," *Journal of Crystal Growth,* Article vol. 72, no. 3, pp. 649-662, 1985.

[93] S. Deville, "Ice-templating, freeze casting: Beyond materials processing," *Journal of Materials Research,* vol. 28, no. 17, pp. 2202-2219, 2013.

[94] S. Deville *et al.*, "Metastable and unstable cellular solidification of colloidal suspensions," *Nature Materials,* vol. 8, no. 12, pp. 966-972, 2009.

[95] J. You *et al.*, "Interfacial undercooling in solidification of colloidal suspensions: analyses with quantitative measurements," *Sci Rep,* vol. 6, p. 28434, 2016.

[96] J.-J. Xu, "Unidirectional Solidification and Mullins–Sekerka Instability," in *Interfacial Wave Theory of Pattern Formation in Solidification*(Springer Series in Synergetics: Springer International Publishing, 2017.

[97] W. W. Mullins and R. F. Sekerka, "Morphological Stability of a Particle Growing by Diffusion or Heat Flow," *Journal of Applied Physics,* vol. 34, no. 2, pp. 323-329, 1963.

[98] W. W. Mullins and R. F. Sekerka, "Stability of a Planar Interface During Solidification of a Dilute Binary Alloy," *Journal of Applied Physics,* vol. 35, no. 2, pp. 444-451, 1964.

[99] S. M. Miller, X. Xiao, and K. T. Faber, "Freeze-cast alumina pore networks: Effects of freezing conditions and dispersion medium," *Journal of the European Ceramic Society,* vol. 35, no. 13, pp. 3595-3605, 2015.

[100] K. A. Jackson and J. D. Hunt, "Transparent compounds that freeze like metals," *Acta Metallurgica,* vol. 13, no. 11, pp. 1212-1215, 1965.

[101] K. Araki and J. W. Halloran, "Porous Ceramic Bodies with Interconnected Pore Channels by a Novel Freeze Casting Technique," *Journal of the American Ceramic Society,* vol. 88, no. 5, pp. 1108-1114, 2005.

[102] S. S. L. Peppin, J. A. W. Elliott, and M. G. Worster, "Solidification of colloidal suspensions," *Journal of Fluid Mechanics,* Article vol. 554, pp. 147-166, 2006.

[103] J. M. H. Schollick *et al.*, "Segregated Ice Growth in a Suspension of Colloidal Particles," *The Journal of Physical Chemistry B,* vol. 120, no. 16, pp. 3941-3949, 2016.

[104] S. S. L. Peppin, M. G. Worster, and J. S. Wettlaufer, "Morphological instability in freezing colloidal suspensions," *Proceedings of the Royal Society A: Mathematical, Physical and Engineering Sciences,* Article vol. 463, no. 2079, pp. 723-733, 2007.

[105] L. Hadji, "Morphological instability induced by the interaction of a particle with a solid-liquid interface," *European Physical Journal B,* vol. 37, no. 1, pp. 85-89, 2004.

[106] T. Abe and T. Yano, "Freezing and Ice Structure Formed in Protein Gels AU - Miyawaki, Osato," *Bioscience, Biotechnology, and Biochemistry,* vol. 56, no. 6, pp. 953-957, 1992.

[107] C. Hoose and O. Möhler, "Heterogeneous ice nucleation on atmospheric aerosols: A review of results from laboratory experiments," *Atmospheric Chemistry and Physics,* Review vol. 12, no. 20, pp. 9817-9854, 2012.

[108] B. Zobrist, C. Marcolli, T. Peter, and T. Koop, "Heterogeneous ice nucleation in aqueous solutions: the role of water activity," *J Phys Chem A,* vol. 112, no. 17, pp. 3965-75, 2008.

[109] B. J. Murray, S. L. Broadley, T. W. Wilson, J. D. Atkinson, and R. H. Wills, "Heterogeneous freezing of water droplets containing kaolinite particles," *Atmospheric Chemistry and Physics,* vol. 11, no. 9, pp. 4191-4207, 2011.

[110] B. J. Murray and E. J. Jensen, "Homogeneous nucleation of amorphous solid water particles in the upper mesosphere," *Journal of Atmospheric and Solar-Terrestrial Physics,* vol. 72, no. 1, pp. 51-61, 2010.

[111] R. J. Herbert, B. J. Murray, T. F. Whale, S. J. Dobbie, and J. D. Atkinson, "Representing time-dependent freezing behaviour in immersion mode ice nucleation," *Atmospheric Chemistry and Physics,* vol. 14, no. 16, pp. 8501-8520, 2014.

[112] D. Niedermeier *et al.*, "Heterogeneous ice nucleation: exploring the transition from stochastic to singular freezing behavior," *Atmospheric Chemistry and Physics,* vol. 11, no. 16, pp. 8767-8775, 2011.

[113] R. Chow, R. Blindt, R. Chivers, and M. Povey, "The sonocrystallisation of ice in sucrose solutions: primary and secondary nucleation," *Ultrasonics,* vol. 41, no. 8, pp. 595-604, 2003.

[114] A. E. Delgado, L. Y. Zheng, and D. W. Sun, "Influence of Ultrasound on Freezing Rate of Immersion-frozen Apples," *Food and Bioprocess Technology,* vol. 2, no. 3, pp. 263-270, 2009.

[115] B. Li and D.-W. Sun, "Effect of power ultrasound on freezing rate during immersion freezing of potatoes," *Journal of Food Engineering,* vol. 55, no. 3, pp. 277-282, 2002.

[116] K. Nakagawa, A. Hottot, S. Vessot, and J. Andrieu, "Influence of controlled nucleation by ultrasounds on ice morphology of frozen formulations for pharmaceutical proteins freeze-drying," *Chemical Engineering and Processing: Process Intensification,* vol. 45, no. 9, pp. 783-791, 2006.

[117] M. D. Luque de Castro and F. Priego-Capote, "Ultrasound-assisted crystallization (sonocrystallization)," *Ultrasonics Sonochemistry,* vol. 14, no. 6, pp. 717-724, 2007.

[118] E. Xanthakis, A. Le-Bail, and H. Ramaswamy, "Development of an innovative microwave assisted food freezing process," *Innovative Food Science & Emerging Technologies,* vol. 26, pp. 176-181, 2014.

[119] M. Dalvi-Isfahan, N. Hamdami, E. Xanthakis, and A. Le-Bail, "Review on the control of ice nucleation by ultrasound waves, electric and magnetic fields," *Journal of Food Engineering,* vol. 195, pp. 222-234, 2017.

[120] M. Orlowska, M. Havet, and A. Le-Bail, "Controlled ice nucleation under high voltage DC electrostatic field conditions," *Food Research International,* vol. 42, no. 7, pp. 879-884, 2009.

[121] E. Xanthakis, M. Havet, S. Chevallier, J. Abadie, and A. Le-Bail, "Effect of static electric field on ice crystal size reduction during freezing of pork meat," *Innovative Food Science & Emerging Technologies,* vol. 20, pp. 115-120, 2013.

[122] S. Wei, X. Xiaobin, Z. Hong, and X. Chuanxiang, "Effects of dipole polarization of water molecules on ice formation under an electrostatic field," *Cryobiology,* vol. 56, no. 1, pp. 93-9, 2008.

[123] J. D. Hunt and K. A. Jackson, "Nucleation of Solid in an Undercooled Liquid by Cavitation," *Journal of Applied Physics,* vol. 37, no. 1, pp. 254-257, 1966.

[124] R. Hickling, "Transient, High-Pressure Solidification Associated with Cavitation in Water," *Physical Review Letters,* vol. 73, no. 21, pp. 2853-2856, 1994.

[125] T. Okada, Y. Iwai, and K. Awazu, "A study of cavitation bubble collapse pressures and erosion part 1: A method for measurement of collapse pressures," *Wear,* vol. 133, no. 2, pp. 219-232, 1989.
[126] P. Schuck *et al.*, "Recent advances in spray drying relevant to the dairy industry: A comprehensive critical review," *Drying Technology,* vol. 34, no. 15, pp. 1773-1790, 2016.
[127] E. C. Needs, "Effects of long-term deep-freeze storage on the condition of the fat in raw sheep's milk," *Journal of Dairy Research,* vol. 59, pp. 49-55, 1992.
[128] D. D. Muir, "Reviews on the Progress of Dairy Science: Frozen concentrated milk," *Journal of Dairy Research,* vol. 51, pp. 649-664, 1984.
[129] M. Pazzola *et al.*, "The Effect of Long-term Freezing on Renneting Properties of Sarda Sheep Milk," *Agriculturae Conspectus Scientificus,* vol. 78, no. 3, pp. 275-279, 2013.
[130] W. L. Wendorff, "Milk composition and cheese yield," in *Proceedings of the 7th Great lakes Dairy Sheep Symposium*, Ithaca, 2002.
[131] A. L. Marquez, G. N. Salvatore, R. G. Otero, J. R. Wagner, and G. G. Palazolo, "Impact of freeze-thaw treatment on the stability of calcium-fortified soy beverages," *Lwt-Food Science and Technology,* vol. 62, no. 1, pp. 474-481, 2015.
[132] M. Spannuth, S. G. Mochrie, S. S. Peppin, and J. S. Wettlaufer, "Particle-scale structure in frozen colloidal suspensions from small-angle x-ray scattering," *Phys Rev E Stat Nonlin Soft Matter Phys,* vol. 83, no. 2 Pt 1, p. 021402, 2011.
[133] L. P. Voutsinas, M. C. Katsiari, C. P. Pappas, and H. Mallatou, "Production of yoghurt from sheep's milk which had been concentrated by reverse osmosis and stored frozen. 2. Compositional, microbiological, sensory and physical characteristics of yoghurt," *Food Research International,* Article vol. 29, no. 3-4, pp. 411-416, 1996.
[134] S. E. Duncan, G. L. Christen, and M. P. Penfield, "Rancid Flavor of Milk: Relationship of Acid Degree Value, Free Fatty Acids, and Sensory Perception," *Journal of Food Science,* vol. 56, no. 2, pp. 394-397, 1991.
[135] P. Young, "Deep-frozen storage of frozen ewe's milk," *Sheep Dairy News,* no. 4, p. 41, 1987.
[136] M. S. Koschak, O. Fennema, C. H. Amundson, and J. Y. Lee, "Protein Stability of Frozen Milk as Influenced by Storage Temperature and Ultrafiltration," *Journal of Food Science,* vol. 46, no. 4, pp. 1211-1217, 1981.
[137] P. Walstra, J. T. M. Wouters, and T. J. Geurts, *Dairy science and technology*. Boca Raton: CRC Taylor & Francis, 2006.
[138] S. Y. Wong and R. W. Hartel, "Crystallization in Lactose Refining—A Review," *Journal of Food Science,* vol. 79, no. 3, pp. R257-R272, 2014.
[139] C. V. Morr, "Chemistry of milk proteins in food processing," *J Dairy Sci,* vol. 58, no. 7, pp. 977-84, Jul 1975.
[140] K. Jouppila and Y. H. Roos, "Glass Transitions and Crystallization in Milk Powders," *Journal of Dairy Science,* Article vol. 77, no. 10, pp. 2907-2915, 1994.
[141] K. Jouppila, J. Kansikas, and Y. H. Roos, "Glass Transition, Water Plasticization, and Lactose Crystallization in Skim Milk Powder," *Journal of Dairy Science,* Article vol. 80, no. 12, pp. 3152-3160, 1997.
[142] Y. H. Roos, "Importance of glass transition and water activity to spray drying and stability of dairy powders," *Le Lait,* vol. 82, no. 4, pp. 475-484, 2002.
[143] Y. H. Roos, "Water in Dairy Products: Significance," in *Encyclopedia of Dairy Sciences (Second Edition)*, J. W. Fuquay, Ed. San Diego: Academic Press, 2011, pp. 707-714.
[144] P. Schuck, E. Blanchard, A. Dolivet, S. Méjean, E. Onillon, and R. Jeantet, "Water activity and glass transition in dairy ingredients," *Le Lait,* vol. 85, no. 4-5, pp. 295-304, 2005.
[145] P. Gallo *et al.*, "Water: A Tale of Two Liquids," *Chemical Reviews,* vol. 116, no. 13, pp. 7463-7500, 2016.
[146] G. Vuataz, "The phase diagram of milk: a new tool for optimising the drying process," *Le Lait,* vol. 82, no. 4, pp. 485-500, 2002.

[147] M. L. Williams, R. F. Landel, and J. D. Ferry, "The Temperature Dependence of Relaxation Mechanisms in Amorphous Polymers and Other Glass-forming Liquids," *Journal of the American Chemical Society,* vol. 77, no. 14, pp. 3701-3707, 1955.
[148] M. Peleg, "On the use of the WLF model in polymers and foods," *Crit Rev Food Sci Nutr,* vol. 32, no. 1, pp. 59-66, 1992.
[149] A. H. J. Paterson, G. D. Ripberger, and R. P. Bridges, "Measurement of the viscosity of freeze dried amorphous lactose near the glass transition temperature," *International Dairy Journal,* vol. 43, pp. 27-32, 2015.
[150] C. M. Chen and K. Yamauchi, "Change of Salt Distribution in Milk During Frozen Storage and Its Partial Reversion after Thawing," *Agricultural and Biological Chemistry,* Article vol. 33, no. 9, pp. 1333-1341, 1969.
[151] M. A. De La Fuente, T. Requena, and M. Juárez, "Salt Balance in Ewe's and Goat's Milk during Storage at Chilling and Freezing Temperatures," *Journal of Agricultural and Food Chemistry,* Article vol. 45, no. 1, pp. 82-88, 1997.
[152] L. Van Den Berg, "pH changes in buffers and foods during freezing and subsequent storage," *Cryobiology,* vol. 3, no. 3, pp. 236-242, 1966.
[153] O. J. McCarthy, "Milk | Physical and Physico-Chemical Properties of Milk," in *Encyclopedia of Dairy Sciences (Second Edition)*, J. W. Fuquay, Ed.: Academic Press, 2002, pp. 467-477.
[154] M. C. Katsiari, L. P. Voutsinas, and E. Kondyli, "Manufacture of yoghurt from stored frozen sheep's milk," *Food Chemistry,* vol. 77, no. 4, pp. 413-420, 2002.
[155] B. H. Webb and S. A. Hall, "Some Physical Effects of Freezing upon Milk and Cream," *Journal of Dairy Science,* vol. 18, no. 5, pp. 275-286, 1935.
[156] S. K. Singh and S. Nema, "Freezing and Thawing of Protein Solutions," in *Formulation and Process Development Strategies for Manufacturing Biopharmaceuticals* F. Jameel and S. Hershenson, Eds.: John Wiley & Sons, 2010, pp. 625-675.
[157] X. Tang and M. J. Pikal, "The Effect of Stabilizers and Denaturants on the Cold Denaturation Temperatures of Proteins and Implications for Freeze-Drying," *Pharmaceutical Research,* vol. 22, no. 7, pp. 1167-1175, 2005.
[158] X. C. Tang and M. J. Pikal, "Measurement of the kinetics of protein unfolding in viscous systems and implications for protein stability in freeze-drying," *Pharm Res,* vol. 22, no. 7, pp. 1176-85, 2005.
[159] B. S. Bhatnagar, R. H. Bogner, and M. J. Pikal, "Protein Stability During Freezing: Separation of Stresses and Mechanisms of Protein Stabilization," *Pharmaceutical Development & Technology,* Article vol. 12, no. 5, pp. 505-523, 2007.
[160] C. R. Fonseca *et al.*, "Storage of refrigerated raw goat milk affecting the quality of whole milk powder," *Journal of Dairy Science,* vol. 96, no. 7, pp. 4716-4724, 2013.
[161] A. K. Yamazi, T. S. Moreira, V. Q. Cavicchioli, R. C. K. Burin, and L. A. Nero, "Long cold storage influences the microbiological quality of raw goat milk," *Small Ruminant Research,* vol. 113, no. 1, pp. 205-210, 2013.
[162] A. A. L. Tribst, L. R. Ribeiro, B. R. d. C. Leite Junior, M. M. de Oliveira, and M. Cristianini, "Fermentation profile and characteristics of yoghurt manufactured from frozen sheep milk," *International Dairy Journal,* vol. 78, pp. 36-45, 2018.
[163] S. G. Anema, "Age Gelation, Sedimentation, and Creaming in UHT Milk: A Review," *Comprehensive Reviews in Food Science and Food Safety,* vol. 18, no. 1, pp. 140-166, 2019.
[164] J. A. Lucey, "Formation and Physical Properties of Milk Protein Gels," *Journal of Dairy Science,* vol. 85, no. 2, pp. 281-294, 2002.
[165] J. A. Lucey, "Cheese | Rennet-Induced Coagulation of Milk," in *Encyclopedia of Dairy Sciences*, J. W. Fuquay, Ed. San Diego: Academic Press, 2011, pp. 579-584.
[166] J. A. Lucey and H. Singh, "Formation and physical properties of acid milk gels: a review," *Food Research International,* vol. 30, no. 7, pp. 529-542, 1997.

[167] D. S. Horne, "Casein Interactions: Casting Light on the Black Boxes, the Structure in Dairy Products," *International Dairy Journal,* vol. 8, no. 3, pp. 171-177, 1998.

[168] Y. Lu, D. J. McMahon, and A. H. Vollmer, "Investigating cold gelation properties of recombined highly concentrated micellar casein concentrate and cream for use in cheese making," *Journal of Dairy Science,* Article vol. 99, no. 7, pp. 5132-5143, 2016,

[169] Y. Lu, D. J. McMahon, L. E. Metzger, A. Kommineni, and A. H. Vollmer, "Solubilization of rehydrated frozen highly concentrated micellar casein for use in liquid food applications," *Journal of Dairy Science,* vol. 98, no. 9, pp. 5917-5930, 2015.

[170] D. F. Newstead, G. Paterson, S. G. Anema, C. J. Coker, and A. R. Wewala, "Plasmin activity in direct-steam-injection UHT-processed reconstituted milk: Effects of preheat treatment," *International Dairy Journal,* vol. 16, no. 6, pp. 573-579, 2006.

[171] S. G. Anema, "Storage stability and age gelation of reconstituted ultra-high temperature skim milk," *International Dairy Journal,* vol. 75, pp. 56-67, 2017.

[172] P. J. Fellows, "22 - Freezing," in *Food Processing Technology (Fourth Edition)*, P. J. Fellows, Ed.: Woodhead Publishing, 2017, pp. 885-928.

[173] Y. H. Hui, *Handbook of frozen foods* (Food science and technology: 133). New York : Marcel Dekker, 2004.

[174] A. E. Delgado and D. W. Sun, "Heat and mass transfer models for predicting freezing processes - a review," *Journal of Food Engineering,* vol. 47, no. 3, pp. 157-174, Feb 2001.

[175] D. J. Cleland, A. C. Cleland, R. L. Earle, and S. J. Byrne, "Prediction of thawing times for foods of simple shape," *International Journal of Refrigeration,* vol. 9, no. 4, pp. 220-228, 1986.

[176] Q. T. Pham, "Modelling heat and mass transfer in frozen foods: a review," *International Journal of Refrigeration,* vol. 29, no. 6, pp. 876-888, 2006.

[177] K. J. Valentas, E. Rotstein, and R. P. Singh, "Handbook of Food Engineering Practice." CRC Press, 1997.

[178] L. B. A. Tyree Jr., North, Oak Brook, IL, 60521), Missig, James R. (Joliet, IL), Rhoades, George D. (La Grange, IL), "Cryogenic cabinet freezer," United States, 1982. Available: http://www.freepatentsonline.com/4356707.html.

[179] S. O. Awonorin, "An appraisal of the freezing capabilities of tunnel and spiral belt freezers using liquid nitrogen sprays," *Journal of Food Engineering,* vol. 34, no. 2, pp. 179-192, 1997.

[180] D. D. N. Duarte, DE, US), John, Candice (Quebec, CA), Mortenson, Stephanie (Edmonton, CA), "VERTICAL COUNTER-FLOW IMMERSION FREEZER," United States, 2015. Available: http://www.freepatentsonline.com/y2015/0184915.html.

[181] G. A. T. Temple, CA), Kirkwood, Donald W. (Oakville, CA), Milankov, Bosko (Mississauga, CA), "Process for freezing or chilling," United States, 1987. Available: http://www.freepatentsonline.com/4655047.html.

[182] P. H. I. Gibson, GB2), Taylor, Robert I. (Guildford, GB2), "Freezing a liquid," United States, 1984. Available: http://www.freepatentsonline.com/4479363.html.

[183] J. K. Walters, "Prilling," 2006.

[184] S. Shen and A. M. Wolsky, "Energy and materials flows in the production of liquid and gaseous oxygen," United States 1980-08-01 1980, Available: https://www.osti.gov/servlets/purl/6574363.

[185] M. Antonelli, U. Desideri, R. Giglioli, F. Paganucci, and G. Pasini, "Liquid Air Energy Storage: A Potential Low Emissions and Efficient Storage System," *Energy Procedia,* vol. 88, pp. 693-697, 2016.

[186] M. T. Kalichevsky, D. Knorr, and P. J. Lillford, "Potential food applications of high-pressure effects on ice-water transitions," *Trends in Food Science and Technology,* Review vol. 6, no. 8, pp. 253-259, 1995.

[187] B. Li and D. W. Sun, "Novel methods for rapid freezing and thawing of foods - a review," *Journal of Food Engineering,* vol. 54, no. 3, pp. 175-182, 2002.

[188] B. Li and D.-W. Sun, "Novel methods for rapid freezing and thawing of foods – a review," *Journal of Food Engineering,* vol. 54, no. 3, pp. 175-182, 2002.
[189] H. Sojoudi, M. Wang, N. D. Boscher, G. H. McKinley, and K. K. Gleason, "Durable and scalable icephobic surfaces: Similarities and distinctions from superhydrophobic surfaces," *Soft Matter,* Review vol. 12, no. 7, pp. 1938-1963, 2016.
[190] K. K. Varanasi, T. Deng, J. D. Smith, M. Hsu, and N. Bhate, "Frost formation and ice adhesion on superhydrophobic surfaces," *Applied Physics Letters,* vol. 97, no. 23, p. 234102, 2010.
[191] Y. Wang, J. Xue, Q. Wang, Q. Chen, and J. Ding, "Verification of icephobic/anti-icing properties of a superhydrophobic surface," *ACS Appl Mater Interfaces,* vol. 5, no. 8, pp. 3370-81, 2013.
[192] D. K. Mandal, A. Criscione, C. Tropea, and A. Amirfazli, "Shedding of Water Drops from a Surface under Icing Conditions," *Langmuir,* Article vol. 31, no. 34, pp. 9340-9347, 2015.
[193] E. Stamatiou, J. W. Meewisse, and M. Kawaji, "Ice slurry generation involving moving parts," *International Journal of Refrigeration,* Article vol. 28, no. 1, pp. 60-72, 2005.
[194] E. M. Drewett and R. W. Hartel, "Ice crystallization in a scraped surface freezer," *Journal of Food Engineering,* Article vol. 78, no. 3, pp. 1060-1066, 2007.
[195] C. S. Rao and R. W. Hartel, "Scraped surface heat exchangers," *Critical Reviews in Food Science and Nutrition,* Review vol. 46, no. 3, pp. 207-219, 2006.
[196] E. B. Jafa, NY, US), Abashkin, Vasilii (St. Petersburg, RU), Balanev, Andrey (St. Petersburg, RU), Martsinovskiy, Georgy (St. Petersburg, RU), Vasiliev, Vladimir (St. Petersburg, RU), Verbitsky, Mikhail (Stoughton, MA, US), "Ice making and harvesting," United States, 2016. Available: http://www.freepatentsonline.com/9528737.html.
[197] T. J. A. Paskach, IA), Schroeder, William D. (Ames, IA), "Continuous system and method for producing frozen food products," United States, 2003. Available: http://www.freepatentsonline.com/6510890.html.
[198] W. L. Morrison, "Method of preparing a frozen food product," United States, 1962. Available: http://www.freepatentsonline.com/3068105.html.
[199] B. C. S. Inc. (2015, 28/12/2016). *Industrial Ice Making Machines*. Available: http://berg-group.com/products/ice-making/5-to-50-tons-shell-ice-machines/
[200] B. C. S. Inc. (2015, 28/12/2016). *A Juicy Job for a Cool Machine*.
[201] R. H. Perry, D. W. Green, and J. Maloney, O., *Perry's Chemical Engineers' Handbook Seventh Edition*. New York: McGraw-Hill, 1999.
[202] S. Peters-Erjawetz, J. Ulrich, M. Tiedtke, and R. W. Hartel, "Milk fat fractionation by solid-layer melt crystallization," *Journal of the American Oil Chemists' Society,* vol. 76, no. 5, pp. 579-584, 1999.
[203] M. J. A. L. Groux, CH), Fayard, Gilles (Epalinges, CH), Jimenez-laguna, Antonio (Lausanne, CH), "Frozen concentrated milk and preparation thereof," United States, 2001. Available: http://www.freepatentsonline.com/6207213.html.

Chapter 2: Equipment.

2.1 Chapter Summary

There are several pieces of equipment that were used regularly in the course of my investigations. These are described in depth in this chapter.

2.2 Differential Scanning Calorimeter

Differential scanning calorimetry was carried out using a Q2000 differential scanning calorimeter (TA instruments, New Castle, DE, USA. Instrument # 970001.901) with an RCS40 cooling system (TA instruments, New Castle, DE, USA. Accessory # 972507.902). Calibration was conducted according to manufacturers' instruction using MilliQ water, and high-purity indium, bismuth and tin standards.

All calibrations and measurements were conducted using Tzero aluminium hermetic pans and lids (TA instruments, New Castle, DE, USA. Consumable # 901683.901 and 901684.901), sealed with a Tzero sample press (TA instruments, New Castle, DE, USA. Accessory # 901600.901) according to manufacturer's instructions.

2.3 Rheology

Rheological measurements were conducted using the suite of instruments available to the School of Food and Advanced Technology, Massey University (Palmerston North, New Zealand).

The instruments used were Anton Paar MCR301 (Serial # MCR301876728) and MCR 302 (Serial #MCR30281518692) computerised rheometers (Anton Paar GmbH, Graz, Austria) equipped with a C-PTD200 Peltier temperature control system (Anton Paar GmbH, Graz, Austria). A double-gap geometry, DG 26.7 (Anton Paar GmbH, Graz, Austria) was used.

2.4 Optical Microscope

Optical microscopy was conducted using an Olympus CHA microscope with an MTV-3 camera mount and an Olympus NKF 3.3x LD photo microscope eyepiece (Olympus Corporation, Tokyo, Japan). For most observations a Nikon E4/0.10 4x objective lens (Nikon Corporation, Tokyo, Japan) was used.

An STC-MC202USB (Omron Sentech Co. ltd, Ebina, Japan) C-mount USB CCD camera was used for low-speed observations. A Megaspeed MS40K (Mega Speed Corporation, Minnedosa, Manitoba Canada) C-mount high-speed monochrome CMOS camera was used for high frame-rate observations.

The custom-built stage discussed in Chapter 4 was used for most microscopy work, some initial experiments were conducted with an Instec HCS622V cold stage, controlled by a mK2000 Temperature Controller (Instec Inc., Boulder, CO, USA).

2.5 Scanning Electron Microscope

Scanning Electron Microscopy was conducted at the electron microscope suite at the Victoria University of Wellington (Wellington, New Zealand). A JEOL 6500F (JEOL Ltd, Akishima, Japan) equipped with a Gatan Alto 2500 cryo preparation chamber and cold stage (Gatan Inc., Leicester, U.K.) was used to capture SEM images. A slush nitrogen chamber was used to freeze samples for imaging. Further details of sample preparation are given in the relevant chapters.

2.6 Centrifuges

For low-speed centrifuge work, an Heraeus Multifuge 1 S-R centrifuge (Thermo Fisher Scientific, Inc., Waltham, MA, USA) was used.

To separate caseins a Sorvall ™ WX Ultra 100 ultracentrifuge (Thermo Fisher Scientific, Inc., Waltham, MA, USA) was used.

2.7 Kjeldahl Distillation.

Assays for Kjeldahl nitrogen were carried out using a Foss Tecator 2006 Digestor (FOSS, Hilleroed, Denmark) and a Kjeltec™ 2100 distillation unit (FOSS, Hilleroed, Denmark). Direct titration of 0.1M HCl was used to determine N content.

2.8 Elemental Analysis.

An Agilent 4210 Microwave Plasma Atomic Emission Spectrometer (MP-AES) (Agilent Technologies, Santa Clara, CA, USA) equipped with an ASX-520 Autosampler (Teledyne CETAC Technologies, Omaha NE, USA) was used to determine the level of elements present in samples.

2.9 Freezer Space

The freezers used for storage were industrial style storage freezer rooms in the Massey University Food Pilot Plant (Palmerston North, New Zealand). The freezer rooms were installed in 2010. The freezers have multiple temperature sensors, which are logged electronically. The data from the room temperature sensor (located on the freezer wall) two product probes are archived. The temperature control system uses a combination of room temperature and freezer evaporator discharge air temperature for control. Each freezer undergoes a defrost cycle of approximately 30 minutes at regular intervals. For the freezers set to -10°C, -20°C and -30°C defrost cycles occur every 8 hours. For the freezer set to -20°C, the defrost cycle occurs every 12 hours.

2.10 Miscellaneous Equipment.

A Brabantia Turbo Hand Blender (Brabantia, Valkenswaard, Netherlands) was used to coarsely homogenise some samples prior to sampling.

An APV 2000 benchtop high-pressure homogeniser (APV systems, Albertslund, Denmark) was used to process samples as discussed further in Chapter 5.

The surface tension of samples was measured with a SITA science line t100 (SITA Messtechnik GmbH, Dresden, Germany) laboratory bubble pressure tensiometer.

To isolate casein micelles from ovine milk, a benchtop scale ultrafiltration unit was used. This consists of a Pellicon ®Tangential Flow Filtration System with a Pellicon ® Mini Cassette Holder and a Pellicon ®2 0.1 µm Durapore 0.1 m^2 filter membrane (Merck Millipore, Burlington, MA, USA).

Coolant for small scale experimental set-ups was cooled and circulated by a Julabo FL300 Recirculating Cooler (Julabo GmbH, Seelbach, Germany). A 50% ethylene glycol solution in water was used as coolant). This was used for the cold-stage and bridgeman furnace microscope.

For large scale cooling loads a Patton Pak PZB600 coolant chiller (Patton, Auckland, New Zealand) was used as part of the experimental set-ups discussed in Chapters 2 and 7.

A Maximator S40-SS high-pressure air driven pump (Maximator GmbH, Nordhausen, Germany) was used to develop the feed pressure required for the continuous tubular freezer covered in Chapters 7 and 8. Driving air was provided by building compressed-air service at 8 Bar, or by N_2 from compressed gas bottles if building compressed air service was unavailable.

A Carbolite Muffle Furnace was used to ash samples for proximate analyses and elemental analyses.

A Thermo Scientific ™ Orion 3 Star Benchtop pH meter (Thermo Fisher Scientific, Inc., Waltham, MA, USA) was used in all pH measurements. Before each session of measurements the pH meter

was calibrated with pH4 and pH7 calibration buffers according to the manufacturer's instructions

2.11 Software

Image analysis was conducted using the FIJI open source image analysis platform [1], with feature recognition carried out with the Trainable Weka Segmentation plugin package[2].

Data processing was conducted with Microsoft Excel 2016 and 2019 (Microsoft Corporation, Redmond, WA, USA), and statistical analyses were conducted with the open source R statistical programming language [3] or with Minitab Version 18 (Minitab LLC., State College, PA, USA).

Mathematical modelling work was conducted using the Matlab R2017b mathematical programming language and environment (The MathWorks, Inc., Natick, MA, USA).

Figures were constructed using Excel, R, Minitab or Matlab as appropriate, and Photoshop CC 19 (Adobe Inc., Mountain View, CA, USA) was used to prepare figures for publication. Photoshop CC19 was used to adjust brightness and contrast of Micrographs to improve legibility. Photoshop was used to prepare composite images from several micrographs.

Equipment designs, and technical drawings were prepared using SolidWorks 2017 (Dassault Systèmes SE, Paris, France)

2.12 References

[1] J. Schindelin *et al.*, "Fiji: an open-source platform for biological-image analysis," *Nat Methods,* vol. 9, no. 7, pp. 676-82, 2012.

[2] I. Arganda-Carreras *et al.*, "Trainable Weka Segmentation: a machine learning tool for microscopy pixel classification," *Bioinformatics,* vol. 33, no. 15, pp. 2424-2426, 2017.

[3] R. C. Team, "R: A language and environment for statistical computing," ed. Vienna, Austria: R Foundation for Statistical Computing, 2014.

Chapter 3: Development of a Rolling Droplet Freezer and Falling Film Freezer.

3.1 Chapter Summary

This chapter discusses some of the preliminary work conducted on freezing, some work on selected properties of ovine milk, the development of a pilot falling-film freezer and selected trials involving this freezer.

3.2 Introduction

At the outset of the project, in 2015, the project aimed to develop a "rolling droplet freezer" which would operate by forming small droplets of liquid milk, and rolling them down an inclined plate with a superhydrophobic surface. The milk would be frozen by a cold counter-current air flow. The frozen milk would roll into a storage bin located below the inclined plate.

The size, milk flow, air flow and air temperatures of this freezer needed to be determined.

In order to develop this freezer, the following engineering problems would need to be solved, and research areas investigated:

- Droplet behaviour on superhydrophobic surfaces.
- The relative contributions to heat transfer from convection, conduction through the superhydrophobic surface, radiation and sublimation.
- The freezing behaviour of rolling milk droplets on superhydrophobic surfaces, focusing on the level of supercooling that would occur, the nucleation rate in droplets, and the freezing temperature profile of a milk droplet.
- How the milk quality was affected by this freezing method, with a focus on the behaviour of proteins and fat globules during the freezing process.
- How to reliable dispense droplets in a freezing environment without fouling nozzles with frozen product.

Preliminary proof of concept work was completed in 2015 by a fourth-year engineering student [1], who investigated the freezing of water droplets rolling in the inside of a rolling ring coated with a superhydrophobic surface. This was found to be a feasible method of freezing liquids. Some still images taken from a high-speed video of a freezing droplet are shown below.

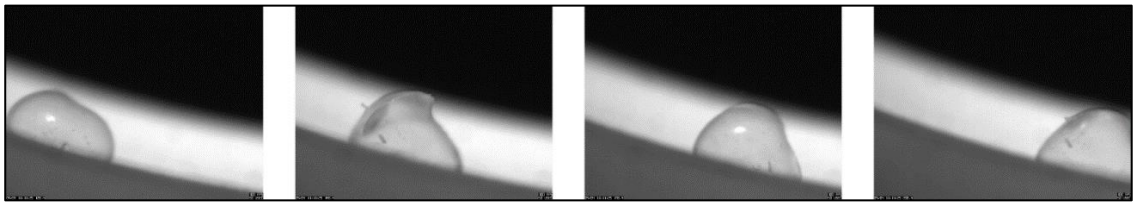

Figure 3-1: A rolling droplet of water after 14 s in a -30°C blast freezer. The droplet is still mostly liquid, though some crystals can be seen.

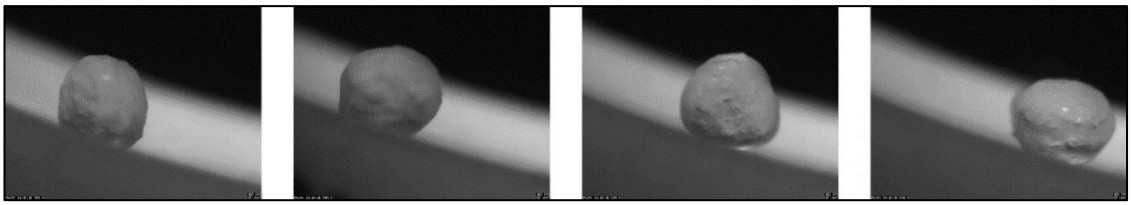

Figure 3-2: A rolling droplet of water after 40s in a -30°C blast freezer. A solid shell of ice has formed. Bubbles can be seen, a result of dissolved gases coming out of solution during freezing.

The original research aims for 2016, the first year of my PhD, are discussed in the following section.

3.3 Research Aims for the Development of a Rolling Droplet Freezer.

In order to develop the freezer and optimise its operation the freezing behaviour of a rolling droplet needed to be investigated. The results of the work conducted in 2016 would have been used to develop a mathematical model of the freezing behaviour of a rolling droplet.

A droplet rolling along a surface displays a resistance to rolling, similar to rolling frictional resistance. This can be seen as a droplet "climbing" up the wall of a rolling ring, and was seen in Mariel Catapang's preliminary work[1] and in literature[2]. This is believed to be as a result of internal viscous dissipation in the droplet, and deformation of the droplet along the droplet/surface contact line[3]. Work was planned to investigate the effect of viscosity, density and surface tension on the rolling resistance of droplets.

A freezing droplet will demonstrate a phenomenon known as "subcooling" or "supercooling"[4] where the fluid cools below its equilibrium freezing temperature before nucleation occurs, following which a fraction of the fluid instantaneously freezes and the temperature of the droplet rises toward the fluid's equilibrium freezing temperature. It was planned to investigate the freezing temperature profile and nucleation rate of the droplet in two different environments: A sessile drop on a cooled superhydrophobic surface, and a single droplet suspended in a freezing airflow. Determination of the nucleation behaviour of the droplets would be vital to the design of the freezer, as the nucleation behaviour determines the freezing profile of the droplet and this freezing profile determines the time required to reach a desired droplet temperature.

The single suspended droplet experiment was designed with a droplet suspended from an analytical balance on a thin wire thermocouple. This experiment would have determined the level of sublimation that occurs, allowing an energy and mass balance to be conducted on the freezing droplets[5]. This would have been important for the operation of a rolling droplet freezer as sublimation and de-sublimation of water could affect the quality of product and could lead to frosting on refrigeration coils or freezer surfaces. One weakness of this experiment is that droplets in a quiescent system could nucleate at different temperatures when compared to a rolling droplet, however the dynamics of the mass and energy balances during freezing could be explored with this experiment

An investigation of the thermal and physical properties of sheep milk was also planned. In order to accurately model the behaviour of a rolling, freezing droplet, the heat capacity, equilibrium freezing temperature, latent heat of freezing and rheological properties of milk are needed. The thermal conductivity of milk is also of interest, however, as a fluid it is difficult to disentangle the effects of convective heat transfer and it can be predicted within the accuracy of most measurement methods by equations such as those given in the Food Properties Handbook[6]. The surface tension of milk is an important parameter for understanding the behaviour of a rolling droplet.

3.4 Work Conducted on Droplet Freezing

3.4.1 Rolling Droplet Settling Angle.

A droplet rolling on a rolling ring will "climb" the ring from the point of view of an observer, settling at a point higher than the lowest point of the system. The tangential angle to the horizontal, at this settling point, is referred to as the "settling angle".

The proof-of-concept studies collected data on the settling angle of a droplet rolling on a superhydrophobic surface on the interior of a rolling ring, and the shape of the droplet. The settling angle was determined from image analysis of high-speed videos of rolling freezing droplets. These data were used by the student to construct a behaviour map describing the behaviour of the droplets as a function of size and tangential velocity.

I used the data collected to investigate the relationship between the settling angle and the rotational velocity of the droplets. This relationship would allow an equation to be developed to describe the rolling resistance of the droplets. This rolling resistance would have affected the terminal velocity of the droplets rolling down the plate which would affect several design parameters of the rolling droplet freezer, such as plate angle, air velocity, and the freezer size/ residence time relationship.

It was found that the rotational velocity of the droplet was a statistically significant predictor of the tangent of the settling angle.

The settling angle could be predicted by the following equation, with ω being the droplet rotational velocity, and a and b being empirically determined coefficients:

$$\theta_{settling} = \tan^{-1}(a * \omega_{droplet} + b) \quad (3\text{-}1)$$

The R^2 of the relationship was low, at 0.73, as can be seen in Figure 3-3. Further work was planned to gather more data on the relationship between rotational velocity and rolling resistance.

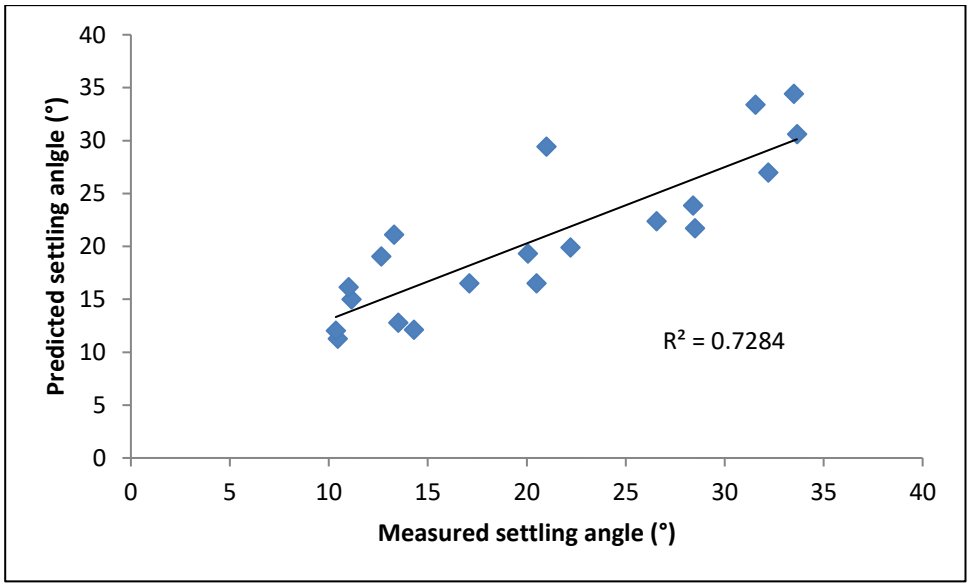

Figure 3-3: Droplet settling angle predicted from equation (3-1) vs. measured settling angle. N=20.

In order to investigate the relationship between the physical properties of the liquid, and the droplet settling angle, an experimental rig was designed. The rig consisted of a ring, with a

superhydrophobic inner surface placed on a pair of rollers, driven by a speed-controlled motor. The settling angle of the droplet would be measured with a high-speed camera.

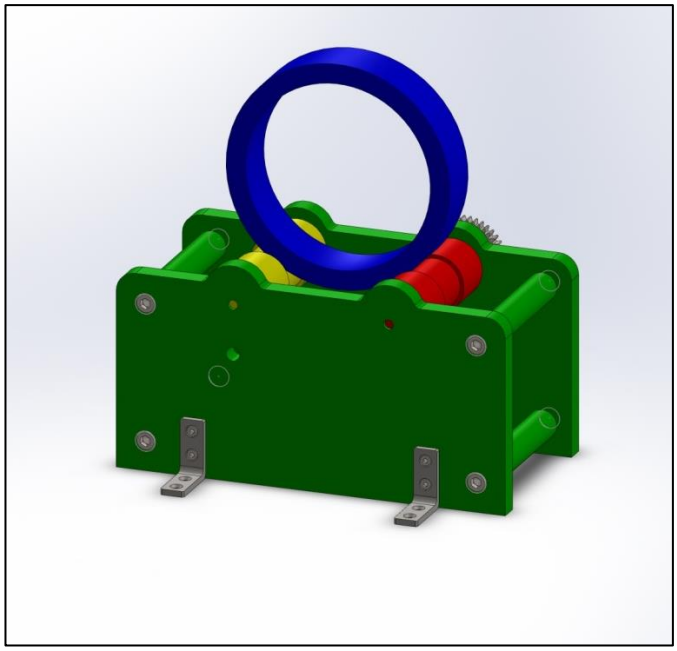

Figure 3-4: A rolling ring to investigate droplet behaviour. A microprocessor-controlled motor would have driven the red drive roller, which drives the replaceable ring (blue). The ring would have varied diameters and surface treatments, and the settling angle of droplets with different sizes and droplet properties would have be investigated at varied tangential velocities.

Experimental equipment to measure the nucleation rates of quiescent milk droplets on superhydrophobic surfaces was designed. The equipment consisted of an aluminium plate onto which superhydrophobic surfaces could be mounted. The plate could be cooled to -30°C by a thermoelectric cooler (or Peltier module) which rejected heat into a water-cooled copper block. The cooled plate was placed inside a housing and an IR transparent window was mounted above the plate. A thermal imaging camera would monitor the temperature of droplets on the surfaces, and detect the temperature rise that occurs upon droplet nucleation. This principle has been previously used to investigate the nucleation of pure water droplets[7, 8].

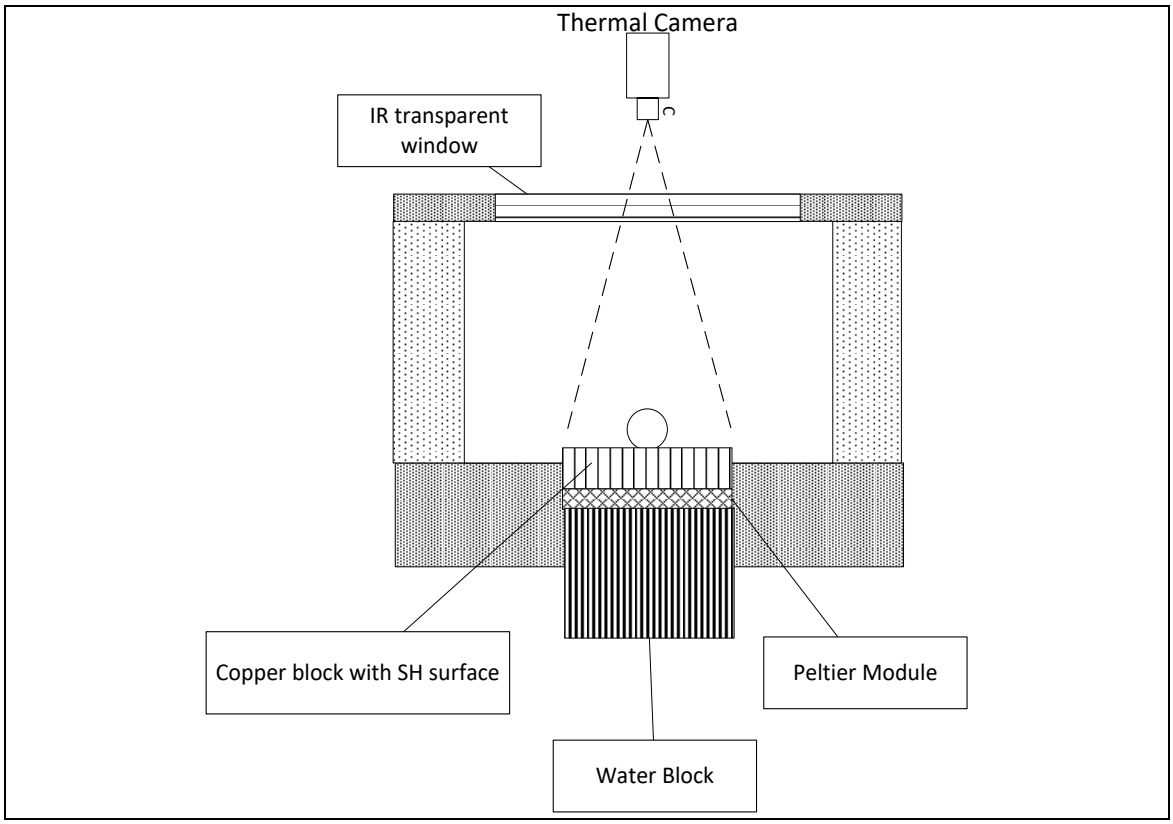

Figure 3-5: Droplet nucleation experiment concept. The thermoelectric cooler would cool the superhydrophobic surface at varying rates and the temperature of a population of droplets would be measured by IR videography to determine nucleation rates of milk drops on superhydrophobic surfaces.

This cooled plate could also have been used with a high-speed camera to investigate the impact of milk droplets on cooled superhydrophobic surfaces. This principle has been used to study the interaction between impacting droplets and superhydrophobic surfaces by several authors[9-11]

The apparatus to measure the freezing and mass loss profiles of a suspended droplet was also designed. It consisted of a thin wire thermocouple, on which a droplet would be placed, suspended below a balance. The droplet would be exposed to a cold, dry, air flow of known temperature and velocity and the data collected. A high-speed camera would record video of the freezing process. Similar methods have been used to study the freezing of pure water[5], food solutions[4] and cocoa butter [12].This is shown in Figure 3-6 below.

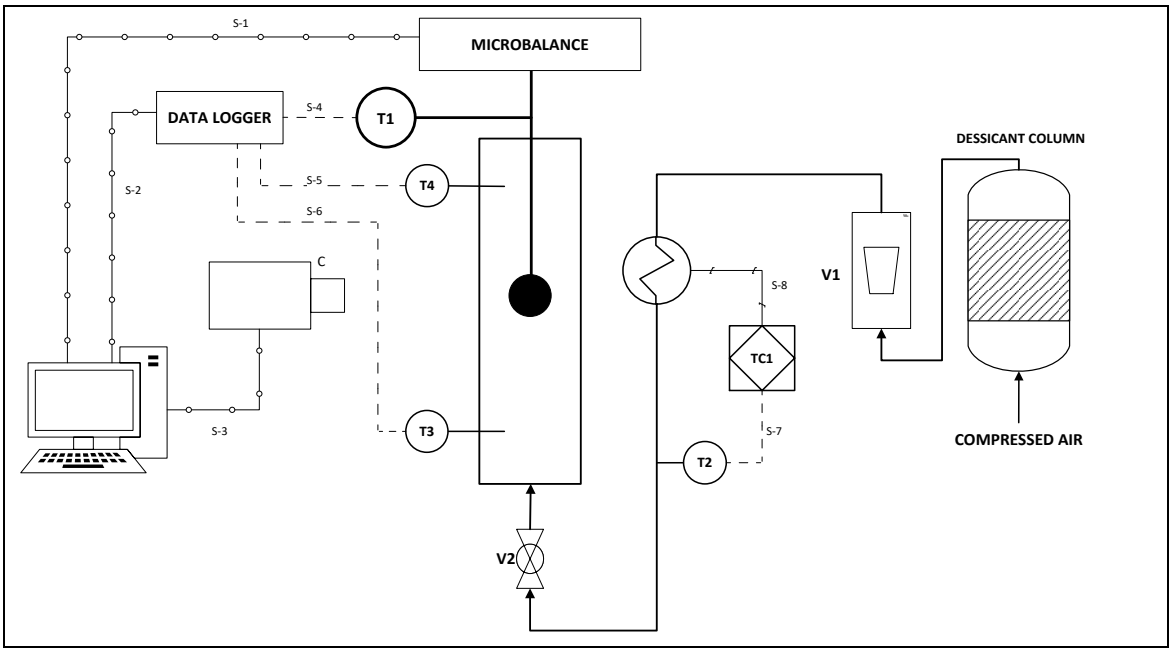

Figure 3-6: Single droplet freezer. This would measure mass and temperature changes occurring in a droplet as it is frozen, to allow verification of numerical models. A droplet would be suspended from the balance on a thermocouple, T1. A cool dry airflow would be controlled by rotameter V1, and its temperature controlled by T2 and TC1. The air temperature at the inlet and outlet of the drying chamber would be measured by thermocouples T3 and T4 respectively. A camera would video the droplet as it freezes. Temperatures T1, T3 and T4, video, and mass readings would be recorded on a computer.

Droplet generators needed to be developed for the full-scale freezer. These droplet generators would need to form a droplet with a diameter of ca 3mm approximately once per second. This would have been achieved with banks of orifices. The size of the orifice needed to be determined, and the effects of non-circular orifices needed to be investigated. Backlit high-speed videography was used to image the formation of droplets with different orifice sizes and angles.

The work to develop the droplet generator was largely done by post-doctoral fellow Georg Ripberger; however, I assisted with collecting high speed video data. Still images from the high-speed videography are shown in Figure 3-7 below.

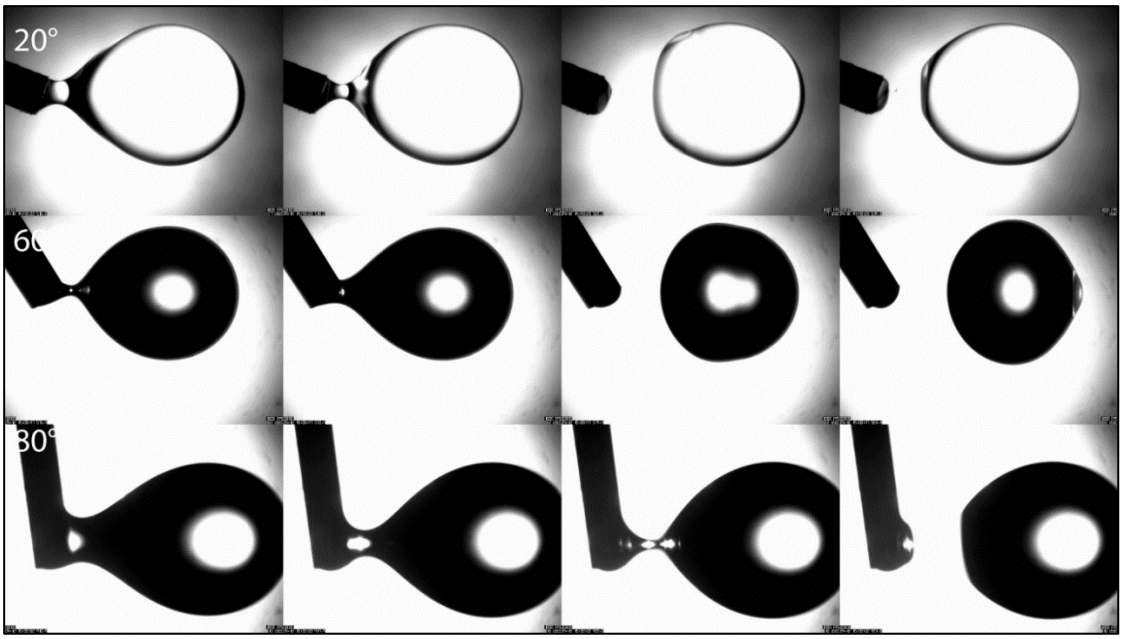

Figure 3-7: Droplets generated from needles at 20°,60° and 80°.

Detailed design had been completed and components were purchased for the experiments described above, when the decision to change the freezing method was made. It was decided to discontinue work on rolling droplets, and to focus on flake freezing. The experiments into droplet behaviour, nucleation, and freezing described above were therefore not conducted.

3.4.2 Freezing Sheep Milk

The degree of supercooling that could occur in sheep milk would have a great effect on the design of a rolling droplet freezer. Initial measurements of the degree of supercooling were conducted with a TA Q2000 DSC, described in detail in Chapter 2. The temperature vs time profiles of several runs are shown in Figure 3-8 and Figure 3-9 . As can be seen, the sessile droplets of re-constituted milk at 18% total solids nucleated at a temperature of -12°C to -15°C, whereas pure water nucleated at -22°C This indicated that large degrees of supercooling could be achieved with sheep milk, despite the presence of milk proteins and fats which might act as nucleation sites.

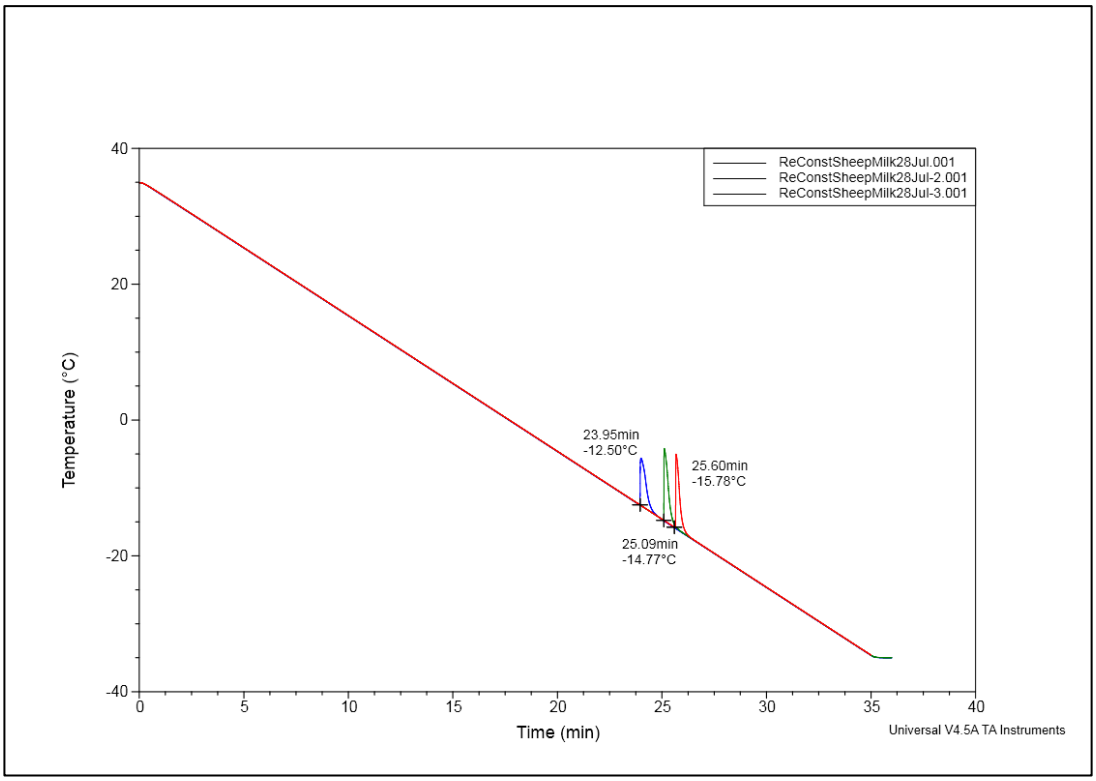

Figure 3-8: Temperature vs. time profiles of ca. 10 mg samples of reconstituted sheep milk being cooled in sealed DSC pans at a rate of 2 Kmin^{-1}. The temperatures at which nucleation occurred are labelled.

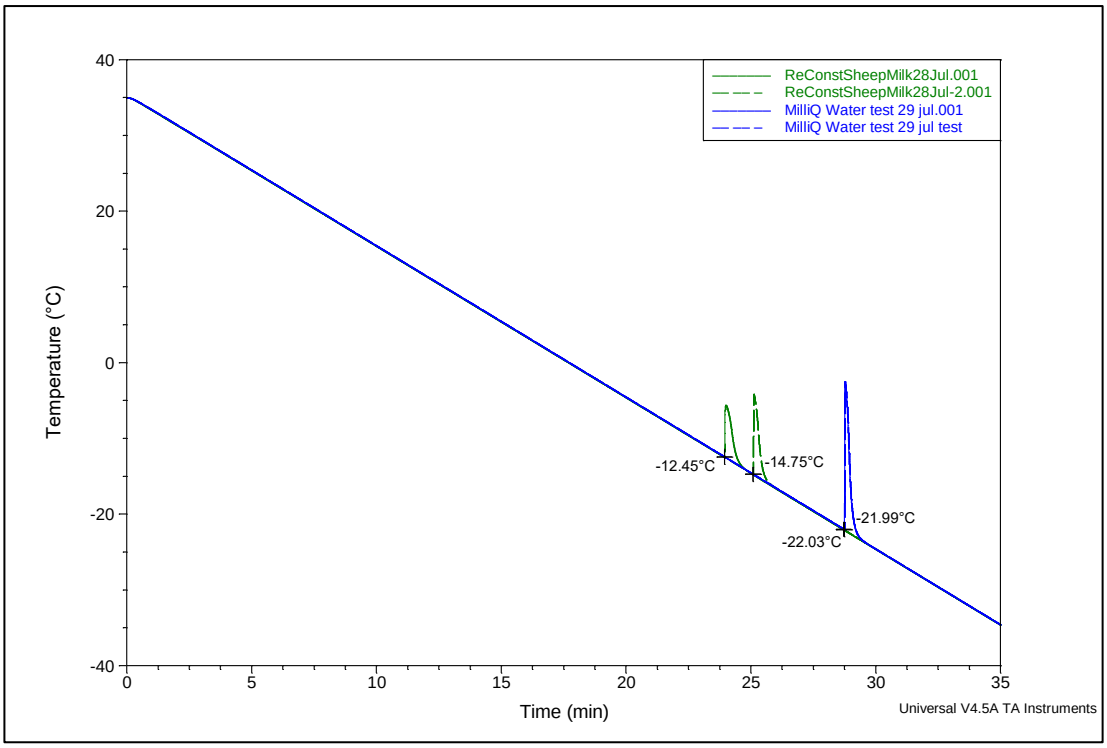

Figure 3-9: Temperature vs. time profiles of ca. 10 mg reconstituted sheep milk and MilliQ water being cooled in sealed DSC pans at a rate of 2 Kmin^{-1}. The temperatures at which nucleation occurred are labelled. MilliQ water shows a higher degree of supercooling before nucleation.

3.4.3 Mathematical Model of Rolling Droplets

The data collecting in the rolling ring, freezing profile and nucleation measurement would have been used to develop a mathematic model of the freezing phenomena in rolling droplets.

The model would have incorporated the following factors:

- Heat transfer from convection, conduction and radiation
- A treatment of supercooling and nucleation frequency as a function of temperature and cooling rate.
- Solute partitioning and freeze concentration in the unfrozen section.
- The direction of ice growth would be determined by modelling the system with inward moving freezing fronts, and a mixed phase system. The model that best predicted the experimentally determined temperature profiles would be selected.
- The effect of rolling on the freezing phenomena. This would involve the following:
    - The terminal velocity of the droplet on an incline surface, based on air resistance and rolling resistance.
    - Increased or decreased convection due to the tangential velocity of the rotating air/liquid interface.
    - Mixing of components, and advection-based heat transfer.

With the change in freezing method in July 2016, the work on this model ceased.

3.5 Measurement of the Physical Properties of NZ Sheep Milk

3.5.1 Introduction

In order to model the freezing behaviour of a rolling droplet accurately or that of a falling film of liquid milk, the heat capacity, initial freezing temperature, latent heat of freezing, surface tension and rheological properties of milk are needed. Work is being done at Massey University to developed breeding value models of dairy sheep. By collaborating with these researchers, a source of fresh raw sheep milk, and its compositional data, could be obtained.

These compositional data allow relationships between composition and properties to be developed.

In this section, the measurements of viscosity, composition, freezing temperature and surface tension are discussed.

The heat capacity measurements and latent heat measurements will be discussed in Chapter 6

The surface tension measurements were unable to be conducted with the fresh raw milk due to equipment availability and the limited shelf life of raw milk. These measurements were conducted with milk reconstituted from powder. These measurements were expected to be less affected by the changes due to processing.

3.5.2 Methods

Individual milk samples were collected from the herd during the afternoon milking at a sheep dairy farm in the Hawkes Bay. These samples were approximately 20-50mL in volume and were collected from a proportional sample of each individual animals' production using an ICAR-approved milk meter designed for goat dairy, and therefore represented a sample of the whole milking.

The collected samples were then refrigerated at 4°C until analysed. All samples were analysed within 72 hours of collection.

The sample viscosity was measured using an Anton Paar Physica MCR302 computerised rheometer fitted with a double gap (DG 26.7) measurement geometry, and a Peltier controlled

temperature cell. The viscosity was measured at shear rates of 1 s^{-1} to 100 s^{-1}. Several samples were selected at random and the viscosity was measured for a temperature sweep of 5°C to 55°C.

The particle size distribution was measured using a Mastersizer 3000.

The composition of the individual samples and the equilibrium freezing temperature was determined by the company Milk Test NZ (Hamilton NZ) from samples that had been collected the previous afternoon milking.

To estimate the surface tension of whole sheep milk, whole sheep milk powder (Spring Sheep Dairy NZ) was reconstituted to total solids levels of 10,15,20,25, and 30%. The samples were placed in a water bath, which allowed the temperature to be varied in 5°C increments from 5°C to 40°C. Surface tension was measured using a SITA science line t100 tensiometer. Tensiometer bubble lifetimes were 8,000 ms up to a total solid concentration of 20%, and 20,000 ms for higher total solids samples. Each measurement was the average of 10 consecutive readings, and each temperature/concentration combination was measured in triplicate.

Detailed descriptions of all analytical equipment used are given in Chapter 2.

3.5.3 Results and Discussion

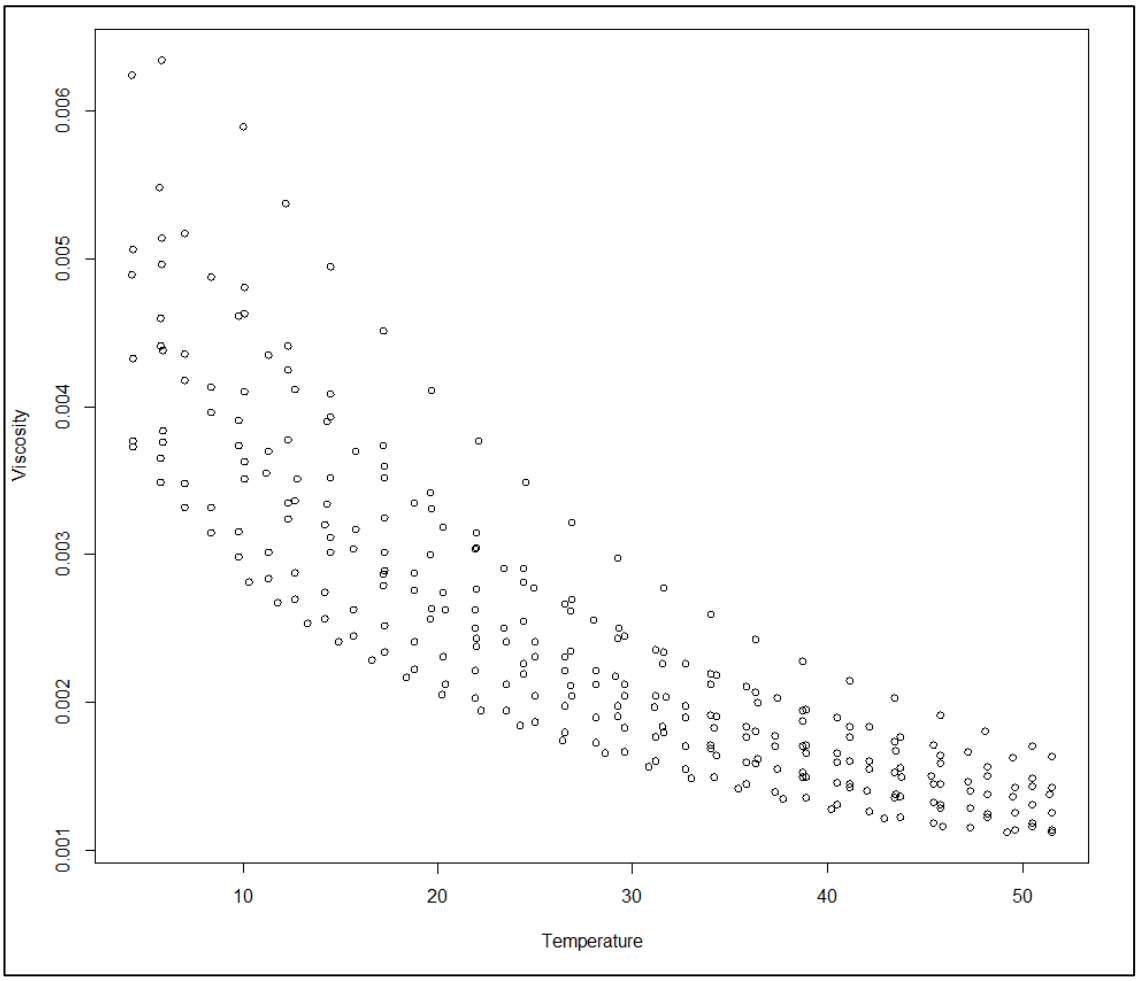

Figure 3-10: Measured viscosity (Pa.s) data from all samples plotted against temperature (°C).

As can be seen in Figure 3-10 above there is an inverse relationship between the temperature of the milk and its viscosity. This is most likely due to the decrease in water viscosity with increasing temperature.

The considerable vertical displacement of the curves is due to the differing solids contents between the milk samples. The solids of the milk, as determined by the external contractor varied from 13.95% to 23.59 %.

The flow behaviour of the samples was found to be Newtonian at shear rates between 1 s^{-1} and 1000 s^{-1}.

Linear Regression models were fitted in R[13], using the components of the milk as predictor values for viscosity at 20°C. These were evaluated, and the most effective model was of the form:

$$\mu = A * \%Fat + B * \%SNF + C \quad (3\text{-}2)$$

where SNF is the solids non-fat.

The coefficients of the fitted equation and their significance values are shown below. For this analysis DF=42.

Table 3- 1: Coefficients for viscosity prediction equation (3-2).

Coefficient	Value	P value
A	$6.57*10^{-5}$	0.034
B	$4.51*10^{-4}$	$1.29*10^{-6}$
C	$-2.76*10^{-3}$	0.00185

Figure 3-11 plots the predicted values of viscosity against the measured values. The R^2 was 0.589.

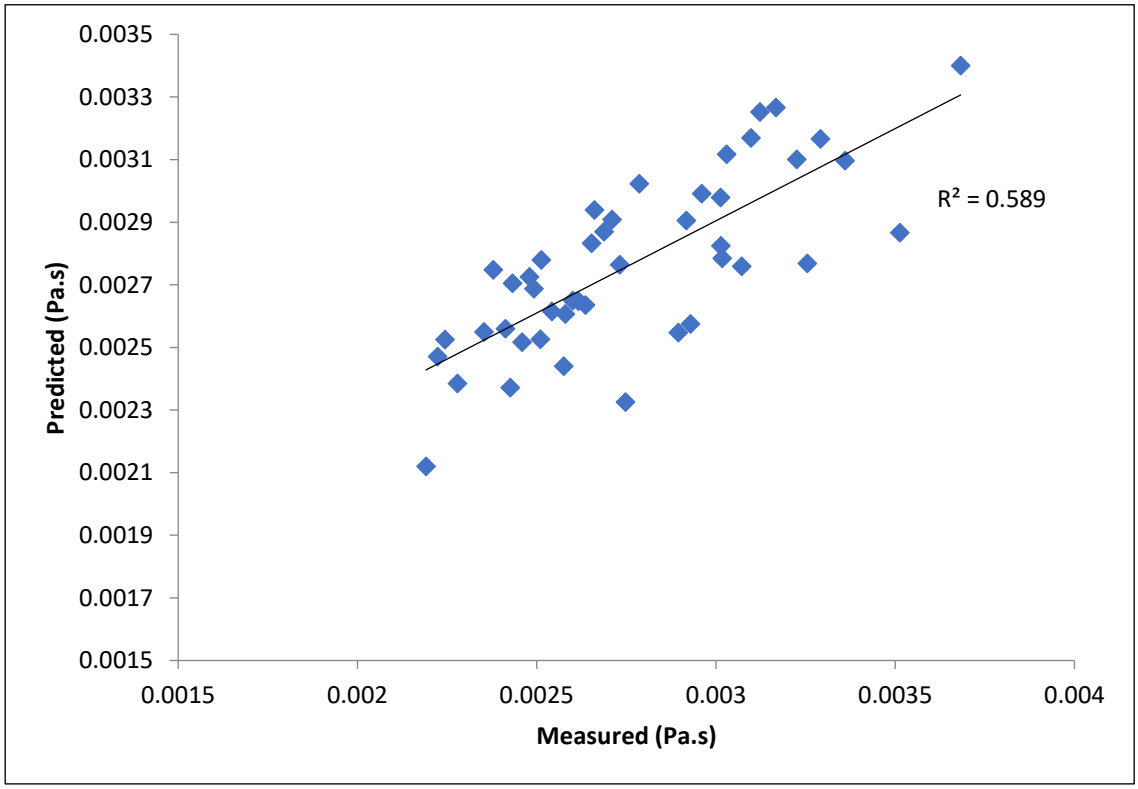

Figure 3-11: Values of viscosity predicted by equation(3-2), and the coefficients in Table 3- 1 vs. measured values.

Six samples were chosen at random to be evaluated across a range of temperatures, from 5 to 55°C. The collected data are shown in Figure 3-10.

This was added to the linear regression model above and evaluated in R, to create a model of the form:

$$\mu = A * \%Fat + B * \%SNF + C * \ln T + D \quad (3\text{-}3)$$

The coefficients of the fitted equation and their significance values are shown below.

Table 3-2: Coefficients for temperature dependent viscosity prediction equation (3-3)

Coefficient	Value	P value
A	$7.94*10^{-5}$	$1.39*10^{-9}$
B	$6.03*10^{-4}$	$<2*10^{-16}$
C	$-1.5*10^{-3}$	$<2*10^{-16}$
D	$-1.51*10^{-4}$	0.737

The values predicted by this model are plotted against the measured values in Figure 3-12. The R^2 of this model is 0.891, for N=290.

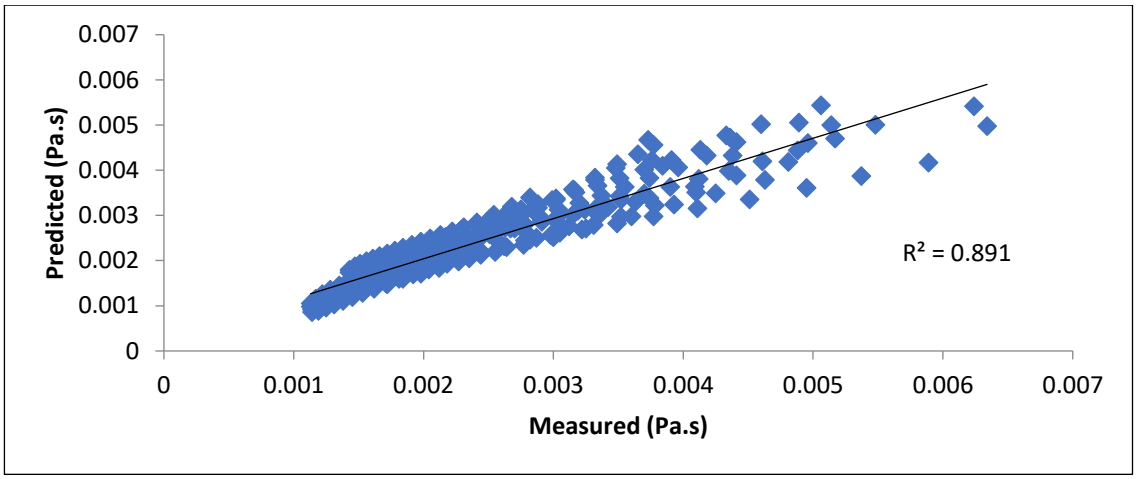

Figure 3-12: Viscosity predicted according to equation (3-3), using coefficients from Table 3-2 vs. measured values. N=290.

Table 3-3: Measured compositional values and compositional values of NZ sheep milk. SCC is somatic cell count, Dx 50 is the median diameter of the particles in the milk.

Nutritional Composition and Processing Properties of NZ Sheep Milk. N=45				
Property	**Mean**	**SD**	**min**	**max**
Total Solids (%)	18.12	1.82	13.95	23.59
Fat (%)	6.75	1.50	3.66	11.83
Protein (%)	5.75	0.60	4.53	6.91
Lactose (%)	4.92	0.23	4.2	5.37
Freezing Point (°C)	-0.56	0.01	-0.577	-0.531
SCC (cells/mL)	1,260,000	3,680,000	20,900,000	11,000
Viscosity @ 20°C (Pa.S)	0.0028	0.0004	0.0022	0.0037
Dx 50 (µm)	4.56	1.31	3	9.2

In comparison, a separate program to measure the properties of NZ sheep milk [14] has published the following compositional data:

Table 3-4: Nutrition composition of sheep milk, adapted from[14].

Nutritional Composition of NZ Sheep Milk		
Component	**Mean**	**Range**
Water (% by Difference)	81.9	78.3-84.7
Total Protein (%)	6.2	5.2-7.7
Casein	4.7	4.1-5.0
Whey	1.0	0.78-1.40
Non-Protein Nitrogen	0.053	0.04-0.12
Fat	6.1	4.4-7.0
Lactose	4.8	4.7-5.1
Ash	0.91	0.89-0.93
Total Solids	18.1	15.3-21.7

The measured values of the surface tension at the measured temperature and concentration points are shown in Figure 3-13, along with the values calculated from a relationship derived by least squares regression.

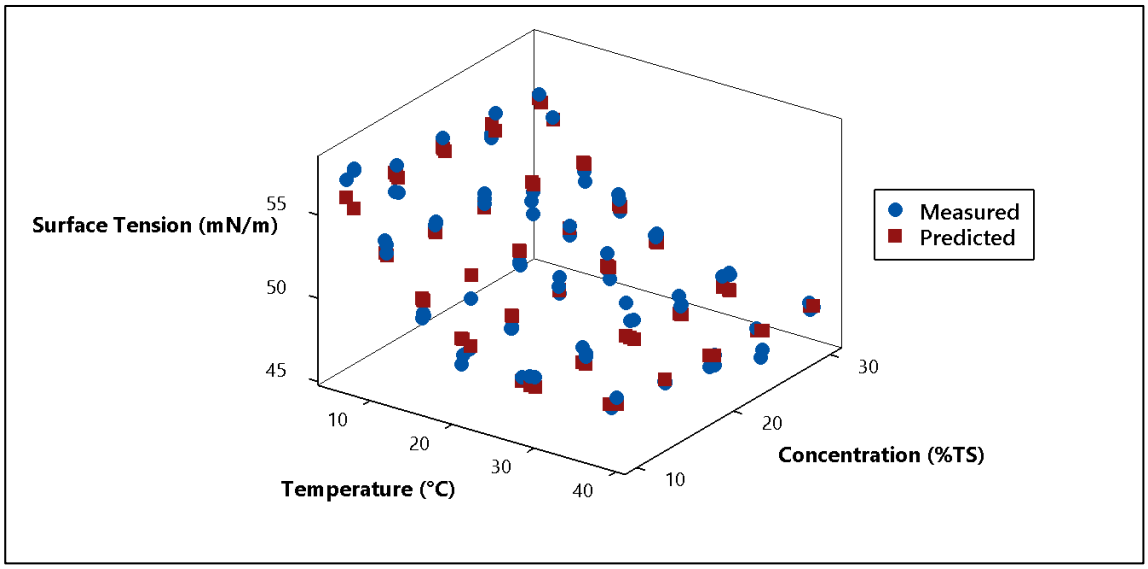

Figure 3-13: Surface tension of ovine milk vs temperature and milk concentration. Measured values, and values predicted from least squares fit.

The surface tension was strongly dependent on temperature, decreasing with increasing temperature, weakly dependent on concentration, with a small decrease as the milk concentration increases. There was no significant interaction between concentration and temperature. Models with quadratic terms for both temperature and concentration and first order interactions were evaluated. After removal on non-significant terms a model of the form $\sigma = A * \%TS + B * T + C * T^2 + D$ was fitted to the measured data by least squares regression. The values fitted to the model are shown in Table 3-5.

Table 3-5:Model parameters for the surface tension of ovine milk.

Parameter	*A*	*B*	*C*	*D*	R^2
Value	-0.0464	-0.7650	0.01198	60.381	91.2%

The range of surface tension values measured includes those which have been reported previously [15]. These values have only been reported at a single temperature, so the development of a relationship that describes the surface tension as a function of temperature

and concentration is valuable. Figure 3-14 shows the measured and predicted surface tension values, compared with data for pure water[16].

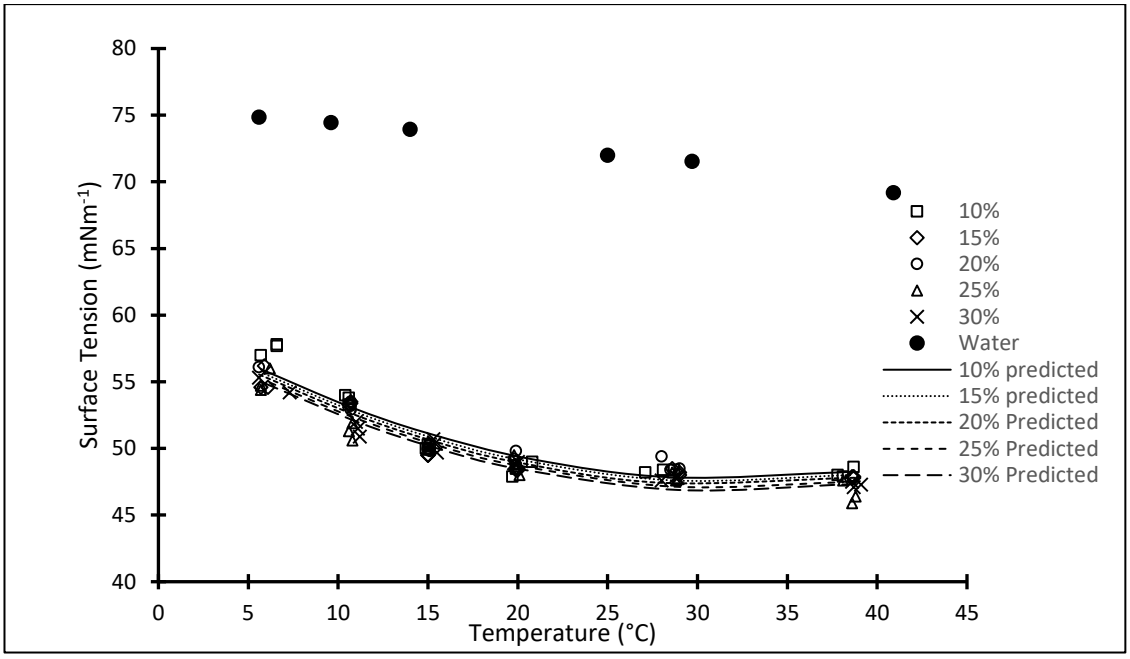

Figure 3-14: The surface tension of reconstituted ovine milk as measured and predicted. The surface tension of pure water is shown as a comparison.

3.6 Change of Approach

Methods of fabrication required for the rolling droplet freezer were investigated.The design of the droplet distributor became a source of difficulty. The requirement for a reliable, robust, cheap, and sanitary droplet generator, making 3 mm droplets was difficult to achieve in a freezing environment.

The corrugated sheets required for the rolling droplet system would need to be fabricated by rolling, and custom rollers would have been required. These rollers would cost in the region of $100,000. The corrugated sheets would also have needed to meet very tight tolerances to allow some methods of surface modification under consideration. These sheets would only be affordable at production scale but would be unaffordable during development.

The manifold design for the droplet generator would have cost approximately $1,300 to manufacture, and as 48 manifolds were required, the cost to manufacture these for the prototype unit would have been approximately $60,000. As sources estimate that there will be around 55 small sheep dairy farms[17], there would only a small production run, reducing manufacturing economies of scale.

Ice adhesion was also a source of concern. There are two different wetting states for fluids on a superhydrophobic surface: The Cassie-Baxter and Wenzel wetting states [18]. The Cassie-Baxter state traps a volume of air in the microstructure of the surface, below the liquid, while in the Wenzel state the liquid is present in the microstructure of the surface. This can occur in condensing atmospheres, and is linked to much greater adhesion forces between the liquid and the surface [18].Tests conducted on the rolling ring freezer in 2015 had shown that there was a tendency for ice to adhere on areas of condensation on superhydrophobic surfaces. This behaviour has also been reported in the literature around superhydrophobic and icephobic surfaces [18], especially for condensing atmospheres[19, 20] [21], and temperatures below -20°C to -25°C[11]. This would cause severe operational difficulties, as ice adhesion could easily lead to blockages between the closely packed corrugated plates, which would be difficult to

detect during operation, and difficult to resolve without raising the temperature of the system above freezing.

This would also require that the air within the freezer be kept absolutely dry to prevent any de-sublimation, and that it must be dried completely after CIP to ensure that no moisture remained within the freezer where it could act as a source for static ice growth.

These factors meant that the rolling droplet freezer was rapidly diverging from its requirements of robustness, reliability and low cost, suited to on-farm or near-farm operation.

3.6.1 Flake Freezers.

The flake freezer approach offered a method with several advantages, as discussed in Chapter 1:

- Increased heat transfer through liquid convection and conduction through metal shells, rather than forced air convection, conduction through a small contact zone and radiation.
- Insensitivity to condensing conditions.
- Ease of fabrication- no need for precision engineered droplet distributors, or custom rollers/dies.
- Ease of scale up.
- Proven designs.
- Less sensitive to off-nominal conditions
- Ease of control- can adjust for flowrate fluctuation.
- Geometry may be more suitable for CIP
- Lower technical risk during development.

Two concepts were identified as suitable for our aims, Scraped Surface Flake Ice Freezers and Falling Film Flake Ice Freezers.

It was decided that a prototype system be constructed where both concepts could be evaluated for suitability.

3.7 Work Conducted on Developing Flake Freezers

3.7.1 Concepts for Prototype

3.7.1.1 Falling Film Freezer

While falling films have been used as freeze concentration equipment, the operating conditions of the milk freezer will be rather different to those found in falling film freeze concentration equipment, which uses ice growth rates of 0.01-1 μms^{-1} to separate ice and solutes [22-24]. Even slow freezing has a fairly high partition coefficient, with values of approximately 0.45 being recorded for freezing front velocities of 2 μms^{-1} [25]. Moreno et al [26] found partition coefficients close to 1 with 15 wt% coffee at ice growth rates of 4μms^{-1}.

It is hoped that increasing this ice growth by several orders of magnitude should trap solutes within the ice structure, as rapid directional freezing has been shown to capture solutes between and within ice crystals[27]. This will be accomplished by increased heat transfer coefficients and greater temperature differences. The freezing front velocity in our pilot unit is expected to be between 40 and 70 μms^{-1}. Using the relationship given by Chen and Chen[25] for whole milk, the partition coefficient in a falling film freezer with an ice growth rate of 70 μms^{-1} is expected to be 10.3. This is clearly impossible. The relationship was developed for ice growth rates between 0 and 2 μms^{-1} and therefore is inapplicable to such high ice growth rates.

The concept of the falling film freezer is shown in Figure 3-15, which shows the operating cycle for the falling film freezer concept.

1. A vertical tube is completely wetted on the outside by a falling film of product, and on the inside by a falling film of coolant.
2. The high heat transfer coefficients of the falling films coupled with the large ΔT between the coolant and product causes a layer of frozen product to grow rapidly on the outside of the vertical tube.
3. Once the frozen product has reached the desired thickness, the product flow is shut off. The coolant flow continues and cools the frozen product to the desired end temperature.
4. The frozen product is detached
    a. A pulse of heat is applied to the interior surface of the tube, melting a thin layer of product
    b. The frozen product, lubricated by a thin film of fluid, falls from the outside of the tube onto an ice breaking /ice transport device located below, which breaks the ice up and transports into a storage bin.
    c. The development of functional surfaces with low ice adhesion strength may allow ice to be removed by vibration, or with a reduced heat input.

Similar devices are used extensively in the fishing industry to produce industrial ice for fish preservation[28], although it is unlikely that an off-the-shelf unit would be suited to on-farm dairying use, or regular CIP.

Figure 3-16 represents the flows of product, coolant, and heat during the cycle as a function of time. A major focus of the next two years of work will be to optimise these cycle times to obtain a high-quality product, at the highest throughput and lowest cost possible.

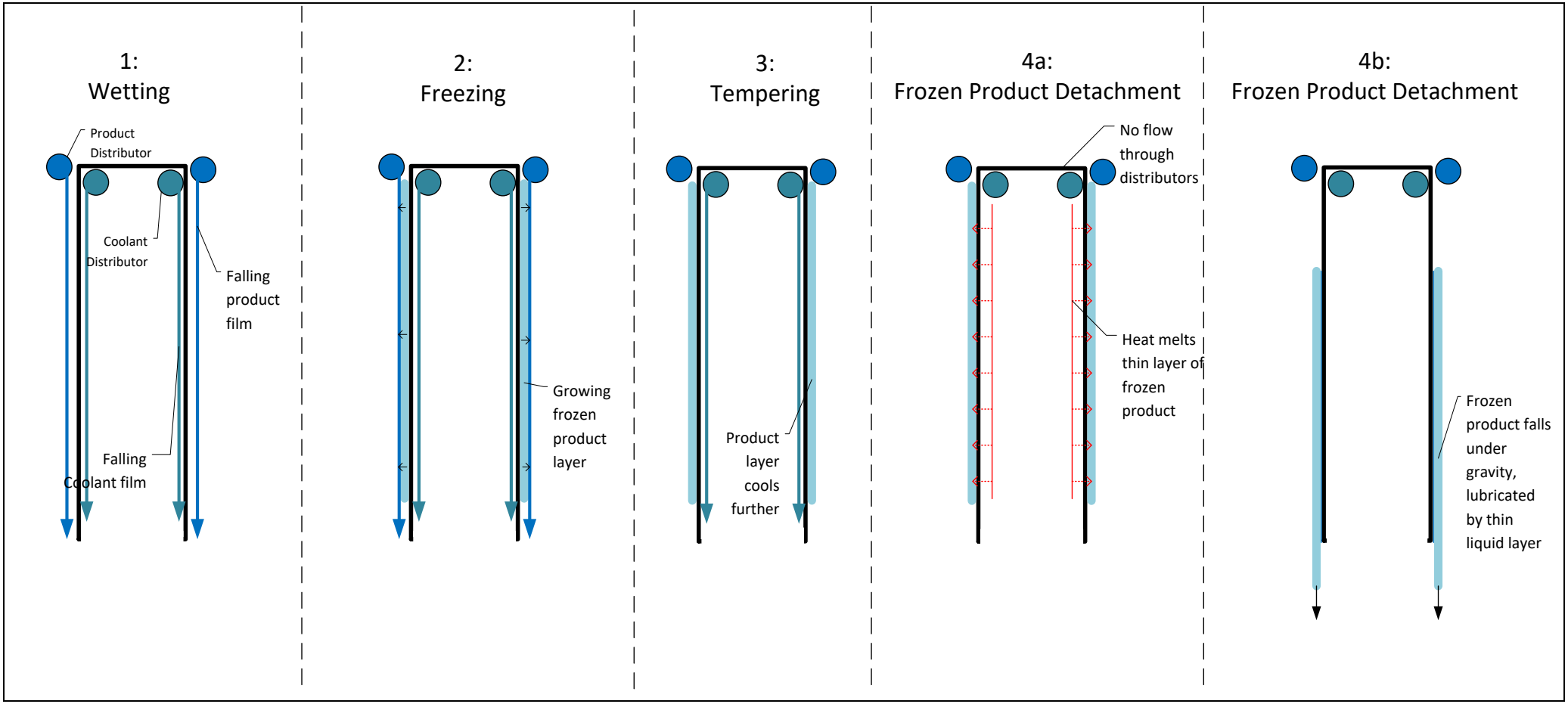

Figure 3-15: Falling film freezer concept. There are 4 stages in the freezing cycle. First the cooled surface is wetted with product, and a layer of frozen product is formed on the cooled surface. The product flow is stopped and the frozen product cools to a final temperature. The product is detached by applying a pulse of heat which melts a thin layer of product. This thin liquid layer allows the frozen shell of product to fall off under gravity.

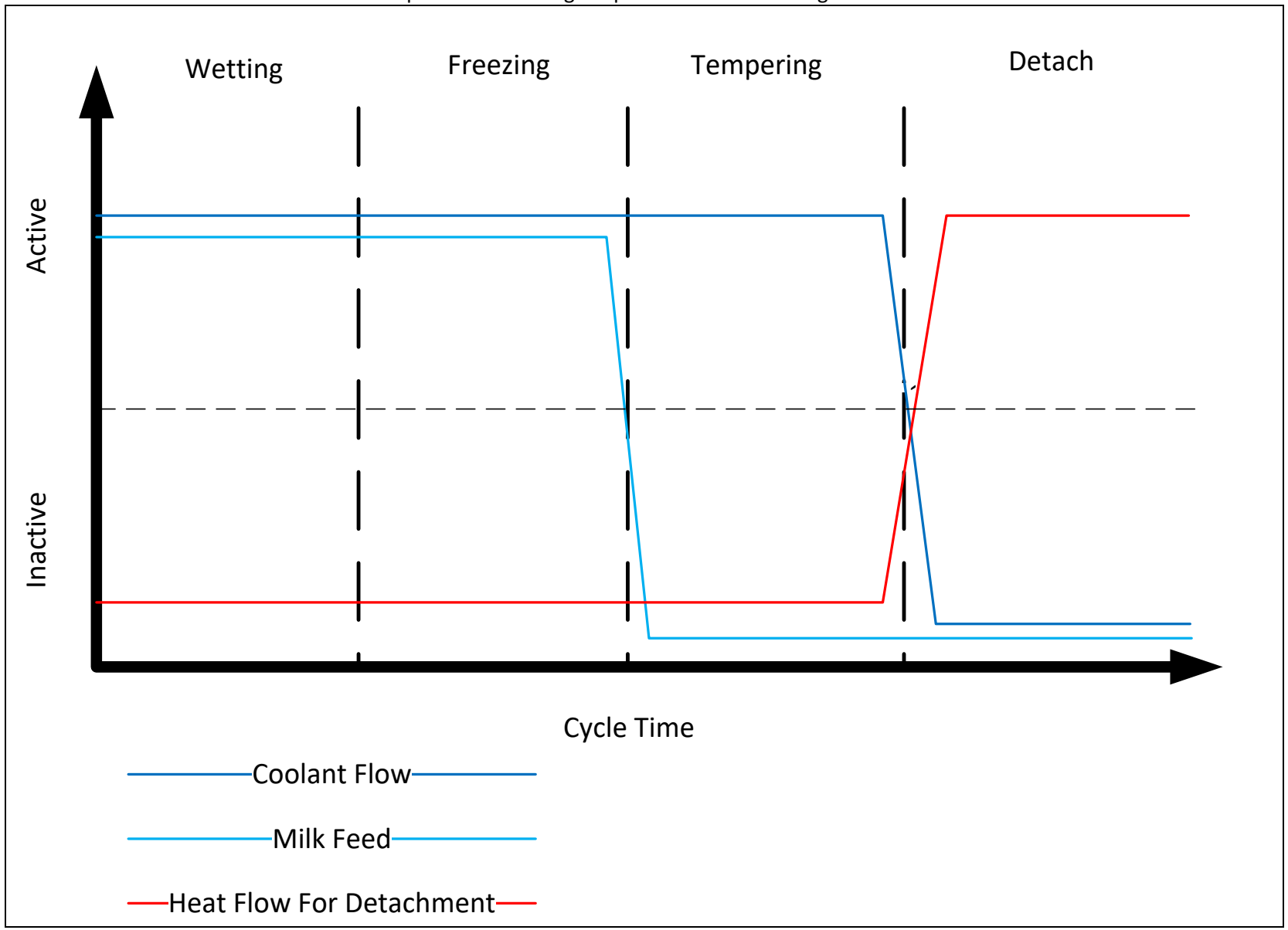

Figure 3-16: Flows of coolant, milk , and heat in a freezing cycle as shown in Figure 3-15.

3.7.2 Rotating Drum Freezer

In Figure 3-17 A below, shows the other concept for the rapid milk freezer, a rotating drum freezer. This is a concept that has been demonstrated with food products such as broccoli[29]. In this concept, which is also illustrated in Figure 3-17 B, a distributor located at the top half of the freezer distributes a film of milk onto the surface of the rotating drum. The drum surface is cooled by an internal spray of liquid coolant as shown in Figure 3-17 C. The coolant distributor can be optimised to give the maximum heat transfer coefficient for a given flow of coolant, thereby minimising the size and cost, and heat gains from the environment of the freezer.

The film of milk freezes rapidly onto the surface of the drum and continues to rotate with the drum. Once the frozen milk has rotated past the flowing film, it continues to cool and harden, until it reaches the desired temperature.

The frozen milk is removed by a scraper blade, and then stored.

The operation of this freezer can be altered by adjusting the diameter of the drum, the rotational speed of the drum, the flows of milk and coolant, and the height of the scraper blade.

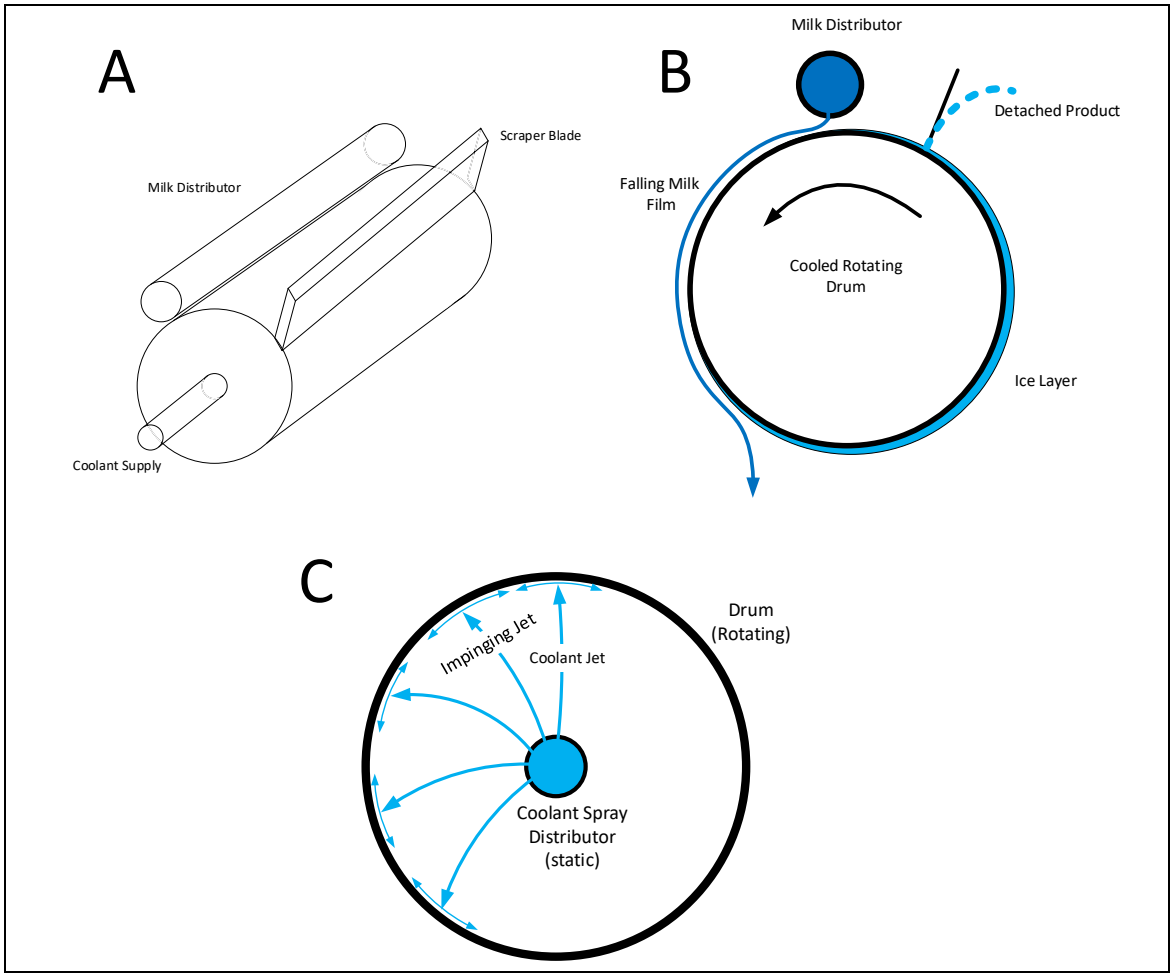

Figure 3-17: A) 3-D view of rotating drum freezer. B) Product flows at the exterior of a rotating drum freezer. C) Coolant flows inside rotating drum freezer.

A process flow diagram showing the major flows and components of the pilot falling film freezer is shown in Figure 3-18. In this freezer, milk is stored in the reservoir at approximately 4°C, and coolant is maintained at a set value between -10°C and -30°C by the chiller unit. To freeze milk, the milk is pumped through the distributor at the top of the freezer, and the coolant is pumped through freezer. The falling film of milk freezes to the surface of the freezer and any unfrozen milk is collected in a sump and returned to the distributor.

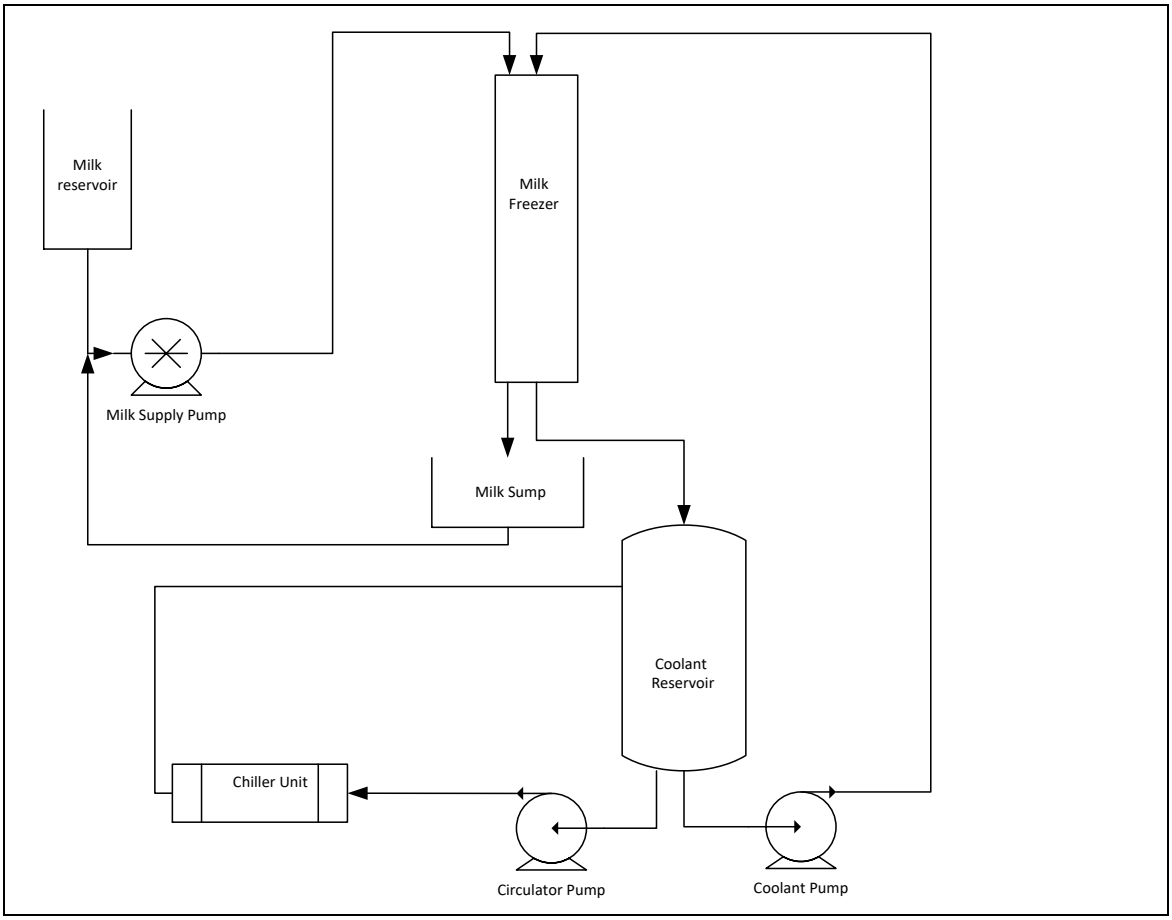

Figure 3-18: Process flow diagram for a pilot falling film freezer. Milk to be frozen is pumped to the freezer, and unfrozen milk running off the freezer is collected in a sump, when the sump is full it is recycled to the feed. The coolant is pumped in one loop from the reservoir to the freezer, and in a separate loop from the reservoir to a chiller unit. Frozen product is removed from the surface of the milk freezer.

An example of a process flow diagram for the falling film freezer in an on-farm setting is shown in Figure 3-19. In this application a single chiller unit provides cooling for the freezer and the milk storage vat.

Coming out of the milking machine, the milk is first pre-cooled by cold water. A glycol coolant loop operating at 2°C then cools the milk to approximately 2-4°C for short term storage in an insulated vat. The heat gained by the glycol loop is removed by the coolant tank, which is held a low temperature (-10°C to -30°C) by the chiller unit.

From the short-term storage, the milk is pumped to the falling film freezer where it is frozen by the coolant, which is pumped to the interior of the falling film freezer. The detached ice is then stored in an insulated and cooled storage bin.

The size of the chiller can be reduced by increasing the size of the coolant tank, and using it as a store of cold energy, and by increasing the size of the milk storage tank and operating the freezer over a longer period than a single milking. Operating over a longer period reduces the peak

power consumption of the freezer, and reduces the fraction of operating time spent in start-up and chill-down of the freezer.

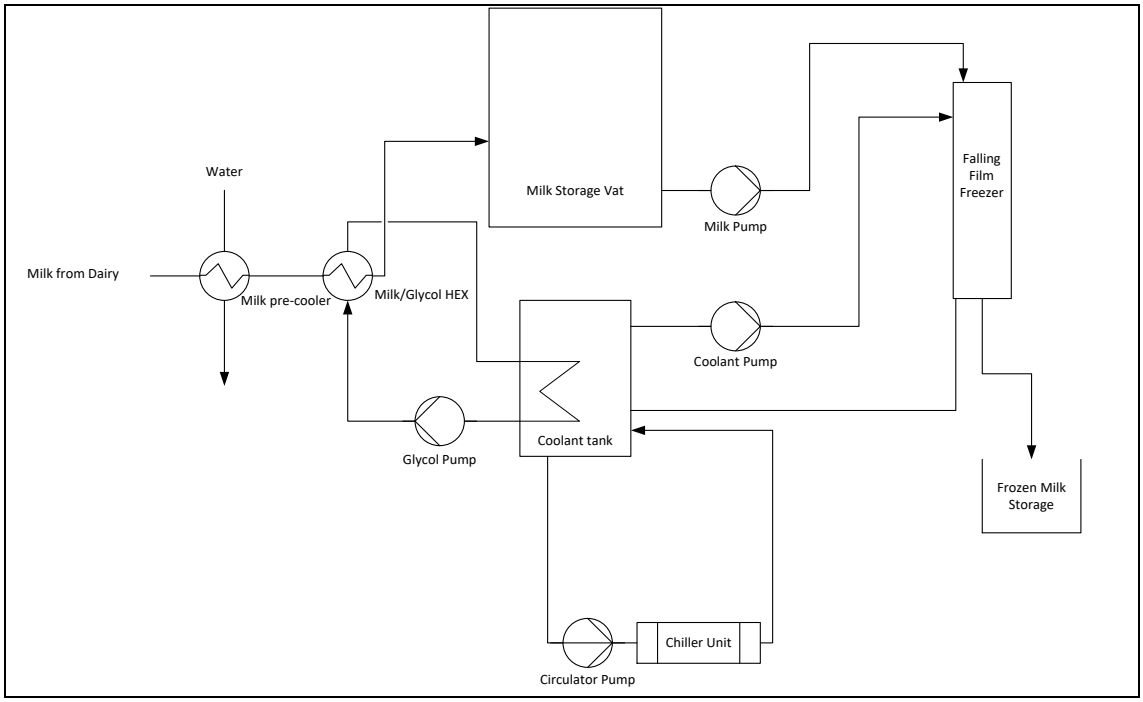

Figure 3-19: Process flow diagram for a falling film freezer in an on-farm setting. This is essentially the same as the system in Figure 3-18, however a glycol loop using the coolant tank as a heat sink to cool milk to the vat storage temperature is added.

3.7.3 Coolant Selection

There were two possibilities for removing heat from the product: direct expansion of refrigerant, or falling coolant films. Each option had advantages and disadvantages.

- Direct expansion advantages:
  - Higher coolant side heat transfer coefficients.
  - Possibility of using hot gas defrost.
  - Low risk of contamination of product in the event of a coolant leak.
- Direct expansion disadvantages
  - More complicated pressure safe and gas tight construction needed.
  - Higher internal refrigerant pressure is a challenge from a food-safety perspective. Loss of integrity in the heat exchanger could cause refrigerant to leak into the food product. It is likely that future regulations would require double-walled heat exchanger construction.
  - Increased difficulty in control.
  - Environmental impacts if any leakage occurs.
  - The range of affordable, high performance refrigerants is limited due to environmental regulations[30]
  - Difficulty in swapping freezer geometry to evaluate concepts.
  - Difficulty is combining both falling film and scraped surface systems in one unit.
- Falling film coolant advantages.
  - Construction does not need to be pressure tight
  - Controls of flow and temperature is decoupled- can alter temperature and flow separately
  - Can easily change geometries
    - This will be important when trialling functional surfaces.

  - Same coolant system can be used for both scraped surface and falling film freezers.
- Falling film coolant disadvantages.
  - Lower coolant side heat transfer coefficient.
  - Care needed in selection of coolant to ensure food safety.
  - Need to use a double-walled tube to ensure food safety.- These are readily available for a number of industrial applications [31], but thermal performance is reduced.

Falling Film coolant was selected as it was felt that ease of control, fabrication and modification were more valuable in a lab scale pilot unit than the increased heat transfer. Heat transfer in both cases is more limited by the product flow than the coolant.

3.7.4 Detail Design of Falling Film Freezer.

3.7.4.1 Evaluation of Heat Transfer Fluid

As a falling film of coolant is to be used to remove heat from the product, a particular coolant formulation needs to be selected. Several different heat transfer fluids were evaluated.

The ideal fluid would have a freezing point 5-10°C lower than the minimum expected operating temperature (MEOT), in order to prevent ice formation in the chiller unit. The fluid would also have a low viscosity and high volumetric heat capacity at MEOT, reducing the circulation volume and pumping power required, and increasing the heat transfer coefficient. A higher heat transfer coefficient allows for a smaller heat transfer area and system, faster ice front growth rates and greater flexibility in operating conditions for the pilot unit.

The fluids evaluated were:

- 60% propylene glycol solution
- 50% Ethanol solution
- 29% $CaCl_2$ solution
- 22% LiCl solution
- Duratherm XLT-120, an organic compound based HTF.
- Paratherm LR, an aliphatic hydrocarbon based HTF.
- Dynalene HC-50, a potassium formate solution based HTF.
- Temper-55

The falling film heat transfer coefficient (h, $Wm^{-2}k^{-1}$) of these solutions was calculated as a function of irrigation rate expressed as mass flow per unit perimeter length (Γ ,$kgm^{-1}s^{-1}$), according to the equations for subcooled falling film heat described in section 7.4.2.3 of this chapter. The heat transfer coefficient was evaluated using the fluid properties at a temperature of -30°C.

The following figure shows the coolant side falling film heat transfer coefficients for a range of mass flows.

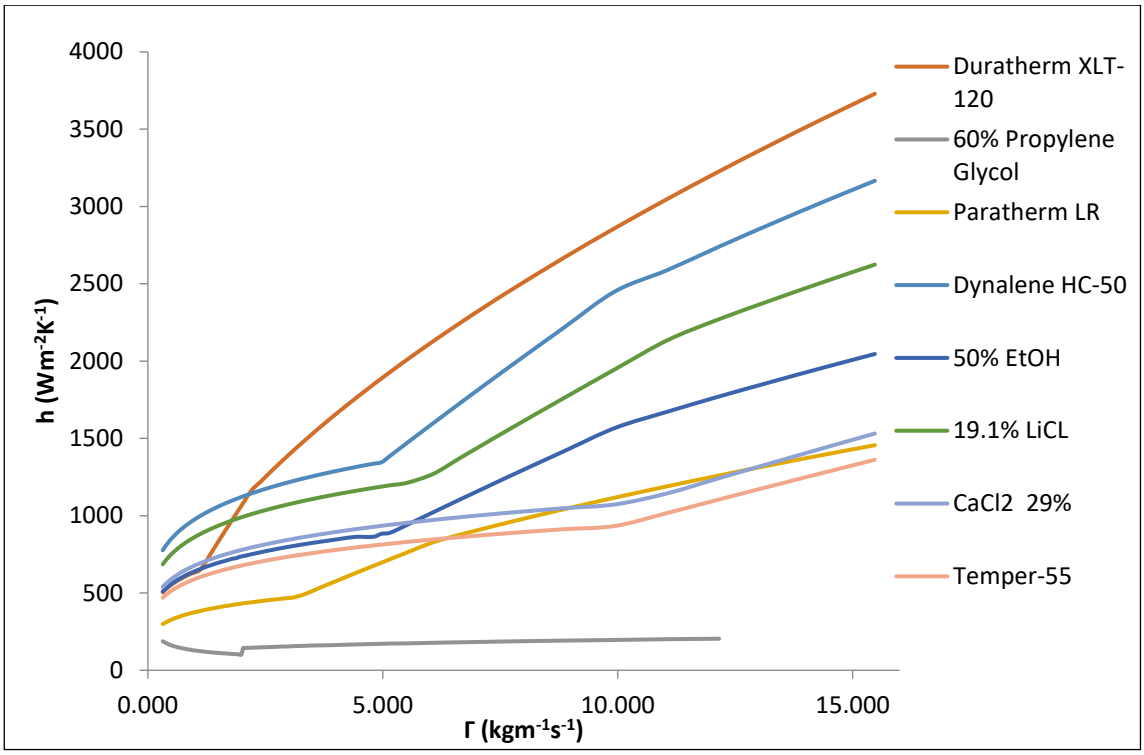

Figure 3-20: Coolant side heat transfer coefficient for several different HTFs. The film heat transfer coefficient is shown as a function of coolant irrigation rate.

As can be seen, 60% propylene glycol was predicted to be the lowest performing fluid of all evaluated. This was largely due to its high viscosity (330 mPa.S) at -30°C[32]. Propylene glycol also has a volumetric heat capacity of 3.399 $kJL^{-1}K^{-1}$.

Duratherm XLT-120 was the highest performing, largely due to a low viscosity of 2.83 mPa.S. However, this product was only available for export from the US in volumes of over 200 L, making it impractical for the pilot unit.

Dynalene HC-50 is a potassium formate based solution, and had a high performance due to a low viscosity.

A 50% Ethanol solution would be an affordable solution, with an acceptable heat transfer coefficient, a volumetric heat capacity of 3.094 $kJL^{-1}K^{-1}$, and a viscosity of 14.6 mPa.S. However, the flash point of this solution would be 24°C, meaning that during start-up and shut down, the system could contain a large volume of flammable gases. It would not be possible to reduce the concentration of Ethanol further, as the freezing point of 50% Ethanol is -37°C, therefore any lower concentration would run the risk of freezing in the chiller unit's heat exchanger.

3.7.4.2 Falling Film Flow and Heat Transfer Calculations

3.7.4.2.1 Minimum Wetting Rate

In order to operate as a falling film, the mass flow per unit length (represented by Γ, kg/m.s) over the surface must be above a certain value. Above the value, called the Minimum Wetting Rate (MWR), the fluid flow wets the entire surface. Below this value, stable dry patches appear, and the fluid flow does not cover the entire surface.

For efficient operation the surface of the freezer should be fully wetted throughout operation. Fully wetting surface will promote even ice growth, and efficient use of the available heat transfer surface.

Perry's Chemical Engineer's Handbook suggests that the MWR is between 0.03-0.3 $kgm^{-1}s^{-1}$ for water at room temperature[33].

As the fluid flowing has different properties to water at 20°C it is necessary to calculate the MWR for the product.

The Hartley-Murgatroyd model [34] calculates the minimum wetting rate (Γ_{min}, $kgs^{-1}m^{-1}$) for an isothermally flowing film with the following equation:

$$\Gamma_{\min} = 1.69\left(\frac{\mu\rho}{g}\right)^{\frac{1}{5}}\left(\sigma(1-cos\theta_{CA})\right)^{3/5} \quad (3\text{-}4)$$

Where μ is the fluid viscosity in Pa.S, ρ is the fluid density in kgm^{-3}, σ is the surface tension of the fluid in Nm^{-1}, and θ is the contact angle of the fluid on the surface. This equation has been tested for milk of various concentrations, and has been found to predict the MWR well for concentrations below 20% TS. Above this concentration the equation is conservative and predicts a higher MWR than that measured experimentally[35].

El-Genk and Saber[36] reviewed several models for MWRs and developed an analytical model for MWRs. They compared this with published experimental data to develop the following empirical expression, with units as for equation (3-4).

$$\Gamma_{\min} = \left(\frac{\rho\mu\sigma^3}{g}\right)^{0.2}(0.67(1-cos\theta_{CA})^{0.623} + 0.26(1-cos\theta_{CA})^{2.09}) \quad (3\text{-}5)$$

These equations were used to calculate the MWR for the coolant and the milk. The coolant MWR, with 22% LiCl as the coolant, calculated as 0.3 $kgm^{-1}s^{-1}$ using the Hartley-Murgatroyd model and 0.2 $kgm^{-1}s^{-1}$ using the El-Genk and Saber model.

For sheep's milk at 4°C, the MWR was calculated as 0.2 $kgm^{-1}s^{-1}$ using the Hartley-Murgatroyd model and 0.1 $kgm^{-1}s^{-1}$ using the El-Genk and Saber model.

In both cases the more conservative value was used as the basis for further calculations.

As can be seen from the above equations, the MWR is dependent upon the contact angle of the fluid on the surface, so this will need to be determined accurately in future experimental work.

As an ice layer forms, the MWR of the milk will drop rapidly as the contact angle of milk on ice should be low. The contact angle of water on ice has been measured as 12±1° [37].

This may allow operational parameters to be tuned to the ideal conditions for each stage of the operating cycle, such as dropping the milk flow rate low enough that no recycling is necessary.

3.7.4.2.2 *Film Flow, Thickness and Velocity*

The Reynolds number of a falling film is as follows [33]:

$$Re = \frac{4\Gamma}{\mu} \quad (3\text{-}6)$$

Flow will be laminar at Reynolds numbers of less than 2,000. For Reynolds numbers above 25 surface waves appear on the liquid film.

The average thickness of a laminar falling film is given by the following equation [33]:

$$\delta = \left(\frac{3\Gamma\mu}{\rho^2 g}\right)^{1/3} \quad (3\text{-}7)$$

The average film velocity is therefore

$$V_{film} = \frac{\Gamma}{\rho\delta} = \frac{g\rho\delta^2}{3\mu} \tag{3-8}$$

Assuming no drag at the gas/liquid interface, the velocity profile *u(x)* where *x*=0 at the solid surface and *x*=*δ* at the gas/liquid interface is described by:

$$u = 1.5V_{film}\left[\frac{2x}{\delta} - \left(\frac{x}{\delta}\right)^2\right] \tag{3-9}$$

These equations are suitable for liquids with a viscosity below about 1mPa.s in a viscous flow regime. However liquids with higher viscosities have lower film thicknesses than would be expected from pure viscous flow behaviour, with a significant deviation for high viscosity liquids (>10-25 mPa.s)[33, 38].

For turbulent flow the average thickness can be estimated to within ±25% :

$$\delta = 0.304\left(\frac{\Gamma^{1.75}\mu^{0.24}}{\rho^2 g}\right)^{1/3} \tag{3-10}$$

The average film velocity can be calculated as in equation (3-8) above.

For all the above equations, *g* can be replaced by $gsin\beta$ for a plate inclined an angle β with the horizontal.

3.7.4.2.3 *Heat Transfer Coefficient*

The heat transfer coefficient between the bulk of a non-evaporating falling film and the wall it flows over can be calculated by the following models[31].

For pure laminar flow, without waves or turbulence (i.e. Reynolds numbers below 25) the Hewitt and Hall-Taylor model can be used:

$$h = \frac{280}{141}\left(\frac{\rho^2 g k^3}{3\mu\Gamma}\right)^{\frac{1}{3}} = \frac{280}{141}\left(\frac{4\rho^2 g k^3}{3\mu^2}\right)^{\frac{1}{3}} Re^{-\frac{1}{3}} \tag{3-11}$$

An empirical correlation is given by Wilke[39] that includes effects from turbulence and waves:

$$\frac{h\delta}{k} = C_o Re^m Pr^{0.344}$$

$\boldsymbol{Re}$	$\boldsymbol{C_o}$	$\boldsymbol{m}$
< 1600	0.029	0.533
$1600 < Re < 3200$	$0.212\text{x}10^{-3}$	1.2
> 3200	$0.181\text{x}10^{-2}$	0.933

(3-12)

For $Re < 1600$ equation (3-7) is used to calculate δ. For $Re > 1600$ equation (3-10) is used.

For Re <25, equation (3-11) was used and for Re>25 equation (3-12) was used to calculate the heat transfer coefficients for the milk side and coolant side falling films, for a range of mass flows, the results are plotted below:

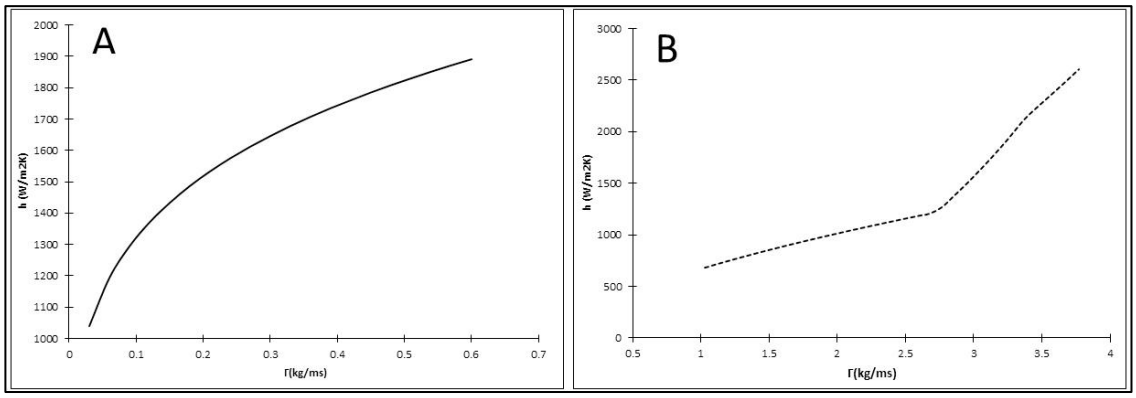

Figure 3-21: The influence on irrigation rate (Γ) on : A) Milk side heat transfer coefficients for the falling film freezer. B) Coolant side heat transfer coefficients for the falling film freezer, using 22% LiCl as an HTF.

With an outside diameter of 76 mm for the pipe, the films are predicted to have the following properties.

Table 3-6: Film properties under operating conditions.

	Coolant	**Product**
Composition	22% m/m LiCl solution	Raw Sheep Milk
MWR ($kgm^{-1}s^{-1}$)	0.31	0.17
Γ ($kgm^{-1}s^{-1}$) under operating conditions	5.6	0.18
Re	1500	200
δ (mm)	2.7	0.58
V (ms^{-1})	0.73	0.30
h ($Wm^{-2}k^{-1}$)	1200	1500

3.7.4.2.4 *Overall Heat Transfer Coefficient.*

As the diameter of the falling film freezer's heat transfer surface is more than 2 orders of magnitude larger than its wall thickness it can be modelled as a planar surface without significant loss of accuracy (The difference between internal and external area is less than 2%) . In this case the overall heat transfer coefficient can be calculated as follows:

$$\frac{1}{U} = \frac{1}{h_{in}} + \frac{x_{wall}}{k_{wall}} + \frac{1}{h_{out}} \tag{3-13}$$

With a wall constructed of 0.5 mm 304 stainless steel, and the convective heat transfer coefficients given in Table 3-6, the overall heat transfer coefficient between the bulk of the falling coolant film and the falling milk film is estimated as 740 $Wm^{-2}k^{-1}$ with no ice layer present.

At the end of the freezing cycle, when a 3 mm thick ice layer is present, the overall heat transfer coefficient is estimated as 380 $Wm^{-2}k^{-1}$.

During the tempering cycle, when the heat is flowing out of the ice layer into the coolant, the heat transfer coefficient from the coolant bulk to the wall/ice interface is estimated as 1500 W/m^2k. The heat transfer coefficient from the coolant bulk to the ice/atmosphere interface is estimated as 520 $Wm^{-2}k^{-1}$.

3.7.4.2.5 *Ice growth rate*

Assuming an equilibrium freezing temperature of -0.6°C, an overall heat transfer coefficient of 730 $Wm^{-2}k^{-1}$, and a nominal coolant inlet temperature of -30°C, the heat flux of the freezer is 21 kWm^{-2}. This translate to an ice growth rate of 68 μms^{-1}, at the beginning of the

freezing cycle. At the end of the cycle the ice growth rate is 35 µms^{-1}. This is around 2 orders of magnitude higher than the ice growth rate found in falling film freeze concentration equipment [22, 40].

3.7.4.3 Coolant Supply Design

3.7.4.3.1 Chiller Selection

In order to freeze 50 L of milk per hour, approximately 4.6 kW of heat needs to be removed, as well as the pumping energy. The desired operating temperature is -30°C. A search of commercially available units and discussion with commercial refrigeration suppliers led to the selection of a Pattonpak PZB600W chiller unit.

This unit integrates a stainless-steel brazed plate heat exchanger, digital temperature controller and low temperature protection. The unit is designed to be installed external to a building to service a heat load inside. The unit has a capacity of 5.1 kW at -30°C, and 32°C ambient.

3.7.4.3.2 Pressure Head Requirement

The pressure head the pump needs to develop across the coolant loop can be summarised as being made of the following components:

- Pressure drop due to friction in piping,
- Pressure drop due to static head,
- Pressure drop due to flow through pipe fittings and shutoff valves
- Pressure drop in control valves
- Pressure drop in Flow meter

The following diagram shows a schematic of the major pressure drops.

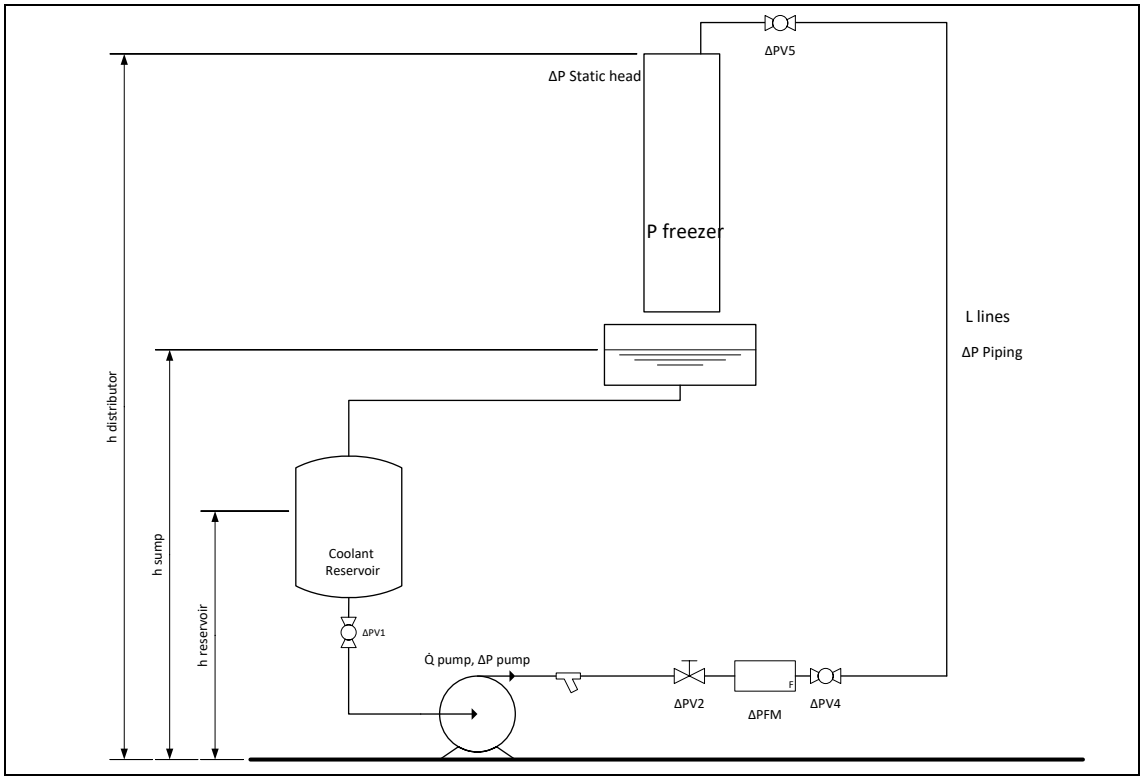

Figure 3-22: Schematic of pressure drops in main coolant loop.

Mathematically this can be represented as follows:

$$\Delta P_{loop} = \Delta P_{piping} + \Delta P_{Static} + \Delta P_{Fittings} + \Delta P_{Control\ Valve} + \Delta P_{Flow\ Meter} \quad (3\text{-}14)$$

The pressure drops from the pipe fittings can be subsumed by the frictional pipe losses by using the equivalent pipe length method.

The frictional pressure drops can be calculated by the Darcy-Weisbach equation[33]:

$$\Delta P = f_D * \frac{\rho}{2} * \frac{u^2}{Di} * L_{eq} \quad (3\text{-}15)$$

The static pressure can be calculated by the following equation:

$$\Delta P_{Static} = \rho * g * (H_{distributor} - H_{sump}) \quad (3\text{-}16)$$

The pressure drop across the control valve is calculated using the K_V value of the valve, a measure of how much flow the valve allows for a pressure drop of 1Bar.

$$\Delta P = \left(\frac{\dot{V}}{K_v}\right)^2 * SG \quad (3\text{-}17)$$

In the above equation, SG is the specific gravity of the fluid, $\dot{V}$ is the fluid flow in m^3hr^{-1} and ΔP is in bar.

The pressure drop across the flow meter was calculated from data provided by the manufacturer.

Using the above equations, the system curves for the coolant supply shown in Figure 3-23 A were calculated.

The same coolant loop is used for the rotating drum design with two differences:

- The static head is lower
- The coolant is distributed through the inside of the drum by a series of nozzles that spray the coolant onto the interior surface.

The rotating drum distributor has been designed to have a velocity across the orifices of 10 ms^{-1}, at a nominal flow of 3 m^3hr^{-1}. A discharge coefficient of 0.61, the discharge coefficient for a sharp-edged orifice, was assumed.

The system curves for the rotating drum freezer system are shown in Figure 3-23 B

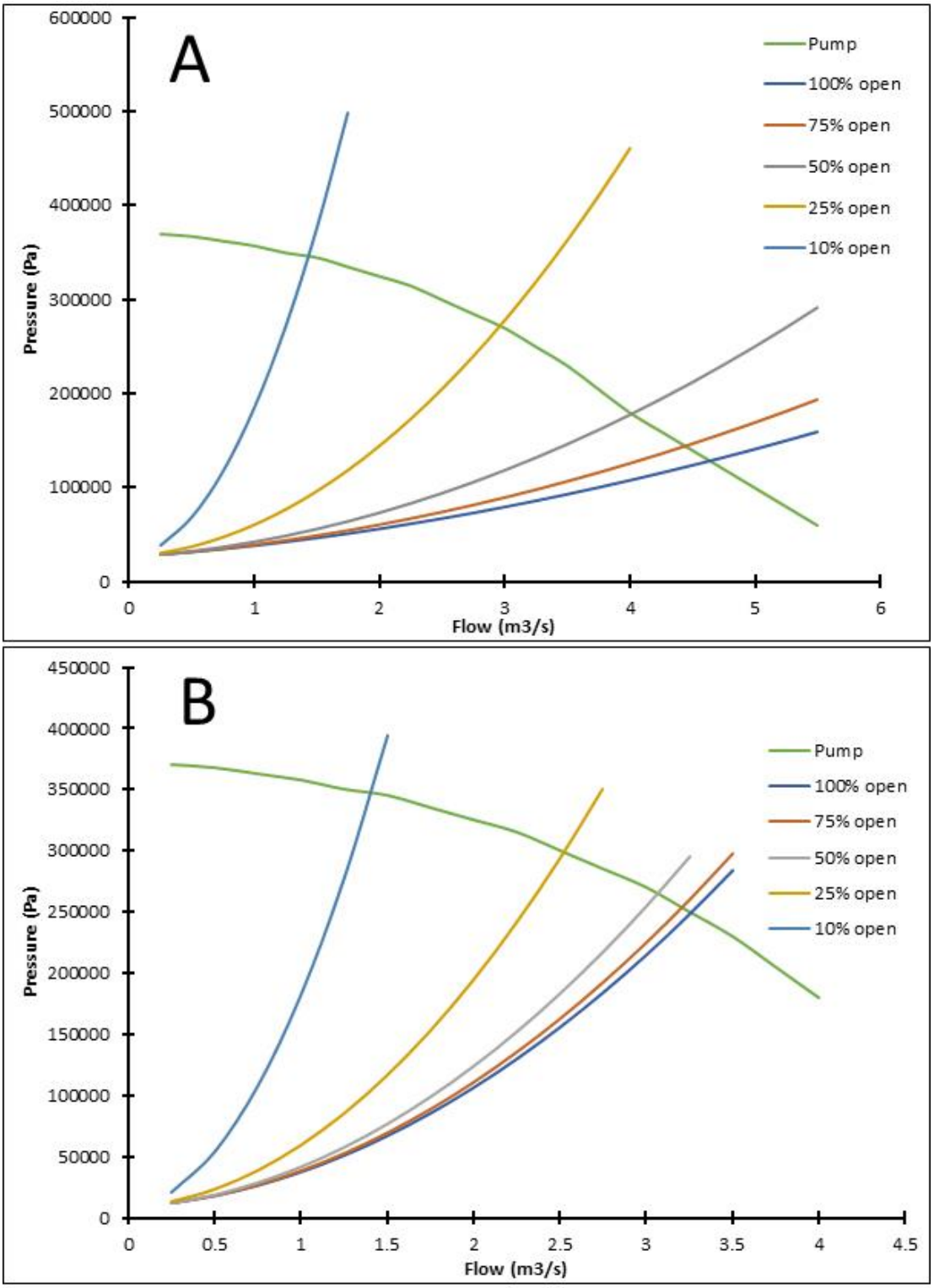

Figure 3-23: A) Pump and system curve for the falling film freezer, showing the pressure drop as a function of valve position and coolant flowrate. B) Pump and system curves for the rotating drum freezer.

3.7.4.3.3 *Pump Selection*

In order to reduce the risk of corrosion from the heat transfer fluid, a stainless-steel pump was preferred. The flow, head, and temperature requirements for the pump were sent to several pump suppliers, and the most economic selection was chosen.

The pump selected was a Lowara 3HM05S05M 0.5 kW multistage centrifugal pump. The pump curve is shown in Figure 3-23.

3.7.4.3.4 *Energy Balance*

An energy balance was conducted across the freezer system. The main heat loads are the following:

- Heat loads from piping
- Heat loads from pump inefficiency
- Heat loads through tank walls.
- Heat load due to product freezing.
- Heat loads from convection to the falling film freezer.

This can be represented mathematically as follows:

$$Q_{chiller} = Q_{piping} + Q_{pump} + Q_{tank} + Q_{convection} + Q_{freezing} \quad (3\text{-}18)$$

The heat loads calculated are summarised in the following table, assuming 20mm of insulation on the piping and tank, an operating temperature of -30°C, and an ambient temperature of 20°C.

Table 3-7: Heat loads on chiller.

Source	Heat Load(W)
Piping	166
Tank	59
Pump Inefficiency	350
Convection to Freezer	153
Product Freezer	4300
Chiller Power	5100

The available chiller power will be sufficient to freeze approximately 47 $kghr^{-1}$ of milk.

3.7.4.3.5 *Temperature Control.*

The temperature within the coolant reservoir will be controlled by the chiller unit, using a feedback control strategy. The coolant temperature will be monitored with a PT100 RTD.

If this control proves inadequate, a bypass loop can be added from the freezer coolant return line to the freezer coolant pump suction line, with a motorised valve to provide fine temperature control by controlling the mixing in warmer coolant from the return line

3.7.4.4 Pilot Unit P&ID and Space Requirements.

A P&ID diagram for the pilot freezer is shown below. A floor plan for the falling film freezer and the laboratory where it was located is also shown below.

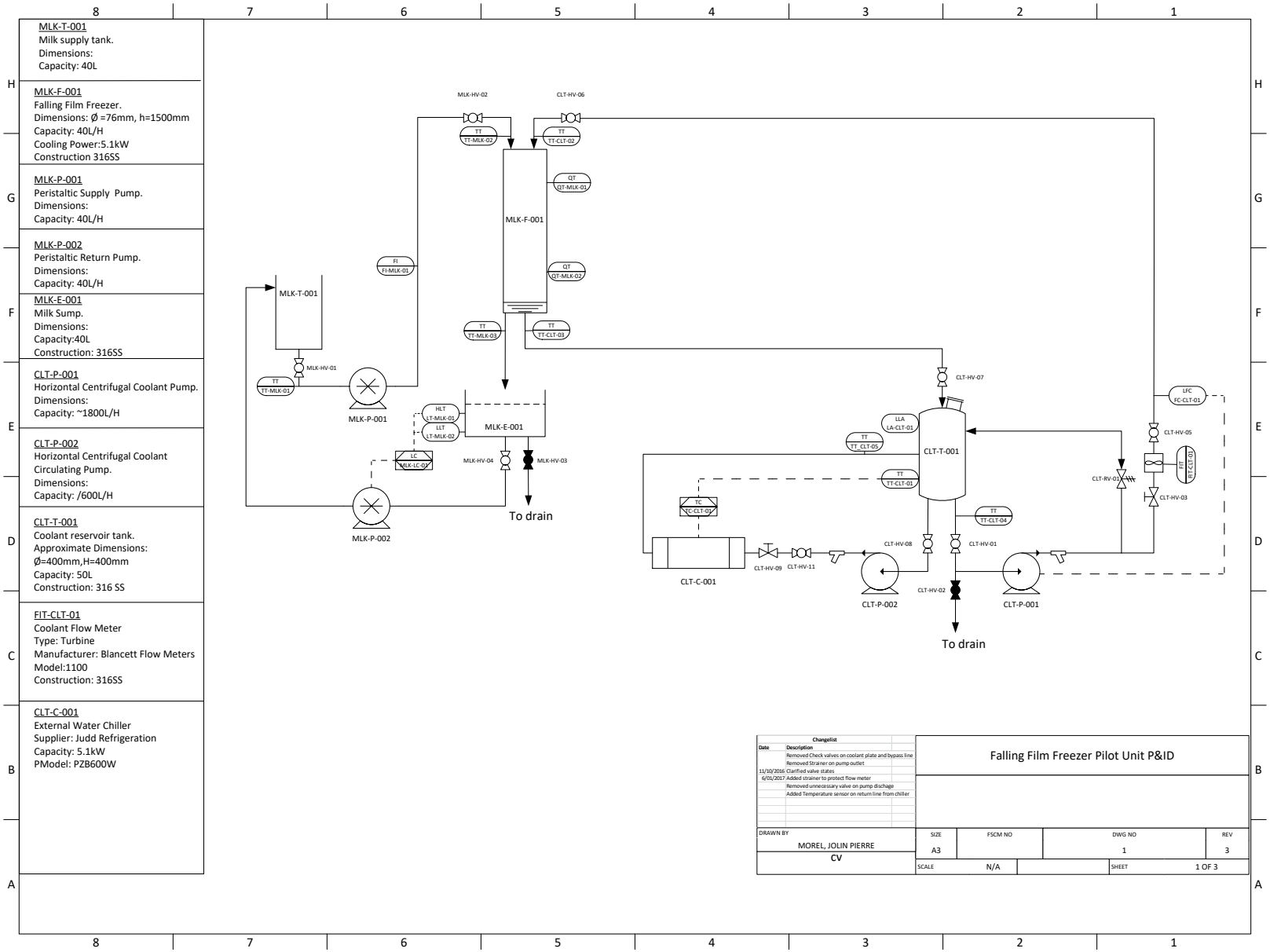

Figure 3-24: Pilot Freezer P&ID, showing piping, equipment, instrumentation, and valving as built for pilot scale unit.

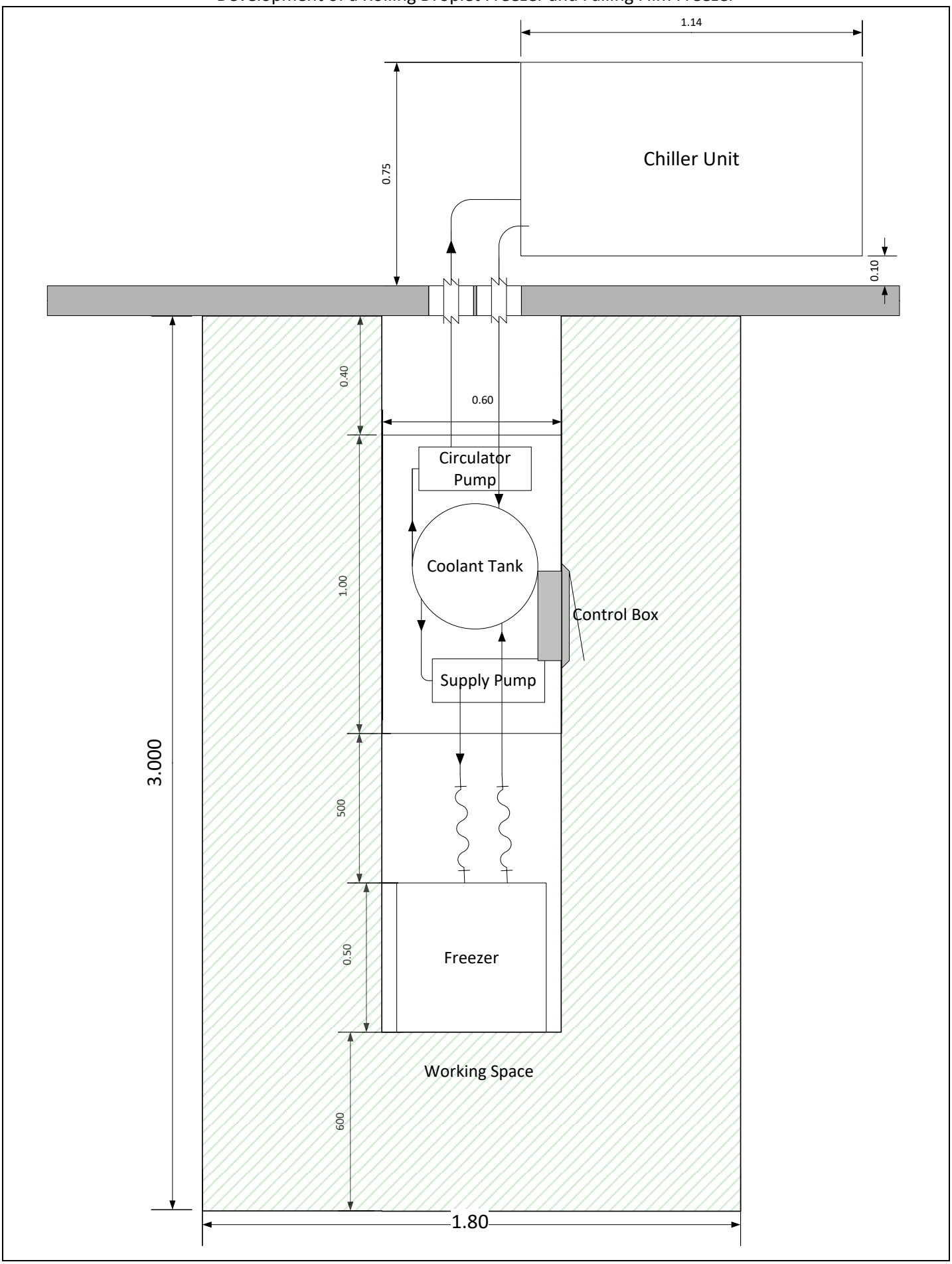

Figure 3-25: Floor space required for the Falling Film Freezer pilot unit.

3.8 Experimental Work Conducted on Falling Film Freezer

3.8.1 Flowmeter Calibration

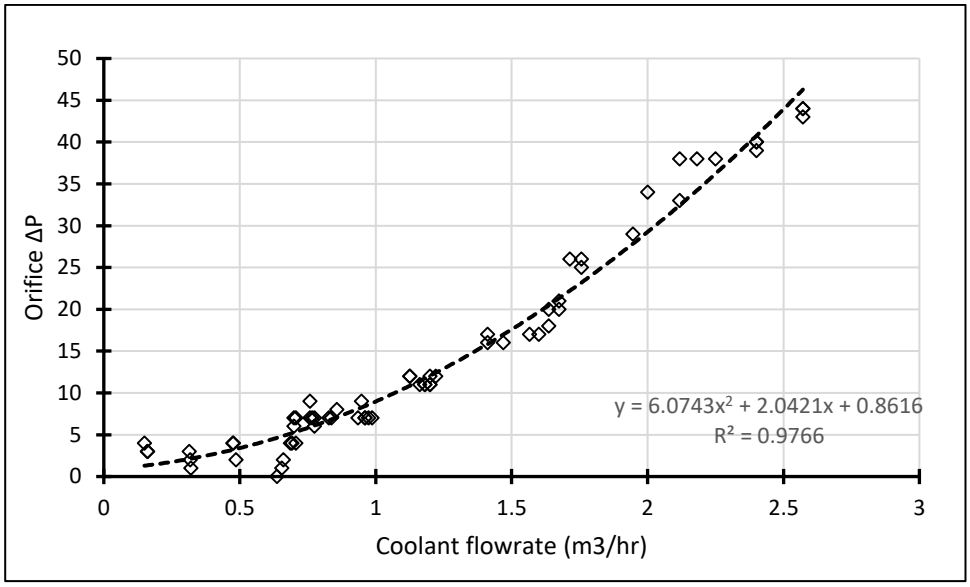

Figure 3-26: Calibration curve for orifice plate flowmeter.

A set of trials were conducted to calibrate the response of the orifice plate flowmeter to coolant flowrate. The flowrate was measured manually with a calibrated scale and stopwatch, with the control valve set to different locations to control flowrate. The ΔP across the orifice plate was measured. The measured response to flow is shown in Figure 3-26. As can be seen, a quadratic equation is an effective descriptor of the response.

3.8.2 Ice Detachment

The heat detachment of ice was tested initially by flushing hot water at 50°C through the coolant flow passage of the falling film freezer, and thereby achieving a significant heat flux. The initial heat flux was estimated at 31 kWm^{-2}.

Tap water was frozen onto the surface of the freezer with coolant temperatures of -30°C and -15°C. The ice layer was grown to thickness of 5 mm or 10 mm. Water at 50°C was then flushed through the coolant side.

This successfully detached flakes of frozen water. The ice expanded and cracked as is shown in Figure 3-28. This cracked ice then detached and fell off in flakes of significant size and thickness. A detached flake of ice approximately 10mm in thickness is shown in Figure 3-27.

Figure 3-27: Ice flake of approximately 10mm thickness detached by rapid heating of the internal tube surface.

Having proven the principle with pure water ice, the detachment of frozen milk by the application of heat was evaluated.

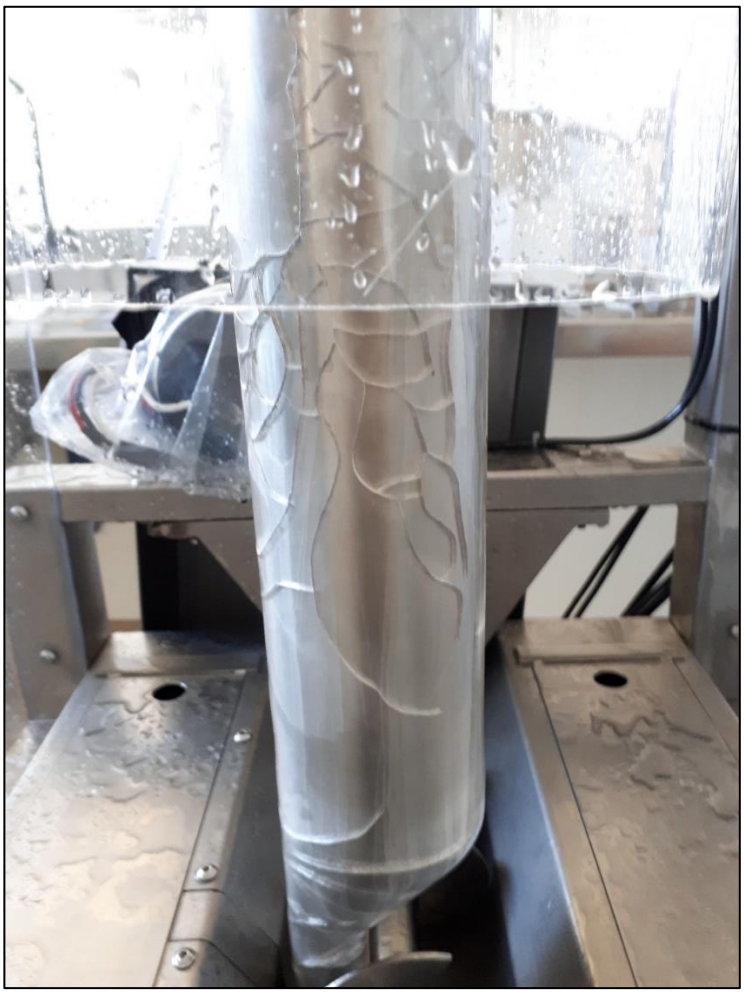

Figure 3-28: Cracking of water ice layer (approx. 5mm thickness) during rapid heating of internal surface of freezer tube.

3.8.3 Milk Detachment

After the successful detachment of pure water ice, the detachment of frozen milk was attempted.

Ovine milk was prepared from whole sheep milk powder to a solids concentration of 20%. A layer of milk approximately 5mm thick was frozen onto the surface of the freezer, then allowed to temper to the coolant temperature before the application of heated water to the coolant side of the freezer. This was attempted at coolant (and final product, assuming equilibrium at wall) temperatures of -30°C, -20°C and -15°C.

Unlike the proof of concept trial with frozen water, no cracking was observed in any frozen milk samples at any temperature. Frozen milk did not detach like frozen pure water, rather samples would melt significantly while still remaining attached to the surface.

Figure 3-29: Frozen milk on the surface of the falling film freezer.

Frozen ovine milk appeared much less brittle than pure water ice. It was decided that this method of detachment would not be effective based on the experience of these proof of concept trials.

Initially it was planned to conduct a series of evaluations on the detachment process, to allow detachment time to be well characterised, as a function of frozen milk temperature and heating power, allowing the operating cycle to be completely modelled and optimised. This was abandoned with the failure of these proof of concept trials.

It was instead decided to evaluate other conventional methods of detachment, such as a mechanical scraper, and unconventional methods such as impact or vibration. This is described later in the chapter.

3.8.4 Partition Coefficient

The partition coefficient is a measurement of the relative concentration of solute in the liquid and solid phases and is calculated as $\overline{K} = \frac{C_s}{C_L}$. This parameter is important for describing the performance of a freeze concentration system, or the behaviour of solutes during the freezing process. Work conducted on freeze-concentration of aqueous solutions shows that the partition is proportional to the freezing front velocity v_f and inversely proportional to the freezing point depression of the system [25].

The partition coefficient of the whole ovine milk was evaluated at several different freezer operating temperatures.

Whole ovine milk was prepared from powder to a total solids concentration of 20%. This was frozen on the falling film freezer and samples removed at 5-minute intervals. Samples of the unfrozen milk running off the bottom of the freezer were also collected at 5-minute intervals.

The total solids content of the samples was determined gravimetrically by forced air drying after pre-drying over steam, following AOAC method 990.19 [41].

In general, the total solids concentration of the frozen milk was lower than that of the unfrozen milk, indicating that separation occurs between the solid and liquid phase.

The partition coefficients measured are shown in Table 3-8. These were collected at a constant product flowrate. This affects the partition coefficient as shown in [25], where the generalised expression for partition coefficient in a falling film freeze concentrator incorporates the effect of product flow past the growing ice. Higher flowrates have been shown to reduce the partition coefficient of sucrose solutions in falling film freeze concentrators [42]. The milk partition coefficient was also evaluated at a single whole milk concentration of 20% whole milk. The partition coefficient has been linked to the freezing point depression of the solution [25]. As the freezing point depression of milk increases with increased milk concentration [6]. For increased milk concentrations, the partition coefficient will be expected to increase, whereas it will likely decrease with decreased milk concentration. This has been shown experimentally by other authors who have evaluated the performance of falling-film freeze-concentrators with concentrated milks [42].

Table 3-8: Partition coefficients determined from falling film freezer trials.

Freezer Operating Temperature (°C)	**Partition Coefficient $\overline{K} = \frac{C_s}{C_L}$.**	
	$\overline{x}$	σ
-30	0.946	0.112
-18	0.926	0.021
-15	0.866	0.065

The partition coefficient of whole ovine milk in this study is significantly higher than that previously published in the freeze concentration field [25, 43], however during extended

processing runs as experienced during freezing on farm there significant freeze concentration would occur, especially for higher operating temperatures. This would not be ideal and would lead to an inhomogeneous product and may affect operating conditions during longer processing runs.

The partition coefficient increased with decreased freezer operating temperature, as this increased the driving force behind ice growth, therefore increasing the ice growth rates, and forcing higher levels of milk components to be incorporated into the ice matrix [23]. The relationship between ice growth rate and solute incorporation has been found in many other products that have been freeze-concentrated [22, 26, 44-46]. This is discussed further in Chapter 4 from a microscopic point of view, with reference to the interaction between particles and advancing solidification interfaces, and the effect of the ice growth rate on the morphology of this advancing interface.

3.8.5 Milk Distributors

The correlations for MWR used during the system design assumed that the surface wetted was flat rather than curved, however the radius of the tube is much(~80x) larger than the calculated film thickness at the MWR, so the divergence from the assumption of a flat surface is negligible.

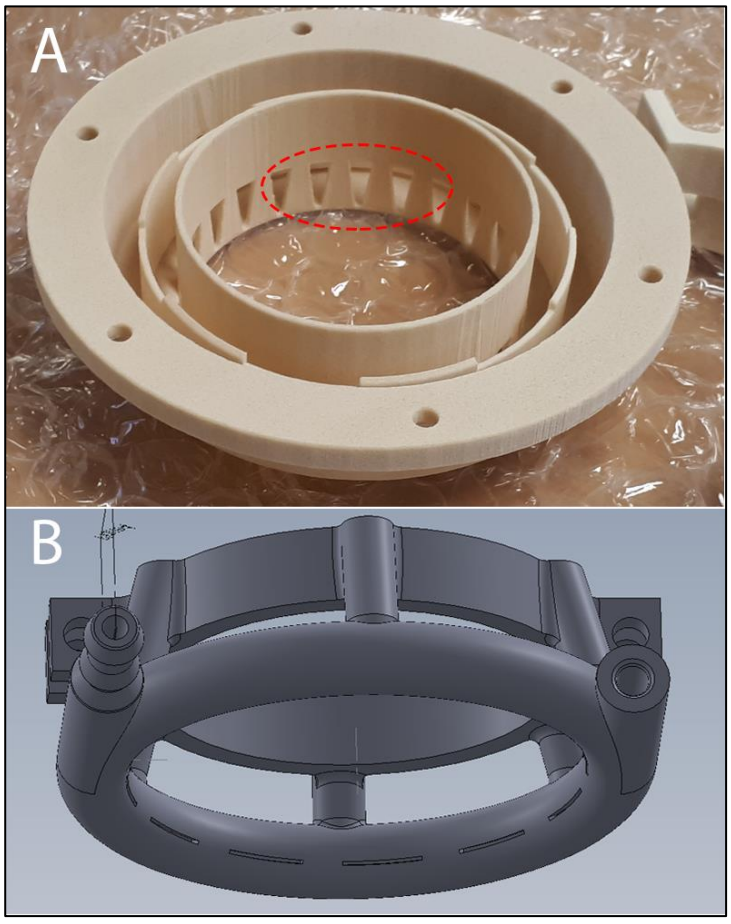

Figure 3-30: Two designs for distributors. A: The internal weir discussed in section 3.8.5.2 . B: The sheet distributor discussed in section 3.8.5.3.

To achieve even distribution of milk at flowrates near the MWR, the milk needed to be evenly distributed at the top of the freezer. Several different types of distributor were trialled.

3.8.5.1 Jet Distributor

The first distributor consisted of a series of jets directed through holes inwards towards the outer surface of the freezer tube.

This distributor was found to have several issues which made it unsuitable for application on a commercial unit.

There were higher areal flowrates at the intersections of adjacent impinging jets, which impeded full wetting of the tube surface, requiring flowrates in excess of the calculated MWR for full wetting of the surface. As the increased product flow would decrease the partition coefficient and increase the energy requirement this was undesirable.

Misalignment of the jets, or unequal flow through the jets as a result of fouling would also lead to partial wetting at flowrates above the calculated MWR. This reduced the effective heat transfer area of the freezer and was undesirable. A further shortcoming of the jet distributor was splattering caused by spray-spray interactions between adjacent impinging jets. This splattering could cause fouling of the freezer in areas that would be difficult to reach during clean-in-place procedures, complicating cleaning of the system. This would be unacceptable during commercial operation.

3.8.5.2 Weir Distributor

To mitigate several of the issues identified with the jet distributor and to increase tolerance to varying flowrate a distributor was constructed in the shape of an internally facing V-notch weir, stood off 3-5 mm from the external surface of the tube. Milk would overflow the weir, fill the space between the tube and weir, and then flow down the surface. This distributor is shown in Figure 3-30.

This distributor performed acceptably during trials, fully wetting the surface at slightly above the MWR. There was no spray-spray interaction, so product spattering was minimal, as was fouling of surfaces that would not be cleaned-in-place.

However, the narrow space between the weir and the freezer surface impeded operation when milk flow was lowered and for milk tempering and removal. The surface tension of milk was sufficient for a liquid bridge to remain between the surface and the weir when flow was stopped. During the tempering step, this bridge would freeze, forming a blockage that prevented the weir from operating after one freezer cycle. A larger standoff was required; however, this was not feasible for the wetting rates used on this freezer.

3.8.5.3 Sheet Distributor

Due to the blockages formed during operation, the weir distributor was replaced by a distributor consisting of a series of flat slots at an angle of 30° below horizontal, through which frozen milk could flow in thin sheets, stood-off 6 mm from surface to prevent surface tension forming liquid bridges that would freeze when the product flow was stopped.

Preliminary trials indicated that this distributor performed acceptably.

3.8.6 Modifications for Milk Detachment

The heating method of fluid detachment proved ineffective, as discussed in section 8.3, so mechanical methods of frozen milk detachment were evaluated.

3.8.6.1 Scraper

A circular scraper was fitted to the tube. The internal diameter of the scraper was slightly larger than the exterior diameter of the freezer tube. The scraper was actuated by hand for the preliminary tests.

Water ice was easily removed by a circular scraper. Water ice was brittle and rigid and would flake or crack when bending forces were applied by a scraper lifting a section of ice from the freezer surface. The ice/surface bond would fail in a peel mode and then fall from the freezer surface.

Despite frozen milk having a lower adhesion strength to stainless steel than water ice [47], it was more difficult to remove from the freezer surface by scraping, as it was less brittle and rigid. When bending forces were applied by forcing a scraper under a section of frozen product, that section would peel and detach, leaving the remainder of the product still attached to the surface. This meant that rather than acting as an inclined wedge removing large sections of solid, the scraper had to remove areas of frozen milk by shear. This is illustrated schematically in Figure 3-31.

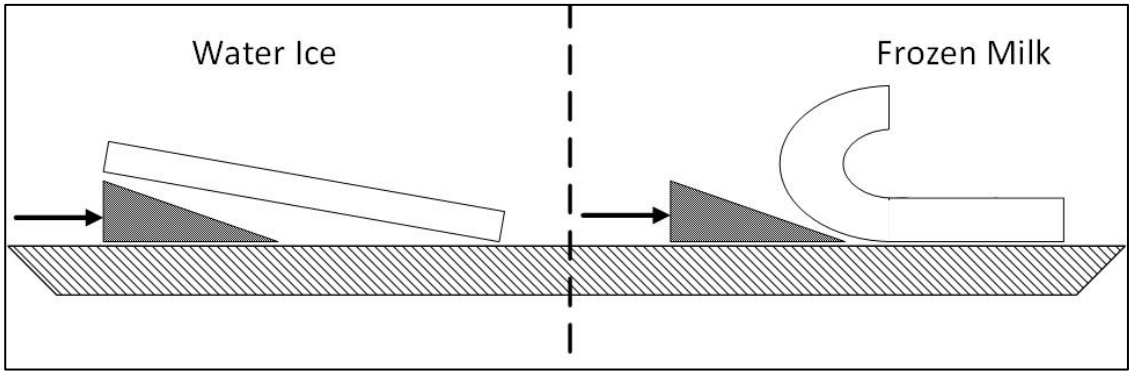

Figure 3-31: Difference in detachment behaviour between water ice and frozen milk. Water ice is brittle and would detach in large flakes. Frozen milk would "curl" or "peel" off a cooled surface.

3.8.7 Scraper Trial

The scraper was a close fit the surface of the freezer, and in initial trials generally operated effectively. However, in some trials the scraper would "ride up" over ice if started on already icy section of tube. This was worse for frozen milk, as frozen milk was less brittle than water.

The scraper was designed to start above the wetted section of the freezer tube to prevent liquid freezing between the scraper and tube surface and allow the scraper to start at an ice-free section of tube, so it could effectively remove the product.

Alternative physical methods were evaluated. These included physical impact, flexion of the tube surface and ultrasonic de-icing. These all generally rely on the brittle nature of ice, and its response to a mechanical input differing from that of the substrate it is adhered to. The difference in response would lead to failure of the adhesive bond between the substrate and the ice.

Physical impact was evaluated by impacting a 2.5 kg mass with an impact energy of ~25 J onto the surface of the frozen material, or a section of tube which was free of frozen material. The frozen material was either frozen milk or pure water ice.

The impact of the mass onto the surface of water ice would lead to cracking and detachment of large sections of ice. Impact of the mass on to the surface of frozen milk had no comparable effect, beyond impact marks on the surface of milk. The milk remained attached.

Detaching the frozen product by flexing the surface was proposed. A similar method is used to deice the leading edge of the wings of small aircraft, where inflation of a rubber "boot" forces the brittle ice to deform, crack and detach. As this would require significant modifications to the freezer surface it was not pursued further.

Ultrasound has been used to de-ice helicopter blades[48], turbine blades[49], freezer coils[50, 51] and flat sheets[52, 53]. This works by exploiting the differences in response to ultrasonic waves by a substrate and the frozen substance, which leads to cracking in brittle ice, and localised areas of high forces normal to the surface, causing detachment of the frozen substance. While this would be an elegant method of de-icing, and would be an investigation into a substrate/ frozen substance combination not previously examined in literature, no further development of this method of removing the frozen product was conducted.

It was decided that the lowest risk option, the further development of a scraper, would be pursued. While other systems may have been conceptually elegant or interesting, ultimately a low-risk and effective system was needed, given the development aims of the project and the commercial imperatives driving the work.

Ultimately the successful development of the continuous tubular freezer (discussed in Chapters 7 and 8) placed all work on the falling film freezer on hold, as it presented a radically simpler, more compact, and more hygienic system, which deserved the majority of developmental time and resources. As a result, the operational behaviour of the falling film freezer was not completely evaluated, nor were the models envisaged at the outset of the work completed. The testing of detachment of frozen milk from functional surfaces was not completed as this work became less relevant with the change in focus to the continuous tubular freezer.

3.9 Conclusions

In this work preliminary measurements of selected properties of ovine milk in an NZ context were conducted. Ovine milk collected from a farm ranged from 14% to 23.6% total solids. The viscosity of ovine milk can be described with a high level of accuracy (R^2=0.89 for 290 measurements) as a function of % fat, %SNF and the temperature of the milk. The surface tension of ovine milk can be described by a function of % total solids and temperature.

Preliminary evaluations of nucleation during cooling in samples of ovine milk was measured. Sessile droplets of milk nucleated at higher temperatures than pure water cooled under identical conditions.

A number of designs for on-farm freezers were evaluated. Initially a rolling droplet freezer was selected as the most promising direction for development. These results were further analysed and used to develop a set of research aims and plan experimental work to study the phenomena occurring the freezing of a droplet rolling over a superhydrophobic surface.

The condensing atmosphere resulting in transitions to a Wenzel wetting state from a Cassie-Baxter wetting state would have reduced the reliability of the system. In addition, the fabrication costs of the system would have likely been excessive for system intended for wide deployment on small farms. As a result, the work on the rolling droplet freezer was abandoned, and developmental work was shifted to flake freezing.

Two embodiments were evaluated and designed. As the physical processes underlying a drum freezer and falling film freezer are similar, a falling-film freezer was constructed, which would remove ice via heat detachment, as this would require more development effort. Iterative component design was applied to the distributor.

The application of heat was effective for detaching ice, but was ineffective for milk, due to the different mechanical properties of milk. The system was modified with the addition of a vertical mechanical scraper, which underwent iterative design.

The partition coefficient of ovine milk during falling film freezing was found to be significantly higher ($\overline{K}$=0.946 at -30°C) than published values for whole milk in freeze-concentration literature. The partition coefficient increased with lower freezer operating temperatures.

A full set of experiments to fit experimental data to generalised models of partition coefficient behaviour [25] was not conducted due to development of continuous tubular freezer.

The development of the falling-film freezer was abandoned due to development of the technically superior continuous tubular freezer described in Chapters 7 and 8.

3.10 List of Symbols

Symbol	Description	Units
$\%Fat$	Fat content of sample	%
$\%SNF$	Solids-Non-Fat content of sample	%
$\%TS$	Solids content of sample	%
a, b	Coefficients for eqn. (3-1)	
A, B, C, D	Coefficients for eqns. (3-2), (3-3) and (3-4).	
C_L	Solute concentration in liquid phase	$g_{solute}/g_{solution}$
C_s	Solute concentration in solid phase	$g_{solute}/g_{solution}$
C_o	Coefficient for eqn. (3-12).	
Di	Piping diameter	m
f_D	Darcy friction factor	
g	Acceleration due to gravity	ms^{-2}
h	Falling film heat transfer coefficient.	$Wm^{-2}K^{-1}$
H	Height	m
h_{in}	Internal film heat transfer coefficient for freezer	$Wm^{-2}K^{-1}$
h_{out}	External film heat transfer coefficient for freezer	$Wm^{-2}K^{-1}$
k	Fluid thermal conductivity	$Wm^{-1}K^{-1}$
$\overline{K}$	Partition Coefficient	
k_{wall}	Thermal conductivity of freezer wall	$Wm^{-1}K^{-1}$
K_v	Valve flow characteristic	
Pr	Prandtl number	
Q	Heat load	W
Re	Reynolds number	
SG	Specific Gravity of fluid	
T	Temperature of sample	$°C$
u	Velocity within film at location 'x'	ms^{-1}
U	Overall heat transfer coefficient for freezer	$Wm^{-2}K^{-1}$
$\dot{V}$	Fluid volumetric flowrate	m^3s^{-1}
V_{film}	Average velocity of laminar falling film	ms^{-1}
x	Distance from solid surface within film	m
x_{wall}	Thickness of freezer wall	m
β	Angle of surface to horizontal	
Γ_{min}	Minimum wetting rate of a falling film	$kgs^{-1}m^{-1}$

Symbol	Description	Units
δ	Average thickness of laminar falling film	m
ΔP	Pressure Drop	Pa
θ_{CA}	Contact angle between fluid and surface.	°
$\theta_{settling}$	Settling angle of a droplet rolling in a rotating ring.	°
ρ	Density of fluid	kgm^{-1}
μ	Dynamic viscosity	$Pa.S$
σ	Surface tension	Nm^{-1}
$\omega_{droplet}$	Rotational velocity of droplet	$°s^{-1}$

3.11 References

[1] M. Catapang, "Preliminary Investigation of a Rolling Droplet Freezer," Massey University School of Engineering and Advanced Technology, Palmerston North, New Zealand, 2015.

[2] E. Burkarter, L. S. Berlim, W. H. Schreiner, and C. K. Saul, "Spinning droplets on superhydrophobic surfaces," *Physics of Fluids,* vol. 22, no. 1, p. 012102, 2010.

[3] L. Mahadevan and Y. Pomeau, "Rolling droplets", *Physics of Fluids,* vol. 11, no. 9, pp. 2449-2453, 1999.

[4] J. P. Hindmarsh, A. B. Russell, and X. D. Chen, "Experimental and numerical analysis of the temperature transition of a freezing food solution droplet," *Chemical Engineering Science,* vol. 59, no. 12, pp. 2503-2515, 2004.

[5] J. P. Hindmarsh, A. B. Russell, and X. D. Chen, "Experimental and numerical analysis of the temperature transition of a suspended freezing water droplet," *International Journal of Heat and Mass Transfer,* vol. 46, no. 7, pp. 1199-1213, 2003.

[6] S. Rahman, *Food Properties Handbook*. CRC Press, 1995.

[7] A. Alizadeh *et al.*, "Dynamics of ice nucleation on water repellent surfaces," *Langmuir,* vol. 28, no. 6, pp. 3180-6, 2012.

[8] K. Li *et al.*, "Investigating the effects of solid surfaces on ice nucleation," *Langmuir,* vol. 28, no. 29, pp. 10749-54, 2012.

[9] R. Hays, D. Maynes, and J. Crockett, "Thermal transport to droplets on heated superhydrophobic substrates," *International Journal of Heat and Mass Transfer,* Article vol. 98, pp. 70-80, 2016.

[10] H. Li, I. V. Roisman, and C. Tropea, "Influence of solidification on the impact of supercooled water drops onto cold surfaces," *Experiments in Fluids,* Article vol. 56, no. 6, 2015.

[11] V. Bahadur, L. Mishchenko, B. Hatton, J. A. Taylor, J. Aizenberg, and T. Krupenkin, "Predictive model for ice formation on superhydrophobic surfaces," *Langmuir,* vol. 27, no. 23, pp. 14143-50, 2011.

[12] A. M. Talhat, V. Y. Lister, G. D. Moggridge, J. R. Rasburn, and D. Ian Wilson, "Development of a single droplet freezing apparatus for studying crystallisation in cocoa butter droplets," *Journal of Food Engineering,* vol. 156, pp. 67-83, 2015.

[13] R. C. Team, "R: A language and environment for statistical computing," ed. Vienna, Austria: R Foundation for Statistical Computing, 2014.

[14] L. Day, M. Broadhurst, and L. Samuelsson. (2016) New Zealand Sheep Milk-nutritional composition. *Food New Zealand*. 20,21.

[15] W. L. W. George F.W. Haenlein, "Sheep Milk," in *Handbook of Milk of Non-Bovine Mammals*, Y. W. Park, Ed.: Blackwell Publishers, 2006.

[16] M. A. Floriano and C. A. Angell, "Surface tension and molar surface free energy and entropy of water to -27.2.degree.C," *The Journal of Physical Chemistry,* vol. 94, no. 10, pp. 4199-4202, 1990.

[17] G. Hutching. (2016, 28/12/2016). *Government and private enterprise to spend $31.4m to develop sheep milk industry*. Available: http://www.stuff.co.nz/business/farming/83552095/government-and-private-enterprise-to-spend-314m-to-develop-sheep-milk-industry

[18] H. Sojoudi, M. Wang, N. D. Boscher, G. H. McKinley, and K. K. Gleason, "Durable and scalable icephobic surfaces: Similarities and distinctions from superhydrophobic surfaces," *Soft Matter,* Review vol. 12, no. 7, pp. 1938-1963, 2016.

[19] K. K. Varanasi, T. Deng, J. D. Smith, M. Hsu, and N. Bhate, "Frost formation and ice adhesion on superhydrophobic surfaces," *Applied Physics Letters,* vol. 97, no. 23, p. 234102, 2010.

[20] Y. Wang, J. Xue, Q. Wang, Q. Chen, and J. Ding, "Verification of icephobic/anti-icing properties of a superhydrophobic surface," *ACS Appl Mater Interfaces,* vol. 5, no. 8, pp. 3370-81, 2013.
[21] D. K. Mandal, A. Criscione, C. Tropea, and A. Amirfazli, "Shedding of Water Drops from a Surface under Icing Conditions," *Langmuir,* Article vol. 31, no. 34, pp. 9340-9347, 2015.
[22] E. Hernández, M. Raventós, J. M. Auleda, and A. Ibarz, "Concentration of apple and pear juices in a multi-plate freeze concentrator," *Innovative Food Science & Emerging Technologies,* vol. 10, no. 3, pp. 348-355, 2009.
[23] J. Sanchez, E. Hernandez, J. M. Auleda, and M. Raventos, "Review: freeze concentration technology applied to dairy products," *Food Sci Technol Int,* vol. 17, no. 1, pp. 5-13, 2011.
[24] Z. L. Zhang and R. W. Hartel, "A multilayer Freezer for freeze concentration of liquid milk," *Journal of Food Engineering,* vol. 29, no. 1, pp. 23-38, 1996.
[25] P. Chen and X. D. Chen, "A generalized correlation of solute inclusion in ice formed from aqueous solutions and food liquids on sub-cooled surface," *Canadian Journal of Chemical Engineering,* Article vol. 78, no. 2, pp. 312-319, 2000.
[26] F. L. Moreno, M. Raventós, E. Hernández, and Y. Ruiz, "Behaviour of falling-film freeze concentration of coffee extract," *Journal of Food Engineering,* vol. 141, pp. 20-26, 2014.
[27] A. Kramer, K. Wani, J. H. Sullivan, and I. Shomer, "Freeze concentration by directional cooling," *Journal of Food Science,* vol. 36, no. 2, pp. 320-322, 1971.
[28] R. American Society of Heating, E. Air-Conditioning, R. American Society of Heating, and E. Air-Conditioning, "2014 Ashrae handbook: Refrigeration," 2014.
[29] C. Marizy, A. Le Bail, J. C. Duprat, and Y. Reverdy, "Modelling of a drum freezer. Application to the freezing of mashed broccoli," *Journal of Food Engineering,* vol. 37, no. 3, pp. 305-322, 1998.
[30] (2017). *New Zealand's phase down of hydrofluorocarbons to ratify the Kigali Amendment to the Montreal Protocol and associated supporting measures: Consultation Document*. Available: https://www.mfe.govt.nz/sites/default/files/media/Climate%20Change/hfc-consultation-doc.pdf
[31] W. M. Rohsenow, J. P. Hartnett, and Y. I. Cho, Eds. *Handbook of heat transfer*, 3rd ed. New York: McGraw-Hill, 1998.
[32] D. C. Company, "Engineering and Operating Guide for DOWFROST and DOWFROST HD Inhibited Propylene Glycol-based Heat Transfer Fluids," ed, 2008.
[33] R. H. Perry, D. W. Green, and J. Maloney, O., *Perry's Chemical Engineers' Handbook Seventh Edition*. New York: McGraw-Hill, 1999.
[34] D. E. Hartley and W. Murgatroyd, "Criteria for the break-up of thin liquid layers flowing isothermally over solid surfaces," *International Journal of Heat and Mass Transfer,* vol. 7, no. 9, pp. 1003-1015, 1964.
[35] S. Paramalingam, J. Winchester, and C. Marsh, "On the fouling of falling film evaporators due to film break-up," *Food and Bioproducts Processing,* vol. 78, no. C2, pp. 79-84, 2000.
[36] M. S. El-Genk and H. H. Saber, "Minimum thickness of a flowing down liquid film on a vertical surface," *International Journal of Heat and Mass Transfer,* vol. 44, no. 15, pp. 2809-2825, 2001.
[37] C. A. Knight, "The contact angle of water on ice," *Journal of Colloid and Interface Science,* vol. 25, no. 2, pp. 280-284, 1967.
[38] M. L. Jackson, "Liquid films in viscous flow," *AIChE Journal,* vol. 1, no. 2, pp. 231-240, 1955.
[39] W. Wilke, "Wärmeübergang an Rieselfilme," VDI-Verlag, Düsseldorf, 1962.

[40] J. M. Auleda, M. Raventós, and E. Hernández, "Calculation method for designing a multi-plate freeze-concentrator for concentration of fruit juices," *Journal of Food Engineering,* vol. 107, no. 1, pp. 27-35, 2011.
[41] G. W. Latimer, *Official methods of analysis of AOAC International*. Rockville, Md: AOAC International, 2016.
[42] P. Chen, X. D. Chen, and K. W. Free, "An experimental study on the spatial uniformity of solute inclusion in ice formed from falling film flows on a sub-cooled surface," *Journal of Food Engineering,* vol. 39, no. 1, pp. 101-105, 1999.
[43] B. Habib and M. Farid, "Freeze concentration of milk and saline solutions in a liquid–solid fluidized bed," *Chemical Engineering and Processing: Process Intensification,* vol. 46, no. 12, pp. 1400-1411, 2007.
[44] L. Bayindirli, M. Ozilgen, and S. Ungan, "Mathematical-Analysis of Freeze Concentration of Apple Juice," *Journal of Food Engineering,* vol. 19, no. 1, pp. 95-107, 1993.
[45] S. K. Ratkje and O. Flesland, "Modeling the Freeze Concentration Process by Irreversible Thermodynamics," *Journal of Food Engineering,* vol. 25, no. 4, pp. 553-567, 1995.
[46] J. Sánchez, Y. Ruiz, M. Raventós, J. M. Auleda, and E. Hernández, "Progressive freeze concentration of orange juice in a pilot plant falling film," *Innovative Food Science & Emerging Technologies,* vol. 11, no. 4, pp. 644-651, 2010.
[47] T. Loho *et al.*, "A tensile technique for measuring frozen products adhesion strength: Application to stainless steel/frozen milk interaction," *Journal of Food Engineering,* p. 109772, 2019.
[48] J. L. Palacios, E. C. Smith, Y. Zhu, and J. L. Rose, "Global ultrasonic shear wave anti-icing actuator for helicopter blades," in *Annual Forum Proceedings - AHS International*, 2007, vol. 2, pp. 1512-1520.
[49] H. Habibi, L. Cheng, H. Zheng, V. Kappatos, C. Selcuk, and T. H. Gan, "A dual de-icing system for wind turbine blades combining high-power ultrasonic guided waves and low-frequency forced vibrations," *Renewable Energy,* Article vol. 83, pp. 859-870, 2015.
[50] H. Tan, G. Xu, T. Tao, X. Sun, and W. Yao, "Experimental investigation on the defrosting performance of a finned-tube evaporator using intermittent ultrasonic vibration," *Applied Energy,* vol. 158, pp. 220-232, 2015.
[51] H. Tan, G. Xu, T. Tao, S. Zhang, and A. Luo, "Investigation on the ultrasonic propagation mechanism and its application on air-source heat pump defrosting," *Applied Thermal Engineering,* vol. 107, pp. 479-492, 2016.
[52] J. Palacios, E. Smith, J. Rose, and R. Royer, "Ultrasonic de-icing of wind-tunnel impact icing," *Journal of Aircraft,* Article vol. 48, no. 3, pp. 1020-1027, 2011.
[53] D. Li and Z. Chen, "Experimental study on instantaneously shedding frozen water droplets from cold vertical surface by ultrasonic vibration," *Experimental Thermal and Fluid Science,* vol. 53, pp. 17-25, 2014.

Chapter 4: Ice Morphology in Frozen Ovine Milk.

4.1 Chapter Summary

Ovine milk was separated into several fractions: whole sheep milk, skim sheep milk, and a casein-free sheep milk ultracentrifugate. A simulated sheep milk ultrafiltrate was prepared by formulation from pure compounds. These liquids along with pure water were frozen at freezing front velocities from 0.5 μms^{-1} to 50 μms^{-1} and the interface morphologies were observed.

The advancing ice interface displayed several different morphologies. The interface generally became more complicated as the freezing front velocity increased. The transitions between interface morphologies occurred at lower velocities as the number of components in the system increased e.g. transitions occurred at lower velocities in samples with casein micelles than in samples without. The feature spacing in advancing interfaces decreased with increasing freezing front velocity.

Raw ovine milk was frozen rapidly with unidirectional heat flow (DF), slowly in a larger volume with no dominant heat flow direction (SF), and extremely rapidly by immersion in liquid nitrogen (RF). These samples were imaged using scanning electron cryomicroscopy (Cryo-SEM), and the ice morphology and distribution of milk solids was analysed.

There were significant differences in ice morphology between the RF, DF, and SF samples imaged by Cryo-SEM, with the ice crystals and milk solids trapped between ice crystals being significantly smaller in DF samples. Ice crystals in DF samples were mostly aligned with the direction of heat flow and had a lamellar form. In some SF samples, crystalline lactose was observed. None was observed in DF samples. there was an extremely fine network of ice crystals and unfrozen solids observed in RF samples.

4.2 Introduction.

Frozen storage has been proposed for sheep milk, and has been found to be appropriate under certain conditions[1, 2]. However it has also been linked to decreases in total solids, fats and non-fat milk solids[3],development of rancid flavours[4], increased coagulation time and decreased curd firmness in cheese making[5], casein destabilisation [6] and formation of insoluble complexes [2]. These effects are linked to the temperature of storage [7], the speed of freezing [8], the crystallisation of lactose [9, 10], and the salt balance in the unfrozen phase [4, 7, 10].

A greater understanding of the freezing process should allow freezing conditions to be selected that can minimise the damage caused by the freeze/thaw process.

The time and temperature of storage have a significant effect on the storage stability of milk. Storage below -20°C is recommended, with stability decreasing at higher temperatures[7]. At temperatures of -27°C or below, the high viscosity of the unfrozen phase, and low kinetic energy of the milk components limits both crystallization of lactose and aggregation of protein.

Wendorff [1, 6] concludes that ovine milk should be frozen rapidly and stored at -27°C for maximum stability, and if milk is stored at -12°C, then it should not be stored for longer than 3 months.

Rapid freezing has also been recognised for a long time as a method of preserving the fat emulsion in milk, as it prevents fat separation and the growth of large destructive ice crystals [8].

Work conducted on freeze-concentration of aqueous solution shows that the partition coefficient $\overline{K} = C_s/C_l$, where C_s and C_l are the concentrations of the solute in the solid and liquid respectively, is proportional to the freezing front velocity v_f and inversely proportional to the freezing point depression of the system[11].

$$\overline{K} \propto f(v_f), \overline{K} \propto 1/f(\Delta T_{FPD}) \quad (4\text{-}1)$$

Rapid freezing involves large temperature gradients and therefore ice growth velocities that predominate in a single direction, parallel to the established temperature gradient.

Milk is a multi-phase system; incorporating a soluble phase containing salts, lactose, and soluble proteins; a colloidal protein phase of casein proteins together with colloidal salts in micelles [12]stabilised sterically and electrostatically by κ-casein; and an emulsion of milk fat globules coated with a phospholipid and protein rich membrane. As a result, the freezing front in milk must interact with a complicated system of particles with different sizes and surface properties.

The interaction of advancing solid/liquid interfaces with particles, and the morphology of these advancing interfaces has been studied extensively in the metallurgical sciences, and in food and pharmaceutical processing science[13]. The interaction between living cells and advancing ice fronts has been observed and modelled[14].The survival of red blood cells during cryopreservation, has been studied from the point of view of directional freezing, and survival rates linked to freezing speeds and unfrozen liquid concentration [15].

Freeze texturing is a method to produce structure in meat analogues, similar to the traditional Japanese method of producing frozen soybean curd called kori-tofu[16, 17]. An ice front moving parallel to the heat flux forms a network of needles or dendrites of ice in the protein, which persists as structured pores when the liquid is melted and removed. The fineness of this network increases as freezing front velocity increases[18].

Freeze-drying, or lyophilisation, is the removal of water from a substance by sublimation of frozen water (at or) below atmospheric pressures. The quality of freeze-dried products is generally high, but the cost of this drying method is also high, so freeze drying is typically used for high-value, heat sensitive food and pharmaceutical products. The morphology of the ice in the product significantly affects the performance of freeze drying, and the characteristics of the final product [16]. Slow freezing generally leads to larger crystal sizes, larger pores and increased mass transfer through the pores upon drying. Directional freezing leading to parallel ice crystals with low tortuosity may increase mass transfer in one direction, useful in the freeze drying of foods [16].

However, despite the importance of the freezing step in frozen storage and a range of food processing steps, the morphology of ice in frozen milk has received limited study. Therefore, the work in this study aimed to investigate the effects of freezing front velocity and milk components on the morphology of frozen milks.

A 'Bridgeman furnace' [19]and Cryo-SEM were used to study the interaction between freezing front velocity and ice morphology in directionally frozen milk. A Bridgeman furnace allows the microscopic observation of freezing fronts at different freezing front velocities. Cryo-SEM is a method of electron-microscopy that allows the imaging of water rich samples without dehydration and chemical fixation. It has been used to study the structure of milk fat globule membranes in native milk and fat globule dispersions[20]. This makes it an ideal method to study the structure of ice in milk samples, with minimum changes due to sample preparation processes.

4.3 Materials and Methods.

4.3.1 Cryo-SEM

4.3.1.1 Materials and Equipment

Fresh Sheep milk was collected from a local farm and stored in a liquid form up 48 hours below 4°C until frozen for analysis. A subsample of this milk was stored at-80°C until nutritional analysis.

Details of the equipment used in this chapter is given in detail in Chapter 2.

4.3.1.2 Methods.

The raw sheep milk was frozen according to the following methods:

Slow frozen (SF) samples: Six samples of milk (100 mL) were added to 100 mL plastic containers, and placed inside two polystyrene insulated boxes. One box was placed inside a freezer at -10°C, and the other in a freezer at -30°C. The temperature profiles during freezing were measured with datalogging temperature probes inserted into representative containers and these are shown in Figure 4-1. After 48 hours frozen storage the frozen milk was removed from the plastic containers and shattered under liquid nitrogen to yield samples an appropriate size for SEM imaging (5-10 mm). The shattered samples were then stored at -80°C until imaging to prevent any further ice crystal growth, or any changes due to various forms of recrystallization.

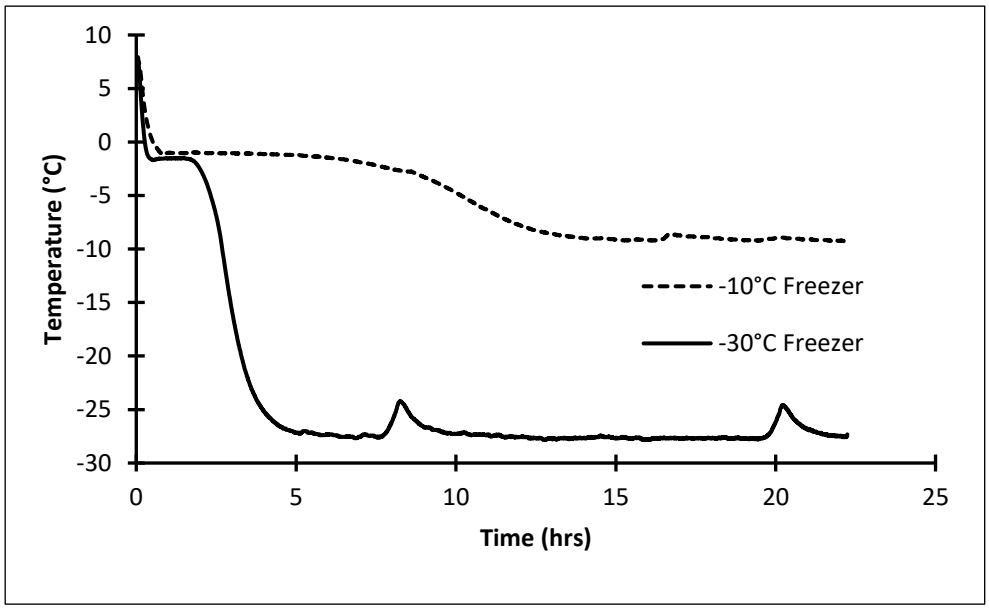

Figure 4-1: Temperature profiles during the slow freezing of milk samples.

Directionally Frozen (DF) samples: An aluminium plate with interior cooling channels was cooled with the Julabo FL300 chiller (discussed in Chapter 2) operating at -20°C. Raw Milk was placed in a mould on the plate to a thickness of 3 mm and removed with a cooled knife once it was fully frozen. The flake of directionally frozen milk was placed in a pre-cooled container and stored at -80°C until imaging.

A second directionally frozen sample was prepared by placing a microscope mounting stub on a cooled aluminium plate, and then freezing a flake onto this surface: this was removed with the sample attached and stored at -80°C until imaging. This allowed imaging perpendicular to the direction of crystal growth.

To prepare extremely rapidly frozen milk, a droplet of milk was placed on a stub on the cryo-SEM mount, and then immersed in liquid nitrogen under vacuum. This frozen droplet was transferred immediately to the electron microscope after freezing.

Imaging was conducted at the Electron Microscopy facility at Victoria University of Wellington, using a JEOL 6500F Scanning Electron Microscope, with Gatan Alto 2500 cryo unit attached.

All samples were prepared according to the following steps:

1. Sample is loaded into the cryo-chamber and cooled to -120°C.
2. The sample is sheared to present a fresh internal surface for imaging.
3. The sample temperature is raised to -95°C and held for 7 minutes to erode ice from fracture face and improve structure clarity.
4. The sample is sputtered with Platinum for 3 120s cycles, and then loaded into the SEM.

Image analysis of collected micrographs was conducted using the Fiji image processing package[21], an open source software package based on ImageJ [22].

4.3.2 Directional Freezing.

4.3.2.1 Methods

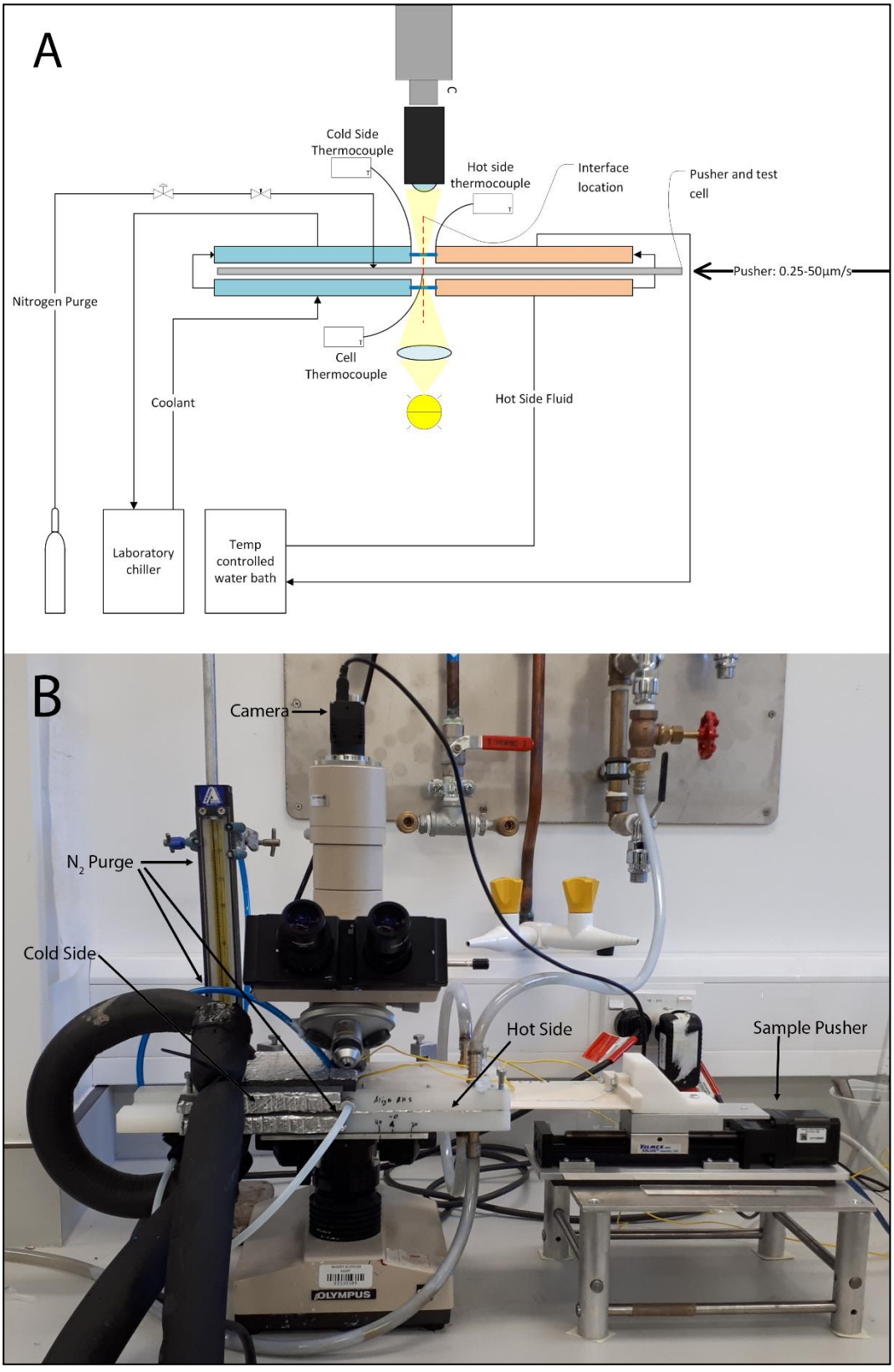

Figure 4-2: The microscope system for observing the morphology of advancing ice fronts, as described in section 3.2.1A schematic of the system is shown above, and the system as installed is shown below.

The directional freezing system consists of a microscope with a USB connected camera, a custom stage with two pairs of aluminium plates with coolant channels, and a system to move a test cell between the two pairs of plates. One pair of temperature-controlled plates was maintained at room temperature and the other maintained below freezing by a Julabo FL-300 chiller, using a 50% solution of ethylene glycol as a coolant. This is shown schematically in Figure 4-2 A, and as installed in Figure 4-2 B.

An aliquot (75 µL) of each solution to be tested was sandwiched between two microscope slides with the edges sealed by vacuum grease to reduce evaporation of test solution. This is shown in Figure 4-3. The test cell is placed in a 3-D printed pusher which is moved by a Velmex XSlide (Velmex, Inc., Bloomfield, NY, USA) motorised linear slide.

The linear slide controlled the speed between 0.25 μms^{-1} to several mms^{-1}. The system was run at speeds of up to 50 μms^{-1} in order to allow sufficient heat transfer between the test cell and the plates.

Dry Nitrogen is introduced into the cold stage and the region around the windows of the cold stage to prevent condensation and consequent frost growth from interfering with the observation of freezing in sample cells.

Thermocouples were placed at the edges of the temperature-controlled plates closest to the freezing interface to monitor the temperature gradient across the interface. A third, thin-wire welded-tip thermocouple with a tip diameter of 75µm was placed at the centre of the long side of the test cell to monitor the temperature gradient experienced as the cell moved between the plates.

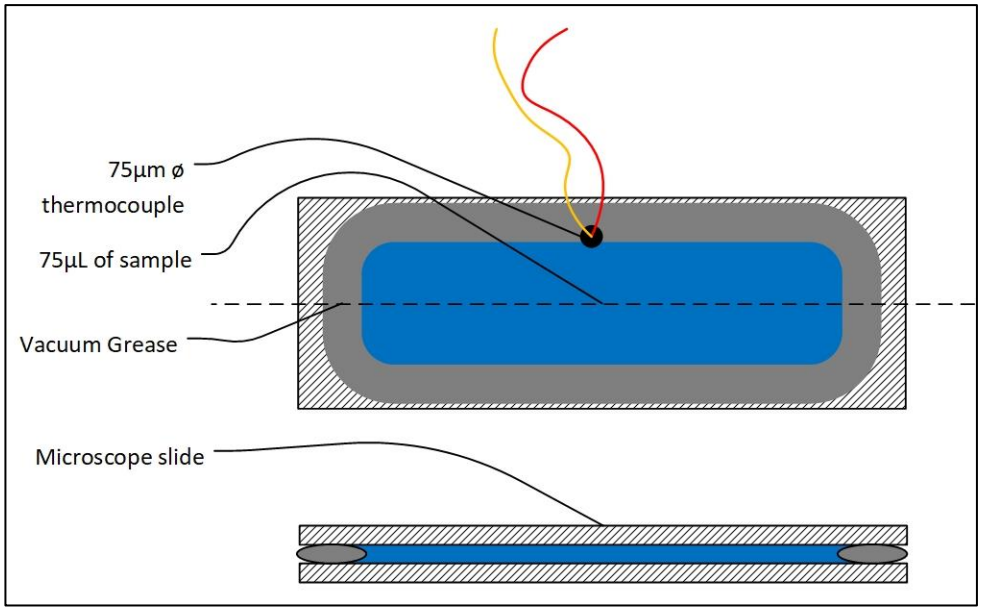

Figure 4-3: Assembly of microscope slides, showing the position of thermocouple and vacuum grease used to seal the test sample. A top view and section view are shown.

As the spatial temperature gradient is fixed by the temperature of the two pairs of plates and the distance between them, the freezing interface is in a fixed location relative to the microscope, corresponding to the equilibrium freezing temperature at a given freezing front velocity. As the freezing interface is in a fixed location relative to these two pairs of plates, the freezing interface advances from the perspective of sample when the sample cell is moved at a fixed velocity from the hot set of plates to the cool set. The slide velocity therefore corresponds exactly to the freezing front velocity.

The freezing interface is observed using a Nikon 4x objective lens. Image analysis was conducted using the Fiji image processing package[21], an open source software package based on ImageJ [22].

4.3.2.2 Materials

The test solutions studied were as follows:

- RO-water
- Simulated Sheep Milk Ultrafiltrate (SSMUF)
- Whole Raw sheep milk (WSM)
- Skim sheep milk (SSM)
- Sheep milk ultracentrifuge supernatant. (SMUC)

SSMUF is a buffer simulating the soluble phase of milk, with the omission of soluble proteins. The composition is shown in Table 4-1. It was prepared by following the method for bovine SMUF as described by Jenness and Koops[23], adjusted by the ratio of ultrafiltratable salts in ovine and bovine milk [24], with the addition of lactose to the concertation commonly found in ovine milk.

Table 4-1: Composition of the SSMUF sample observed in directional freezing studies.

Solute	Concentration ($mmolL^{-1}$)
KH_2PO_4	5.31
K_2HPO_4	6.81
$K_3C_6H_7O_7.2H_2O$	0.15
$Na_3C_6H_7O_7.2H_2O$	2.45
$CaCL_2.2H_2O$	0.97
$Mg_3(C_6H_5O_7)_2.9H_2O$	8.14
KOH	1.00
K_2CO_3	5.08
Lactose	2.74

Milk was collected from a local farm and preserved by the addition of NaN_3 to a concentration of 30 ppm. NaN_3 was chosen due to its effectiveness at low concentrations, minimising the change in colligative properties due to the addition of preservative. The milk was stored at or below 4°C until further preparation or analysis.

Skim Milk was obtained by centrifuging milk at 3000 g for 20 minutes at 20°C. The fat was removed, and the skimmed milk was reserved for analysis and ultracentrifugation.

The casein phase of the milk was removed from the milk by ultracentrifugation at 80,000 g for two hours at 20°C. This temperature was selected to reduce the amount beta-casein solubilised. The resulting serum phase was reserved for analysis and the casein was discarded.

The total solids of the prepared milk samples were determined according to AOAC method 990.20 [25]. Crude Protein was determined by a Kjeldahl method adapted from AOAC method 991.20 utilising a Kjeltec KT200 distillation system [25]. Fat was determined according to AOAC method 989.05 [25]. The ash content was determined according to AOAC method 945.46 [25]. Lactose was determined by difference.

The sheep milk serum is free from micellar casein and therefore its protein fraction consists mostly of whey and other soluble proteins. This value was used to estimate the relative compositions of casein and whey in all samples.

Table 4-2: Composition of samples observed in directional freezing studies. All values are % m/m.

Milk	Fat	Protein	Whey	Casein	Ash	Lactose	Total Solids	Aqueous Phase	Water
Whole Sheep Milk (WSM)	6.90	5.43	1.03	4.40	0.92	3.81	17.05	88.70	82.95
Skimmed Sheep Milk (SSM)	0.39	5.63	1.43	4.23	1.00	5.23	12.27	95.38	87.73
Sheep Milk Serum (SMUC)	0.25	1.52	1.52	0	0.52	5.58	7.92	99.75	92.08

4.3.3 Very-High-Speed Freezing

Samples were placed on microscope slides and these slides were placed on the chilled plate of an Instec HCS622V cold microscope stage. Glycol coolant at -16°C was pumped through the cooled stage, and the stage was maintained above freezing with a resistive heater. When the resistive heater was turned off the stage and sample cooled rapidly, and the sample supercooled. The sample nucleated suddenly and the resulting rapid recalescence was imaged at 500 fps with a Megaspeed MS40K high speed camera mounted on the microscope, through a 10x objective lens and a 3.3x eyepiece lens. The temperature profile and the nucleation temperature were recorded using the thermocouples in the cold stage.

4.4 Results and Discussion

Ovine milk and its fractions are very far from the ideal or model systems often used in colloidal freezing studies. The colloidal dispersion in milk consists of fat globules, casein micelles and globular whey proteins in a solution of milk salts, lactose and other small components [12].

The size of the colloidal particles varies significantly, with fat globules in unhomogenised sheep-milk being, on average, 3.30 µm in diameter, and casein micelles averaging ca. 193 nm in diameter[26]. The whey proteins are dispersed at a molecular level[27].

The aqueous phase consists mostly of low molecular weight solutes, and therefore the colligative properties of this phase can be approximated by Raoult's law. The freezing point depression in raw ovine milk is primarily due to the lactose and salt content of the milk [12], which results in a freezing point of -0.57°C [26].

Milk composition can also vary significantly as a result of seasonality[28], length of lactation[29], nutrition[30], parity[31], farming system[31], breed [32]and inter-animal variations. The complexity of this system makes quantitative, mechanistic description of the behaviour of the advancing ice interface in ovine milk or milk fractions very difficult.

The majority of work investigating the freezing of colloids has considered model systems of monodisperse particles in precisely defined liquid phases. These particles are typically ceramics, polymers, glasses or metals, and the liquid phases are commonly water, or organic solvents such as camphor or tert-butyl alcohol[33]. When these studies consider inter-particle interactions, they typically use a hard sphere model, which may not be suitable for the colloidal components of milk. One of the only other areas where the colloidal freezing of materials of comparable complexity is considered in detail is the study of frost heave, where're relatively pure ice lenses

form in freezing soils[34]. In these studies, predictive models are based upon bulk soil properties, as models based on ice physics are “a nightmare to understand” [35].

4.4.1 Very-High-Speed Freezing

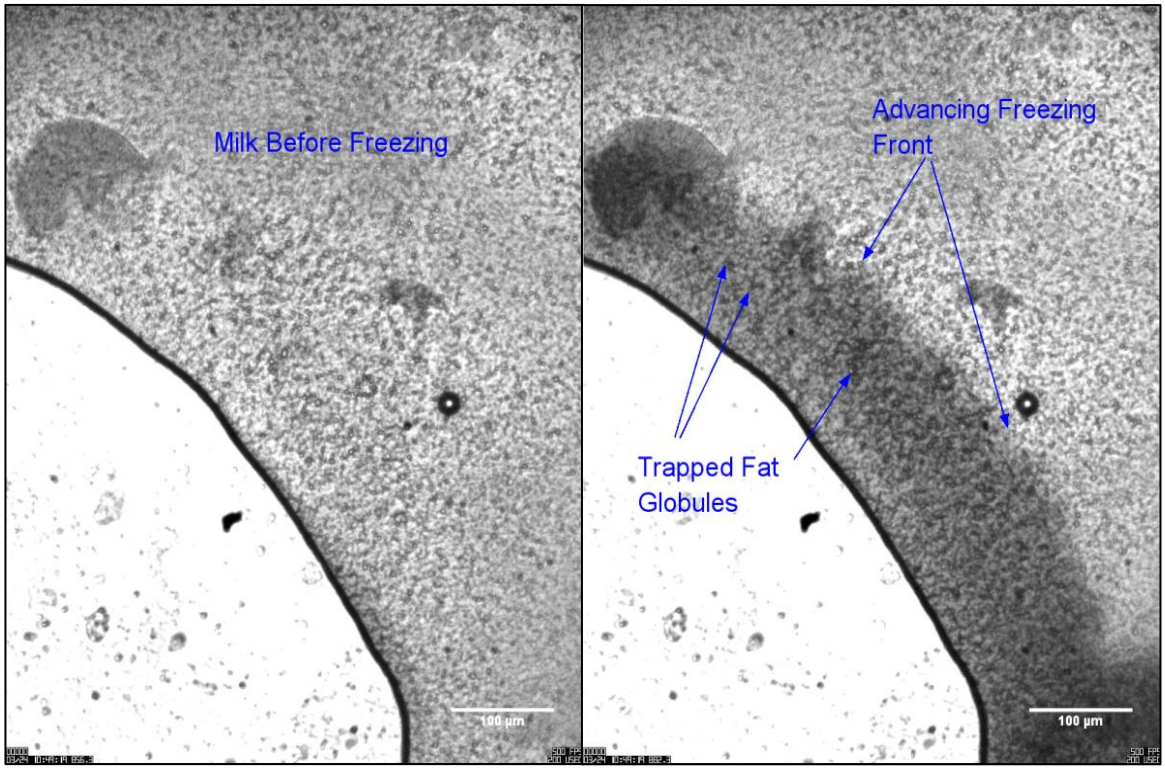

Figure 4-4: An advancing freezing front in milk being frozen at very high freezing front speeds after supercooling and nucleation. Nucleation in the sample occurred at the air/fluid interface seen at the the bottom left of each image. The left hand image is the sample immediately prior to nuclearion. The sample approximately 10ms after nucleation is seen on the right. The darker area is the frozen region. Milk globules are engulfed and trapped in place by this advancing freezing front.

Samples typically nucleated at a temperature of -8°C to -9°C. This is higher than the typical nucleation temperature seen in DSC studies, as described in Chapters 3 and 6. Milk sandwiched between slides has a larger contact area than sessile droplets in DSC pans, so heterogenous nucleation rates are higher. A typical cooling curve is shown in Figure 4-5. The freezing front velocities (as determined the previously calibrated image field size, and camera frame rate) of milk frozen at very high speeds averaged 21.2 mms^{-1}, with a standard deviation of 4.8 mms^{-1}. The freezing front in these tests was dendritic in form, with extremely fine dendrites. Freezing began at three-phase (milk/air/slide) interfaces. In all tests the fat globules were entrapped within the advancing ice front. These freezing front velocities are comparable to those found in the literature for crystal growth rates in highly supercooled water, and is at the limit of diffusion driven crystal growth for the measured degrees of supercooling[36].

It is also difficult to supercool large volumes of liquid reliably, as homogenous nucleation is probabilistic and volume dependent, therefore a stable nucleus is more likely to form in a large volume at a given degree of supercooling or supersaturation than a small volume. Large volumes also tend to have a larger number of sites for heterogenous nucleation.

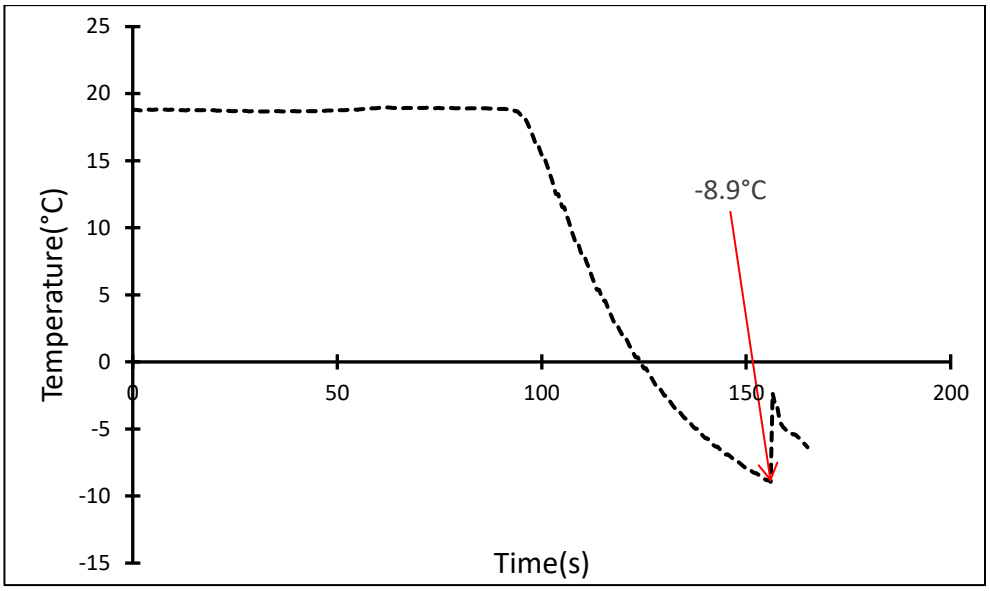

Figure 4-5: A typical cooling curve during microscopy studies of the freezing of supercooled ovine milk. The nucleation temperature of -8.9°C is labelled. Nucleation can be detected by the sudden increase in temperature as a result of the release of latent heat.

The combination of extremely high required heat fluxes, and the difficultly of reliably supercooling large volumes, makes exploiting supercooling in order to form a fine ice structure infeasible on a large scale. Therefore, the ice growth behaviour observed in these studies is unlikely to be representative of that found in products frozen by industrially common freezing methods. Pressure assisted freezing, which is discussed more in Chapter 1, may be used to form fine ice networks, however the extremely high-pressure requirements mean that it is not yet commercially applied.

4.4.2 Controlled Speed Directional Freezing

4.4.2.1 Temperature Gradients

The spatial temperature profile experienced by selected samples is shown in Figure 4-6. There is some variation in the initial temperature read by the temperature probe, as the initial position of the probe varied between runs, however the temperature gradient experienced by the probe in the temperature region of interest was identical between runs.

Table 4-3: Cooling rates experienced by a region of sample as it appraches and passes the freezing front.

Cooling Rate		
V_f	**Cooling Rate (Ks^{-1})**	**Cooling Rate ($Kmin^{-1}$)**
2 μms^{-1}	0.005	0.3
5 μms^{-1}	0.013	0.8
10 μms^{-1}	0.027	1.6
20 μms^{-1}	0.050	3.0
30 μms^{-1}	0.075	4.5

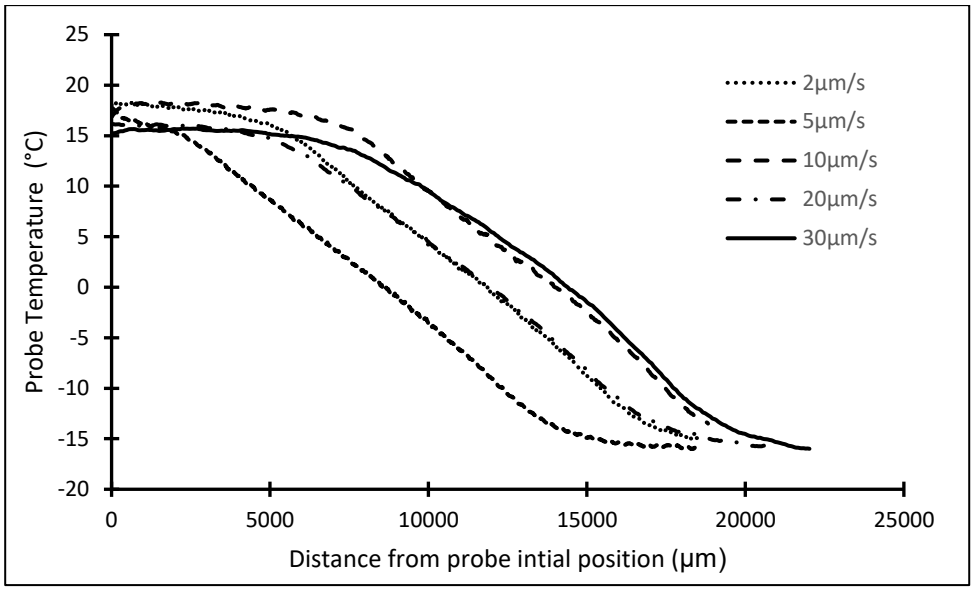

Figure 4-6: Temperature profiles indicative of those experienced by samples being frozen in the custom microscope stage described in section 3.2.1. A 0.75 mm welded tip thermocouple probe was placed at the centre of the long axis of the sample slide, and the temperature measured as it moved from the hot side to the cold side. As can be seen in the graph, samples experienced identical spatial temperature gradients, despite differing sample velocities.

The temperature histories experienced by the probe in selected runs are shown in Figure 4-7. While the temperature profiles are the same between tests run at different freezing front velocities, the probe measurements confirm that the cooling rate is significantly larger at the higher speeds, and that for the speeds tested is not limited by heat transfer into the experimental cell.

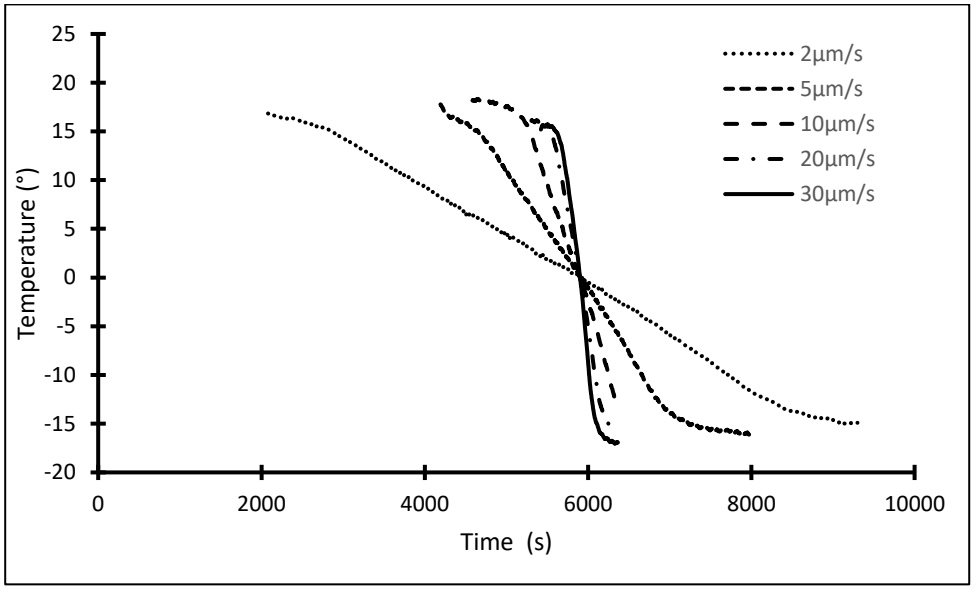

Figure 4-7: Temperature histories of those experienced by samples being frozen in the custom microscope stage. The profiles were measured with a 0.75 mm welded tip thermocouple attached to the centre of the long axis of the sample slide. This time-based temperature profile shows the cooling rates experience by a region of sample as it travels through the microscope stage.

The cooling rates experienced by a region of sample as it goes through the phase transition are shown in Table 4-3. These cooling rates were determined from the straight-line portions of the temperature histories in Figure 4-7.

4.4.2.2 Morphology Map in sheep milk

Similar to colloidal systems encountered in freeze casting, sheep milk and its fractions display a number of different morphologies as v_f increases. The morphology also changes as the fluid being frozen changes. The fluids frozen ranged from RO water, to the very complex milk system. The morphologies observed are shown in Figure 4-8. In (A), the interface is planar. The columnar interface is shown in subsections (B)-(E). In (D) and (E) the columnar interface begins to show instabilities of its own. In (D), this is present as splitting at the tip of the columns, and sinusoidal variations on the hot side of the columns (the side of the columns facing the bulk of the melt and towards a higher temperature). In (E), the columns no longer display tip splitting, but appear more needle-like, with small sinusoidal variations on the hot side. These variations can continue to grow into short parabolic or columnar fingers as can be seen in (F). These side branches, and the main brain can also be very sharp and needle-like, as is shown in (G). Two dendritic forms of growth are shown in (H) and (I).

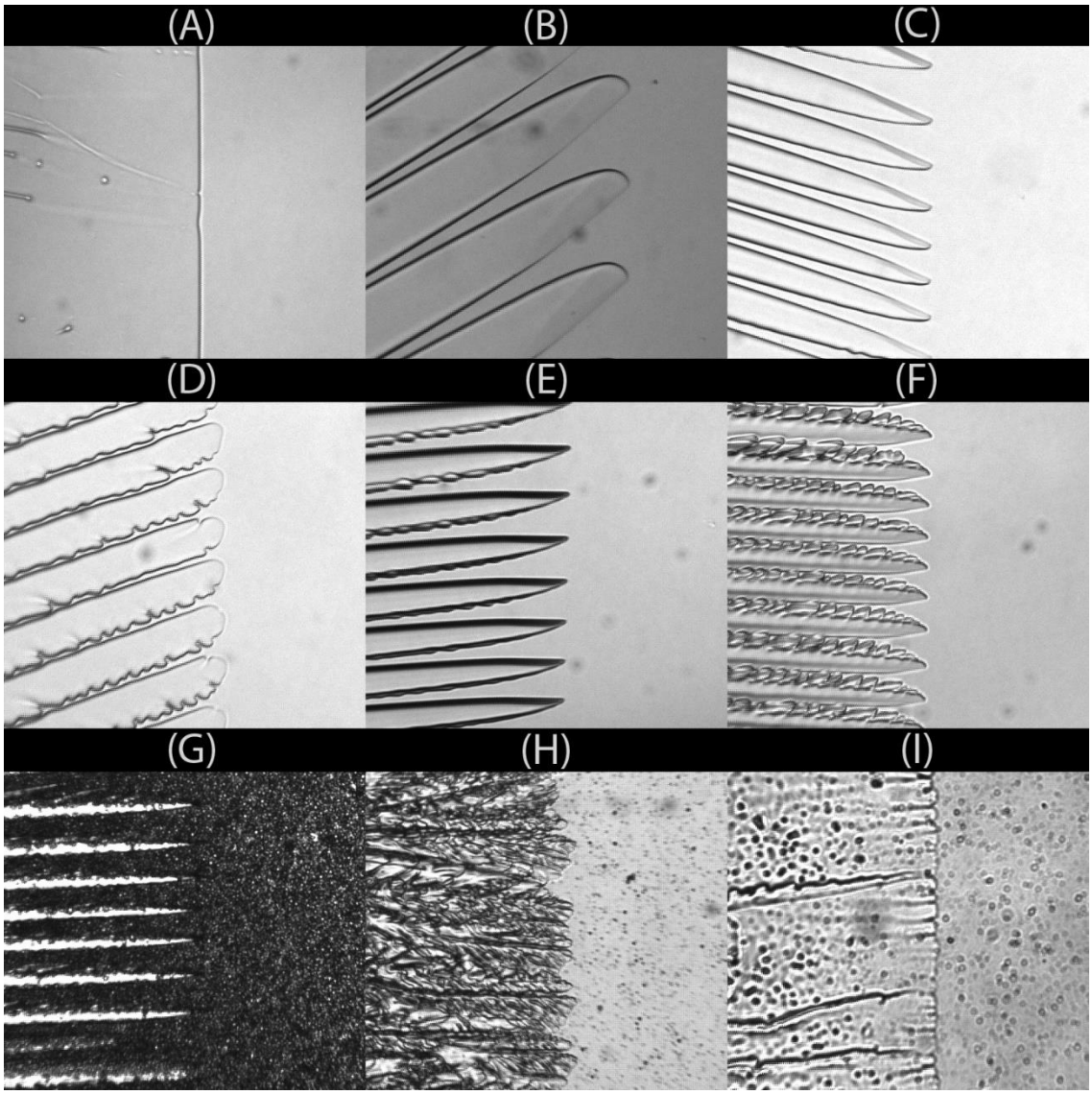

Figure 4-8: Morphologies observed in an advancing ice/fluid interface. A planar interface is shown in (A), columnar interfaces are shown in (B) and (C). Columnar interface with ripples on the hot side of the columns are shown in (D), (E) and (F), with the ripples being larger on (F). In (H) there are secondary needle-like columns on the hot side of the columns, and the columns themselves are needle-like in form. (G) shows a highly dendritic interface. (I) Shows an interface which is dendritic but appears planar at the leading edge. All images were captured during this study. (A)-(F) are images of morphologies in SSMUF, (G) and (I) are images of morphologies in SSM, and (H) is an image of a morphology in WSM. v_f varied from 0.5- 50 μms^{-1}.

The interface morphologies are mapped as a function of the v_f and the "complexity" of the fluid in Figure 4-9. Morphology maps have been presented in freeze-casting literature [37], these maps display behaviour as a function of particle size and v_f, for a number of systems. However, these systems are considerably simpler than milk, having pure solvents, or tightly defined solutions as a continuous phase, and typically monodisperse particle size distributions. The particles used are themselves significantly simpler, as are their interactions with the solvent and solutes, and each other. Therefore, a map of morphology against particle size and v_f would be inappropriate, and an arbitrary "complexity" axis was used in place of particle sizing.

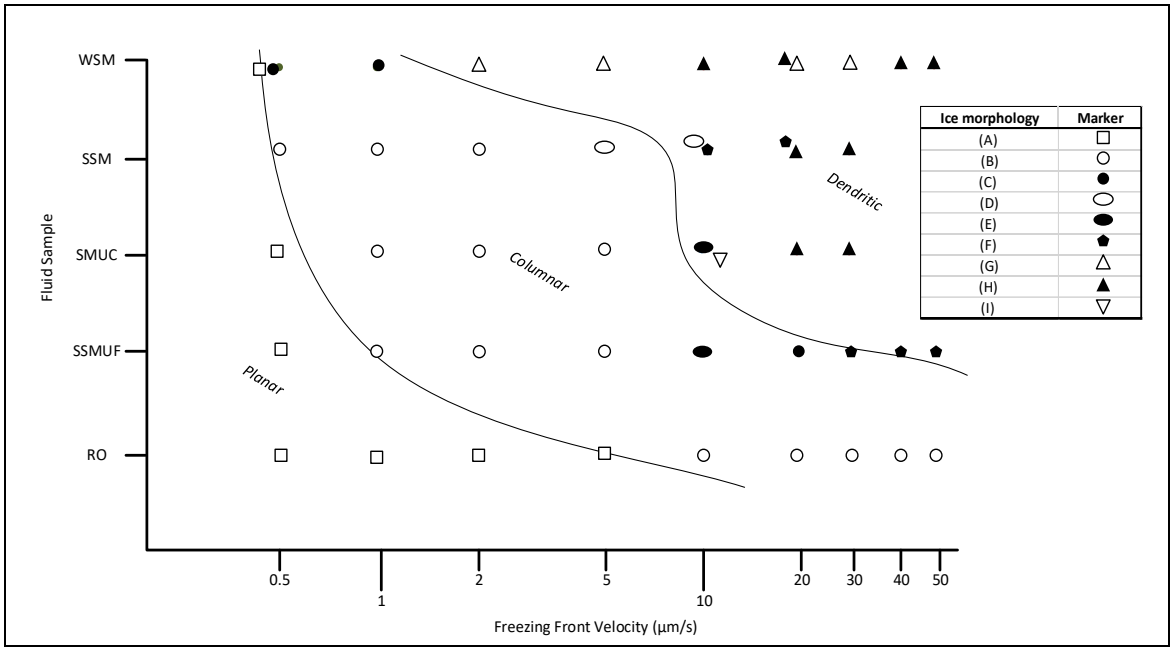

Figure 4-9: A map of the morphologies encountered in advancing ice/fluid interfaces in milk fractions at constant spatial temperature gradient of ~360Kmm^{-1} and varying freezing front velocities. The freezing front velocity is presented on a logarithmic scale, and the fluids tested are listed in increasing "complexity". Examples of morphologies encountered are shown in Figure 4-8. The regions of the map corresponding to various morphologies are labelled.

As the aim of this study is not to provide a quantitative and fully predictive description of the system, but rather a qualitative explanation of the complex behaviour of freezing milk, this axis of increasing milk complexity is effective. Each milk fraction adds a new factor to the behaviour of the system; Pure water is affected by the interaction between the thermal gradient and freezing front velocity, and the surface energy and crystal growth kinetics at the advancing interface; SSMUF adds the effects of solute species being rejected and diffusing away from the interface, and effects of the solute concentration gradient near the interface, and the surface energy of the interface; SSMUC introduces molecular scale whey protein species and their interaction with the interface; More significant colloid interactions are introduced with the casein micelles in SSM (approximately 190 nm); With WSM, the colloidal fat system (approximately 3µm) also interacts with the interface.

The critical speed for the transitions between interface morphologies differs between fluids studied and tends to decrease for the more complex fluids. Mechanisms governing instability formation are covered in section 4.2.3 below .

In RO water, a planar interface is maintained until 5 µms^{-1}, at a spatial temperature gradient of 38 Kcm^{-1}. Between 5-10 µms^{-1} the planar interface transitions to a columnar interface. No transitions to dendritic growth were seen for the speeds or temperature gradients studied.

In SSMUF the interface was planar at 0.5 μms^{-1} ; transition from planar to columnar interface occurred at a freezing front velocity of 0.5-1 μms^{-1}. The interface was columnar until 50 μms^{-1}, with ripples on the hot side of the columns occurring above 10 μms^{-1}, and the columns having short secondary fingers above 30 μms^{-1}.

The advancing interface in SMUC transitions from a planar interface to columnar at a freezing front velocity of 0.5-1 μms^{-1}, and displayed dendritic growth over 10 μms^{-1}; however some samples at 10 μms^{-1} had columnar interfaces. Indeed, in several samples two different interface morphologies were present at different regions of the interface, indicating that the transition between different morphologies may be the result of differing initial conditions or initial crystal orientations.

The interface in SSM was columnar even at v_f= 0.5 μms^{-1}. The transition to dendritic growth occurs at 20 μms^{-1}. At 20 μms^{-1}, some samples also showed needle-like growth with large side branches. At 30 μms^{-1} and above all samples showed a dendritic interface.

In WSM, the interface was columnar above 0.5 μms^{-1}, and became dendritic at v_f >2 μms^{-1}. At v_f > 10 μms^{-1} some samples displayed needle like interfaces with large side branches.

The α-value of a solvent is calculated from the latent heat ΔH_f at the equilibrium temperature T_f the gas constant R and a factor dependent on the crystallographic environment of the interface ξ.

$$\alpha = \frac{\Delta H_f \xi}{R T_f} \tag{4-2}$$

This value determines whether crystal growth occurs in a dendritic or faceted manner. Dendritic growth generally occurs when α<1[38]. The entropy of melting h_E/RT_E of water is approximately 2.6 JK^{-1} [39, 40], yet water readily forms dendrites, as ξ has a typical maximum of 0.5-1 for the close packed crystal plane and less for others. This effect of plane on the dendritic growth characteristics could cause some samples to display both dendritic and columnar growth under identical conditions, due to the interface being imaged at a location where two crystals of different orientation are growing in parallel.

The spacing of columnar and needle-like interface features during freezing was measured. The distance from the most advanced tip of one feature to the most advanced tip of the next feature was considered the feature spacing. Where interfaces displayed planar or highly dendritic morphology the spacing was not measured.

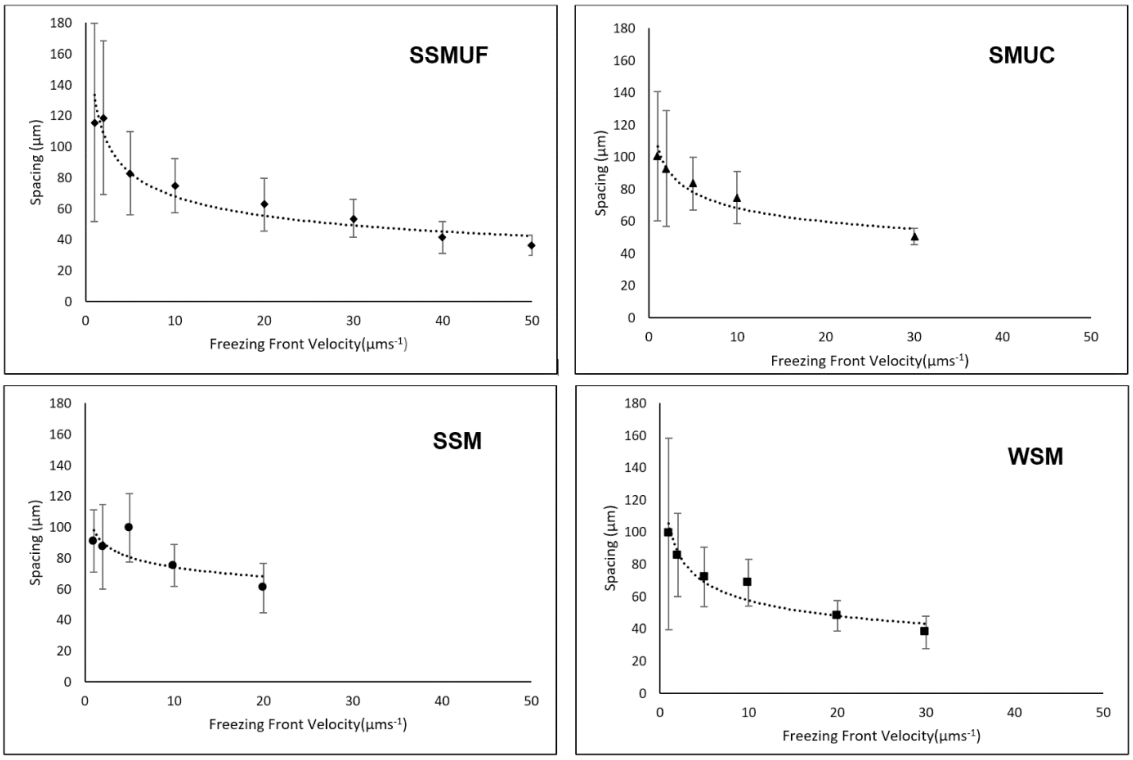

Figure 4-10: Feature spacing in advancing interfaces follows a power law relationship with interface speed. The measured values for feature spacing are plotted against speed above, along with power law fitted trendlines. Error bars are ±1σ of the feature spacing observed across all runs and all features at a particular set of conditions. Observations which were highly dendritic are not shown, due to the lack of repeatable features.

Figure 4-10 A-D shows the feature spacing for each milk fraction measured. The relationship between feature spacing λ and interface velocity v_f in freezing water-based colloids has been described as a power law ($\lambda = A \cdot v_f^{-n}$) by several authors [37, 41, 42]. Power law curves were fitted to the results for each fluid and the prefactor A and exponent n , and the results are shown in Table 4-4

Table 4-4: Power-law curve parameters for the lines of best fit as shown in Figure 4-10.N refers to the number of trials conducted to get the data points for a particular graph.

Fluid	A	n	N	R^2	TSS	ESS	RSS
SSMUF	133	0.29	24	0.93	0.253	0.236	0.017
SMUC	107	0.19	15	0.92	0.054	0.050	0.004
SSM	98.1	0.12	15	0.57	0.028	0.016	0.012
WSM	105	0.26	18	0.92	0.123	0.113	0.010

The prefactor A has been reported to increase with increasing solid phase volume [37].This is fairly constant in all the samples measured, despite the variation in total solids from roughly 5% to 17%, however the particle loadings vary from 0% to approximately 12 % , and most previous freeze casting work considers particle loadings higher than this level. An increased A value may be seen in concentrated milks, if further work is done to investigate these. The exponent n has been reported to show a dependence on particle size in alumina suspensions, with n decreasing as particle size decreases [42], varying from 0.67 to 1. Various other colloid freezing studies have reported n values from 0.33 to 0.7[41] . Unfortunately, the fluids in these studies were simple systems of water and colloidal particles, with the possible addition of binding agents or dispersants, yet there was no attempt made to predict spacing quantitatively [37]. There is a range of particle sizes found in ovine milk, rather than a monodisperse suspension as found in

other work. The particle interactions in ovine milk are more complicated than those in other studies, which may lead to n being outside of the range observed in previous water-based studies. As can be seen in Figure 4-10, the variance of feature spacing decreased as the freezing front velocity increased in all samples. This may be due to the greater kinetic driving force destabilising the interface when v_f increases. This reduces the effect of initial conditions and stochasticity on the destabilisation of the interface, which predominates at lower speeds leading to larger variation in feature spacing.

Previous workers have developed a predictive model for alumina by combing traditional solidification theories with the two-phase Stefan problem[41]. The Neumann solution to the Stefan problem was used to derive the magnitude of the steady-state freezing front velocity, Λ. Λ was linked with models describing feature size and freezing conditions in lamellar and dendritic growth, and the exponents in the regression models were similar to those found in many metallic and non-metallic environments. It was found that regression models fit more effectively when dispersion media properties rather than slurry properties were used to calculate Λ.[43] This methodology may prove useful for food colloid systems once the freezing rate approximates a steady state, and provided sufficient data are available to calculate Λ. This may be of particular use to calculate properties of interest in freeze-drying.

Engulfment of fat globules was observed in all samples of WSM with v_f>0.5 µms^{-1}, and partial engulfment was seen in WSM samples with v_f=0.5 µms^{-1}, some rejection was observed below this speed. The engulfment of fat globules was also seen in the electron micrographs of directionally frozen milk, but not seen in slowly frozen milk. This is discussed further in section 4.3 below.

Due to the limitations of the optical microscopy setup, it was not possible to view the behaviour of the casein micelles and their interaction with the advancing ice interface. It may be possible to view this directly if a customised cooling stage is developed for use with confocal microscopy. It is possible to see the relative amounts of particle engulfment in the electron micrographs that are presented in section 4.4.3 , and this is discussed there.

4.4.2.3 Perturbations and Growth from Perturbations.

It is well known that in many directional freezing or solidification systems a planar interface becomes unstable and transitions to a more complex interface. This phenomenon is known as Mullins-Sekerka instability[44]. This change in morphology is determined by the interaction between macroscopic driving forces, supersaturation or supercooling, and the microscopic properties of the interface, surface tension, interfacial energy and crystal growth kinetics.

Mullins and Sekerka found that infinitesimal perturbations at the interface of a growing spherical crystal can either decrease over time, or increase and lead to unstable growth if the perturbation is above a critical radius[45].This analysis was extended to planar surfaces with a sinusoidal perturbation of infinitesimal initial amplitude [46], which showed that if the perturbations grew, the interface would become unstable. This is illustrated in Figure 4-11. In a unidirectionally advancing solidification interface in a pure melt in a 2-dimensional system, there is a degree of supercooling ahead of the interface caused by the balance between the crystal growth rate as a function of supersaturation and the thermal gradient of the system. Growing crystals must reject heat into this region, and the thermal gradient can be shown as a series of isotherms, or isopotential lines ahead of the interface as shown in Figure 4-11.

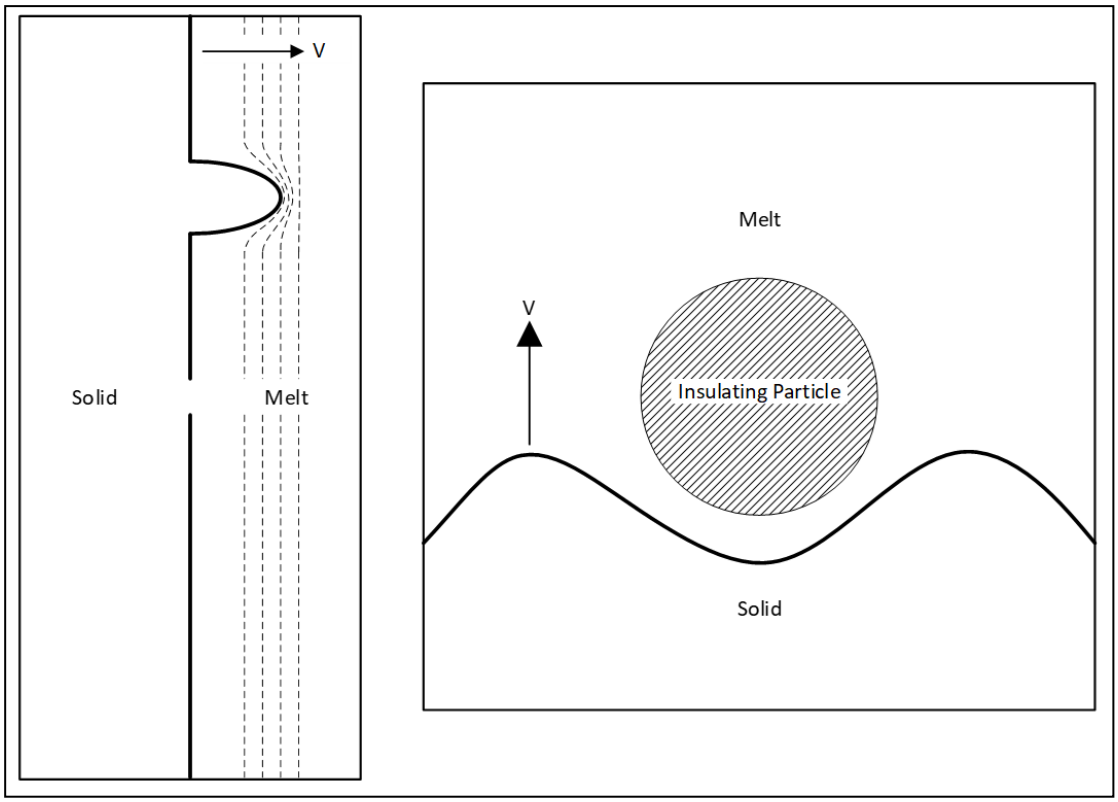

Figure 4-11: A perturbation from a planar interface experiences higher thermal gradients, or chemical potential gradients (as represented by the dotted isolines) than the pure planar interface. This increases crystal growth rates at the tip of the perturbation and favours interface destabilisation. The interaction with an insulating particle is also shown. Heat and/or solutes are rejected ahead of the interface. The insulating particle increases the resistance to heat or mass flow through the particle, causing the interface to grow more rapidly in regions away from this particle.

If a sharp perturbation exists, the isopotential lines bunch up near the perturbation, steepening the chemical potential gradient and the growth rate at the perturbation. This would make it kinetically favourable for an interface to break up into a number of perturbations. This is described in terms of heat removal, but the phenomenon is equally applicable to mass transport, and diffusion of solute to the growing interface.

However, a complicated interface with a number of perturbations would have a significantly larger interfacial area, and a larger interfacial energy, which is thermodynamically unfavourable. The increased curvature of the interface at perturbations also leads to an increase in the chemical potential of the perturbed region as a result of the Gibbs-Thomson effect. This decreases the chemical potential gradient between the melt and the solid and reduces the growth rate.

An analogous situation to thermal diffusion from an advancing gradient also occurs for chemical species in any system other than a pure melt. The solubility of solutes in a solidified solvent, such as ice, is significantly lower than the solubility in the liquid solvent. This causes a chemical potential gradient to form in front of the advancing interface [16]. The effect of this chemical gradient can be seen when comparing the behaviour of SSMUF and RO water samples. The thermal diffusivities of both samples are similar; however, the chemical species present in SSMUF cause a chemical gradient ahead of the interface to be formed as solutes are rejected from the solid water. This creates an additional driving force favouring the destabilisation of the interface, which is why SSMUF samples showed a transition to columnar growth morphology at freezing speeds roughly an order of magnitude lower than RO water samples.

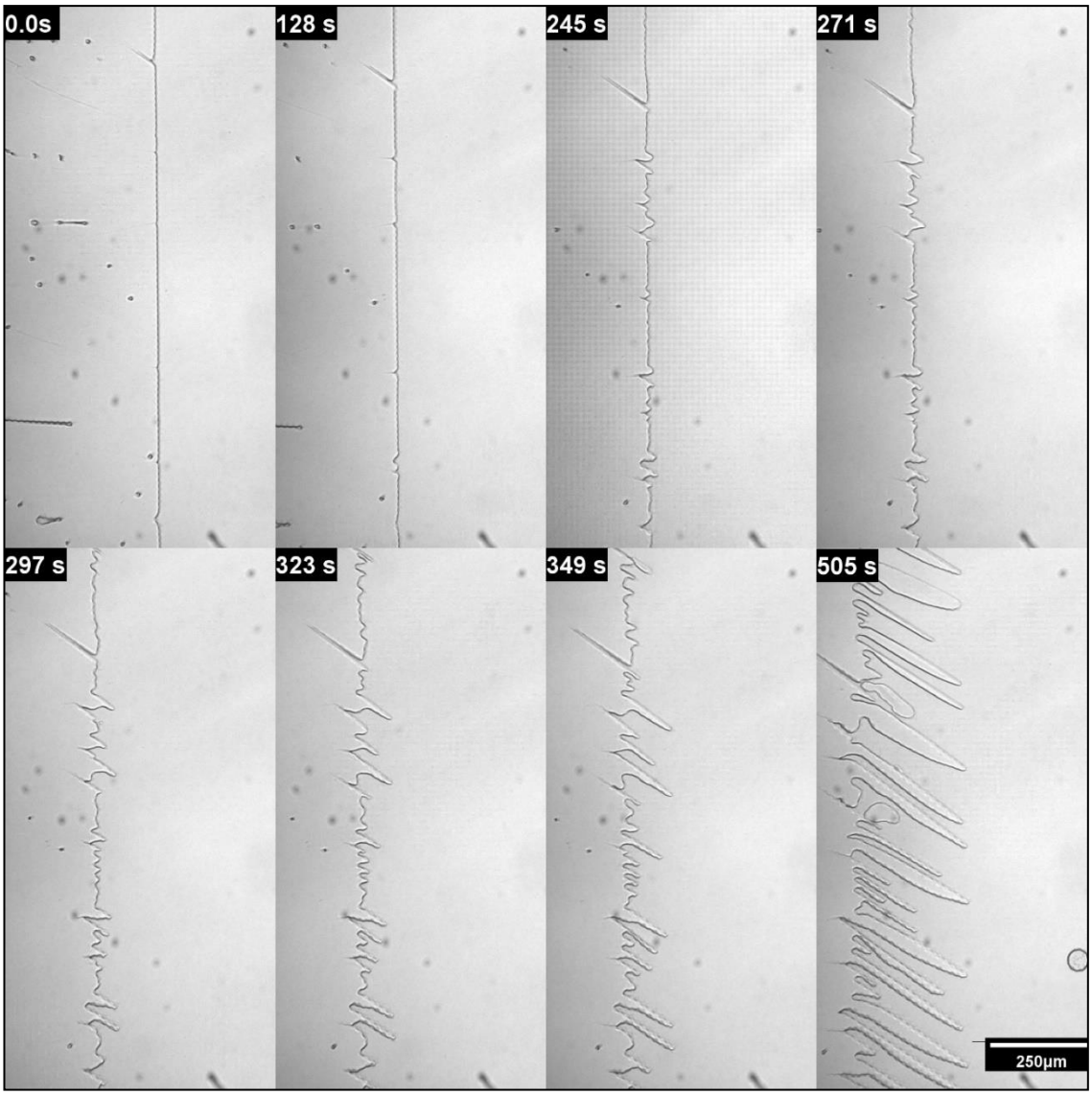

Figure 4-12: Instability formation in an freezing front advancing (from left to right) in SSMUF. v_f=1 µms^{-1}, and G=37 Kcm^{-1}. This is illustrative of the transition from a planar ice front to a columar morphology at lower freezing front velocities.The location of the front in each image is fixed relative to the camera. In the first image the interface beween the solid (left hand side of the interface) and liquid (right hand side) SSMUF is planar. Small sinusoidal perturbations can be seen after 128 s. The furthest advanced perturbations experience greater chemical and thermal gradients and can be seen to grow at a higher rate than other parts of the interface.

The formation of instabilities in an advancing ice front is illustrated in Figure 4-12, which shows the transition of an ice front from planar to columnar in SSMUF, where V_f=1 µms^{-1}, and G=37 Kcm^{-1}. Sinusoidal perturbations are formed in the planar ice front, the rate of this disturbance is affected by the degree of supercooling and the temperature gradient. Below a certain threshold these perturbations disappear, however above this the perturbations are reinforced and continue to grow to form stable columns. The rejection of solutes ahead of the growing ice front also leads to a region of increased solute concentration, and therefore lower equilibrium freezing temperature. Ahead of this zone, the liquid may have a lower solute concentration and be supercooled. This is an unstable situation called constitutional supercooling [47], and is illustrated in Figure 4-13. If any perturbation penetrates the region of maximum solute concentration ahead of the interface, it will enter a supercooled region and may grow rapidly.

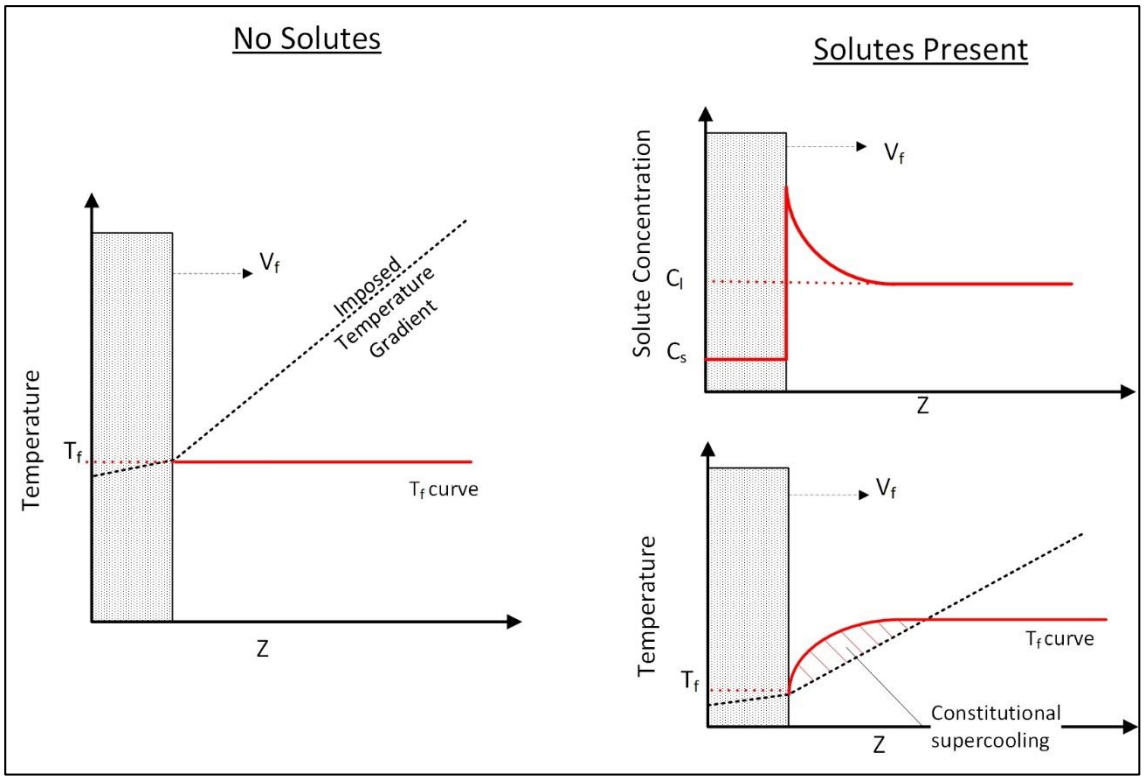

Figure 4-13: Graphical illustration of constitutional supercooling. An interface advances into the melt with a velocity v_f. Where there are no solutes the freezing temperature is constant, and the imposed temperature gradient is always above the freezing temperature in the liquid phase. When solute is present, rejection from the advancing solid phase leads to an increased solute concentration ahead of the interface, as shown at top right. This increased solute concentration decreases the freezing temperature, so the temperature gradient imposed now results in a supercooled volume of liquid ahead of the interface. Adapted from [48].

At temperatures near the equilibrium freezing temperature growth of ice crystals in the primary and secondary prismatic planes is orders of magnitudes higher than in the basal plane direction, therefore sideways growth into the supercooled region between is lower. However, if there is a sufficient spatial temperature gradient then the relative growth rates of the crystal faces can vary with spatial position. Solutes are also rejected into the area between crystals, reducing the equilibrium freezing temperature in these regions and the degree of supercooling present. This further reduces the growth of ice in these directions and leads to the formation of lamellar or columnar ice morphology, dependent upon the ice growth rate and solution properties[42] .
This also selects for crystals oriented in the direction of heat flux in steady state growth, as those crystals whose preferred growth direction is perpendicular to the heat flux will be "outgrown" by those aligned with the heat flux[19]. Dendrites form on the face of the columns/lamella closest to the warm region[19].
The growth of a stable columnar interface from a planar interface at higher velocities is shown in Figure 4-14. This transition occurred in a sample of SSMUF, with v_f =20 µms^{-1}, and G=35 Kcm^{-1}. The transition sequence is different to the lower velocity transition seen in Figure 4-12. At the lower speed sinusoidal initial variations [46] grew directly into columns. The balance between crystal growth parallel to the temperature gradient and crystal growth perpendicular to the temperature gradient, into the sub-cooled inter-column area, determined the stable column spacing. At higher speeds, the interface remains stable until the decreased temperature at the interface overcomes the constitutional supercooling. Sinusoidal perturbations grow, the leading perturbations at a higher rate than others. From these leading columns, a fractal network of dendrites grows sideways into the sub-cooled surrounding fluid. From the warm side of these dendrites, a stable interface of equal width columns then emerges, and is maintained during the crystal growth experiment. The area of dendritic growth corresponds to the zone of fluid that is

supercooled, and once the dendrites reach the fluid at the equilibrium freezing temperature the growth morphology changes to a steady state morphology driven by the thermal gradient, the ice growth rate, and the properties of the sample. The dendrites form at an angle of approximately 60° to the main branch, indicating that this growth is occurring along the a-axis of the ice crystals. The degree of supercooling at the interface at the initiation of dendritic growth can be estimated from the spatial displacement of the interface relative to the equilibrium freezing line, and the spatial temperature gradient. For the transition shown in Figure 4-14, the supercooling can be estimated as 0.47°C.
The spacing of these columns is governed by the same balance growth of parallel to the heat flow and growth sideways into the supercooled interstices, and the fluid properties in these interstices.

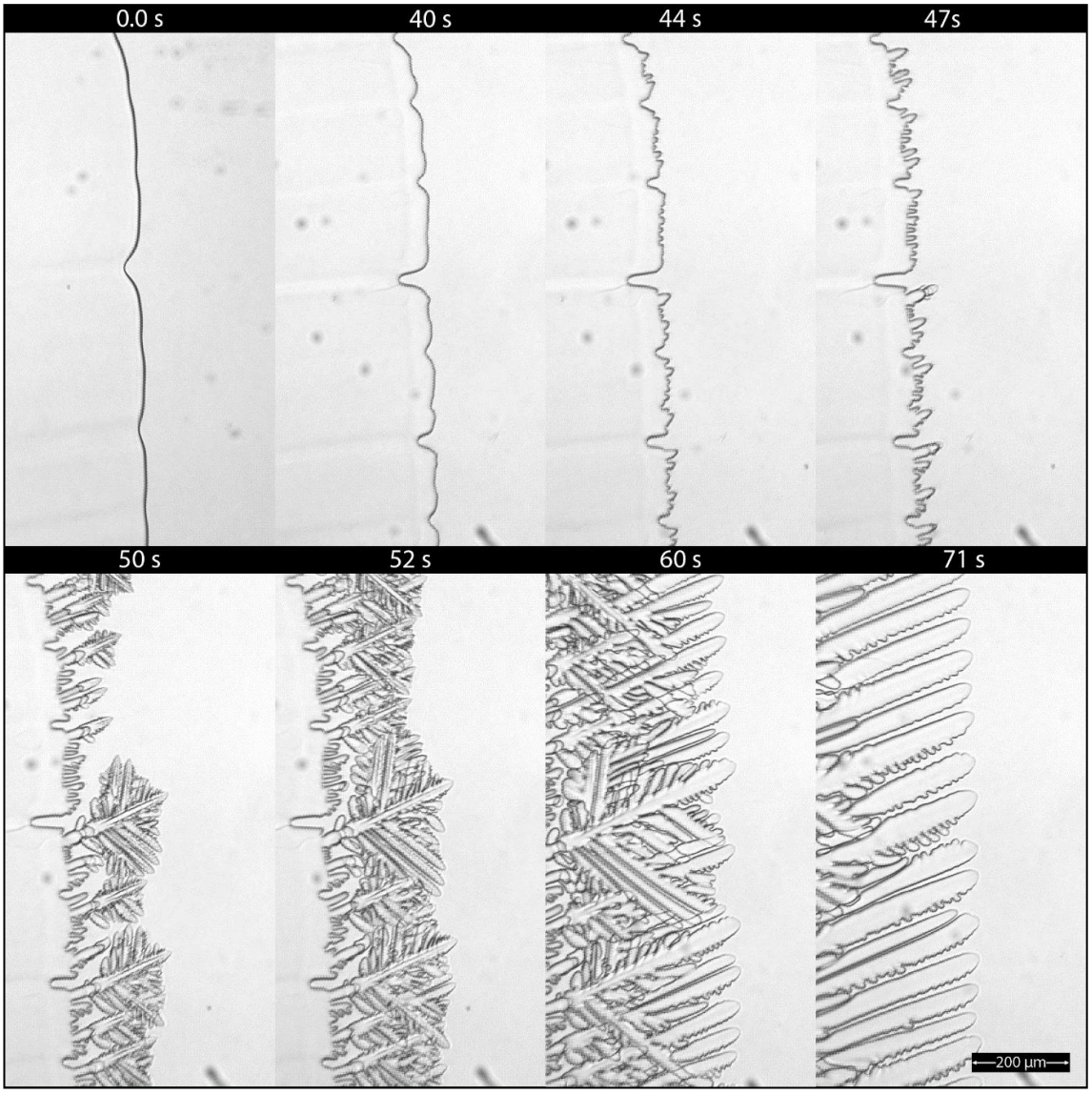

Figure 4-14: Formation of a columnar interface from an initial planar interface in SSMUF. v_f=20ms^{-1} and G=37 Kcm^{-1}. The interface transitions through an intermediate dendritic morphology seen in the images at 50s, 52s and 60s.

This transition from randomly oriented ice crystals during the initial crystal growth phase to crystals aligned with the temperature gradient during steady state growth has also been observed in the directional freezing of ice in alumina suspensions, where the random growth occurs during the growth into the supercooled zone, and once the supercooled zone has been frozen, columnar growth occurs along the line of equilibrium freezing temperature [49].

As can be seen in the morphology map in Figure 4-9, this critical speed for this transition decreases as each new milk component is added to the system. The addition of solutes in SSMUF leads to a significant decrease in the critical speed when compared to RO water. This decrease in critical velocity may be the result of two factors. The first factor is the presence of a chemical as well as a thermal gradient ahead of the interface which promotes the destabilisation of the interface due to constitutional supercooling[48]. The second factor is the reduction of the interfacial energy because of the solute concentration in the liquid, which reduces the thermodynamic penalty imposed by a greater interfacial energy.

The addition of particles reduces the critical speed for a transition from a planar interface below the onset speed of the Mullins-Sekerka instability[50]. As a particle with differing thermal conductivity to the melt is pushed ahead of the interface, it induces a change in the thermal profile ahead of the interface. An insulating particle can lead to a reversal in the thermal gradient as the gap between it and the interface decreases, and heat is rejected more easily through the solid phase[50]. This is illustrated in Figure 4-11. This phenomenon may be responsible for the critical velocity being lower in samples with casein micelles and fat globules (SSM and WSM), as these particles can interact with advancing ice interfaces.

4.4.3 Cryo-Electron Micrographs of Frozen Milk.

Cryo-Scanning Electron Microscopy as described in sections 4.3.1 and 2.5 was used to image the ice morphology of samples frozen at different rates.

Electron micrographs of the milk frozen by immersion in liquid nitrogen are shown in Figure 4-13. From this micrograph it can be seen that there is a separation between the milk solids (which appear as the rippled structure in the image) and the ice even at this high freezing speed. The ice has formed dendritic structures at this high growth speed. This has been observed in colloids at extremely high freezing rates where it is referred to as an isotropic interface due to the lack of significant lamellar or dendritic structures[37]. In order to prevent ice crystallisation, and form a glassy solid it would be necessary to cool the milk to approximately -130°C, (the glass transition temperature of ovine milk at 18% total solids as determined by the Gordon-Taylor equation [51]) fast enough to prevent ice formation.

Fat globules and the outlines of regions where they were located before the sample was fractured can also be seen in Figure 4-15 A. The average thickness of the solids bands is below 1μm.

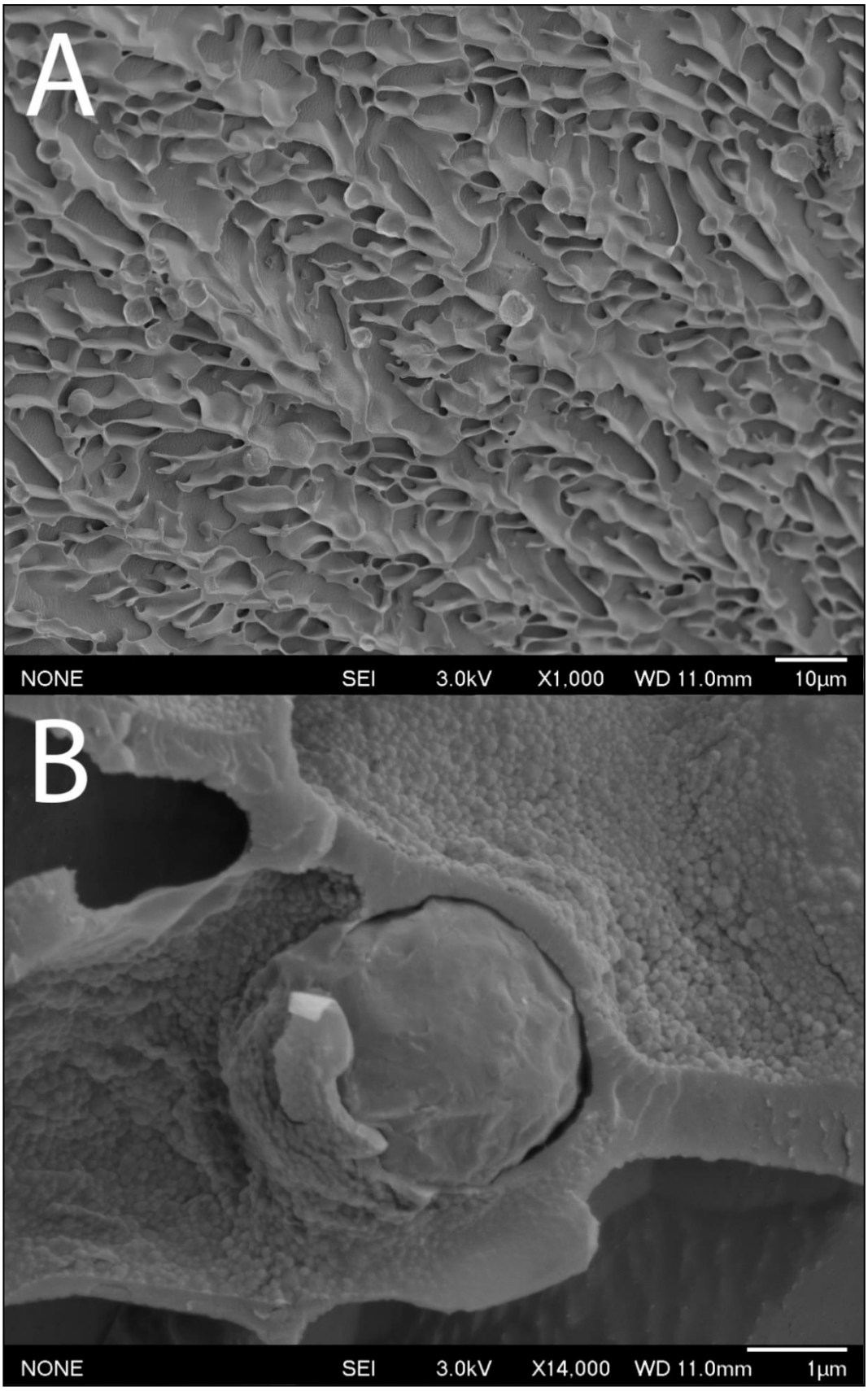

Figure 4-15:A) Highly dendritic network of milk solids observed in ovine milk frozen by immersion in liquid nitrogen. Eroded areas are observed where ice crystals have been removed by sublimation during sample preparation. B) A milk fat globule engulfed in milk proteins in ovine milk frozen by immersion in liquid nitrogen. Overlapping casein micelles are also observed as small spherical structures.

At higher magnification, as shown in Figure 4-15 B, the bands can be seen to be made of casein micelles. The bands have a grainy appearance and are comprised of spherical structures approximately 100-200 nm in diameter, which corresponds to the diameter of casein micelles in ovine milk[26].

When directionally frozen at moderate freezing speeds (approximately 15 μms^{-1}) the ice crystals grow in a columnar fashion, rejecting the solids into thin parallel bands between the crystals. The long axes of the crystals are aligned with the direction of heat flow, this can be seen in Figure 4-16. This behaviour is also observed in the optical microscope observations described earlier in this chapter.

The fat globules are rejected from the growing ice crystals and are typically found in the inter-crystal space. Some can be observed in the ice crystal space, indicating that they were engulfed by the advancing ice crystal. For an advancing flat ice interface, the particle will be engulfed if the ice front velocity is above the critical velocity for the particle [42, 52]. This is discussed in greater detail in section 1.6.3.1. The critical ice velocity for an advancing flat ice interface is given by:

$$v_c = \frac{\Delta\sigma d}{3\eta r}\left(\frac{a_o}{d}\right)^n \tag{4-4}$$

Where d is the distance to the ice interface, η is water viscosity, a_o is water intermolecular distance, r is particle radius (radius of gyration for polymers), and $\Delta\sigma$ is the surface free energy change, given by:

$$\Delta\sigma = \sigma_{sp} - (\sigma_{lp} + \sigma_{sl}) \tag{4-5}$$

The inverse relationship between r and v_c is why some fat globules were engulfed in the ice crystals, whereas the casein micelles which are roughly an order of magnitude smaller [26], would have a v_c roughly an order of magnitude higher.

The v_c calculation is based on a simplified analysis of a dilute system, with an advancing planar front. The actual velocity at which particles are engulfed may differ from the calculated value, the relative magnitude of the critical velocities for casein micelles and fat globules helps to explain the distribution of milk components in the frozen milk samples.

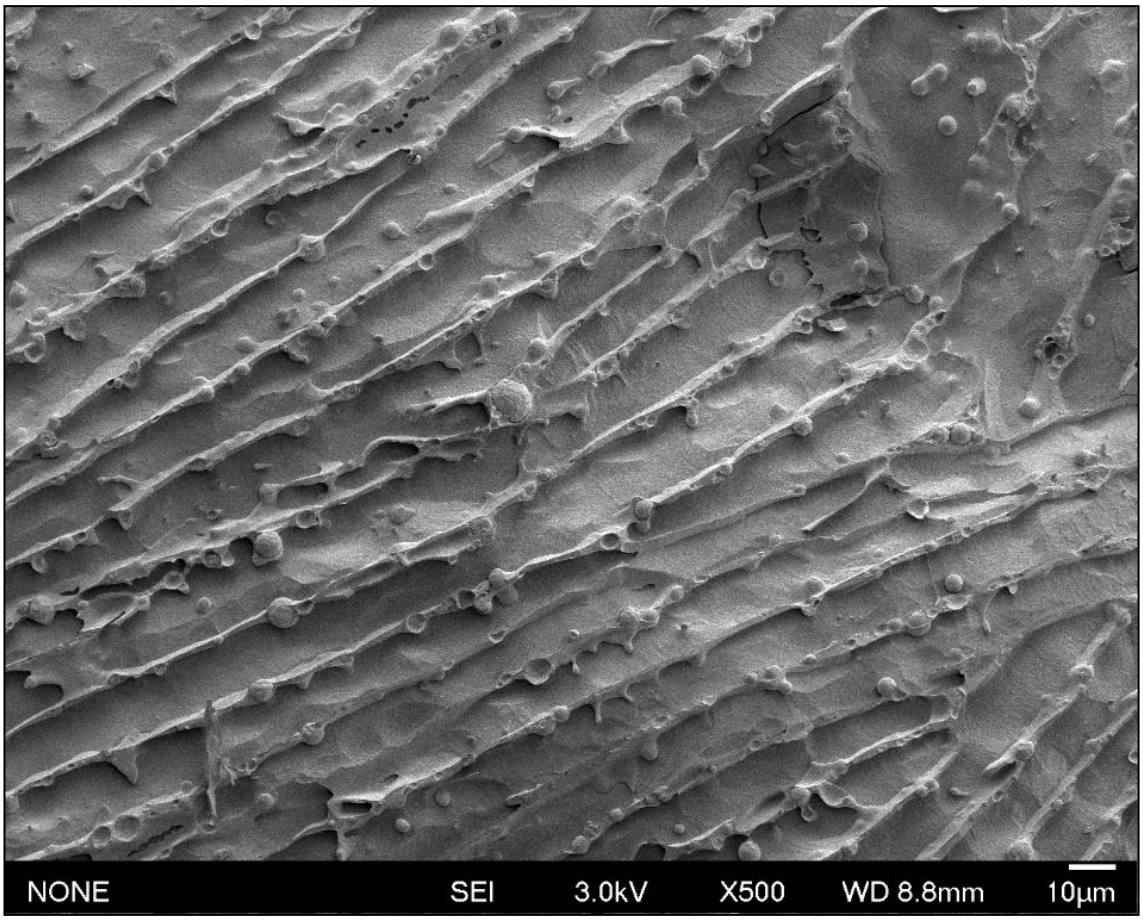

Figure 4-16: Lamellar ice growth seen in scanning electron micrographs of directionally frozen milk. View is in a plane parallel to the direction of heat flow and ice growth. The "eroded" areas between bands are where ice cyrstals were present before sublimation was used to highlight the frozen structures. The bands present are the milk solids, which were rejected into the inter-crystalline spaces during freezing. Fat globules can be seen as the round structures present in the bands (some indentations can be seen. These were left by fat globules that were lost when the sample was fractured for imaging). Fat globules can also be seen in the areas previously occupied by ice crystals.

The lamellar morphology of the ice crystals in directionally frozen milk can be further seen in Figure 4-17. As can be seen in the views perpendicular to ice growth direction, the crystals are oriented into lamellae, with a low aspect ratio (width: height). The median aspect ratio is 2.4:1. The frequency distribution of the aspect ratio of the lamellar ice crystals is shown in Figure 4-19 A. As the aspect ratio is significantly larger than 1, it is appropriate to refer to the crystals as having a lamellar morphology, rather than columnar. This lamellar morphology is commonly found in freeze-cast ceramics that use water as a solvent[33]. Parallel to the growth direction the narrow axis of the lamellae can be seen, as can flatter regions where the sample shear plane intersects the wide axis of the lamellae.

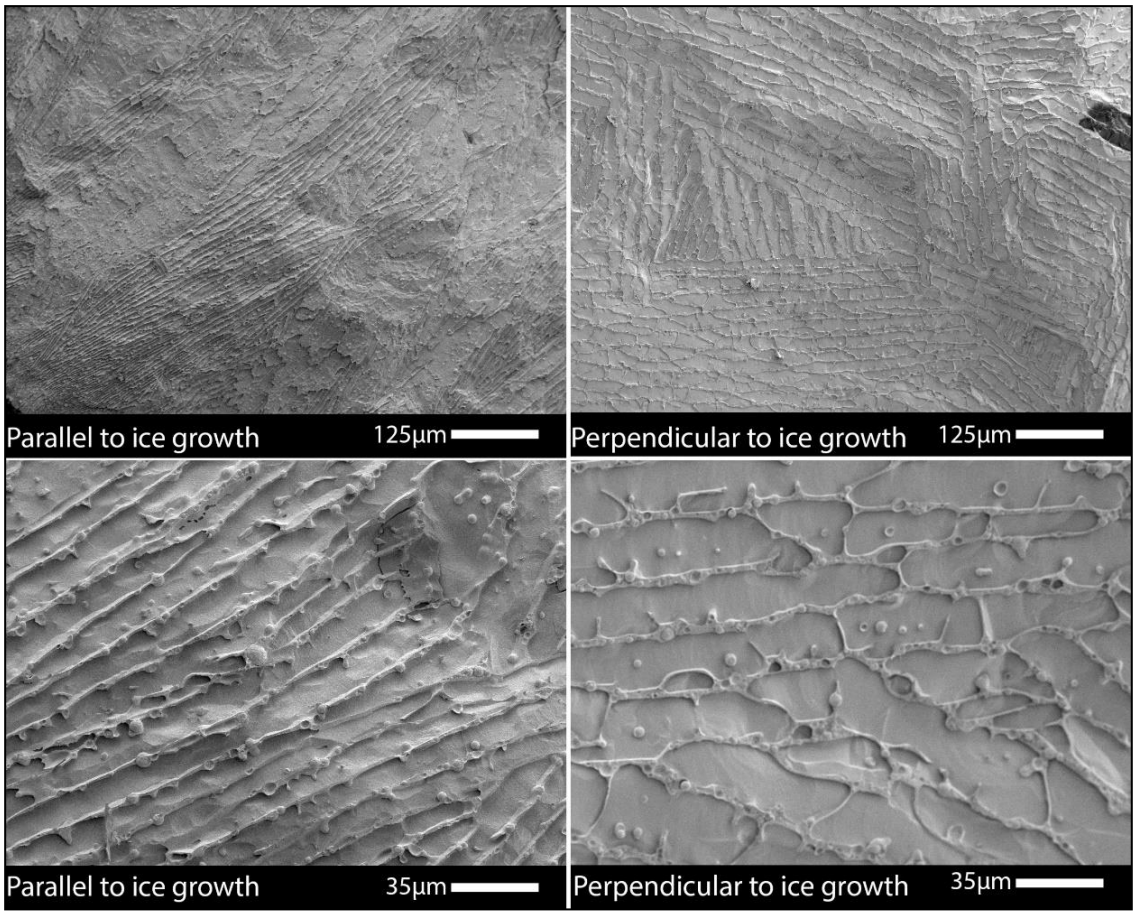

Figure 4-17: Cryo-SEM images of ice crystals in directionally frozen milk, imaged in a plane parrallel to ice growth direction and heat flux, and in a plane perpendicular to to ice growth direction and heat flux. Two maginfications are shown, to illustrate features across two length scales. Further description of the features present is given in Figure 4-14.

The ice crystals imaged in a plane parallel to the direction of heat flux are ordered largely in a single orientation, as is shown in the micrographs in Figure 4-17. When ice crystals are imaged in a plane perpendicular to the direction of heat flux, several orientations can be observed. This is seen in the micrographs in Figure 4-17. The orientation of the crystals in these two planes, and their cross-sectional area as seen in image plane are shown in Figure 4-19 B. When viewed in a plane parallel to the heat flux and ice growth direction, the crystals are more highly aligned than crystals viewed in a plane perpendicular to the direction of heat flux.

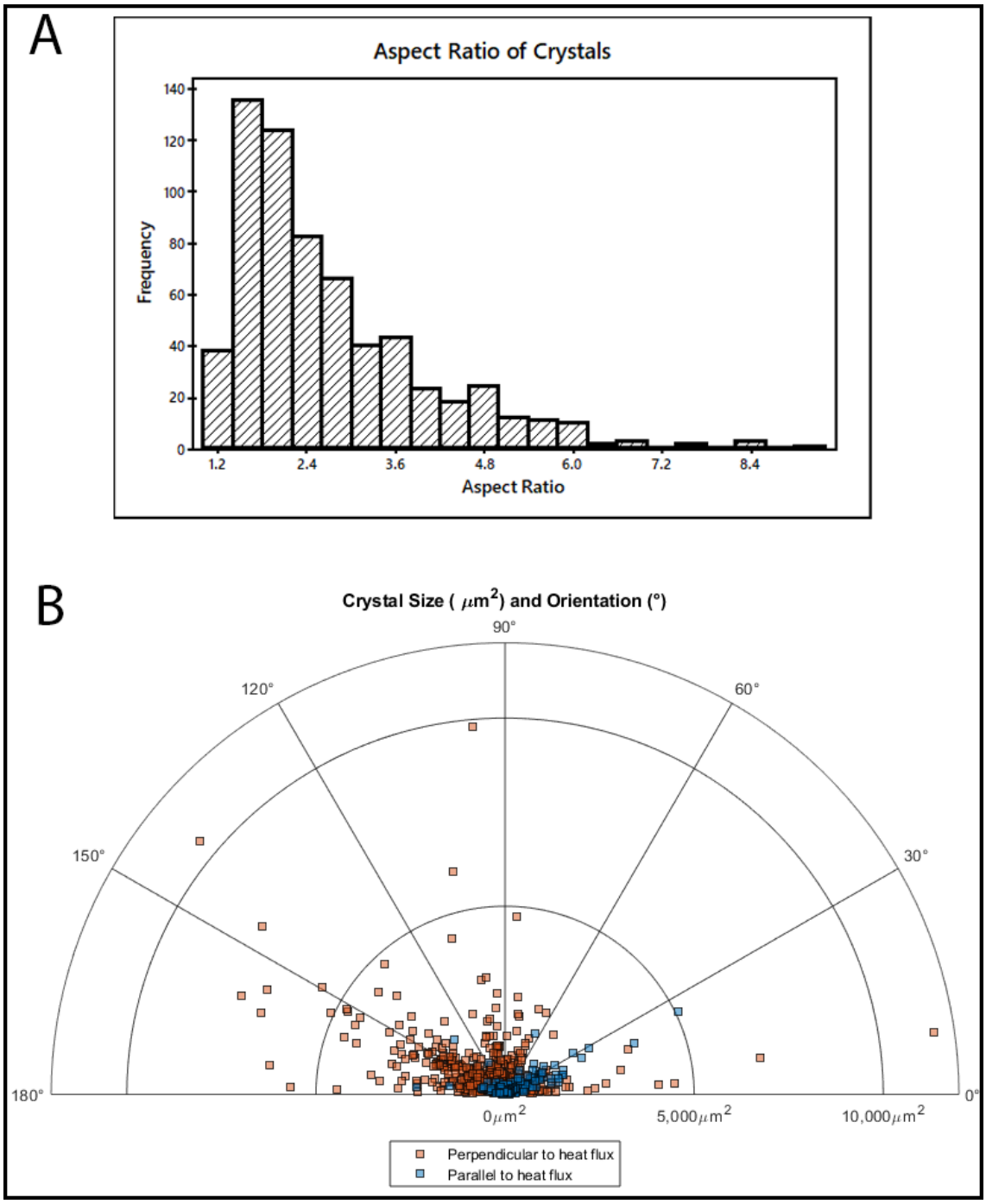

Figure 4-18: A) The aspect ratio, determined from the Feret dimensions, of crystals in DF samples, such as shown in Figure 4-15, when imaged on a plane perpendicular to the heat flux. Aspect ratio appears to follow a lognormal distribution B) The crystal size and orientation distributions of crystals both parallel and perpendicular to the heat flux. Orientation is the angle of the long axis of observed crystals relative to the image horizontal plane.

Electron-micrographs of milk frozen slowly are shown in Figure 4-20. In these samples, the solutes have been rejected into thick bands between spaces which once held large ice crystals. There is little apparent directionality to the ice crystals. No engulfing of fat globules in ice crystals is seen, as v_f may be significantly lower than v_c for fat globules. The average thickness of milk solids bands is 55± 49 (std dev) µm, compared with 3.2±1.5 µm for directionally frozen milk samples. The size of the ice crystals could not be estimated from the electron-micrographs as they were larger than the field of view of the SEM, even at the lowest magnification.

The size of the milk solids bands could limit the size of any protein aggregates formed during frozen storage. This could have an effect on the sensory acceptability of freeze-thawed milk; soft particles above approximately 80 µm in size can be perceived as "gritty", and hard particles above 20 µm are perceived as "gritty"[53]. The slowly frozen samples could form aggregates of over 80 µm in size, which could be perceptible, however the limited size of the milk solids bands in the directionally frozen milk would reduce the size of any aggregates and their effect on perceived texture.

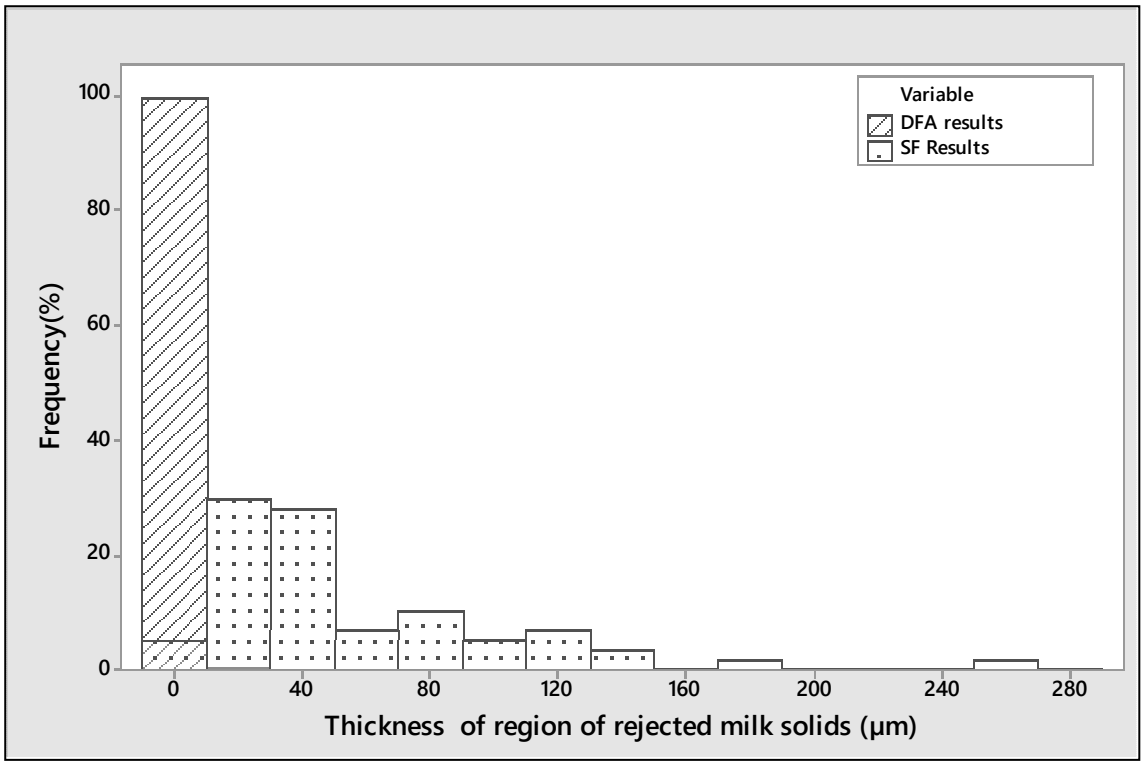

Figure 4-19: Histogram of the measured thickness of milk solids regions observed in cryo-electron micrographs of directionally frozen (DFA) (such as shown in Figure 4-14 and Figure 4-15) and slowly frozen (SF) milk samples (such as shown in Figure 4-18 and Figure 4-19).

In some studies, model ceramic systems have been aggregated together so that their attractive Van der Waals forces ensure aggregate stability after thawing. This has been observed in 32 nm colloidal silica spheres [54], and in a mixture of nano-scale γ-alumina and micron scale α-alumina[55]. While the nature of these colloidal dispersions is significantly different from milk, these studies nonetheless demonstrate that stable dispersions can be disrupted by the freeze-thaw process.

As discussed elsewhere in this thesis, in samples of ovine milk maintained at high frozen storage temperatures, (>-10°C) for sufficient time, a gel forms and a cream layer can no longer be separated from the destabilised milk. This may be a result of a network of destabilised proteins surrounding the fat globules and preventing them from separating. The fat globules were surrounded by proteins in micrographs of samples frozen slowly and stored at both -10°C and -30°C, and the overall ice morphology of these samples showed little difference. However, milk stored at -30°C still behaved like fresh milk after thawing and showed little particle aggregation. This suggests that the destabilisation of the milk discussed elsewhere was as a result of changes occurring during the storage time, rather than the freezing process alone.

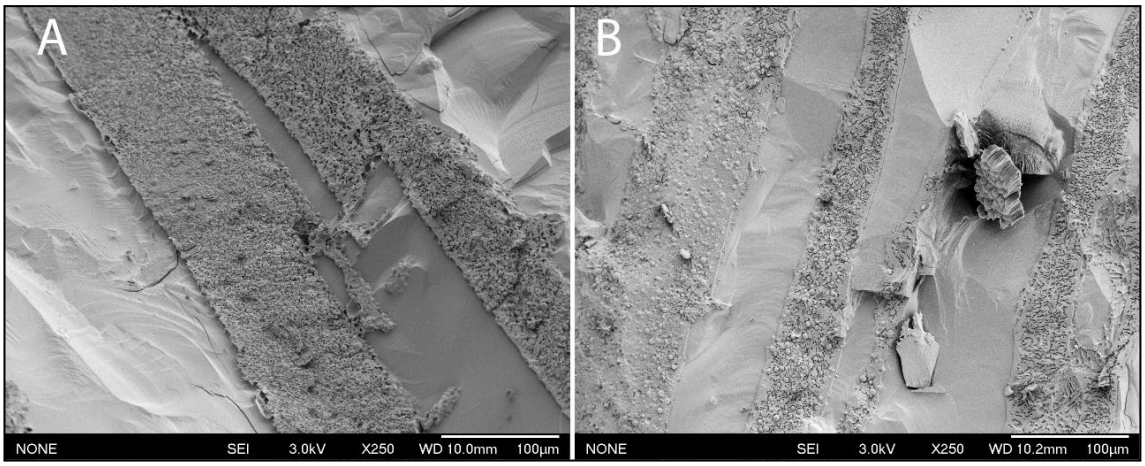

Figure 4-20: Large bands of rejected milk solids in electron micrographs of samples of ovine milk that were frozen slowly and stored at -10°C (A) and -30°C(B).

4.4.3.1 Lactose Crystallisation.

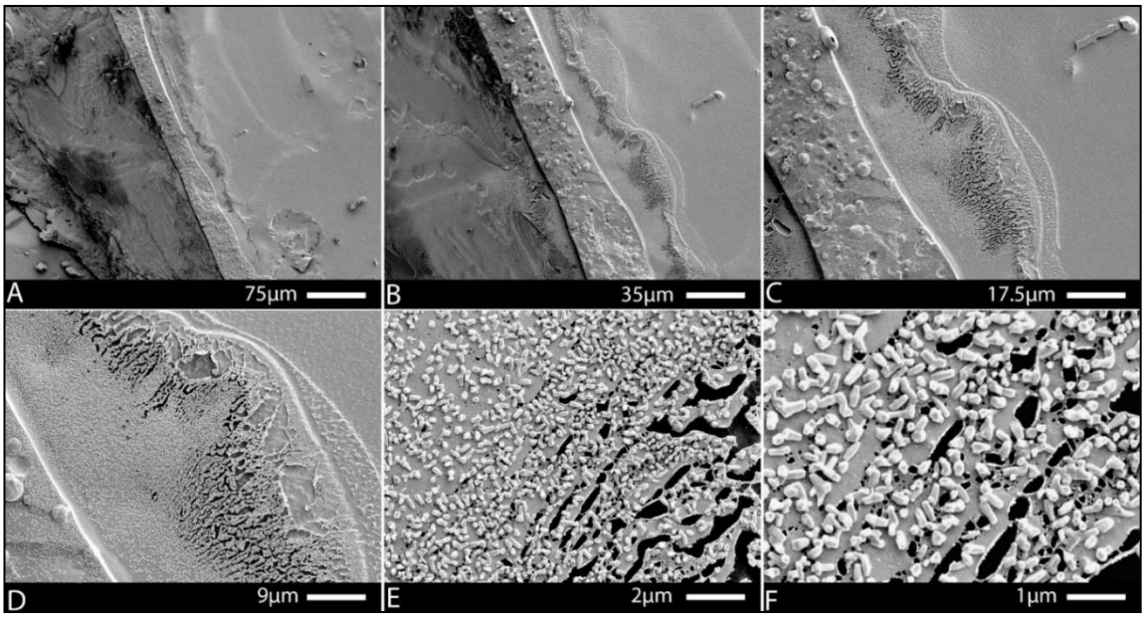

Figure 4-21: Possible lactose crystallisation observed in a sample of ovine milk that was frozen slowly and stored at -30°C until imaging.Images A-F are the same region at increasing levels of maginfication. A milk solids band is seen between two ice crystals in A, and this is the area magnified.

The white crystal-like structures seen in Figure 4-21 are most likely lactose crystals: No structures that could be identified as bacteria were seen in any micrographs. The white particles are on average approximately 400nm long. This is smaller than most bacterial cells with the exception of mycoplasma species, which are spherical. The particles have a distinct faceted appearance similar to prismatic crystals of lactose monohydrate formed at high lactose crystal growth velocities, or tomahawk shaped lactose crystals[56] . There are also tetrahedral clusters of white particles visible , which are unlike the crystal forms typically reported for lactose[9, 56].These are shown in Figure 4-22. According to Paterson [56], there are very few reports of clustered lactose in the literature, all of which suggests this occurs at high levels of supersaturation. The extremely small crystals observed, and the large number present also suggests that the crystals formed at high levels of supersaturation, due to the large nucleation rates that would be needed to form such a large number of crystals in system with no secondary

nucleation from attrition of seed crystals. The crystals are also significantly smaller than typically observed, being on sub-micron scale, whereas a lot of the previous work on lactose crystallisation deals with crystals 10's to 100's of µm in size. There are limited references to nanocrystalline lactose in literature: In the skin of partially crystallised dairy powders, which contained lactose crystal clusters and crystals 200 nm in length[33][57], and in the athermal milling of crystalline lactose which was studied by XRD and may lead to the formation of lactose nanocrystals [58].

The distribution of lactose is not uniform. The crystallised lactose is mostly located in the regions close to milk solids bands, and in the milk bands. The rejection of lactose ahead of the freezing front leads to the formation of regions of supersaturated lactose solution at the boundaries between ice crystals. This may become a supercooled glass if cooled far enough. In the case of slowly frozen milk the supersaturated lactose solution was held in conditions that allowed for nucleation and crystal growth. Soluble lactose has been found to have a cryoprotectant effect in frozen milk[59], so its crystallisation in the slowly frozen samples may contribute to quality loss. This may also indicate that the slowly frozen milk spent significant time well above the system's T_g which allowed lactose to crystallise. As discussed in chapter 6, in whole ovine milk a melting onset transition, where the system viscosity drops low enough to allow ice formation, occurs at -25°C, and the glass transition would occur at approximately -34°C. The lactose in milk stored at -30°C is in an extremely viscous environment that would supress crystal nucleation. As discussed in chapter 5, assuming the viscosity of the unfrozen phase follows WLF kinetics, it will increase by 5 orders of magnitude from -10°C to -28°C. The lactose in the system is supersaturated below a temperature of approximately -2°C to -3°C. As a result, the longer the temperature of the system is maintained between -3°C and -25°C to -30°C there is a greater likelihood of lactose crystallising. This more rapid cooling of milk in the directionally frozen samples means that the system reaches a highly viscous state where lactose crystallisation is supressed by the high viscosity. The role of lactose crystallisation in storage destabilisation of frozen milk has been suggested by previous authors[1, 7, 60], but the cryo-SEM images in this chapter are a possible detection of crystalline lactose present in slowly frozen samples but not in rapidly frozen samples.

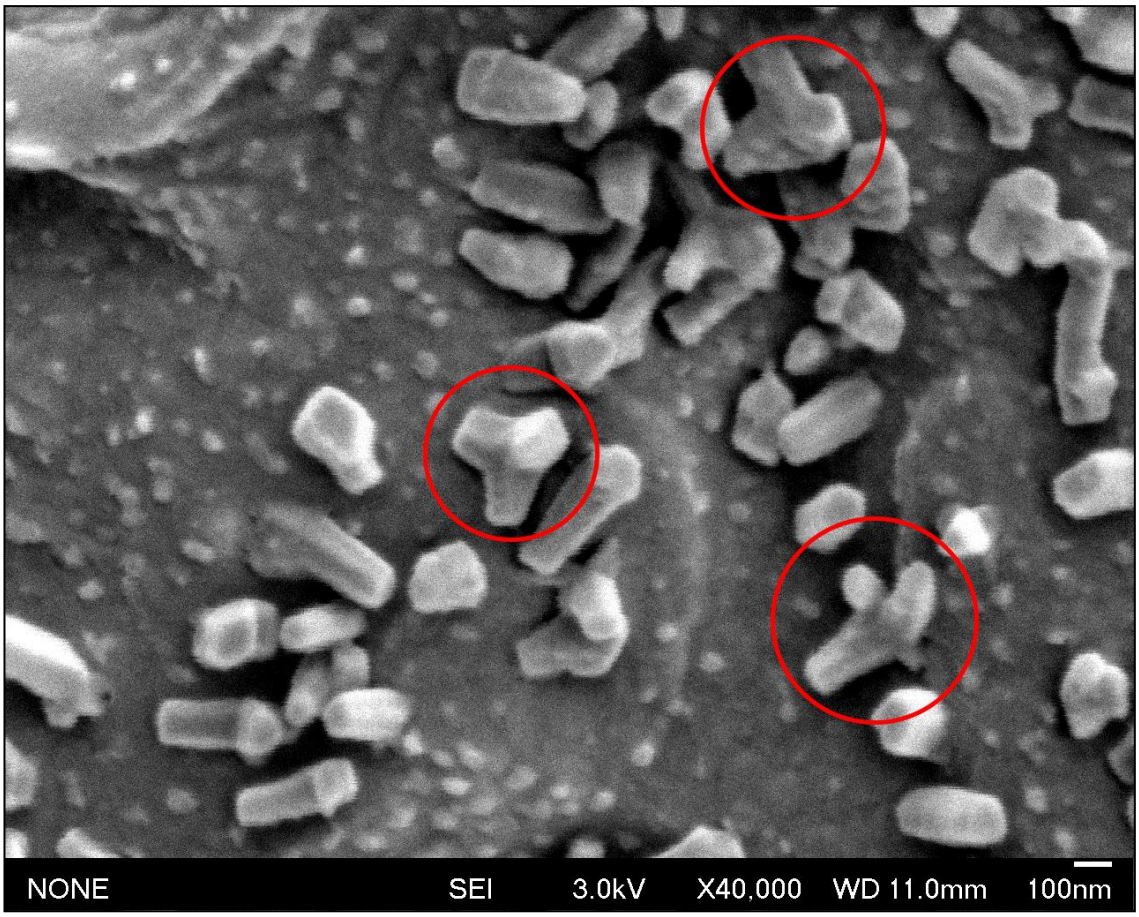

Figure 4-22: Possible lactose crystals in electron micrographs of slowly frozen ovine milk that was stored at -30°C. Clustered crystals are circled in red.

4.5 Engineering Relevance

The freezing front velocities selected in this work are realistic for the range of conditions that will be encountered in common food processing systems.

The freezing front velocity can be directly related to the heat flux of a freezing system as follows:

$$Q = \Delta H_f * \rho_{ice} * v_f \tag{4-6}$$

Where Q is the heat flux, in Wm^{-2}, ΔH_{fus} is the latent heat in Jkg^{-1}, ρ_{ice} is the density of ice in kgm^{-3}, and v_f is the ice front velocity in ms^{-1}.

Using a slightly conservative ΔT value of 20K, the U value required to achieve a given v_f can be calculated. This is plotted in Figure 4-23, with the U values typical of industrial freezers shown [61].

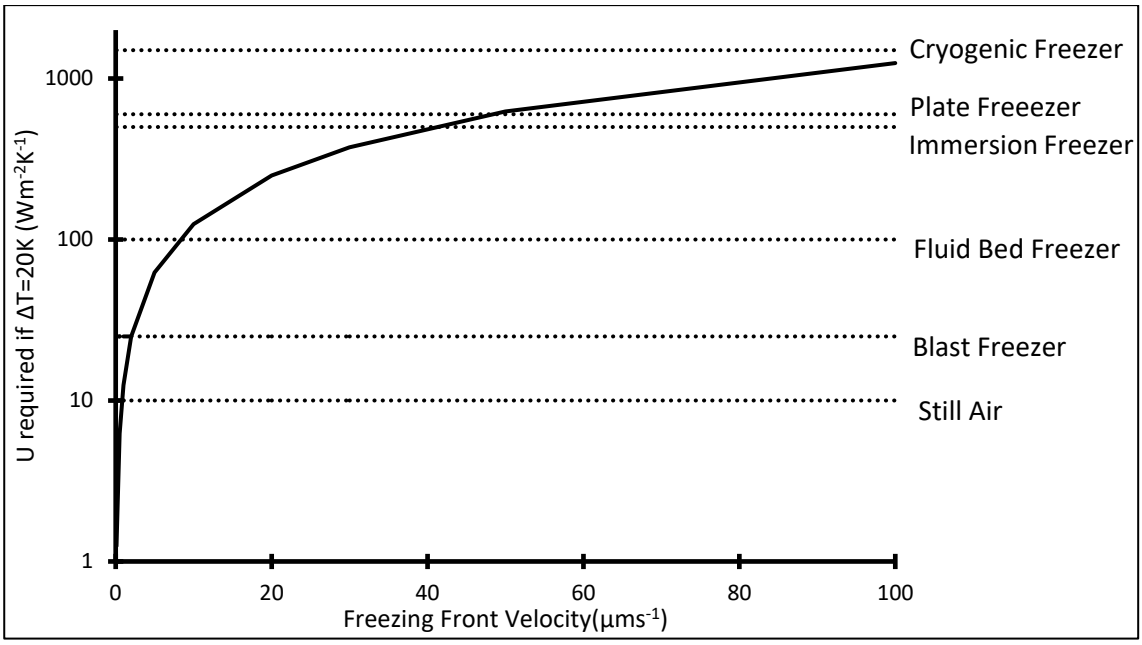

Figure 4-23: Freezing front velocities acheivable by commercial freezing methods.

However, these U values are surface properties and are only achievable in the absence of any appreciable ice thickness. Achieving high ice growth rates in the presence of an ice layer requires a large ΔT. Once a 2.5 mm thick layer of ice is present, maintaining a v_f of 20 µms^{-1} requires a ΔT across the ice layer of 25K, 30 µms^{-1} requires a ΔT across the ice layer of 37 K and this increases linearly with increased ice thickness.

The morphology of a frozen product also affects the mass transfer rates achievable during freeze-drying. As freeze-drying is a possible processing step following directional freezing, the freeze-drying performance may be able to be optimised by optimising the freezing step. Generally speaking, high freezing speeds lead to poor mass transfer rates during primary freeze drying [62] due to increased resistance to mass flow in pores due to small pore sizing. However, it is possible that directionally aligned main columns gives primary porosity in one direction with side dendrites leading to secondary porosity which may complicate this analysis. The higher total surface area in rapidly frozen sample may increase mass flow rates of vapour during the secondary drying phase. This is a rate-determining step for high total solids products. Some papers have discussed predictive models for the effect of freezing front velocity on the porosity, tortuosity, and surface area of a sample [41]. These factors are important for modelling mass transfer during the freeze-drying process.

4.6 Conclusions

Whole Sheep Milk, Skim Sheep Milk, Sheep Milk UltraCentrifuge supernatant, Simulated Sheep Milk Ultrafiltrate and RO water were frozen with v_f varying from 0.5 µms^{-1} to 50 µms^{-1} and the interface morphology was observed.

The observed interface morphology changed as v_f increased, from planar to columns, to columns with secondary dendrite growth, to dendritic growth. A map of morphology against v_f and fluid was constructed. Transitions to more complicated morphologies occurred at lower temperatures in more complicated fluids. The feature spacing in the freezing front followed a power law relationship with v_f. In general, milk behaves like other water-based colloids.

Directionally frozen (DF) and slow frozen (SF) were imaged with Cryo-SEM. There was a distinct difference in morphology observed in the DF and SF samples. The DF samples had a highly anisotropic frozen morphology consisting of lamellar ice crystals with the long crystal axis

aligned with the direction of heat flux. The SF samples had large ice crystals with large bands of milk solids between the crystals. There was no distinct orientation to the SF samples. Crystalline structures approximately 400nm in length, which may have been lactose, were also observed in some SF samples but were absent in all DF samples. Samples of raw milk were frozen by direct immersion into liquid nitrogen. These samples had a dendritic ice morphology with separation of milk components from ice crystals.

4.7 List of Symbols

Symbol	Description	Units
A	Feature spacing pre-factor	
a_0	Water intermolecular distance	m
C_l	Solute concentration in liquid phase	g_{solute}/g_{liquid}
C_s	Solute concentration in solid phase	g_{solute}/g_{solid}
d	Particle distance to interface.	m
$\overline{K}$	Partition Coefficient	
n	Feature spacing exponent	
Q	Heat flux	Wm^{-2}
r	Particle radius (or radius of gyration for macromolecules)	m
R	Gas constant	$JK^{-1}\,mol^{-1}$
T_f	Equilibrium freezing temperature	K
v_c	Critical freezing front velocity for particle engulfment	ms^{-1}
V_f	Freezing front velocity	ms^{-1}
α	Solvent α-value	
ΔH_f	Latent heat of fusion/freezing/crystallisation	$Jmol^1$
ΔT_{FPD}	Freezing point Depression	K
$\Delta\sigma$	Surface free energy change on engulfment	Jm^{-2}
η	Water viscosity	$Pa.s$
λ	Feature spacing	μm
ξ	Crystallographic factor	
ρ_{ice}	Density of ice	kgm^{-3}
σ_{lp}	Surface energy between particle and liquid	Jm^{-2}
σ_{sl}	Surface energy between liquid and solid	Jm^{-2}
σ_{sp}	Surface energy between particle and solid	Jm^{-2}

4.8 References

[1] W. L. Wendorff, "Freezing Qualities of Raw Ovine Milk for Further Processing," *Journal of Dairy Science,* vol. 84, pp. E74-E78, 2001.

[2] P. Young, "Deep-frozen storage of frozen ewe's milk," *Sheep Dairy News,* no. 4, p. 41, 1987.

[3] E. C. Needs, "Effects of long-term deep-freeze storage on the condition of the fat in raw sheep's milk," *Journal of Dairy Research,* vol. 59, pp. 49-55, 1992.

[4] D. D. Muir, "Reviews on the Progress of Dairy Science: Frozen concentrated milk," *Journal of Dairy Research,* vol. 51, pp. 649-664, 1984.

[5] M. Pazzola *et al.*, "The Effect of Long-term Freezing on Renneting Properties of Sarda Sheep Milk," *Agriculturae Conspectus Scientificus,* vol. 78, no. 3, pp. 275-279, 2013.

[6] W. L. Wendorff, "Milk composition and cheese yield," in *Proceedings of the 7th Great lakes Dairy Sheep Symposium*, Ithaca, 2002.

[7] M. S. Koschak, O. Fennema, C. H. Amundson, and J. Y. Lee, "Protein Stability of Frozen Milk as Influenced by Storage Temperature and Ultrafiltration," *Journal of Food Science,* vol. 46, no. 4, pp. 1211-1217, 1981.

[8] B. H. Webb and S. A. Hall, "Some Physical Effects of Freezing upon Milk and Cream," *Journal of Dairy Science,* vol. 18, no. 5, pp. 275-286, 1935.

[9] S. Y. Wong and R. W. Hartel, "Crystallization in Lactose Refining—A Review," *Journal of Food Science,* vol. 79, no. 3, pp. R257-R272, 2014.

[10] C. V. Morr, "Chemistry of milk proteins in food processing," *J Dairy Sci,* vol. 58, no. 7, pp. 977-84, 1975.

[11] P. Chen and X. D. Chen, "A generalized correlation of solute inclusion in ice formed from aqueous solutions and food liquids on sub-cooled surface," *Canadian Journal of Chemical Engineering,* Article vol. 78, no. 2, pp. 312-319, 2000.

[12] O. J. McCarthy, "Milk | Physical and Physico-Chemical Properties of Milk," in *Encyclopedia of Dairy Sciences (Second Edition)*, J. W. Fuquay, Ed.: Academic Press, 2002, pp. 467-477.

[13] H. Kiani and D.-W. Sun, "Water crystallization and its importance to freezing of foods: A review," *Trends in Food Science & Technology,* vol. 22, no. 8, pp. 407-426, 2011.

[14] A. Chang, J. A. Dantzig, B. T. Darr, and A. Hubel, "Modeling the interaction of biological cells with a solidifying interface," *Journal of Computational Physics,* vol. 226, no. 2, pp. 1808-1829, 2007.

[15] H. Ishiguro and B. Rubinsky, "Mechanical Interactions between Ice Crystals and Red Blood Cells during Directional Solidification," *Cryobiology,* vol. 31, no. 5, pp. 483-500, 1994.

[16] G. Petzold and J. M. Aguilera, "Ice Morphology: Fundamentals and Technological Applications in Foods," *Food Biophysics,* vol. 4, no. 4, pp. 378-396, 2009.

[17] M. Watanabe, "Freeze Texturing of Food Materials by Ice-nucleation with the Bacterium Erwinia ananas AU - Arai, Soichi," *Agricultural and Biological Chemistry,* vol. 50, no. 1, pp. 169-175, 1986.

[18] T. Abe and T. Yano, "Freezing and Ice Structure Formed in Protein Gels AU - Miyawaki, Osato," *Bioscience, Biotechnology, and Biochemistry,* vol. 56, no. 6, pp. 953-957, 1992.

[19] S. Deville, *Freezing Colloids: Observations, Principles, Control, and Use*. Cham, Switzerland: Springer International Publishing, 2017.

[20] J. Luo *et al.*, "Cryo-SEM images of native milk fat globule indicate small casein micelles are constituents of the membrane," *Rsc Advances,* vol. 4, no. 90, pp. 48963-48966, 2014.

[21] J. Schindelin *et al.*, "Fiji: an open-source platform for biological-image analysis," *Nat Methods,* vol. 9, no. 7, pp. 676-82, 2012.

[22] C. T. Rueden *et al.*, "ImageJ2: ImageJ for the next generation of scientific image data," *BMC Bioinformatics,* vol. 18, no. 1, p. 529, 2017.

[23] R. Jenness and J. Koops, "Preparation and properties of a salt solution which simulates milk ultrafiltrate," *Netherlands Milk and Dairy Journal,* vol. 16, pp. 153-164, 1962.
[24] C. Holt and R. Jenness, "Interrelationships of constituents and partition of salts in milk samples from eight species," *Comp Biochem Physiol A Comp Physiol,* vol. 77, no. 2, pp. 275-82, 1984.
[25] G. W. Latimer, *Official methods of analysis of AOAC International*. Rockville, Md: AOAC International, 2016.
[26] G. F. W. Haenlein and W. L. Wendorff, "Sheep Milk," in *Handbook of Milk of Non-Bovine Mammals*, Y. W. Park, Ed.: Blackwell Publishers, 2006.
[27] P. F. Fox, "Milk | Introduction," in *Encyclopedia of Dairy Sciences (Second Edition)*, J. W. Fuquay, Ed. San Diego: Academic Press, 2011, pp. 458-466.
[28] A. Sevi, M. Albenzio, R. Marino, A. Santillo, and A. Muscio, "Effects of lambing season and stage of lactation on ewe milk quality," *Small Ruminant Research,* vol. 51, no. 3, pp. 251-259, 2004.
[29] V. Pavic, N. Antunac, B. Mioc, A. Ivankovic, and J. L. Havranek, "Influence of stage of lactation on the chemical composition and physical properties of sheep milk," *Czech Journal of Animal Science,* vol. 47, no. 2, pp. 80-84, 2002.
[30] G. Pulina, A. Nudda, G. Battacone, and A. Cannas, "Effects of nutrition on the contents of fat, protein, somatic cells, aromatic compounds, and undesirable substances in sheep milk," *Animal Feed Science and Technology,* vol. 131, no. 3-4, pp. 255-291, 2006.
[31] R. Bencini and G. Pulina, "The quality of sheep milk: a review," *Australian Journal of Experimental Agriculture,* vol. 37, no. 4, p. 485, 1997.
[32] H. Sakul and W. J. Boylan, "Evaluation of U.S. sheep breeds for milk production and milk composition," *Small Ruminant Research,* vol. 7, no. 3, pp. 195-201, 1992.
[33] S. Deville, S. Meille, and J. Seuba, "A meta-analysis of the mechanical properties of ice-templated ceramics and metals," *Sci Technol Adv Mater,* vol. 16, no. 4, p. 043501, 2015.
[34] J. M. Schollick *et al.*, "Segregated Ice Growth in a Suspension of Colloidal Particles," *J Phys Chem B,* vol. 120, no. 16, pp. 3941-9, 2016.
[35] S. Deville, "Ice-templating, freeze casting: Beyond materials processing," *Journal of Materials Research,* vol. 28, no. 17, pp. 2202-2219, 2013.
[36] A. Criscione, D. Kintea, Ž. Tuković, S. Jakirlić, I. V. Roisman, and C. Tropea, "Crystallization of supercooled water: A level-set-based modeling of the dendrite tip velocity," *International Journal of Heat and Mass Transfer,* vol. 66, pp. 830-837, 2013.
[37] T. Waschkies, R. Oberacker, and M. J. Hoffmann, "Investigation of structure formation during freeze-casting from very slow to very fast solidification velocities," *Acta Materialia,* vol. 59, no. 13, pp. 5135-5145, 2011.
[38] K. A. Jackson and J. D. Hunt, "Transparent compounds that freeze like metals," *Acta Metallurgica,* vol. 13, no. 11, pp. 1212-1215, 1965.
[39] K. Araki and J. W. Halloran, "Porous Ceramic Bodies with Interconnected Pore Channels by a Novel Freeze Casting Technique," *Journal of the American Ceramic Society,* vol. 88, no. 5, pp. 1108-1114, 2005.
[40] U. G. Wegst, M. Schecter, A. E. Donius, and P. M. Hunger, "Biomaterials by freeze casting," *Philos Trans A Math Phys Eng Sci,* vol. 368, no. 1917, pp. 2099-121, 2010.
[41] S. M. Miller, X. Xiao, and K. T. Faber, "Freeze-cast alumina pore networks: Effects of freezing conditions and dispersion medium," *Journal of the European Ceramic Society,* vol. 35, no. 13, pp. 3595-3605, 2015.
[42] S. Deville, E. Saiz, and A. P. Tomsia, "Ice-templated porous alumina structures," *Acta Materialia,* vol. 55, no. 6, pp. 1965-1974, 2007.
[43] J. M. Nokes *et al.*, "Reduced Blood Coagulation on Roll-to-Roll, Shrink-Induced Superhydrophobic Plastics," *Advanced Healthcare Materials,* Article vol. 5, no. 5, pp. 593-601, 2016.

[44] J.-J. Xu, "Unidirectional Solidification and Mullins–Sekerka Instability," in *Interfacial Wave Theory of Pattern Formation in Solidification*(Springer Series in Synergetics: Springer International Publishing, 2017.

[45] W. W. Mullins and R. F. Sekerka, "Morphological Stability of a Particle Growing by Diffusion or Heat Flow," *Journal of Applied Physics,* vol. 34, no. 2, pp. 323-329, 1963.

[46] W. W. Mullins and R. F. Sekerka, "Stability of a Planar Interface During Solidification of a Dilute Binary Alloy," *Journal of Applied Physics,* vol. 35, no. 2, pp. 444-451, 1964.

[47] J. You *et al.*, "Interfacial undercooling in solidification of colloidal suspensions: analyses with quantitative measurements," *Sci Rep,* vol. 6, p. 28434, 2016.

[48] S. Deville *et al.*, "Metastable and unstable cellular solidification of colloidal suspensions," *Nature Materials,* vol. 8, no. 12, pp. 966-972, 2009/12/01 2009.

[49] A. Lasalle *et al.*, "Ice-templating of alumina suspensions: Effect of supercooling and crystal growth during the initial freezing regime," *Journal of the American Ceramic Society,* Article vol. 95, no. 2, pp. 799-804, 2012.

[50] L. Hadji, "Morphological instability induced by the interaction of a particle with a solid-liquid interface," *European Physical Journal B,* vol. 37, no. 1, pp. 85-89, 2004.

[51] K. Jouppila and Y. H. Roos, "Glass Transitions and Crystallization in Milk Powders," *Journal of Dairy Science,* Article vol. 77, no. 10, pp. 2907-2915, 1994.

[52] N. O. Chung, M. K. Lee, and J. Lee, "Mechanism of freeze-drying drug nanosuspensions," *Int J Pharm,* vol. 437, no. 1-2, pp. 42-50, 2012.

[53] J.-X. Guinard and R. Mazzucchelli, "The sensory perception of texture and mouthfeel," *Trends in Food Science & Technology,* vol. 7, no. 7, pp. 213-219, 1996.

[54] M. Spannuth, S. G. Mochrie, S. S. Peppin, and J. S. Wettlaufer, "Particle-scale structure in frozen colloidal suspensions from small-angle x-ray scattering," *Phys Rev E Stat Nonlin Soft Matter Phys,* vol. 83, no. 2 Pt 1, p. 021402, 2011.

[55] J. Zheng, D. Salamon, L. Lefferts, M. Wessling, and L. Winnubst, "Ceramic microfluidic monoliths by ice templating," *Microporous and Mesoporous Materials,* vol. 134, no. 1, pp. 216-219, 2010.

[56] A. H. J. Paterson, "Lactose processing: From fundamental understanding to industrial application," *International Dairy Journal,* vol. 67, pp. 80-90, 2017.

[57] D. Mahlin, J. Berggren, G. Alderborn, and S. Engström, "Moisture-induced surface crystallization of spray-dried amorphous lactose particles studied by atomic force microscopy," *Journal of Pharmaceutical Sciences,* https://doi.org/10.1002/jps.10503 vol. 93, no. 1, pp. 29-37, 2004.

[58] J. F. Willart, V. Caron, R. Lefort, F. Danède, D. Prévost, and M. Descamps, "Athermal character of the solid state amorphization of lactose induced by ball milling," *Solid State Communications,* vol. 132, no. 10, pp. 693-696, 2004.

[59] C. V. Morr, "Chemistry of milk proteins in food processing," *Journal of dairy science,* Review vol. 58, no. 7, pp. 977-984, 1975.

[60] P. Walstra, J. T. M. Wouters, and T. J. Geurts, *Dairy science and technology*. Boca Raton: CRC Taylor & Francis, 2006.

[61] P. J. Fellows, "22 - Freezing," in *Food Processing Technology (Fourth Edition)*, P. J. Fellows, Ed.: Woodhead Publishing, 2017, pp. 885-928.

[62] J. C. Kasper and W. Friess, "The freezing step in lyophilization: Physico-chemical fundamentals, freezing methods and consequences on process performance and quality attributes of biopharmaceuticals," *European Journal of Pharmaceutics and Biopharmaceutics,* vol. 78, no. 2, pp. 248-263, 2011.

Chapter 5: Frozen Storage of Ovine Milk

5.1 Chapter Summary

If milk is thawed immediately after freezing, then it is essentially undamaged. No significant changes were seen in samples stored frozen for 1 or 3 days. Deleterious effects happen over time. A series of trials was conducted to measure the extent and pace of change under various storage conditions. Raw ovine milk was collected and stored frozen at -10°C, -18°C and -28°C for periods up to 8 weeks. The milk was tested after thawing to evaluate changes in the particle size, pH, viscosity, colour and heat coagulation time. The effects of heating and high-pressure homogenisation of thawed milk on particle size, viscosity and colour were also evaluated. The level of protein in the serum phase of the milk was measured across the storage time for each storage temperature, as was the distribution of Ca^{2+} ions. The viscosity of milk and its response to heat was measured after 6 months storage at -18°C.

Thermally reversible gels were formed after at least 4 weeks storage at -10°C, as seen by increases in viscosity, increases in particle size and the formation of a gel. There were no trends in pH or serum protein levels observed over the storage period, however the Ca^{2+} concentration decreased in samples stored at -10°C and -18°C. It is suggested that a gel is formed by steric interaction and interaction with the concentrated solute environment when milk solids are concentrated into volumes between ice crystals and this gel is stabilised by Ca^{2+} ions. This gel is weak and when thawed milk is heated, the kinetic energy of particles overcomes the binding energy of the particles.

Homogenisation was able to break apart agglomerated of milk solids formed during frozen storage.

Sintering and agglomeration of particles could affect the bulk handling behaviour of frozen milks, so the effect of storage under an applied static load was tested on whole ovine milk at -10°C and -18°C, and concentrated milk at -18°C and -25°C. Frozen ovine milk sintered after storage at -10°C but remained free-flowing after storage at -18°C. Concentrated milk sintered after storage at -18°C and remained free-flowing after storage at -25°C. This may be a result of the greater fraction of unfrozen milk at higher storage temperatures, and lower viscosity of the unfrozen milk at higher storage temperatures.

5.2 Introduction

Frozen storage has been proposed for sheep milk, and has been found to be appropriate under certain conditions[1, 2]. However it has also been linked to decreases in total solids, fats and non-fat milk solids[3],development of rancid flavours[4], increased coagulation time and decreased curd firmness in cheese making[5], casein destabilisation [6] and formation of insoluble complexes [2]. These effects are linked to the temperature of storage [7], the speed of freezing [8], the crystallisation of lactose [9, 10], and the salt balance in the unfrozen phase [4, 7, 10].

The pH of the unfrozen phase in frozen electrolyte solutions can change significantly due to the incorporation of ionic impurities in ice and the formation of local electric gradients[11].

Under some freezing and frozen storage conditions, the formation of insoluble gels and insoluble protein aggregates was noted. The protein composition of these insoluble fractions is of interest as an understanding of their composition may shed light on their formation, and how to prevent it.

Heat treatment is a key process in the dairy industry, and the majority of milk collected undergoes it[12]. Ovine and caprine milks have lower heat stability than bovine milk [13] which is related to differences in the mineral composition of the two milks. As frozen storage affects the salt balance of the system[14], this storage may also affect the heat stability of the milk. The heat stability of sheep's milk is affected significantly by the time of year at which the milk is collected[15]. Calcium contents have been reported stable throughout a lactation season[16], though some authors have demonstrated that the mineral content of ovine milk varies significantly over a year[17]

A widely used method to determine heat stability is the "subjective heat stability test" [18], where a sealed glass tube containing milk is immersed in an oil bath at 140°C and agitated until coagulation is observed.

To determine total calcium content samples were dry ashed then dissolved in HNO_3 and analysed by MP-AES. To determine soluble calcium, the casein micelles and associated calcium were separated from serum by ultracentrifugation at 80,000g for 2hrs[19]. The supernatant was prepared as above and then analysed as for total calcium.

During storage of frozen milk pellets there was a concern that the small amount of unfrozen water, when combined with pressure at the contact points between particles, could lead to "sintering", where particles bridge at contact points, leading to the bulk becoming an agglomeration, rather than a free-flowing product. This could make product handling more difficult, and should be avoided if possible. The conditions under which milk samples would sinter together were evaluated.

5.3 Materials and Methods

Raw sheep milk was collected from the bulk tank of a commercial sheep milk farm located in Wairarapa, New Zealand in September 2018. The milk was kept below 5°C until analysis and freezing. All analyses on raw milk were conducted within 48 hours of collection. Subsamples of milk were stored below 2°C for up to 72 hours for proximate analysis, as discussed in section 3.2.

Aliquots (100 mL) of milk samples in 100 mL sample containers were placed in insulated bins to simulate the slow freezing that would occur in a bladder or bucket in a blast freezer.

Samples were frozen and stored in walk-in freezers at -10°C, -18°C, and -28°C to -30°C, for periods of 1,3 days, 1,2,3,4,6,8 weeks. The samples will therefore be referred to by their storage temperature and time, i.e. "-10°C 4 Weeks sample".

5.3.1 Equipment

Details of all equipment used in this work, including manufacturer and country of origin, are given in Chapter 2.

5.3.2 Proximate Analysis

The total solids content was determined gravimetrically by forced air drying after pre-drying over steam, following AOAC method 990.19. The fat content was determined gravimetrically by Mojonnier extraction, according to AOAC method 989.05[20]. The Ash content was measured by drying followed by ashing at 550°C according to AOAC method 945.46. Crude protein was determined from the total nitrogen, measured by the Kjeldahl method, following AOAC method 991.20. Lactose was estimated by difference.

5.3.3 Sintering During Storage

5.3.3.1 Ovine Milk

Ovine milk (20 L) was reconstituted from whole ovine milk powder, supplied by Spring Sheep Dairy (NZ), to a concentration of 18% total solids. The milk was frozen in a 5 mm layer in

trays approximately 10 mm deep in a walk-in freezer room set at -20°C. Further details of these freezers are given in section 2.9. The frozen milk was then manually broken into flakes with a thickness of 5 mm, and length and width of approximately 30 mm, and placed into acrylic cylinders (ID 240 mm, and depth 200 mm). A rigid circular plate was placed on top of the milk flakes, and a 10 kg mass, simulating the pressure of approximately 500 mm of milk flakes, was placed on the circular plate. The cylinders containing the frozen milk flakes were placed in sealed containers in walk-in freezers held at -10°C and -18°C. The sealed container reduced the likelihood of sublimation or desublimation occurring.

After 4 months frozen storage the samples were removed from the freezer and the particles were observed for signs of sintering, agglomeration, or deformation. The original location of the circular plate was marked with indelible marker to provide a reference against which deformation and settling could be observed.

5.3.3.2 Concentrated Bovine Milk

A further sintering test was conducted using concentrated bovine milk, to simulate evaporated milk. Milk was reconstituted to 35% from whole milk powder. The simulated evaporated milk was frozen into cylinders approximately 15 mm in diameter and 30-90 mm long, placed into acrylic cylinders (ID 240 mm, and depth 200 mm). A rigid circular plate was placed on top of the simulated evaporated milk pellets, and a 20 kg mass, simulating the pressure of approximately 1000 mm of milk pellets, was placed on the circular plate. The cylinders containing the frozen milk pellets were placed in sealed containers in walk-in freezers held at -18°C and -25°C. No samples were stored at -10°C, as it was expected that the higher total solids level would lead to extensive sintering at -10°C, based on results from the previous sintering trial.

After 2.5 months frozen storage the samples were removed from the freezer and the pellets were observed for signs of sintering, agglomeration, or deformation. The original location of the circular plate was marked with indelible marker to provide a reference against which deformation and settling could be observed.

5.3.4 pH Measurement.

The pH was measured in freshly thawed samples with a benchtop pH meter, calibrated at pH 4.00 and pH 7.00 with Merck CertiPUR reference buffer solutions (Merck KGaA, Darmstadt, Germany)before each series of measurements. Measurements were carried out at 20°C. Measurements were conducted in triplicate.

5.3.5 Soluble and Total Calcium Fractionation.

To determine the total and soluble fractions of the milk samples after storage, a method was required for separating the micellar casein system and its associated colloidal calcium phosphate from the serum, without changing the solute makeup of the liquid phase. Destabilising and precipitating casein by adjustment of the system pH was unsuitable. Ultracentrifugation was used to separate the casein phase[19]. The procedure for sample preparation is represented graphically in Figure 5-1.

Fat globules were removed by centrifugation at 3000 g for 20 minutes at 20°C. A sample of the skim milk was retained for analysis. The remaining skim milk was centrifuged at an average (spatial) acceleration of 80,000 g for 2 hours at 20°C[19].

The serum supernatant was collected. Skim milk and serum were stored frozen below -25°C in an industrial walk-in freezer for long term storage before elemental analysis.

5.3.6 Atomic Emission Spectroscopy

The samples were prepared for elemental analysis following a procedure adapted from AOAC official method 991.25[20], with a smaller dilution factor for the ash samples to account

for the lower mass fraction of calcium in milk compared to cheese, and MP-AES used in place of AAS.

All glassware used was soaked overnight in 5% HNO_3 and rinsed with milli-Q water before drying and use.

Samples were placed in pre-weighed porcelain sample crucibles. Crucibles had been washed in 5% HNO_3 and milli-Q water, and then placed in a furnace at 550°C overnight. These crucibles were transferred to desiccators and stored until needed for sample preparation. Samples were dried over a steam bath, then ashed overnight at 550°C [21, 22].

The ash content was determined gravimetrically, then the ash was dissolved in 2.5 mL of 6M HNO_3. An aliquot (5 mL) of 1% $LaCl_3$ solution was added (for a final concentration of 0.1% La) and the samples were made up to 50 mL with MilliQ water. Samples were gravity filtered through low ash filter papers (Whatman 541).

Calcium content was determined using an Agilent 4210 MP-AES as described in section 2.8 at a wavelength of 704.815 nm. A calibration curve was generated with standards at 2, 20, 200 and 1000 ppm Ca^{2+}, prepared from $CaCO_3$ and 6M HNO_3.

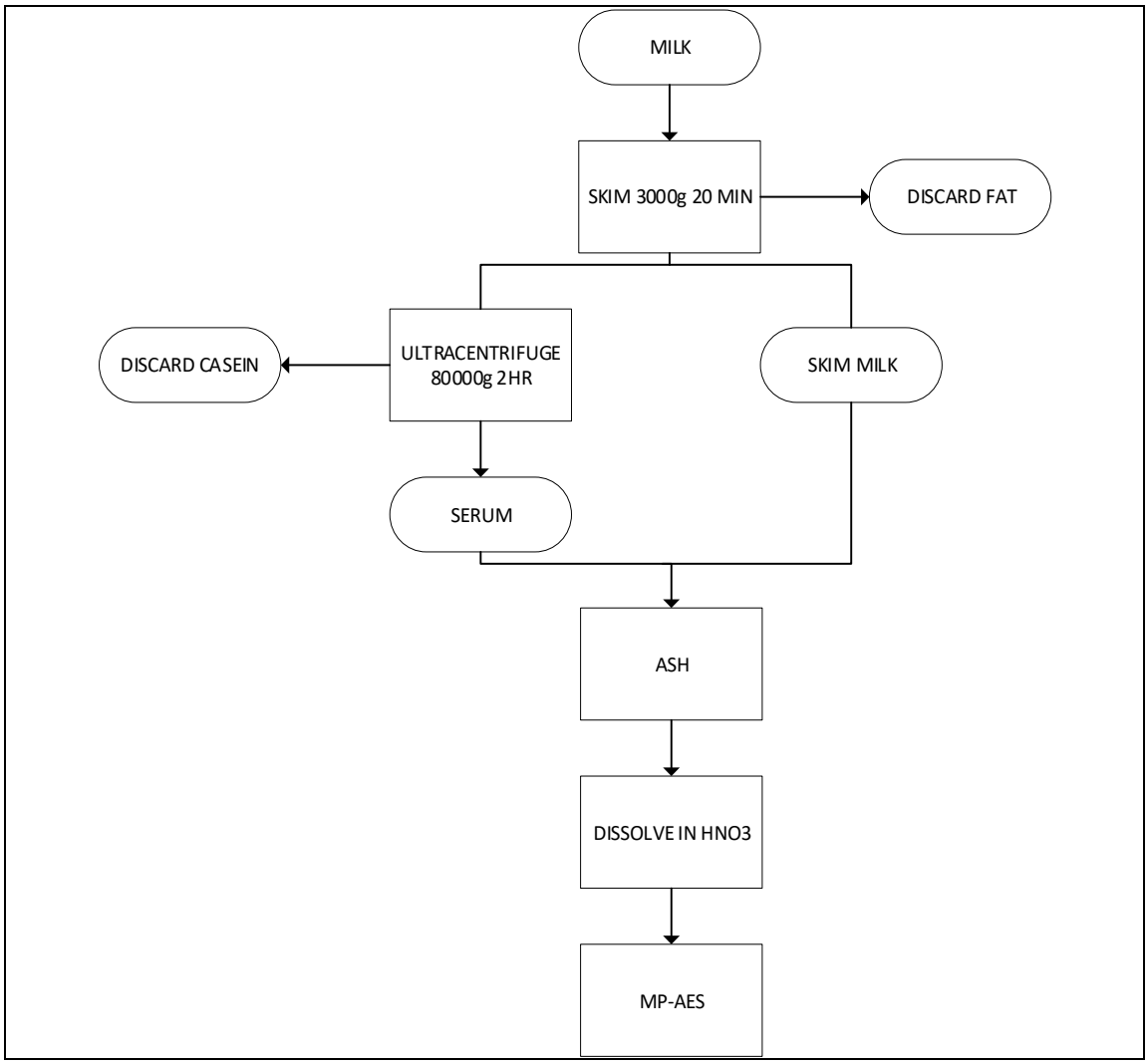

Figure 5-1: Preparation of samples for elemental analysis.

5.3.7 Determination of Serum Protein Concentration

To evaluate the extent of any solubilisation of casein proteins during the freezing and thawing process, or the incorporation of whey proteins during freezing and thawing, the crude protein concentration of the serum phase was measured. The serum fraction was isolated by ultracentrifugation as described in section 3.5. Crude protein was determined by the Kjeldahl method. Due to time and sample volume restraints, these measurements were conducted in singlicate.

5.3.8 Homogenisation

To evaluate the effect of high-pressure homogenisation on the properties of freeze-thawed milk, samples were tested as follows: Each frozen sample was thawed in a waterbath at 20°C. All samples thawed within 60 minutes. A 150 mL aliquot was then heated to 60°C. The aliquots were then homogenised in an APV 2000 benchtop high pressure homogeniser, with a pressure at the first stage of 20 MPa, and a second stage pressure of 4 MPa. The samples were recycled through the homogeniser for 3 passes. Subsamples were taken for analysis after the heating step and after each pass through the homogeniser.

Colorimetric measurements, particle size distribution and flow curves were collected for the subsamples. The homogenisation testing was conducted in singlicate.

5.3.8.1 Colorimetry

Colour measurements were conducted with a Konica Minolta CR-400 Chroma Meter. Samples of milk were placed in a petri dish and placed on top of the sensing aperture. A shade was lowered over the apparatus to prevent interference from ambient light, and the colour profile was then measured. Data was recorded in the CIELAB colour space.

5.3.8.2 Particle Size Measurements.

Particle sizes were measured by dynamic light scattering, using a Malvern Mastersizer 2000. For model fitting, the particles were treated as spherical with a refractive index of 1.46, and an absorption index of 0.001[23]. Samples of milk were dispersed in RO water.

5.3.9 Heat Stability

Milk samples were adjusted to the desired pH by the addition of 1M HCl or 1M NaOH. 5 mL of sample was transferred to an 8 mL Wheaton sample vial (224884), and sealed with a phenolic resin cap.

Sealed vials were attached to a mounting plate by spring clips and lowered into an oil-bath at 140°C. Vials were rocked at a rate of 10 min^{-1}. The time was recorded at first appearance of a coagulated solid. Readings from vials which leaked and released significant volumes of bubbles were discarded.

A pH range of 6.2 to 7.0, with increments of 0.2 was selected as typical of ovine milk pH [24], including possible deviations due to storage and processing conditions.

5.3.10 Viscosity

Viscosity measurements were conducted with an Anton Paar MCR301 computerised rheometer fitted with a double-gap geometry. A shear rate sweep from 10 s^{-1} to 1000 s^{-1} at a temperature of 20°C was conducted for each sample. These measurements were conducted in triplicate. Measurements were taken after the heating step, and after each pass through the homogeniser.

5.3.11 Thawing temperature and time effect on viscosity

Milk was frozen in 100mL sample containers and stored at or below -25°C for 6 months. Milk was thawed in waterbaths at 4°C, 21°C, 30°C, 50°C, and left in water baths for 1,2,4 hours.

Viscosity was measured at 20°C and at a shear rate of 230s^{-1}, with an Anton Paar MCR 301 computerised rheometer fitted with a double-gap geometry

Particle size was measured with a Malvern Mastersizer 3000. For model fitting, the particles were treated as spherical with a refractive index of 1.46, and an absorption index of 0.001. Samples of milk were dispersed in RO water.

5.4 Results

5.4.1 Composition

The composition of the milk was as follows:

Table 5-1: Measured composition of sheep milk used in this study. Error bars are 95% CI for mean, N=3.

Component	% m/m
Total solids	17.69 ± 0.004
Crude protein	6.53 ± 0.03
Fat	5.76 ± 0.04
Ash	1.02 ± 0.02

This composition is well within the expected range of compositions for sheep milk as reported by many authors [25].

5.4.2 Sintering During Storage.

5.4.2.1 Ovine Milk

The samples were removed from the freezer after 4 months storage. The frozen milk flakes stored at -10°C displayed some sintering and agglomeration, with flakes sticking together when the cylinders were inverted. There was also deformation of the flakes, with the flakes having a 5-10 mm lower bed depth than when storage was started. This was an approximate 10% reduction in height.

Milk flakes stored at -18°C displayed no noticeable agglomeration, deformation or sintering, the bed depth was the same as at the start of the storage period, and the particles flowed easily when the cylinders were inverted.

1.1.1 Concentrated Bovine Milk

The simulated evaporated milk pellet stored at -18°C, the cylinders showed some flattening (flats ~12mm wide) where they had been in direct contact with the circular plate. The pellets strongly adhered to each other, so the mass could be lifted as a unit, and individual cylinders were difficult to detach manually. The bed of frozen cylinders had decreased approximately 10-15 mm in height during the storage period.
The concentrated milk cylinders stored at -25°C showed no noticeable deformation and remained free-flowing after the storage period.
The temperature logs from the freezers are shown in Figure 5-2 below:

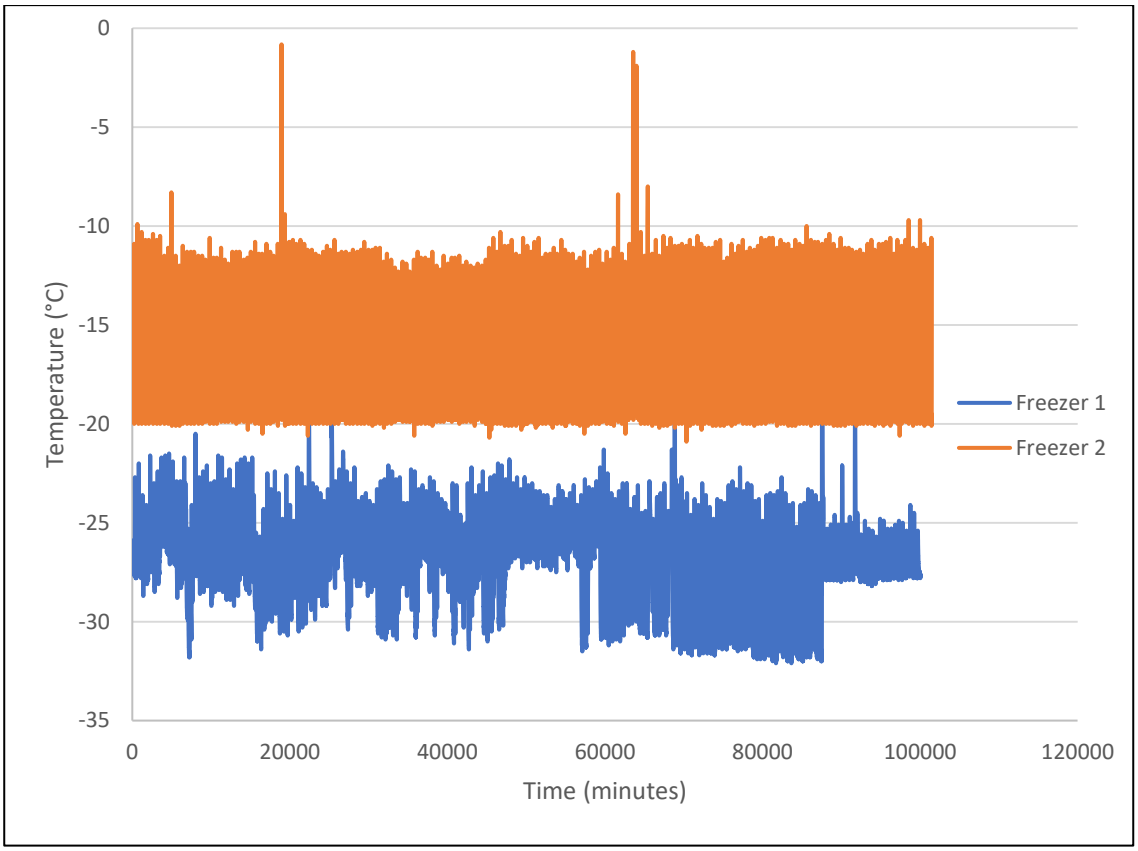

Figure 5-2: Temperature log from the storage freezers during the storage of frozen concentrated milk.

The total time above certain temperatures is shown in Table 5-2. These are the temperatures measured by the freezer control system, not necessarily the temperature measured inside the container with the frozen pellets.

Table 5-2: Cumulative fraction of time the freezers were above a given temperature.

FREEZER 1			FREEZER 2		
TEMP (°C)	**Total time over (min)**	**% of total time**	**TEMP (°C)**	**Total time over (min)**	**% of total time**
0	0	0.0	***0***	0	0
-5	0	0.0	***-5***	70	0.1
-10	0	0.0	***-10***	165	0.2
-15	0	0.0	***-15***	4745	4.6
-20	165	0.2	***-20***	100295	98.8
-25	12245	12.2	***-25***	101490	100
-30	84785	84.7	***-30***	101490	100

5.4.3 General Observations

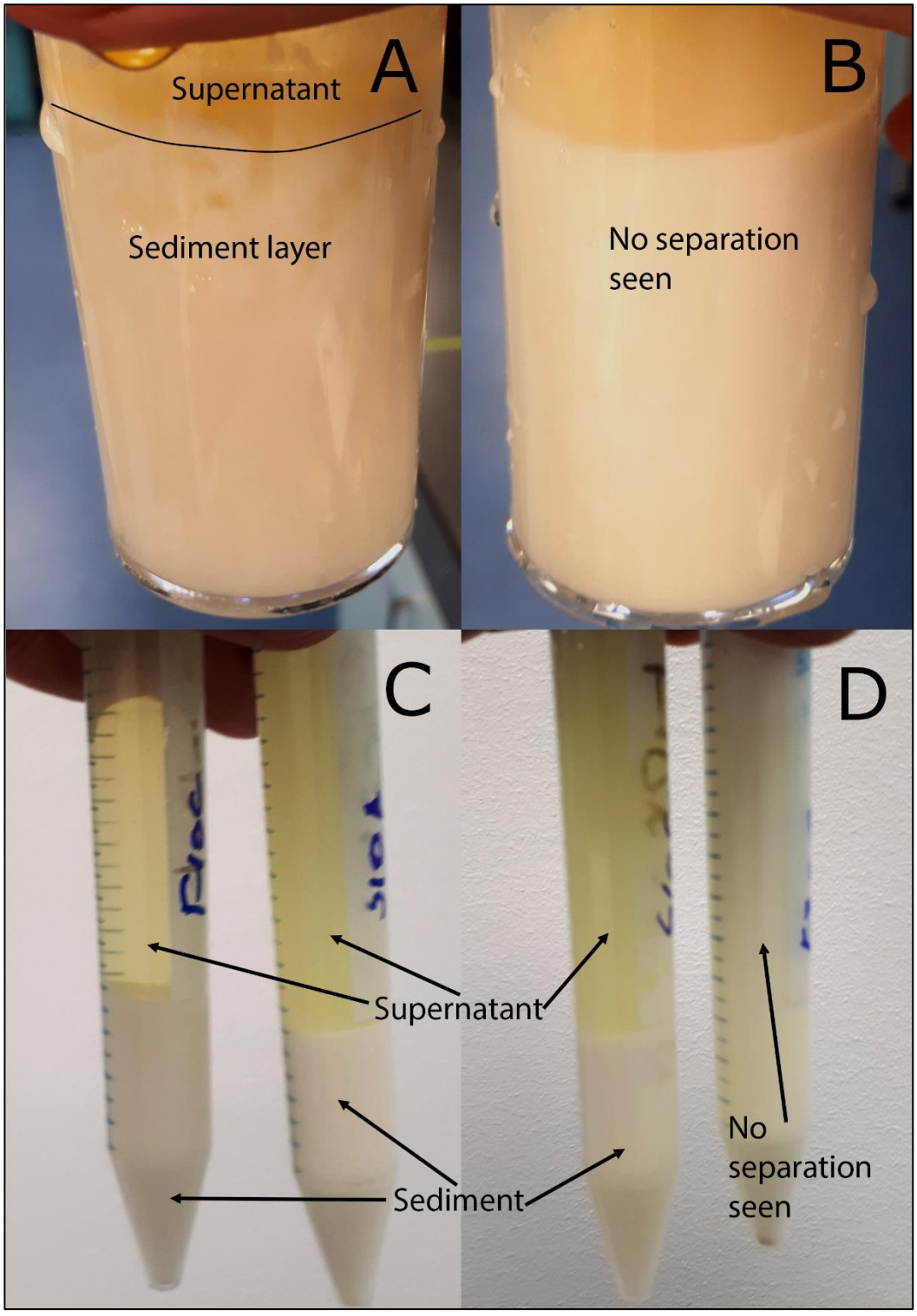

Figure 5-3: Separation of milk stored at -10°C for longer than 4 weeks (A). Comparison with milk stored below -25°C for an identical time (B). The effect of centrifugation (1,500 g x10 minutes) on these samples is shown in C and D. The milk stored at -10°C separated into a sediment and supernatant. Milk stored below -25°C did not separate under centrifugation.

After 1 week's storage at -10°C flecks were observed with the naked eye after thawing. After 4 and 8 weeks, milk stored at -10°C displayed a significant volume of sediment, similar in appearance to curdled milk. At -18°C after 8 weeks some small flecks were observed upon thawing, but little sediment. Milk stored below -25°C never displayed any flecks or signs of

protein sedimentation. After 8 weeks there was an appearance of a small volume of free fat on the surface after thawing.

This separation is shown in Figure 5-3 in section A. Milk stored at -10°C then showed a gel-like sediment layer and a serum supernatant layer. In section B: milk that was stored below -25°C for the same time period, shows no separation. In C two samples of milk stored at -10 °C for longer than 4 weeks then thawed at 20°C and centrifuged (less than 60 minutes after thawing) at 1500 g for 10 minutes; the separation into a sediment and supernatant can be seen clearly. In D, milk stored below -25°C then thawed , and treated to the same centrifugation treatment (right-hand centrifuge tube) as milk stored at -10°C (left-hand tube) shows no separation, whereas the separation in the -10°C milk can be clearly seen.

After centrifugation the cream could be separated from the majority of samples, as it formed a distinct layer above the skim milk. However, in milk stored at -10°C for 4 weeks and 8 weeks, no cream layer was present. After centrifugation the milk separated into a gel-like sediment and a clear supernatant.

After heating to 60°C with stirring, the sediment observed in thawed -10°C 4-week samples appeared to disperse, returning the milk to a normal appearance. The sediment also appeared to disperse after 24-48 hours of refrigerated storage. The sediment appeared to re-disperse more slowly after 8 weeks of frozen storage when compared to the sediment present after 4 weeks of frozen storage for all samples showing sediment.

5.4.4 pH

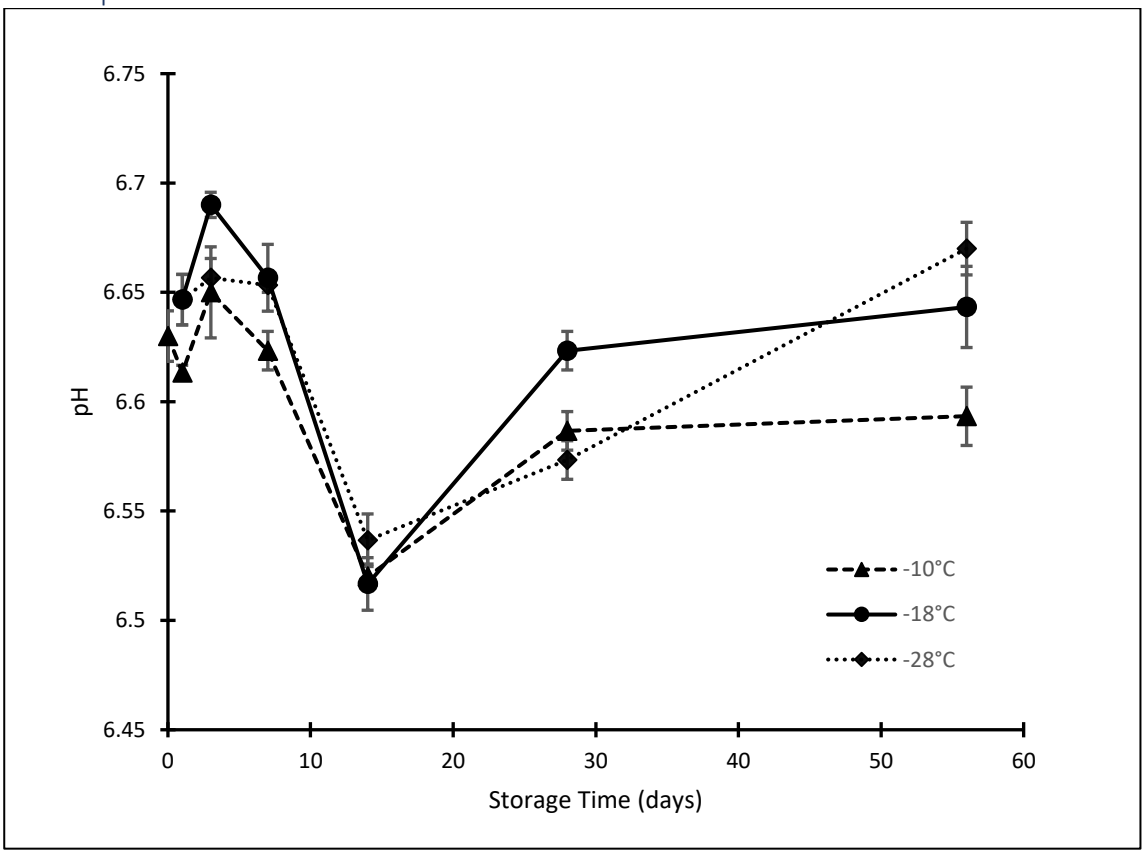

Figure 5-4: pH of Ovine milk measured after frozen storage at -10°C, -18°C and -28°C for up to 56 days. Error bars are standard error of the mean.

The pH evolution over time is shown in Figure 5-4, with the values, and the results of an ANOVA test presented in Table 5-3. The error bars in Figure 5-4, and the error terms in Table 5-3, are the standard error of the mean. As can be seen, there was no clear trend of increase or

decrease in the pH over the storage time, for any of the storage conditions. There was a significant difference between the pH of the unfrozen milk and milk stored for 2 weeks at all storage temperatures. There was no significant difference between the unfrozen milk and all the milk stored for less than 2 weeks, or greater than 2 weeks. This may be an instrumental effect that was only present when these samples were measured. All the pH values recorded were within the range of pH values previously reported for ovine milk [25]

Table 5-3: pH of samples immediately after frozen storage and thawing. Error bars are 95% CI for mean. Treatments that do not share a superscript are different. All measurements were conducted in triplicate: p<0.05.

	Storage Temperature (°C)		
Storage Time (days)	**-10**	**-18**	**-28**
Unfrozen	6.63 ± 0.01^{abcde}		
1	6.61 ± 0.00^{bcde}	6.62 ± 0.01^{bcde}	6.65 ± 0.01^{abcd}
3	6.65 ± 0.02^{abc}	6.69 ± 0.02^{a}	6.66 ± 0.00^{ab}
7	6.62 ± 0.01^{bcde}	6.65 ± 0.01^{ab}	6.65 ± 0.01^{abc}
14	6.52 ± 0.01^{g}	6.51 ± 0.01^{g}	6.54 ± 0.01^{fg}
28	6.58 ± 0.01^{def}	6.62 ± 0.02^{bcde}	6.57 ± 0.01^{efg}
56	6.59 ± 0.01^{cdef}	6.64 ± 0.01^{abcd}	6.67 ± 0.01^{ab}

5.4.5 Calcium Fraction

The serum calcium concentrations decreased through the storage time in samples stored at -10°C and -18°C. The milk stored at -10°C showed an increase in the Ca^{2+} concentration in the 56 day samples, when compared to 28 day samples though this may merely be a redistribution of the Ca^{2+} from the sediment to the serum during the time before separation, as has been suggested may occur in previous work looking at mineral distribution during frozen storage [14]. There was a small decrease in serum Ca^{2+} concentration when milk was stored at -28°C.

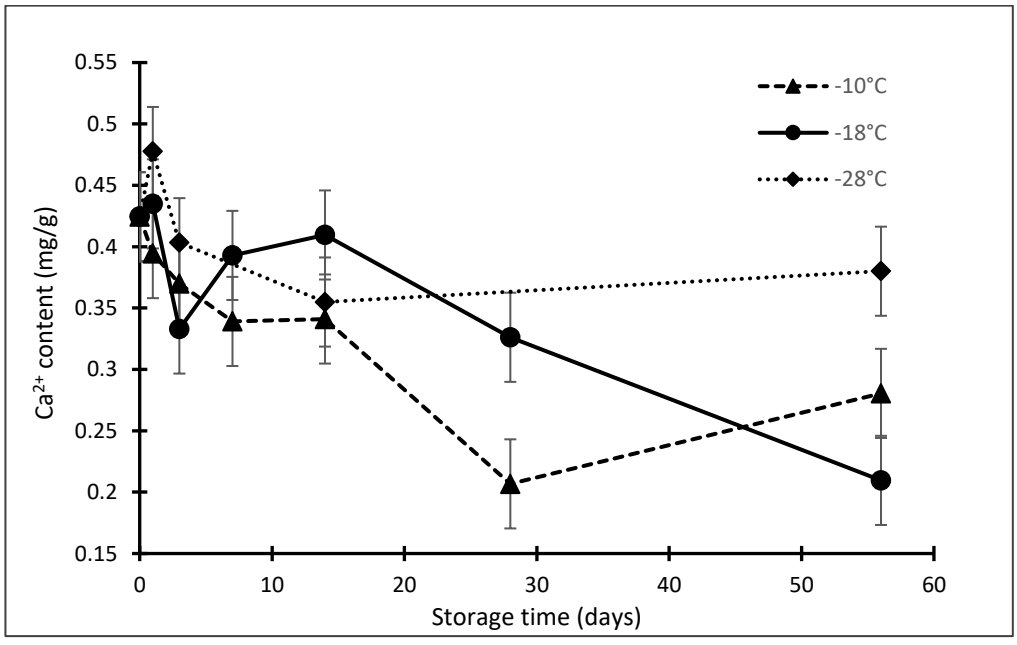

Figure 5-5: Ca^{2+} concentration in the serum phase (or supernatant phase in gelled samples), as determined from MP-AES analysis of ashed samples. Samples were stored at -10°C, -18°C and -28°C for up to 8 weeks (56 days).Error bars are 1σ.

The Ca^{2+} concentration in the sediment or gels formed after storage was 68% higher than that of skimmed milk. The total Ca^{2+} concentrations in selected milk samples are shown in Table 5-4.

Table 5-4: Calcium concentration in selected samples after frozen storage. Reported standard deviation for serum samples is the pooled standard deviation.

Sample Conditions			***Ca^{2+} Concentration (mg/g)***	
Storage time (days)	**Storage Temperature (°C)**	**Phase**	$\bar{x}$	σ
Unfrozen	Unfrozen	Serum	0.424	0.036
Unfrozen	Unfrozen	Skim milk	2.14	0.13
56	-10	Sediment	3.82	0.17
56	-10	Serum	0.280	0.036
56	-18	Serum	0.210	0.036
56	-30	Serum	0.380	0.036

5.4.6 Protein Solubilisation

There was no apparent change in the protein concentration during the storage period. The measured protein concentration in the milk serum phase are shown in Figure 5-6.

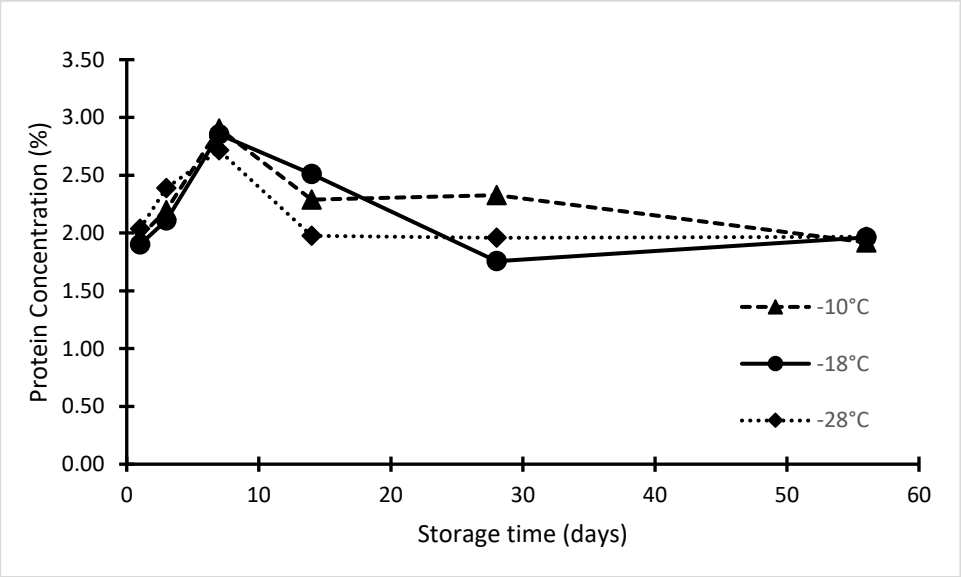

Figure 5-6: Protein concentrations in milk serum phase. In samples stored at -10°C for 4 weeks and 8 weeks, the protein concentration is that of the supernatant after gentle centrifugation.

There was also no consistent change in the concentration of protein in the supernatant fraction separated from milk which was stored at -10°C for 4 weeks and 8 weeks, indicating that there was little incorporation of whey proteins into the sediment/curd network observed, and nor was there any breakdown and solubilisation of casein proteins that would cause them to enter the soluble phase.

5.4.7 Heat stability

The measured heat stability curves are shown in Figure 5-7. The values presented are the average of triplicate measurements. In measurements where a leak was detected, the value was discarded. It is well known that there are two types of milk with regards to heat stability, type A where the heat stability displays a local maximum at approximately pH 6.7-6.8, and type B, where the heat stability shows no maximum and increases with increased pH[26]. As can be seen from the curves in Figure 5-7, ovine Milk is a type A milk with a maximum heat stability at pH 6.7-6.8. Frozen storage does not cause the milk to change from a type A milk to a type B milk,

the general shape of the curves was the same for all combinations of frozen storage temperature and storage time.

One-way ANOVA tests were performed for each set of data at a given pH to see if there were significant differences between the heat coagulation time at any combination of storage time and storage period. This was conducted using Minitab 18. There were no significant differences between the measured HCT for any combination of storage time and storage period.

The mean HCT measured for each combination of storage temperature, storage time and heat treatment pH is shown in Table 5-8.

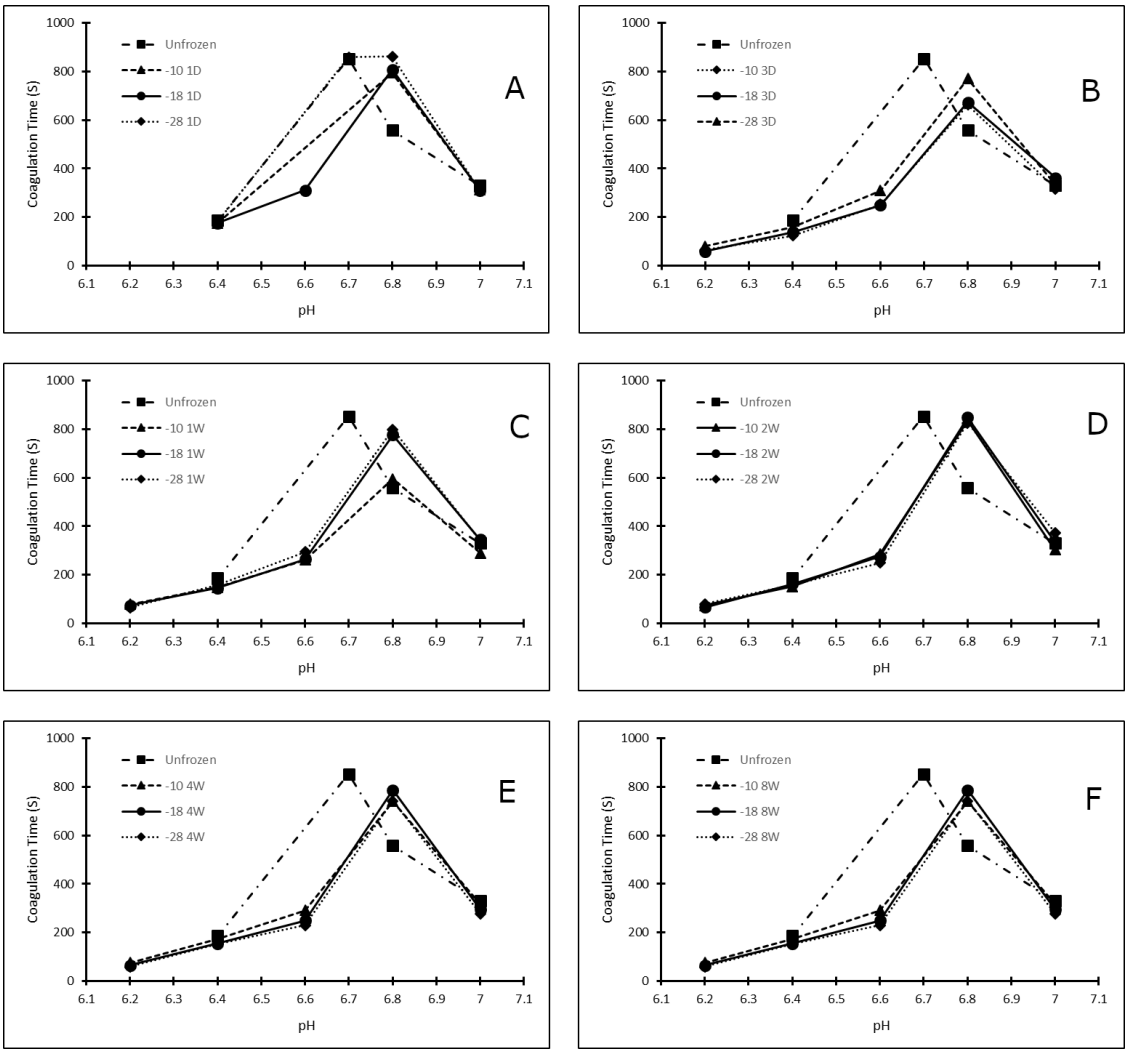

Figure 5-7: Heat stability curves for milk stored frozen for A: 1 day, B: 3 days, C: 1 week, D: 2 weeks, E: 4 weeks and F: 8 weeks.

5.4.8 Homogenisation

5.4.8.1 Viscosity

This viscosity of samples was measured after thawing and before heating for homogenisation, with the shear rate being ramped from 10 to 1000 s^{-1}. The majority of samples displayed Newtonian flow behaviour. In Figure 5-8 the viscosity at a shear rate of 230 s^{-1} is plotted against storage time for each storage temperature. A shear rate of 230 s^{-1} was selected as it is representative of the viscosity at all points for a Newtonian sample and is well within the region of high accuracy for the rheometer used.

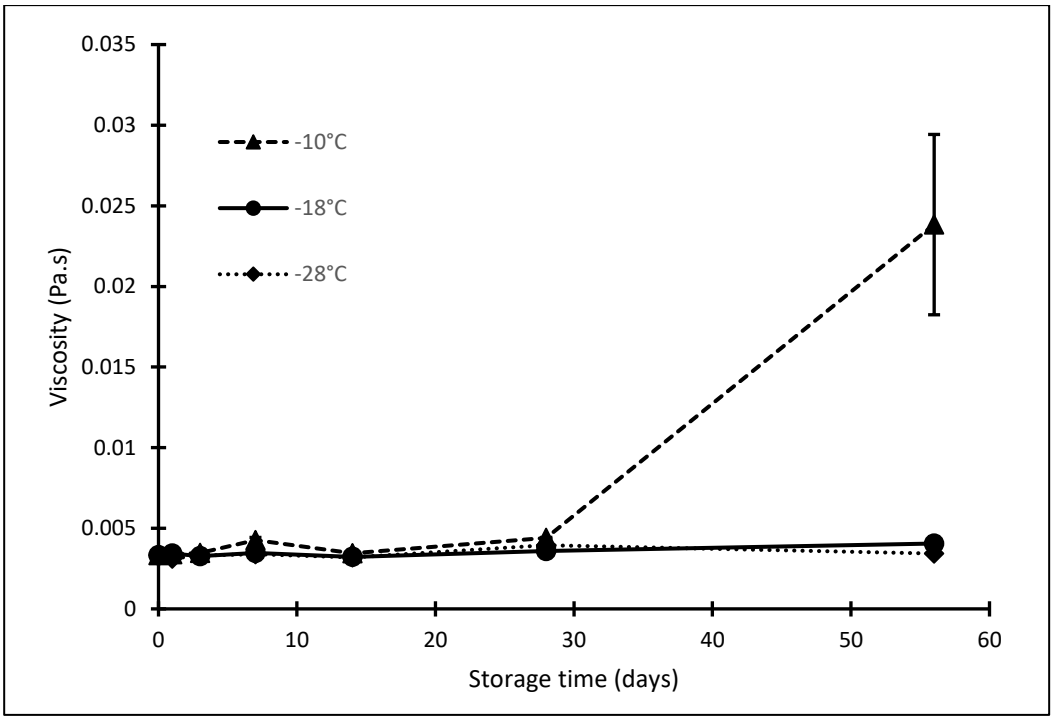

Figure 5-8: Viscosity at 230s^{-1} of raw ovine milk samples stored at -10°C,-18°C and -28°C for up to 8 weeks.

The viscosity of thawed samples was roughly constant for samples stored at -18°C and -28°C. The viscosity for milk stored at -10°C was constant until 14 and 28 days of storage, when an increase in viscosity was observed. After 56 days (8 weeks) of storage at -10°C the viscosity was observed to increase greatly, as did the variability of the measured viscosity.

The milk stored at -10°C for 8 weeks also displayed non-Newtonian characteristics on thawing. No other samples did. This can be seen in the curves of viscosity as a function of shear rate shown in Figure 5-9 A. The curving of the graph below a shear rate of approximately 50s^{-1} is a rheometer artefact.

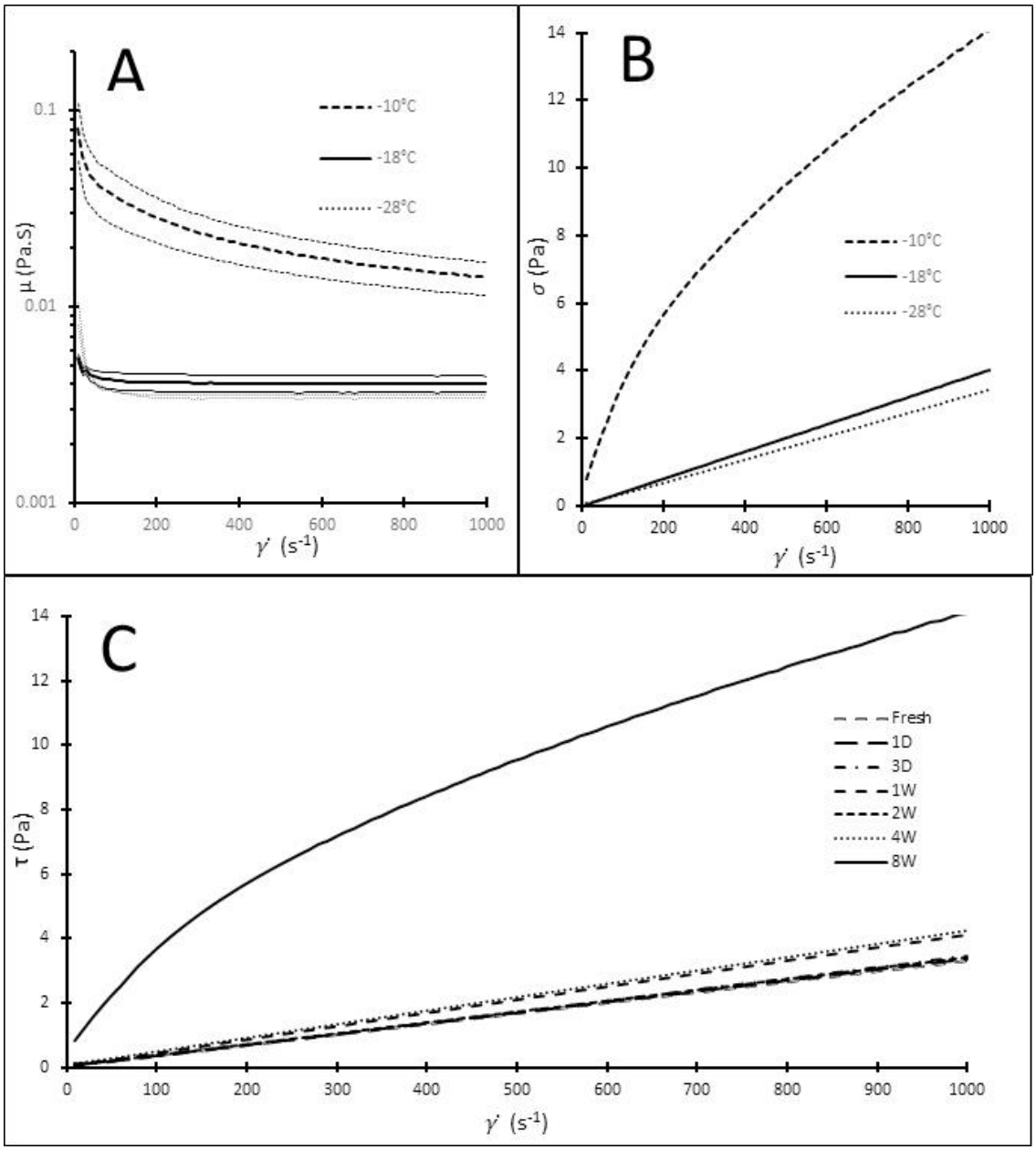

Figure 5-9: A: The viscosity of ovine milk stored for 8 weeks at -10°C, -18°C and -28°C and then thawed. Dotted lines represent 95% CI for curves. B: Shear stress as a function of shear rate in ovine milk, after 8 weeks of storage at -10°C, -18°C and -28°C. C: Shear stress as a function of shear rate in ovine milk after storage at -10°C . Measurements are shown for shear rates up to 1000s^{-1}.

The non-Newtonian behaviour of milk stored at -10°C for 8 weeks can also be clearly seen in the shear stress/shear rate curve shown in Figure 5-9 B

This develops after 8 weeks of storage, however increases in viscosity can be seen after 2 and 4 weeks, as seen by the larger gradient in the shear stress/shear rate curves in Figure 5-9 C.

The homogenisation process, involving the stirred heating of the thawed milk to 60°C, followed by 3 passes through a homogeniser, at a primary valve pressure of 20 MPa and a secondary valve

pressure of 4 MPa, led to changes in the viscosity and particle size of the milk. The viscosity of samples during the homogenisation process is shown in Figure 5-11.

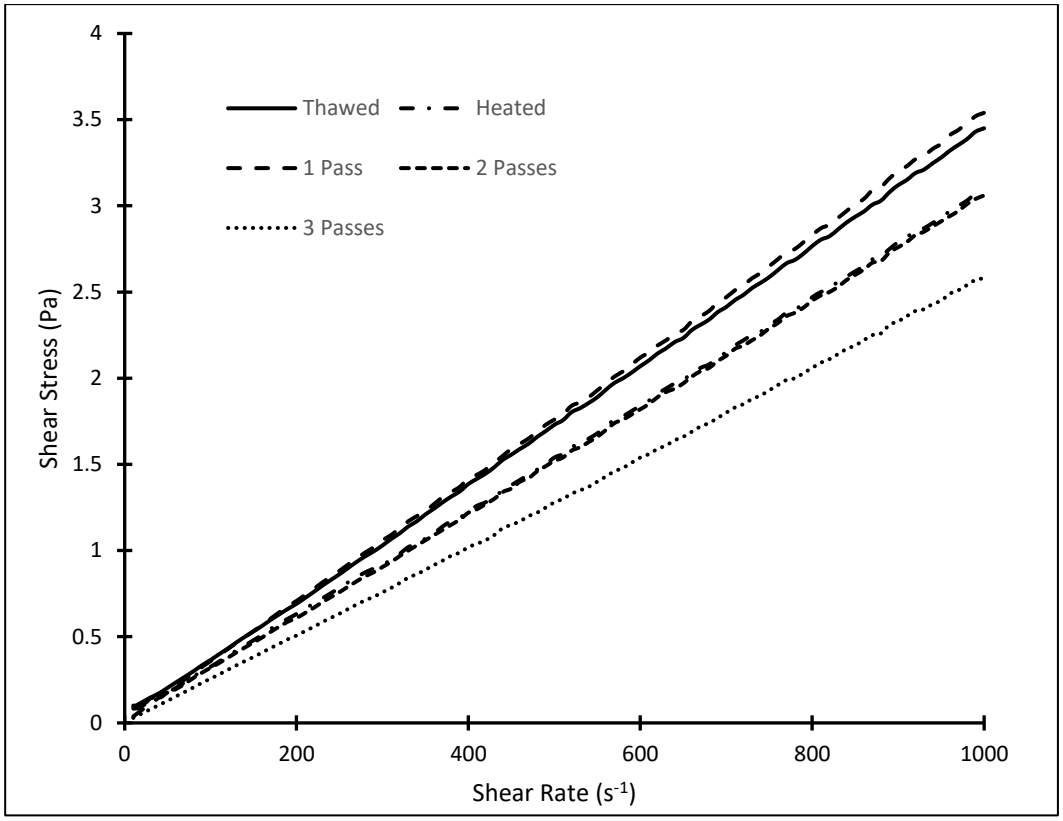

Figure 5-10: Flow curves of ovine milk stored at -28°C for 8 weeks, after various stages of the homogenisation process.

The flow curves from a typical set of measurements (-28°C for 8 weeks) are shown in Figure 5-10. All flow curves in Figure 5-10 show a linear relationship between shear rate and shear stress, confirming Newtonian flow behaviour for samples before and after homogenisation, with the exception of the samples stored at -10°C when for 8 weeks, which were non-Newtonian prior to homogenisation.

For each treatment, a power law equation was fitted to the shear stress/shear rate curve to describe flow behaviour of the milk where τ is the shear stress, $\dot{\gamma}$ is the shear rate, K is the flow consititency index and n is the flow behaviour index:

$$\tau = K\dot{\gamma}^n \quad (5\text{-}1)$$

The fitted values for K and n are given in Table 5-9.

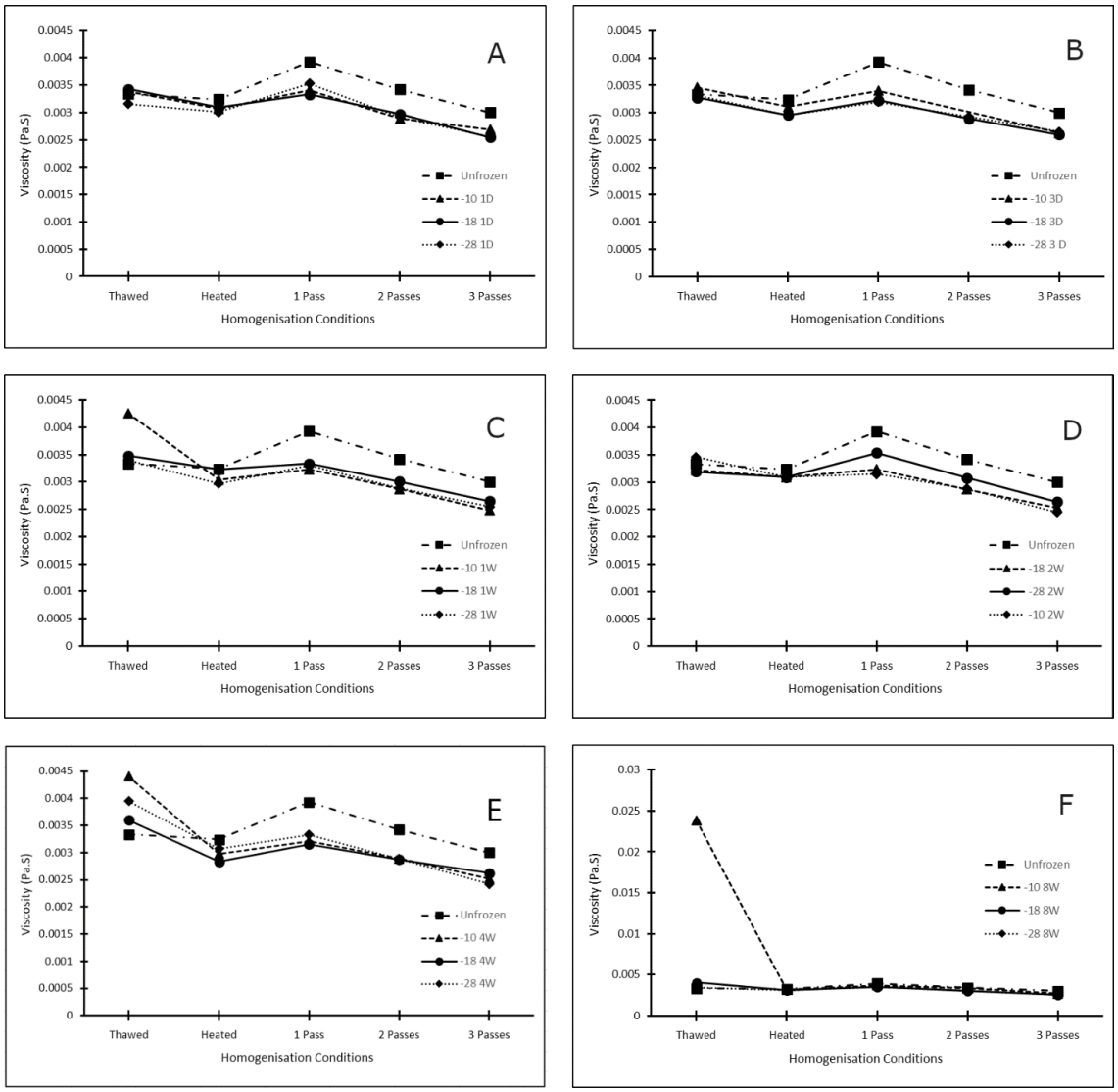

Figure 5-11: Viscosity at 230 s^{-1} for milk that has been thawed, heated to homogenisation temperature, and recycled through the homogeniser for 1, 2 and 3 passes. Milk stored frozen for A: 1 day, B: 3 days, C: 1 week, D: 2 weeks, E: 4 weeks and F: 8 weeks.

There was no apparent change in the viscosity of freshly thawed samples stored at -18°C and -28°C, when compared with the unfrozen sample for all storage times. An increase in viscosity can be seen for freshly thawed samples stored at-10°C for 1, 4 and 8 weeks, with a dramatic increase in the viscosity seen after 8 weeks at -10°C.

A simple application of heat reduced viscosity in all samples by 5-20%. A small increase in viscosity after 1 pass through the homogeniser was seen in all samples, followed by a small decrease in viscosity over the remaining two passes.

There is an order of magnitude decrease in viscosity in the milk stored at -10°C for 8 weeks after being heated to 60°C, before homogenisation. This is seen in Figure 5-11 F. The flow behaviour of this milk sample also changes from non-Newtonian to Newtonian, after the application of heat, as can be seen in the flow curves in Figure 5-12.

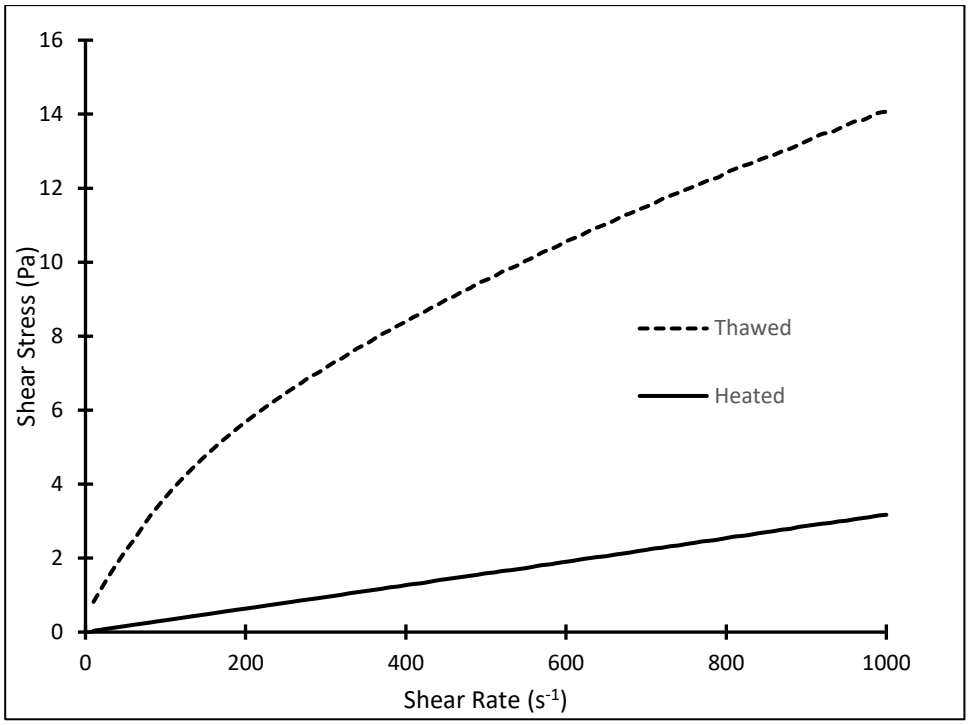

Figure 5-12: Flow behaviour of milk stored at -10°C for 8 weeks immediately after thawing, and after heating to 60°C. Curves recorded at 20°C.

The flow behaviour index of this sample before heating was 0.59. As the flow behaviour index was below 1, the fluid can be considered to have pseudoplastic behaviour. There was no apparent yield stress detected. In this test, the time dependence of the flow behaviour was not measured, so whether the -10°C 8-week milk was thixotropic could not be determined. After heating the flow behaviour index had increased to 1.00, indicating classical Newtonian flow behaviour.

5.4.8.2 Particle Sizes

The particle sizes of milk decrease significantly after the first pass through the homogeniser, with the volume mean of all samples dropping from a range of 2.22 µm to 4.69 µm, to a range of 0.46 µm to 1.34 µm. There was a further decrease in particle size after the second and third passes through the homogeniser, dropping to a range of 0.86 µm to 0.295 µm.

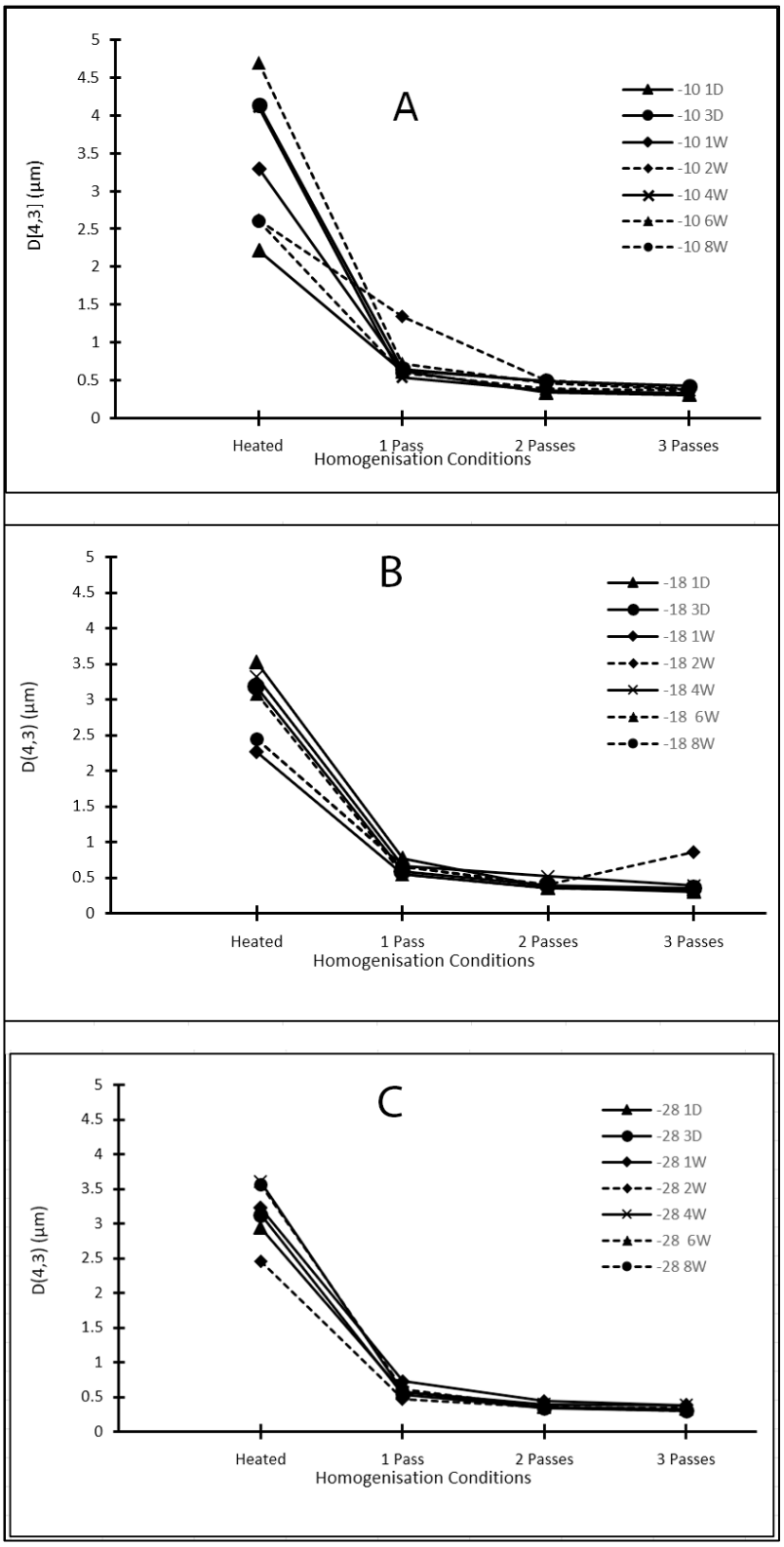

Figure 5-13: Particle size (volume weighted mean) of milk stored frozen after homogenisation treatments. A: Milk stored at -10°C, B: Milk stored at -18°C, and C: Milk stored at -28°C.

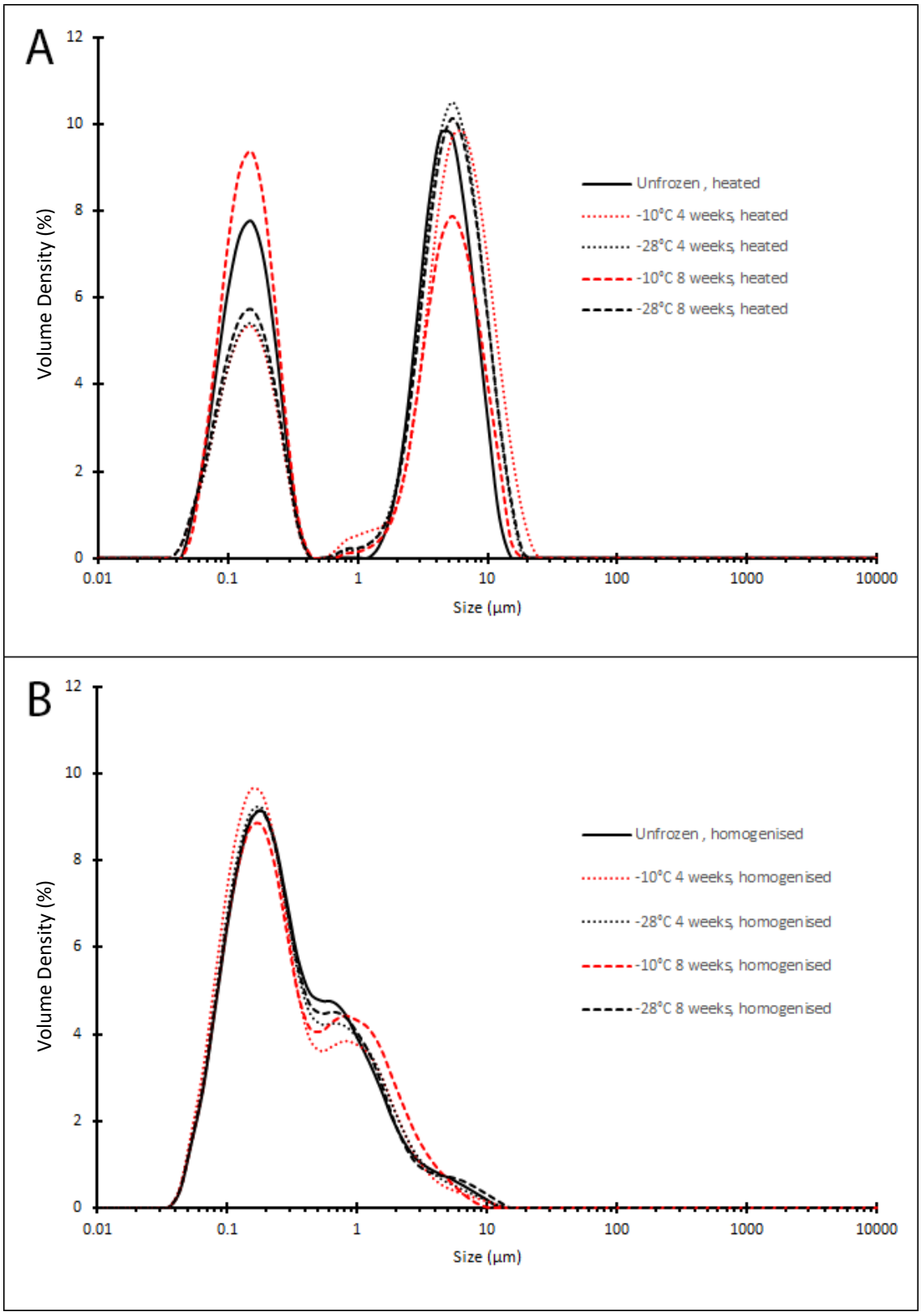

Figure 5-14: Particle size distributions of milk stored at -10°C and below -28°C for 4 weeks and 8 weeks. A: After heating to 60°C and before homogenisation. B: After homogenisation. The peaks at approximately 0.1-0.2 µm correspond to casein micelles in the samples, and the peak and shoulder in the 1-10 µm range correspond to fat globules in the samples.

The particle size distributions of selected samples before and after homogenisation are shown in Figure 5-14. As can be seen, the particle size distribution changes from a bimodal distribution to one with a single broad peak.

5.4.8.2.1 *Preliminary Measurements*

A preliminary set of measurements was conducted prior to this trial. In these preliminary trials, samples of raw ovine milk were collected from a farm in the Manawatu, and stored for 4 and 8 weeks, at -10°C and below -25°C.

The general observations for this preliminary storage trial agreed with the trial discussed in this chapter, with significant volumes of a gel-like sediment being found in samples stored at -10°C for 4 weeks and 8 weeks. The particle size distributions of these samples were measured as discussed in section 3.8.2. However, whereas the measurements shown in Figure 5-13 and Figure 5-14 were measured after heating the samples to 60°C, the measurements in the preliminary trial were conducted immediately after thawing. Volume density particle size distribution of unfrozen milk from the preliminary as shown in Figure 5-15 B which reveals two large peaks, and a third smaller peak. The first, with peak maximum at approximately 150 nm, corresponds to the typical casein micelles in ovine milk. The second has a peak maximum at 4.9 µm, which corresponds to the fat globules in the milk. The third peak was broad, and low and had a peak at ~600 µm. This is likely due to some creaming or agglomeration in the raw milk.

In milk that was stored at -10°C, during the preliminary trial, after 4 weeks of storage, the peak at 150 nm had significantly decreased in area, as had the peak at 4.9µm, and a new peak with a maximum at 43µm was observed. After 8 weeks of storage, there were no particles detected in the size range of the casein micelles, there was a single large peak, with a maximum at 154 µm. In milk that was stored below -25°C during the preliminary trial, there was no significant shifting of the peaks at 64 nm and 4.9 µm. The third peak decreased in area, however, there was no difference in the volume fraction of particles greater than 11 µm in diameter between the unfrozen samples, and the samples stored frozen for 8 weeks.

Figure 5-15 A shows the change in the surface area weighted average diameter over the storage period observed during this preliminary trial. Below -25°C, there was no significant increase in this mean diameter. At -10°C there was an increase of almost 3 orders of magnitude, increasing from 89 nm to 58 µm.

In comparison, the particle size distributions shown in Figure 5-14, do not show any an agglomeration during the storage period at -10°C or -28°C. This is likely due to the heating step prior to measurement, which disrupts the agglomerates seen in Figure 5-15. This is also noticed in the decreased viscosity after the heating of samples discussed in sections 4.8.1 and 4.9.

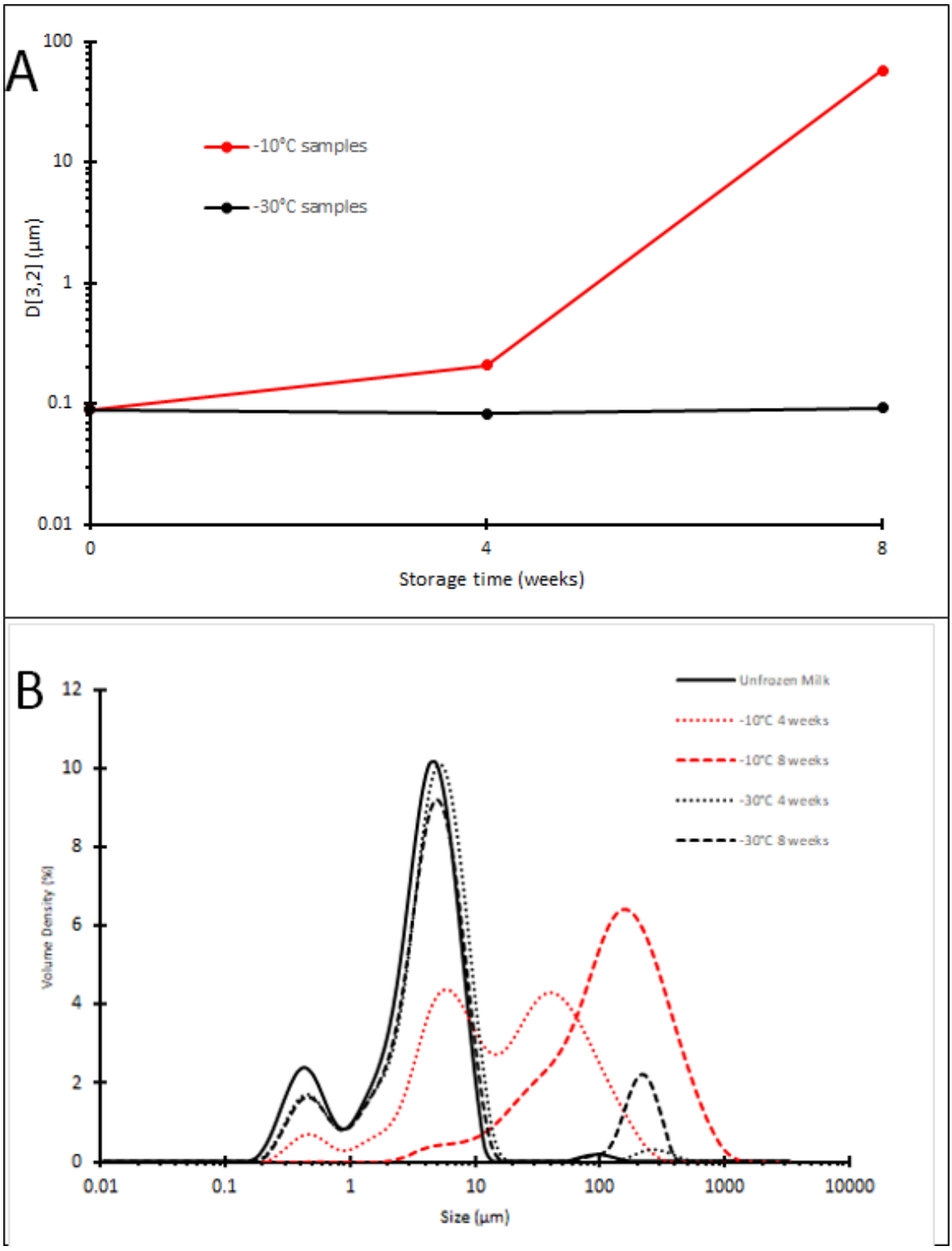

Figure 5-15: A: Evolution of D[3,2] (surface area weighted mean) of thawed ovine milk after storage at -10°C and below -28°C for 4 and 8 weeks during the preliminary storage trial . This is constant for samples stored below -28°C, and increased for samples stored at -10°C . B: Change in particle size distributions during the preliminary storage. During storage at -10°C showed aggregation with the formation of a large peak at 154µm. The peaks at approximately 0.1-0.2 µm correspond to casein micelles in the samples, and the peaks in the 1-10 µm range correspond to fat globules in the samples. Larger peaks correspond to protein and fat aggregates.

5.4.8.3 Colorimetry

The CIELAB colour space is a method of quantifying colour commonly used in the food industry[27]. It uses three co-ordinates, L*, a* and b*. L* describes the lightness or luminosity of the product and is usually depicted on the vertical axis. The green-red axis is described by a*,

with positive values for reddish colours and negative values for greenish. Blue-yellow is described by b*, with positive values for yellowish colours and negative for blueish. The whiteness index (WI) is calculated with formula (5-2) [28]. The yellowness index (YI) is a measure of the degree of yellowness of the sample, and can be calculated by formula (5-3)

$$WI = 100 - \sqrt{(100 - L^*) + a^{*2} + b^{*2}} \quad (5\text{-}2)$$

$$YI = 142.86\frac{b^*}{L^*} \quad (5\text{-}3)$$

The YI and WI for all measured samples are plotted in Figure 5-16; Values for the thawed and heated samples, and the samples after 3 passes through the homogeniser are given in Table 5-6 and Table 5-7.

There was a significant decrease in whiteness index after storage and thawing and warming. The magnitude of this decrease in WI increased over the storage period. The decrease in whiteness was seen in samples stored at all temperatures. The whiteness of the samples increased significantly after the first pass through the homogeniser.

The yellowness of the sample was found to increase in all samples thawed after 8 weeks of frozen storage. The yellowness increased after the first pass through the homogeniser, and then decreased over subsequent passes.

A Pearson correlation test was used to evaluate if a relationship existed between WI and YI, and no significant correlation was found, so it is appropriate to discuss the two values separately.

A backwards elimination stepwise selection algorithm was conducted to select terms for a pair of regression models describing the responses of WI, and YI. The predictor terms evaluated were the homogenisation treatment, the temperature, the first and second order polynomial terms for storage time, and the first order interaction between time and temperature. The criteria for term elimination was α=0.05, and the model was required to be hierarchical at each step.

After removing the WI values at a storage time of 3 days, which were found to be outliers with an unduly large effect on the fitted equation, the following equations describing the change in whiteness during frozen storage were developed:

$$WI = 84.77 - 0.1413ST + 0.001776ST^2 \quad (5\text{-}4)$$

where WI is the white index of the milk, and ST is the storage time in days. For samples after homogenisation, equation (5-4) is modified by replacing the constant term (84.77 in equation (5-4)) with the values in Table 5-5.

Table 5-5: Intercept values for equation (5-4) for each homogenisation treatment.

Homogenisation treatment	Regression intercept
Heated	84.77
1 Pass	86.69
2 Passes	87.31
3 Passes	87.66

The storage temperature was not a significant predictor, and neither was the storage temperature/storage time interaction. The R^2 of the model is 0.726, for 156 observations.

A similar regression procedure was followed to develop a model for YI. The first and second order polynomial terms for storage time were found to be significant predictors, as was the homogenisation treatment, but not storage temperature. The R^2 of the model was low, at 0.45, so the model is not presented here.

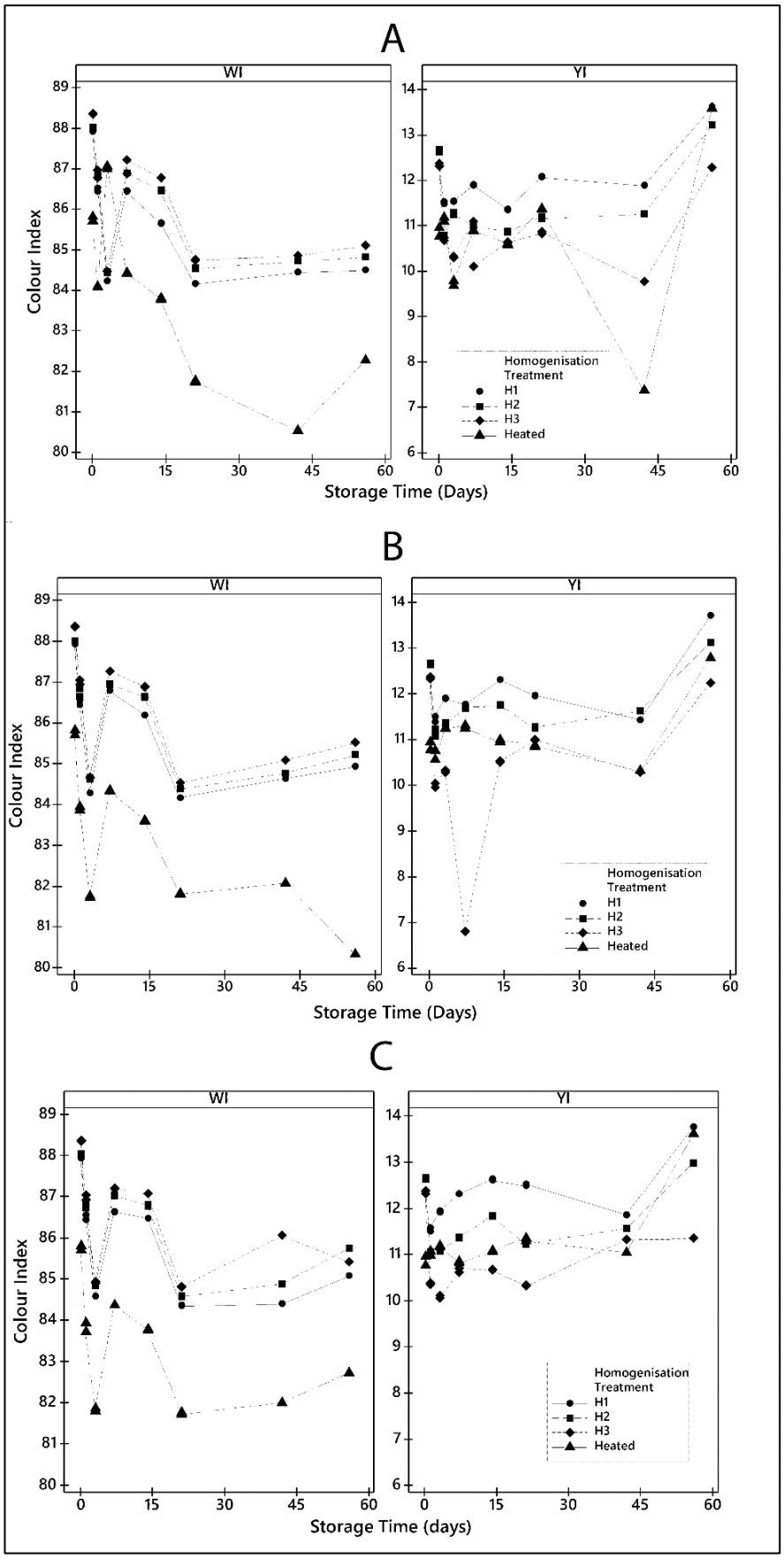

Figure 5-16: Colour Indices of ovine milk after frozen storage and homogenisation. A: -10°C storage temperature, B: -18°C, C: -28°C.

5.4.9 Thawing Temperature and Time Effects on Viscosity

Viscosity decreased after thawing and holding at 21°C, 30°C and 50°C. Viscosity was almost constant for 4°C.

The viscosity decrease was greatest for 50°C, decreasing from 3.3 mPa.S to 2.6 mPa.S, with a smaller decrease measured for 30°C, 3.3 mPa.S to 2.9 mPa.S and a much smaller decrease measured for 21°C. This is shown in Figure 5-17 below.

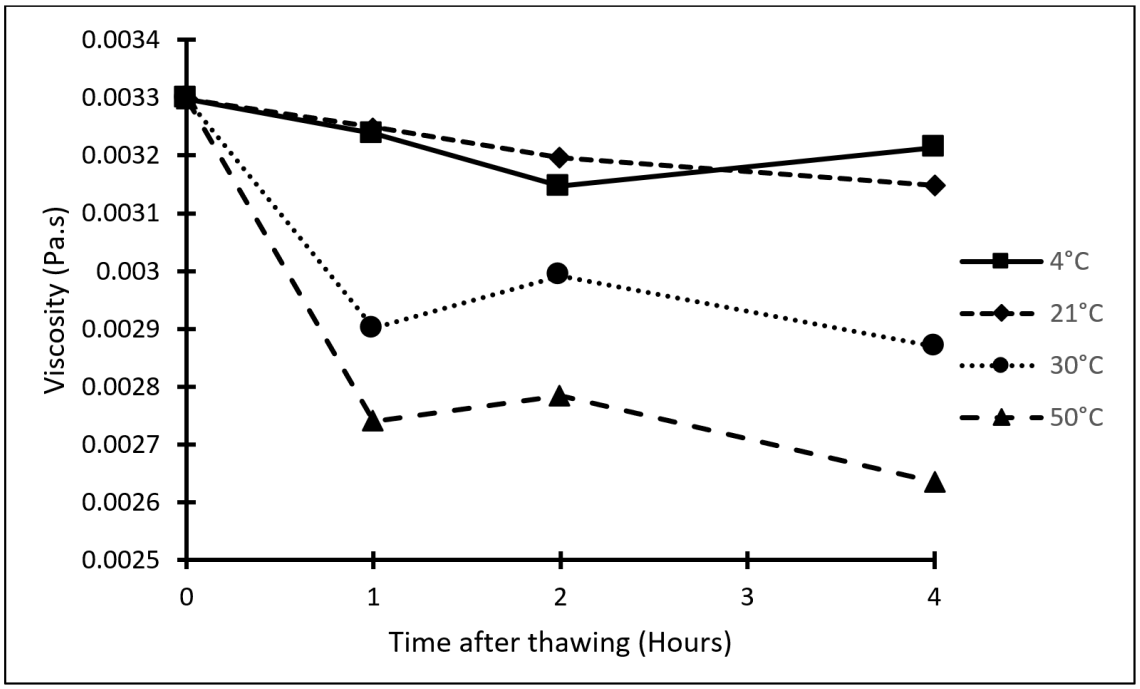

Figure 5-17: Milk samples were stored below -25°C for 6 months and then thawed in water baths and held at constant temperature for up to four hours. The evolution of the samples viscosity is shown above. There is no significant drop in viscosity during storage at 4°C, a slight decrease in viscosity occurs during storage at 21°C. At 30°C and 50°C the viscosity of milk drops signiicantly after being held for 1 hour.

The greatest decrease in viscosity occurs during the first hour after thawing and storage at temperatures of 30°C and 50°C. Between 1 and 4 hours after thawing a smaller decrease occurs. Both 30°C and 50°C samples followed a similar curve, but the total decrease in viscosity was lower in the 30°C sample. The viscosity of the 21°C sample decreased linearly with time from 3.3 mPa.s to 3.1 mPa.s.

5.5 Discussion

5.5.1 Sintering

The results of the trial indicate that if a free-flowing product is desired after frozen storage then frozen whole ovine milk should be stored at or below -18°C, as no sintering is seen at this temperature. The test was conducted when flakes were the assumed geometry, as flake freezing was then the planned method. This is a worst-case scenario, as flakes will give larger interparticle contact areas than spheres or short cylinders.

Sticking between particles occurs when viscous flow of liquid forms a liquid bridge between adjacent particles. Refreezing of this viscous liquid then forms solid linkages between particles[29].The difference between the samples stored at -10°C and -18°C can be explained by considering the difference in volume of unfrozen liquid in each sample, as is discussed further in Chapter 6. At both temperatures the samples are above the glass transition temperature and above the maximally freeze-concentrated temperature [30], so unfrozen water will be present in both samples. The volume of unfrozen liquid in whole ovine milk is approximately 4.5x greater

at -10°C than at –18°C. This unfrozen water will change the mechanical properties allowing sintering and deformation to occur. Unfrozen water may also migrate to the interparticle contact points and solidify if temperature cycling occurs. A similar effect is seen in frozen sucrose solutions, which have a lower creep strength at higher frozen storage temperatures, due to the increased volume of the unfrozen phase [31]. Another factor that will decrease creep strength at -10°C is the decreased viscosity of the unfrozen phase, which may be 2 orders of magnitude greater at -18°C than at -10°C. This is discussed further later in this chapter, in regard to the mechanics and kinetics of milk gel formation. At temperatures lower than -18°C further sintering is unlikely as the unfrozen fraction is further reduced.

Temperature cycling may also be a factor leading to the sintering of samples, where a rise in the storage temperature may cause a volume of frozen water to melt, which can form interparticle bridges that re-freeze on subsequent cooling. A similar process occurs during the temperature cycling of powders in storage at high humidity, where liquid bridges form and the crystallisation occurs in these bridges when moisture is removed[32]. Cycling is expected to be a greater issue at higher temperatures than lower as similar temperature swings of compatible magnitude lead to larger changes in the amount of unfrozen water. For example, the volume of water melted in a 2°C rise at -10°C is 4x greater than the volume melted in a similar temperature rise at -18°C.

The sintering behaviour of the simulated evaporated milk can be similarly explained by the difference in the volume of unfrozen phase between the sample at -18°C and the sample at -25°C. The high concentration of soluble solids in the simulated evaporated milks means that the volume of unfrozen water at -18°C is sufficient to allow sintering under pressure to occur, whereas the lower concentration of solids in whole ovine milk meant that -18°C was sufficiently cold to prevent sintering.

5.5.2 Homogenisation Performance

High-Pressure Homogenisation at 20 MPa/4 MPa effective at returning the particle size, viscosity and colour of frozen stored milk to values similar to that of the fresh homogenised milk.

The heating step alone was effective in returning the particle size and viscosity to values similar to fresh milk, however the colour of the milk was still more yellow and less white than fresh milk, until homogenisation. Decreased whiteness may indicate some agglomeration of the casein micelles, or the presence of free fat.

This indicates that the heating step provided sufficient thermal energy to disrupt the weak gel network present in milk that had been stored at -10°C for 4 and 8 weeks. The high shear forces and extensional forces experienced by the milk during high pressure homogenisation affected the milk system in the same way in both fresh milk and frozen stored milk.

This indicates that heating to homogenisation temperatures and subsequent homogenisation is effective at remedying physical faults caused during frozen storage. This study did not investigate other changes that have been referenced by other authors such as changes in digestibility [4], changes in rennetability[5], development of rancid flavours[4], changes in minor components such as FFAs, or changes in ADV[33], so the effect of the combination of frozen storage and homogenisation on these properties is still not known.

5.5.3 Heat Stability

Previous authors have found differences between the heat stability of various milks. Ovine milk caseins are more mineralised, and less hydrated than bovine milk, which decreases its heat stability in comparison. In addition, the molar β-lactoglobulin to κ-casein ratio differs, which influences the heat stability, with increased resistance as the ratio approaches 1. The smaller micelle size of ovine micelles also affects the heat stability[13, 34-36]. The lower level of κ-casein have been linked to lower heat stability of ovine milk[37]. Changes in the whey/casein

ratio has been linked to changes in heat stability in goat milk, decreasing whey/casein ratio improves heat stability of milk[38]. The changes in the mineral and protein balances may also be why concentrated milks have been found to have lower heat stability[39, 40]. Milk heat stability can be increased by addition of calcium chelating agents such as TSPP or trisodium citrate. The change in heat stability with pH is a result of the changes in mineral species as a result of pH. In goat milk, optimum heat stability is found at pH 6.9. Decreasing the pH increases ionic calcium concentration, shielding negative charges on micelles and leading ultimately to aggregation. Addition of inorganic phosphate increases buffering capacity at pH 7[13, 41]. The storage of milks can also affect the heat stability. Cold storage has been found to lead to β-casein dissociation and calcium phosphate solubilisation, lowering heat stability in goats milk[42].

The changes in composition with seasonality also affect the heat stability. Ewe's milk in Europe has its lowest heat stability (1 min at pH 6.39) in September, higher heat stability (10 min at pH 6.5) in March, and its maximum (18 min pH 6.78) in June [13, 15] . These seasonal changes may be due to the changes in the mineralisation of the milk, as the minerals in milk are important for heat stability.

It is generally difficult to compare from study to study with regard to HCT due to differences in methodology, however comparisons between treatments in a single study are valid. This being said, the heat stabilities measured in this study were similar to those reported elsewhere for ovine milk [13, 15] considering possible differences in measurement techniques. As the values collected in this study were taken from a single, mid-season collection of milk, there were no data collected on the variation with seasonality.

The milk in this study showed similar heat stability regardless of the combination of storage time and temperature. As discussed above the ionic environment of the milk can affect the heat stability, and changes in the serum Ca^{2+} concentration were seen. The lack of difference in heat stability may be due to changes in the calcium and phosphate systems reverting after thawing and before the heat stability test, as has been noted in other studies of the mineral environment of ovine milk[14], returning the freeze-thawed milk to a similar ionic environment as the raw milk.

It is also possible that the heating process allowed reversible changes in the salt distribution to revert before the sample reached the analysis temperature, as the mobility and diffusion rates of salts increases with temperature.

5.5.4 Changes in Milk System Including Gel Formation

The gels formed in ovine milk during frozen storage are unusual in that they appear to be reversible, re-dispersing upon heating. Other milk gels, formed by the action of rennet or acidification are typically irreversible[43].

The application of heat or time leads to the disruption of the network and a reduction in PSD and viscosity, indicating that strong particle-particle interactions are not occurring. This gives another possible method for remedying physical damage upon storage.

There was no long-term trend showing changes in pH in thawed samples, this indicated that the presence of gels in thawed samples may not be linked to the pH driven solubilisation of Colloidal Calcium Phosphate (CCP), which causes acid disruption of casein micelles. Previous studies have found decreases in pH in frozen bovine milk, with a decrease to pH 6.1 observed at -10°C, and a similar decrease at -18°C[44] The acidity of raw ovine milk is similar to that of bovine milk [25]. This is unlikely to be sufficient to destabilise casein on its own.

However, other studies have found that there is a steady loss of soluble calcium during storage at -7°C, which reaches a new constant level after 120 days[45]. Inorganic phosphate was found to drop during the first 60 days of frozen storage. This change was partially reversible after

stirring for 48 hours at 5°C. The protein stability dropped at a similar rate to the Ca^{2+} concentration. Increases in viscosity were also partially reversible on storage [45].

In their study of the stability of frozen milk Koschak et al [7] noted that stability increased with decreasing temperature in previous studies. They also found that removal of Ca^{2+}, and the addition of soluble sugars (or hydrolysis of lactose) increased the stability of milk. It was suggested by these authors[7] that H-bonding between adjacent proteins contributes to destabilisation of milk and this is inhibited by sugars h-bonding to proteins. It was also suggest that Ca^{2+} plays a part in destabilising milk[7]. The link between Ca^{2+} and micelle destabilisation has been noted by other authors who noted slight drops in soluble Ca^{2+} and moderate drops in soluble PO_4^{2+} during frozen storage[14]. The lower drop in soluble component when compared with Chen and Yamauchi's 1969 study[45], was linked to the slow (48hours) thawing, which allowed the salt system to revert to a more normal distribution. In the current study I observed a small decrease in Ca^{2+} seen in samples stored at -10°C for 4 weeks and -18°C for 4 and 8 weeks. This suggests that Ca^{2+} has migrated to the micellar phase in these samples, but not in samples stored below -25°C.

In the current study no change was observed in apparent protein levels in serum phase of milk after frozen storage and thawing, even in samples that formed a gel on thawing. This suggests that the gelation observed is less likely to be due to casein-whey interaction such as found in age gelation of UHT milks[46], as this would lead to changes in the protein levels present in the serum. It is possible however that small levels of whey protein incorporation into the gel network occurred on frozen storage, and this was below the detection limit of the methodology I used. There was also no heating step before frozen storage, however, protein stability is thermodynamically reduced at cold temperatures, leading to a formation known as cold unfolding [47]. This mechanism may be capable of causing whey proteins to denature and interact with caseins.

The Gibbs-Helmholtz equation describes the Gibbs free energy change on denaturation, and can be used to model the temperature variation of the thermodynamic stability of proteins [48]. $\Delta G_D(T)$ is the Gibbs free energy change of denaturation at a temperature T, ΔH_D is the enthalpy change on denaturation, ΔC_P is the difference in heat capacity between the natural and denatured states and T_D is the higher denaturation temperature.

$$\Delta G_D(T) = \Delta H_D\left(1 - \frac{T}{T_D}\right) + \Delta C_p\left[(T - T_D) - T\ln\left(\frac{T}{T_D}\right)\right] \quad (5\text{-}5)$$

ΔG_Dfollows a parabola with the protein stability decreasing both above and below the temperature of maximum stability. Heat denaturation is an endothermic reaction that occurs when the thermal kinetic energy of the protein is increased to the point when the protein chains unfold and expose interior groups, which can then form aggregates[49]

Cold unfolding of globular proteins is an exothermic process[50], that occurs when the hydration of protein non-polar groups becomes thermodynamically favourable at lower temperatures. This causes the polypeptide chain to unfold and expose internal non-polar structures to water[51].

β-Lactoglobulin has been shown to undergo a reversible cold unfolding transition (this is distinct from the thermal denaturation that occurs at higher temperatures) [52] . The cold-unfolding temperature of β-lactoglobulin is decreased by increased concentration, as occurs during freeze-concentration, and is decreased by increasing sugar content, as also occurs during freeze-concentration. It may be possible that cold unfolding contributed to the formation of gels during frozen storage in this study. The kinetics of this cold unfolding have been studied, and found to be dependent on the viscosity of the system, suggesting that in the highly concentrated and

viscous environment of the unfrozen phase in frozen milk, the half-life of the cold unfolding process will be long[53].

Thermally reversible gelation of dairy products has been observed in highly concentrated suspensions of caseins. Panouille et al found that sub-micellar structures can form weak gels at casein concentrations of over 100 gL^{-1}[54]. Lu, McMahon and Vollmer found that cold gelation of concentrated casein in the form of reconstituted milk is thermally reversible [55]. This was linked to casein reduction during diafiltration to form casein concentrate, the micelles dissociate, and protein strands entangle on cooling below a gelation temperature. This occurs at high casein levels. This network is partially stabilised by Ca^{2+} bonding to phosperine residues on protruding protein chains on neighbouring micelles. The network formed is weak and can be reversed by heating. Lu *et al* observed similar gelation behaviour in concentrated micellar casein suspensions where it was linked to interaction between whole, non-dispersed casein micelles, with micelles touching and weak bonds forming between emerging and enmeshing protein chains on the micelle surfaces [56]. These protein gels are also thermally reversible and are thought to occur when the kinetic energy of the casein micelles is reduced, and they lack mobility with their neighbours due to the high casein concentrations. The spheres of hydration are reduced and they overlap [56].

This may be a mechanism which can explain the behaviour of the milk gels observed in this study. During freezing the milk solids are rejected from ice crystals and concentrated into small unfrozen regions ahead of an advancing ice front. The presence of highly concentrated regions of milk solids in frozen samples is confirmed by cryo-SEM images presented in chapter 4. In particular Figure 4-18 shows tightly packed casein micelles.

This tight packing could lead to steric interference between adjacent casein micelles and interaction between protruding protein chains, which form weak bonds. These bonds served to allow a gel to be maintained after thawing. The increased ionic strength in the concentrated unfrozen phase may also reduce electrostatic repulsion by increasing the shielding of the negatively charged surface of the casein micelles.

On thawing the casein micelles once again have scope for movement, however the gel must be disrupted by thermally induced motion of the micelles in the gel. The increased kinetic energy on heating, and increased available volume allows for movement of casein micelles and disruption of networks. This is seen in the behaviour of milk that was thawed and held at different temperatures, as discussed in section 3.11. Here the viscosity of the samples decreased fastest and to the greatest degree when the milk was held at 30°C or 50°C after thawing, and only limited changes were seen in milk held at 4°C. This also explains the disruption of the milk gels formed under storage frozen storage at -10°C for 4 or 8 weeks, which are disrupted by heating to 60°C before homogenisation. This heating provided the thermal energy required to mobilise the casein micelles in the gel.

The gel did not reform when the samples were cooled back down to 4°C after heating or homogenisation, as the casein micelles were dispersed in the original volume of the milk, rather than being trapped in small unfrozen volumes, and so there was no driving force to overcome the stabilising forces in the suspension. This possible mechanism is shown in Figure 5-19. Similar thermally reversible gel behaviour has been observed in highly concentrated micellar casein concentrate (HC-MCC) [56]. However, unlike the freeze-thawed milk in this study, the increased concentration is still present at low temperatures in HC-MCC, so cooling down causes gels to reform. Some literature suggests that this agglomeration can become irreversible after longer storage periods [57].

However, there was no gel formation seen in samples stored frozen below -25°C in the current study, and samples stored at -18°C only showed small flecks after 8 weeks of frozen storage. The

driving forces behind milk gelation, such as reduced water volume, and increased milk solids concentration are more significant below -25°C than at -10°C. It seems that there are likely several factors reducing the reaction rates at the lower storage temperatures. Gel formation may be thermodynamically favoured, but kinetically limited at lower temperatures.

The solids concentration of the unfrozen phase of ovine milk at its maximally freeze-concentrated state, is estimated in Chapter 6 as roughly 85%, which is in a similar range as other milks[30, 58] and food products [59]. The melting onset, which is the upper range of the glass transition, as viscosity drops low enough for crystallisation to occur) is in the range of -25°C (measured for whole sheep milk), to -31°C (measured for sheep milk serum). Literature values of the glass transition have ranges from -38.2°C for freeze dried bovine milk[60], to -28°C and -23°C for T_g for the maximally freeze-concentrated solute matrices of whole milk and skim milk respectively [61].

The concentration of lactose in the unfrozen phase at its maximum concentration of 85% is approximately 20-25%. The viscosity of the unfrozen phase at temperatures above the glass transition can be estimated from the WLF equation[62]. This can be written in two forms [63]:

$$a\text{: } \log_{10} a_T = -\frac{C_1(T - T_S)}{C_2 + T - T_S} \quad or\ b\text{: } \log_{10} a_T = -\frac{17.44(T - T_g)}{51.6 + T - T_g} \tag{5-6}$$

In this equation, a_T is the ratio between the viscosity at temperature T, at the reference temperature T_S, or the glass transition temperature T_g, and C_1 and C_2 are empirical coefficients. Equation (5-6)(a) uses the viscosity at a reference temperature, ideally at least 50°C above T_g, and equation (5-6) (b) uses the viscosity at T_g.

Using equation (5-6) (a), the values for C_1 and C_2 published by Peleg [63], and the viscosity for concentrated lactose solution at 10°C[64], the viscosity of the unfrozen phase at -10°C, -18°C and -28°C can be estimated. These viscosities can also be estimated from the lactose viscosity at T_g, which has been measured at 1.1x10^{14} Pa.s [65], or estimated from 10^{11} to 10^{12} Pa.s[66], and equation (5-6) (b), and using a value for T_g of -31°C. The two curves generated are shown in Figure 5-18.

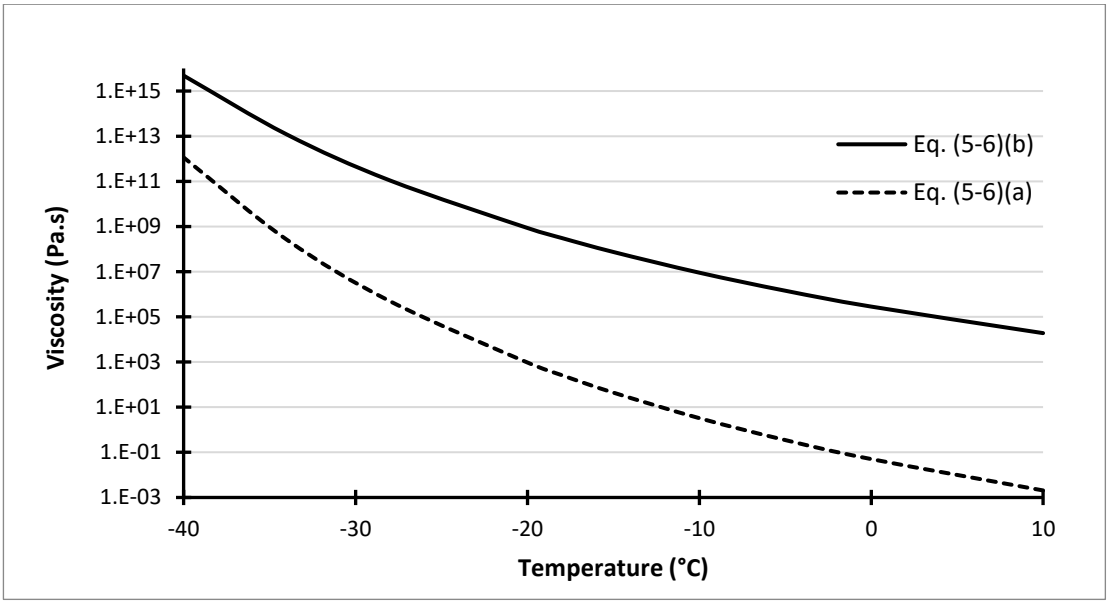

Figure 5-18: Viscosity in the unfrozen phase, estimated using the WLF model, based on the viscosity and behaviour of lactose. The upper curve is based on an extrapolation of viscosity from a glass transition at -31°C, and a viscosity in the glassy state of 10^{12} Pa.s. The lower curve is based on an extrapolation of the viscosity of a 20% Lactose solution at 10°C (2.05x10^{-3} Pa.s).

The uncertainties in T_g, the reliance on a generalised curve coefficient, and the variance in published viscosities at T_g mean that the curve generated by equation (5-6)(a) is likely more accurate. For this reason, the authors of the original WLF model counsel against using equation (1-40) (b) unless absolutely necessary. However, there are limited data in literature about the viscosity of highly freeze-concentrated milks. Nonetheless, the curves generated from the WLF model show an increase in viscosity between -10°C and -18°C of 2 orders of magnitude, and an increase in viscosity between -10°C and -28°C of 5 orders of magnitude.

The concentration factor on a water basis (Q^*,the ratio of g solid/100 g water in the concentrated state to the initial state.) of milk at -28°C, Q^*= 27.7 was larger than that at -10°C, when Q^*=13.9.This would increase some reaction rates *in absence of an increase in viscosity*, however the very large increase in viscosity leads to decreases in reaction rate, despite increased levels of solutes.

Hydrogen bonding at the contact points of adjacent micelles may be supressed by the presence of lactose in solutions. Lactose is supersaturated at all the storage temperatures evaluated. Using the solubility of lactose at 0°C [67] as a rough estimate, and the freezing curves determined in Chapter 6, lactose becomes supersaturated at -2°C in partially frozen ovine milk. As described above, the viscosity of the system increases rapidly with decreased temperature, and may inhibit lactose crystallisation in the samples stored at below -25°C. Lactose may crystallise in samples stored at -10°C, which removes the cryoprotective effect of lactose and decreases the viscosity of the unfrozen phase.

This effect can be influenced by cooling rate, as lactose crystals were detected by cryo-SEM in samples of ovine milk frozen slowly and stored below -25°C (discussed in Chapter 4), as these samples spend long enough in a temperature range where lactose was supersaturated, yet the system was not viscous enough to inhibit crystallisation.

Other mechanisms of bond formation between adjacent micelles will also be suppressed at the high viscosities present at lower temperatures. Linking between protein chains on the micelle surface and whey proteins, or other micelles, requires realignment and mobility of surface located proteins. As the cold unfolding of β-lg is kinetically limited by the high viscosity environment, greatly increasing process half-life (in sucrose solution 2.2 years at -15°C, 2.5×10^4 years at T_g.[53]), it may be that the rearrangement of proteins on the surface of adjacent micelles is similarly affected by increased viscosity, which decreases the amount of agglomeration occurring in samples stored below -25°C. The increased viscosity near T_g will also reduce the rate of progressive dehydration of proteins due to the increased osmotic pressure of the cryo-concentrated phase.

The diffusion of species to and from the micelle surface is limited by highly increased viscosity below -25°C. This is consistent with higher levels of Ca^{2+} migration to the serum phase in -10°C and -18°C samples. As a result, any protein system changes that are a result of changes in the mineral environment of the micelles will occur slower below -25°C when compared to -10°C.

This suggests that best storage stability will be seen in samples stored below -25°C, while at or below -18°C would be suitable for short storage periods of up to 4-8 weeks. Storage at -10°C is not a suitable method for storage of frozen ovine milk.

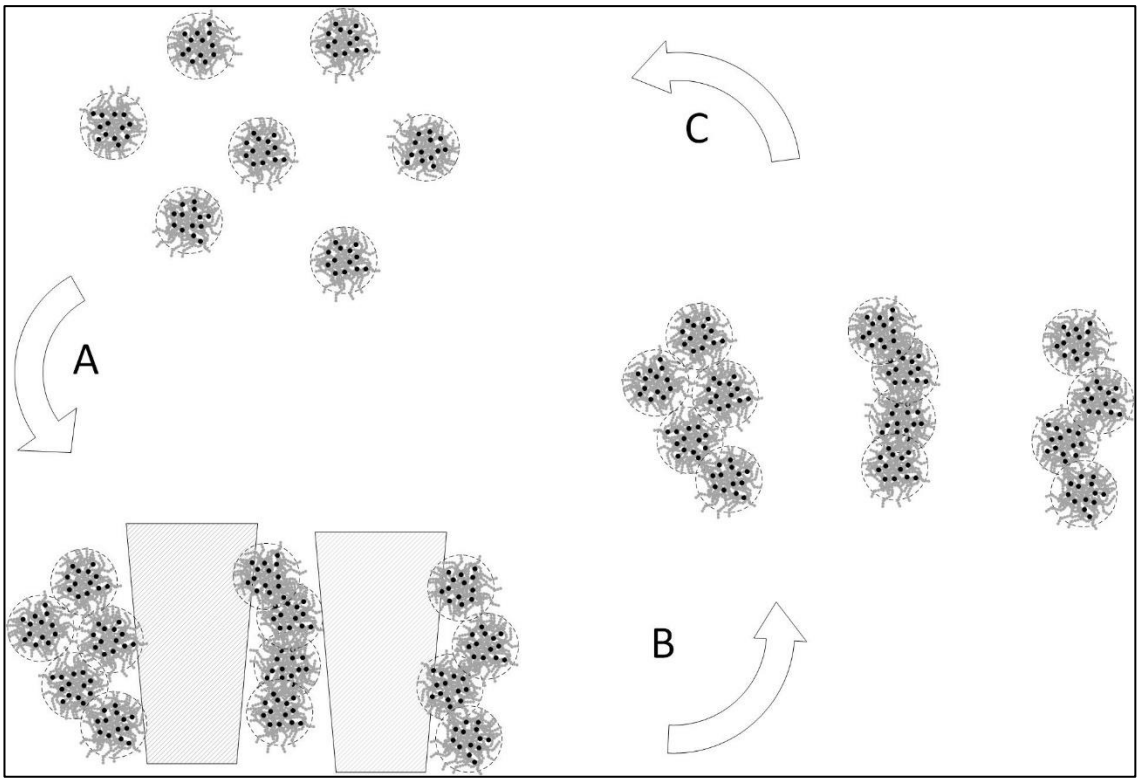

Figure 5-19: Possible mechanism leading to creation of a gel in ovine milk stored frozen at -10°C. A: Freezing form large ice crystals, in with micelles forced into small volumes between crystals. The force of rejection by the ice crystals overcomes the steric and electrostatic repulsion stabilising the micelle suspension. Micelles come into contact and begin to form low strength bonds in the altered solute environment of the highly concentrated inter-crystal regions. B: The ice is melted, and the bonds formed during frozen storage hold the micelles together. There is not enough thermal motion to overcome the attractive force. C: During heating, the thermal motion of micelles causes them to overcome inter-particle bonds and redisperse in the liquid. Species may diffuse to or from the micelle surface as the liquid volume has returned to that of the original milk. The liquid volume is large enough that micelles remain separated by steric and electrostatic repulsion during subsequent cooling to temperatures above freezing.

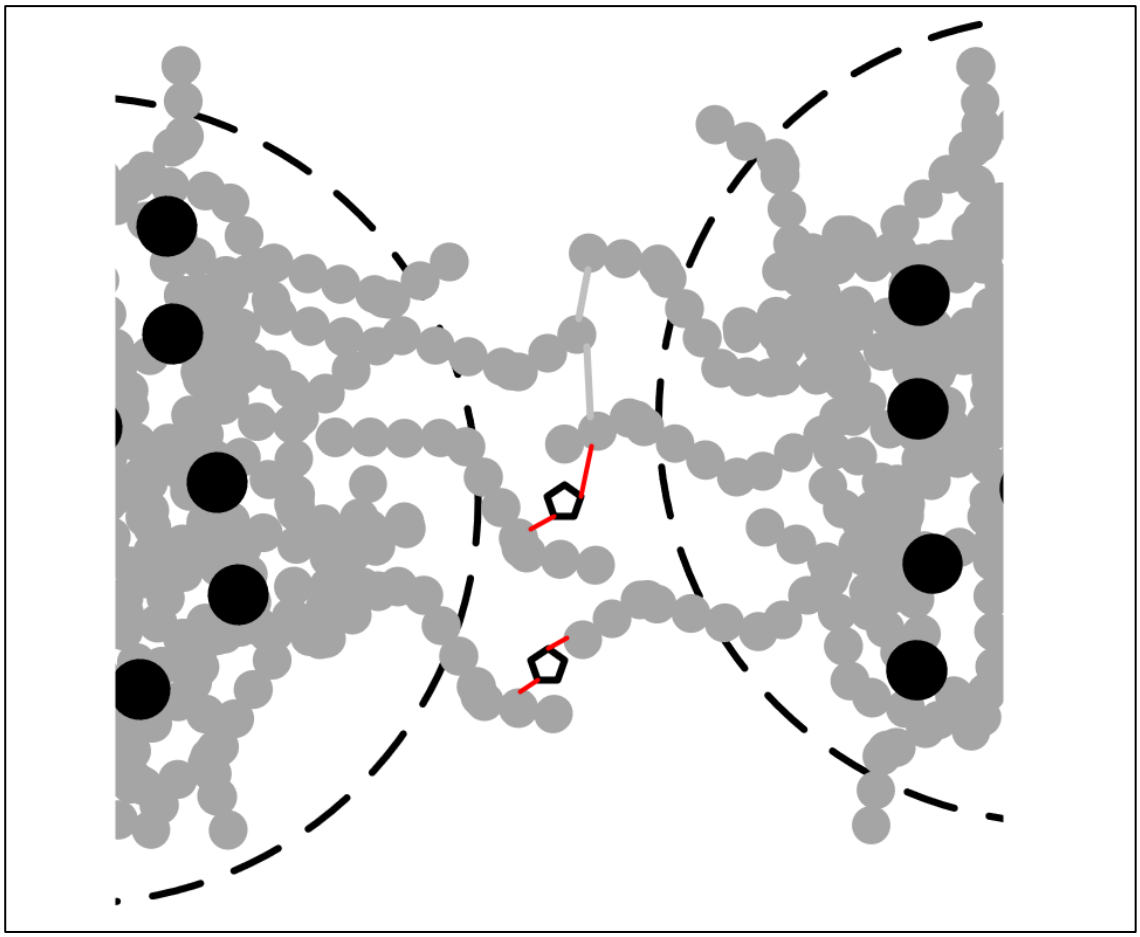

Figure 5-20: Possible mechanisms of binding between two adjacent casein micelles in a frozen sample: Grey line represent hydrogen bonding between adjacent proteins. Pentagons represent Ca^{2+} ions which may form bridges between negative regions on adjacent proteins. Hydrophobic interactions and steric interference may also occur.

5.6 Conclusions

Raw ovine milk was stored frozen at different temperatures for up to 8 weeks, and the changes occurring in a number of factors was measured. Significant agglomeration, and separation into a gel and sediment, was visually observed in samples of milk stored at -10°C, for 4 and 8 weeks. The particle size distribution after heating in all samples was similar to original particle size distribution. Samples stored at -10°C and not heated after thawing showed significant increases in particle size after 4 and 8 weeks of storage. This gelation was accompanied by a significant increase in viscosity, and in milk stored at -10°C for 8 weeks, a change in flow behaviour from Newtonian to Non-Newtonian shear thinning behaviour.

Homogenisation was effective at reducing particle size, viscosity, and yellowness in milk that had been stored frozen and thawed

There was no change in pH as a result of frozen storage, nor were there any changes in serum or supernatant protein levels. Nor were there any significant changes in the heat stability of the milk after frozen storage. However, there was a decrease in the soluble Ca^{2+} concentration after 4 weeks and 8 weeks storage at -18°C and 4 weeks storage at -10°C. This decrease was approximately 50% for -18°C samples, and approximately 34% for samples stored at -10°C.

The storage stability of milk is most likely affected by the viscosity of the unfrozen phase and the state of water in milk during frozen storage. At lower temperatures, near the glass transition temperature, the viscosity of the unfrozen phase increases by several orders of magnitude, which reduces the rate of the phenomena which cause gelation in frozen milk.

For storage periods over 8 weeks, frozen ovine milk should be stored below -18°C and ideally below -25°C. Frozen ovine milk should not be stored at or above -10°C.

In the next chapter, the state of water in milk during freezing and the transitions occurring during freezing are investigated.

5.7 List of Symbols

Symbol	Description	Units
a^*	CIELAB red-green value	
a_T	Ratio of viscosities	
b^*	CIELAB blue-yellow value	
C_1	WLF equation constant	
C_2	WLF equation constant	K
K	Flow consistency index	$Pa.S^n$
L^*	CIELAB lightness value	
n	Flow behaviour index	
ST	Storage time	$days$
T	Temperature	K
T_D	Hot denaturation temperature	K
T_g	Glass transition temperature	K
T_s	Reference temperature for WLF model	K
WI	Whiteness index	
YI	Yellowness index	
ΔC_p	Difference in specific heats between natural and denatured states	$Jmol^{-1}K^{-1}$
ΔH_D	Protein enthalpy change on denaturation	J
$\Delta G_D(T)$	Gibbs free energy change on denaturation	J
$\dot{\gamma}$	Shear rate	s^{-1}
τ	Shear stress in a fluid	Pa

5.8 References

[1] W. L. Wendorff, "Freezing Qualities of Raw Ovine Milk for Further Processing," *Journal of Dairy Science,* vol. 84, pp. E74-E78, 2001.

[2] P. Young, "Deep-frozen storage of frozen ewe's milk," *Sheep Dairy News,* no. 4, p. 41, 1987.

[3] E. C. Needs, "Effects of long-term deep-freeze storage on the condition of the fat in raw sheep's milk," *Journal of Dairy Research,* vol. 59, pp. 49-55, 1992.

[4] D. D. Muir, "Reviews on the Progress of Dairy Science: Frozen concentrated milk," *Journal of Dairy Research,* vol. 51, pp. 649-664, 1984.

[5] M. Pazzola *et al.*, "The Effect of Long-term Freezing on Renneting Properties of Sarda Sheep Milk," *Agriculturae Conspectus Scientificus,* vol. 78, no. 3, pp. 275-279, 2013.

[6] W. L. Wendorff, "Milk composition and cheese yield," in *Proceedings of the 7th Great lakes Dairy Sheep Symposium*, Ithaca, 2002.

[7] M. S. Koschak, O. Fennema, C. H. Amundson, and J. Y. Lee, "Protein Stability of Frozen Milk as Influenced by Storage Temperature and Ultrafiltration," *Journal of Food Science,* vol. 46, no. 4, pp. 1211-1217, 1981.

[8] B. H. Webb and S. A. Hall, "Some Physical Effects of Freezing upon Milk and Cream," *Journal of Dairy Science,* vol. 18, no. 5, pp. 275-286, 1935.

[9] S. Y. Wong and R. W. Hartel, "Crystallization in Lactose Refining—A Review," *Journal of Food Science,* vol. 79, no. 3, pp. R257-R272, 2014.

[10] C. V. Morr, "Chemistry of milk proteins in food processing," *J Dairy Sci,* vol. 58, no. 7, pp. 977-84, 1975.

[11] C. Robinson, C. S. Boxe, M. I. Guzmán, A. J. Colussi, and M. R. Hoffmann, "Acidity of frozen electrolyte solutions," (in English), *Journal of Physical Chemistry B,* Article vol. 110, no. 15, pp. 7613-7616, 2006.

[12] J. E. O'Connell and P. F. Fox, "Heat Treatment of Milk: Heat Stability of Milk," in *Reference Module in Food Science*: Elsevier, 2016.

[13] K. Raynal-Ljutovac, Y. W. Park, F. Gaucheron, and S. Bouhallab, "Heat stability and enzymatic modifications of goat and sheep milk," *Small Ruminant Research,* vol. 68, no. 1, pp. 207-220, 2007.

[14] M. A. De La Fuente, T. Requena, and M. Juárez, "Salt Balance in Ewe's and Goat's Milk during Storage at Chilling and Freezing Temperatures," *Journal of Agricultural and Food Chemistry,* Article vol. 45, no. 1, pp. 82-88, 1997.

[15] D. D. Muir, D. S. Horne, A. J. R. Law, and A. W. M. Sweetsur, "Ovine milk. 2. Seasonal changes in indices of stability," *Milchwissenschaft,* vol. 48, no. 8, pp. 442-445, 1993.

[16] A. Sevi, M. Albenzio, R. Marino, A. Santillo, and A. Muscio, "Effects of lambing season and stage of lactation on ewe milk quality," *Small Ruminant Research,* vol. 51, no. 3, pp. 251-259, 2004.

[17] F. Rincón, R. Moreno, G. Zurera, and M. Amaro, "Mineral composition as a characteristic for the identification of animal origin of raw milk," *Journal of Dairy Research,* vol. 61, no. 1, pp. 151-154, 1993.

[18] D. T. Davies and J. C. D. White, "The stability of milk protein to heat: I. Subjective measurement of heat stability of milk," *Journal of Dairy Research,* Article vol. 33, no. 1, pp. 67-81, 1966.

[19] F. Gaucheron, "The minerals of milk," *Reprod Nutr Dev,* vol. 45, no. 4, pp. 473-83, 2005.

[20] G. W. Latimer, *Official methods of analysis of AOAC International*. Rockville, Md: AOAC International, 2016.

[21] M. O'Sullivan, "Analytical Methods | Proximate and Other Chemical Analyses," in *Encyclopedia of Dairy Sciences (Second Edition)*, J. W. Fuquay, Ed. San Diego: Academic Press, 2011, pp. 76-82.

[22] D. Fitzpatrick and J. D. Glennon, "Analytical Methods | Atomic Spectrometric Techniques," in *Encyclopedia of Dairy Sciences (Second Edition)*, J. W. Fuquay, Ed. San Diego: Academic Press, 2011, pp. 141-145.

[23] M. C. Michalski, V. Briard, and F. Michel, "Optical parameters of milk fat globules for laser light scattering measurements," *Lait,* vol. 81, no. 6, pp. 787-796, 2001.

[24] M. Ramos and M. Juarez, "Milk | Sheep Milk," in *Encyclopedia of Dairy Sciences*, J. W. Fuquay, Ed. Second Edition ed., 2011.

[25] W. L. W. George F.W. Haenlein, "Sheep Milk," in *Handbook of Milk of Non-Bovine Mammals*, Y. W. Park, Ed.: Blackwell Publishers, 2006.

[26] H. Tessier and D. Rose, "Influence of κ-casein and β-lactoglobulin on the Heat Stability of Skimmilk1," *Journal of Dairy Science,* vol. 47, no. 10, pp. 1047-1051, 1964.

[27] P. B. Pathare, U. L. Opara, and F. A.-J. Al-Said, "Colour Measurement and Analysis in Fresh and Processed Foods: A Review," *Food and Bioprocess Technology,* vol. 6, no. 1, pp. 36-60, 2012.

[28] A. M. C. N. Rocha, C. C. A. R. Mota, and A. M. M. B. Morais, "Physico-chemical qualities of minimally processed carrot stored under vacuum," *Journal of Foodservice,* Article vol. 18, no. 1, pp. 23-30, 2007.

[29] R. A. Murti, A. H. J. Paterson, D. L. Pearce, and J. E. Bronlund, "Stickiness of skim milk powder using the particle gun technique," *International Dairy Journal,* vol. 19, no. 3, pp. 137-141, 2009.

[30] G. Vuataz, "The phase diagram of milk: a new tool for optimising the drying process," *Le Lait,* vol. 82, no. 4, pp. 485-500, 2002.

[31] X. Xu, G. Jeronimidis, A. G. Atkins, and P. A. Trusty, "On the yield stress of frozen sucrose solutions," *Journal of Materials Science,* Article vol. 38, no. 2, pp. 245-253, 2003.

[32] A. H. J. Paterson, "Lactose processing: From fundamental understanding to industrial application," *International Dairy Journal,* vol. 67, pp. 80-90, 2017.

[33] S. E. Duncan, G. L. Christen, and M. P. Penfield, "Rancid Flavor of Milk: Relationship of Acid Degree Value, Free Fatty Acids, and Sensory Perception," *Journal of Food Science,* vol. 56, no. 2, pp. 394-397, 1991.

[34] W. L. Claeys *et al.*, "Consumption of raw or heated milk from different species: An evaluation of the nutritional and potential health benefits," *Food Control,* vol. 42, pp. 188-201, 2014.

[35] O. Pellegrini, F. Remeuf, and M. Rivemale, "Evolution des caractéristiques physico-chimiques et des paramètres de coagulation du lait de brebis collecté dans la région de Roquefort," *Lait,* vol. 74, pp. 425-442, 1994.

[36] F. Remeuf, J. Lenoir, and C. Duby, "Étude des relations entre les caractéristiques physico-chimiques des laits de chèvre et leur aptitude à la coagulation par la présure," *Lait,* vol. 69, no. 6, pp. 499-518, 1989.

[37] P. F. Fox and M. C. T. Hoynes, "Heat stability characteristics of ovine, caprine and equine milks," *Journal of Dairy Research,* vol. 43, no. 3, pp. 433-442, 1976.

[38] S. Bouhallab, N. Leconte, Y. Le Graet, and A. Garem, "Heat-induced coagulation of goat milk: Modification of the environment of the casein micelles by membrane processes," *Lait,* Article vol. 82, no. 6, pp. 673-681, 2002.

[39] H. Singh, "Heat stability of milk," *International Journal of Dairy Technology,* Conference Paper vol. 57, no. 2-3, pp. 111-119, 2004.

[40] J. Dumpler and U. Kulozik, "Heat-induced coagulation of concentrated skim milk heated by direct steam injection," *International Dairy Journal,* vol. 59, pp. 62-71, 2016.

[41] A. Montilla and M. M. Calvo, "Goat's Milk Stability during Heat Treatment: Effect of pH and Phosphates," *Journal of Agricultural and Food Chemistry,* vol. 45, no. 3, pp. 931-934, 1997.

[42] K. Raynal-Ljutovac, T. Massouras, and M. Barbosa, "Goat milk and heat treatments," *South African Journal of Animal Sciences,* Article vol. 34, no. 5SUPPL.1, pp. 173-175, 2004.

[43] J. A. Lucey, "Formation and Physical Properties of Milk Protein Gels," *Journal of Dairy Science,* vol. 85, no. 2, pp. 281-294, 2002.

[44] L. Van Den Berg, "pH changes in buffers and foods during freezing and subsequent storage," *Cryobiology,* vol. 3, no. 3, pp. 236-242, 1966.

[45] C. M. Chen and K. Yamauchi, "Change of Salt Distribution in Milk During Frozen Storage and Its Partial Reversion after Thawing," *Agricultural and Biological Chemistry,* Article vol. 33, no. 9, pp. 1333-1341, 1969.

[46] S. G. Anema, "Age Gelation, Sedimentation, and Creaming in UHT Milk: A Review," *Comprehensive Reviews in Food Science and Food Safety,* vol. 18, no. 1, pp. 140-166, 2019.

[47] B. S. Bhatnagar, R. H. Bogner, and M. J. Pikal, "Protein Stability During Freezing: Separation of Stresses and Mechanisms of Protein Stabilization," *Pharmaceutical Development & Technology,* Article vol. 12, no. 5, pp. 505-523, 2007.

[48] S. K. Singh and S. Nema, "Freezing and Thawing of Protein Solutions," in *Formulation and Process Development Strategies for Manufacturing Biopharmaceuticals* F. Jameel and S. Hershenson, Eds.: John Wiley & Sons, 2010, pp. 625-675.

[49] P. L. H. M. P.F.Fox, *Advanced Dairy Chemistry. Volume 1A, Proteins : basic aspects*. Springer US, 2013.

[50] E. Ascolese and G. Graziano, "On the cold denaturation of globular proteins," *Chemical Physics Letters,* vol. 467, no. 1, pp. 150-153, 2008.

[51] P. L. Privalov, "Cold Denaturation of Protein," *Critical Reviews in Biochemistry and Molecular Biology,* vol. 25, no. 4, pp. 281-306, 1990.

[52] X. Tang and M. J. Pikal, "The Effect of Stabilizers and Denaturants on the Cold Denaturation Temperatures of Proteins and Implications for Freeze-Drying," *Pharmaceutical Research,* vol. 22, no. 7, pp. 1167-1175, 2005.

[53] X. C. Tang and M. J. Pikal, "Measurement of the kinetics of protein unfolding in viscous systems and implications for protein stability in freeze-drying," *Pharm Res,* vol. 22, no. 7, pp. 1176-85, 2005.

[54] M. Panouille, D. Durand, T. Nicolai, E. Larquet, and N. Boisset, "Aggregation and gelation of micellar casein particles," *J Colloid Interface Sci,* vol. 287, no. 1, pp. 85-93, 2005.

[55] Y. Lu, D. J. McMahon, and A. H. Vollmer, "Investigating cold gelation properties of recombined highly concentrated micellar casein concentrate and cream for use in cheese making," *Journal of Dairy Science,* Article vol. 99, no. 7, pp. 5132-5143, 2016.

[56] Y. Lu, D. J. McMahon, L. E. Metzger, A. Kommineni, and A. H. Vollmer, "Solubilization of rehydrated frozen highly concentrated micellar casein for use in liquid food applications," *Journal of Dairy Science,* vol. 98, no. 9, pp. 5917-5930, 2015.

[57] P. Walstra, J. T. M. Wouters, and T. J. Geurts, *Dairy science and technology*. Boca Raton: CRC Taylor & Francis, 2006.

[58] P. Walstra, *Dairy Technology*. Boca Raton: CRC Press, 1999.

[59] Y. H. Roos and S. Drusch, "Chapter 4 - Water and phase transitions," in *Phase Transitions in Foods (Second Edition)*, Y. H. Roos and S. Drusch, Eds. San Diego: Academic Press, 2016, pp. 79-113.

[60] A. Pugliese, M. Paciulli, E. Chiavaro, and G. Mucchetti, "Application of differential scanning calorimetry to freeze-dried milk and milk fractions," *Journal of Thermal Analysis and Calorimetry,* vol. 137, no. 2, pp. 703-709, 2018.

[61] Y. H. Roos, "Chapter 9- Reaction Kinetics," in *Phase Transitions in Foods*, Y. H. Roos, Ed. San Diego: Academic Press, 1995, pp. 271-312.

[62] M. L. Williams, R. F. Landel, and J. D. Ferry, "The Temperature Dependence of Relaxation Mechanisms in Amorphous Polymers and Other Glass-forming Liquids," *Journal of the American Chemical Society,* vol. 77, no. 14, pp. 3701-3707, 1955.

[63] M. Peleg, "On the use of the WLF model in polymers and foods," *Crit Rev Food Sci Nutr,* vol. 32, no. 1, pp. 59-66, 1992.

[64] K. R. Morison and F. M. Mackay, "Viscosity Of Lactose And Whey Protein Solutions," *International Journal of Food Properties,* vol. 4, no. 3, pp. 441-454, 2001.

[65] A. H. J. Paterson, G. D. Ripberger, and R. P. Bridges, "Measurement of the viscosity of freeze dried amorphous lactose near the glass transition temperature," *International Dairy Journal,* vol. 43, pp. 27-32, 2015.

[66] K. J. Singh and Y. H. Roos, "Frozen State Transitions in Freeze-Concentrated Lactose-Protein-Cornstarch Systems," *International Journal of Food Properties,* vol. 10, no. 3, pp. 577-587, 2007.

[67] O. F. Hunziker and B. H. Nissen, "Lactose Solubility and Lactose Crystal Formation: I. Lactose Solubility," *Journal of Dairy Science,* vol. 9, no. 6, pp. 517-537, 1926.

5.9 Appendix

Table 5-6: Mean White and Yellow Indices of ovine milk after frozen storage and thawing. Means that do not share a superscript are significantly different (p<0.05).

Storage Temperature	Storage Time (days)	White Index	Yellow Index
Unfrozen	0	85.76 ^{b}	10.85 ^{ghi}
-10°C	1	84.08 ^{d}	11.13 ^{cdefg}
	3	87.03 ^{a}	9.73 ^{k}
	7	84.41 ^{c}	10.88 ^{fghi}
	14	83.79 ^{ef}	10.59 ^{ij}
	21	81.75 ^{j}	11.37 ^{c}
	42	80.52 ^{k}	7.36 ^{l}
	56	82.27 ^{h}	13.60 ^{a}
-18°C	1	83.90 ^{de}	10.65 ^{ij}
	3	81.74 ^{j}	11.24 ^{cde}
	7	84.34 ^{c}	11.28 ^{cd}
	14	83.60 ^{f}	10.97 ^{efgh}
	21	81.81 ij	10.86 ^{ghi}
	42	82.07 ^{hi}	10.32 ^{j}
	56	80.32 ^{k}	12.79 ^{b}
-28°C	1	83.83 ^{ef}	11.02 ^{defgh}
	3	81.83 ^{ij}	11.18 ^{cdef}
	7	84.37 ^{c}	10.83 ^{hi}
	14	83.76 ^{ef}	11.07 ^{cdefgh}
	21	81.74 ^{j}	11.32 ^{cd}
	42	81.99 ^{hij}	11.04 ^{cdefgh}
	56	82.72 ^{g}	13.61 ^{a}

Table 5-7:Mean White and Yellow Indices of ovine milk after frozen storage and thawing, and 3 recirculations through a homogeniser at 20 MPa/4 MPa. Means that do not share a superscript are significantly different (p<0.05).

Storage Temperature	Storage Time	White Index	Yellow Index
Unfrozen	0	88.36 ^{a}	12.34 ^{a}
-10°C	1	86.87 ^{c}	10.70 ^{cdef}
	3	84.46 ^{j}	10.30 ^{efg}
	7	87.05 ^{bc}	10.59 ^{cdefg}
	14	86.78 ^{c}	10.63 ^{cdefg}
	21	84.74 ^{ghij}	10.70 ^{cde}
	42	84.85 ^{ghi}	9.76 ^{g}
	56	85.10 ^{efg}	12.28 ^{ab}
-18°C	1	87.00 ^{bc}	9.99 ^{fg}
	3	84.65 ^{hij}	10.30 ^{efg}
	7	87.27 ^{b}	6.79 ^{h}
	14	86.89 ^{c}	10.51 ^{cdefg}
	21	84.53 ^{ij}	10.99 ^{cde}
	42	85.08 ^{fg}	10.28 ^{defg}
	56	85.51 ^{e}	12.23 ^{ab}
-28°C	1	86.97 ^{bc}	10.36 ^{efg}
	3	84.90 ^{gh}	10.08 ^{fg}
	7	87.20 ^{b}	10.65 ^{cdefg}
	14	87.06 ^{bc}	10.66 ^{cdefg}
	21	84.80 ^{ghi}	10.32 ^{efg}
	42	86.05 ^{d}	11.32 ^{bcd}
	56	85.41 ^{ef}	11.35 ^{bc}

Table 5-8: Heat coagulation time (HCT) of ovine milk after frozen storage. For any particular pH, there were no significant differences ($p<0.05$) in HCT.

Heat Coagulation Time (s)

Storage Temperature (°C)		***-10***						***-18***						***-28***					
pH		**6.2**	**6.4**	**6.6**	**6.7**	**6.8**	**7.0**	**6.2**	**6.4**	**6.6**	**6.7**	**6.8**	**7.0**	**6.2**	**6.4**	**6.6**	**6.7**	**6.8**	**7.0**
Storage time (Days)	***0***																		
	1	*	176	300	*	793	312	*	176	311	*	807	310	*	182	*	858	862	308
	3	66	125	253	*	661	317	60	139	250	*	673	362	81	159	309	*	769	333
	7	80	150	261	*	594	290	75	147	264	*	775	346	66	162	294	*	798	343
	14	75	153	286	*	836	304	68	164	275	*	848	336	81	159	250	*	825	374
	28	77	174	292	*	741	319	66	155	249	*	786	296	61	152	230	*	741	278
	56	59	130	267	*	659	342	71	141	244	*	630	336	62	132	261	*	810	375

Table 5-9: Power-law fluid coefficients for ovine milk after frozen storage and homogenisation treatment. K is the flow consistency index and n is the flow behaviour index.

			Power-Law Fluid Coefficients														
Storage Temperature (°C)			***-10°C***					***-18°C***					***-28°C***				
Homogenisation Treatment			**Thawed**	**Heated**	**1 Pass**	**2 Passes**	**3 Passes**	**Thawed**	**Heated**	**1 Pass**	**2 Passes**	**3 Passes**	**Thawed**	**Heated**	**1 Pass**	**2 Passes**	**3 Passes**
Storage Time (days)	***Unfrozen***	**K**	0.0037														
		n	0.986														
	1	**K**	0.0035	0.0031	0.0034	0.0027	0.0025	0.0036	0.0033	0.0033	0.003	0.0024	0.0031	0.0029	0.0035	0.0028	0.0024
		n	0.996	0.997	1.00	1.01	1.00	0.990	1.00	1.00	1.00	1.01	1.00	1.01	1.00	1.01	1.00
	3	**K**	0.0036	0.0031	0.0034	*	0.0025	0.0037	0.0029	0.0032	0.0029	0.0025	0.0034	0.0029	0.0032	0.0029	0.0025
		n	0.993	1.00	1.00	*	1.01	0.98	1.00	1.00	1.00	1.01	0.997	1.00	1.00	1.00	1.01
Storage Temperature (°C)			***-10°C***					***-18°C***					***-28°C***				
Homogenisation Treatment			**Thawed**	**Heated**	**1 Pass**	**2 Passes**	**3 Passes**	**Thawed**	**Heated**	**1 Pass**	**2 Passes**	**3 Passes**	**Thawed**	**Heated**	**1 Pass**	**2 Passes**	**3 Passes**
Storage Time (days)	***7***	**K**	0.0053	0.0297	0.0032	0.0027	0.0023	0.0037	0.0034	0.0033	0.0029	0.0026	0.0035	0.0028	0.0032	0.0028	0.0024
		n	0.965	1.00	1.00	1.01	1.02	0.992	0.999	1.001	1.01	1.00	0.995	1.01	1.01	1.01	1.01
	14	**K**	0.0038	0.0031	0.0031	0.0025	0.0023	0.0032	0.0031	0.0032	0.0028	0.0024	0.0032	0.003	0.0036	0.003	0.0026
		n	0.985	1.00	1.00	1.00	1.01	1.00	1.00	1.00	1.01	1.01	1.00	1.00	0.999	1.01	1.00
	28	**K**	0.0055	0.0029	0.003	0.0027	0.0023	0.0037	0.0028	0.0029	0.0029	0.0024	0.0041	0.0029	0.0031	0.0026	0.0022
		n	0.962	1.01	1.01	1.01	1.02	0.996	1.00	1.01	1.00	1.02	0.995	1.01	1.01	1.02	1.02
	56	**K**	0.277	0.0031	0.0038	0.0035	0.0030	0.0043	0.0029	0.0034	0.0027	0.0023	0.0036	0.0031	0.0034	0.0029	0.0023
		n	0.59	1.00	0.996	0.991	1.00	0.991	1.01	1.00	1.01	1.02	0.996	0.997	1.00	1.00	1.02

Chapter 6: Phase Behaviour of Ovine Milk

6.1 Chapter Summary

The freezing behaviour of whole ovine milk, skim ovine milk and ovine milk serum was studied via DSC.

The freezing curve of each substance was calculated, with three different methods of partitioning the energy release into latent and sensible contribution tested; the sensible heat being calculated by published values of heat capacity for milk components; the sensible heat being calculated from the measured heat capacity of milk components; and the sensible heat being estimated from the heat capacity of the samples at temperature above and below the freezing transition. This final method was found to be suitable. The effect of assuming a constant latent heat was tested against a more accurate method which accounted for the reduced latent heat below 0°C. The effect of the reduced latent heat on the calculated freezing curve was minimal and was therefore ignored. Melting onset transitions were recorded in all samples.

The final fraction of unfrozen phase of water and therefore the maximally freeze-concentrated solids fraction was calculated from the energy release over the transition, and from the temperature of the melting onset with the Gordon-Taylor equation. The two methods agreed well.

A partial phase diagram for ovine milk was developed.

6.2 Introduction

6.2.1 Freezing of Ovine Milk.

Determining the unfrozen fraction of milk as a function of temperature below the equilibrium freezing temperature will assist in determining frozen storage conditions that minimise quality loss during storage, and will shine light on some of the behaviour of ovine milk during frozen storage. Knowledge of the unfrozen fraction will also assist in the design of commercial and industrial scale freezers for ovine milk, by providing accurate values for heat flows required to reach desired temperatures.

The phase diagram of bovine milk has been investigated [1] , and the freezing point depression curve for bovine skim milk given up to 40% TS [2]. Some work has been done on the equilibrium freezing temperature of ovine milk[3], which allows for detection of adulteration by cryoscopic measurements. However, there has been little detailed investigation of the freezing behaviour of ovine milk, so this study aims to investigate the freezing transition of ovine milk, in the temperature range of -40°C to 20°C.

6.2.2 Differential Scanning Calorimetry and Unfrozen Water.

Differential Scanning Calorimetry (DSC) is a method of thermal analysis that detects thermal transitions in a sample, by measuring the difference in either heat flow or temperature between the sample and an inert reference[4]. The two principles of measurement are known as power compensation and heat flux DSC respectively. Power compensation DSC uses two separate, but identical furnaces and maintains the sample and reference at identical temperatures, measuring the difference in power required to achieve this. In heat flux DSC a single larger furnace holds both the sample and reference and the difference in temperature between the two is measured, which allows the heat flow into the sample to be calculated. In this work heat flux DSC is employed.

DSC is often used to measure phase or thermodynamic changes in dairy products, such as glass transitions in lactose, denaturation of proteins, and melting of fats[4].

A phase change in a pure substance is accompanied by a distinct change in enthalpy which occurs at a single temperature. This would be detected on an ideal DSC trace of heat flow against temperature as a sharp peak at a single temperature, with the enthalpy change of the transition quantified by the area under the DSC peak.

Impurities in water depress the temperature at which this phase change occurs by reducing the chemical potential of the mixture at a given temperature. As freezing occurs when the chemical potential of the liquid mixture reaches the chemical potential of the pure solid. The decreased chemical potential of the mixture means that this is reached at a lower temperature than the pure solvent.

As water freezes as pure ice, the concentration of solutes in the unfrozen phase increases, and the freezing temperature drops further. This is illustrated in the idealised food system phase diagram in Figure 6-1. This continues until the system reaches its maximally freeze-concentrated point, or in some systems, the eutectic point. If the viscosity of the unfrozen system is too great to allow nucleation of solutes at the eutectic point, the concentration of the unfrozen phase may increase beyond the equilibrium eutectic [5]. The maximally freeze-concentrated point is the point at which no further ice is formed during the timeframe of the observations as the food solution has reached a temperature and concentration at which the systems viscosity is too great for crystal growth. Further cooling beyond this results in the formation of a system comprising of ice, and a supersaturated solution or glass [6].

This progressive freezing point depression spreads the peak on a DSC trace across a range of temperatures, until a glass transition or melting onset is detected at the lower temperature of the phase transition. In pure water, It is possible to form a glass if the water is cooled extremely rapidly below 130 K at 1 Bar [7], however in food systems the glass transition occurs at higher temperatures, and lower cooling rates. In freeze dried bovine whole milk powders, a glass transition has been observed at -38.2°C [8]. Other investigators have measured a melting onset temperature of whole milk of -32°C[9].

Food solutions that are cooled rapidly also show non-equilibrium ice formation at temperatures above the equilibrium glass temperatures, and below the melting onset temperatures [6]. However, investigating this region of the ovine milk phase diagram is out of the scope of this work.

This broadening of the DSC peak can be used to determine the unfrozen fraction of a two-phase system at a range of temperatures by tracking the enthalpy change up to a given temperature in the transition and comparing this with the total enthalpy change during the phase change [10].

The unfreezable water can be estimated from the total enthalpy of the DSC heat flux peak, and the enthalpy of freezing of water[2, 7], and this has been found to be independent of initial water concentration, with a unfreezable water content of 0.4 g/gDM [9].

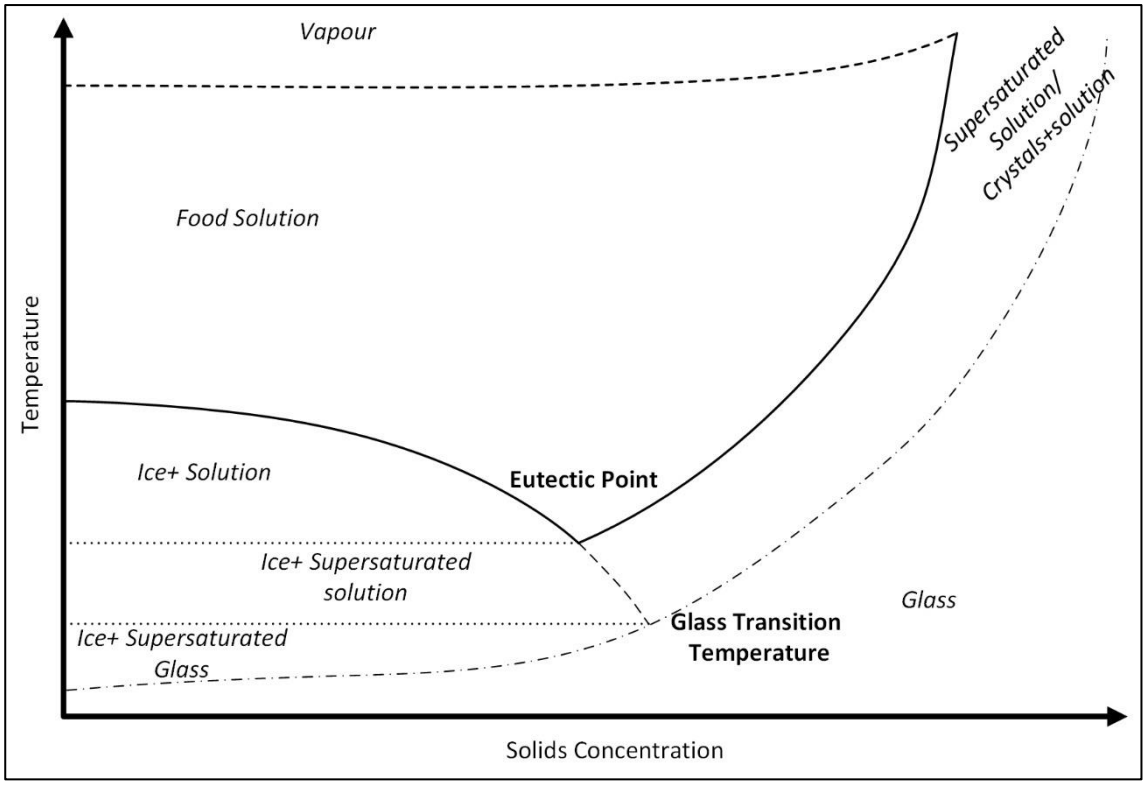

Figure 6-1: An example of a phase diagram for an idealised food solution, adapted from [2] and [11].

6.3 Methods.

6.3.1 Equipment and Software.

Detailed descriptions of the equipment and software used in this experimental work are given in Chapter 2 of this thesis.

6.3.2 Preparation of Milk Fractions.

Ovine Milk was collected from a farm in Palmerston North, New Zealand, and preserved by the addition of NaN_3 to a concentration of 30 ppm. NaN_3 was chosen due to its effectiveness at low concentrations, minimise the change in colligative properties due to the addition of preservative. The milk was stored at or below 4°C until further preparation or analysis. The milk was not heat treated in any fashion. All processing and DSC measurements were conducted within 1 week of collection.

Skim milk was obtained by centrifuging milk at 3000 g for 20 minutes at 20°C. The fat was removed, and the skimmed milk was reserved for analysis and ultracentrifugation.

The casein phase of the milk was removed from the milk by ultracentrifugation at 80,000 g at 20°C for two hours. The serum phase was reserved for analysis and the casein was discarded. Ultracentrifugation was used to remove the casein phase as it did not require adjusting the ionic strength or pH of the fluid. Removing the casein by acid precipitation would lead to changes in the makeup of soluble species in the milk, due to the dissolution of the colloidal calcium phosphate [12]. This change in the soluble species could affect the freezing behaviour system, so a physical method of separation was chosen.

The fat globules collected from the whole milk were dispersed in a volume of RO water identical to the original milk aliquot. This volume of water was separated by centrifuging milk at 3000g at 20°C for 20 minutes, and the fat was re-dispersed in a second volume of water. The fat globules were recovered as above, and then frozen at -80°C in preparation for freeze-drying.

Casein micelles were recovered from skim milk by diafiltration with 7 diavolumes of MilliQ water, using a membrane with a 0.1 µm cutoff. The resulting casein micelle dispersion was then frozen -80°C in preparation for freeze-drying.

Samples of fat globules and casein micelles were freeze dried in a laboratory scale shelf freeze-dryer. After freeze-drying, the dried fat and casein samples were stored in a desiccator below 5°C for up to 4 weeks until analysis.

6.3.3 Compositional Analysis

Total solids were determined according to AOAC method 990.20 [13]. The crude protein content was determined by a Kjeldahl method adapted from AOAC method 991.20, utilising a Kjeltec KT200 distillation system. The fat content was determined according to AOAC method 989.05 [13].The ash content was determined according to AOAC method 945.46 [13]. Lactose was estimated by difference.

6.3.4 Heat Capacities

Triplicate measurements of the dry fat and casein samples were measured using a TA instruments Q2000 DSC, operating in modulated mode. The samples were placed in pre-weighed T-zero aluminium hermetic plans, sealed and then weighed, and thermograms were recorded immediately after weighing.

The heat capacities were measured from -35° to 85 °C, at a heating rate of 3Kmin^{-1}, modulated at a frequency of 100 s^{-1} and an amplitude of 1 K. The cell constant was calibrated using a sapphire standard disc.

6.3.5 DSC Scan for Melting Peak

DSC signals were measured using a TA instruments Q2000 DSC operating in modulated mode.

The samples of milk fractions were placed in pre-weighed T-zero aluminium hermetic plans, sealed and then weighed, and thermograms were recorded immediately after weighing, in order to reduce any mass loss due to evaporation of water.

The sample was equilibrated at 40°C, then cooled to -35°C, and held isothermal for 10 minutes. The DSC signal was recorded between -35°C and 35°C at a heating rate of 1 Kmin^{-1}, modulated at a frequency of 1 min^{-1} and an amplitude of 1 K.

Before the measurements described in this chapter a single sample of skim bovine milk had been cycled from -40°C to 30°C at heating rates of 1 to 10 Kmin^{-1}. The shift of the melting peak maxima was measured and the shift varied from 0.16°C at 1 Kmin^{-1} to 6.04°C at 10 Kmin^{-1}. The shift was 0.28 °C at 2 Kmin^{-1} and at 1.16°C at 5 Kmin^{-1}.

Therefore, a heating rate of 1 Kmin^{-1} was selected to minimise thermal lags during the melting of samples. Further reduction of heating rate may reduce thermal lag further, but will also reduce sensitivity at the same time.

6.3.6 Freezing of Reconstituted Milk Samples.

The equilibrium melting points of concentrated milk solutions and concentrated simulated sheep milk ultrafiltrate (SSMUF) were determined from the steady temperature region on the temperature-time graph of the freezing process. The temperature time graphs were gathered by immersing a T-type thermocouple inside a 50mL sample of the test solution, and then placing the solution in a -80°C freezer. The temperature of the solution was logged every 2 seconds with a Measurement Computing USB-TC datalogger, until the sample reached equilibrium with the freezer. The thermocouples were calibrated in an ice-water slush.

A small number of AgI crystals were added to each sample to prevent supercooling by acting as a nucleation surface.

Whole milk and sheep milk solutions with controlled total solids were made up from commercially available whole sheep milk powder and whole cow milk powder. The solutions were prepared at the following concentrations:

Table 6-1: Concentration of whole milk powders frozen in -80°C freezer.

Sheep and Cow Milks Concentration (% TS)
10
15
20
25
30
40

SSMUF is a buffer simulating the soluble phase of milk, with the omission of soluble proteins. The composition is shown in Table 6-2. It was prepared by following the method for bovine SMUF as in Jenness and Koops[14], adjusted by the ratio of ultrafiltratable salts in ovine and bovine milk [15], with the addition of lactose to the concentration typical of ovine milk[16].

Table 6-2: Composition of SSMUF.

Solute	Concentration ($mmolL^{-1}$)
KH_2PO_4	5.31
K_2HPO_4	6.81
$K_3C_6H_7O_7.2H_2O$	0.15
$Na_3C_6H_7O_7.2H_2O$	2.45
$CaCL_2.2H_2O$	0.97
$Mg_3(C_6H_5O_7)_2.9H_2O$	8.14
KOH	1.00
K_2CO_3	5.08
Lactose	2.74

Higher concentration SSMUF buffers were prepared as above, but with the concentration of solutes adjusted by the concentration levels below:

Table 6-3: Concentrations of SSMUF frozen in -80°C freezer.

SSMUF concentrations
1.0x
1.5x
2.5x
4.0x

6.4 Determination of the Apparent Unfrozen Fraction

In this work, the calculation of apparent unfrozen water was adapted from a method which used calorimetric data to study the freezing curves of NaCl solutions [17] .

The apparent unfrozen water referred to in this work is defined as the fraction of the freezable water which remains unfrozen at a given temperature, as inferred from DSC measurements. Apparent ice fraction is defined in a similar fashion, as the fraction of freezable water frozen at any given temperature. Freezable water is the fraction of water in a sample which freezes between the initial equilibrium temperature and the end of freezing as the temperature of the sample approaches the glass transition. Water that remains unfrozen at the glass transition may not be energetically bound to a compound, and may be thermodynamically able to freeze, however the increase in viscosity prevents any further freezing occurring during experimental period. These two temperatures are determined from features in the DSC curve after compensation for thermal lag as discussed in section 6.4.1.

Two separate algorithms for the estimation of unfrozen fraction were considered. Both rely on the DSC measurements for the total enthalpy change as a function of temperature but differ in how the contribution of sensible heat to the total enthalpy change is estimates. The first estimates the enthalpy change required to heat up varying components of the food solution, using measured or published thermophysical data for the food components, and then completes an energy balance to estimate the latent heat component. The second utilises the DSC trace to estimate the average heat capacities in the frozen and liquid fractions in regions away from the thermal transition, and then completes an energy balance to estimate the latent heat component. As a result, three different methods were considered: The compositional method with published thermal properties, the compositional method with measured heat thermal properties, and the purely DSC based method. These three methods are referred to as FPH, MCC, and SLF respectively.

6.4.1 Thermal Lag Compensation

In an idealised transition, the enthalpy/temperature curve will be non-differentiable at the equilibrium freezing point, as the enthalpy/temperature relationship changes from being solely based on the absorption or loss of sensible heat, to the absorption or loss of latent heat and sensible heat. However, all measured curves are differentiable and show a smooth transition in the region of the equilibrium freezing temperature. This smooth transition reflects the thermal lag occurring within the DSC sample, where the resolution of large transitions is limited by the heat flux out of, or into, the sample pan.

A straight-line approximation of the highest slope region of the enthalpy curve is made, as the highest slope occurs just below the equilibrium freezing temperature. A second straight line approximation is made of the solid-state enthalpy curve and extended to below the approximate equilibrium freezing point.

The equilibrium freezing point is approximated by taking the second derivative of enthalpy/temperature curve and finding where this is equal to zero. This is an inflection point on the enthalpy/temperature curve and is indicative of the end of heat absorption by melting ice, all heat flow beyond this point is due thermal lag and sensible heating of the sample.

The intersection of these two lines is taken as the equilibrium freezing point, and the enthalpy over the phase change is determined. This is shown graphically in Figure 6-2.

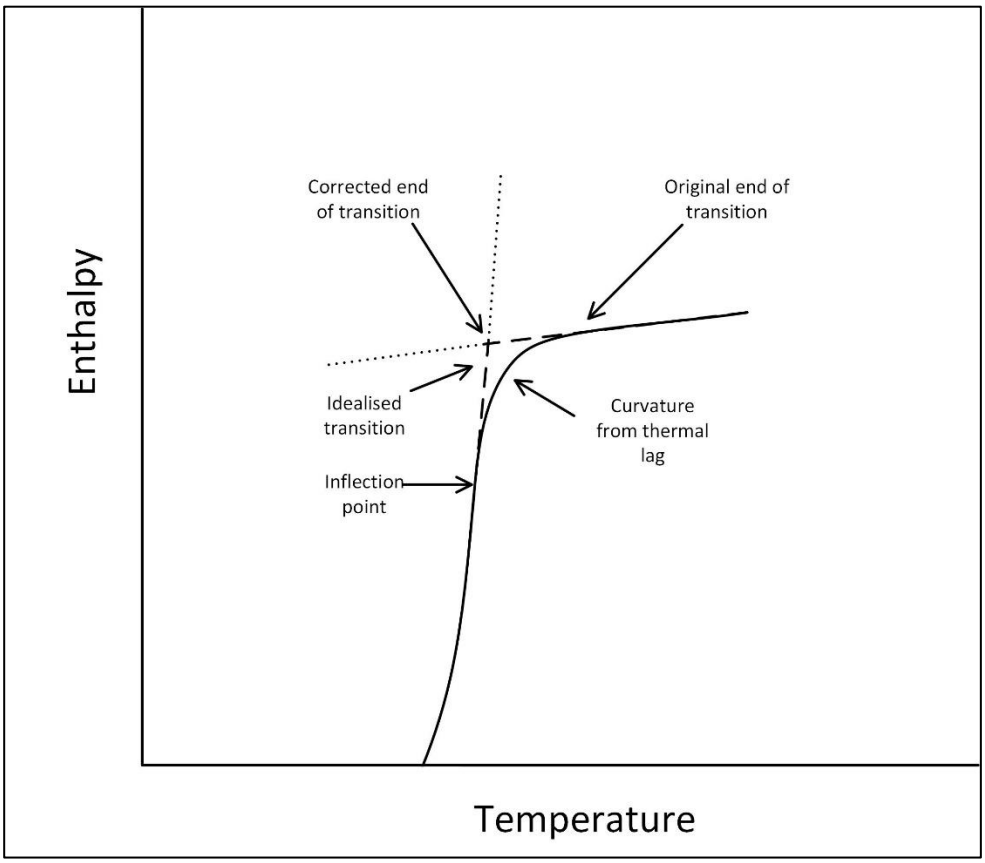

Figure 6-2: Correcting graph curvature due to thermal lag. The dotted lines represent straight line fits near the end of the phase transition.

6.4.2 Compositional Method

The enthalpy change during the transition of a complex food substance from a solid to a liquid is the sum of heat flows from several phenomena. They are as follows:

1. The latent heat required to melt the ice present.
2. The sensible heat required to heat the ice present from its melting point to the final temperature
3. The sensible heat required to heat the unfrozen aqueous phase present from the initial temperature to its melting point.
4. The sensible heat required to heat the discontinuous phases present in the food substance from the initial to the final temperature. In milk these phases are the fat and micellar casein phases.

To determine the sensible heats, an estimation of the liquid and solid faction is needed. This is determined by an iterative process. The zeroth iteration of the fraction of water that is in the solid phase (F_s) was made. This first estimate set F_s to 1 below the equilibrium freezing temperature (T_f), and 0 above T_f. At each temperate T, the two phase heat capacity Cp_{slw} is calculated from equation (6-1), where Cp_{sw} and Cp_{lw} are the solid and liquid water heat

capacities at temperature T. The solid and liquid heat capacities of water were calculated from polynomial estimations available in literature[2].

$$Cp_{slw}(T) = F_S(T) * Cp_{Sw}(T) + \left(1 - F_s(T)\right) * Cp_{lw}(T) \quad (6\text{-}1)$$

The two phase sensible enthalpy of the water component H_{sl} was calculated by integrating equation (6-1) between the initial datum temperature T_0 and T, and multiplying the integral by the water content of the food X_w.

$$H_{slw} = X_w \int_{T_0}^{T} Cp_{slw}(T)dT \quad (6\text{-}2)$$

The enthalpy contributions for the fat and casein, H_{fat} and H_{casein} , in the system were calculated according to equation (6-3) and equation (6-4). These follow the same form as equation (6-2), with the relative values for fat and casein substituted in place of water.

$$H_{fat} = X_{fat} \int Cp_{fat}(T)dT \quad (6\text{-}3)$$

$$H_{casein} = X_{casein} \int Cp_{casein}(T)dT \quad (6\text{-}4)$$

The total enthalpy contribution from the sensible heat of the components H_{sens} was calculated as shown in equation (6-5).

$$H_{sens} = H_{sl} + H_{fat} + H_{casein} \quad (6\text{-}5)$$

The apparent latent heat change to temperature T, $\Delta H'_{fus}(T)$, was calculated by subtracting the sensible heat from the total measured enthalpy change $\Delta H_{total}(T)$.

$$\Delta H'_{fus}(T) = \Delta H_{total}(T) - H_{sens}(T) \quad (6\text{-}6)$$

The greatest value of $\Delta H'_{fus}(T)$ is used as the latent heat of the transition.

$$\Delta H_{fus} = Max[\Delta H'_{fus}(T)] \quad (6\text{-}7)$$

The first iteration of $F_s(T)$ was calculated from the zeroth iteration of the latent heat of the transition ΔH_{fus} and the zeroth iteration of the apparent latent heat up to temperature T, $\Delta H'_{fus}(T)$

$$F_s(T) = 1 - \frac{\Delta H'_{fus}(T)}{\Delta H_{fus}} \quad (6\text{-}8)$$

This set of values of F_s was then used as an input in equation (6-1), and the process was repeated for a second and third iteration. After 3 iterations there was no significant change in the calculated values.

6.4.3 Straight-Line Method

In this method, the onset of melting and the equilibrium freezing temperature were determined from the DSC measurements. Straight line equations were fitted to the enthalpy/temperature curves in the temperature ranges below and above the phase transition.

The onset of melting was determined from the absolute first derivative of the DSC heat flow vs temperature curve. This was used to establish when the heat flow diverged considerable from

a constant as would be observed when latent heat is absorbed by a melting sample. This also appears as a small step change in the heat flow/temperature graph, similar to that seen in a glass transition. This is discussed further in section 5.3.

These straight-line fitted equations were used to determine Cp_s, and Cp_l, the solid and liquid heat capacities. In these regions the enthalpy change is solely due to the sensible heating of the milk components that do not undergo phase change, and the water component away from its phase change. The difference in the heat capacity of the milk components over the temperature range studied is negligible when compared with the heat flow due to the phase change, and the change in specific heat capacity of water from a solid to a liquid.

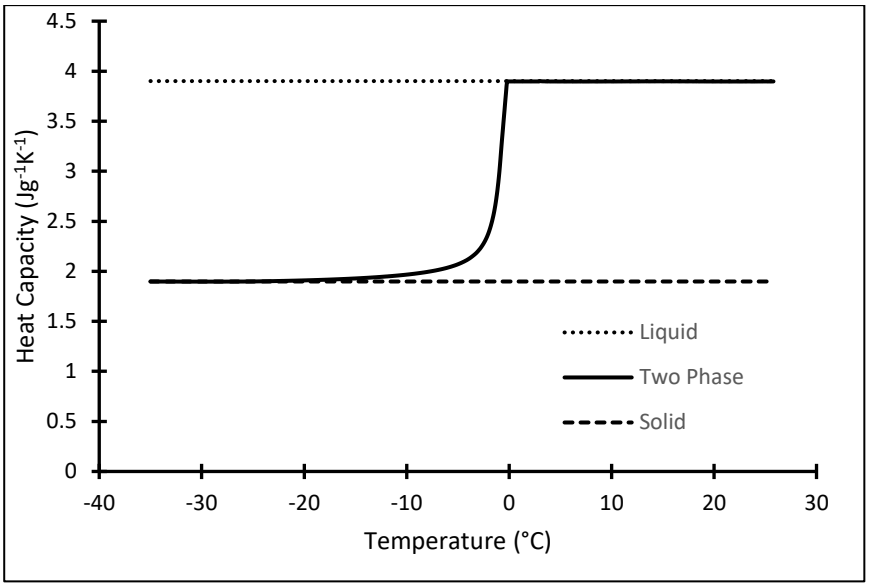

Figure 6-3: Solid, liquid and two-phase heat capacities in whole ovine milk.

By assuming that the heat capacities are constant across the temperature range, the two phase heat capacity Cp_{sl} was solely dependent on the change in apparent ice fraction $F_s(T)$, as shown in equation (6-9). This is shown graphically in Figure 6-3.

$$Cp_{sl}(T) = F_S(T) * Cp_S + (1 - F_s(T)) * Cp_l \quad (6\text{-}9)$$

The zeroth iteration set $Fs(T)$=1 below the T_f, and $Fs(T)$=0 above this temperature. Once $Cp_{sl}(T)$ has been determined, the two-phase sensible heat contribution $H_{sens}(T)$ was calculated by equation (6-10)

$$H_{sens}(T) = \int_{T_0}^{T} Cp_{sl}(T)dT \quad (6\text{-}10)$$

The apparent latent $\Delta H'_{fus}(T)$ was determined at each temperature by equation(6-6), the latent heat of the transition ΔH_{fus} was determined according to equation (6-7), and the apparent ice fraction as a function of temperature was calculated using equation (6-8).

This set of values of F_s was then used as an input in equation (6-9), and the process repeated for a second and third iteration. After 3 iterations there were no significant changes in the calculated values.

The various parts of this enthalpy balance are shown in Figure 6-4.

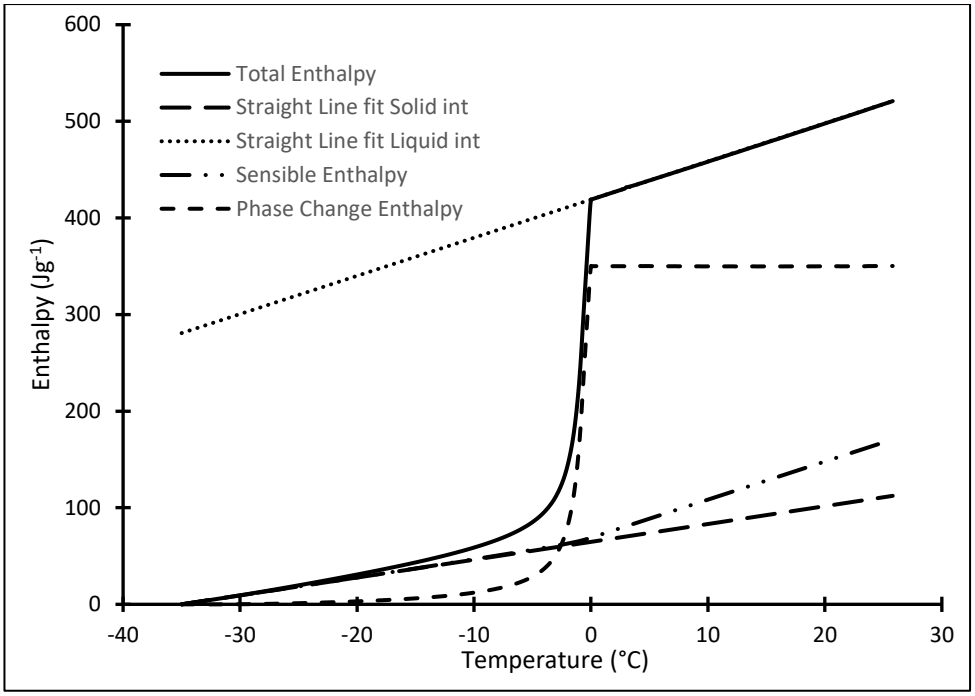

Figure 6-4: Enthalpy balance as described in section 4.3.

6.5 Results and Discussions

6.5.1 Sample Composition

The composition of the samples studied via DSC are shown in Table 6-4. The ash content of the sheep milk serum collected was lower than the skim or whole milk, as the colloidal minerals, associated to the casein micelles were removed with the casein. The composition is within the expected ranges for ovine milk in NZ[18].

Table 6-4: Composition of fluids studied via DSC. Compositions are given in % m/m on a wet basis. Values are averages of triplicate measurements. Errors are the 95% confidence interval for the mean.

Milk Fraction	Fat (%)	Protein (%)	Ash (%)	Lactose (%)	Total Solids (%)	Water (%)
Whole Sheep Milk (WSM)	6.90±0.07	5.4±0.3	0.92±0.06	3.81±1.1	17.1±0.8	83±0.8
Skimmed Sheep Milk (SSM)	0.39±0.03	5.66±0.04	1.00±0.02	5.23±0.03	12.27±0.01	87.73±0.01
Sheep Milk Serum (SMUC)	0.25±0.05	1.52±0.01	0.52±0.02	5.6±0.1	7.9±0.1	92.1±0.1

6.5.2 DSC Curves: Nucleation, Freezing and Melting.

The temperatures at which samples nucleated and began to freeze during the cooling cycles are shown in Figure 6-5, the mean temperatures are shown in Table 6-5. A one-way ANOVA test was performed and there were no significant differences between fluids.

Table 6-5: Mean and standard deviation of nucleation temperatures of samples.

Milk Fraction	Mean Nucleation Temperature (°C)
MilliQ Water	-17.2±2.2
SMUC	-17.3±2.9
SSM	-18.7±1.6
WSM	-14.7±1.9

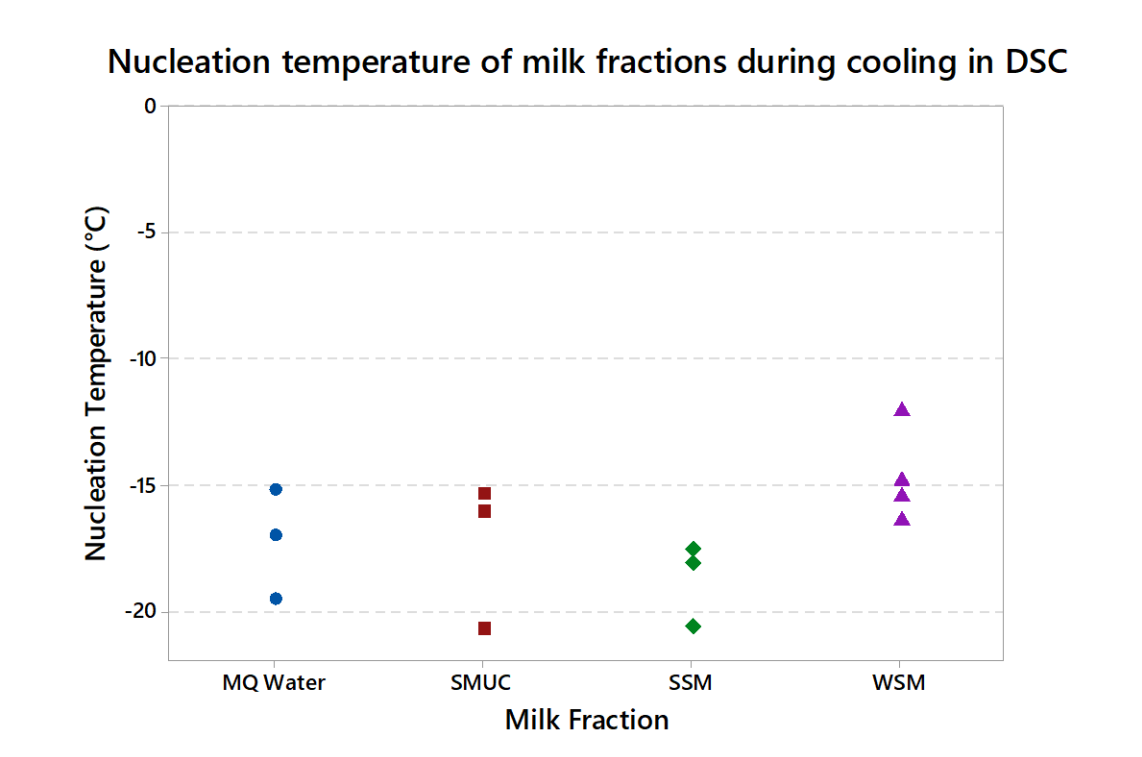

Figure 6-5: Nucleation temperatures observed during the cooling of samples in DSC measurements.

The energy released at nucleation for these samples, and the expected release based upon the total water content, is shown in Table 6-6.

Table 6-6: Energy released upon freezing for Whole Skim Milk (WSM), Skim Sheep Milk (SSM) and Sheep Milk UltraCentrifugate (SMUC) samples. The energy release measured via DSC is compared against the expected energy release($\Delta H_{fus}\ Expected$) , as calculated from the product of the sample water content and the latent heat of freezing at the nucleation temperature ($\Delta H_{fus} H_2O @ T_{nucleation}$).

Sample	$\Delta H_{fus}\ Measured$ $\left(\frac{kJ}{kg}\right)$	$T_{nucleation}$ (°C)	$\Delta H_{fus}\ H_2O\ @T_{nucleation}$ $\left(\frac{kJ}{kg}\right)$	$\Delta H_{fus}\ Expected$ $\left(\frac{kJ}{kg}\right)$	Fraction
WSM B	217	-14.9	302	250	0.87
SSM A	273	-20.6	288	252	1.08
WSM C	262	-16.4	298	247	1.06
SMUC B	260	-15.3	301	277	0.94
WSM D	236	-12.1	308	256	0.92
SSM E	244	-17.5	295	259	0.94
SSM C	234	-18.1	294	258	0.91
SMUC D	263	-16.0	299	275	0.96
SMUC C	268	-6.2	321	295	0.91
WSM A	223	-15.5	300	249	0.89
SSM D	225	-6.6	320	281	0.80
SMUC A	271	-20.7	288	265	1.02

These energy releases are on average within 5% of the expected value calculated from the integral form of the Kirchhoff equation. This confirms that there were no unexpected phenomena occurring during the freezing of samples, which would affect the results during the subsequent heating ramp. All samples were in a solid state before the heating ramp and heat flow measurement.

Raw DSC output curves are shown in Figure 6-6, with the region of the heat flow curves containing the melting onset transition highlighted and expanded to make the presence of this transition visible. Heat flow diverges from steady as the temperature approaches the freezing temperature and peaks at the equilibrium freezing temperature Tf. There is a small (2-4%) thermal lag in the peak after Tf.

Typical absolute integrals of the curves in Figure 6-6 are shown in Figure 6-7. The integral curve can be seen to be approximately linear before and after the melting transition. The slope of this straight-line region is the heat capacity of the solid or liquid sample.

The heat capacity can also be determined from the heat flow curve if the heating or cooling rate of the sample is known. As the variation of heat capacity as a function of temperature is small away from the melting transition, the derivative of the heat flow curve can be used to detect where large changes in the apparent heat capacity occur, and hence the onset of the melting transition. This is illustrated in Figure 6-8. The 1st derivative is plotted on a log axis. The rate of change above approximately 5°C is solely due to the change in the heat capacity of the liquid phase, and gives an indication of the order of magnitude of this phenomena. The increase as a result of the melting can be clearly seen.

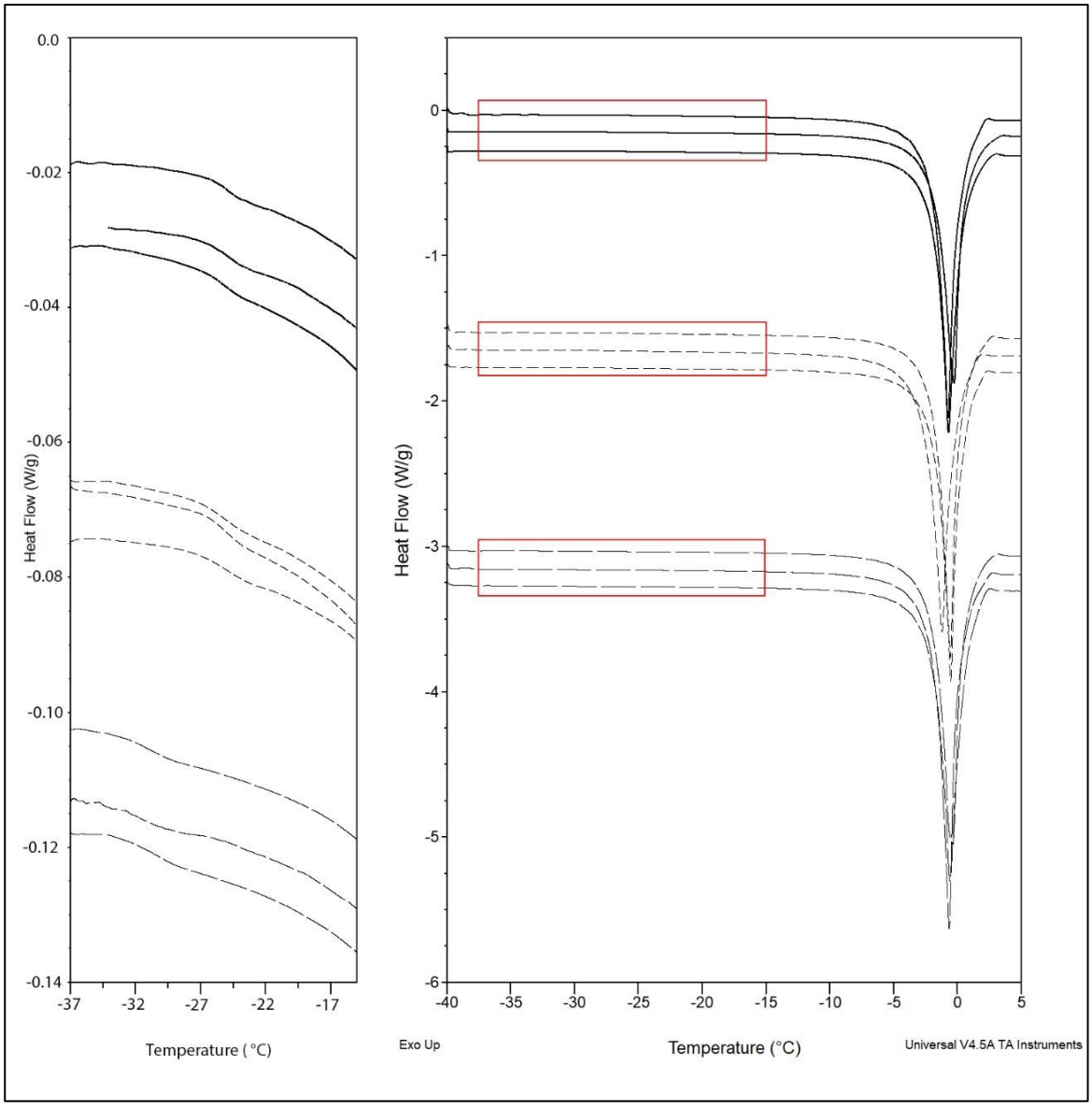

Figure 6-6: DSC curves for whole sheep milk ———, skim sheep milk - - - -, and sheep milk ultracentrifugate— — —. The curve from -40°C to 5°C is shown on the right. The region outlined in the red boxes is shown at larger scale on the left. Step changes can be seen in the curves at left, indicating a melting onset transition. Data is shown before post-processing to remove thermal lag. Curves are shifted vertically to aid in legibility.

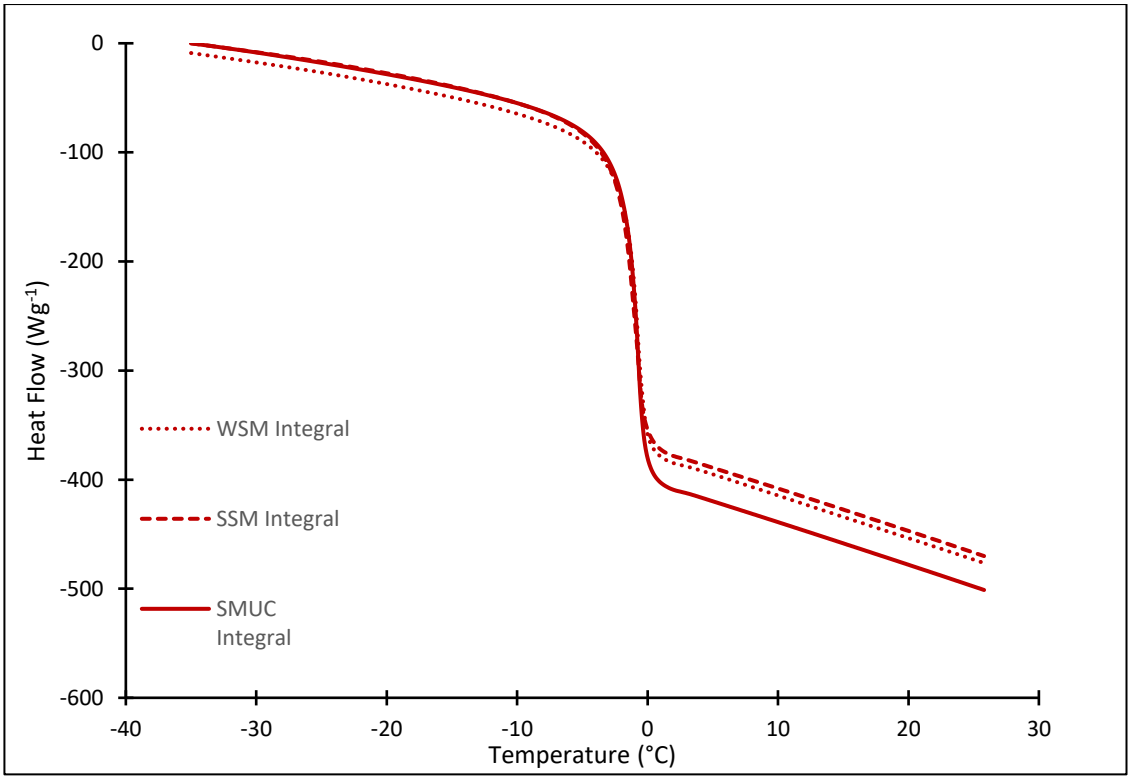

Figure 6-7: Typical absolute integrals (enthalpies) of curves in Figure 6-6 before post-processing to remove thermal lag.

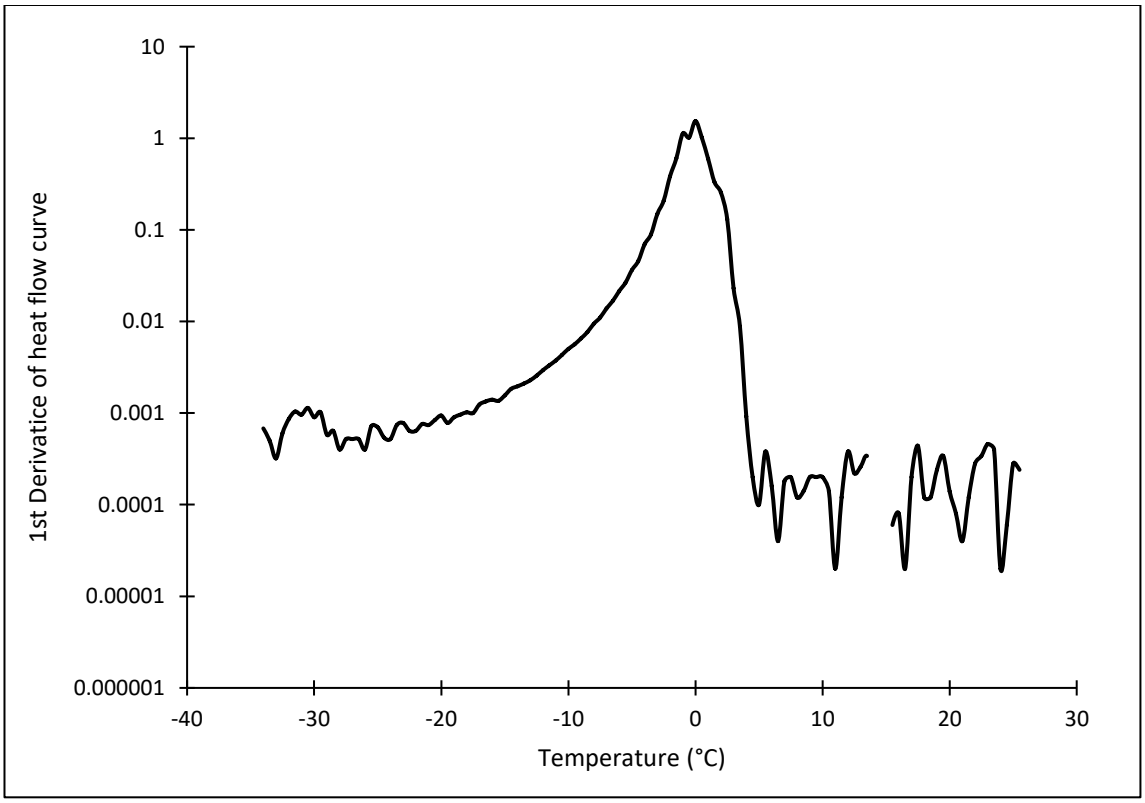

Figure 6-8: 1st Derivative of heat flow curve for a SMUC sample across the temperature range studied.

In the region of the equilibrium freezing temperature, the apex of the heat flow peak can be taken as the equilibrium freezing temperature. As the greatest change in fraction of unfrozen water due to progressive freezing occurs at or just below the equilibrium freezing temperature

the heat flow will be greatest at this point. In an idealised phase transition there would be a discontinuity in the heat flow/temperature graph, or a non-differentiable point in the enthalpy/temperature graph, as is illustrated in the thermal lag correction in Figure 6-2, however the thermal lag spreads this transition out. The equilibrium freezing point can also be estimated from the inflection point in the temperature/enthalpy graph as described in section 4.1.

The equilibrium freezing temperatures as estimated from the two methods described above are shown in the table below. For analysis of apparent unfrozen water, the 2nd derivative method was used to determine the equilibrium freezing temperature, and the end of the melting transition. There were no significant differences between the equilibrium freezing temperatures of each milk fraction. A pairwise t-test showed no significant difference between the two methods of estimating the equilibrium freezing temperature. More accurate measurements can be conducted using a cryoscope, but this was not done in this work. However there was no significant difference ($p<0.05$) between the measured values and previously reported values of the freezing point of sheep milk (-0.617 for raw milk, -0.614 for pasteurised milk) [19].

Table 6-7: Estimated equilibrium freezing temperatures. Error bars are the 95% confidence interval for the mean. N=4.

	Sample		
Estimation Method	**SMUC**	**SSM**	**WSM**
Peak Apex	-0.69±0.13	-0.74+0.32	-0.56±0.15
2nd derivative	-0.58±0.03	-0.72±0.31	-0.56±0.19

The serum phase of the milk appears to be the chief determinant of the initial degree of FPD, as there are no significant differences in the estimated initial freezing points.

6.5.3 Melting Onset

In all samples a small, but distinct, melting onset was observed at low temperatures. This is interpreted as the result of the concentrated unfrozen fraction of the milk transitioning from a glass to a maximally freeze-concentrated liquid, and the initial melting of the pure ice fraction.

Regrettably the DSC available was limited to a minimum temperature of -40°C, which is above the glass transition temperatures reported for a number of dairy systems: The glass transition (T_g) of maximally freeze-concentrated lactose solutions has been measured as -41°C, and the melting onset (T_m) as -31°C [20]. The same study also found that model lactose/protein solutions displayed both higher melting onset temperatures and lower glass transition temperatures when compared to pure lactose systems. The unfrozen aqueous fraction of the milk will be a highly concentrated solution of lactose and milk salts. In spray-dried bovine milk the T_g at a_w=0.155 ($X_w = 0.03$) has been measured at -38.2°C [8], which does not agree with other measurements which report T_g =64°C for whole milk at X_w=0.024[21]. T_m=-32°C has been reported in skimmed bovine milk [21].

A one-way ANOVA was performed to evaluate whether there were significant differences between the mean melting onset temperature of each sample. The temperatures at which melting onsets were observed are shown in Table 6-8.

Table 6-8: Observed Melting Onset in milk samples. Samples with differing superscripts are significantly different. p<0.05. Standard error of mean presented.

Sample	***Melting Onset (°C)***
SMUC	-31±0.7^{a}
SSM	-25.3±0.1^{b}
WSM	-25±0.1^{b}

The individual values of observed melting onsets are shown in Figure 6-9. T_m for whole and skim sheep milks are identical at approximately -25°C, however T_m of sheep milk ultracentrifugate is significantly lower at -31°C. This would indicate that the melting onset temperature of the system is raised by the presence of casein micelles and their associated colloidal salts, but not affected by the presence of milk fat globules.

The glass transition temperature in anhydrous milk protein concentrate powders with higher protein contents (60-80%) has been found to be greater than that in lower protein (40-50%) powders[22]. This effect is expected due to the presence of high molecular weight protein polymers, which can also interact with lactose[23].

The intact casein micelle system can also bind significant quantities of water [24], which may reduce the water: lactose ratio in the unfrozen phase above the glass transition temperature. As the glass transition temperature decreases with increased water activity [21], the increased availability of water in the SMUC samples when compared to casein-containing samples may lead to a higher water activity in the maximally freeze-concentrated state, and therefore a lower glass transition temperature, and possibly a lower melting onset temperature.

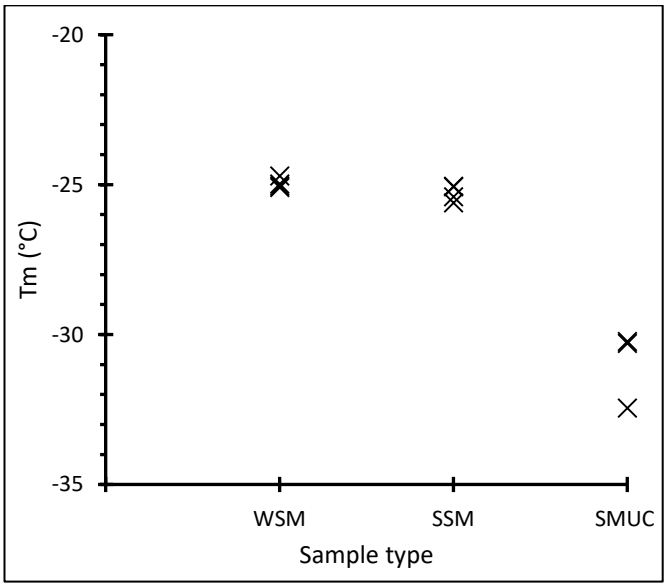

Figure 6-9: Observed melting onset temperatures of samples during heating from -40°C to 20°C.

The insensitivity of the melting onset temperature to the presence of fat globules is expected, as the fat globules can be considered to be a separate phase in the milk system, immiscible with the components that are responsible for the physical transitions during freezing and vitrification. Studies of glass transition in milk powders have found no clear effect of fat content on glass transition temperature[21].

There is essentially zero mobility of species below the glass transition due to the large increase in viscosity, to the order of 10^{12}-10^{13} Pa.s [25]. In the transition zone between the onset of melting and the glass transition the viscosity of the maximally frozen system will increase markedly, which will dramatically reduce reaction rates and diffusion rates, decreasing the rate of spoilage reactions. No recrystallization should occur below this temperature. Oxidation should occur very slowly below the glass transition temperature, and enzyme inactivation may occur in the glassy state [26]. This will increase the storage stability of the frozen milk, as is discussed in other chapters of this thesis.

The DSC method has proven sufficiently sensitive to detect the glass transition temperature during the freezing of concentrated coffee concentrates in other work we are conducting.

6.5.4 Specific Heat Capacity of Milk Components.

The specific heat capacity of the freeze-dried micellar casein fraction isolated (as described in section 3.2), when measured by DSC is shown in Figure 6-10 A. This is the average of triplicate measurements. The specific heat capacity shows an approximately linear increase with temperature, from 0.98 $Jg^{-1}K^{-1}$ at -35°C to 1.81 $Jg^{-1}K^{-1}$ at 30°C. The heat capacity of the isolated protein fraction differs significantly to the curve predicted using literature values of the specific heat of protein [2].

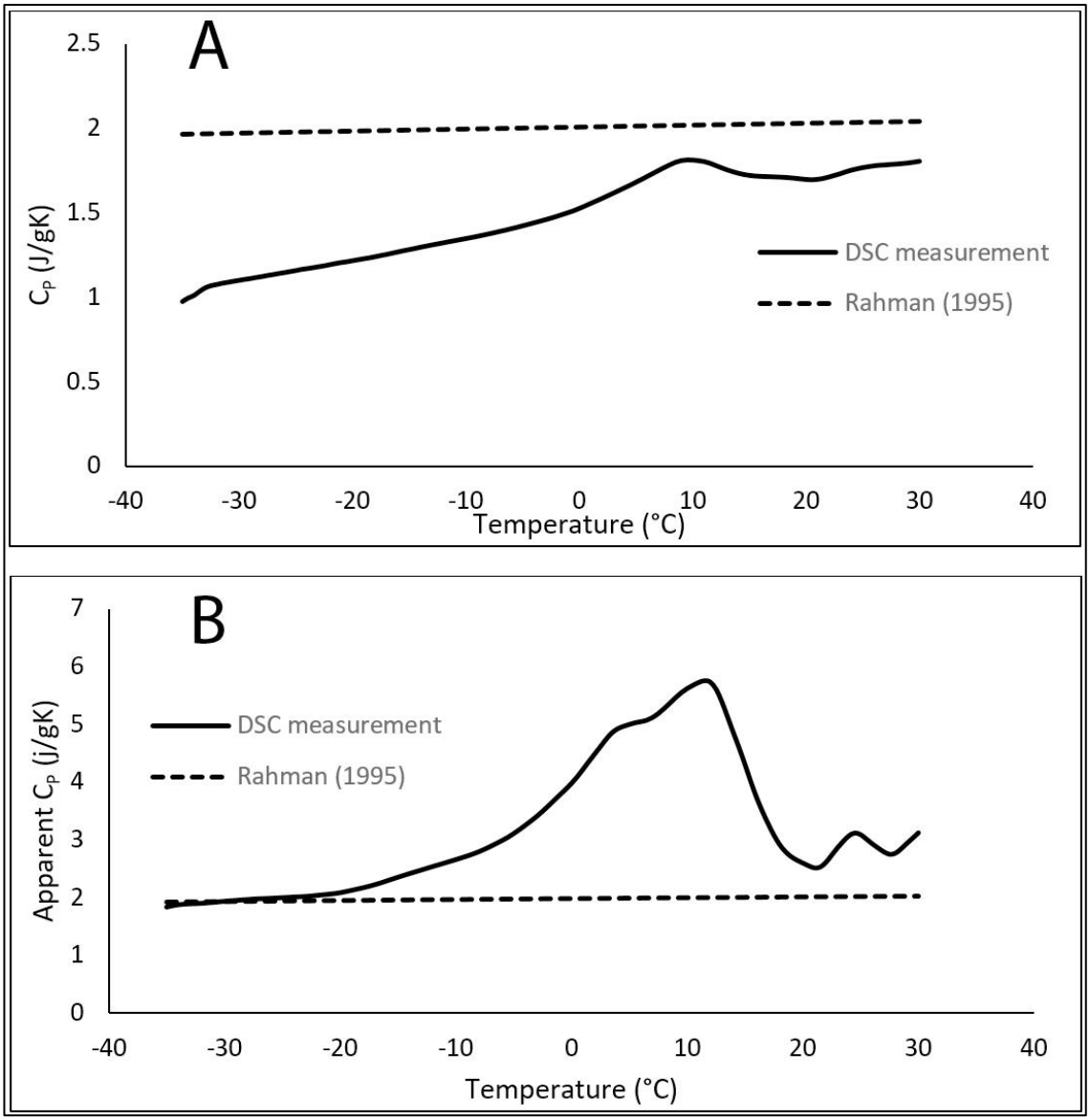

Figure 6-10: A: Measured specific heat capacity of isolated casein with a comparison to literature values. B: Measured apparent specific heat capacity of isolated fat globules with a comparison to literature values.

The apparent specific heat capacity curve of milk fat globules isolated from sheep milk is shown in Figure 6-10 B. The curve is the average of triplicate DSC measurements. This curve is compared with literature values of the specific heat capacity of fats [2]. As can be clearly seen there is a peak which shows an increase in the apparent specific heat from approximately 1.9 $Jg^{-1}K^{-1}$ to approximately 5.7 $Jg^{-1}K^{-1}$ There is a good agreement with the literature values from -35°C to -20°C, when the two curves diverge, and a peak is seen in the measured curve. This peak is likely due to the melting of some components of milk fat, and the latent heat absorbed during this phase transition.

For use in the determination of apparent unfrozen water in milk the integral of the heat capacity is more useful and this was determined from -35°C to 30°C. Polynomial functions of the form shown in equation (6-11) were fitted to the enthalpies of fat and casein with 238.16K (-35°C) selected as a datum point. The polynomial coefficients are shown in Table 6-9.

$$H = k_1\theta^4 + k_2\theta^3 + k_3\theta^2 + k_4\theta + k_5 \quad (6\text{-}11)$$

Table 6-9: Polynomial coefficients for equation (6-11).

	k_1	k_2	k_3	k_4	k_5
Casein Polynomial	-3.0×10^{-6}	3.144×10^{-3}	-1.251	220.8	-14650
Predictor T-value	*-18.81*	*18.58*	*-18.24*	*17.91*	*-17.66*
Predictor P- value	*<0.001*	*<0.001*	*<0.001*	*<0.001*	*<0.001*
Fat Polynomial	-4.1×10^{-5}	4.237×10^{-2}	-17.21	3032	-199900
Predictor T-value	*-21.25*	*20.89*	*-20.50*	*20.09*	*19.68*
Predictor P-value	*<0.001*	*<0.001*	*<0.001*	*<0.001*	*<0.001*

When the total integrals across the temperature range are compared as shown in Figure 6-11, there is a roughly 20% difference between the fat enthalpies determined from published predictive equations [2, 27] and the values measured in this study.

The difference between the measured values for the casein enthalpies determined from published predictive equations [2, 27] and the values measured in this study, with the values calculated using published equations being approximately 55% higher at 0°C.

These differences mean that the published predictive equations evaluated are not suitable for determining the enthalpy contribution of proteins and fats during the melting transition of ovine milk. These equations cannot be used as part of a methodology to determine the apparent ice or unfrozen water fraction of ovine milk.

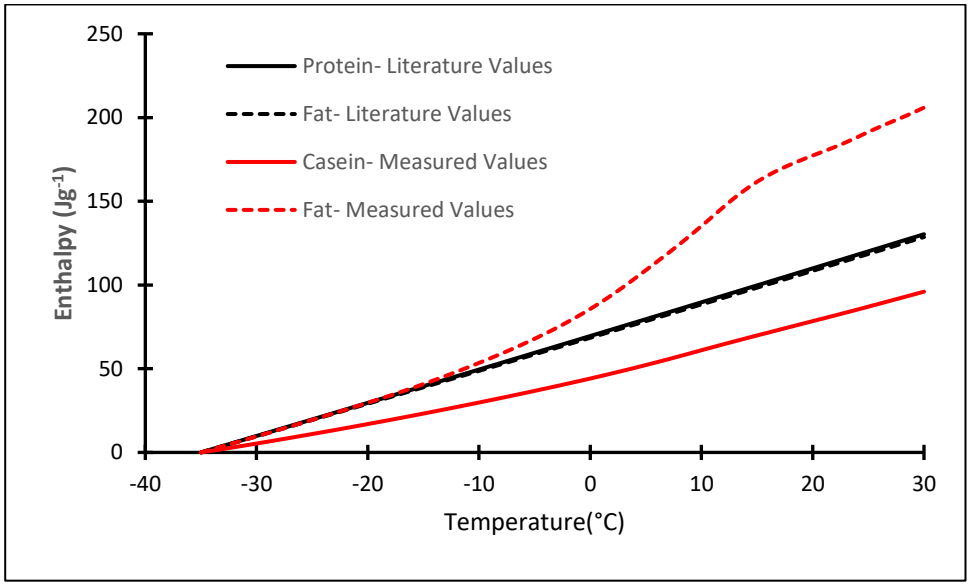

Figure 6-11: Milk fat and casein specific heat integral, comparison between curves calculated from literature values (in black), and those measured experimentally (in red).

6.5.5 Apparent ice and unfrozen water fractions from DSC Curves.

As discussed above, literature values of fat and protein sensible heat were not suitable and were not used further to generate curves of ice and unfrozen water fractions.

When curves generated by subtracting measured values of component sensible heat were evaluated, it was seen that the apparent ice and unfrozen water fractions were not monotonically increasing or decreasing as would be expected if the curves accurately described the phenomena occurring. This occurred as a result of over-estimation of the sensible heat contribution over the transition, and limitations in using separate component sensible heats and enthalpies.

These limitations are two-fold: The first is that any error in the measurement of the sample composition, or the sample mass in the DSC leads to a significant overestimation of the sensible heat contributions near T_M. At temperatures several degrees above T_M, $\frac{dF_s}{dT}$ is large enough that the heat flow due to latent heat masks the comparatively small inaccuracy in the sensible heat estimate.

The second limitation is the non-ideal nature of the major milk components in the highly concentrated state that occurs near T_M. At these temperatures, and the concentration there are limited thermal data available in literature. As a result, correlations that were intended for more commonly encountered temperatures and concentrations were used, which may not accurately represent the thermal behaviour in this region.

Therefore, the method described in section 6.4.2 was unsuitable and data from this is not presented further. Instead, the apparent ice and unfrozen water fractions were estimated using the method discussed in section 6.4.3, which used a single DSC scan per sample and estimated the sensible heat contributions from the regions of the curve outside of the transition.

Apparent ice fraction curves generated by this method are shown in Figure 6-12. Curves for each milk fraction are similar, indicating that the freezing behaviour is governed by the solutes present, which are present in all samples. There are no significant differences in the SSM curves and WSM curves, indicating that the presence of fat globules has minimal effect on freezing behaviour.

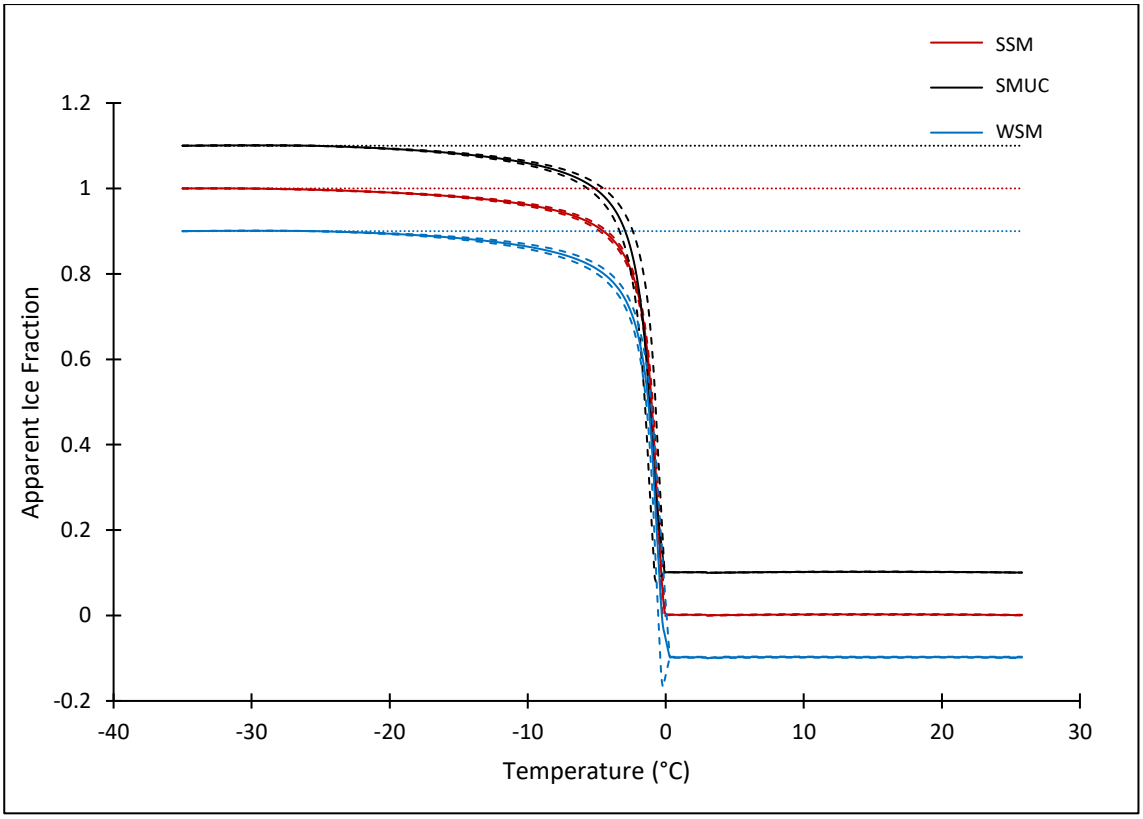

Figure 6-12. Apparent ice fraction as a function of temperature for Sheep Milk UltraCentrifugate(SMUC) , Skim Sheep Milk(SSM) and Whole Sheep Milk (WSM). Curves are average of all replicates and 95% CI for the means are shown as dashed lines. Curves are shifted 0.1 units in the Y-axis. Reference lines at an apparent ice fraction of 1 are shown for each sample.

The unfrozen water over the whole phase transition can be calculated as follows [2]:

$$M_I = \frac{\Delta H_{fus}}{\Delta H fus_{water}} \tag{6-12}$$

Where the enthalpy of the sample peak ΔH_{fus} is given in kJ/kg solute and the M_I is the mass of ice.

$$M_{uw} = \frac{M_{tw} - M_I}{M_{si}} \tag{6-13}$$

The mass of unfrozen water M_{uw} was calculated from M_I, the total mass of water M_{tw} and the mass of solids in the system M_{si}[2]. This value for M_{uw} was used to calculate the solids fraction $X_s(T)$, the water fraction $X_w(T)$ and the lactose fraction $X_l(T)$ in the unfrozen phase. These curves are shown in Figure 6-13. The concentration factor $Q^*(T)$, on a basis relative to water (eg, g solid/g water) can be calculated from the mass fraction of solids at T_f and at a temperature T [28]:

$$Q^* = \frac{X_s(T)\left(1 - X_s(T_f)\right)}{X_s(T_f)\left(1 - X_s(T)\right)} \tag{6-14}$$

$Q^*(T)$ for whole ovine milk during the freezing process is shown in Figure 6-13. Several milk properties such as a_w, mineral equilibria, colligative properties, and diffusion coefficients are proportionally affected by Q^* at a constant temperature, with diffusion constants decreasing,

and the viscosity increasing and becoming non-Newtonian. However, in the concentration process that occurs during freezing, the temperature also affects physical properties of the unfrozen phase. This is discussed further in Chapter 5.

For whole milk the solids concentration at the maximally freeze-concentrated point, $X_S(T_m)$, was calculated as 85±1.6% from equations (6-12) and (6-13). This is similar to published phase diagrams of whole bovine milk calculated from the behaviour of lactose [1], which was determined to be maximally freeze-concentrated at approximately 80% total solids. A maximally freeze-concentrated solids level of approximately 80% has been suggested as typical for a lot of food solutions[6]. A level of bound water in milk has been suggested as 0.4 g/g lactose. In lactose solutions the solids concentration of the maximally freeze-concentrated solution has been found to be 82%, with lower concentrations for mixed protein/carbohydrate systems[20]. The concentration in the unfrozen phase at the melting onset can also be estimated from the temperature of this transition using the Gordon-Taylor equation[29] Estimating $X_S(T_m)$ for whole ovine milk from the Gordon-Taylor equation and coefficient values for bovine milk[1, 20, 21, 30-32] and the measured melting onset point, gives, $X_S(T_m)$=87.5%, which agrees well with the value determined from the energy release, when possible differences between ovine and bovine milk are considered. Using the same method gives $X_s(T_m)$=0.85-0.86 for ovine skim milk, and $X_s(T_m)$ =0.8-0.82 for ovine serum.

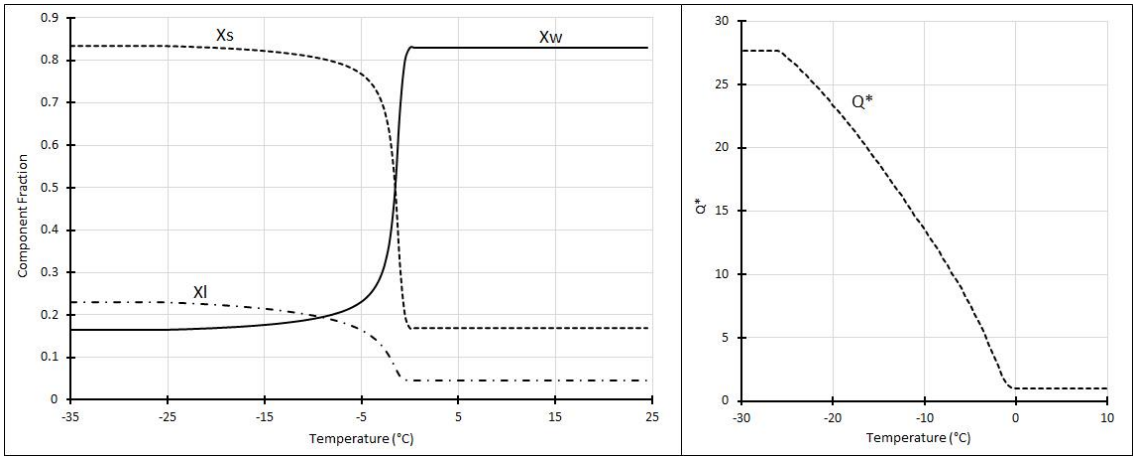

Figure 6-13:Component fractions in the unfrozen fraction in whole ovine milk during freezing. X_S, the total solid fraction, X_W, the water fraction, and X_l, the lactose fraction. The concentration factor Q is also shown.*

The graph of X_s in Figure 6-13 can be used with values for T_m discussed in section 5.3, the values for $X_s(T_m)$ discussed above, and the Gordon-Taylor equation for T_g of bovine milk to draw a partial phase diagram for ovine milk, shown in Figure 6-14.

The glass transition onset for a maximally freeze-concentrated system T_g' is estimated from $X_s(T_m)$ and the Gordon-Taylor equation for T_g of bovine milk. As a result, these values are estimates, as ovine milk has a typically higher protein: lactose ratio (typically 3.4:4.2 for bovine milk [33], 5.4:3.8 for ovine milk used in this work) , which may act to increase T_g values. This is an area for further investigation.

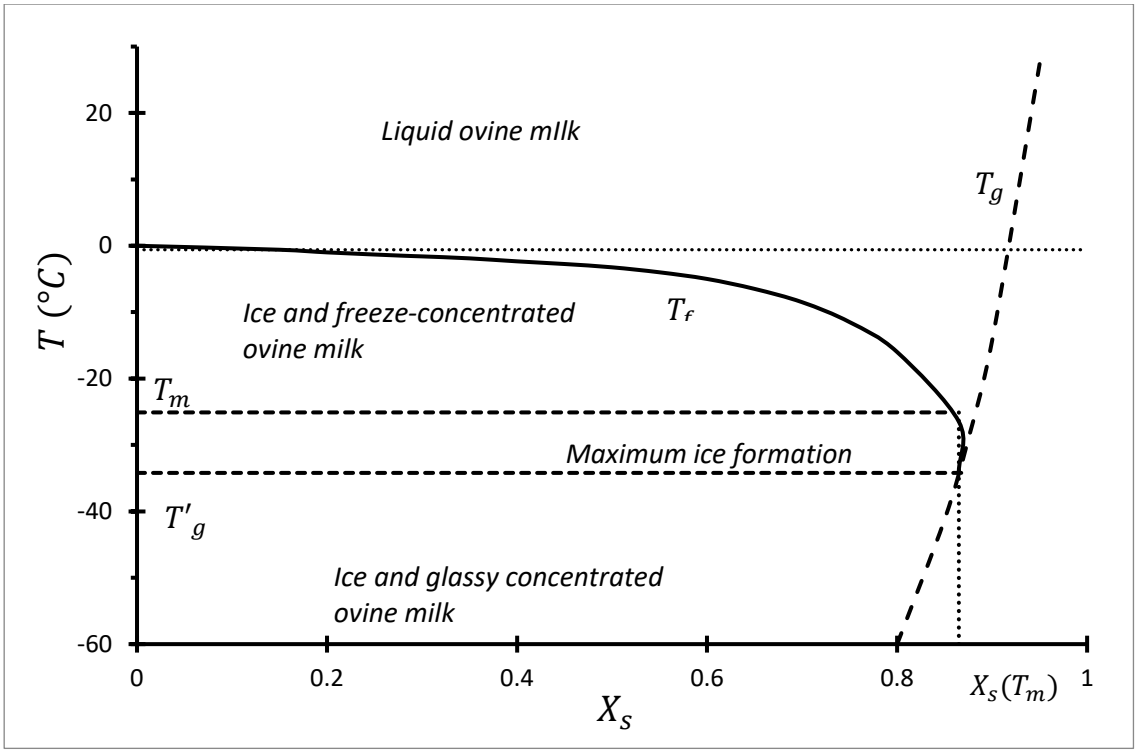

Figure 6-14: Partial Phase Diagram for ovine milk. T_g estimated from the Gordon-Taylor equation fits for whole bovine milk. T_f and T_m determined from DSC study, and $X_s(T_m)$ estimated from energy release during the freezing process.T'_g estimated from the Gordon-Taylor equation and $X_s(T_m)$.

6.5.6 Error Sources in Curve Generation.

6.5.6.1 Reduction of Latent Heat of Water Below 0°C

A possible source of error in this analysis in the handling of the decreased latent heat of water at temperatures below 0°C. The magnitude of this effect is discussed:

There are two different processes reducing the latent heat of water below 0°C: The thermodynamic reduction due to the reversibility of the freezing process, and the reduction of latent heat when water freezes from a metastable state.

The second case is discussed first: The latent heat change on freezing is lower when ice is formed from a metastable state by a non-reversible process, when compared to a change from a reversible process [34]. The latent heat has been measured calorimetrically by other workers and found to be lower than predicted from hydrostatic predictions, indicating higher entropy and free energy state [35]. This is hypothesised to be due to rapid freezing from a metastable state forming polycrystalline ice with stored energy in grain boundaries. This is supported by images of frozen sucrose solutions formed from solutions supercooled below -5°C being polycrystalline. Similar behaviour has been seen in simple solutions of NaCl, at dilute concentrations. Studies investigating water/H_2O_2 solutions have also found similar behaviour. [36] The formation of interstitials in ice reduces latent heat at a rate of approximately 4 eV per interstitial [37]. This reduction in latent heat would be observed in the melting peak if the water in the frozen solution has not had time to anneal to a lower energy state.

As discussed above, this anomalous behaviour of water is seen in measurements of transitions from a metastable state. The resulting solids have a higher entropy, and higher free energy, hence a lower latent heat. During the freezing of a food solution, assuming that the freezing began near T_f, rather than from supercooled liquid, the formation of ice below T_f is not a transition from a metastable state, and will therefore be a reversible transition. Therefore, the

thermodynamic reduction in the latent heat can be considered by itself and can calculated using the integral form of Kirchhoff equation:

$$\Delta H_{fus}(T) = \Delta H_{fus}(T_f) - \int_{T}^{T_f} [Cp_l - Cp_s]dT \quad (6\text{-}15)$$

The heat capacity of water below 0°C increases to a maximum at -45°C. This is well established in literature, with some disagreement between emulsion and bulk studies[38]. This has also been measured from vapour pressure, which also allowed estimation of latent heat of fusion[39] using the integral form of the Clausius-Clapeyron equation:

$$\ln\left(\frac{p_s}{p_l}\right) = \frac{\overline{\Delta H_{fus}}}{R_v}\left(\frac{1}{T_1} - \frac{1}{T}\right) \quad (6\text{-}16)$$

The calculations of the latent heat from the Clausius-Clapeyron equation in the literature match those calculated by the Kirchoff equation. By calculating the latent heat as a function of temperature using the Kirchoff equation as derived by [35], and using the data for liquid water heat capacity from [40] and solid water heat capacity from [2], the curve shown in Figure 6-15 A was derived. This curve shows the latent heat of freezing for water supercooled below 0°C, or it can also be expressed as a ratio of latent heat at a given temperature to Latent heat at 0°C as is shown in Figure 6-15 B

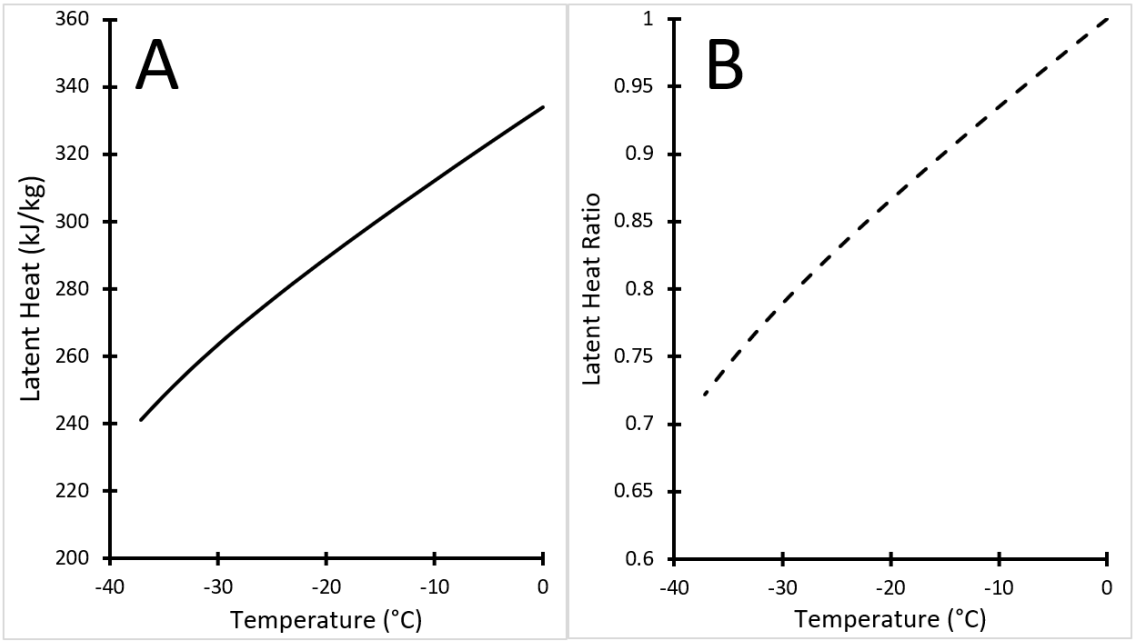

Figure 6-15: Latent heat of water at temperatures below 0°C A: Absolute value. B: Ratio of latent heat below 0°C to the value at 0°C.

The effect of incorporating this reduction in latent heat below 0°C into the algorithms described in section 6.4 was evaluated. The average deviation between curves derived using the uncorrected latent heat and curves corrected for the reduced latent heat was 0.4%. Therefore, the increased accuracy does not justify applying this correction, as this is not a major source of error.

Ice does not superheat under commonly encountered conditions; water will not be present in a metastable form at temperatures above the equilibrium melting temperature for the solution, as the surface of the solid acts as a nucleation site for the formation of liquid [41], and there exists a quasi-liquid pre-melted layer at the surface of bulk ice[42]. Experimental lags before melting have been measured in ultrafast heating studies, however these times are on the order

of picoseconds and therefore can be neglected in this study [43]. It can be assumed that in this study there is no dynamic superheating of ice to temperatures higher than the equilibrium freezing temperature, for a given solution. Therefore, for a given solution in contact with ice, and at a uniform temperature, the temperature corresponds to the equilibrium melting temperature of that solution. None of the ice present can be superheated above its equilibrium freezing temperature. Therefore, the required heat in excess of that required for sensible heating of the sample can all be assigned to the latent heat at the temperature where the heat flow is measured.

6.5.6.2 Thermal lags within DSC samples.

The major contribution to temperature error in this study is the thermal lag within the DSC sample pan itself. This is can become significant when the heat change over a transition is large, sample volumes are large, and heating rates are high. As the liquid-solid phase change in water involves a significant change in enthalpy, the heating rate for this study was set at 1 $Kmin^{-1}$ to reduce thermal lag, and the sample volumes were minimised. Nonetheless a significant thermal lag was observed during the final 2-4% of the thermal transition, due to the large energy requirements of melting. This was compensated for after the fact, but remains a possible source of inaccuracy, as the straight line fitted as a correction may have a somewhat different slope than the idealized curve.

6.5.6.3 Thermal Properties of Milk Components and Advantages of Self-Contained Methods.

When comparing the various algorithms for estimating the apparent ice fraction of partially frozen milk fractions, the “straight line fitting” algorithm is the most effective. The algorithm is “self-contained” which means that no external data are needed. Other methods can lead to compounding errors resulting from inaccuracies in the measurement of the sample mass, or the sample composition.

Methods which calculate the enthalpy contribution of sensible heat of each food component, require highly accurate measurements of the sample composition, and accurate measurement or calculation of the thermal properties of the food components across the entire range of the phase transition. Errors in the above will become highly apparent when the latent heat release is small, as happens near the melting onset transition.

The measured thermal data for food components also need to be representative of each component, in the environment in which it is found for all temperatures. I.e., the heat capacity of a dry casein sample measured at temperatures below T_f, may not be an accurate representation of the actual heat capacity of casein micelles in the in concentrated solutes present below T_f.

Using a single sample in the DSC has other advantages. The measurements and analysis can be done rapidly, without requiring a set of compositional analyses to be conducted. The sample volumes are small, which has advantages when supply of the product is limited, however, this adds complexity to the preparation of the product, requiring it to be homogenous before a sub-sample is taken for DSC analysis.

Other than the requirement for homogeneity, the sample preparation for DSC is simple and rapid, allowing a number of samples and replicates to be measured fairly rapidly.

6.5.7 Freezing of Reconstituted Milk Samples.

To corroborate freezing behaviour as observed by DSC measurements and that seen at a bulk scale, samples of reconstituted milk at several solids levels were frozen in a -80°C freezer, and the temperatures logged. Examples of the freezing curves measured by samples frozen in the -80° freezer are shown in Figure 6-16 and Figure 6-17. The presence of AgI in the samples was mostly successful at preventing supercooling and a subsequent temperature jump upon

nucleation. Small levels of supercooling were observed in some samples. Supercooling was reduced in order to minimise the change in liquid volume, and solute concentration on nucleation and recalescence. If a sample is significantly supercooled, a fraction of the liquid water is removed upon recalescence and the remaining liquid fraction would become more concentrated, decreasing the initial equilibrium freezing temperature Tf. The magnitude of this effect can be estimated from equation (6-17), where $\Delta T_{subcool}$ is the difference between the equilibrium freezing temperature and the nucleation temperature $T_{nucleation}$ [44].

$$X_{wR} = \frac{\Delta H_{fus}}{\Delta T_{subcool} Cp_l} \tag{6-17}$$

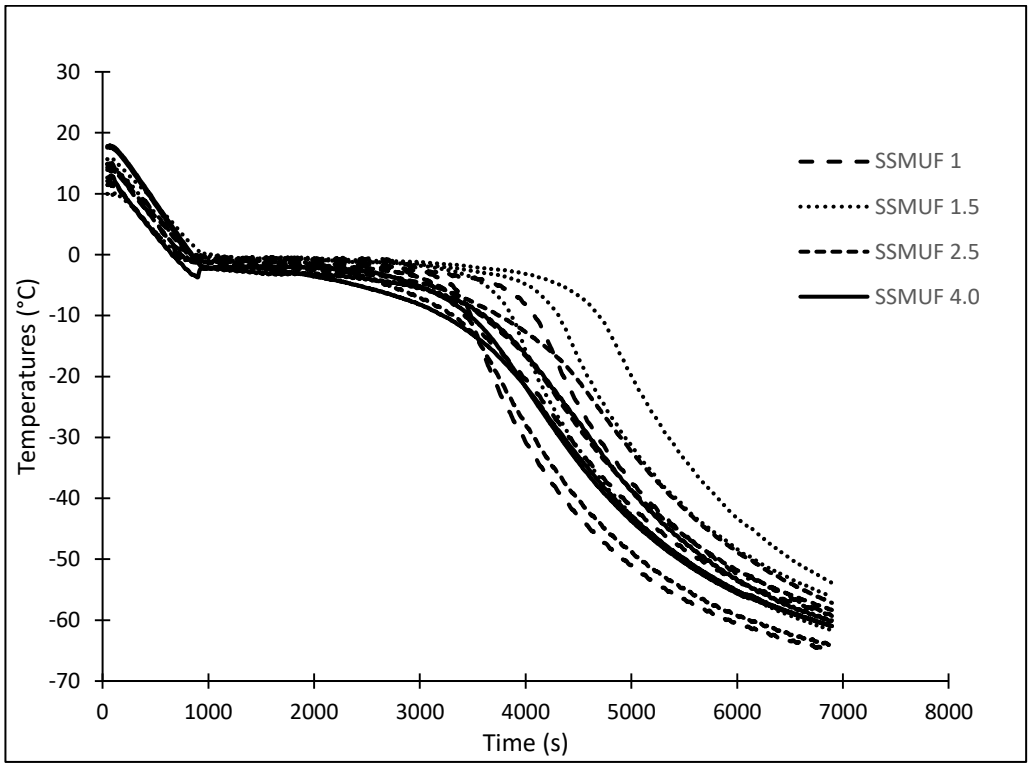

Figure 6-16: Temperature/time curve of SSMUF Samples at 4 different concentrations, corresponding to the 1x, 1.5x, 2.5x , and 4.0x the native salt concetration during freezing in a -80°C freezer.

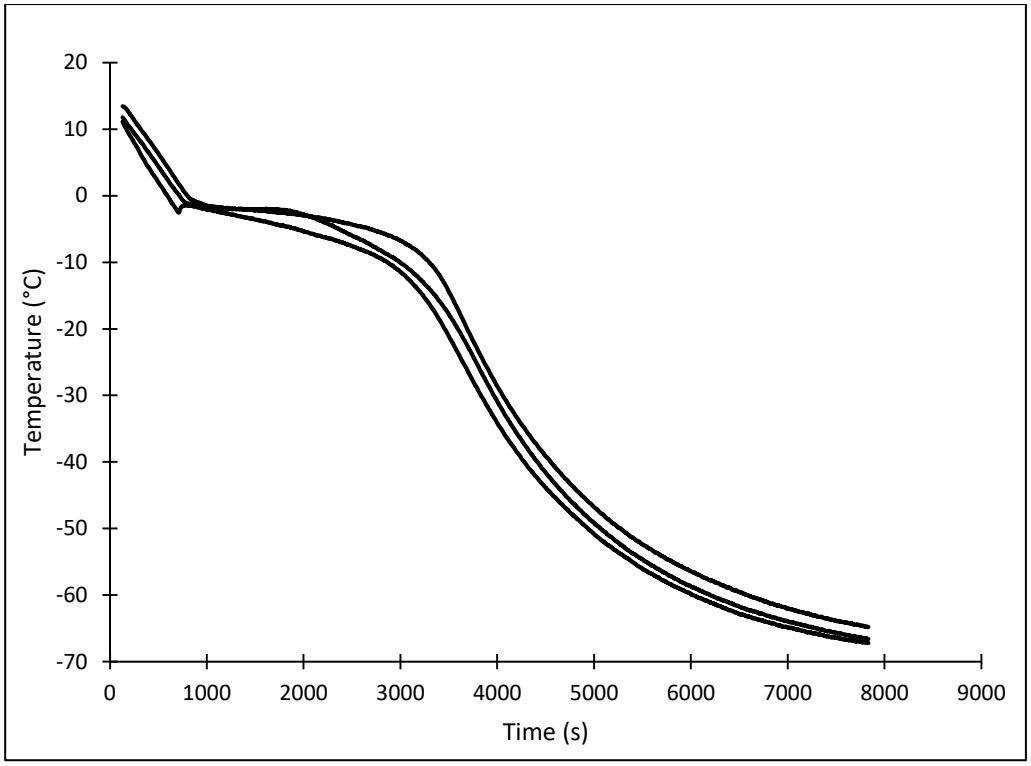

Figure 6-17: Temperature/time curve of 30% TS ovine milk reconstituted from powder during freezing.

The effect of total solids on Tf for each of the tested solutions is plotted in Figure 6-18, showing the averaged freezing temperature of triplicate measurements. Each replicate represents a sample prepared from separate batch of powder, and replicates were carried out on separate days. Error bars represent Figure 6-18A shows the relationship for reconstituted whole cow milk, Figure 6-18B for reconstituted whole sheep milk, and Figure 6-18C for SSMUF.

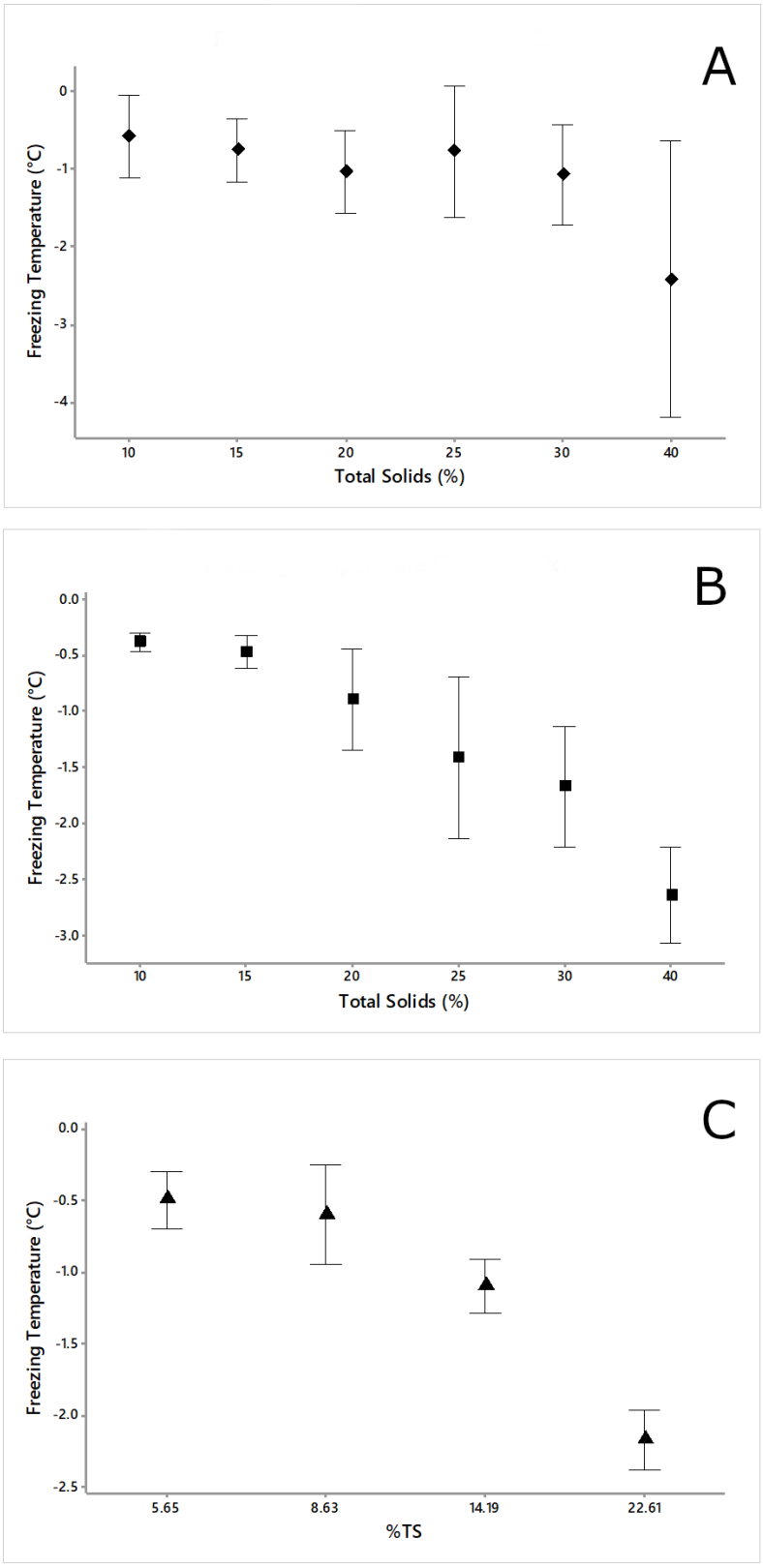

Figure 6-18: Tf vs. %TS for A: Cow milk, B: Sheep milk, C: SSMUF. Error bars represent the 95% confidence interval of the mean.

Quadratic equations of the form shown in equation (6-18) were fitted to the mean freezing temperature values for each solids concentration. There is no constant term in equation (6-18) to ensure that T_f is 0°C for water without dissolved solids.

$$T_f = a_2 C_s + a_3 C_s^2 \tag{6-18}$$

The coefficients for equation (6-18) are shown in Table 6-10 below:

Table 6-10: Quadratic coefficients for freezing point depression curves.

	Coefficient			Coefficient P values				
Sample	**a_2**	**a_3**	**R^2**	**a_2**	**a_3**	**TSS**	**ESS**	**RSS**
Sheep Milk	-2.46×10^{-2}	-1.05×10^{-3}	0.997	0.012	0.004	12.95	12.91	0.04
Cow's Milk	-2.75×10^{-2}	-6.84×10^{-4}	0.955	0.22	0.32	9.70	9.27	0.43
SSMUF	-5.87×10^{-2}	-1.62×10^{-3}	0.997	0.036	0.11	6.54	6.53	0.02

The curves of T_f predicted from the solid concentration according to equation (6-18) are shown in Figure 6-19.The freezing curve derived from the DSC data is also plotted. There is a close alignment between the two curves. Milk was not reconstituted at concentrations above 40%, for several reasons. There is a high degree of difficulty getting full wetting in high total solids (>50%) milk that is reconstituted from powder. The milk reconstituted from powder may not necessarily be indicative of actual behaviour in a highly freeze-concentrated solution, as a separation of components occurs when solids and particles are rejected from advancing ice fronts. This rejection occurs at different rates for different sizes of component. Therefore, the unfrozen freeze-concentrated solution in an intercrystalline space may have differing levels of fats and proteins to a bulk solution at similar total solids concentrations. As a result, the phase change behaviour may differ. This can be seen in some cryo-SEM images of frozen milk presented in chapter 4, where there appears to be a separation between protein and fat rich bands, and regions of dissolved solids, indicated by lactose crystals.

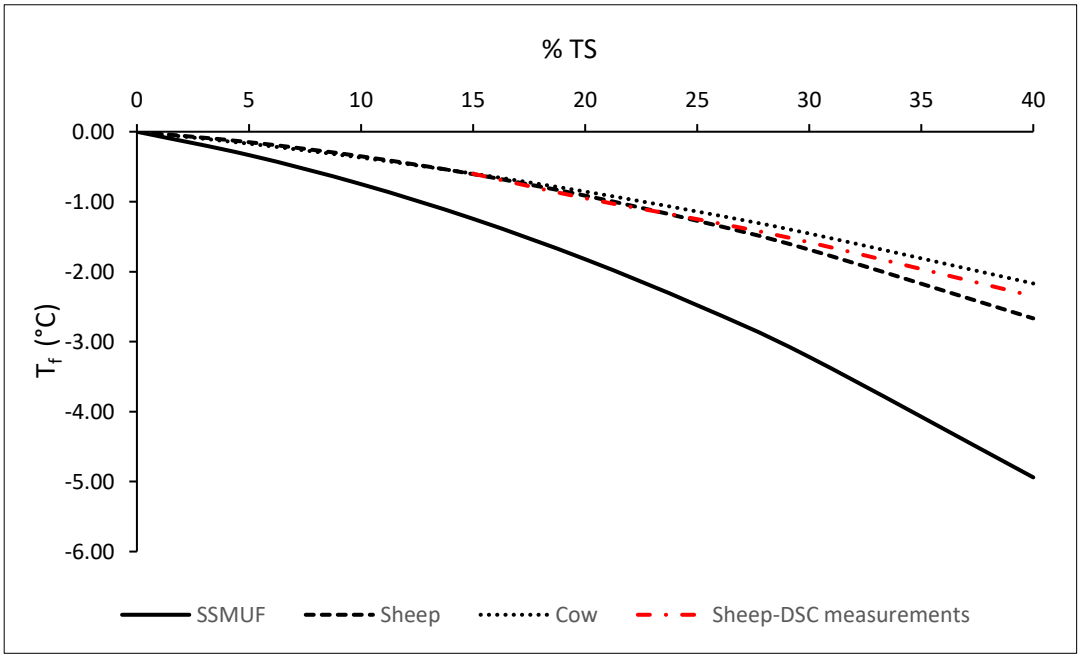

Figure 6-19: Freezing point curves predicted by equation (6-18), using the coefficients in Table 6-10, compared to measured values.

The volume and temperature dependent nature of nucleation in lactose[45] may also lead to differences in the freezing behaviour between a solution made up to a given solids concentration, and an unfrozen inclusion with similar solids content. The sample in the two cases will take different temperature/volume and concentration paths to reach a similar endpoint, so non-equilibrium processes such as lactose crystallisation may not behave similarly in each case. This is further reinforced by the cryo-SEM images presented in chapter 4, where lactose crystallisation is present in one of two samples that were cooled to the same eventual end point but followed different time and temperature paths. As lactose in solution contributes to the freezing and glass transition behaviour in the liquid phase, differences in its state (in an unsaturated solution, supersaturated solution, or crystallised) will lead to differences in freezing behaviour.

6.6 Conclusions

The phase transition behaviour of several milk fractions was studied by DSC and by measuring cooling curves in a freezer. During the cooling phase of the DSC study, the milk fraction samples nucleated at an average temperature of -16.8°C. Supercooling was minimal in the cooling curve experiment, as the addition of AgI promoted nucleation.

The energy release on nucleation is lower at higher degrees of sub cooling, as calculated from the integral form of the Kirchoff equation. The measured energy releases at nucleation were on average within 5% of the predicted values.

During heating from -40°C, the melting onset T_M of the maximally freeze-concentrated sample was observed at between -31°C and -25°C, dependant on sample. The melting onset of SMUC was the same as literature values for maximally freeze-concentrated lactose solutions. The melting onset was higher in SSM and WSM (-25.3°C and -25.0°C respectively).

The equilibrium freezing temperature T_f was determined by two methods, from the peak apex in the DSC curve, and from the second derivative of the enthalpy/temperature curve near the expected T_f. The values determined were within the range of previously published values. There were no significant differences between T_f values estimated for each milk fraction.

The concentration of the maximally freeze-concentrated solution of whole milk $X_s(T_m)$ was determined from the latent heat release, $X_s(T_m)$=0.85±0.016, and from the Gordon-Taylor equation using T_m, $X_s(T_m)$=0.875. These two methods agreed well. Using then Gordon-Taylor equation, $X_s(T_m)$=0.85 for skim milk, and $X_s(T_m)$=0.81 for ovine milk serum. A partial phase diagram of ovine milk was plotted from the data derived from the DSC measurements and the Gordon-Taylor equation. The curve of T_f vs C_s determined from DSC measurements agreed well with that determined from the freezing point of reconstituted milks.

This freezing behaviour may allow the properties of partially frozen milks to be controlled by adjusting their temperature. This may allow the milk to be frozen with novel techniques which exploit this behaviour. One of these techniques is discussed in detail in the next two chapters of this thesis.

6.7 List of Symbols

Symbol	Description	Units
$a_{1\ldots3}$	Quadratic coefficients for FPD	
Cp_{casein}	Casein specific heat.	$Jg^{-1}K^{-1}$
Cp_{fat}	Fat specific heat.	$Jg^{-1}K^{-1}$
Cp_{l}	Liquid-phase specific heat.	$Jg^{-1}K^{-1}$
Cp_{lw}	Water liquid-phase specific heat.	$Jg^{-1}K^{-1}$
Cp_{s}	Solid-phase specific heat.	$Jg^{-1}K^{-1}$
Cp_{sl}	Two-phase specific heat.	$Jg^{-1}K^{-1}$
Cp_{slw}	Water two-phase specific heat.	$Jg^{-1}K^{-1}$
Cp_{sw}	Water solid-phase specific heat.	$Jg^{-1}K^{-1}$
C_s	Solids Concentration	$\%\ Total\ Solids$
F_s	Ice fraction of freezable water.	g/g
H_{casein}	Casein enthalpy.	Jg^{-1}
H_{fat}	Fat enthalpy.	Jg^{-1}
H_{sens}	Total sensible enthalpy.	Jg^{-1}
H_{sl}	Two-phase sensible heat enthalpy.	Jg^{-1}
H_{slw}	Water Two-phase sensible heat enthalpy.	Jg^{-1}
$k_{1\ldots5}$	Polynomial coefficients for fat and casein enthalpy	
M_I	Mass of ice formed during transition	g
M_{si}	Mass of solids in sample	g
M_{tw}	Total mass of water	g
M_{uw}	Mass of unfrozen water	g
p_l	Vapour pressure of liquid solvent	Pa

p_s	Vapour pressure of solid solvent	Pa
R_v	Gas constant	$Jmol^{-1}K^{-1}$
T	Temperature.	$°C$
T_0	Datum temperature	$°C$
T_f	Equilibrium Freezing Temperature.	$°C$
T_g	Glass Transition Temperature	$°C$
T_M	Melting Onset Temperature	$°C$
$T_{nucleation}$	Temperature at which a cooled sample nucleates.	$°C$
X_{casein}	Casein Fraction.	$g/gmilk$
X_{fat}	Fat fraction.	$g/gmilk$
X_l	Lactose Fraction	$g/gmilk$
X_s	Solid fraction	$g/gmilk$
X_{sl}	Aqueous phase fraction.	$g/gmilk$
X_w	Water fraction	$g/gmilk$
X_{wR}	Amount of water frozen on recalescence	$g/gmilk$
X_l	Lactose Fraction	$g/gmilk$
$\Delta H'_{fus}$	Enthalpy change due to phase change from T_0 to T_i	Jg^{-1}
ΔH_{fus}	Total enthalpy change due to phase change.	Jg^{-1}
$\Delta Hfus_{water}$	Enthalpy of fusion of water	Jg^{-1}
ΔT_f	Amount of FPD	$°C$
$\Delta T_{subcool}$	Amount of supercooling	$°C$

6.8 References.

[1] G. Vuataz, "The phase diagram of milk: a new tool for optimising the drying process," *Le Lait,* vol. 82, no. 4, pp. 485-500, 2002.

[2] S. Rahman, *Food Properties Handbook*. CRC Press, 1995.

[3] O. Hanus *et al.*, "Relationship between freezing point and raw ewes' milk components as a possible tool for estimation of milk adulteration with added water,", *Journal of Food and Nutrition Research,* vol. 54, no. 4, pp. 281-288, 2015.

[4] P. Zhou and T. P. Labuza, "Analytical Methods | Differential Scanning Calorimetry," in *Encyclopedia of Dairy Sciences (Second Edition)*, J. W. Fuquay Ed. San Diego: Academic Press, 2011, pp. 256-263.

[5] D. S. Reid, W. Kerr, and J. Hsu, "The glass transition in the freezing process," *Journal of Food Engineering,* vol. 22, no. 1, pp. 483-494, 1994.

[6] Y. H. Roos and S. Drusch, "Chapter 4 - Water and phase transitions," in *Phase Transitions in Foods (Second Edition)*, Y. H. Roos and S. Drusch Eds. San Diego: Academic Press, 2016, pp. 79-113.

[7] O. Mishima and H. E. Stanley, "The relationship between liquid, supercooled and glassy water," *Nature,* Review vol. 396, no. 6709, pp. 329-335, 1998.

[8] A. Pugliese, M. Paciulli, E. Chiavaro, and G. Mucchetti, "Application of differential scanning calorimetry to freeze-dried milk and milk fractions," *Journal of Thermal Analysis and Calorimetry,* vol. 137, no. 2, pp. 703-709, 2018.

[9] H. Kumagai, K. Nakamura, and J. Fujiwhara, "DSC Measurement of Frozen Water in Liquid Foods," *Agricultural and Biological Chemistry,* vol. 49, no. 11, pp. 3097-3101, 1985.

[10] X. D. Chen, W. D. Wu, and P. Chen, "An analytical relationship of concentration-dependent interfacial solute distribution coefficient for aqueous layer freeze concentration," *AIChE Journal,* Article vol. 61, no. 4, pp. 1334-1344, 2015.

[11] Y. H. Roos, "Chapter 4 - Water and Phase Transitions," in *Phase Transitions in Foods*, Y. H. Roos Ed. San Diego: Academic Press, 1995, pp. 73-107.

[12] D. S. Horne, "Casein micelle structure: Models and muddles," *Current Opinion in Colloid & Interface Science,* vol. 11, no. 2-3, pp. 148-153, 2006.

[13] G. W. Latimer, *Official methods of analysis of AOAC International*. Rockville, Md: AOAC International, 2016.

[14] R. Jenness and J. Koops, "Preparation and properties of a salt solution which simulates milk ultrafiltrate," *Netherlands Milk and Dairy Journal,* vol. 16, pp. 153-164, 1962.

[15] C. Holt and R. Jenness, "Interrelationships of constituents and partition of salts in milk samples from eight species," *Comparative biochemistry and physiology. A, Comparative physiology,* vol. 77, no. 2, pp. 275-82, 1984.

[16] M. Ramos and M. Juarez, "Milk | Sheep Milk," in *Encyclopedia of Dairy Sciences*, J. W. Fuquay Ed., Second Edition ed., 2011, ch. 494-502.

[17] J. Leys, P. Losada-Pérez, C. Glorieux, and J. Thoen, "The melting behaviour of water and water–sodium chloride solutions studied by high-resolution Peltier-element-based adiabatic scanning calorimetry," *Journal of Thermal Analysis and Calorimetry,* vol. 129, no. 3, pp. 1727-1739, 2017.

[18] L. Day, M. Broadhurst, and L. Samuelsson. (2016) New Zealand Sheep Milk-nutritional composition. *Food New Zealand*. 20,21.

[19] B. Janštová, P. Navrátilová, M. Králová, and L. Vorlová, "The freezing point of raw and heat treated sheep milk and its variation during lactation," *Acta Veterinaria Brno,* vol. 82, no. 2, pp. 187-190, 2013.

[20] K. J. Singh and Y. H. Roos, "Frozen State Transitions in Freeze-Concentrated Lactose-Protein-Cornstarch Systems," *International Journal of Food Properties,* vol. 10, no. 3, pp. 577-587, 2007.
[21] K. Jouppila and Y. H. Roos, "Glass Transitions and Crystallization in Milk Powders," *Journal of Dairy Science,* Article vol. 77, no. 10, pp. 2907-2915, 1994.
[22] V. Maidannyk *et al.*, "Water sorption and hydration in spray-dried milk protein powders: Selected physicochemical properties," *Food Chemistry,* vol. 304, p. 125418, 2020.
[23] M. Kamrul Haque and Y. H. Roos, "Water Plasticization and Crystallization of Lactose in Spray-dried Lactose/Protein Mixtures," *Journal of Food Science,* Article vol. 69, no. 1, pp. FEP23-FEP29, 2004.
[24] W. Kneifel, A. Seiler, J. N. Dewit, and P. S. Kindstedt, "Water-Holding Properties of Milk Protein Products - a Review," *Food Structure,* vol. 12, no. 3, pp. 297-308, 1993..
[25] Y. H. Roos and S. Drusch, "Physical state and molecular mobility," in *Phase Transitions in Foods (Second Edition)*, Y. H. Roos and S. Drusch Eds. San Diego: Academic Press, 2016, pp. 19-47.
[26] Y. H. Roos, "Phase transitions and structure of solid food matrices," *Current Opinion in Colloid & Interface Science,* vol. 3, no. 6, pp. 651-656, 1998.
[27] Y. Choi and M. Okos, "Thermal properties of liquid foods," 1986.
[28] P. Walstra, J. T. M. Wouters, and T. J. Geurts, *Dairy science and technology*. Boca Raton: CRC Taylor & Francis, 2006.
[29] M. Gordon and J. S. Taylor, "Ideal copolymers and the second-order transitions of synthetic rubbers. i. non-crystalline copolymers," *Journal of Applied Chemistry,* vol. 2, no. 9, pp. 493-500, 1952.
[30] K. Jouppila, J. Kansikas, and Y. H. Roos, "Glass Transition, Water Plasticization, and Lactose Crystallization in Skim Milk Powder," *Journal of Dairy Science,* Article vol. 80, no. 12, pp. 3152-3160, 1997.
[31] P. Schuck, E. Blanchard, A. Dolivet, S. Méjean, E. Onillon, and R. Jeantet, "Water activity and glass transition in dairy ingredients," *Le Lait,* vol. 85, no. 4-5, pp. 295-304, 2005.
[32] Y. H. Roos, "Importance of glass transition and water activity to spray drying and stability of dairy powders," *Le Lait,* vol. 82, no. 4, pp. 475-484, 2002.
[33] C. F. Balthazar *et al.*, "Sheep Milk: Physicochemical Characteristics and Relevance for Functional Food Development," *Comprehensive Reviews in Food Science and Food Safety,* vol. 16, no. 2, pp. 247-262, 2017.
[34] D. Bertolini, M. Cassettari, and G. Salvetti, "Anomalies in the “latent heat” of solidification of supercooled water," *Chemical Physics Letters,* vol. 119, no. 6, pp. 553-555, 1985.
[35] W. Cantrell, A. Kostinski, A. Szedlak, and A. Johnson, "Heat of Freezing for Supercooled Water: Measurements at Atmospheric Pressure," *The Journal of Physical Chemistry A,* vol. 115, no. 23, pp. 5729-5734, 2011.
[36] F. Franks, Ed. *Water: A Comprehensive Treatise*. New York: Springer Science+ Business Media, 1982.
[37] V. F. Petrenko and R. W. Whitworth, *Physics of Ice*. Oxford: Oxford University Press, 2002, p. 392.
[38] E. Tombari, C. Ferrari, and G. Salvetti, "Heat capacity anomaly in a large sample of supercooled water," *Chemical Physics Letters,* vol. 300, no. 5, pp. 749-751, 1999.
[39] N. Fukuta and C. M. Gramada, "Vapor Pressure Measurement of Supercooled Water," *Journal of the Atmospheric Sciences,* vol. 60, no. 15, pp. 1871-1875, 2003.

[40] D. G. Archer and R. W. Carter, "Thermodynamic Properties of the NaCl + H2O System. 4. Heat Capacities of H2O and NaCl(aq) in Cold-Stable and Supercooled States," *The Journal of Physical Chemistry B,* vol. 104, no. 35, pp. 8563-8584, 2000.

[41] C. McBride, C. Vega *, E. Sanz, L. G. MacDowell, and J. L. F. Abascal, "The range of meta stability of ice-water melting for two simple models of water," *Molecular Physics,* vol. 103, no. 1, pp. 1-5, 2005.

[42] B. Slater and A. Michaelides, "Surface premelting of water ice," *Nature Reviews Chemistry,* vol. 3, no. 3, pp. 172-188, 2019.

[43] H. Iglev, M. Schmeisser, K. Simeonidis, A. Thaller, and A. Laubereau, "Ultrafast superheating and melting of bulk ice," *Nature,* Article vol. 439, no. 7073, pp. 183-186, 2006.

[44] X. D. Chen and P. Chen, "Freezing of aqueous solution in a simple apparatus designed for measuring freezing point," *Food Research International,* vol. 29, no. 8, pp. 723-729, 1996.

[45] J. McLeod, A. H. J. Paterson, J. R. Jones, and J. E. Bronlund, "Primary nucleation of alpha-lactose monohydrate: The effect of supersaturation and temperature," *International Dairy Journal,* vol. 21, no. 7, pp. 455-461, 2011.

6.9 Appendices

Table 6-11: Average recorded heat flow and cumulative integral of heat flow from DSC measurements between -35°C and 25°C, and apparent ice fraction as calculated in section 6.5.5 for samples tested in this chapter.

	WSM			SSM			SMUC		
	Heat Flow	Integral	Ice Fraction	Heat Flow	Integral	Ice fraction	Heat Flow	Integral	Ice fraction
Temperature	Wg^{-1}	Jg^{-1}	Xf	Wg^{-1}	Jg^{-1}	Xf	Wg^{-1}	Jg^{-1}	Xf
-34.5	-0.021	-9.77	1.000	-0.026	-0.80	1.000	-0.010	-0.81	1.000
-34	-0.021	-10.62	1.000	-0.027	-1.60	1.000	-0.010	-1.62	1.000
-33.5	-0.021	-11.47	1.000	-0.027	-2.40	1.000	-0.010	-2.43	1.000
-33	-0.021	-12.32	1.000	-0.027	-3.21	1.000	-0.010	-3.26	1.000
-32.5	-0.021	-13.18	1.000	-0.027	-4.02	1.000	-0.010	-4.09	1.000
-32	-0.022	-14.05	1.000	-0.027	-4.84	1.000	-0.010	-4.93	1.000
-31.5	-0.022	-14.91	1.000	-0.028	-5.66	1.000	-0.010	-5.78	1.000
-31	-0.022	-15.79	1.000	-0.028	-6.49	1.000	-0.010	-6.65	1.000
-30.5	-0.022	-16.66	1.000	-0.028	-7.32	1.000	-0.010	-7.53	1.000
-30	-0.022	-17.54	1.000	-0.028	-8.16	1.000	-0.011	-8.42	1.000
-29.5	-0.022	-18.42	1.000	-0.028	-9.00	1.000	-0.011	-9.33	0.999
-29	-0.022	-19.31	1.000	-0.028	-9.85	1.000	-0.011	-10.25	0.999
-28.5	-0.022	-20.21	1.000	-0.029	-10.71	1.000	-0.011	-11.18	0.999
-28	-0.023	-21.12	1.000	-0.029	-11.57	1.000	-0.011	-12.12	0.999
-27.5	-0.023	-22.02	1.000	-0.029	-12.44	1.000	-0.011	-13.07	0.998
-27	-0.023	-22.94	1.000	-0.030	-13.32	1.000	-0.011	-14.03	0.998
-26.5	-0.023	-23.87	1.000	-0.030	-14.22	1.000	-0.011	-14.99	0.998
-26	-0.024	-24.81	1.000	-0.031	-15.13	1.000	-0.011	-15.96	0.997
-25.5	-0.024	-25.77	1.000	-0.031	-16.06	1.000	-0.011	-16.94	0.997
-25	-0.025	-26.75	1.000	-0.032	-17.01	0.999	-0.011	-17.93	0.997
-24.5	-0.025	-27.75	0.999	-0.033	-17.99	0.999	-0.011	-18.92	0.996
-24	-0.026	-28.78	0.999	-0.034	-18.98	0.999	-0.011	-19.93	0.996
-23.5	-0.026	-29.82	0.998	-0.034	-20.00	0.998	-0.011	-20.94	0.995
-23	-0.026	-30.87	0.998	-0.035	-21.03	0.997	-0.011	-21.96	0.994

-22.5	-0.027	-31.93	0.997	-0.035	-22.07	0.997	-0.010	-22.99	0.994
-22	-0.027	-32.99	0.997	-0.035	-23.12	0.996	-0.010	-24.04	0.993
-21.5	-0.027	-34.08	0.996	-0.036	-24.18	0.995	-0.004	-25.09	0.993
-21	-0.028	-35.17	0.995	-0.036	-25.26	0.995	0.019	-26.16	0.992
-20.5	-0.028	-36.27	0.995	-0.037	-26.34	0.994	0.058	-27.23	0.991
-20	-0.028	-37.38	0.994	-0.037	-27.45	0.993	0.001	-28.32	0.990
-19.5	-0.029	-38.51	0.993	-0.038	-28.56	0.992	0.001	-29.42	0.990
-19	-0.029	-39.66	0.992	-0.038	-29.70	0.991	0.001	-30.54	0.989
-18.5	-0.029	-40.82	0.991	-0.039	-30.85	0.990	0.000	-31.67	0.988
-18	-0.030	-42.00	0.990	-0.040	-32.02	0.989	0.000	-32.81	0.987
-17.5	-0.030	-43.19	0.989	-0.040	-33.21	0.988	-0.001	-33.97	0.986
-17	-0.031	-44.41	0.988	-0.041	-34.42	0.987	-0.001	-35.15	0.985
-16.5	-0.031	-45.64	0.987	-0.042	-35.64	0.986	-0.002	-36.35	0.984
-16	-0.032	-46.89	0.986	-0.042	-36.90	0.984	-0.002	-37.57	0.983
-15.5	-0.032	-48.18	0.985	-0.043	-38.18	0.983	-0.003	-38.81	0.982
-15	-0.033	-49.48	0.984	-0.044	-39.49	0.981	-0.004	-40.08	0.980
-14.5	-0.034	-50.82	0.982	-0.045	-40.83	0.980	-0.004	-41.37	0.979
-14	-0.035	-52.19	0.981	-0.046	-42.20	0.978	-0.005	-42.70	0.978
-13.5	-0.035	-53.58	0.979	-0.048	-43.61	0.976	-0.006	-44.06	0.976
-13	-0.036	-55.02	0.977	-0.049	-45.06	0.974	-0.007	-45.46	0.974
-12.5	-0.037	-56.49	0.975	-0.050	-46.55	0.972	-0.008	-46.89	0.973
-12	-0.038	-58.00	0.973	-0.052	-48.09	0.970	-0.009	-48.37	0.971
-11.5	-0.039	-59.56	0.971	-0.054	-49.68	0.968	-0.010	-49.89	0.969
-11	-0.041	-61.18	0.969	-0.056	-51.33	0.965	-0.012	-51.48	0.967
-10.5	-0.042	-62.85	0.966	-0.058	-53.05	0.962	-0.014	-53.12	0.964
-10	-0.044	-64.59	0.964	-0.061	-54.84	0.959	-0.016	-54.84	0.962
-9.5	-0.046	-66.39	0.961	-0.064	-56.72	0.956	-0.018	-56.65	0.959
-9	-0.048	-68.30	0.958	-0.068	-58.71	0.952	-0.020	-58.55	0.956
-8.5	-0.051	-70.30	0.954	-0.072	-60.82	0.948	-0.023	-60.56	0.952
-8	-0.054	-72.43	0.950	-0.077	-63.06	0.943	-0.027	-62.71	0.949
-7.5	-0.058	-74.70	0.946	-0.083	-65.48	0.938	-0.031	-65.01	0.944

-7	-0.063	-77.15	0.941	-0.091	-68.11	0.932	-0.036	-67.52	0.939
-6.5	-0.068	-79.81	0.935	-0.100	-71.01	0.925	-0.042	-70.26	0.934
-6	-0.076	-82.75	0.928	-0.112	-74.24	0.917	-0.051	-73.33	0.927
-5.5	-0.084	-86.03	0.921	-0.127	-77.91	0.908	-0.061	-76.77	0.920
-5	-0.097	-89.78	0.911	-0.147	-82.14	0.896	-0.075	-80.76	0.911
-4.5	-0.112	-94.14	0.900	-0.175	-87.19	0.882	-0.092	-85.41	0.900
-4	-0.134	-99.33	0.886	-0.213	-93.33	0.864	-0.118	-91.10	0.885
-3.5	-0.164	-105.82	0.868	-0.271	-101.20	0.839	-0.153	-98.18	0.867
-3	-0.211	-114.18	0.844	-0.357	-111.73	0.805	-0.209	-107.53	0.842
-2.5	-0.282	-125.73	0.809	-0.498	-126.80	0.754	-0.292	-120.48	0.807
-2	-0.408	-142.97	0.755	-0.731	-149.97	0.673	-0.439	-140.13	0.753
-1.5	-0.620	-171.27	0.665	-1.129	-189.10	0.534	-0.688	-172.25	0.661
-1	-1.033	-224.20	0.493	-1.520	-251.17	0.315	-1.165	-232.55	0.488
-0.5	-1.218	-309.57	0.212	-1.641	-323.07	0.116	-1.474	-332.38	0.195
0	-0.762	-358.33	0.044	-0.832	-354.17	0.000	-0.803	-380.13	0.000
0.5	-0.406	-372.63	0.000	-0.504	-365.97	0.000	-0.440	-395.58	0.000
1	-0.247	-378.80	0.000	-0.304	-372.23	0.000	-0.252	-402.70	0.000
1.5	-0.160	-382.47	0.000	-0.176	-375.97	0.000	-0.144	-406.73	0.000
2	-0.096	-384.93	0.000	-0.097	-378.40	0.000	-0.071	-409.38	0.000
2.5	-0.060	-386.50	0.000	-0.058	-380.10	0.000	-0.022	-410.98	0.000
3	-0.048	-388.00	0.000	-0.059	-381.67	0.000	-0.014	-412.48	0.000
3.5	-0.045	-389.57	0.000	-0.062	-383.50	0.000	-0.018	-414.20	0.000
4	-0.047	-391.33	0.000	-0.063	-385.37	0.000	-0.019	-416.05	0.000
4.5	-0.048	-393.23	0.000	-0.063	-387.23	0.000	-0.020	-417.95	0.000
5	-0.048	-395.10	0.000	-0.063	-389.13	0.000	-0.020	-419.85	0.000
5.5	-0.048	-397.03	0.000	-0.063	-391.03	0.000	-0.020	-421.75	0.000
6	-0.048	-398.97	0.000	-0.063	-392.93	0.000	-0.020	-423.65	0.000
6.5	-0.048	-400.90	0.000	-0.063	-394.80	0.000	-0.020	-425.55	0.000
7	-0.048	-402.83	0.000	-0.063	-396.70	0.000	-0.020	-427.45	0.000
7.5	-0.049	-404.77	0.000	-0.063	-398.60	0.000	-0.020	-429.38	0.000
8	-0.049	-406.73	0.000	-0.064	-400.50	0.000	-0.020	-431.30	0.000

8.5	-0.049	-408.63	0.000	-0.064	-402.40	0.000	-0.020	-433.20	0.000
9	-0.049	-410.60	0.000	-0.064	-404.30	0.000	-0.021	-435.10	0.000
9.5	-0.049	-412.60	0.000	-0.064	-406.20	0.000	-0.021	-437.03	0.000
10	-0.049	-414.53	0.000	-0.064	-408.13	0.000	-0.021	-438.95	0.000
10.5	-0.049	-416.50	0.000	-0.064	-410.07	0.000	-0.021	-440.88	0.000
11	-0.049	-418.47	0.000	-0.064	-411.97	0.000	-0.021	-442.80	0.000
11.5	-0.049	-420.47	0.000	-0.064	-413.90	0.000	-0.021	-444.75	0.000
12	-0.049	-422.40	0.000	-0.064	-415.80	0.000	-0.021	-446.70	0.000
12.5	-0.049	-424.37	0.000	-0.064	-417.73	0.000	-0.021	-448.63	0.000
13	-0.049	-426.33	0.000	-0.065	-419.67	0.000	-0.021	-450.58	0.000
13.5	-0.049	-428.33	0.000	-0.065	-421.63	0.000	-0.021	-452.55	0.000
14	-0.049	-430.27	0.000	-0.065	-423.57	0.000	-0.021	-454.50	0.000
14.5	-0.049	-432.23	0.000	-0.065	-425.50	0.000	-0.021	-456.45	0.000
15	-0.049	-434.17	0.000	-0.065	-427.40	0.000	-0.021	-458.38	0.000
15.5	-0.049	-436.13	0.000	-0.065	-429.40	0.000	-0.022	-460.35	0.000
16	-0.049	-438.07	0.000	-0.065	-431.33	0.000	-0.022	-462.30	0.000
16.5	-0.049	-440.00	0.000	-0.065	-433.27	0.000	-0.022	-464.28	0.000
17	-0.049	-441.97	0.000	-0.065	-435.23	0.000	-0.022	-466.23	0.000
17.5	-0.049	-443.90	0.000	-0.065	-437.20	0.000	-0.022	-468.23	0.000
18	-0.049	-445.83	0.000	-0.065	-439.13	0.000	-0.022	-470.15	0.000
18.5	-0.049	-447.77	0.000	-0.065	-441.13	0.000	-0.023	-472.13	0.000
19	-0.049	-449.73	0.000	-0.066	-443.07	0.000	-0.023	-474.08	0.000
19.5	-0.049	-451.67	0.000	-0.065	-445.07	0.000	-0.023	-476.08	0.000
20	-0.049	-453.60	0.000	-0.066	-447.00	0.000	-0.024	-478.03	0.000
20.5	-0.049	-455.57	0.000	-0.066	-449.00	0.000	-0.025	-480.00	0.000
21	-0.049	-457.53	0.000	-0.066	-450.97	0.000	-0.025	-482.00	0.000
21.5	-0.049	-459.47	0.000	-0.066	-452.97	0.000	-0.026	-483.95	0.000
22	-0.049	-461.43	0.000	-0.066	-454.90	0.000	-0.031	-485.95	0.000
22.5	-0.049	-463.37	0.000	-0.066	-456.90	0.000	-0.066	-487.93	0.000
23	-0.049	-465.37	0.000	-0.066	-458.87	0.000	-0.067	-489.95	0.000
23.5	-0.049	-467.37	0.000	-0.066	-460.90	0.000	-0.067	-491.95	0.000

24	-0.050	-469.33	0.000	-0.066	-462.87	0.000	-0.067	-493.95	0.000
24.5	-0.050	-471.33	0.000	-0.067	-464.87	0.000	-0.067	-495.98	0.000
25	-0.050	-473.33	0.000	-0.067	-466.87	0.000	-0.067	-497.95	0.000

Chapter 7: Development and Testing of a Continuous Tubular Freezer.

7.1 Chapter Summary

A method was proposed for continuous freezing into a substantially frozen product by pumping through a smooth-bored cooled tube. This exploited the progressive freezing of ovine milk discussed in Chapter 6, and the formation of dendritic or columnar ice discussed in Chapter 4 to form a plug of solid product lubricated by unfrozen product. This was trialled for a range of foodstuffs and temperatures on a benchtop scale rig with an internal tube diameter of 4.2mm. The apparent ice fraction of samples tested on the small-scale system was evaluated by the method discussed in Chapter 6. Products extruded continuously in an apparently solid form. The pumping pressure required for operation increased as the temperature decreased, and the solid fraction (at the outlet temperature) increased.

7.2 Introduction

Several freezer concepts were evaluated at the outset of the project. These are discussed in detail in Chapter 1. During testing of a falling film freezer it was found that the mechanical properties of milk ice differed significantly from those of water ice and that this made the detachment of frozen milk ice from the surface of the falling film freezer by a short melt-back cycle problematic. This is discussed further in Chapter 3. The elasticity displayed by the frozen milk caused issues during melt-back detachment, but it was thought that this might be exploited in other ways.

The possibility was raised of creating a slush and then freezing it solid by controlling the heat flow distribution in a straight pipe. There have been slush ice makers developed that control the supercooling in a cooled tube by causing nucleation at a pre-determined location. This allows controlled amounts of heat to be removed from the slush, and the ice fraction of the slush to be controlled [1].

As discussed in Chapter 6, there is a significant proportion of unfrozen water in frozen milk at temperatures just below the initial freezing temperature. It was suggested that this may allow a plug of milk to be substantially frozen into a tube, from the outside in, and then extruded by the pressure behind the plug. The unfrozen liquid fraction would serve to lubricate the frozen milk plug and allow it to be extruded. The high rate of freezing at the interface between the cooled tube and the slowly moving milk was hypothesised to lead to the formation of a highly dendritic region, as discussed in Chapter 4, at the perimeter of the freezing plug, with a significant volume fraction of unfrozen liquid. This would limit the shear strength, and adhesion strength of the milk at the milk/ tube interface and reduce the force required to extrude the frozen product. Under steady state continuous flow conditions, the frozen plug would be free to expand ahead of the freezing location, toward the outlet of the freezer, preventing significant normal forces at the tube/plug interface as a result of the expansion of milk upon freezing.

Informed by the ice growth studies in Chapter 4, ice crystal growth was hypothesised to be predominantly radial and aligned with to the dominant heat flows in the freezer.

The crystalline orientation of the ice grown in this freezer was not expected to have any significant effect on the hoop stresses resulting from ice expansion during freezer: There is minimal anisotropy in the expansion of water on freezing- The unit cell of ice is 0.3% shorter in the c-axis, and compressibility along this axis is only slightly reduced[2]. Moreover, it is difficult to reliably form crystals with a uniform crystalline orientation[3], so it was expected that crystals

growing inside the freezer would have a range of orientations. The expansion on freezing was expected to be reduced across any limited temperature range, when compared to the freezing transition in pure water, as a fraction of the liquid was expected to remain unfrozen and so not contribute to the expansion. The presence of solutes and particles in the fluid which do not expand on freezing was also expected to limit expansion. The stress resulting from expansion may also be reduced as unfrozen liquid may allow crystals to slip relative to one-another. Finally, the freezing plug may also be free to expand distally.

The high rate of freezing should also limit radial mass flows of solutes due to freeze-concentration effects, as discussed in Chapters 1 and 3. It is known that the partition coefficient ($K = C_s/C_l$) increases with ice growth rate[4], so maintaining a high average ice growth rate was expected to limit the formation of a solute-depleted exterior region and solute-rich interior with reduced freezing point.

It was hypothesized that the adhesion of frozen product to the wall would be reduced by either a lubricating layer of unfrozen liquid, or a reduction in ice volume at the interface between the frozen product and the wall. This hypothesis was investigated as part of the work discussed in this chapter and the next chapter.

Regardless of the actual method governing adhesion to the wall, some physical relationships between operating parameters, fluid properties and system conditions could be postulated. These guided the design of the proof of concept experiments and assisted in the design of the lab-scale prototype system. The relationships between the radius, length, fluid properties and required pressure is described below.

The adhesion force at the frozen plug/ wall interface is estimated to be proportional to the perimeter of the interface, and the length of the frozen section:

$$F_{adhesive} \propto K_{adhesive} * 2\pi r_{plug} * L_{plug} \tag{7-1}$$

The extrusion force behind the plug is the product of the area of the plug, and the pressure of the liquid behind the plug:

$$F_{extrusion} = \pi r_{plug}^2 * P_{liquid} \tag{7-2}$$

It was expected that the pressure required to extrude the frozen product would be insensitive to the superficial velocity of the product in the freezer. Higher superficial velocities in a tube will lead to increased pressure drop due to flow resistance, as described by the Darcy-Weisbach equation:

$$\frac{\Delta \mathrm{P}}{L} = f_D \cdot \frac{\rho}{2} \cdot \frac{v^2}{D} \tag{7-3}$$

The pressure required to extrude the product was expected to be several orders of magnitude higher than that required to overcome resistance to flow, so frictional pressure losses can be ignored. When estimated from published ice adhesion strength values (<10 kNm^{-2}) for icephobic surfaces [5] this pressure was initially calculated as roughly 10-20MPa.

The apparent adhesion strength may be a function of solids concentration, surface roughness, surface energy, temperature of the frozen milk, and apparent ice fraction. It may also be a function of the normal force resulting from ice pressure on the exterior wall:

$$K_{adhesive} = f(X_s, Ra, \sigma, T_{milk}, F_{ice}) \tag{7-4}$$

The extrusion force must be greater than the adhesion force to extrude the solid plug.

$$F_{extrusion} > F_{adhesive} \tag{7-5}$$

Therefore, while temperature, surface properties, and fluid properties are held constant, the pressure required to move a frozen plug was postulated to be inversely proportional to the plug diameter. This would work in favour of scaling to larger diameters during scale up.

$$P_{liquid} \propto \frac{1}{r_{plug}} \tag{7-6}$$

This is shown graphically in Figure 7-1, which shows the adhesion force for a given length increasing linearly with radius (assuming no changes in operating conditions), and the required pressure to overcome this adhesion force and extrude product decreasing with increased radius.

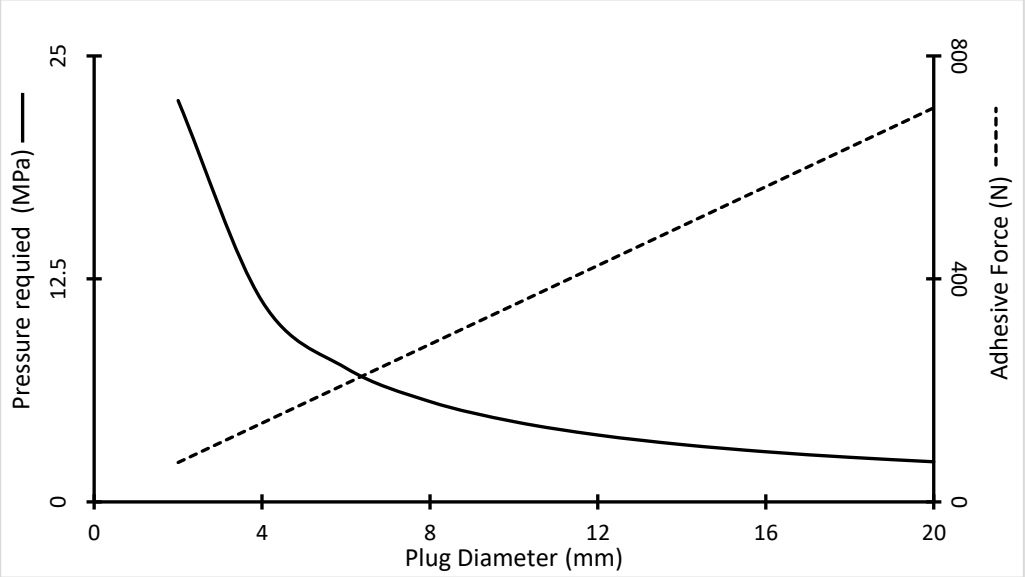

Figure 7-1: Adhesion force and Pressure required to extrude a 1m section of frozen product at -6°C (an apparent adhesion strength of 11kNm^{-2}) as a function of frozen product plug diameter for an exemplar product. The adhesion force increases in linear relationship with plug diameter is it is a function of the contact area between the tube wall and frozen plug. The pressure required to extrude a given length of pipe decreases in a linear relationship with the cross-sectional area of the plug.

However, as the plug diameter increases, so would the characteristic distance for heat transfer, increasing the requisite residence time to form a frozen plug, and therefore the length of tube required (and the interfacial area for adhesion) also increases.

Proof of concept experiments were conducted to test whether this freezing method was feasible. These experiments also tested the suitability of this freezing method for substances beyond ovine milk. Further experimental work was conducted to test the influence of coolant temperature and product flowrate on the behaviour of the system, the expected scale-up behaviour of the system, and to test whether methods to reduce the floor-space of the system were feasible.

The behaviour of the system was expected to be strongly dependant on the apparent ice fraction of the aqueous phase, and so this was estimated using calorimetric methods for the feedstocks tested. This methodology was discussed earlier in Chapter 6, and is simple, rapid and suitable to many liquid samples so it used here.

The expected heat flows and ice growth behaviours discussed earlier will lead to an expected ice morphology which can be verified by optical microscopy of samples taken from the freezer, and Cryo-SEM of frozen samples. This microscopy work might also answer questions such as

whether the frozen product is lubricated by a thin layer of unfrozen liquid as it is extruded, whether fats and other solids trapped at the interface serve to lubricate the frozen product, or whether the ice fraction at the wall is reduced and therefore less ice is adhered to the wall, reducing the adhesion strength between the wall and the frozen product. This work is discussed in detail in the next chapter.

Finally, areas of further interest will be briefly discussed, including the processing of other products with this system, and the use of this system as a preparatory step for other processing.

7.3 Methods

7.3.1 Materials

Reconstituted sheep milk was prepared to total solids concentrations of 15%, 18% and 23% by weight from whole sheep milk powder (Spring Sheep Dairy, Auckland NZ). Samples were reconstituted by stirring with a magnetic stirrer at 40°C for 30 minutes after the slow addition of the correct mass of powder. Samples were degassed under vacuum and stored below 4°C for up to 48 hours before use.

Other samples evaluated were as follows:

1. Coffee extract at 20° Brix
2. Commercial orange juice (Keri Premium Orange Juice, Coco-Cola Amatil (NZ) Ltd, Auckland NZ) Total solids 10.3 % by vacuum drying, 10.2° Brix.
3. Fruit smoothie mixes (Kaitahi, Waverley, NZ).
4. Gold kiwifruit pulp, seedless with a total solids content of 16.1%.

The fruit smoothie mixes had the following composition, as reported by the packaging nutritional information:

Table 7-1: Composition of smoothies tested during product proof of concept trials.

Component (% m/m)	Smoothie 1	Smoothie 2	Smoothie 3
Fat	0	1.42	2.50
Protein	1.75	1.25	2.42
Dietary fibre	4.5	3.25	4.75
Carbohydrates	13	11.75	9.75
Sugars	9	9.5	7.5
Water	85	85.6	85.3

The coffee extract was received as a freeze-dried powder and was stored in an oxygen and moisture impermeable bag below 4°C until it was reconstituted to a target of 20° Brix according to a published relationship between coffee % solids and °Brix [6]. The refractive index of reconstituted coffee extract was measured immediately following reconstitution and it was stored below 4°C for less than 24 hours before testing.

The gold kiwifruit pulp was prepared from Zespri SunGold kiwifruit (Zespri International Ltd., Mount Maunganui, NZ). Kiwifruit were blanched at 90°C for 60s and peeled. The peeled fruit were pulped in a food processor and then passed through a 1.6mm screen to remove seeds. The pulp was then pulped further in the food processor and passed through an 800µm screen. This pulp was vacuum packed and stored at -80°C until use. The pulp was thawed at room temperature before testing. The total solids content was determined by vacuum drying at 70°C for 18 hours.

7.3.2 Equipment.

Further details of laboratory equipment, microscopy equipment, and software packages used can be found in Chapter 2.

7.3.2.1 4.2mm Diameter Freezer Description.

A schematic of the initial benchtop unit is shown in Figure 7-2 below. The annular heat exchanger consisted of an 800 mm long section of stainless-steel tube, 6 mm OD and 4.2 mm ID, with ends deburred. The coolant jacket was a 500 mm length of 12.7 mm OD stainless steel tube, leaving an annulus of 2.5 mm for coolant flow. The heat exchanger was insulated with 15 mm polyurethane foam insulation.

Heat was removed by a 50% ethylene glycol/water solution chilled by a Julabo FL300 laboratory chiller. The inlet and outlet temperatures of the coolant were measured with a pair of T-type thermocouples.

Milk is pumped by displacing a piston inside a high-pressure reservoir. RO water is pumped into the reservoir behind the piston by a Waters model 600E multi-solvent delivery unit, capable of a maximum flowrate of 20 mL/minute. The reservoir is a cylinder of 316 stainless steel, with an OD of 100 mm, bore diameter of 45 mm, and a total reservoir volume of 350 mL. Reservoir end caps are 25 mm thick plates of 316 stainless steel.

Pressure is monitored by a pressure indicator built into the HPLC pump, and a Wika “type 2” pressure gauge with a measurement range of 0-690 Bar. For some experiments the Julabo FL300 was replaced by the coolant circulator unit described in section 3.7.4.3

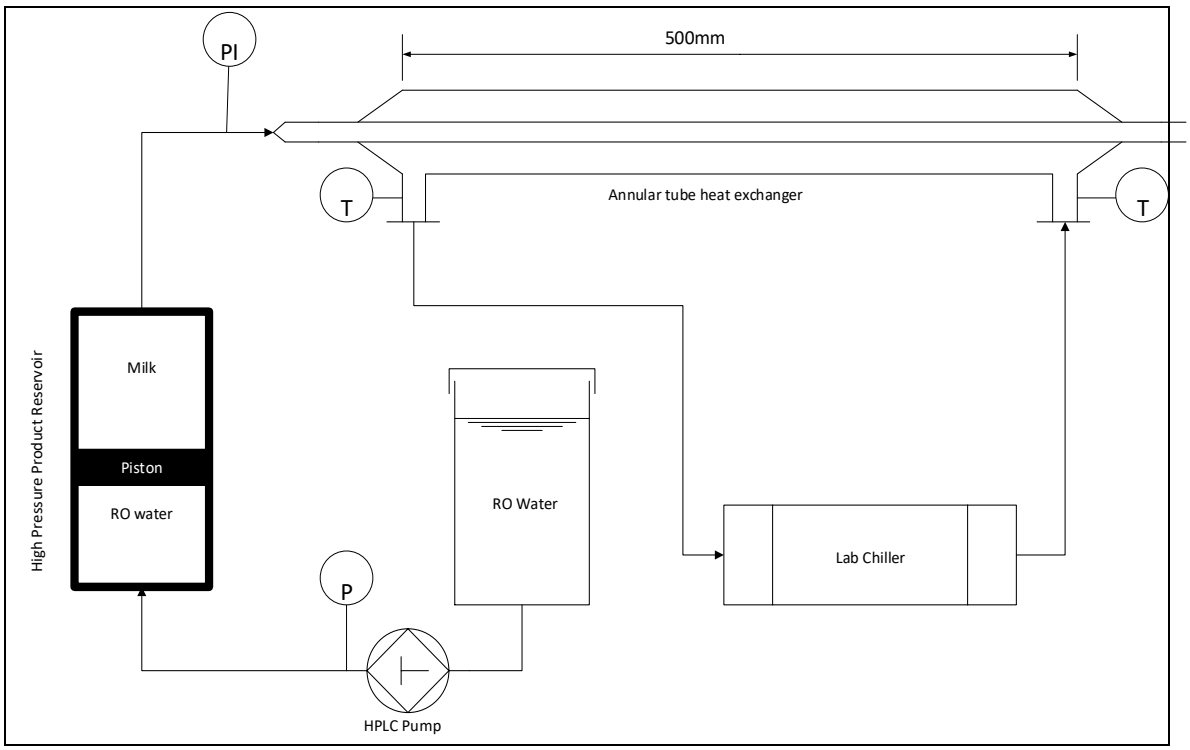

Figure 7-2: Schematic of the 4.2 mm diameter freezer. Product to be frozen (i.e. milk) is placed in the high-pressure reservoir. The piston in the high-pressure reservoir is displaced by RO water pumped by a Waters 600E multisolvent delivery system. The product is pumped through jacketed tube with an internal diameter of 4.2 mm, an external diameter of 6 mm and a cooled length of 500 mm. Coolant (50% ethylene glycol solution) is chilled and circulated by a Julabo FL300 circulating chiller. Pressure is indicated by a Wika type 2 pressure gauge with a range of 0-690 Bar, and temperatures are recorded by T-type thermocouple.

7.3.2.1.1 *Typical Experimental Procedure for 4.2mm Diameter Freezer.*

The typical experimental procedure for a trial of a product using the 4.2 mm diameter freezer was as follows:

1. The high-pressure reservoir was filled with the product to be tested at room temperature and was assembled. The reservoir was connected to the outlet of the HPLC pump and to the inlet of the 4.2 mm diameter freezer.
2. The HLPC pump was primed and then used to displace sufficient fluid to fill the 4.2 mm diameter freezer. Once liquid product flowed from the freezer the flow at the HPLC pump was stopped.
3. The lab chiller was started, and coolant flow begins. The temperature was set to the desired test temperature. Thermocouple readings were logged with a USB-Temp data logger. Once the coolant had reached the set temperature, it was held isothermal for 10 minutes, the desired flowrate was set at the HPLC pump, and the pump started.
4. If the product flowed out as a liquid, the pump was stopped, and the system was left to cool further, before the pump was restarted. If liquid flow persists this was noted, and the coolant set temperature was reduced, while the pump was stopped to allow the product to freeze.
5. Once the product extruded as a solid, the pressure reading on the pressure gauge, the set temperature, the inlet temperatures and the flow rates were noted.
6. The coolant temperature was varied, and the pressure required for solid product extrusion was noted once the system reached steady state at the new temperature, and at least one tube volume of product was extruded.
7. Any solid product would be collected in rigid sample containers held at 30° to the vertical. The impact of a solid product against the far inner wall of the container would provide the force required to break the product into lengths of approximately 3-10 tube diameters. The sample collection containers were filled with liquid nitrogen to immediately cool the sample to preserve the ice structure of the sample for further analysis.

Frozen samples were stored at -80°C to prevent crystal structure changes resulting from recrystallization, or Ostwald ripening.

7.3.2.2 10.2mm Straight Freezer

This freezer was essentially the same as the 4.2 mm diameter freezer as described in section 3.2.1, with the following differences:

1. The inner tube length was been increased to 1200 mm,
2. The inner tube diameter ID was 10.2 mm, OD was 12 mm. At a typical flowrate of 10mL/minute the residence time was 588s.
3. The outer tube internal diameter was 20 mm, giving an annular space of approximately 4mm. Coolant superficial velocity in the annulus was 1.8 ms^{-1}.

7.3.2.2.1 *Typical Experimental Procedure for 10.2mm Straight Freezer*

The experimental procedure when using 10.2 mm Straight Freezer diameter was essentially identical to the procedure used with the 4.2 mm diameter freezer.

7.3.2.3 10.2 mm Spiral Tubular Freezer Description.

In order to increase throughput of the freezer, the refrigeration power must be increased, and the amount of heat removed increased. The freezer is essentially a heat exchanger, and the heat flow from product to coolant can be approximated as a function of the overall heat transfer coefficient U, the heat transfer area A, and the temperature difference between the coolant and the product.

$$\dot{Q}_{freezer} \approx UA\Delta\mathrm{T} \quad (7\text{-}7)$$

Increasing any of these factors will increase the heat flow, however one of the easiest to change on scale-up is the heat transfer area. The heat transfer area can be increased by changing the cross-section profile of the tube to one that has a greater ratio of perimeter to cross sectional area, increasing the diameter of the tube, or increasing the cooled length of the tube.

Modifying the cross-sectional profile of the tube could lead to difficulties with fabrication, and increase cost, so was not appropriate for a freezing system intended to minimise capital expenditures. Complicated geometries could also increase the risk of difficulties being encountered during CIP.

Increasing the diameter increases the external area of the tube where heat transfer occurs, however this also increases the characteristic distance of the system, increasing the resistance to heat transfer to the centre of the product, and increasing the required residence time. This is an area where the trade-offs between increased resistance to heat flow, increased heat transfer area, increased residence time, and reduced feed pressure requirements can be optimised further.

Increasing the heat transfer area by increasing the length of the tube is simple from a conceptual, analytical and manufacturing viewpoint. The post-doctoral fellow collaborating on this project developed the concept of forming the tube into a spiral, increasing the length of the tube while minimising the physical size of the freezer. A constant radius spiral also maintains a constant geometry for a frozen plug.

A schematic of the system is shown in Figure 7-3 below. The coolant system described in Chapter 2 was connected to the freezer. The feed was pumped into the system by a Maximator S40-SS air driven pressure intensifier. The pressure intensifier has a 1:39 ratio of drive pressure to output pressure, and a maximum rated pressure of 390 Bar. The pump was driven by a cylinder of oxygen free-nitrogen, or a commercial air compressor. The flow of liquid feed was controlled by varying the air drive flow with a needle valve.

Three thermocouples measured the coolant temperature in the annular space surrounding the freezer tube. The pressure of the feed was indicated at the pump outlet with a Wika “type 2” pressure gauge with a range of 0-690 Bar and recorded with a pressure transducer. The 4-20 mA output from the transducer was converted to 0-2 V for logging by an MCC USB-Temp data logger.

Coolant was cooled and circulated by a Julabo FL300 laboratory chiller for initial trials. For further trials and demonstrations, coolant was cooled and circulated by the chiller unit initially intended for use with the falling-film freezer, as described in Chapter 3.

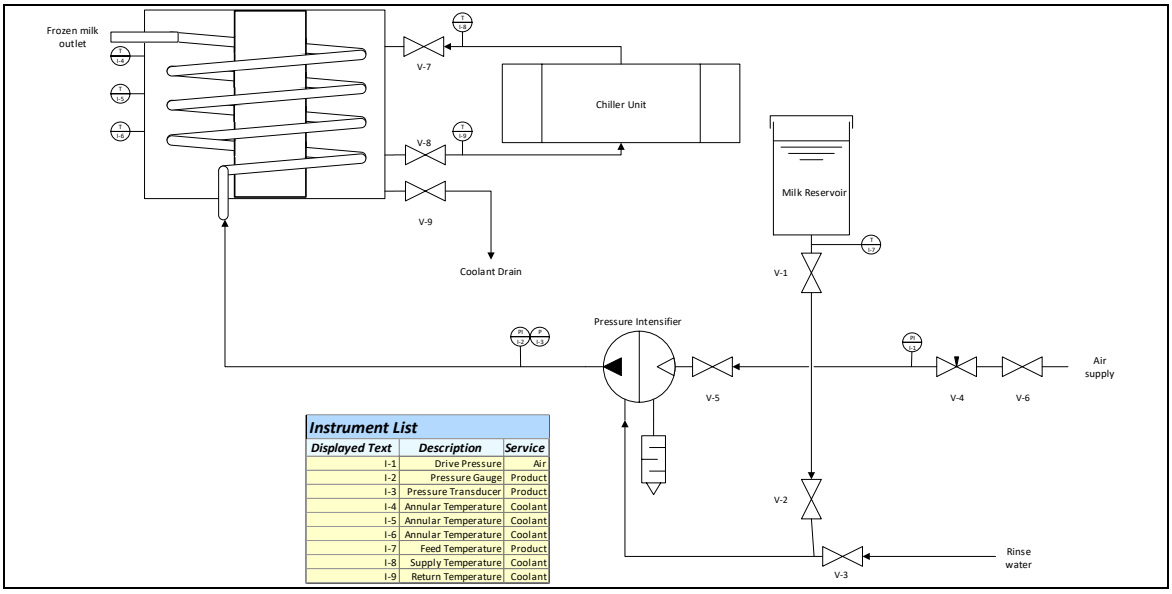

Figure 7-3: Schematic of the Spiral Freezer. Coolant (50% ethylene glycol solution) is circulated around the annular space around the freezer tube by the chiller unit described in Chapter 3. Product to be frozen (i.e. milk) is held in a 20L plastic reservoir in a domestic refrigerator. Product is pumped by a Maximator S40-SS air-driven pressure intensifier. Air is supplied by a building air supply, or a nitrogen gas bottle, with pressure with a downstream pressure control gauge. Flow is regulated by a needle valve on the air supply. The pressure of the feed is indicated at the pump outlet with a Wika "type 2" pressure gauge (range of 0-690Bar). Freezing occurs in the spiral tube, which has a length of 4.5m, and an internal diameter of 10mm.

The 10.2 mm spiral freezer tube is shown in Figure 7-4. The product enters through the tube at the base of the coolant space and leaves through the tangential exit at the top. Coolant flows in an annulus around the spiral tube, between the exterior wall of the coolant space, and a central plug (not shown). The coiled tube has a length of 4.5 m, and internal diameter of 10 mm, and a spiral radius of 150 mm. The annulus around the tube has an internal diameter of 100 mm and an external diameter of 200 mm.

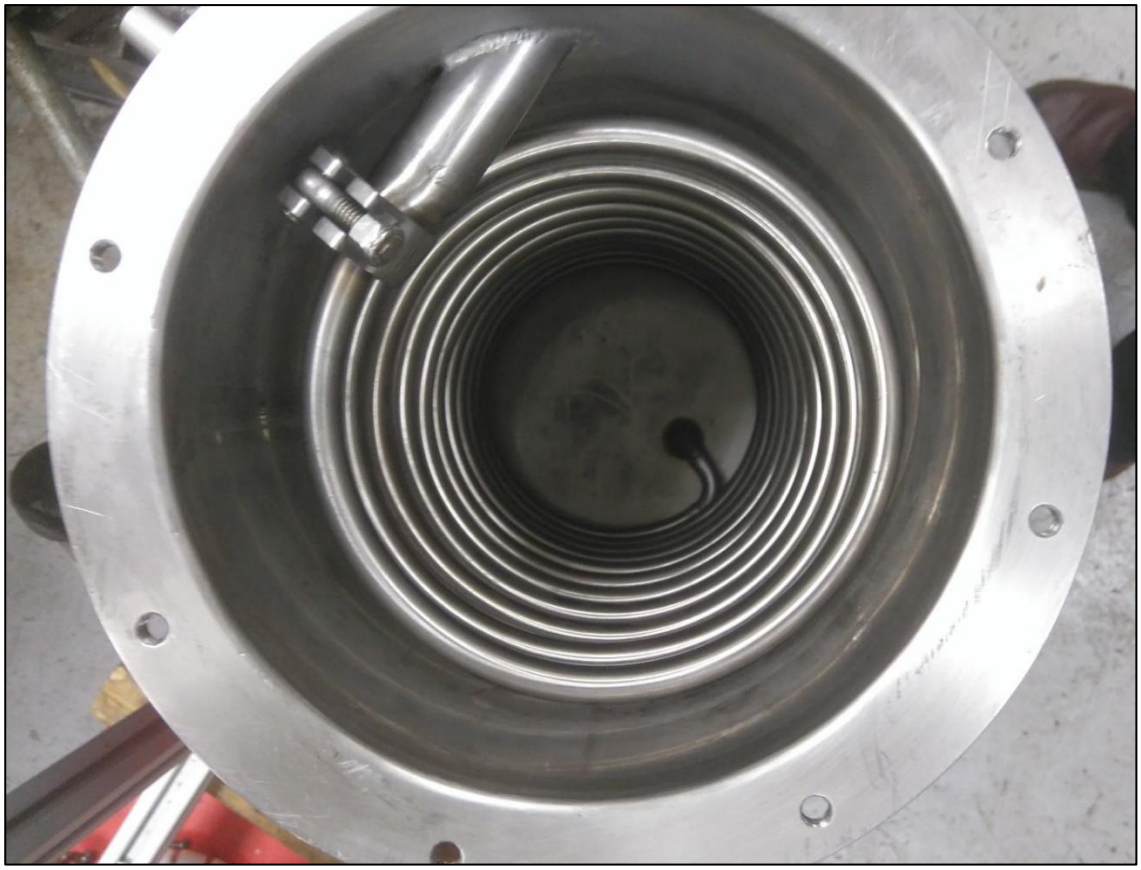

Figure 7-4: Spiral Freezer tube, showing the spiral construction and the exterior of the coolant annulus. The plug that forms the annulus is not shown.

7.3.2.3.1 *Typical Experimental Procedure for 10.2 mm Spiral Freezer.*

Prior to use, the 10.2 mm spiral freezer was cleaned using a CIP procedure as follows: The system was rinsed thoroughly with hot water. A solution of caustic detergent was then flushed through the system and recirculated several times. After a contact time of at least 30 minutes the caustic detergent was drained, and the system was rinsed. A cold solution of acidic detergent was then flushed through the system and recirculated. After a contact time of at least 30 minutes the acid detergent was drained, and the system was then rinsed with cold water. The system was then drained and prepared for trials. After use a similar CIP procedure was used. If the system was to be used in the near future for a study involving microbial testing then it was stored filled with an iodophor sanitiser solution, which was drained before trials.

The coolant temperature in the coolant reservoir was controlled by the external refrigeration unit. The temperature was set at this unit, and the coolant circulated through it to bring the coolant to the desired temperature.

The product reservoir was filled, and product was pumped through the freezer until the freezer tube was full. Once the coolant was at the desired temperature the coolant supply pump was activated to pump coolant around the exterior of spiral freezer tube. The temperature of the coolant surrounding the spiral was logged at 3 points with a USB-Temp data logger, as was the temperature in the coolant reservoir.

Once the product was frozen, the air-driven high-pressure pump was activated. The pressure developed was varied by controlling the gas supply pressure with a regulator, and the gas flow was controlled with a needle valve. The voltage produced by the pressure transducer was logged with a USB-Temp data logger and converted to a pressure reading at a later time. The state of the product leaving the freezer was noted.

The frozen product was collected in a pre-cooled container, or in a container with liquid nitrogen to keep it cold for further use.

7.3.3 Determination of Apparent unfrozen water

Subsamples from each product tested on the tube freezer were reserved and stored below 4°C for less than 48 hours to be investigated by DSC. Measurements were conducted with a pre-calibrated TA instruments Q2000 DSC. Approximately 10-20mg of samples were sealed in TZero Aluminium pans and placed in the DSC. The samples were equilibrated at -40°C and then heated at 1 $Kmin^{-1}$ to 35°C with a purge gas flow of 50mL/min of instrument-grade nitrogen. The frozen water as a function of temperature was determined from the heat flow curve according to the straight-line fitting procedure described in Chapter 6.

7.3.4 Ovine Milk Trials

Ovine milk trials were carried out for conditions that would encompass the vast majority of operating conditions and milk compositions that are likely to be encountered in commercial operation.

The ovine milk concentrations of 15%, 18% and 23% corresponded to the mean, and upper and lower limits, for 95% of ovine milk encountered in NZ (as shown in Table 3-3 and Table 3-4). These were frozen at a range of operating temperatures in order to study the effect of operation temperature on the required pressure, and apparent adhesion strength, for extrusion. The lower limit of operating temperature was set during trials by pressure limitations of experimental equipment. The temperature was raised during trials until extruded product were considered too soft to be effectively handled using bulk solids handling equipment. This was a subjective judgement on the part of the researchers.

7.3.5 Product Proof of Concept Trials

In order to evaluate the suitability of this freezing method for a range of food products, samples of liquid food products to be evaluated were tested on the 4.2mm diameter freezer using the methodology described in section 3.2.1.1. The samples evaluated are described in detail in section 3.1.

7.4 Results and Discussion

7.4.1 Product proof of concept.

All products tested on the 4.2mm diameter extruded in a solid form. A feed flow of 2.5mL/min, corresponding to a residence time of 166s, allowed for steady state operation of the freezer, and trial length was limited solely by the volume of the high-pressure reservoir. The freezer was operated in excess of 1 hour for each individual product trial. The equilibrium freezing points , T_f, were determined from the DSC curves as discussed in Chapter 6.Coolant temperature rise across the freezer was low, on average -0.44°C. Coolant temperature listed below is the average of inlet and outlet.

Table 7-2: Pressures and operating temperatures recorded during proof of concept trials

Sample	T_f (°C)	Temperature(°C)	Pressure (MPa)
20.4°Brix Coffee Extract	-1.2	-7	Still Liquid
		-9.8	2
		-11.5	3.5
		-13.6	7.5
		-14.6	12
10.3°Brix Orange Juice	-0.8	-14.5	8
Smoothie 1	-1.5	-9	12 initial, 1.5-2.2 at steady state.
Smoothie 2	-1.5	-7	4 initial, 1.5 steady state
Smoothie 3	-1.5	-7	8 initial 1.0 steady state
Gold kiwifruit pulp	-1.7	-9	1.25
		-9.5	1.75
		-10.5	2.5
		-12	4.5
		-13	6
		-13	6.5

These steady state operating pressures are plotted against the difference between operating temperature and product equilibrium freezing temperature, $T_{op} - T_f$, in Figure 7-5. As can be seen from the plotted pressures of the trials, the relationship between pressure and $T_{op} - T_f$ is monotonically increasing, as also seen in trials with sheep milk and reconstituted milk in Figure 7-11. The relationship in Figure 7-5 can be described by equation (7-8) , where the P_{liquid} is given in MPa and $T_{op} - T_f$ is in °C . For 14 observations, r^2=0.91.

$$P_{liquid} = -0.95\left(T_{op} - T_f\right) - 5.1 \tag{7-8}$$

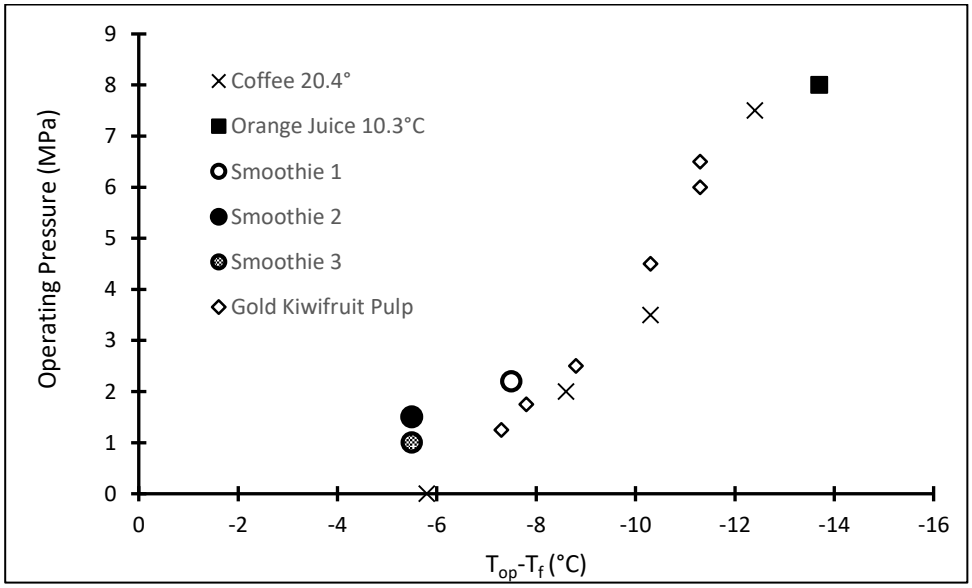

Figure 7-5: Operating pressures required for extrusion from the 4.2mm diameter freezer of several feedstocks at a range of temperatures. Residence times were between 166s and 208s.

Figure 7-6 shows representative images from the proof of concept experiments. These trials demonstrated the suitability of this freezing method for a variety of liquid and paste food products.

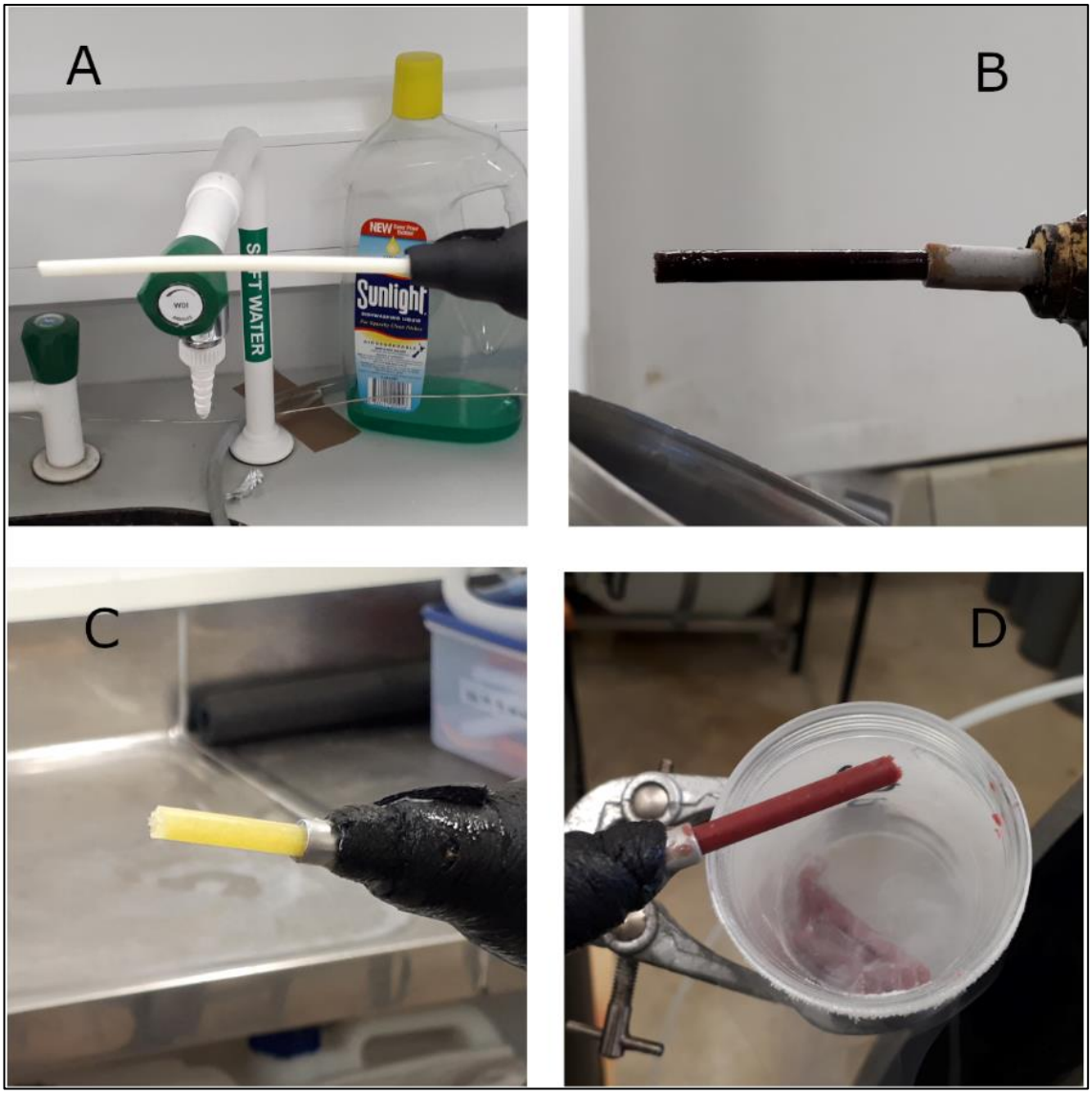

Figure 7-6: Product being extruded from the 4.2mm freezer during proof of concept trials. The residence time for the pictured trials was 166s. A: Extrusion of 15% TS ovine milk. B: Extrusion of 20.4° Brix coffee extract. C: Extrusion of 10.2° Brix orange juice. D: Extrusion of a fruit smoothie mix.

These trials show that the freezing method is applicable to products with a significant fat proportion such as the ovine milk, a significant level of fibres such as the smoothie mixes, and products with neither fats not suspended fibres such as the coffee and orange juice samples.

7.4.2 Apparent Unfrozen Water and Ice Fractions

The DSC heat flow curves from -40°C to 20°C for several products are shown in Figure 7-7, as is the curve for pure water. The water peak displays a significant amount of peak spreading after the onset due to thermal lag within the sample, but the peak onset is at 0°C. The other curves have less distinct peak onsets due to the progressive melting of the solutions. The peak apexes are all lower than 0°C, with the exception of the pure water sample.

The amount of freezable water frozen at any given temperature was calculated and plotted from -35°C to 20°C, giving a curve of apparent ice fraction vs. temperature. These curves are shown in Figure 7-8, along with the idealised curve for water. As can be seen, there are significant apparent unfrozen water fractions present at temperatures below 0°C

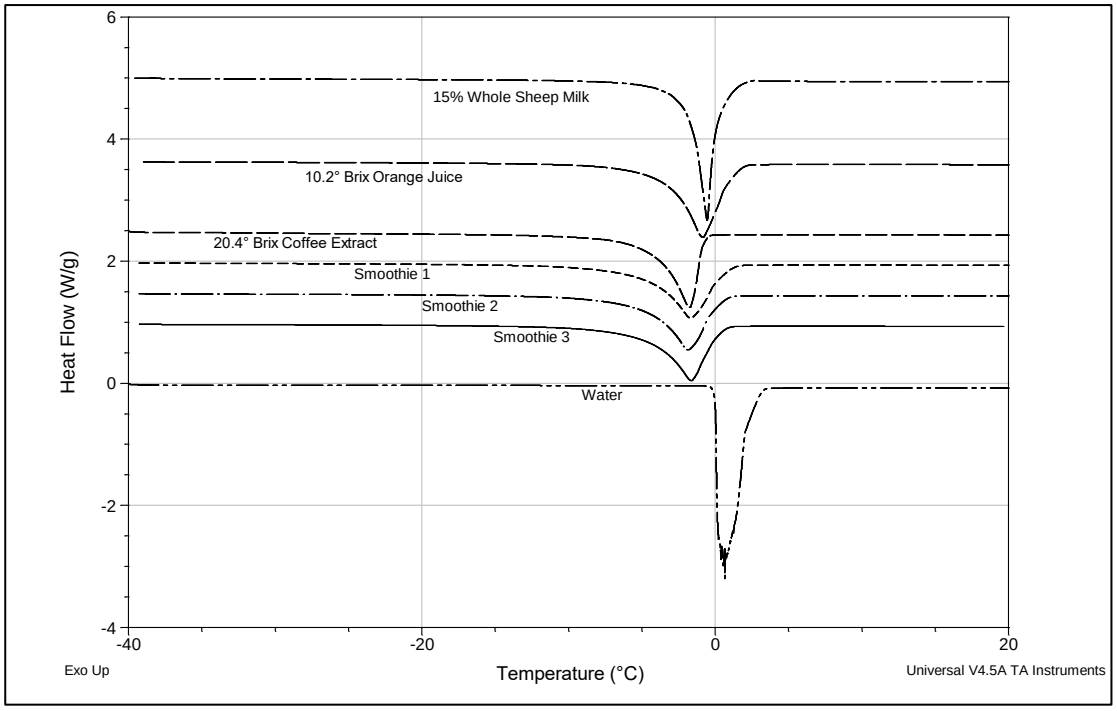

Figure 7-7: DSC curves of selected products with pure water for reference. Products were heated at 1Kmin^{-1} from -40°C to 20°C .Curves are shifted vertically for visual clarity, with the exception of RO water. . and the less obvious peak onsets when compared to water, which has a distinct and steep onset at its melting point of 0°C.

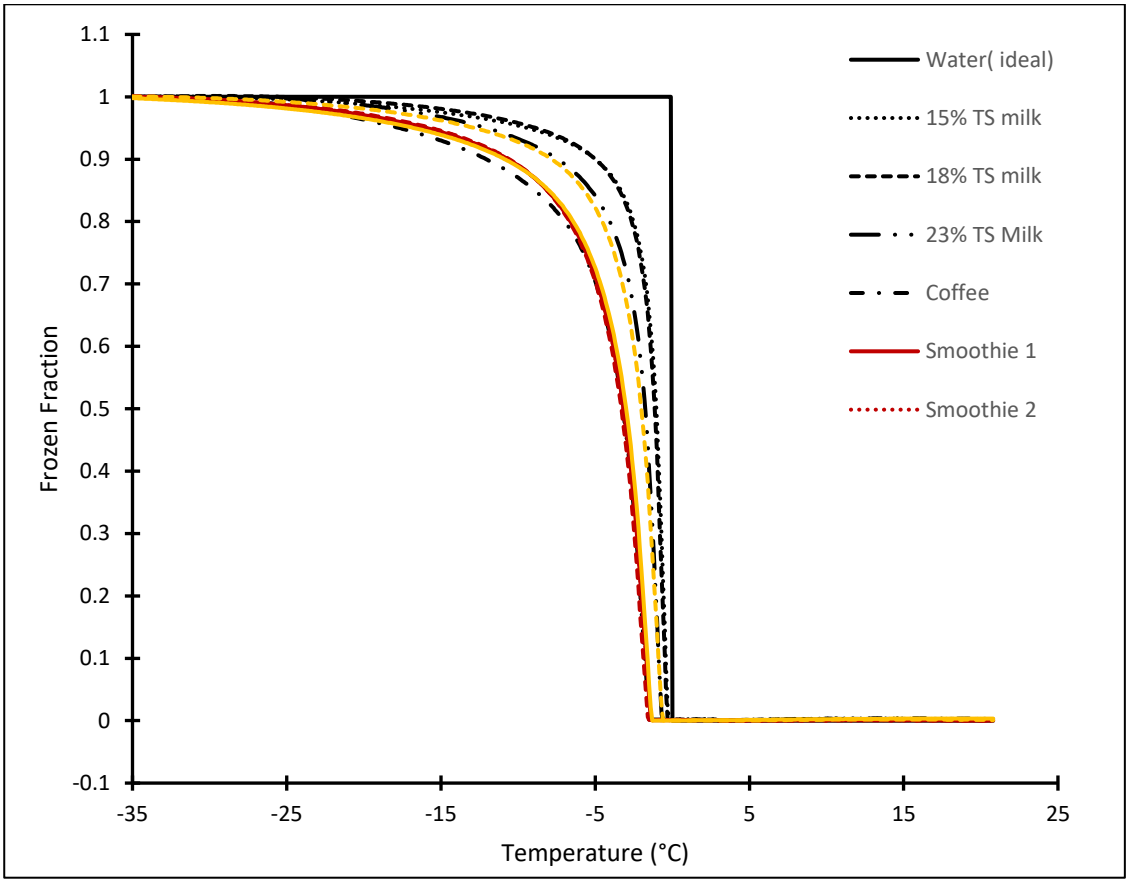

Figure 7-8: Apparent ice fractions for various products tested on freezer with the idealised water transition(all water freezes at the 0°C) as reference. The apparent ice fraction is the fraction of freezable water (water that is frozen at -35°C) that is frozen at any temperature, not a fraction of total water. Apparent ice fractions were determined from DSC measurements.

7.4.3 Effect of Apparent Ice Fraction on Pressure

As postulated in section 7.2, the extrusion of the frozen plug requires a significant pressure to be developed by the pump. This pressure is orders of magnitude higher than that required to pump a liquid through the same tube at the same flowrates. Therefore, the pressure required for liquid flow can be ignored when measuring the pressure required to extrude the frozen plug and determining the apparent adhesion strength between the milk and the wall for a given set of conditions. This was confirmed by experimental data as there was no relationship between residence time (i.e. superficial velocity) and pressure required.

A scatter plot of the pressures developed during operation of the 4.2 mm diameter freezer against the difference between operating temperature and sample equilibrium freezing temperature , $T_{op} - T_f$, is shown in Figure 7-9 . The concentration of the milk used in each run is shown in the scatterplot.

The pressure required to extrude the frozen milk increases with increasing $T_{op} - T_f$. Each milk concentration demonstrates a similar relationship between $T_{op} - T_f$ and pressure.

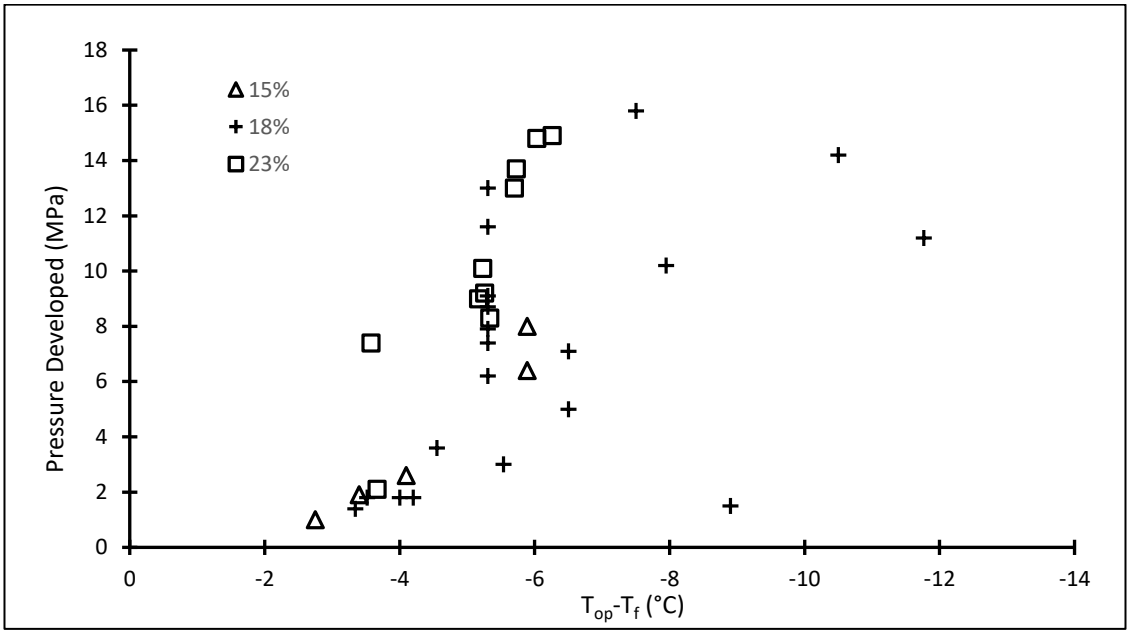

Figure 7-9: Pressure developed at various $T_{op} - T_f$ during operation of the 4.2mm diameter freezer during trials of reconstituted ovine milk at 3 different solids levels. Solids levels presented are % m/m on a wet basis. Residence times for these samples were between 139s and 208s.

The apparent adhesion strength described in equation (7-1) was calculated from a force balance of equations (7-1), (7-2) and (7-5) is plotted against temperatures for all milk compositions in Figure 7-10. The apparent adhesion strength is described in kNm^{-2}, as it is calculated as the force required to detach and extrude the frozen plug, divided by the interfacial area. This interfacial area is calculated assuming that the frozen plug is the entire cooled length of the tube. This apparent adhesion strength could also be described as the ultimate shear strength of the plug/wall interface.

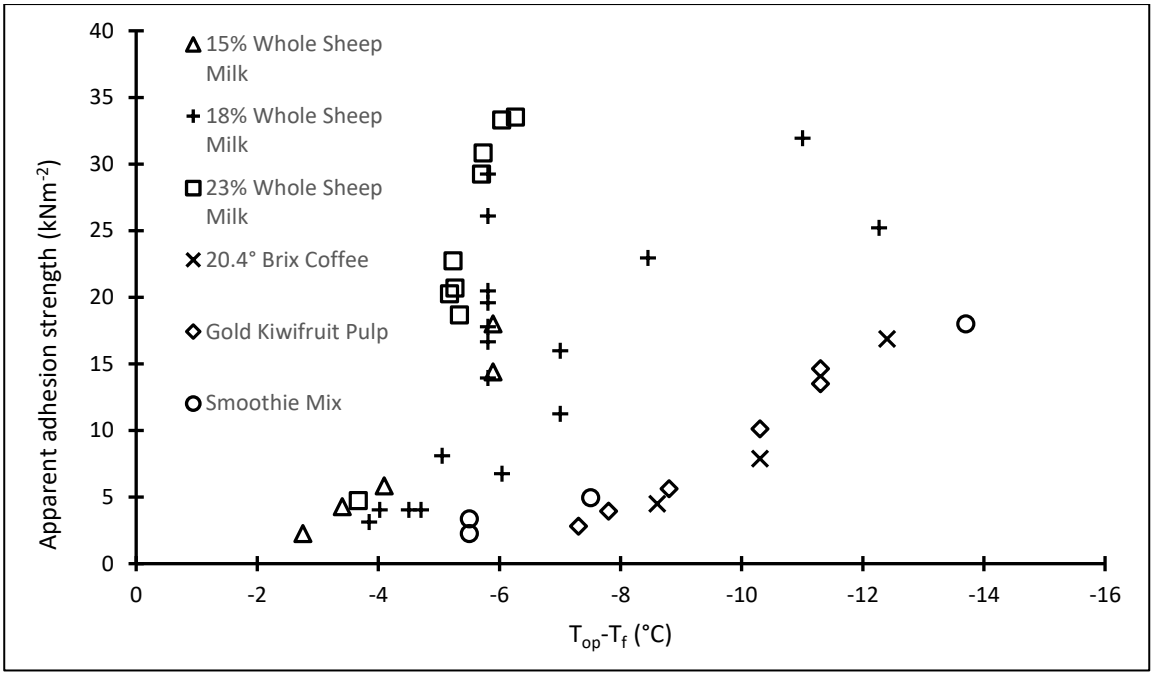

Figure 7-10: Apparent adhesion strength at various freezer operating temperatures for reconstituted ovine milk and other products trialled. Where solids concentrations are given, these are %m/m on a wet basis. The apparent adhesion strength is calculated from pressure developed in 4.2mm diameter freezer, the cross-sectional area of the plug and the area in contact with the freezer wall assuming that the frozen plug is the entire cooled length of the tube.

This increase in pressure requirement and apparent adhesion strength with increased $T_{op} - T_f$ is most likely due to the increase in apparent ice fraction with decreasing temperature, discussed in section 7.4.2 The increased apparent ice fraction may increase the volume fraction of solid ice at the plug/wall interface. The ice morphology at the interface is discussed in detail in Chapter 8. Increased ice fraction at the interface will increase the strength of this interface as more of the interface is able to bear a load. For example, if there is an area of 100mm^2 of product in contact with the freezer wall, a frozen product with a homogenous apparent ice fraction of 0.85 at the wall would have 85mm^2 of ice in contact with the wall, and 15mm^2 of unfrozen liquid in contact. At lower ice fractions this interface has a significant liquid phase which cannot transfer a load between the plug and the wall. This leads to the ice at the interface shearing at a lower stress, and therefore less pressure being required to extrude the plug.

The relationship between the apparent ice fraction and apparent adhesion strength for each milk composition tested is shown in Figure 7-11, as is the relationship for other products tested in the product proof of concept trials. This relationship appears linear, for the ranges of apparent ice fractions present in the tested temperatures.

The apparent pressure required to extrude frozen milk at 23% total solids appeared to be greater than for other products. This may be a result of different ice structure in samples of more concentrated milk, which alters the apparent adhesion strength. It may be a result of increased viscosity in the unfrozen phase, which has been linked to different mechanical properties in frozen sucrose solutions[7]. There was a significant variability in the results for 18% TS whole milk. This work was the first conducted with the small diameter freezer, so this increased variability may be a result of less controlled operation parameters in the first trials conducted on a novel piece of equipment.

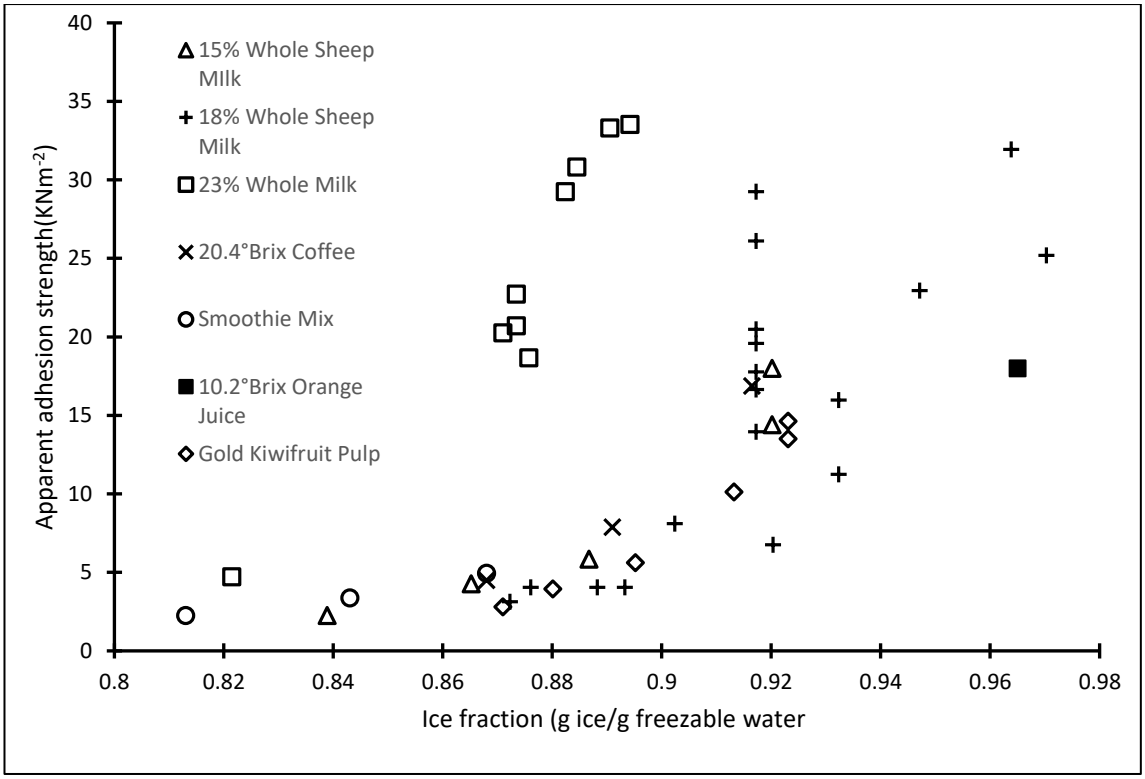

Figure 7-11: Apparent adhesion strengths as a function of apparent ice fraction for reconstituted milk at 15%, 18% and 23% TS are shown, as are other products tested. The apparent adhesion strength is calculated from pressure developed in 4.2mm diameter freezer, the cross-sectional area of the plug and the area in contact with the freezer wall assuming that the frozen plug is the entire cooled length of the tube. The apparent ice fraction is determined from DSC measurements as discussed in 3.3. Residence times for these samples were between 139s and 208s.

7.4.4 Scale-Up Trials: 10.2mm Straight Freezer and 10.2 mm Spiral Freezer

Only one successful trial was recorded with the 10.2 mm Straight Freezer, as a pinhole leak formed at a weak weld on the product size. Nevertheless, the trial suggested that the operating pressure at a given temperature did decrease with an increase in diameter, when the increased interfacial area was accounted for. As the 10.2 mm Spiral Freezer was available when the pinhole leak occurred, it was decided to conduct further trials with the 10.2 mm Spiral Freezer, rather than repair the 10.2mm Straight Freezer.

The 10.2 mm spiral freezer operated successfully and was used to produce kilogramme scale quantities of frozen milk from raw ovine milk for use in a storage trial for a separate research trial. In a typical run of the 10.2 mm spiral freezer, the operating temperature was -5°C, and the maximum operating pressure was 20MPa. A total of 6kg of product was frozen over a 45-minute period. Accounting for the increased interfacial area of this freezer, the pressure was within expected limits: The freezer diameter was approximately 250% that of the 4.2mm diameter freezer, whereas the 10.2 mm spiral freezer is 1,000% longer. This gives an expected pressure scaling factor of roughly 170%.

The operating pressure for ovine milk at 18% solids at -5°C on the 4.2nmm diameter freezer varied from 6MPa to 13MPa. When increased by 170% to scale up to the 10.2nmm spiral freezer as above, the expected operating pressure was 10MPa to 22 MPa. The observed pressure was within this expected range. The residence time for trials on this scale freezer varied from 123s

to 184s. Figure 7-12 shows frozen milk being extruded from the outlet of the 10.2 mm Spiral freezer.

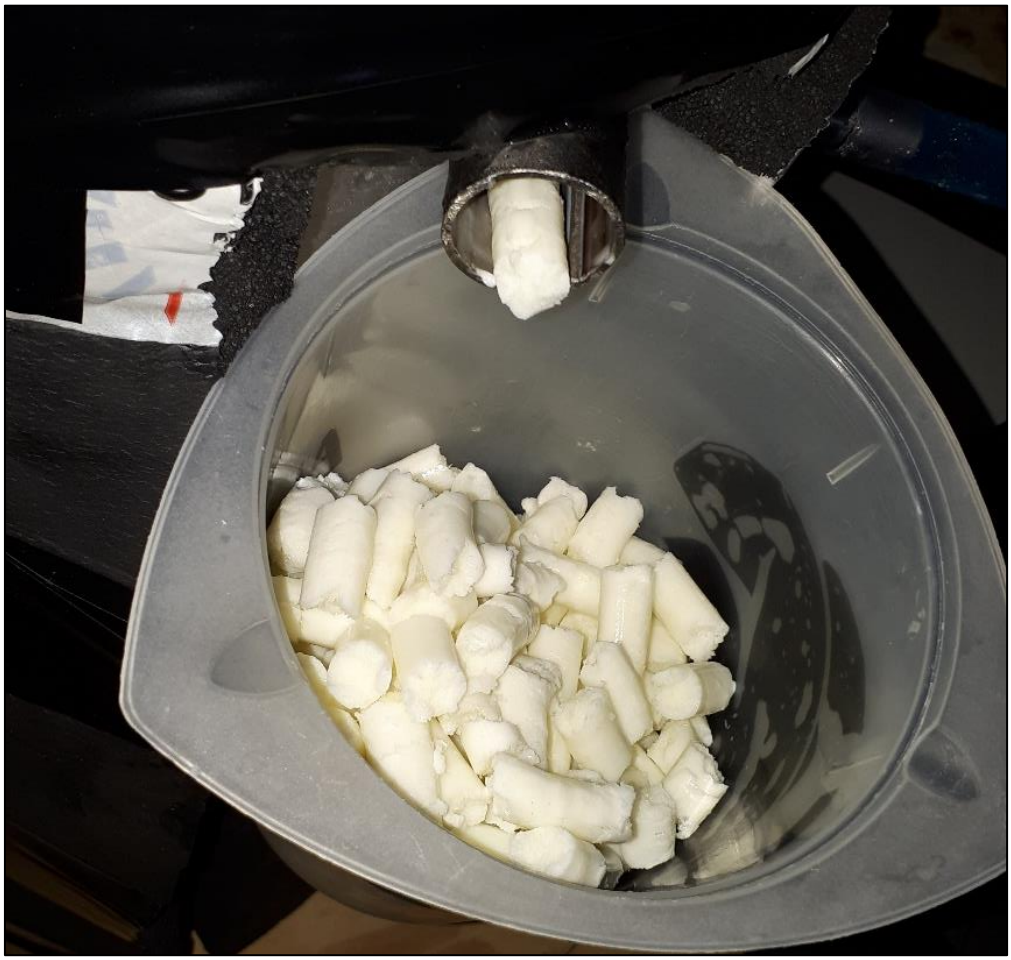

Figure 7-12: Frozen milk being extruded from the outlet of the 10.2 mm Spiral Freezer. Freezer operating temperature was -6°C. Pellets of frozen milk are approximately 10mm diameter 20-30mm long.

7.5 Further Applications and Research

7.5.1 New Products

As has been shown in section 4.1 this freezing method can be applied to a range of food products. It is suggested that this method could be applied to a range of other products such as:

- Meat by-products or extracts
- Colostrum
- Sauces
- Evaporated milk at 50% TS in place of a spray drier
- RTD/RTE foodstuffs
- Anything displaying sufficient freezing point depression to allow for the progressive freezing that enables this process.

There is the possibility of using this system outside of the food industry. It is still an open question whether freezing point depression is required for the method to work, or whether the presence of a sufficient fraction of non-ice substance at the frozen product/ tube wall interface will be sufficient for operation. If it is the latter, then there is a possibility of freezing an oil/water emulsion or a suspension of solid particles. This would allow this methodology to be applied to

certain applications in the materials science industry, such as the production of porous ceramic extrusions by the extrusion of the frozen product, followed by freeze drying and a binding process such as sintering [8]. These ceramics could have applications as filter media or biomimetic scaffolds.

7.5.2 Use as a Preparatory Step for Further Processing

This single step freezing process which forms discrete particles of frozen product will likely be suitable as a preparatory freezing step for freeze-dried products. Many manufacturers of freeze-dried products prefer to freeze the products prior to loading the drier rather than freezing on the trays, in order to maximise dryer through-put. The continuous freezing process also has an advantage in that it forms free-flowing particles which can be easily handled by continuous freeze-dryers.

However, there may be both advantages and disadvantages to this freezing method, when applied as a preparatory step for freeze-drying and research needs to be done to evaluate the freeze-drying performance of continuously tubular frozen products.

In samples of products frozen on a cooled plate with a free product surface, such as occurs when freeze-dryer trays are used for the freezing step, the rate-limiting factor for drying can be the macroscopic concentration of solutes at the top of the sample, leading to a layer of glassy concentrate at the vacuum/sample interface which reduces mass transfer[9]. Products frozen using this tubular freezer may have higher effective mass transfer rates due to higher surface-area/ volume ratios than bulk frozen samples. However, if a concentrated solute layer exists at the vacuum sample interface, this could reduce the mass transfer rates during freeze drying. This should be evaluated as part of future work into this freezing process.

However, the mass diffusion coefficient D in freezer drying is related to feature spacing of ice crystals, λ, with larger ice crystals leading to shorter primary drying times[10], so the smaller feature space resulting from the rapid freezing in the CTF method may limit the achievable mass transfer rates. In contrast, directional freezing of products in vials has been linked to lower primary drying times when compared with vials which supercooled and nucleated, given more homogenous ice structures. This is due to better heat conduction through the directionally aligned ice crystal, and directional continuous porosity which allowed higher sublimation rates without increasing pressure in the freeze-dried cakes[11]. Increased supercooling is linked with higher primary drying times due to smaller pore networks as a result of rapid recrystallization [12]. This situation may be analogous to that encountered in pellets form by the CTF process, which have radially aligned ice crystals, and which will form radially aligned pores on drying, which may decrease the resistance to mass flow out of the pellet.

As a preliminary test of freeze-drying suitability, samples of frozen 20.4° Brix coffee extract, fruit pulps and frozen smoothie mixes have been vacuum-freeze-dried successfully. Mass flow rates have not yet been compared against tray frozen samples of identical characteristic distance, so no conclusions can yet be drawn on relative mass flow rates. Figure 7-13 shows several samples after vacuum-freeze-drying. No collapse during the freeze-drying process was noted. Some change in coloration was seen as a result of the freeze-drying process, but this was also observed in other products that had been freeze-dried after conventional freezing on a cooled belt and is likely due to the removal of water and changes in the surface morphology affecting the scattering of light at the particle surface.

Figure 7-13:Samples of product that was vacuum freeze-dried after rapid freezing and extrusion. A: 20.4° Brix coffee extract. B-D: Fruit smoothie mixes.

Pellets frozen by the CTF process can be packaged direct into bags as a frozen product for either the consumer market, or into larger bags as item of commerce for business to business trade.

7.6 Conclusions

A novel continuous freezer for liquid food products was conceived, based on the behaviour of rapidly advancing ice fronts and the progressive freezing of milk. The continuous freezer was found to be effective for a wide range of liquid food products at a several scales.

The 4.2 mm diameter freezer operated as hypothesised, with solid product being extruded by high pressure liquid feed. The freezer was capable of continuously extruding the following products; whole sheep milk, at a range of solids concentrations; orange juice; concentrated coffee extract; gold kiwifruit pulp; and smoothie mixes.

The pressure required to extrude all frozen products from the freezer increased as the magnitude of $T_{op} - T_f$ increased. The residence time for samples on the 4.2mm diameter freezer varied from 166s to 208s.

The pressure required to extrude the sample, and therefore the adhesion strength between the sample and the tube wall increased as the fraction of freezable water frozen increased. Samples with frozen fraction from 0.8 to 0.98 were extruded during this study.

Frozen milk at 23% total solids appeared to follow a different curve, with a greater adhesion strength for a given temperature or frozen fraction than comparable products.

The freezer concept scaled to larger sizes, with a single successful extrusion of product from a 10.2 mm internal diameter straight freezer, and a series of successful trials with the 10.2mm Spiral Freezer. The 10.2 mm spiral freezer operated with a residence time of 123-184s at an operating temperature of -5°C and an operating pressure of 20 MPa.

Vacuum freeze-drying was effective for a variety of product pellets frozen by this method.

The ice morphology of products frozen in this freezer, the heat flows occurring during the freezing process, scaling relationships, and work done to develop a commercial scale unit are discussed in the next chapter.

7.7 List of Symbols

Symbol	Description	Units
A	Heat transfer area in freezer	m^2
$F_{adhesive}$	Force of product adhesion.	N
$F_{extrusion}$	Force required to extrude frozen product	N
F_{ice}	Normal force of ice against freezer wall.	N
$K_{adhesive}$	Coefficient of product adhesion/ adhesion strength	Nm^{-2}
L_{plug}	Length of frozen product plug	m
P_{liquid}	Liquid product pressure in freezer	Pa
$\dot{Q}$	Heat flow in freezer	W
Ra	Surface roughness	μm
r_{plug}	Radius of frozen product plug	m
T	Temperature	$°C$
T_f	Product equilibrium freezing temperature	$°C$
T_{op}	Freezer operating temperature	$°C$
U	Overall heat transfer coefficient in freezer	$Wm^{-2}K^{-1}$
X_{ice}	Apparent ice fraction	$g_{ice}/g_{\text{freezeable water}}$
X_s	Solids fraction in product	$g/g_{product}$
σ	Surface energy	Jm^{-2}

7.8 References

[1] A. Le Bail and D. Michel, "Continuous Method for Partially Crystallising a Solution and a Device for Carrying Out Said Method," Patent EP1711244B1, 2009-07-29, 2009.

[2] B. Pamuk, P. B. Allen, and M. V. Fernández-Serra, "Insights into the Structure of Liquid Water from Nuclear Quantum Effects on the Density and Compressibility of Ice Polymorphs," *The Journal of Physical Chemistry B,* vol. 122, no. 21, pp. 5694-5706, 2018.

[3] M. J. Shultz, A. Brumberg, P. J. Bisson, and R. Shultz, "Producing desired ice faces," *Proceedings of the National Academy of Sciences,* vol. 112, no. 45, p. E6096, 2015.

[4] P. Chen and X. D. Chen, "A generalized correlation of solute inclusion in ice formed from aqueous solutions and food liquids on sub-cooled surface," *Canadian Journal of Chemical Engineering,* Article vol. 78, no. 2, pp. 312-319, 2000.

[5] K. Golovin, S. P. R. Kobaku, D. H. Lee, E. T. DiLoreto, J. M. Mabry, and A. Tuteja, "Designing durable icephobic surfaces," *Science Advances,* vol. 2, no. 3, p. e1501496, 2016.

[6] F. L. Moreno *et al.*, "Rheological Behaviour, Freezing Curve, and Density of Coffee Solutions at Temperatures Close to Freezing," *International Journal of Food Properties,* vol. 18, no. 2, pp. 426-438, 2014.

[7] X. Xu, G. Jeronimidis, A. G. Atkins, and P. A. Trusty, "On the yield stress of frozen sucrose solutions," *Journal of Materials Science,* Article vol. 38, no. 2, pp. 245-253, 2003.

[8] S. Deville, *Freezing Colloids: Observations, Principles, Control, and Use*. Cham, Switzerland: Springer International Publishing, 2017.

[9] M. Kochs, C. Körber, I. Heschel, and B. Nunner, "The influence of the freezing process on vapour transport during sublimation in vacuum-freeze-drying of macroscopic samples," *International Journal of Heat and Mass Transfer,* vol. 36, no. 7, pp. 1727-1738, 1993.

[10] A. Hottot, S. Vessot, and J. Andrieu, "A Direct Characterization Method of the Ice Morphology. Relationship Between Mean Crystals Size and Primary Drying Times of Freeze-Drying Processes," *Drying Technology,* vol. 22, no. 8, pp. 2009-2021, 2004.

[11] M. Rosa, J. M. Tiago, S. K. Singh, V. Geraldes, and M. A. Rodrigues, "Improving Heat Transfer at the Bottom of Vials for Consistent Freeze Drying with Unidirectional Structured Ice," *AAPS PharmSciTech,* vol. 17, no. 5, pp. 1049-59, 2016.

[12] A. Petersen, G. Rau, and B. Glasmacher, "Reduction of primary freeze-drying time by electric field induced ice nucleus formation," *Heat and Mass Transfer,* vol. 42, no. 10, pp. 929-938, 2006.

Chapter 8: Continuous Tubular Freezer- Ice Morphology, Modelling, and Scale-up.

8.1 Chapter Summary

The ice morphology of selected products frozen by the continuous freezer described in Chapter 7 was investigated by optical microscopy and scanning electron cryo-microscopy (Cryo-SEM). The ice morphology was found to be predominantly radial parallel to the expected heat flows in the freezer. The ice crystals increased in size closer to the centre of frozen plugs and were highly dendritic at the plug/wall interface. There was no obvious continuous layer of lubricating liquid observed at the external surface of the plugs, however there were many inclusions of unfrozen liquid implying a reduced volume fraction of ice at the plug/wall interface.

The expected scaling relationships of the freezer system are developed from first principles. A simplified model of the heat flows within the freezer was developed. This model was solved numerically for a number of initial conditions, and the results of the modelling agreed with the expected scaling behaviour. The required residence time was found to decrease with increased radial heat flux and decreased radius. The required length appeared to be invariant with regards to radius for a given flowrate and areal heat flux. An overview of possible enhancements and optimisations is given, but detailed optimisation work is outside of the scope of this chapter.

Finally, work carried out to develop a possible commercial-scale system is discussed, as are various possible embodiments which may allow further scale-up of the system. The heat transfer area for the freezer may be increased by using a number of parallel tubes, or by using an annular product flow path.

8.2 Introduction

As discussed in the previous chapter, a freezer suitable for liquid food products was conceived, and it was hypothesised that it would operate as follows:

- Rapid freezing forms a dendritic network of ice crystals (as illustrated in Chapter 4) at the interface between the product and a cooled wall.
- The dendritic network of ice crystals entraps liquid and may prove fragile.
- A certain fraction of this liquid remains unfrozen at the freezer's operating temperature due to the progressive freezing of solute-containing water (as discussed in Chapter 6).
- This unfrozen liquid would reduce the adhesion of frozen product to the cooled wall, either by acting as a lubricant, or by reducing the volume fraction of ice in contact with the wall and available to distribute stresses.
- This reduced adhesion would allow the frozen product to be extruded by feeding the product into the freezer with a high-pressure pump. The pressure of the feed acting on the cross-sectional area of the plug would develop forces great enough to overcome the reduced wall adhesion.

This method of operation is shown graphically in Figure 8-1, which shows the hypothesised effects of freezing rate (v_f) and temperature on product being frozen in a tubular freezer, assuming unfrozen liquid inclusions reduced the volume fraction of ice at the wall.

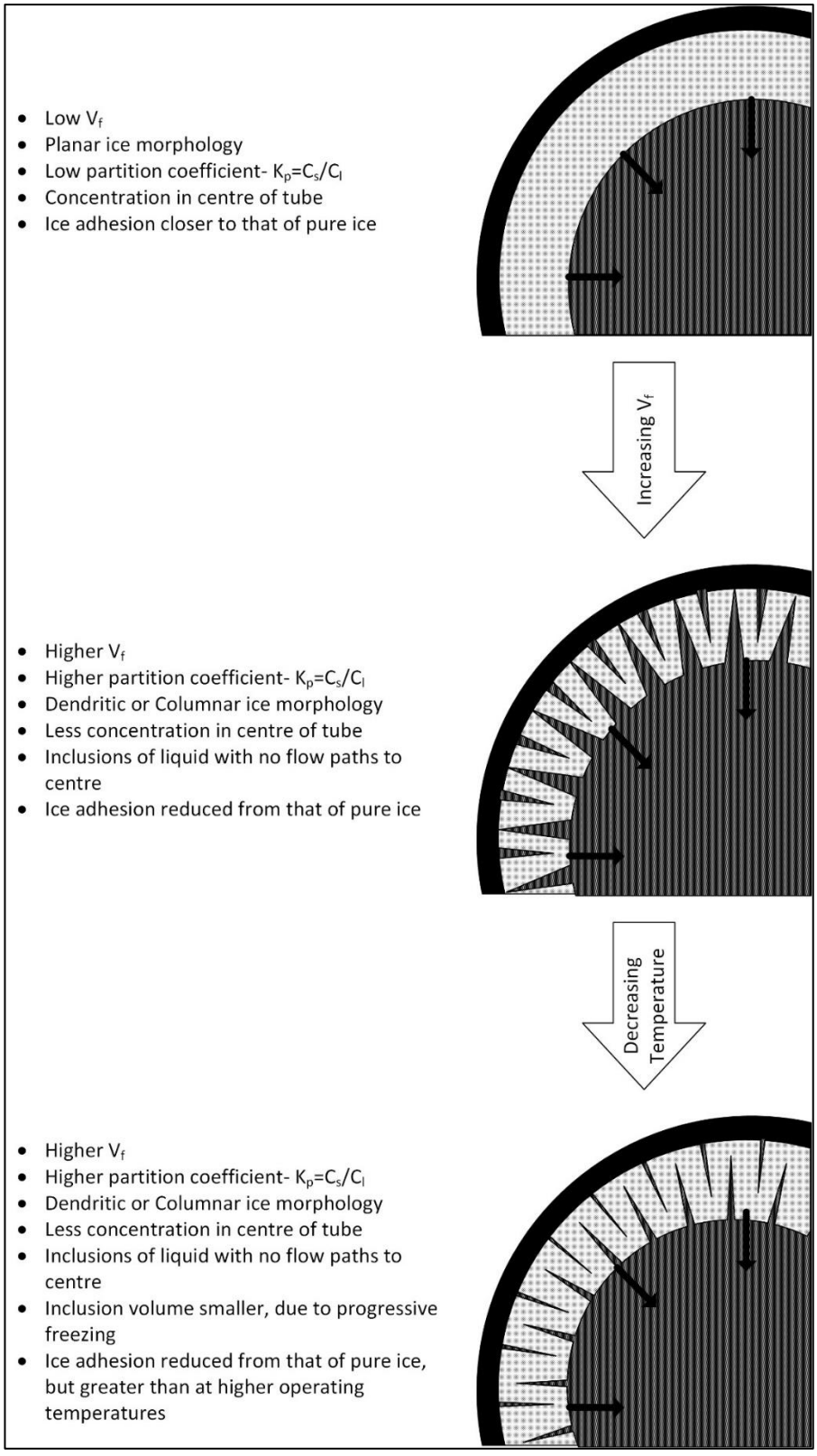

Figure 8-1: Hypothesised operating mechanisms of the continuous tubular freezer and ice growth behaviour inside the tubular freezer.

These hypotheses were partially tested on a benchtop scale using a freezer with a cooled length of 500mm and an internal diameter of 4.2mm and at larger scale using a freezer with a cooled length of 4500mm (wound in a spiral) and an internal diameter of 10.2mm, as discussed in Chapter 7. At both of these scales the freezer operated effectively on a range of products with

operating pressure increasing as the difference between operating temperature and product equilibrium freezing temperature increases, and as the frozen fraction increased.

While the operation of the system was demonstrated in the previous chapter, the hypotheses about ice growth behaviour and operating principles could not be confirmed by operational observations alone. Ice morphology can shed light on the heat flows within the system, and the ice morphology may also help in understanding the mechanism that governs the adhesion strength between the product and the freezer. To investigate the ice morphology in frozen product, and test hypotheses about its relationship with adhesion strength, optical microscopy and cryo-SEM were used.

Basic heat transfer relationships and energy balances were used in the previous chapter to develop expected relationship between freezer dimensions and operating conditions. These relationships may be useful for parametric modelling of the system.

There are a number of possible avenues for enhancing performance of a freezer like the one discussed in this chapter, many of which are well established in heat exchanger design literature.

Numerical modelling is a useful tool for many scientific applications, and can be used to study the effect of operating temperature, product flowrate and freezer diameter on heat transfer within the freezer, and to see the effect of these factors on the ice distribution within a freezer during observation. Due to the interlinked nature of the anisotropic thermal properties of the system, the apparent ice fraction of the product, and the temperature of a region of the freezer, numerical solutions to the system of equations may be more appropriate than semi-analytical solutions. A simplified partial differential model of the heat flow can be developed, and the output from its solution could be compared against the expected scaling relationships developed from energy balances and basic heat transfer relationship to explore the scaling behaviour, and guide scale-up efforts..

The goal of the project underlying this thesis was to develop a freezer suitable for the on-farm freezing of sheep milk. Therefore, designs for a commercial prototype unit need to be canvassed. These might consider: Piping and instrumentation diagrams (P&ID) which comprehensively show the required equipment, piping, instrumentation, and valving for a food-safe on-farm unit; Layouts showing the components, temperatures and air pressures needed for a food-safe unit and possible embodiments of the continuous tubular freezer which may allow further scale-up of the system.

8.3 Methods

8.3.1 Materials

Reconstituted sheep milk was prepared to a total solids concentration of 15% by weight from whole sheep milk powder (Spring Sheep Dairy, Auckland NZ). Samples were reconstituted by stirring with a magnetic stirrer at 40°C for 30 minutes after the slow addition of the correct mass of powder. Samples were degassed under vacuum and stored below 4°C for up to 48 hours before usage.

Commercial orange juice (Keri Premium Orange Juice, Coco-Cola Amatil (NZ) Ltd, Auckland NZ) was purchased from a local supermarket. The total solids content was determined to be 10.3 % by vacuum drying at 70°C for 18 hrs, or measured as 10.2° Brix at 20°C. The orange juice was in liquid form on purchase and was stored below 4°C until testing. The orange juice container was shaken before testing to redistribute any pulp or sediment present.

Raw Ovine Milk was collected from a local farm. The composition was determined according to the methodology discussed in section 5.3.2, and was 15% total solids, 5.4% protein, (4.3%

casein), 3.7% fat, 4.8% lactose, 0.92% ash. The milk had been stored frozen between -18°C and -20°C for 20 days prior to thawing at 20°C and being re-frozen in the tube freezer.

8.3.2 Equipment.

Further details of laboratory equipment, microscopy equipment, and software packages used can be found in Chapter 2.

8.3.3 4.2mm Diameter Freezer Description and Operation.

Chapter 7 gives a detailed description of this freezer, and a detailed description of the experimental procedure used to gather data and collect samples. For the purposes of microscopy, frozen samples were collected under liquid nitrogen and stored at -80°C to prevent crystal structure changes resulting from recrystallization, or Ostwald ripening.

8.3.4 Microscopy of Frozen Samples

Ovine milk made up to 15%TS from WMP was frozen in the 4.2mm diameter freezer. The frozen samples captured under liquid nitrogen were then transferred to a -30°C freezer for 24 hours until microscopy.

An optical microscope with C-mount camera attachment was placed in a -30°C freezer overnight to allow it to reach thermal equilibrium. A secondary light was mounted at an oblique angle to the microscope stage to allow for reflected light microscopy. An attempt at using a microtome failed due to solidification of lubricating oils, so samples were carefully sectioned in the axial and transverse planes with a razor at -30°C.

8.3.4.1 Cryo-SEM of Frozen Sections.

To discern the structure of product frozen in the tube freezer in greater detail than that achievable with optical microscopy, sections of frozen product were imaged via Cryo-SEM. The samples frozen were as follows:

1. Raw Ovine Milk
2. Commercial orange juice.

Both samples were frozen on the 4.2mm diameter freezer described in Chapter 7, at set flow rates of 2mL/min, giving a residence time of 208s. The set temperature for the coolant was -5°C for the Ovine Milk samples, and -12.5°C for the Orange Juice samples.

Frozen samples captured under LN2 were packed in dry ice and stored for 24-72 hours before sample preparation for cryo-SEM.

Imaging was conducted at the Electron Microscopy facility at Victoria University of Wellington, using a JEOL 6500F Scanning Electron Microscope, with Gatan Alto 2500 cryo unit attached.

Samples were frozen into sample holders with the addition of Tissue-Tek Optimal Cutting Temperature (O.C.T.) compound (Sakura Finetek Japan Co., Ltd., Tokyo, Japan) to enhance sample adhesion. Samples, tools, and sample holders were cooled in liquid nitrogen to prevent reheating and re-melting the sample during the mounting process. The orientation of mounted samples and their fracture planes is shown in Figure 8-2.

Once loaded into the preparation chamber the samples were held at -120°C for 20 minutes, fractured and then sublimated at -95°C for 7 minutes to expose structures on the fractured face. The samples were sputter coated with Palladium then loaded onto the SEM stage.

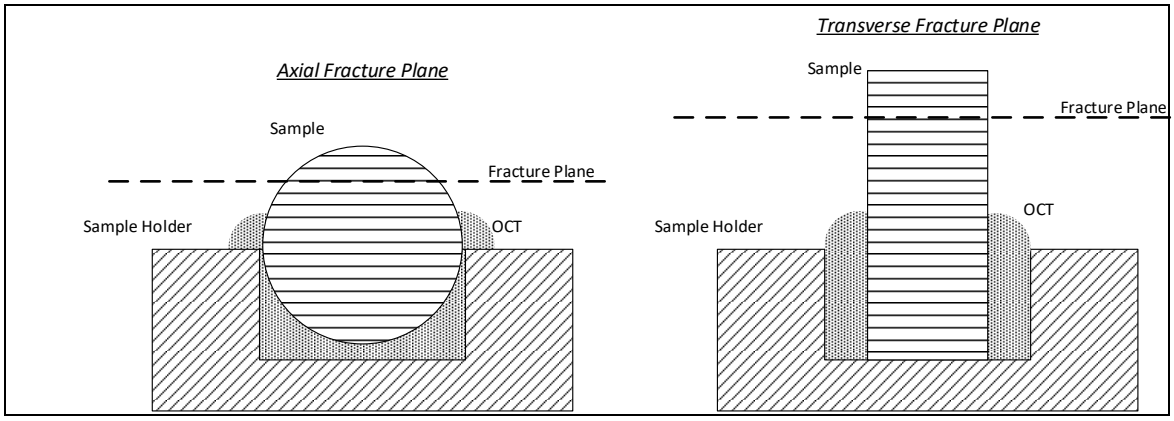

Figure 8-2: Sample mounting for cryo-SEM. Cylindrical plugs of frozen product are frozen to sample holders with Optimal cutting temperature (OCT) compound in two orientations, to allow imaging of ice morphology in two directions. The fracture planes of the two orientations are shown. The same nomenclature for fracture planes is used for optical microscopy images.

To analyse ice crystal size and shape in the cryo-SEM images, the FIJI image analysis software [1] was used. Segmentation of images into regions of ice crystals and concentrated solids was carried out using the Trainable Weka Segmentation plugin[2]. Statistical analysis was carried out using Minitab® Statistical Software. Further details of these software programs are given in Chapter 2.

8.4 Results

8.4.1 Optical Microscopy

The ice structure in the frozen plug was anisotropic and showed distinctly ordered structures in both the axial and transverse planes. The ice morphology can also be seen to vary with radial position, i.e. the ice at the interface of the plug and tube wall was geometrically different to ice further from the interface.

The images in Figure 8-3 were captured using a 4x objective lens and a 3.3x camera eyepiece lens.

Transverse slices of the frozen plug are shown in Figure 8-3 A and B, and these show several interesting features that can be understood by reference to the phenomena discussed in Chapter 4.

The ice crystals were columnar/lamellar in form and are oriented radially. This indicates that the heat flow was predominantly radial, which can also be deduced from a consideration of the geometry of the system and where heat removal occurs. The columnar/lamellar form of the ice also indicates that the freezing front velocity was high enough to lead to this morphology, rather than planar ice growth.

At the perimeter of the frozen plug, the ice shows a complicated morphology that appeared fractured or dendritic. This could be due to either mechanical stresses at the interface between a sliding plug and a stationary wall, or a result of the high freezing front velocity predominating at the plug/wall interface, or a combination of the two factors.

A combination of the two factors was most probable, as the freezing front at the tube/plug interface would be subject to a greater temperature gradient, and freezing front velocity, than experienced further into the plug. For a residence time of 208s in this freezer, the average ice growth rate is at least 10.1μms^{-1}. This would lead to a dendritic structure as this ice growth rate is within the dendritic range for ovine milk as shown in Chapter 4. As the structure at the interface contains ice dendrites and unfrozen water, its adhesion strength should be lower than

that of the bulk of the plug[3, 4]. Any factures that occur due to ice adhering to the wall and then breaking/detaching will occur in this region, and this could contribute to the discorded structure at the perimeter of the plug.

Breakage of ice at the wall may also cause secondary nucleation as the crystals adhered to the wall will act as seeds for further ice growth. This may allow for the rapid growth of small crystals near the wall, leading to a rapid formation of interspersed volumes of concentrated unfrozen liquid and ice.

The transverse slices displayed sectors of parallel crystals, arranged radially, with chaotic zones where two converging sectors merge. The chaotic areas are highlighted in Figure A and B, as are the radial sectors of parallel ice crystals. The direction of ice crystal growth is shown with the overlaid arrows in the figures. This crystal morphology is similar to that encountered in metallurgical fields with round bar stock formed via continuous casting[5] , which also arises from the radial heat flow from the centre of a cooling and solidifying melt.

Detachment of the frozen plug could occur by shearing of the dendritic ice structure at the plug perimeter, as discussed previously, or the entirety of the frozen plug could detach from the wall at the exact interface between the ice and the wall and be lubricated by the unfrozen liquid fraction. As the wall has not been polished, there is significant surface roughness that could lead to a strong ice-wall interface. It is inferred then that the detachment of the frozen plug is a result of the dendritic network at the outside of the plug shearing, leaving a certain amount of ice adhered to the wall. Further testing with polished surfaces and low surface energy surfaces that affect the theoretical adhesion strength between ice and the wall material may help to understand the method of detachment in greater detail. The Cryo-SEM images presented later in this chapter are also helpful when attempting to describe the adhesion behaviour of the system.

Figure 8-3 C shows the ice morphology in a representative axial slice of a frozen plug frozen at a set temperature of -5°C. The ice crystals are generally parallel in direction and are narrow in form. The ice has grown in parallel to the centripetal heat flow, with a high enough freezing front velocity to form columnar/lamellar ice crystals, as discussed in Chapter 4. The average centre-centre size of the ice columns/lamellae in the axial slices was 46µm with a standard deviation of 14µm.

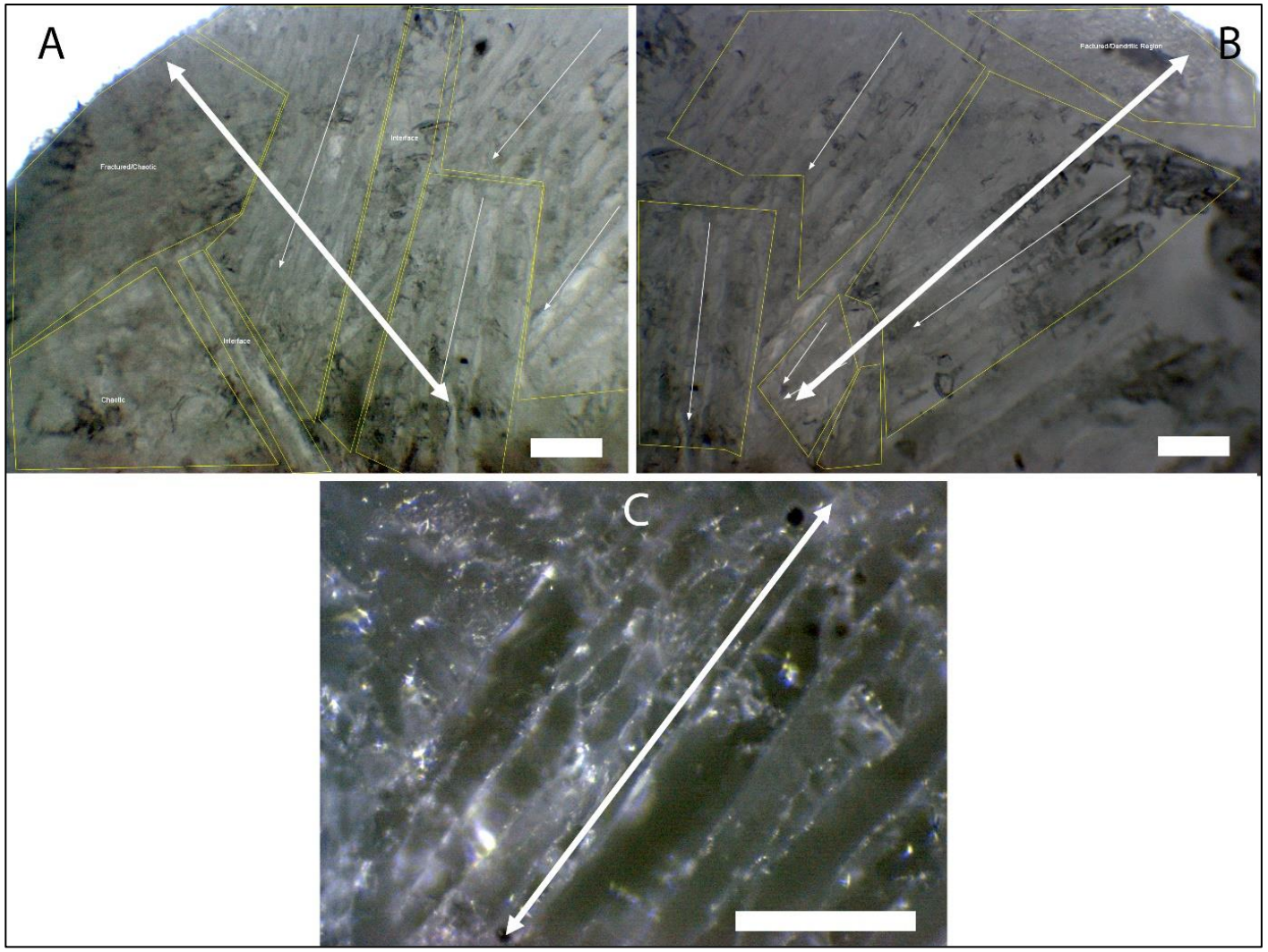

Figure 8-3: A and B: Ice morphology in a transverse slice of frozen plug imaged by optical microscopy. Regions of crystals with major axes aligned in similar directions are outlined. C. Crystal morphology in a slice along the polar axis. The exterior of the plug, i.e. the region in contact with the freezer wall, is at the top left in image A and the top right of image B. Scale bars are 200µm. Image C is away from the wall. The primary heat flow and ice growth direction in A and B is radially in from the wall, and in C the heat flow and ice growth direction are from the top right of the image. These are indicated by the double-headed arrows.

8.4.2 Scanning Electron Cryo-Microscopy

Figure 8-4 shows the ice crystal structure in a sample of raw ovine milk frozen on the 4.2mm diameter freezer. The figure is a composite of images taken at 40x magnification, looking at a transverse fracture plane in the sample. Figure 8-5 is an image of same sample as Figure 8-4 composited from images taken at 150x magnification. The ice morphologies in samples frozen on the 4.2mm diameter freezer were similar to those observed by optical microscopy and are similar to what would be predicted from the ice morphology behaviour described in Chapter 4. Due to the more effective microscopy method, it is easier to determine features present in these images.

In the cryo-micrographs of frozen milk samples, the visible ridges are interpreted as being milk solutes, dominated by casein micelles and amorphous lactose, and the valleys are ice crystals that were partially removed by sublimation during sample preparation. Areas of extensive ridging imply zones with appreciable unfrozen liquid. This analysis is similar for cryo-micrographs of orange juice, however rather than being milk solids the solutes that make up ridges are low molecular weight carbohydrates, primarily in an amorphous state.

The average area of the ice crystals parallel to the fracture plane increased as the distance from the edge of the frozen plug increased. This indicates that the heat flow decreased due to the insulating effect of ice and the spacing of interface features increased as the distance from the exterior of the plug increased. The relationship between interface features and freezing front velocity (a function of heat flow) is discussed further in Chapter 4. Freezing front velocities will have increased at the centre of the tube, however this is not seen in the ice morphology of frozen samples, as a result of collisions and interactions between advancing ice crystals There may also be a change due to the solute environment as a result from freeze-concentration.

The direction of crystal growth appeared to be generally radial, from the exterior to the plug, aligned with the expected heat flow in the sample.

The initial crystallographic orientation of ice nuclei affects crystal growth orientation, so the regularity of the radial ice distribution was lower than would be expected if orientation were solely dependent on heat flow. Radially growing crystals may also “foul” each other as they approach the centre of the plug, and change the alignment of crystals. This is appeared to be more prevalent in milk than in orange juice, as can be seen by the greater apparent radial symmetry in micrographs of orange juice samples.

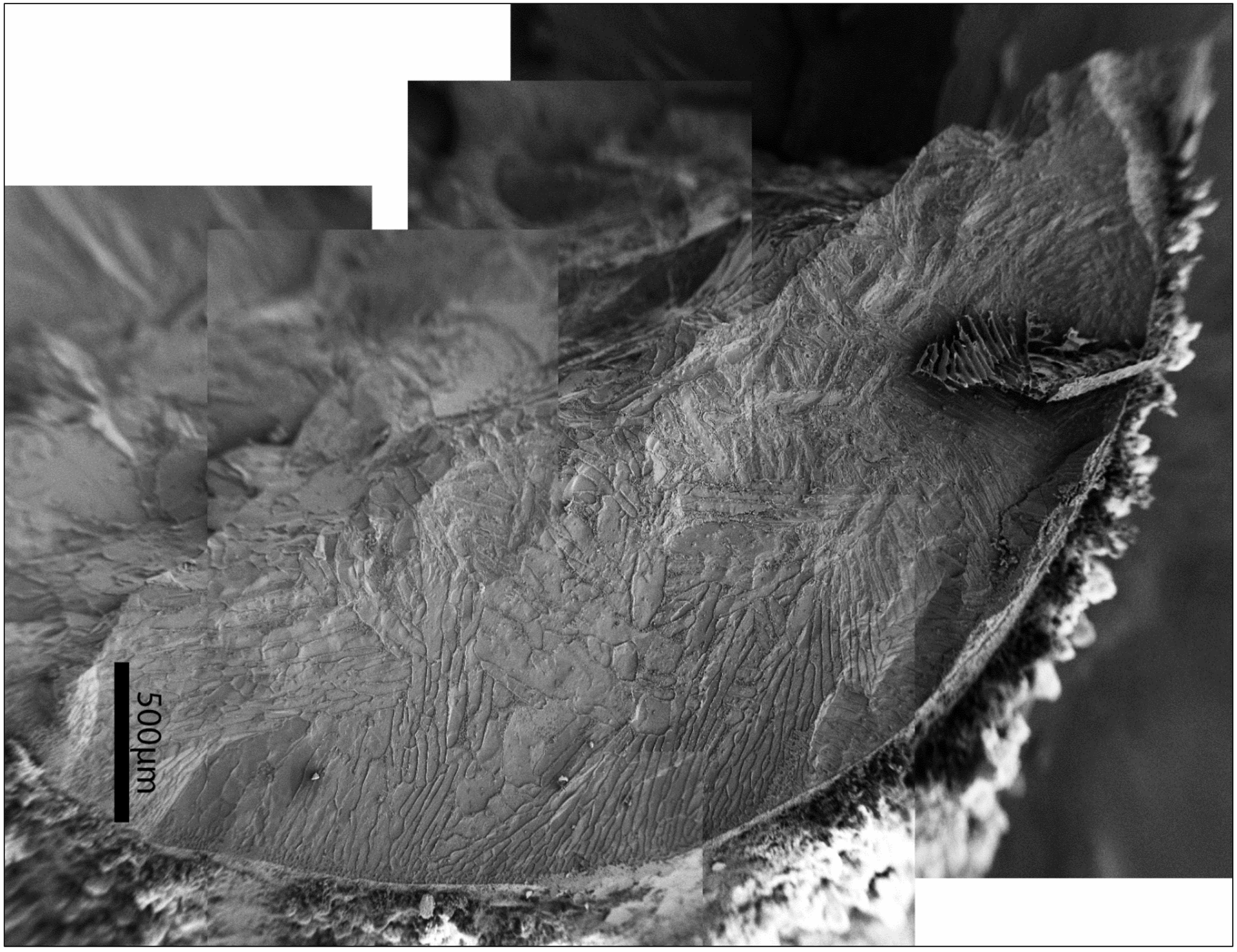

Figure 8-4: Fracture face of sample of milk frozen on 4.2mm diameter freezer. Composite of images at 40x magnification. Imaged by Cryo-SEM. The fracturing process broke the core roughly in half along the long axis of the core. The curved surface at the right is the contact surface with the freezer wall (some hoarfrost, typical of Cryo-SEM preparation, can be seen.). At left is where the centre of the core would be located. The predominant ice growth and heat flow direction is radially inwards from the exterior wall.

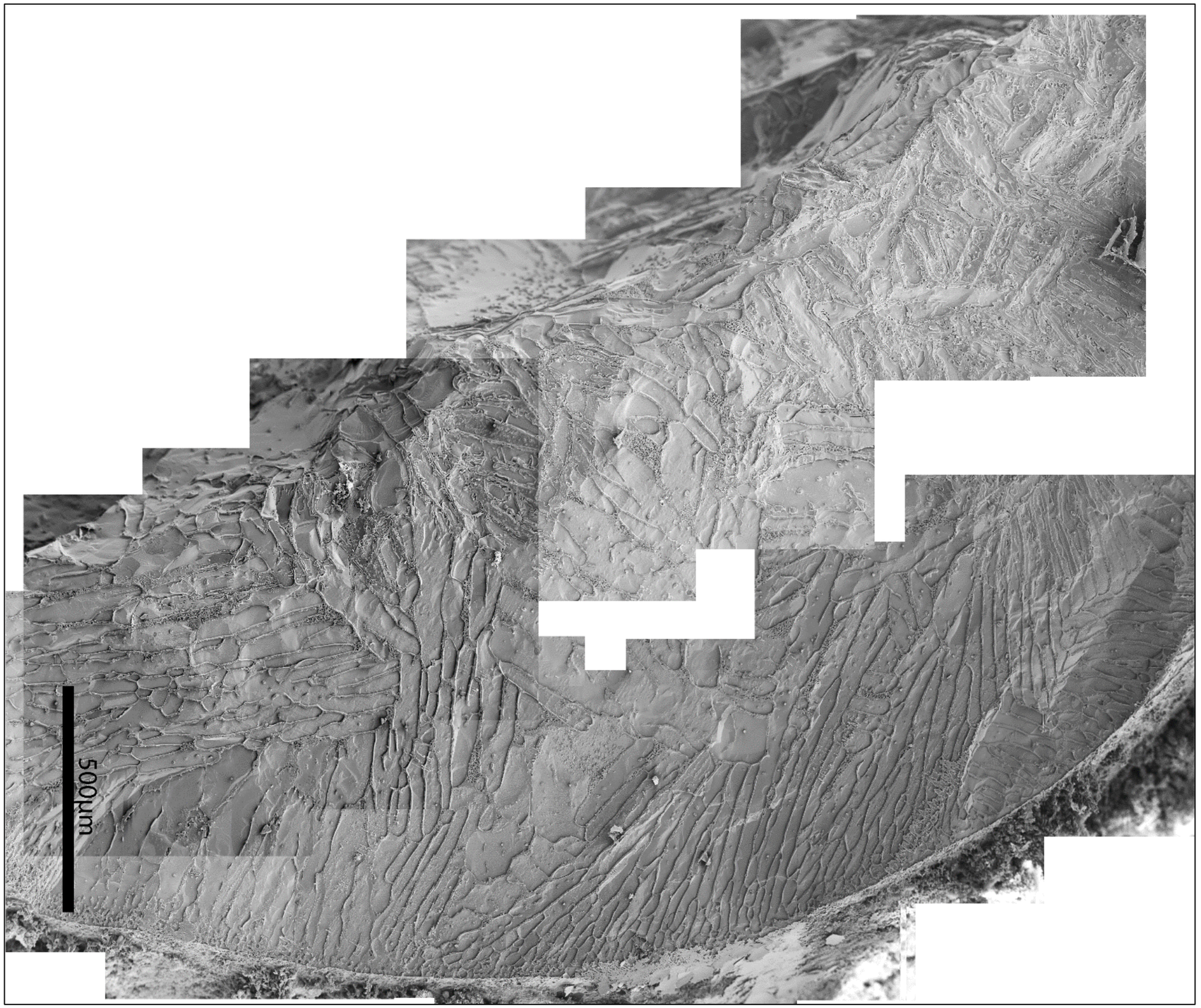

Figure 8-5:Fracture face of sample of milk frozen on 4.2mm diameter freezer. Composite of images at 150x magnification. Imaged by Cryo-SEM. The fracturing process broke the core roughly in half along the long axis of the core. The curved surface at the right is the contact surface with the freezer wall (some hoarfrost, typical of Cryo-SEM preparation, can be seen.). At left is where the centre of the core would be located. The predominant ice growth and heat flow direction is radially inwards from the exterior wall.

At the wall of the sample, where the highest growth rates are likely, the ice crystal structure was fine, and showed less obvious alignment. From the cryo-SEM images, it can be seen that this was a result of the patterns formed by the advancing ice front, rather than being mechanical damage due to shear in the freezer. This morphology is shown in Figure 8-6. Initial crystal gowth may occur into a slightly supercooled melt, which leads to high growth rates and the formation of dendrites. This is shown in Chapter 4, and has been observed in studies investigating the structure of frozen colloids[6] [7], and model food systems [8]. It is sometimes referred to as a "homogenous" or "Equiaxed" zone.

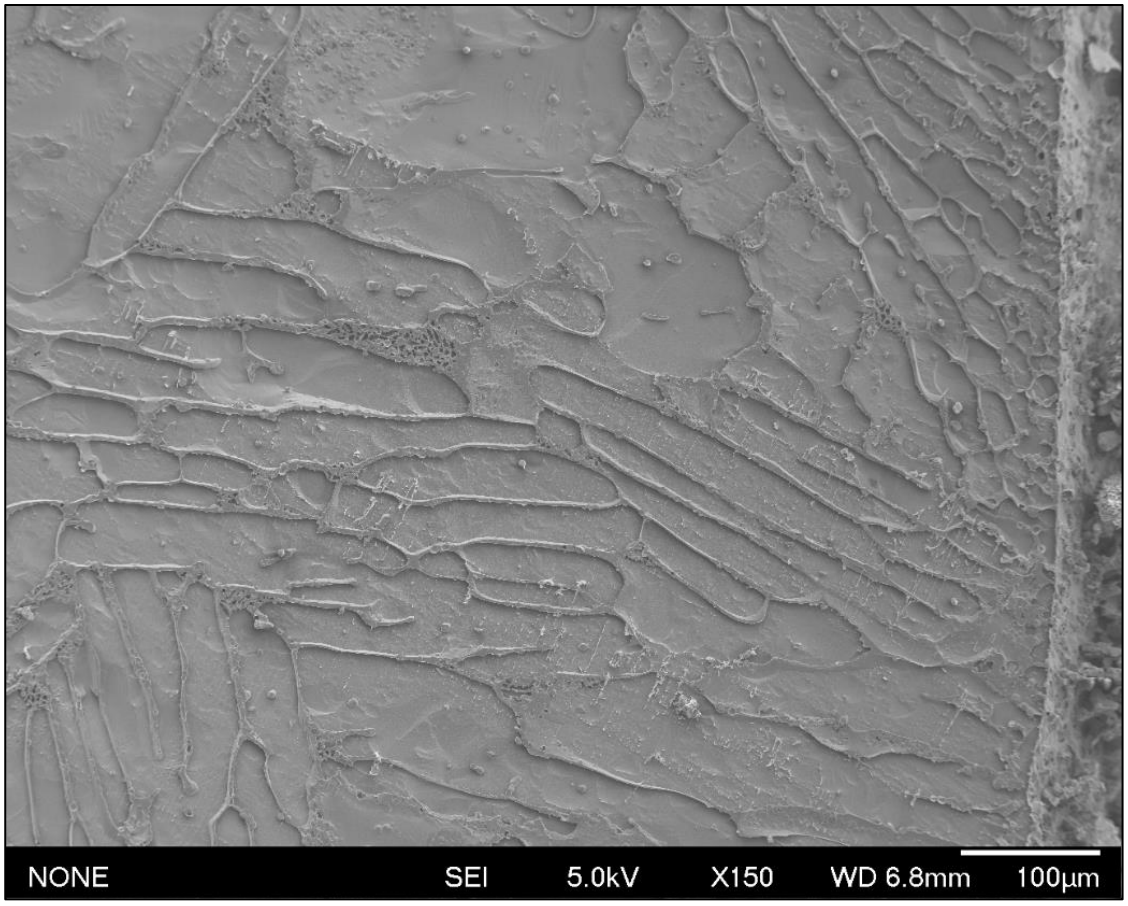

Figure 8-6: Frozen sample morphology at the frozen plug/freezer wall interface. The sample is a plug of raw ovine milk, imaged on a transverse fracture plane by Cryo-SEM .The frozen plug/wall interface is seen at the far right of the image, 50µm from the edge of the image. Hoarfrost is observed past this (a consequence of Cryo-SEM preparation). The heat flow and ice growth direction is from the right of the sample to the left.

Once the heat involved in supercooling has been removed, if the heat flux and the ice growth rate is sufficient, a dendritic or tree-like morphology results. As discussed in section 4.4.2.2, in ovine milk this transition to dendritic growth happens at ice growth rates of 2-5μm^{-1}. When heat flow decreases due to increased ice thickness, a columnar or lamellar ice morphology becomes established, generally parallel to the direction of heat flow. For the samples tested, the average ice growth rate (as determined from the residence time in the freezer) was 10.1μms^{-1}.

Although there are significant volumes of unfrozen liquid trapped in the ice structure near the wall, there is no uninterrupted layer of unfrozen liquid apparent at the wall. If an uninterrupted layer of unfrozen liquid was present at the wall that would suggest that the limited adhesion strength observed could be the result of this liquid acting as a lubricant.

The volumetric proportion of unfrozen liquid at varying distances from the exterior surface of the frozen plug of raw ovine milk was estimated by measuring the fraction of a transect drawn

concentric with the exterior surface that was solute ridge. A series of such arcs were measured on the image in Figure 8-6 and are shown in Figure 8-7. The unfrozen liquid volume is enriched in the exterior 50-100 µm, slightly enriched at a distance of 150 µm from the exterior, and no enrichment is apparent further into the frozen plug. This unfrozen liquid fraction enrichment could limit ice adhesion strength near the tube wall.

This enrichment may be the result of increased liquid pressure at the centre of the freezing plug leading to a radial bulk liquid flow outward to the freezer wall, where the final unfrozen liquid fraction is greater than that in the bulk sample. While it is reasonable to assume some inward radial displacement of unfrozen liquid as the crystals grown inward, once crystals reach the centre of the plug and compete for available volume, the direction of bulk liquid flow is expected to reverse. The solute concentration in the unfrozen liquid at any radial location is unlikely to be different from that determined by the equilibrium freezing temperature. i.e., the concentration of liquid in the unfrozen liquid in a region at -10°C is the same as that in a sample of the same product held at eqilibirum at -10°C. As this unfrozen liquid flows towards the colder plug exterior, some will freeze, maintaining the equilibrium between temperature and concentration. The bulk flows occurring are not expected to occur at timeframes faster than the diffusion limited ice growth rate.

As shown in chapter 4, If ice growth is columnar, the ice growth rate is greatest in the axis aligned with the heat flux, with lower ice growth velocities sideways into the intercrystalline melt. It is likely that columnar ice crystals will intersect in the centre of the frozen plug before the intercrystalline spaces have solidified, which will lead to an increase in liquid pressure in the centre of the freezing plug and outward radial liquid flow. Micrographs show that unfrozen liquid regions in the plug are in communication with each other, allowing this bulk liquid flow.

This should be treated with caution as the micrographs used for this analysis were from a single sample of raw ovine milk, and more data are needed before it can be shown whether this phenomenon is common to all samples frozen with a continuous tubular freezer.

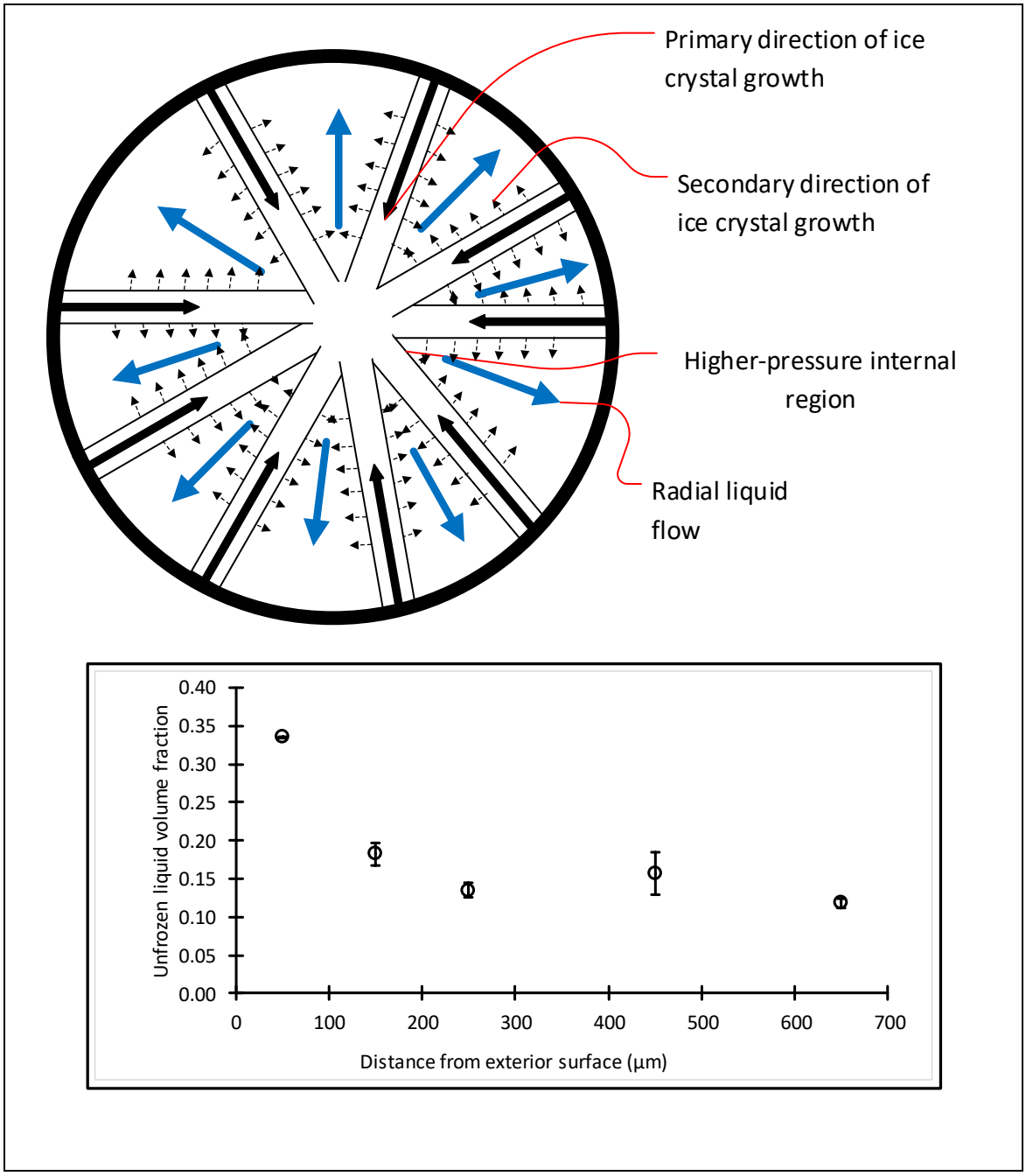

Figure 8-7: Apparent solute fraction in a frozen plug of raw ovine milk as a function of the distance from the exterior surface. A possible mechanism for this enrichment is shown graphically: The ice crystals grow with the greatest velocity in the direction aligned with heat flux. This is labelled as the primary direction of ice growth. The collision of these crystals at the centre of the freezing plug, along with slower secondary growth from the sides of the columns leads to a higher liquid pressure at the centre of the plug, which in turn leads to a radial liquid flow to the exterior of the freezing plug.

The relationship between ice fraction and mechanical properties of frozen food solutions has been observed in other studies; The rigidity of partially freeze-concentrated frozen food solutions is affected by the fraction of ice present [9]; The adhesion strength of frozen bovine milk on stainless steel substrates increases with decreased temperature, and this effect was linked to the decreased volume fraction of unfrozen liquid at the milk/stainless steel interface as the temperature decreases [4]; The yield stress of frozen sucrose solutions has also been found to increase with decreased temperature, as a result of the increased levels of concentrated unfrozen solution[10].

The existing literature, the observed ice behaviour, and the relationship between adhesion strength and apparent ice fraction all support the hypothesis that the reduction of ice volume compared to pure ice, as a result of dendritic ice growth trapping volumes of unfrozen liquid and radial movement of unfrozen liquid, reduces the adhesion strength at the wall. Further, if the ice/unfrozen liquid matrix at the wall is modelled as a porous material then a generalised mixing rule would be appropriate for describing mechanical properties[3], and the adhesion strength will monotonically decrease with increased unfrozen liquid fraction at the wall.

Much like the frozen milk plug, the ice crystal structure in a plug of frozen orange juice was predominantly radial, this is shown in Figure 8-8. Ice crystals can be identified in micrographs as eroded areas between bands of solutes. The size of ice crystals was analysed from micrographs in ImageJ image analysis software. The size of the ice crystals decreased at the exterior of the plug, when compared to the centre of the plug. The ice crystal size within 850µm of the plug exterior was significantly smaller than the ice crystal size within a radius of 850µm of the centre of the plug, however in both regions there were significant variations in particle size as shown in Table 8-1.

Table 8-1: Dimensions of ice crystals exposed on fracture face in orange juice. Variations shown are standard deviation for values, and the 95% confidence interval for the difference. The area is the cross-sectional area of the ice crystals exposed at the fracture face.

Dimension	**Centre of frozen plug** N=321	**Exterior of frozen plug** N=403	**Difference**
Area (µm^2)	3610±5380	1330±2610	2280±640
Feret length (µm)	129±126	83.7±76	45.7±15.6
Feret minima (µm)	36.0±30.8	22.4±21.1	13.5±4.0
Aspect ratio	4.11±3.07	4.54±2.74	0.43±0.43

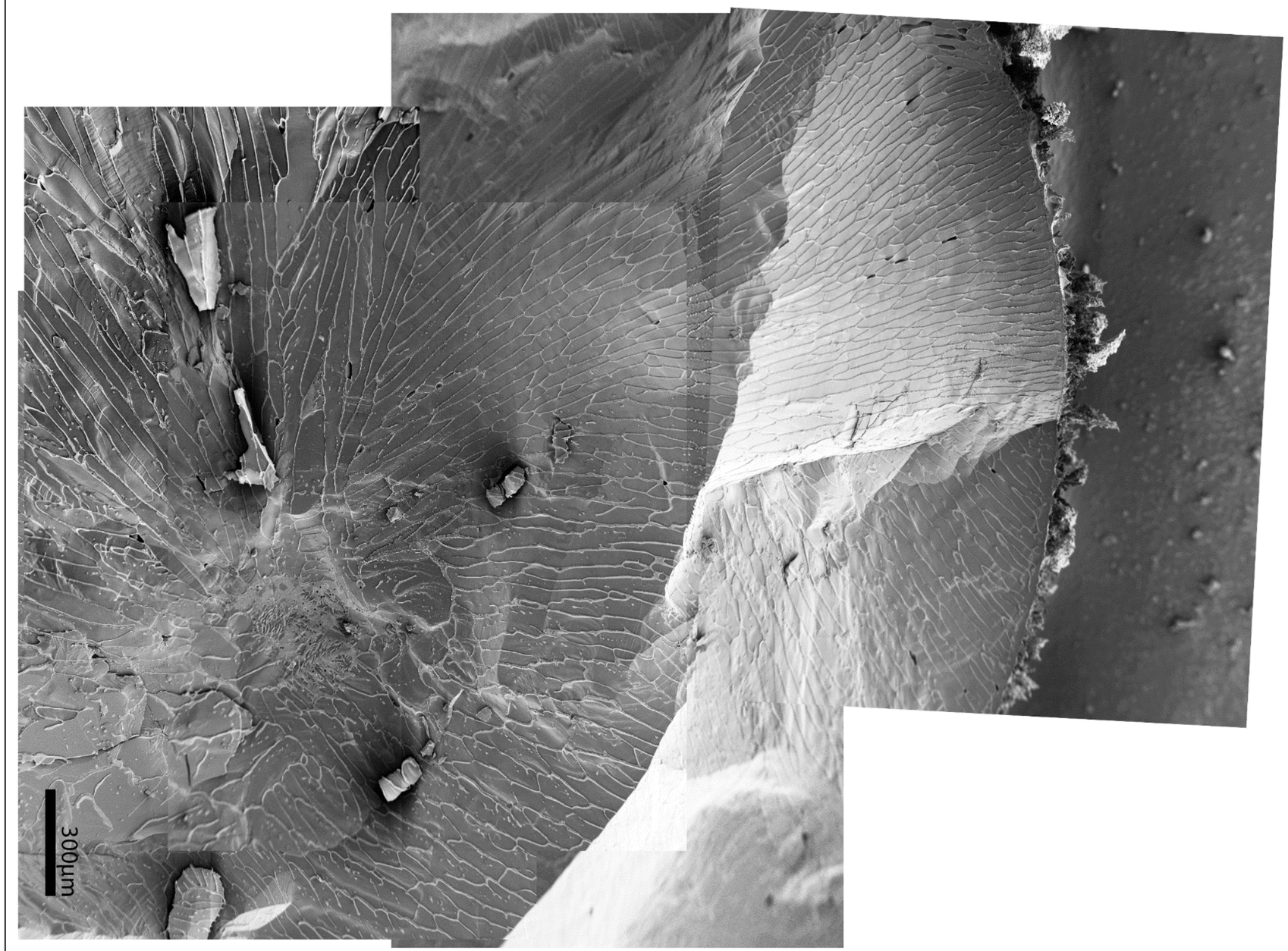

Figure 8-8: Fracture face of a sample of orange juice frozen on the 4.2mm diameter freezer. Composite of images at 40-100x magnification. Imaged by Cryo-SEM. The exterior of the frozen plug can be seen at the top of the image (hoarfrost can also be seen), and the centre of the frozen plug is located approximately 600-900µm from the bottom edge of the image. Heat flow and ice growth was radial from external edges to the centre of the frozen plug.

This page intentionally left blank.

The angular distribution of ice crystals at the centre of the solid plug was fairly even, as shown in Figure 8-9, illustrating the predominantly radial direction of the crystal growth.

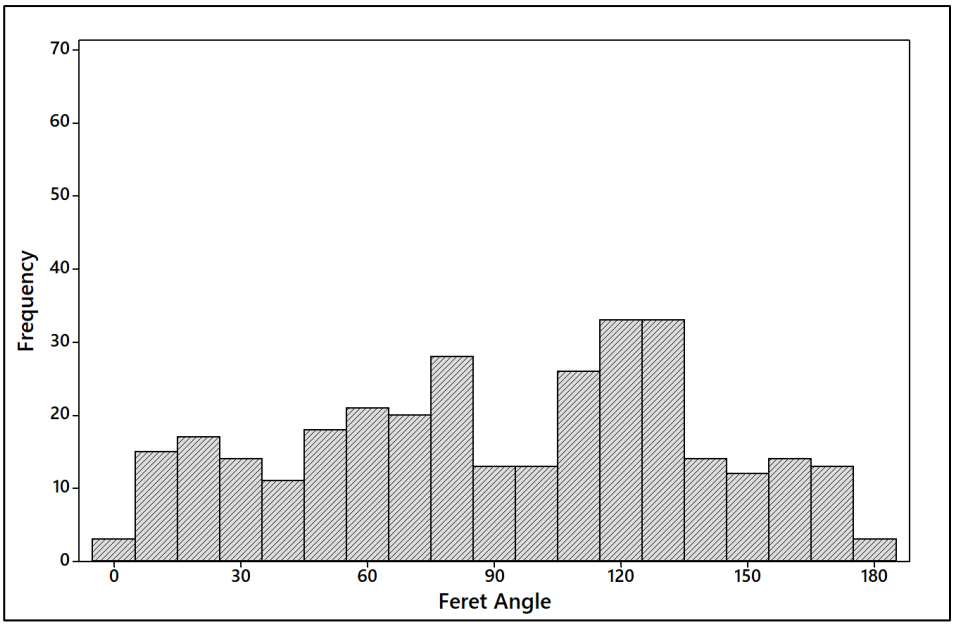

Figure 8-9: Histogram of ice crystal angles in the centre of a frozen plug of orange juice. Angles were determined from the Feret maxima and minima of ice crystals exposed at the fracture plane, and are the angle of the long axis of these cross-sections an arbitrary horizontal.

The morphology of the ice crystals in the core of orange juice shown in Figure 8-8 is analysed further for a region located 700µm to 1400 µm from the external edge. The size of crystals in this region follows a loglogistic distribution with a large number of smaller crystals, and a tail of larger crystals. The median area exposed on the fracture plane was 1070µm^2 and the mean area was 3770 µm^2. Some of the smaller crystals may be a cross-section of a larger columnar crystal out of the plane of the image

The crystal aspect ratio, derived from the ratio of the long and short Feret diameter, follows lognormal distribution. The median aspect ratio was 2.9 and the mean aspect ratio was 3.5.

The radial distribution of the crystals was measured by plotting the angle of the long axis of all crystals with an aspect ratio greater than 3 against the radial position of the crystals' centroid. There was a linear relationship between the two plotted angles with an R^2=0.78 for 140 observations. This indicated that the crystals were aligned radially, with long axes pointed to the centre of the frozen plug. These measurements are summarised in Figure 8-10.

.

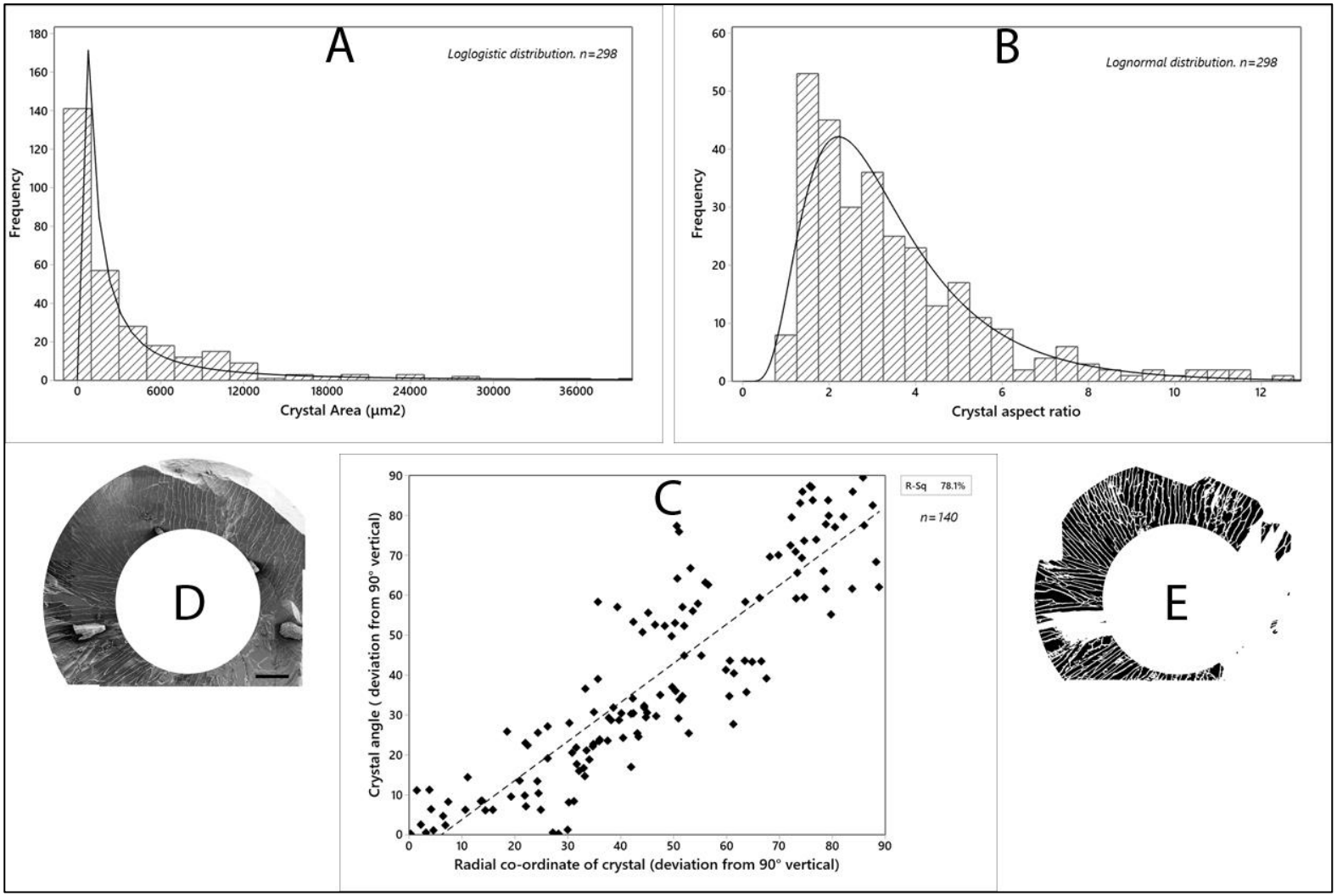

Figure 8-10: Analysis of the crystal size, shape and orientation of the region of the orange juice core located 700-1400µm from the external surface of the core. D shows the masked region, and E shows the particle shapes extracted from this image. The size histogram of these crystals is shown in A. The crystal size appears to follow a loglogistic distribution. The distribution of the aspect ratio of the crystals is shown in B. The radial distribution of the crystals is illustrated in C. The angle of the crystals to vertical is plotted against the radial co-ordinates of the centroid of the crystals, excluding crystals with an aspect ratio below 3. These angles align, indicating that ice crystals grow radially inwards.

There was a small layer of glassy solid at some areas on the exterior of the orange juice samples as shown in Figure 8-11, however this may be a result of sample handling causing a small degree of melting at the exterior, as this was not seen on frozen milk samples, and orange juice has a higher degree of freezing point depression making it more susceptible to melting at the exterior during handling. Despite this thin layer, the morphology of the sample more than ~20µm from the edge is unaffected by melting during handling.

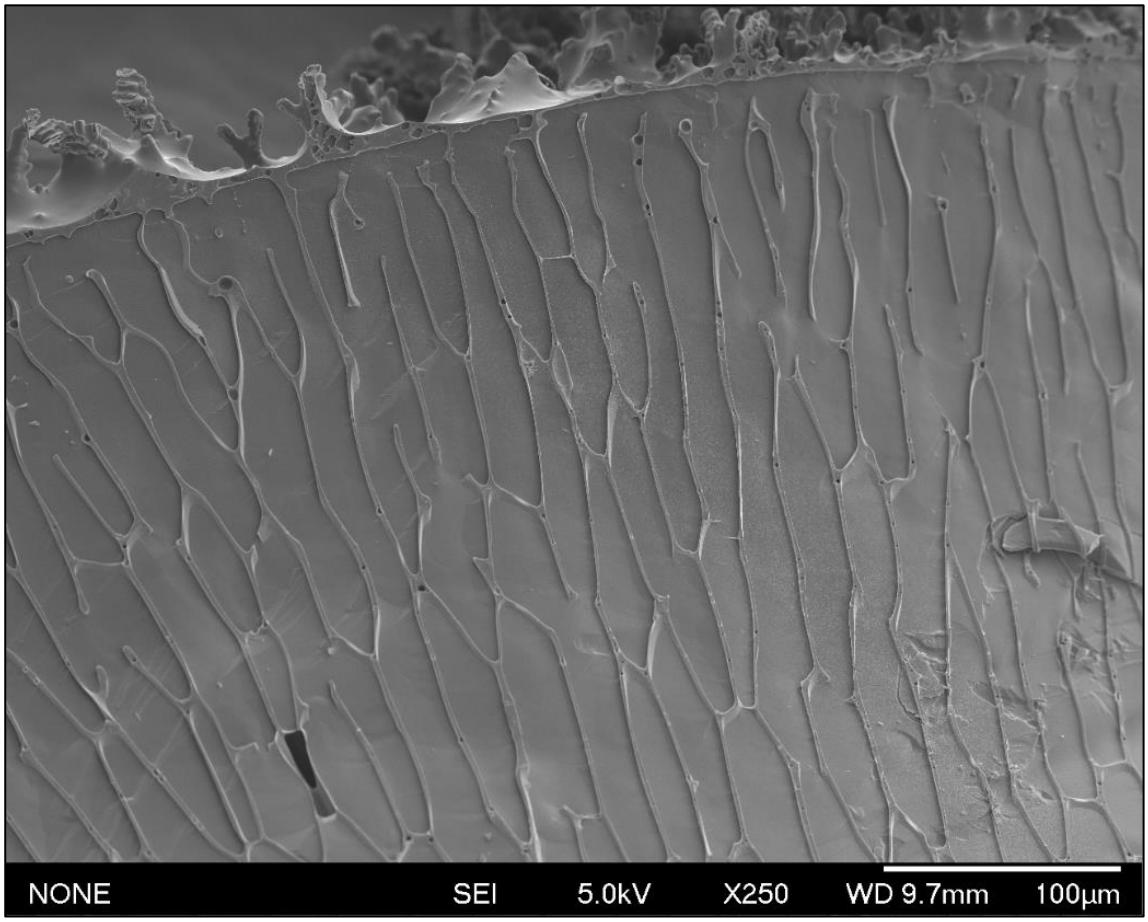

Figure 8-11:Frozen sample morphology at the frozen plug/freezer wall interface at 250x magnification. Sample is a frozen plug of Orange Juice, imaged on a transverse fracture plane by Cryo-SEM. The exterior of the frozen plug is located at the top of the image. Heat flow and ice growth is radial inwards from this exterior.

Some crystallisation of solutes in orange juice can be observed at 13,000x magnification in the micrographs in Figure 8-12, however, the majority of the solute was in a glassy state. The crystalline structures observed were extremely small, approximately 150nm in length.

No crystallisation of lactose was observed in any of the frozen plugs of ovine milk, indicating that this freezing method did not promote crystallisation, unlike the slowly frozen samples discussed in Chapter 4.

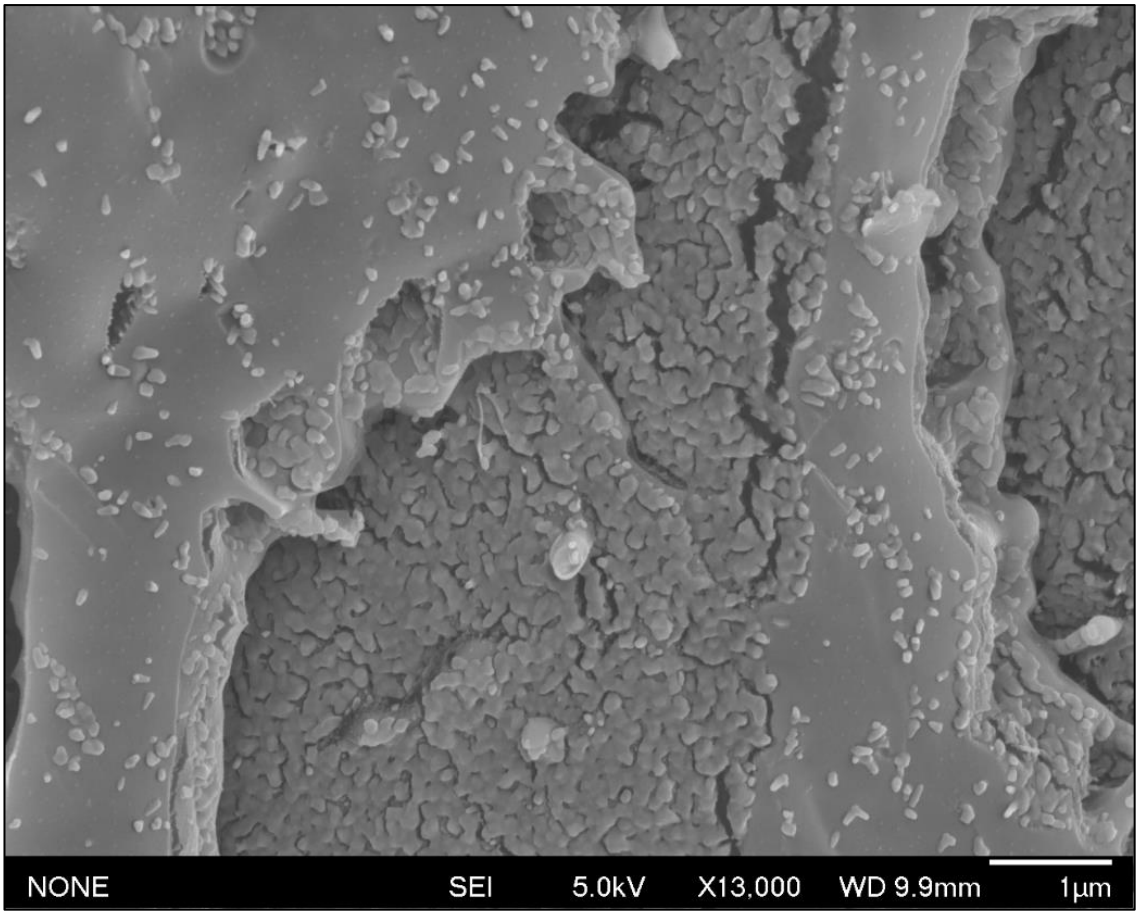

Figure 8-12: Concentrated solute region in orange juice sample at 13,000x magnification. Imaged by Cryo-SEM. Some crystallisation of solute may have occurred.

8.4.3 Comparison to ice structure in other products

There are a number of other freezing methods used in food processing, and the ice morphology formed by these processes may differ from that seen shown in the electron-micrographs in this chapter. The ice morphology of products frozen by the continuous tubular freezer consists of dendritic crystals at the wall, with radial columnar crystals growing toward the centre of the plug. The crystals may once again become dendritic at the centre of the tube as the ice growth rate increases again (discussed in section 8.6.5.2). The ice structure is solely a result of the product and the operational parameters of the freezer and the absence of any external mixing or scraping devices.

One of the most common products made by a continuous freezing method is Ice-cream. Ice-cream is a multiphase product with ice crystals, fat crystals and air bubbles in a continuous phase of unfrozen ice-cream mix. These ice crystals are typically disc-shaped[11] in the final product. The crystals form as dendrites on the cooled wall of the freezer, which has a temperature of approximately -20°C. These dendrites are removed by the scraper and mixed into the bulk where they become rounded by recrystallisation, isomass rounding, and related processes[12]. The air injection typical to ice-cream also reduces the 'hardness' of the mixture, which is also controlled by controlling the temperature of the semi-frozen mixture.

Scraped surface freezers are similar to ice-cream freezers in that dendritic ice is formed at the cooled wall before being broken off and transported to the bulk by the scraper, where crystals become rounded by various ripening processes[11].

Freeze crystallisers aim to form very pure ice, and to achieve this they grow ice with a very low v_f. Progressive freeze crystallisers achieve this by having low heat transfer rates at the wall to form bulk layer of pure ice[13]. Suspension freeze crystallisers aim to have a high crystallisation rate to ensure larger growth area and low v_f[14]. This is achieved by separating nuclei formation (which occurs in a scraped surface heat exchanger which forms a large population of crystal nuclei) and crystal growth (which occurs slowly in a separate vessel, or in a separate volume of the scraped surface freezer). Ice crystals formed are rounded and have minimal solute incorporation.

The closest analogue to this freezer in terms of ice morphology are freezers where is ice formed on cooled surfaces and allowed to grow for an extended time period without mechanical disturbance, such as falling film or drum freezers. Falling film freezers have been found to generate a similar ice structure, with ice crystal size increasing as a layer of ice forms between the cooled surface and the freezing product[15]. The continuous tubular freezer was conceived after studies intended to understand the ice growth morphologies in a falling film freezer.

8.5 Optimisation and Scaling

8.5.1 System Heat and Mass Flow

A schematic illustrating the heat and fluid and mass flows that occur during the steady state formation of a frozen milk plug is shown in Figure 8-13.

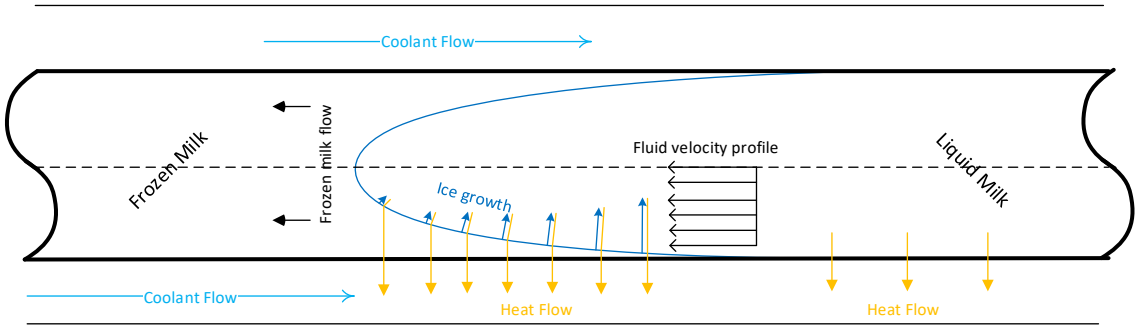

Figure 8-13: Heat and mass flows in continuous tube freezer. The ice profile is expected to show a parabolic profile as shown in by the blue line. This is distinct from the fluid velocity profile as indicated by the parallel arrows. For initial analysis this profile is assumed to be uniform.

The flowrates are low, and the flow is laminar for all tested and simulated systems (ranging from Re=3 in the smallest-scale tests to Re=400 for the largest simulation).However, rather than the fluid having a parabolic velocity profile characteristic of Poiseuille flow, it is assumed for the purposes of this chapter that a uniform velocity profile exists due to the frozen plug ahead of the liquid milk. In reality, flow patterns will be more complex and there may also be radial mixing resulting from convection driven by the temperature gradients in the freezer. Convection would be more predominant as diameter increases.

Heat should flow in a predominantly radial direction, due to the significantly smaller distance radially vs longitudinally, and the high heat transfer driving force due to the flow of coolant around the tube.

Ice grows radially inwards, aligned with the heat flow. The ice growth rate should decrease initially as the thickness of the ice layer increases, before increasing again as the area of interface decreases at the centre of the plug. As a result, the initial dendritic morphology transitions to a columnar ice morphology. This ice layer would not possess a “sharp” interface such as would be found in pure water or on a cooled tube operating as a progressive freeze-concentrator[16], rather the interface would very likely be a “mushy” layer of mixed ice and unfrozen solution trapped between ice columns.

Partial differential models describing heat and mass flow within the system can be used to optimise the product and coolant flows to allow the greatest throughput for a given geometry, and a preliminary one is presented in section 8.6.

8.5.2 Surface Finish

It may be possible to reduce the adhesion strength between the frozen milk plug and the inner surface of the tube by altering the surface properties of the tube. Examples of these alterations include:

1. Reducing the surface roughness by mechanical polishing
2. Reducing the surface roughness by electro-polishing.
3. Modifying the surface to have a lower surface energy via coating with low surface energy chemicals.
4. Ion-beam indentation [17].

These modifications may reduce the force required to extrude the frozen product and the pump pressure requirement. This would reduce the energy costs of operating the freezer and may decrease the capital expenditure, if the cost of surface coating is offset by lowered pump requirements. The results of initial pilot trials indicate that the freezer is feasible without surface modification to standard heavy gauge stainless steel piping. The technical readiness of these modifications should be monitored and may be implemented as they become feasible.

8.5.3 Product and Coolant Temperatures

Heat exchangers (HEX) can be broadly classified as cross flow, co-current flow, or counter-current flow. The two types applicable to the operation of the continuous freezer are co-current and counter-current.

In co-current flow, the fluid in both the hot side and cold side of the HEX enter at the same end, and the flow to the exit is parallel. The temperature difference is greatest at the entry to the HEX and smallest at the exit. The exit temperature of the hot side cannot be lower than the exit temperature of the cold side.

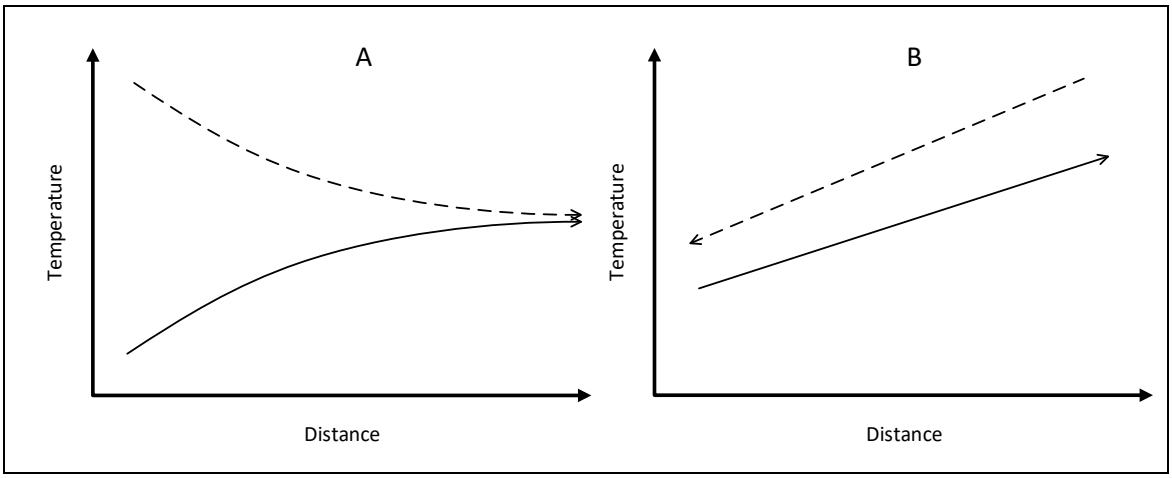

Figure 8-14: Temperature profiles in A: a co-current HEX, and B: a counter-current HEX

In a counter-current arrangement the hot and cold fluids enter at different ends of the HEX, and the temperature difference across the heat exchanger is constant. The log-mean temperature difference (LMTD) is higher, and this makes a counter-current arrangement most efficient for a given area and heat transfer coefficient. The hot side outlet temperature can be lower than the cold side outlet temperature. The temperature-distance profiles characteristic of a counter-current heat exchanger are shown in Figure 8-14 B.

For the tubular freezer under discussion the thermal profiles will deviate from the ideal, due to the phase change of the water in milk.

While a counter-current arrangement is most efficient from a thermal design perspective it may not be the most effective. A co-current arrangement is attractive for this application as it allows for a closer approach to the desired final temperature. Because the adhesion force appears to increase as temperature decreases, it is important to control where heat flow occurs and ensure that temperatures at the wall at the freezer exit are not too cold, or ice fraction too high.

While co-current flow reduces the average temperature difference and increases the required heat transfer area, heat transfer enhancements on the coolant side of the tube can increase the overall heat transfer coefficient and reduce the area required.

As control of the wall temperature of the freezer outlet is vital to its performance, a co-current flow pattern allows for monitoring and control of the coolant temperature at this point and was chosen for current embodiments of the freezer.

8.5.4 Heat Transfer Enhancements.

Heat transfer can be controlled in different sections by modifying the external geometry of the tube, or by altering the flow path of liquid coolant surrounding the tube. These heat transfer enhancements reduce the effective thermal resistance and therefore increase the heat transfer for a given area and temperature difference.

Heat transfer enhancements work by increasing the effective heat transfer area, such as extended surfaces or fins, or decreasing the thickness of the boundary layer by increasing turbulence near the heat exchanger walls, such as turbulators or swirl generators[18]. The Thermal Performance Factor (TPF) describes the effectiveness of enhancements as the ratio of heat transfer increase to friction increase:

$$\eta = \frac{\frac{Nu}{Nu_0}}{\left(\frac{f}{f_0}\right)^{1/3}} \tag{8-1}$$

Heat transfer enhancements can also be classified as active, passive or compound[19]. Active methods involve some external device augmenting heat transfer by vibrating the surfaces, pulsing the fluid flow, stirring the fluid, inducing fluid flow by electrostatic fields, or removing evolved vapours to reduce the insulating effect of gas. Passive devices were discussed above, and compound devices are combinations of the two other approaches.

Heat transfer enhancements can also be selectively added to areas of the tube where increased heat transfer is desired, or to compensate for low temperature differences near the freezer exit.

At Bi>1.0 coolant side heat transfer enhancements lose effectiveness. The Biot number for all realistic film heat transfer coefficients is significantly greater than unity, for both fully solid and fully liquid tube contents, for larger diameter tubes, indicating that internal thermal gradients will be significant, as will internal resistance to heat flow. The Biot number only approaches unity for small diameter freezers with low film heat transfer coefficients: Bi=1 for a 5mm diameter tube, full of liquid product with k=0.5 $Wm^{-1}K^{-1}$, and cooled with h=200 $Wm^{-2}K^{-1}$. For a 20mm diameter tube, full of liquid product with k=0.5 $Wm^{-1}K^{-1}$, and cooled with a more likely h=1000 $Wm^{-2}K^{-1}$, Bi=20, indicating that a significant internal heat gradient would exist.

The current embodiment of the freezer uses passive devices to enhance heat transfer performance to allow for shorter freezer lengths and reduced operating pressures.

8.5.5 Coolant Selection

In the system, there are two broad classes of refrigerant which can be used: A primary refrigerant, boiling at the exterior surface of the freezer tubes, or a secondary refrigerant, such as a glycol solution, which is cooled by an external chiller unit.

A primary refrigerant will generally have a higher coolant-side heat transfer coefficient than a secondary coolant, as heat is transferred by boiling, rather than convection[20], however this may be of limited benefit for larger diameter tubes where Bi >> 1.0.

A secondary refrigerant can have a cross-flow, counter-current or co-current flow direction, as discussed above. While the temperature of the coolant will not necessarily be constant across the length of the freezer tube, and the coolant-side heat transfer coefficient will likely be lower than with a primary refrigerant, a secondary refrigerant can serve as a store of cold energy. While the freezer is not operating, a large reservoir of secondary refrigerant can be cooled and then used during the freezing process, reducing the size of the chiller unit required.

A secondary refrigerant may also be easier to control, by throttling the refrigerant flow around the freezer tubes.

The current embodiment of the freezer uses a secondary coolant, as it simplifies system construction and control during system start-up, and the large internal resistance to heat transfer reduces the benefit of implementing a primary refrigerant system.

8.5.6 Scaling Relationships

The tube length and diameter will have a significant impact on the thermal performance of the system, and the pressure requirements to extrude the frozen product. Increasing the heat transfer area by increasing the tube diameter is possible. However, the characteristic distance of the system increases with the diameter, increasing the resistance to heat transfer to the centre of the system, making this method less efficient than increasing tube length. The amount volume of product to be frozen per unit heat transfer area will also increase as diameter increases, a larger diameter tube will require a longer residence time for freezing to occur.

Increasing the heat transfer area by increasing tube length maintains the characteristic distance of the system and therefore the resistance to heat transfer does not increase with increased heat transfer area. The surface area of the product/wall interface increases linearly with increased heat transfer surface area. The ratio of cross-sectional area to interfacial area increases linearly with increased length, so the increase in extrusion pressure requirement should be directly proportional to the increase in heat transfer area.

The relationships between length, diameter, and operating conditions are discussed in this section. These relationships may prove useful for preliminary calculations, optimisation studies, and scaling-up from experimental small-scale data, and studying the maximum capacity practical for single tube elements. For more in-depth design work, 2D or 3D numerical heat transfer equations, coupled with finite element modelling of the physical properties of the system should be used.

8.5.6.1 Residence Time

A given volume of milk must reside in the tube for a sufficient length of time to allow sufficient heat removal from said volume to freeze the milk to the desired final ice fraction.

$$Heat\ required\ to\ freeze\ volume\ of\ milk = Heat\ removed\ via\ heat\ transfer \tag{8-2}$$

$$L_{tube}\pi r_{tube}^2 \rho_{product} \Delta H_{fus} X_{ice,f} = 2L_{tube}\pi r_{tube}\phi_q \tau \tag{8-3}$$

This gives a relationship for the mean residence time, τ:

$$\tau = \frac{r_{tube}\rho_{product}\Delta H_{fus}X_{ice,f}}{2\phi_q} \quad (8\text{-}4)$$

8.5.6.2 Radius and Required Pressure.

Described in equation (7-6). The pressure required for extrusion for a constant length, temperature and set of fluid properties is inversely related the radius of the freezer : $P_{liquid} \propto \frac{1}{r_{tube}}$

8.5.6.3 Heat Transfer, Residence Time, Length and Pressure

The required length of the tube can be calculated from the residence time and the superficial velocity in the tube as follows

$$\dot{v_s} = \frac{\dot{m}_{product}}{\rho_{product}\pi r_{tube}^2} \quad (8\text{-}5)$$

$$L_{tube} = \dot{v_s}\tau \quad (8\text{-}6)$$

Tube length can be expressed as a function of fluid properties, heat transfer properties, tube radius, and product flowrate:

$$L_{tube} = \frac{\Delta H_{fus}X_{ice,f}\dot{m}_{product}}{2\pi r_{tube}\phi_q} \quad (8\text{-}7)$$

If it is assumed that the system is designed so that the length of the frozen plug is a constant fraction of the total tube length, and this fraction is invariant with changes to radius, flowrate and average heat flux, then the pressure required for product extrusion can be estimated by combining equations (7-1), (7-2), and (7-5) and equation (8-7):

$$L_{plug} = X_{plug}L_{tube} \quad (8\text{-}8)$$

$$P_{liquid} = \frac{2K_{adhesive}L_{plug}}{r_{tube}} \quad (8\text{-}9)$$

$$P_{liquid} = \frac{2K_{adhesive}X_{plug}\dot{m}_{product}\Delta H_{fus}X_{ice,f}}{\pi\phi_q r^2} \quad (8\text{-}10)$$

It can be clearly seen from equation (8-10) that for a given flowrate through a tube, latent heat requirements and adhesion strength, the pressure requirement is inversely proportional to the product average heat flux and the square of the radius.

This relationship between heat flux, and tube radius will be the key focus for optimisation of the system.

8.5.7 Satisfying Scaling Relationships and Design Constraints.

The relationship between mass flow, heat flux, radius and required pressure applies to a single tube. The most effective method of scaling up for higher product throughputs is likely to be finding the optimum combination of mass flow, radius and heat flux achievable for the selected product and coolant method and construct multiples of this tube. The pressure requirement for several identical tubes in parallel is identical for a single tube, and the flow rate increases linearly with increased tube numbers. The power requirement for a pump is

proportional to the product of flowrate induced and pressure developed. Higher pressure pumps, valves and fittings and controls increase cost and complexity more than simply increasing the flowrate requirement of the pump.

Several possible embodiments of a multiple tube design are shown in Figure 8-24 A-C. Multiple tubes may be operated in parallel. These tubes may be each fed by individual pumps, or from a manifold fed by a single pump. The tubes may each be individually isolated by valves to allow for operation at off-design conditions.

A further possible arrangement is to construct the system so an internal tube runs coolant through the centre of the product zone, this annular arrangement is shown in Figure 8-24 D. This reduces the characteristic distance for a given cross-sectional area, however the perimetric area will increase when compared to a circular cross section of identical product flow area. The relationship described by equation (8-10) can be updated to calculate the pressure requirement for an annular heat transfer arrangement, where r_2 and $r_1$are the exterior and interior dimensions of the annulus which contains the product:

$$P_{liquid} = \frac{2K_{adhesive}X_{plug}\dot{m}_{product}\Delta H_{fus}}{\pi\phi_q(r_2^2 - r_1^2)} \quad (8\text{-}11)$$

8.6 Numerical Modelling of a Continuous Tubular Freezer

In order to assist in the design of a commercial prototype tube freezer a mathematical model of heat flow and phase change within the tube was developed.

This model was intended primarily as a “ball-parking” effort to allow basic dynamics and ice growth rates to be investigated, and provide sizing information for the design of a heavily instrumented full-scale prototype. Data gathered from this future prototype could be used to support a more detailed modelling effort, which includes the effect of phenomena that have been omitted in this model.

8.6.1 Conceptual Design of Model

The system is modelled as a straight tube, with a 2-dimensional cylindrical geometry, an unsteady-state partial differential model is solved using an implicit solver, with a backwards time difference and 2nd order central finite-difference discretisation scheme. This is illustrated in Figure 8-13.

The latent heat of the transition is accounted for by the apparent heat capacity method which is appropriate given the wide range of temperatures over which the phase change transition occurs, the apparent heat capacity, enthalpy, and ice fraction follow the curves determined for whole ovine milk by DSC studies presented Chapter 6.

The phase change transition modelled does not include the total temperature range of the transition that was covered in Chapter 6. While whole ovine milk still has unfrozen water present until it reaches a maximally freeze concentrated stage at a temperature of -25°C, and the ideal storage temperature for long term storage is above -28°C, the tubular freezer as described in this chapter and the previous chapter requires a certain volume fraction of unfrozen liquid to operate. This unfrozen liquid is required to reduce the adhesion of the frozen plug to the freezer wall.

As a result, the system will not be modelled under conditions that will result in milk undergoing a complete freezing transition. Then effective end of freezing will be assumed to have occurred when the product reaches an apparent ice fraction that is sufficient for it to behave like a solid. If the apparent ice fraction is too low, the product will be too fragile for extrusion, or act as a slurry. From experimental work in Chapter 7, whole ovine milk was observed to extrude from

the small diameter freezer at an apparent ice fraction above 0.85, and this value was used when tracking ice front locations during this analysis.

8.6.1.1 Model Assumptions

The model is based on the following assumptions:

- Uniform velocity profile within the tube. This is justified in the solid as limited mixing is expected to occur, due to the lack of mixing force in the solid. The velocity profile in the liquid is assumed to be uniform to simplify model development, and as actual velocity profiles are not known.. The superficial velocities in the tube are low, and heat flows in the radial direction is high. Therefore, the effect of advection and a parabolic velocity profile is negligible when compared to conductive heat transfer.
- Mass-flow in the radial direction is negligible, and freeze concertation occurs within a matrix fixed in volume and location. There is no axial or radial anisotropy in the distribution of solutes. This is a simplifying assumption for these heat transfer calculations. There are likely some diffusive and convective mass flows occurring, but modelling these is beyond the scope of this work.
- Due to the wide distribution of the freezing transition there is no sharp phase change boundary, instead there is a mushy layer of increasing ice fraction as radial distance increases. Therefore, the central assumption of the Classical Stefan problem, a smooth phase-change boundary defined at the equilibrium freezing temperature, is not met. Methods which avoid the requirement to specify a sharp phase change front and better models the freezing behaviour of foods[21, 22].
- Coolant is a uniform temperature along the length of the simulated system-This is justified, as most experimental and pilot systems tested thus far have effectively run with a 'cross-flow' coolant path, where coolant flowrates and patterns are significantly in excess of product flows and so there is very little temperature difference between inlet and outlet.
- The overall heat transfer coefficient (U value) is constant along the length of the simulated system.
- The change in volume is ignored, as the radius is constrained and the change is gradual, contributing to an increase in the downstream velocity. The velocity change is minimal.
- As velocity is constant, and the velocity profile in constant, the movement of fluid can be simulated by iterating the position of each cell at each time step.

8.6.2 Mathematical Description

8.6.2.1 Product Side

The heat flows for a representative volume in the system, away from system boundaries can be described as follows:

$$Change\ in\ enthalpy = (Heat\ conducted\ in - Heat\ conducted\ out)$$

Or, in the form of a standard heat transfer equation:

$$\rho C_p \frac{\delta\theta}{\delta t} = \nabla(\kappa \nabla\theta) \tag{8-12}$$

In an axisymmetric cylindrical co-ordinate system this becomes:

$$\rho C_p \frac{\delta\theta}{\delta t} = \frac{\kappa}{r}\frac{\delta\theta}{\delta r} + \frac{\delta}{\delta r}\left(\kappa \frac{\delta\theta}{\delta r}\right) + \frac{\delta}{\delta z}\left(\kappa \frac{\delta\theta}{\delta z}\right) \tag{8-13}$$

The thermal conductivity k, varies with the increasing ice fraction X_{ice} in the node, as does the apparent heat capacity C_p. However, due to the arrangement of ice crystals parallel to the heat flow, the thermal conductivity will also be different in the axial (z) and radial (r) directions. The thermal conductivity of a one dimensional system with parallel solid and liquid layers can be modelled using the Kopelman(1966) model [23]. This model effectively reduces to a simple volumetric average rule in direction parallel to the ice and solid layers. Simple volumetric average rules for prediction of thermal conductivity have been used in literature modelling the heat flow during directional freezing [24, 25].

The solid volume fraction is calculated as follows:

$$\epsilon_s = \left[1 + \left(\frac{1}{X_{ice}} - 1\right)\left(\frac{\rho_s}{\rho_l}\right)\right]^{-1} \tag{8-14}$$

From this the thermal conductivity parallel to the layers k_{pa}, and perpendicular to the layers k_{pe}, are calculated:

$$\kappa_{pa} = k_l\left[1 - \epsilon_s\left(1 - \frac{\kappa_s}{\kappa_l}\right)\right] \tag{8-15}$$

$$\kappa_{pe} = \kappa_l\left[\frac{\kappa_s}{\epsilon_s\kappa_l + \kappa_s(1-\epsilon_s)}\right] \tag{8-16}$$

Heat transfer in the axial (z) direction occurs perpendicular to the ice layers, and the perpendicular thermal conductivity (k_{pe}) will be used. In the radial (r) direction, the parallel thermal conductivity (k_{pa}) will be used.

8.6.2.2 Coolant Side

For simplicity in the initial models , the coolant is assumed to have a significantly higher mass flow rate than the milk, so the coolant temperatures is uniform along the length of the simulated system, and there is a constant film heat transfer along the length of the tube.

8.6.2.3 Boundary Conditions

8.6.2.3.1 *Centreline of Tube: r=0.*

At $r = 0$, a singularity exists, as well as a symmetry boundary condition, this can be resolved by utilising L'Hôpital's rule:

$$\frac{1}{r}\frac{\delta\theta}{\delta r} \rightarrow \frac{\delta^2\theta}{\delta r^2} \tag{8-17}$$

$$\frac{\delta\theta}{\delta t} = \frac{\kappa}{\rho C_p}\left(2\frac{\delta^2\theta}{\delta r^2} + \frac{\delta^2\theta}{\delta z^2}\right) \tag{8-18}$$

8.6.2.3.2 *At Convective Boundary with Coolant*

At a node on the convective boundary $r = r_{max}$, heat is lost by convection to constant temperature coolant.

$$U(\theta_{coolant} - \theta_{rmax}) = -\kappa \frac{\delta\theta}{\delta r} \quad (8\text{-}19)$$

8.6.2.3.3 *At Tube Entry*

At the entry to the tube, $z = 0$ the product temperature is fixed.

$$\theta_{z=0} = \theta_{inlet} \quad (8\text{-}20)$$

8.6.2.3.4 *At Tube Exit*

The exit of the tube $z = z_{max}$, there is an insulated boundary:

$$\frac{\delta\theta}{\delta z} = 0 \quad (8\text{-}21)$$

8.6.2.4 Discretisation of Model

The model was discretised using a backwards time difference and a spatial 2nd order central difference scheme. Figure 8-15 illustrates a node used for the discretisation equation. This implicit method for solving the heat equation is numerically stable for all sizes of time step.

As thermal conductivity values at adjacent nodes may differ, the thermal conductivities between two adjacent nodes are evaluated at the mean temperature of these nodes [26].

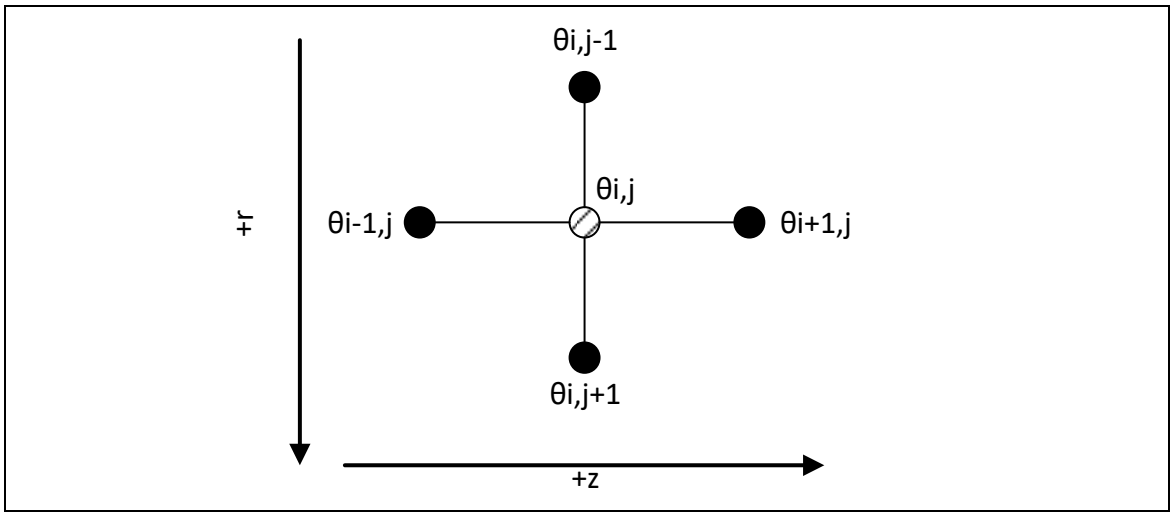

Figure 8-15: A node away from boundaries

8.6.2.4.1 *At a Node Away from Any Boundaries*

$$\frac{\delta^2\theta}{\delta r^2} = \frac{\theta_{i,j-1} - 2\theta_{ij} + \theta_{i,j-1}}{\Delta r^2} \quad (8\text{-}22)$$

$$\frac{1}{r}\frac{\delta\theta}{\delta r} = \frac{\theta_{i,j+1} - \theta_{i,j-1}}{2r\Delta r} \quad (8\text{-}23)$$

$$\frac{\delta^2\theta}{\delta z^2} = \frac{\theta_{i+1,j} - 2\theta_{ij} + \theta_{i-1,j}}{\Delta z^2} \quad (8\text{-}24)$$

$$\frac{\theta_{i.j}^{k+1}-\theta_{i.j}^{k}}{\Delta t}=\frac{\kappa_{pa}}{\rho C_p}\left(\frac{\theta^{k+1}{}_{i,j-1}-2\theta_{ij}^{k+1}+\theta_{i,j-1}^{k+1}}{\Delta r^2}+\frac{\theta_{i,j+1}^{k+1}-\theta_{i,j-1}^{k+1}}{2r\Delta r}\right)+\frac{\kappa_{pe}}{\rho C_p}\left(\frac{\theta_{i+1,j}^{k+1}-2\theta_{ij}+\theta_{i-1,j}^{k+1}}{\Delta z^2}\right) \tag{8-25}$$

8.6.2.4.2 *At a Node on the Convective Boundary*

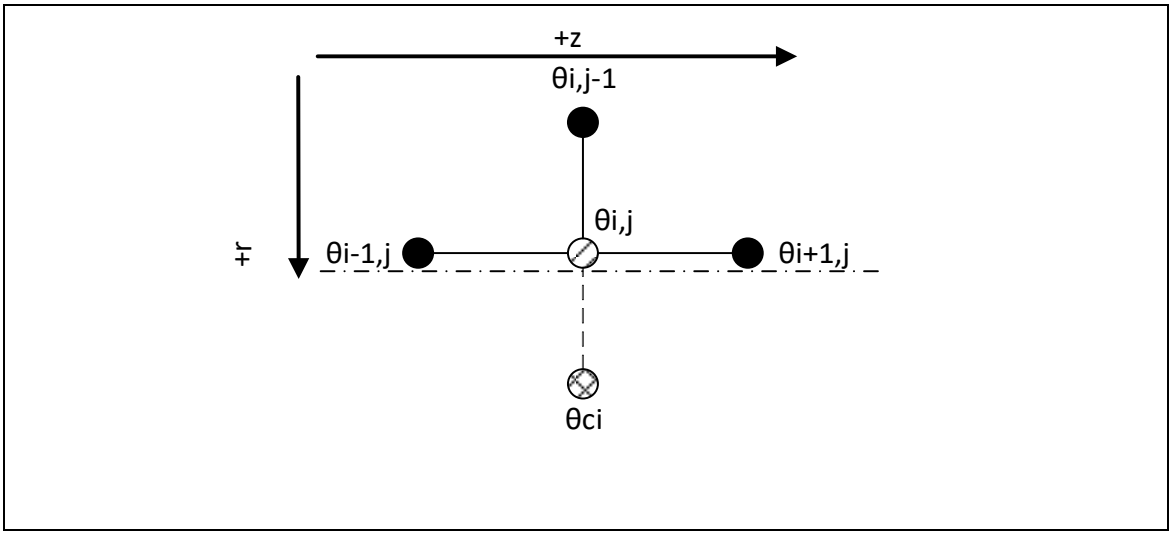

Figure 8-16: A node on the convective boundary between coolant and tube. R_{max} is located at the dotted line. The coolant node indicated by the cross-hatched dot is an imaginary node for programming purposes.

The boundary condition at these nodes is described in equation (8-19), it is discretised with a backwards difference in the radial direction and central difference in the axial direction as follows. $r_{j-\frac{1}{2}}$ is the radius halfway between the external node and the next interior node.

$$\frac{\theta_{i.j}^{k+1}-\theta_{i.j}^{k}}{\Delta t}=\frac{A_{r_{max}}}{V_{conv}}\frac{U}{\rho C_p}\left(\theta^{k}c_i-\theta_{i,j}^{k}\right)+\frac{A_{r_{j-\frac{1}{2}}}}{V_{conv}}\frac{K_{pa}}{\rho C_p}\left(\frac{\theta_{i,j-1}^{k+1}-\theta_{i,j}^{k+1}}{\Delta r}\right)+\frac{\kappa_{pe}}{\rho C_p}\left(\frac{\theta_{i+1,j}^{k+1}-2\theta_{ij}+\theta_{i-1,j}^{k+1}}{\Delta z^2}\right)$$
$$V_{conv}=\pi\left(r_{max}^2-r_{j-\frac{1}{2}}^2\right)\Delta z \tag{8-26}$$
$$A_{r_{max}}=2\pi\Delta z r_{max}$$
$$A_{r_{j-\frac{1}{2}}}=2\pi\Delta z r_{j-\frac{1}{2}}$$

8.6.2.4.3 *At a Node on the Tube Entry Boundary*

As the temperature is fixed, the discretisation at this boundary is simple:

$$\theta_{0,j}^{k+1}=\theta_{inlet} \tag{8-27}$$

8.6.2.4.4 *At a Node on the Tube Exit Boundary.*

In order to simulate an adiabatic boundary in the axial direction a synthetic node, $\theta_{i+1,j}$,is added and defined as:

$$\theta_{i+1,j}^{k+1} = \theta_{i,j}^{k+1} \tag{8-28}$$

Therefore, there is no heat flow in the axial direction as:

$$\kappa \frac{\delta\theta}{\delta z} = 0 \tag{8-29}$$

8.6.2.4.5 *At the Centre of the Tube, Where r=0.*

This can be written as follows, for programming at $r = 0$.

$$\frac{\delta^2\theta}{\delta r^2} = \frac{\theta_{i,j-1} - 2\theta_{ij} + \theta_{i,j-1}}{\Delta r^2} \tag{8-30}$$

$$\frac{\delta\theta}{\delta r} = 0, \qquad \frac{\theta_{i,j-1} - \theta_{i,j+1}}{2\Delta r} = 0, \qquad \theta_{i,j-1} = \theta_{i,j+1} \tag{8-31}$$

$$\frac{\delta^2\theta}{\delta r^2} = \frac{2\left(\theta_{i,j+1} - \theta_{i,j}\right)}{\Delta r^2}, at\ r = 0 \tag{8-32}$$

A discretisation for the $\frac{\delta^2\theta}{\delta r^2}$ term was given in equation (8-24). The full discretisation is given below:

$$\frac{4\kappa_{pa}}{\rho C_p}\frac{\left(\theta_{i,j+1}^{k+1} - \theta_{i,j}^{k+1}\right)}{\Delta r^2}, + \frac{\kappa_{pe}}{\rho C_p}\left(\frac{\theta_{i+1,j}^{k+1} - 2\theta_{ij}^{k+1} + \theta_{i-1,j}^{k+1}}{\Delta z^2}\right) = \frac{\theta_{i.j}^{k+1} - \theta_{i.j}^{k}}{\Delta t} \tag{8-33}$$

8.6.3 Solution Algorithm

The solution algorithm for the unsteady state model is shown in Figure 8-17.

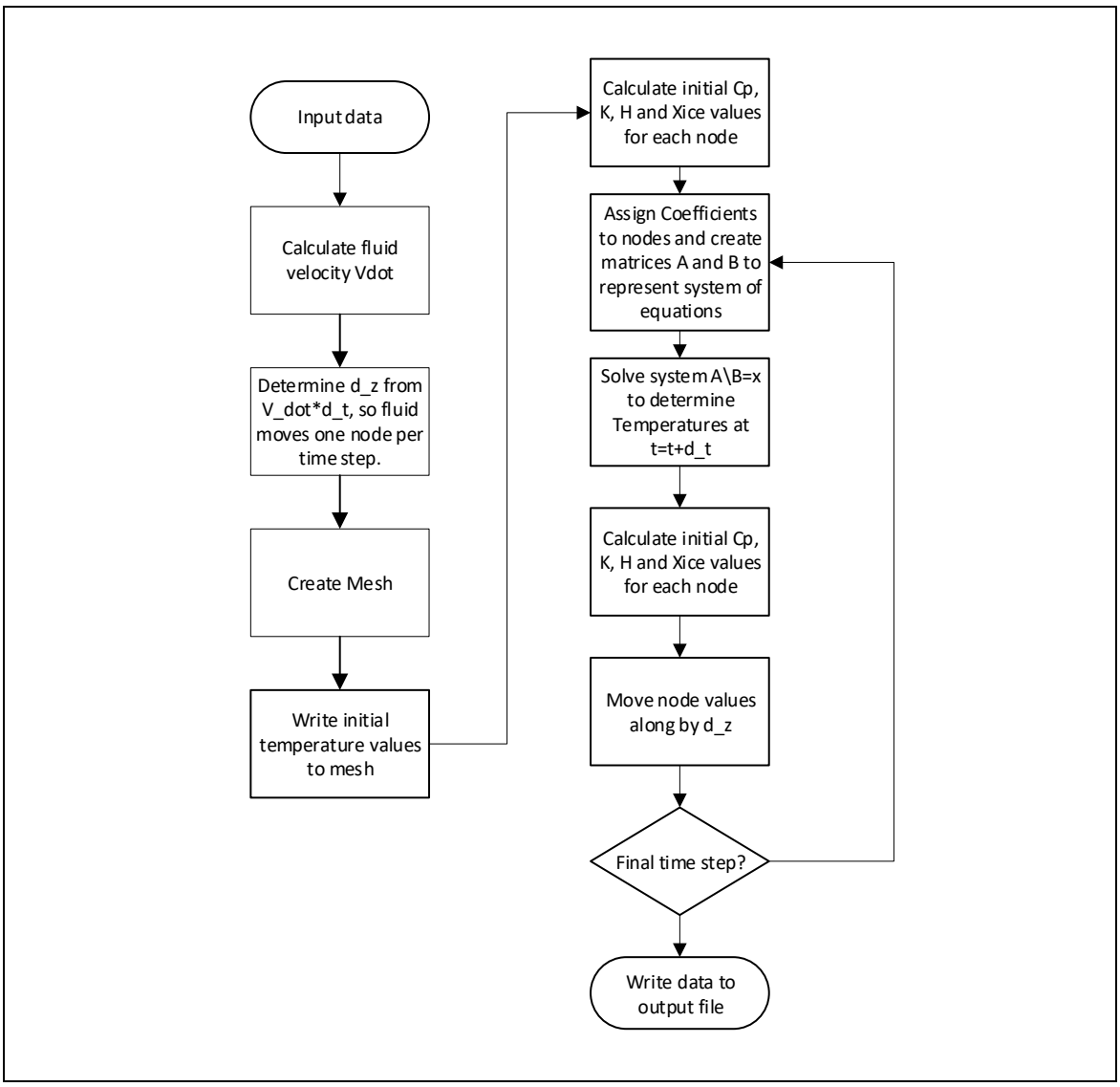

Figure 8-17: Solution algorithm for model

The model was programmed in MATLAB R2017b. Details of software are provided in section 2.11.

8.6.4 Model Input Parameters

The model was run with a range of input conditions. These are summarised in the Table 8-2:

Table 8-2: Initial conditions for model runs

Coolant Heat Transfer Coefficient ($Wm^{-2}K^{-1}$)	Inlet Temperature (°C)	Length (m)	Coolant Temperature (°C)	Product Flowrate ($kghr^{-1}$)	Tube Diameter (mm)
1100	4	25	-5	10	10
			-7.5	20	20
			-10	30	
			-12.5	40	
		40	-5	10	30
			-7.5	20	50
			-10	30	
			-12.5	40	

The coolant heat transfer coefficient is a typical value for liquid-liquid heat transfer in a tubular heat exchanger (Table 11-3, Perry's Chemical Engineers' Handbook, 7th ed.[27]). For detailed design this value should be replaced with one determined for the specific combination of coolant properties and tube exterior geometry selected.

The apparent heat capacity Cp over the temperature range of interest was determined from DSC data presented in Chapter 6 of this thesis, as was the apparent ice fraction over the temperature range. From these data the axial and radial thermal conductivities were calculated from equations (8-16)-(8-18). The apparent heat capacity includes the latent heat spread of the progressive freezing transition, and thus is significantly greater near the equilibrium freezing temperature. These values are shown in Figure 8-18.

Initial liquid phase conductivity above the freezing point was set as 0.55 $Wm^{-1}K^{-1}$, which is in the range of thermal conductivities reported for liquid milk[28], and aligns with values measured by the author using the transient hot-wire technique (not presented in this thesis). Solid phase thermal conductivity was set initially at 2.3 $Wm^{-1}K^{-1}$ at -35°C using a parallel model, and milk component thermal conductivities [23].

Thermal conductivity could be estimated in greater detail by incorporating the effect of varying solid and liquid composition on thermal conductivity. The solid and liquid phase composition will vary during the freezing process as a result of rejection of solutes from the growing ice front. However, for the purposes of this model this should be sufficiently accurate.

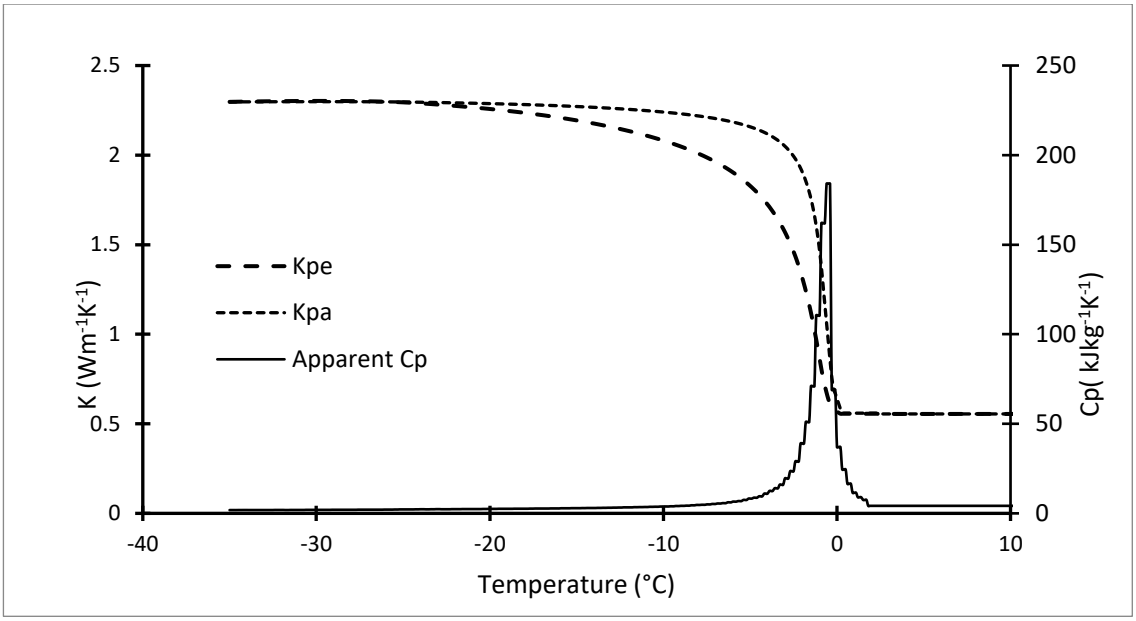

Figure 8-18: Curves of apparent heat capacity and axial (Kpe) and radial (Kpa) thermal conductivities. These were determined from the apparent ice fraction data presented earlier in the thesis. Thermal conductivities were determined by Kopelman's 1966 model for one-directional layered anisotropic materials.

8.6.5 Model Results

Implicit PDE solving algorithms are inherently stable for all time steps, however the truncation error of a backwards difference discretisation is a first order error, and scales with the time step. The relative error of the model was evaluated for a subsection of the total length at time steps from 0.25s to 15s. A timestep of 1 s was selected as being a compromise between reducing truncation error, and simulation time. There are no macro-scale heat transfer or phase transfer processes which are expected to occur within a single time step.

The required length is the length required for the ice fraction in the centre of the simulated zone across two successive axial nodes to differ by less than 1%, and be over 85% of the ice fraction at a simulated position from the inlet of 25m for 10 mm and 20 mm diameter, and 40m for 30 mm and 50 mm. The time to reach steady state after the application of cooling is determined as the time for the average temperature difference for each node across two time steps to be less than an absolute value of 0.001K.

The outputs of the modelling work are discussed in this section. The plots of temperature, and ice fraction and tables of required length and residence time are presented in the appendix of this chapter.

Contour plots of the temperature and ice fraction for freezers with a diameter of 10 mm, 20 mm, 30 mm, and 50mm are shown in Figure 8-26 to Figure 8-33, and the freezer conditions and required lengths, residence times, and average ice growth rate are shown in Table 8-3 to Table 8-6.

The contour plots represent an axisymmetric slice, with the centreline on the left and the coolant surface on the right. The fluid inlet is at the bottom and the outlet at the top.

Temperature and ice fraction plots are presented for steady-state operation.

The temperature profile and the ice fraction profile are roughly parabolic in shape.

8.6.5.1 Model Validation

8.6.5.1.1 *Comparison against analytical solutions and predictive equations.*

The required residence time were compared against simple predictive models for freezing time. The system was modelled as an infinite cylinder, and the freezing times were calculated using Plank's Equation[29], Pham's equation [30]and Salvadori and Mascheroni's equation[29].

The average absolute deviation between the residence time as predicted by the model and by the predictive equations was 10% for Pham's equation, 10% for Salvadori and Mascheroni's equation, and 15% for Plank's equation.

Figure 8-19 shows a scatter plot of the residence time predicted by the model in this chapter and freezing times as predicted by the above equations. Residence times measured in the commercial scale up times below are also highlighted.

The generally close agreement between the required residence times predicted by the model and the freezing times predicted by well-established analytical solutions indicate that the results should be suitable for the intended purpose of sizing a protype unit.

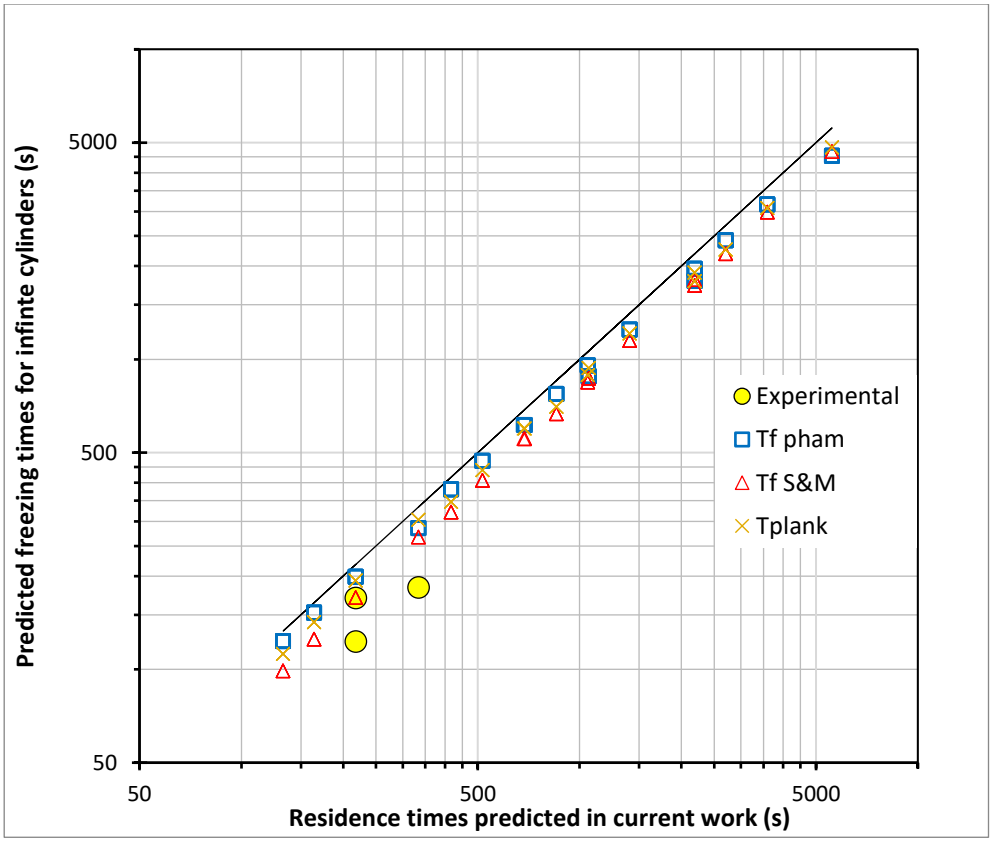

Figure 8-19:Residence time predicted by present work plotted against freezing times for infinite cylinders predicted by several equations. Residence times measured during scale-up trials are plotted as open circles.

8.6.5.1.2 *Comparison against commercial scale-up trials.*

While a full set of validation trials for the model presented was not possible due to time and material constraints, some limited validation can be done with data from experimental runs conducted on the 10.2 mm Spiral Freezer, and commercial scale-up work being conducted at the time of the writing of this thesis.

Experiments with the 10.2 mm Spiral Freezer were reported in Chapter 7. During operation at -5°C, with a cooled length of 4500 mm products were frozen with residence times of 123s to 184s. The throughput was approximately 6-8 $kghr^{-1}$.

Commercial scale-up trials were conducted by a partner company during the writing of this thesis. The trials were conducted using a freezer based off the designs presented in this thesis, and adapted the chiller unit described in Chapter 3 and the high-pressure feed system used for the 10.2 mm spiral freezer discussed in Chapter 7. These trials reported pulsed operation at a residence time of approximately 120-180s for a 12 mm ID freezer operating at -7°C for freezers with cooled lengths of 600 mm and 1200 mm. Cooled sections used spiral fins to increase coolant-side heat transfer coefficients.

These results are similar to the model results, which predicted required residence times of 210s for 10 mm ID freezers operating at -7.5°C.

Unfortunately, it was not possible to measure the internal temperature and ice profiles of the products during these freezer trials to validate the predicted temperature and ice profiles. Further work with specialised experimental equipment should be considered to validate the predictions made by this model.

8.6.5.2 Residence times and ice growth rates

The length required is primarily a function of flow through the tube, and the operating coolant temperature, which is a proxy for average heat transfer. This is expected from the scaling relationships described in section 5.7. The required lengths are plotted in Figure 8-20 as are the relationships between residence time and the heat fluxes and heat flows for different freezer diameters. As can be seen from plot C, the required residence time, is inversely proportional to the average heat flux and is directly proportional to the tube diameter. This agrees with the relationships shown in equation (8-4). Plot A indicates that the residence time is independent of flowrate and is instead proportional to the diameter and operating coolant temperature (related to heat flux).

Tables of the lengths and residence time for each freezer diameter and set of operating conditions are presented in the appendix.

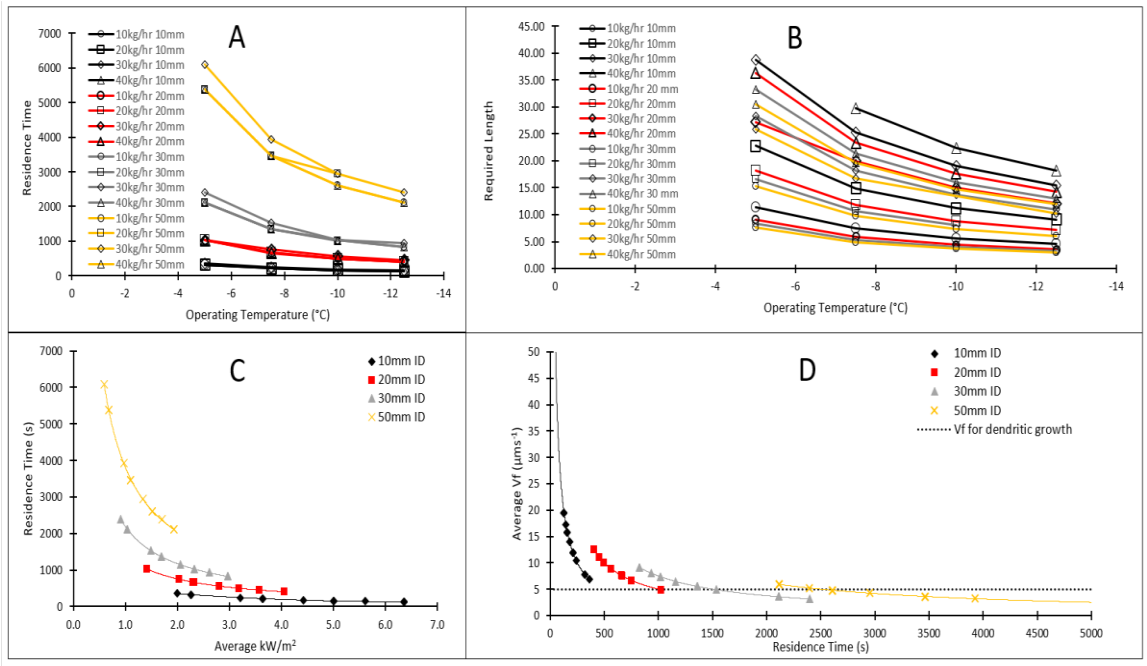

Figure 8-20: Various relationships between operating conditions as determined by numerical modelling. A: Residence time required as a function of flowrate, diameter, and operating temperature. B: Required length as a function of flowrate, diameter, and operating temperature. C: Residence time as a function of the average heat flux at the exterior of the tube and the interior diameter of the freezer. D: The average ice front velocity as a function of residence time, and the interior diameter. The dotted line represents the ice front velocity at which the interface morphology for whole ovine milk was observed to transition between columnar and dendritic forms, as discussed in section 4.4.2.2.

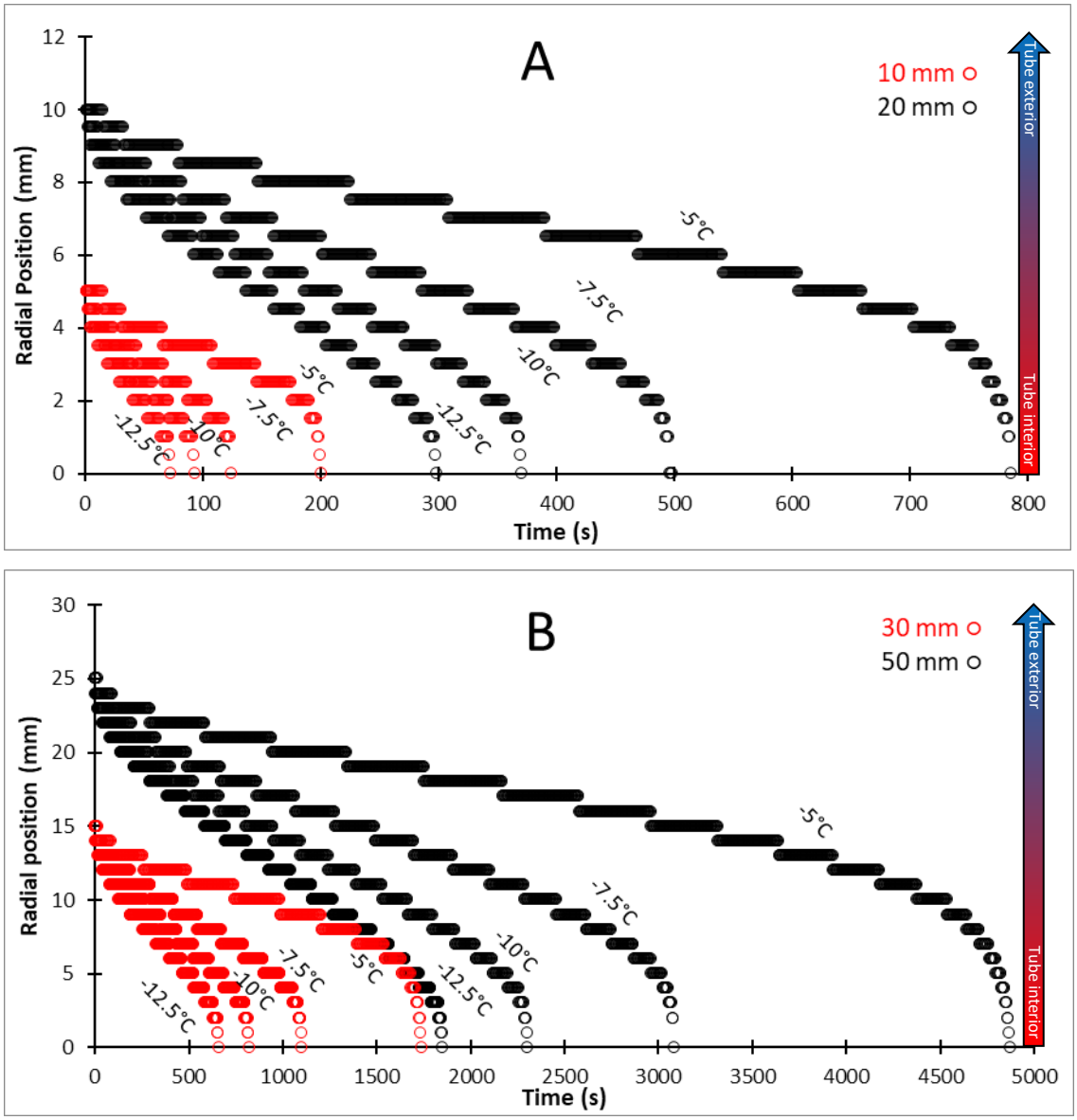

Figure 8-21: Radial position of ice front over time for all combinations of operating temperature and tube diameter. The radial direction of heat flow is indicated by the arrows at the right. Tube exterior is at the top of each graph, and tube interior is at the base.

For this analysis the ice front is assumed to be located within a node when the nodal apparent ice fraction first reaches 85%. The nodal position of the ice front as a function of time is shown in Figure 8-21. There is a high ice growth rate at the exterior of the tube where the product is in direct contact with the cooled wall. This ice growth rates decreases as an ice layer increases the resistance to heat flow from the ice front. However, near the interior of the tube there is a very high ice growth rate as the ratio of the area in contact with coolant and the area of the ice front becomes very large and overcomes the heat transfer resistance resulting from the increased thickness of the ice layer.

This shown mathematically in equation , where the ice growth rate is shown as a function of the radius of the plug, the radial position of the interface and the properties of the ice and latent heat, and the temperature difference across the cylindrical ice layer. The first term dominates as r_{ice} tends to zero: $\lim_{r_{ice}\to 0} \frac{1}{r_{ice}} = \infty$. The second term dominates as r_{plug}/r_{ice} tends to one: $\lim_{r_{plug}/r_{ice}\to 1} \frac{1}{\ln(r_{plug}/r_{ice})} = \infty.$

$$v_f = \frac{1}{\rho \Delta H_{fus} r_{ice}} \cdot \frac{\Delta\theta \kappa_{ice}}{\ln\left(r_{plug}/r_{ice}\right)} \quad (8\text{-}34)$$

This can also be seen in the steady-state contour plots of ice fraction and temperature shown in the appendix. The isothermal contours, and shape of the freezing front at steady-state show different gradients to the horizontal at different radial positions. If the gradient of the ice front is high, this indicates that the radial position of the ice front is moving slowly with respect to its longitudinal displacement caused by product flow through the freezer. Areas of the freezer with a low gradient indicate that the radial position of the ice front rapidly with respect to the product flow through the freezer. This is seen at the exterior and interior of the freezer, where the ice front velocity is greatest.

As discussed in Chapter 4, feature size decreases as ice front velocity increases. The higher ice growth rates at the exterior predicted by this modelling, explain the ice morphology seen in Cryo-SEM images presented earlier in this chapter showing ice crystals which are smaller at the exterior of the frozen plug than the interior.

The average ice growth rate (v_f) determined from the diameter of the system and the residence time. v_f ranges from 4.6 µms^{-1} for initial conditions of 10 kghr^{-1} product, with a coolant temperature of -5°C and a freezer diameter of 50mm, to 38.9 µms^{-1} for a coolant temperature of -12.5°C and a freezer diameter of 10mm. This is plotted for the simulation results in Figure 8-20 D. As can be seen in Figure 8-20 D, for large diameters, and long residence times, the average v_f can drop below the v_f required for dendritic ice formation. At intermediate distances from the exterior of the tube ice growth rates will be lower than the average, and these low ice growth rates may result in gross separation of solutes at the interior.

At large diameters, this separation of solutes at the interior may cause the underlying principle of the freezer to break down.

8.6.5.3 Required Operating Pressure

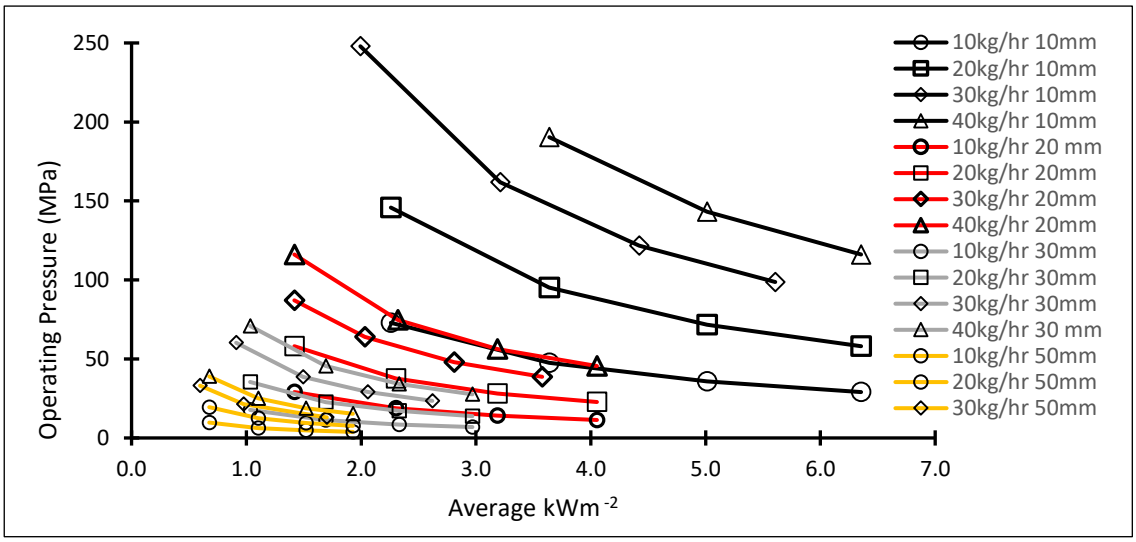

Figure 8-22: The required operating pressure as a function of heat transfer to the exterior of the freezer, flowrate and freezer internal diameter, assuming an apparent adhesion strength of 14 kPa, and sufficient tube length to reach steady state by the outlet.

Assuming a realistic apparent adhesion strength as measured in section 7.4.4, the graph shown in Figure 8-22 can be constructed, which shows maximum expected operating pressures as a function of flowrate, heat fluxes, and interior diameter of the tube. As can be seen in the figure larger diameter tubes have lower operating pressures for a given flowrate and exterior heat

transfer rate, as expected from the relationships between pressure and cross-sectional area given in Chapter 7. The operating pressure also decreases as the average heat flux increases, due to higher average heat fluxes decreasing the required length of the freezer and required area for heat transfer for a given flowrate. The reduced area leads to a lower ice adhesion strength.

However, as the average ice growth rate decreases as the tube diameter increases, as discussed in section 8.6.5.2 , the tube diameter cannot be arbitrarily increased in order to decrease operating pressure, as this will reduce ice growth rates to the point where solute separation could occur. As a result, a balance must be struck between maximising ice growth rates and decreasing operating pressure.

An upper limit of 20-30mm may be appropriate to maintain high ice growth rates while minimising operating pressures as much as practicable. The pressure requirements also indicate that the best option to achieve a given flowrate for a particular diameter may be to parallelise freezer tubes, rather than extend the tube length. More detailed modelling which incorporates mass transfer phenomena should be carried out on this system to expand upon the heat transfer modelling. This mass transfer modelling will allow for optimisation of the diameter of the system, aiming to maximise diameter while maintaining v_f sufficient to prevent solute separation.

Optimisation of heat transfer will also be effective at reducing the required freezer length, and required pressure, while maintaining high ice growth rates.

As the operating pressure is directly related to the adhesion, then icephobic coating should effectively reduce the required operating pressure. There are literature reports of smooth icephobic surfaces which reduce adhesion by a factor of 10, when compared to structural materials such as steel [31]. The application of such a material to the interior of the freezer should result in a decrease in operating pressure and should be investigated further.

8.7 Commercial Prototype Design

8.7.1 P&ID

A P&ID describing a possible prototype is shown in Figure 8-23. The system depicted in the P&ID performs the following function in a food-safe environment:

1. Freezes a product supplied from a cooled vat.
2. Transfers the frozen product to a storage container in a cooled food-safe environment.
3. Stores frozen product in the cooled food-safe environment.
4. Contains equipment to CIP the cooled vat, the freezer, and the transfer lines between equipment.
5. Contains instrumentation to monitor the system for process control and for food safety assurance.
6. Allows safe and effective start-up and shut-down of the system.

The freezing process occurs as follows. The product to be frozen is stored in the feed tank (E-1) until required. This tank is cooled by a coolant loop circulated by a pump (E-10), and stirred by an agitator (E-8). The temperature in the feed tank is monitored and controlled by a temperature controller (I-5), which allows cold coolant into the coolant loop by actuating a solenoid valve (V-5). The coolant bleeds through a check valve (V-4), into the coolant loop and out through an orifice to the coolant return line. The feed tank can be isolated with a manually operated butterfly valve (V-1).

The product passes a manually operated freezer isolation valve (V-2) and is pumped by a positive displacement pump (E-2) into the freezer (E-3) where it is frozen as described earlier in this

chapter. The positive displacement pump is driven by a variable speed drive (E-4 and I-1), which is controlled in part by a pressure indicator and controller (I-2), which allows flow only while a sufficient pressure drop is detected across the freezer, indicating that frozen product is present at the outlet. Coolant flow to the chiller is controlled by a solenoid valve (V-6), with an additional start-up loop which allows finer control of coolant flow on start-up by actuating a solenoid valve (V-19). To drain the system of product during shutdown, or wash fluid after CIP, a fail open solenoid valve (V-3) is provided, which flows to a tundish.

Frozen product flows through a cooled large diameter tube to the storage container (E-5), in a cooled insulated space. The temperature at the outlet of this tube is monitored and used for control (I-3). This space is cooled by a fin fan heat exchanger (E-6). Coolant to this heat exchanger is controlled by a solenoid valve (V-7), which is controlled by a temperature controller monitoring the temperature in the cooled space (I-4). This space is maintained at a positive pressure to prevent contamination of the frozen product. External air is driven through a HEPA filter (E-17) by a forward curved blower (E-16), and then supplied to the storage space.

Coolant is supplied by a coolant supply pump (E-9), and its temperature is maintained by a chiller on the coolant return line (E-15) which is controlled by a temperature controller (I-7) on the insulated coolant reservoir (E-7) . A coolant bypass valve (V-8) allows coolant to be recirculated during start-up.

Water for CIP and for general purposes is supplied through a pair of ball valves (V-18 and V-17) The CIP tank (E-11) can be isolated by a butterfly valve (V-9), and drained to a tundish through a normally closed butterfly valve (V-10). The CIP pump (E-13) transfers the solution through an inline heater (E-12), controlled by a downstream temperature controller (I-9). CIP flow can be diverted to the feed tank by a normally closed valve (V-11), and into the main freezer line by a normally closed valve (V-12). A drain valve (V-13) and CIP return valve (V-14) are also located nearby. A CIP bypass valve is located around the high-pressure pump (V-16). This allows for sufficient velocity in the freezer tube to achieve CIP. The high-pressure pump(E-2) discharge can be cycled back to the suction side during CIP to ensure it is well cleaned. CIP fluids are returned to the CIP tank by a pump (E-14).

Some valving may be replaced by a flow-plate in order to reduce capital costs, and ensure product security without the expense of double block-and-bleed valving. These valves are outlined on the P&ID.

8.7.2 Food Safety

Food safety is ensured by a hierarchy of precautions. The primary factor that ensures food safety is the development of effective procedures and practices which ensure food safety is maintained. These are collectively referred to as “good operating practices” and can include:

- Monitoring animal health.
- Cleanliness during collection of milk.
- Development and implementation of effect SOPs for system operation.
- Effective record-keeping, and prompt handling of deviations from normal operation.
- Effective tracking of product.

The first layer of physical protection is that system is designed to operate at temperatures that minimise the growth of microbial hazards. The mechanical design of the system is the next level of protection. The system will be designed and constructed to relevant standards, in order to reduce the possibility of microbial growth in the system. The system will have smooth internal surfaces with no dead legs or crevices in order to reduce stagnant areas, and to allow simple cleaning. It is also designed to drain by gravity to reduce the water activity in the environment. All food contact surfaces will be made from non-corroding materials, food grade to prevent the

formation of rough areas where bacterial growth can easily occur. The system is isolated from the atmosphere by two concentric barriers. The primary barrier is the freezer construction, which does not allow liquid product to contact the atmosphere during operation. The secondary barrier is the system housing, which is intended to operate at a positive pressure over the external environment, prevent ingress of dirt or bacteria. The system is protected against coolant leaks by two main principles, the first is the extreme pressure difference between the product environment during freezing and the coolant loop. If a leak develops in the coolant/product barrier, the product will leak into the coolant rather than the other way around. The second is that only food-safe coolants will be used.

The system will also be cleaned regularly by CIP, and is designed to allow this to be effective at destroying microbial contamination, and the removal of biofilms, or dirt and other substrates that support microbial growth. This cleaning is a necessary component of food safety, but cannot entirely compensate for failings in other levels of protection.

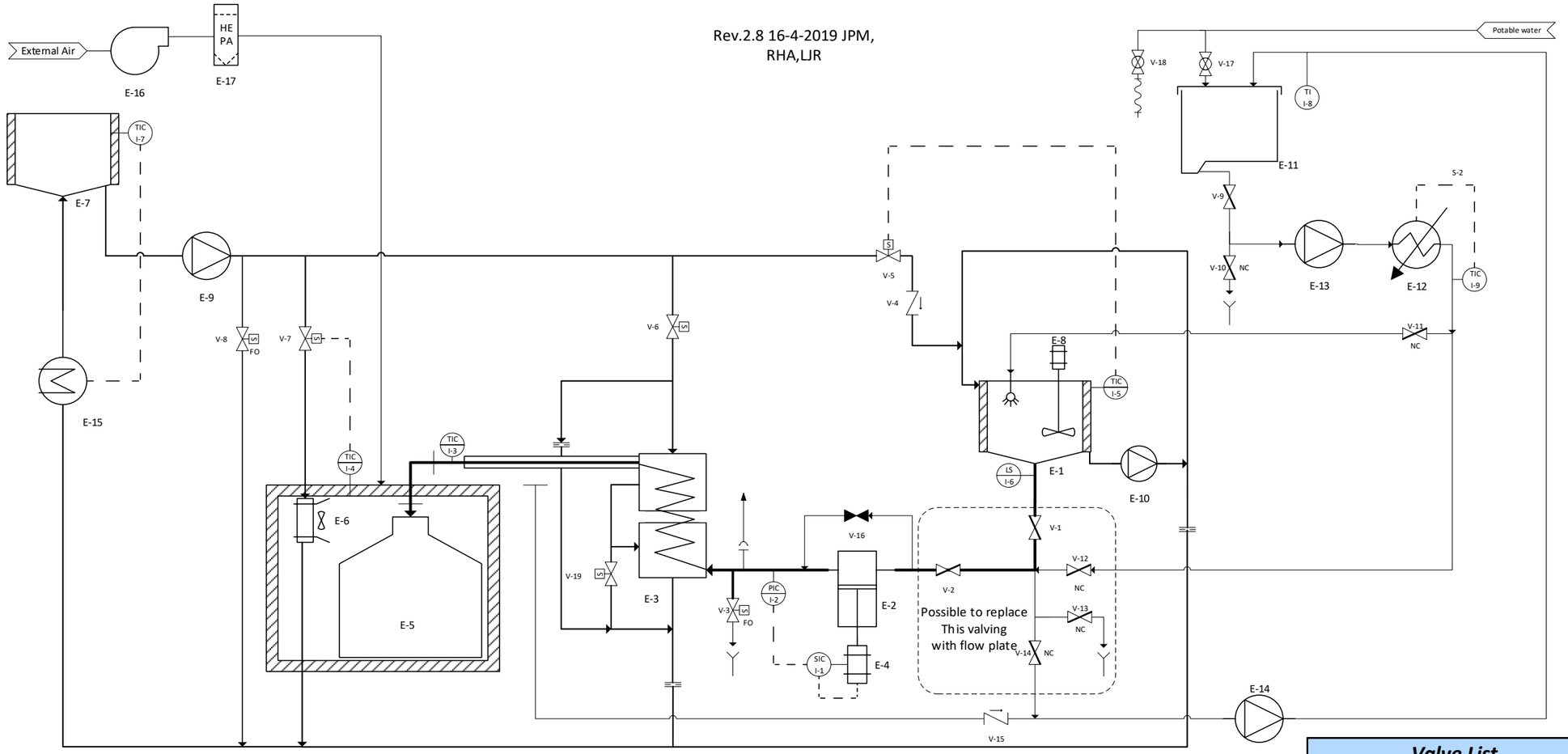

Equipment List

Displayed Text	Description
E-1	Product feed tank
E-2	High pressure feed pump
E-3	Spiral freezer
E-4	Feed pump motor+ VSD
E-5	Storage IBC
E-6	Air cooling unit
E-7	Coolant storage tank
E-8	Feed tank agitator
E-9	Coolant supply pump
E-10	Feed tank coolant circulator pump
E-11	CIP tank
E-12	CIP supply heater
E-13	CIP supply pump
E-14	CIP return pump
E-15	Coolant chiller
E-16	Forward curved blower
E-17	Hepa air filter

Instrument List

Displayed Text	Description	Service
I-1	Variable speed drive	
I-2	Pressure Controller	Product
I-3	Freezer exit temperature	Product
I-4	Temperature controller	Chilled Air
I-5	Temperature controller	Product
I-6	Level controller	Product
I-7	Supply Temperature	Coolant
I-8	Return temperature	CIP
I-9	Supply temperature controller	CIP

Lines

Product

Coolant

Air

CIP

Signals

Valve List

Displayed Text	Description
V-1	Feed tank isolation
V-2	Freezer isolation
V-3	Fail-open drain valve
V-4	Coolant injection check valve
V-5	Tank coolant CV
V-6	Chiller coolant CV
V-7	Air coolant CV
V-8	Coolant bypass valve
V-9	CIP tank isolation
V-10	CIP tank drain
V-11	CIP spray isolation
V-12	CIP supply isolation valve
V-13	System drain valve
V-14	CIP return
V-15	CIP return check valve
V-16	Pump CIP bypass
V-17	CIP fill valve
V-18	Washdown hose valve
V-19	Freezer startup bypass valve

Figure 8-23: A P&ID drawing of a commercial prototype, displaying all equipment, vessels, instruments, valves, services, lines, and signals required.

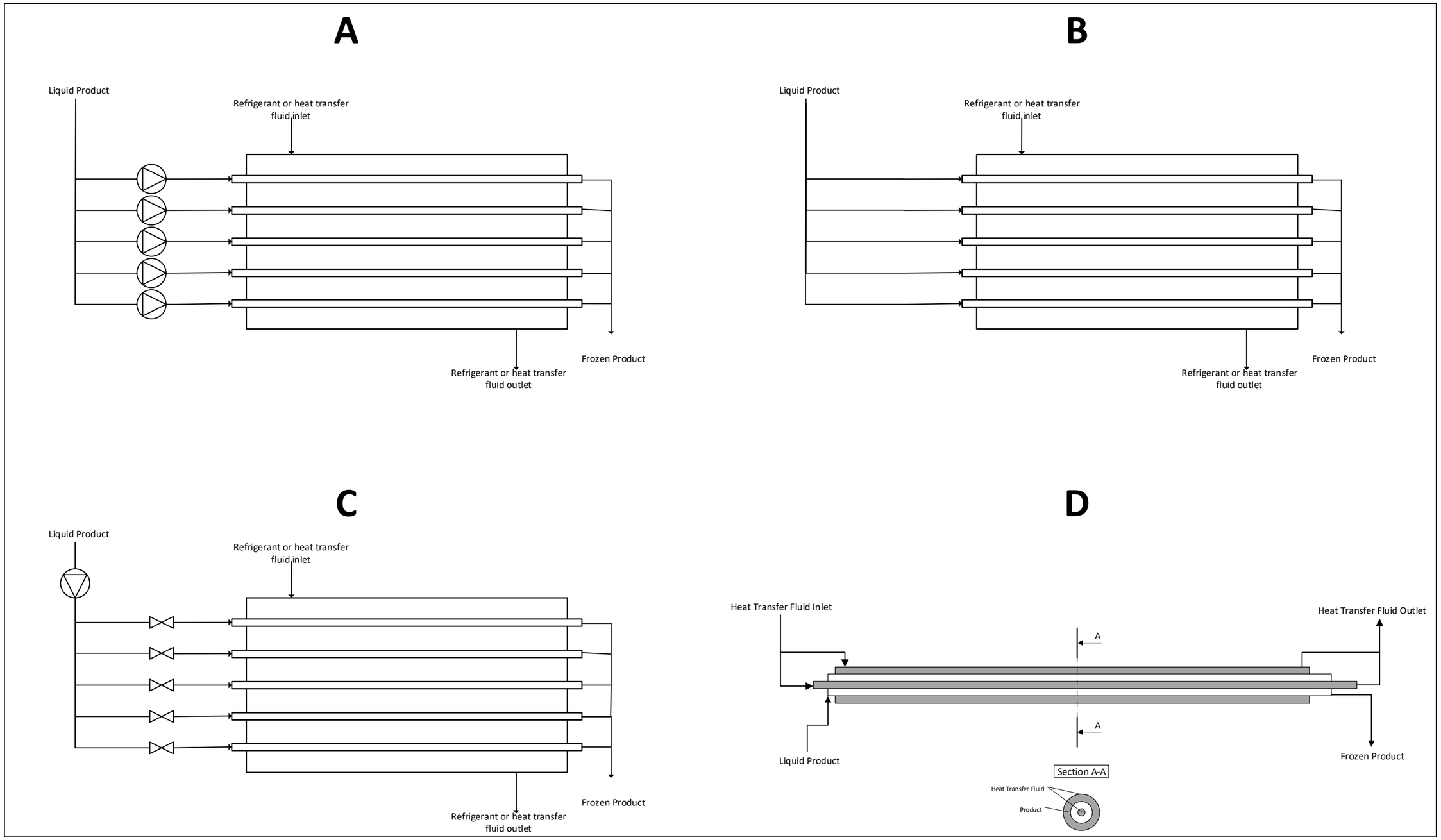

Figure 8-24: Several possible embodiments for a product and coolant flow in a continuous freezer. A) Multiple tubes driven by multiple pumps. B) Multiple tubes driven by one pump, no valving. C) Multiple tube from one pump, isolation valving. D) Annular arrangement of coolant and product

8.7.3 System Layout

Two possible layouts for a commercial prototype system are shown in Figure 8-25, one layout (B) incorporates a single intermediate bulk container(IBC) for storage of frozen product, the other (A) is designed to hold 3 IBCs to allow for loading, or possibly swing-over filling of more than one IBC in an operating session.

Each layout illustrates possible locations for the freezer, high pressure pump, coolant reservoir, air handling units to supply cool filtered air to the unit and preserve positive pressure, CIP systems to clean the system, valving and control locations and refrigeration systems, and access for product and operators.

The expected operating temperatures are also shown on the layouts. IBC storage areas are to be kept below -25°C, and are insulated from the rest of the unit. The area containing the freezer and coolant bank is to be kept at approximately 4°C, and is insulated from the external environment and the CIP area. The CIP area is kept separate to minimise heat transfer between the tank of hot CIP fluid and the rest of the unit.

Some valving may be replaced by a flow-plate in order to reduce capital costs.

This page intentionally left blank.

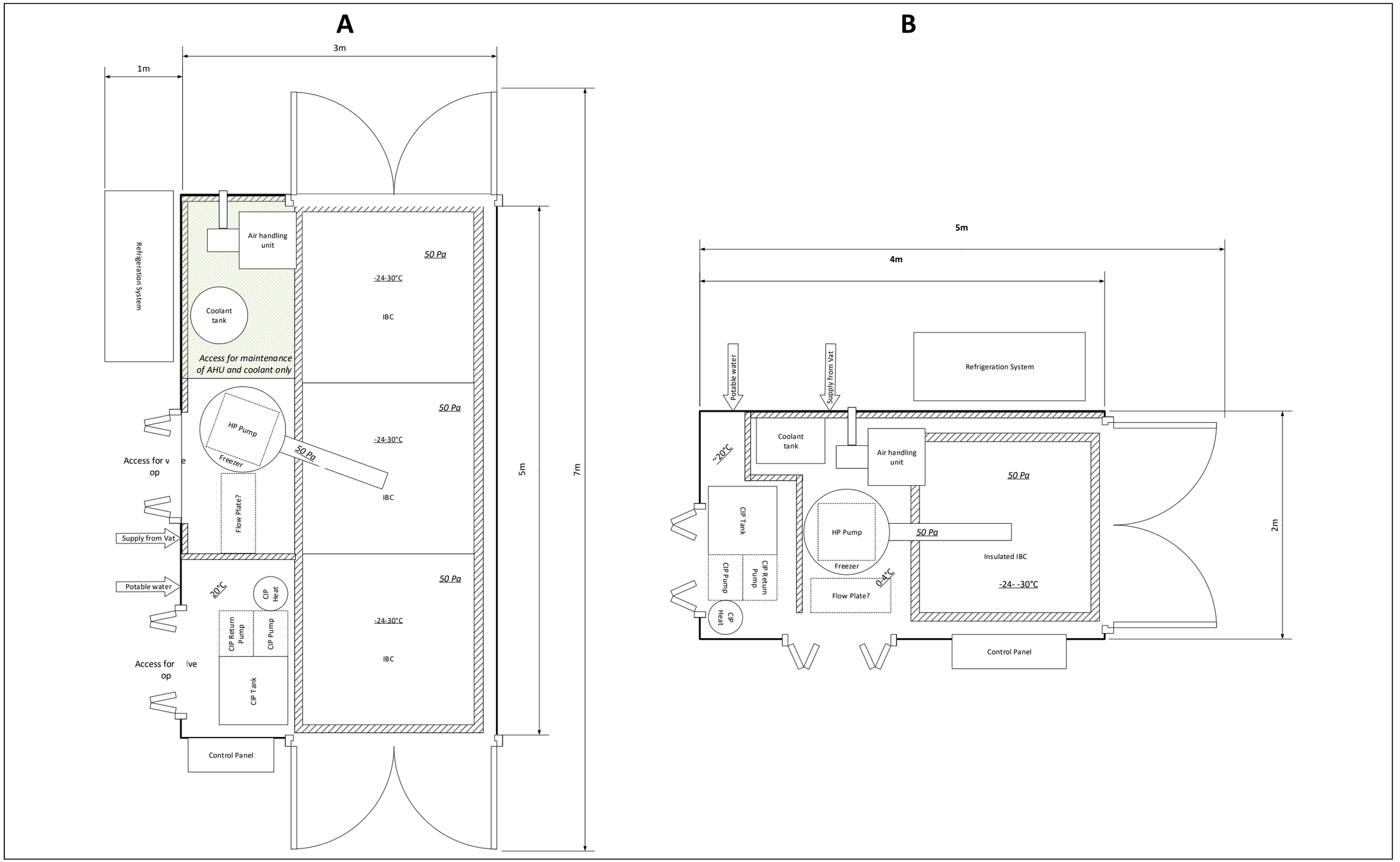

Figure 8-25: Two layouts for a commercial prototype system. A is a maximal embodiment with three IBCs stored. B is a minimal embodiment designed to fit within a 20ft shipping container and a single IBC. All items are realistic sized and located in appropriate locations. Temperatures and pressures required within areas of the system to ensure food safety are shown.

This page intentionally left blank.

8.7.4 Suitability for On-Farm Use

8.7.4.1 Reliability

The system is expected to have a high level of reliability in an on-farm environment. There are minimal moving parts involved, and the parts that are moving are high pressure, which are commercial off-the-shelf units. Thermal cycling is minimised, which should reduce reliability and lifespan issues resulting from this. Further reliability can be achieved by replacing automated valving with a flow plate, at the cost of a small increase in labour requirements. Electronic interlocking can be implemented to prevent common errors that may lead to damage of the system, such as operating pumps against a closed valve.

8.7.4.2 Ease of Use

Minimal product handling will be required. The product can be taken directly from storage vats to final storage vessels (as a frozen product), without any requirement for human interaction.

The system is suitable for high levels of automation, allowing unattended operation. If utmost reliability is wanted, then a small decrease in automation will be encountered, as automated valving will be replaced by a flow plate. However, this will only require human interaction during start-up and CIP.

8.8 Conclusions

The ice morphology in frozen plugs studied using optical microscopy and scanning electron cryo-microscopy showed predominantly radial ice crystals, as expected from the heat fluxes involved. Ice crystals at the exterior of the frozen plugs, near the product/wall interface were significantly smaller than those further in. Crystals were columnar in form, with the long axes radially aligned. The ice morphology supports the hypothesis that trapped solutes at the frozen product/wall interface reduce the apparent ice adhesion of the product ,relative to that of pure ice, by reducing the fraction of ice adhered to the surface, and allowing movement of ice crystals relative to one-another, rather than serving as an uninterrupted lubricating layer between the frozen plug and the wall.

Ice morphology was similar for samples of raw ovine milk, and single-strength orange juice. Glass regions were seen in between ice crystals, indicating that these regions were liquid before immersion in LN_2. There was no lactose crystallisation observed in raw ovine milk samples, and there was limited sugar crystallisation observed in orange juice samples.

Scaling relationships suggested that the required residence time, and therefore required freezer length would decrease as the radial heat flux of the system increased, and the radius decreases. Numerical modelling showed that, in agreement with these relationships, required residence times decreased with increased heat flux and decreased radius. The pressure required for extrusion increases as radius decreases. The average freezing front velocity decreases as the freezer tube radius and residence time increases. If this drops below the velocity required for gross solute entrapment, then the operating principle of the freezer breaks down. The balance of required pressure and required ice growth rate gave a probable maximum practical diameter for the simulated conditions of 30 mm.

8.9 List of Symbols

Symbol	Description	Units
A	Heat transfer area in freezer	m^2
f	Friction factor	
f_0	Original friction factor	
$F_{adhesive}$	Force of product adhesion.	N
$F_{extrusion}$	Force required to extrude frozen product	N
$K_{adhesive}$	Coefficient of product adhesion/ adhesion strength	Nm^{-2}
L_{plug}	Length of frozen product plug	m
L_{tube}	Length of freezer tube	m
$\dot{m}_{product}$	Product flowrate in freezer	kgs^{-1}
Nu	System Nusselt number	
Nu_0	Unenhanced Nusselt Number	
P_{liquid}	Liquid product pressure in freezer	Pa
$\dot{Q}$	Heat flow in freezer	W
r_1	Internal radius of annular freezer	m
r_2	External radius of annular freezer	m
Ra	Surface roughness	μm
r_{ice}	Radius of ice front location	m
r_{plug}	Radius of frozen product plug	m
r_{tube}	Internal radius of freezer tube	m
T	Temperature	$°C$
U	Overall heat transfer coefficient in freezer	$Wm^{-2}K^{-1}$
v_f	Freezing front velocity.	
$\dot{v}_s$	Superficial product velocity in freezer	ms^{-1}
$X_{ice,f}$	Final ice fraction in product	$g_{ice}/g_{freezable\ water}$
X_{plug}	Fraction of freezer length frozen	
X_s	Solids fraction in product	$g/g_{product}$
ΔH_{fus}	Latent heat of freezing	Jkg^{-1}
η	Thermal performance factor	
κ_{ice}	Thermal conductivity of ice	$Wm^{-1}K^{-1}$
$\rho_{product}$	Average density of product in tube	kgm^{-3}
σ	Surface energy	Jm^{-2}
τ	Residence time	s
ϕ_q	Heat flux in freezer	Wm^{-2}
For PDE model		
$A_{r_{max}}$	Area of convective boundary	m^2
$A_{r_{j-\frac{1}{2}}}$	Area of shell between convective boundary node and next radial node	m^2

C_p	Heat capacity of substance	$Jkg^{-1}K^{-1}$
i, j, k	Node indices in the radial, longitudinal and time directions.	
r	Radial position in cylindrical co-ordinates	m
r_{max}	Radial position of convective boundary	m
$r_{j-\frac{1}{2}}$	Radial position $\Delta r/2$ from convective boundary	m
t	Time	s
V_{conv}	Volume of node at convective boundary	m^3
X_{ice}	Ice fraction	$g_{ice}/g_{freezable\ water}$
γ	Angular position in cylindrical co-ordinates	m
z	Longitudinal position in cylindrical co-ordinates	m
ϵ_s	Solid phase volumetric fraction	
θ	Temperature	$°C$
κ	Thermal conductivity	$Wm^{-1}K^{-1}$
κ_l	Liquid phase thermal conductivity	$Wm^{-1}K^{-1}$
κ_{pa}	Thermal conductivity parallel to layers	$Wm^{-1}K^{-1}$
κ_{pe}	Thermal conductivity perpendicular to layers	$Wm^{-1}K^{-1}$
κ_s	Solid phase thermal conductivity	$Wm^{-1}K^{-1}$
ρ	Density of substance	kgm^{-3}
ρ_l	Liquid phase density	kgm^{-3}
ρ_s	Solid phase density	kgm^{-3}

8.10 References

[1] J. Schindelin *et al.*, "Fiji: an open-source platform for biological-image analysis," *Nat Methods,* vol. 9, no. 7, pp. 676-82, 2012.

[2] I. Arganda-Carreras *et al.*, "Trainable Weka Segmentation: a machine learning tool for microscopy pixel classification," *Bioinformatics,* vol. 33, no. 15, pp. 2424-2426, 2017.

[3] J. Shaocheng, G. Qi, and X. Bin, "Porosity dependence of mechanical properties of solid materials," *Journal of Materials Science,* Article vol. 41, no. 6, pp. 1757-1768, 2006.

[4] T. Loho *et al.*, "A tensile technique for measuring frozen products adhesion strength: Application to stainless steel/frozen milk interaction," *Journal of Food Engineering,* p. 109772, 2019.

[5] W. Wolczynski, A. Ivanova, P. Kwapisiński, and E. Olejnik, *Structural Transformations Versus Hard Particles Motion in the Brass Ingots*. 2017.

[6] A. Lasalle *et al.*, "Ice-templating of alumina suspensions: Effect of supercooling and crystal growth during the initial freezing regime," *Journal of the American Ceramic Society,* Article vol. 95, no. 2, pp. 799-804, 2012.

[7] T. Waschkies, R. Oberacker, and M. J. Hoffmann, "Investigation of structure formation during freeze-casting from very slow to very fast solidification velocities," *Acta Materialia,* vol. 59, no. 13, pp. 5135-5145, 2011.

[8] M. Kochs, C. Körber, I. Heschel, and B. Nunner, "The influence of the freezing process on vapour transport during sublimation in vacuum-freeze-drying of macroscopic samples," *International Journal of Heat and Mass Transfer,* vol. 36, no. 7, pp. 1727-1738, 1993.

[9] G. Blond, "Mechanical properties of frozen model solutions," *Journal of Food Engineering,* vol. 22, no. 1, pp. 253-269, 1994.

[10] X. Xu, G. Jeronimidis, A. G. Atkins, and P. A. Trusty, "On the yield stress of frozen sucrose solutions," *Journal of Materials Science,* Article vol. 38, no. 2, pp. 245-253, 2003.

[11] E. M. Drewett and R. W. Hartel, "Ice crystallization in a scraped surface freezer," *Journal of Food Engineering,* Article vol. 78, no. 3, pp. 1060-1066, 2007.

[12] K. L. K. Cook and R. W. Hartel, "Mechanisms of Ice Crystallization in Ice Cream Production," *Comprehensive Reviews in Food Science and Food Safety,* vol. 9, no. 2, pp. 213-222, 2010.

[13] G. Petzold and J. M. Aguilera, "Centrifugal freeze concentration," *Innovative Food Science & Emerging Technologies,* vol. 20, pp. 253-258, 2013.

[14] R. W. Hartel and L. A. Espinel, "Freeze Concentration of Skim Milk," *Journal of Food Engineering,* vol. 20, no. 2, pp. 101-120, 1993.

[15] F. L. Moreno *et al.*, "Volatile compounds, sensory quality and ice morphology in falling-film and block freeze concentration of coffee extract," *Journal of Food Engineering,* vol. 166, pp. 64-71, 2015.

[16] O. Miyawaki, L. Liu, Y. Shirai, S. Sakashita, and K. Kagitani, "Tubular ice system for scale-up of progressive freeze-concentration," *Journal of Food Engineering,* vol. 69, no. 1, pp. 107-113, 2005.

[17] J. Leveneur, J. Morel, M. Trompetter, R. Archer, T. Loho, and J. Kennedy, "Reducing frozen dairy product adhesion by controlling the surface properties of stainless steel," presented at the 9th International Conference on Advanced Materials and Nanotechnology (AMN9), Wellington, NZ, 2019. Poster.

[18] C. Maradiya, J. Vadher, and R. Agarwal, "The heat transfer enhancement techniques and their Thermal Performance Factor," *Beni-Suef University Journal of Basic and Applied Sciences,* vol. 7, no. 1, pp. 1-21, 2018.

[19] M. Sheikholeslami, M. Gorji-Bandpy, and D. D. Ganji, "Review of heat transfer enhancement methods: Focus on passive methods using swirl flow devices," *Renewable and Sustainable Energy Reviews,* vol. 49, pp. 444-469, 2015.

[20] W. M. Rohsenow, J. P. Hartnett, and Y. I. Cho, Eds. *Handbook of heat transfer*, 3rd ed. New York: McGraw-Hill, 1998.

[21] A. C. Cleland and R. L. Earle, "A comparison of methods for predicting the freezing times of cylindrical and spherical foodstuffs," *Journal of Food Science,* https://doi.org/10.1111/j.1365-2621.1979.tb03422.x vol. 44, no. 4, pp. 958-963, 1979.

[22] Q. T. Pham, "Modelling heat and mass transfer in frozen foods: a review," *International Journal of Refrigeration,* vol. 29, no. 6, pp. 876-888, 2006.

[23] S. Rahman, *Food Properties Handbook*. CRC Press, 1995.

[24] S. M. Miller, X. Xiao, and K. T. Faber, "Freeze-cast alumina pore networks: Effects of freezing conditions and dispersion medium," *Journal of the European Ceramic Society,* vol. 35, no. 13, pp. 3595-3605, 2015.

[25] U. G. Wegst, M. Schecter, A. E. Donius, and P. M. Hunger, "Biomaterials by freeze casting," *Philos Trans A Math Phys Eng Sci,* vol. 368, no. 1917, pp. 2099-121, 2010.

[26] C. Bonacina and G. Comini, "On the solution of the nonlinear heat conduction equations by numerical methods," *International Journal of Heat and Mass Transfer,* vol. 16, no. 3, pp. 581-589.

[27] R. H. Perry, D. W. Green, and J. Maloney, O., *Perry's Chemical Engineers' Handbook Seventh Edition*. New York: McGraw-Hill, 1999.

[28] L. A. Minim, J. S. R. Coimbra, V. P. R. Minim, and J. Telis-Romero, "Influence of Temperature and Water and Fat Contents on the Thermophysical Properties of Milk," *Journal of Chemical & Engineering Data,* vol. 47, no. 6, pp. 1488-1491, 2002.

[29] A. E. Delgado and D. W. Sun, "Heat and mass transfer models for predicting freezing processes - a review," *Journal of Food Engineering,* vol. 47, no. 3, pp. 157-174, 2001.

[30] Q. T. Pham, "Simplified equation for predicting the freezing time of foodstuffs," *International Journal of Food Science & Technology,* https://doi.org/10.1111/j.1365-2621.1986.tb00442.x vol. 21, no. 2, pp. 209-219, 1986.

[31] K. Golovin, S. P. R. Kobaku, D. H. Lee, E. T. DiLoreto, J. M. Mabry, and A. Tuteja, "Designing durable icephobic surfaces," *Science Advances,* vol. 2, no. 3, 2016.

8.11 Appendix

Contour plots of the temperature and ice fraction for freezers with a diameter of 10 mm, 20 mm, 30 mm, and 50mm are shown in Figure 8-20 to Figure 8-27, and the freezer conditions and required lengths, residence times, times to reach steady-state and average ice growth rate are shown in Table 8-3 to Table 8-6.

The contour plots represent an axisymmetric slice, with the centreline on the left and the coolant surface on the right. The fluid inlet is at the bottom and the outlet at the top.

Temperature and ice fraction plots are presented for steady-state operation.

Table 8-3: Results from runs of model for a 10mm diameter freezer.

Run	Diameter (mm)	Coolant Temperature (°C)	Product Flow ($kghr^{-1}$)	Required Length (m)	Required residence time (s)	V_f average (μms^{-1})
A	10	-5	10	11.4	322	15.5
B	10	-5	20	22.8	322	15.5
C	10	-5	30	34.2	322	15.5
D	10	-5	40		0	
E	10	-7.5	10	7.4	210	23.8
F	10	-7.5	20	14.9	210	23.8
G	10	-7.5	30	22.00.3	210	23.8
H	10	-7.5	40	29.7	210	23.8
I	10	-10	10	5.6	158	31.6
J	10	-10	20	11.2	158	31.6
K	10	-10	30	16.8	158	31.6
L	10	-10	40	22.4	158	31.6
M	10	-12.5	10	4.5	128	39.0
N	10	-12.5	20	9.1	128	39.0
O	10	-12.5	30	13.6	128	39.0
P	10	-12.5	40	18.1	128	39.0

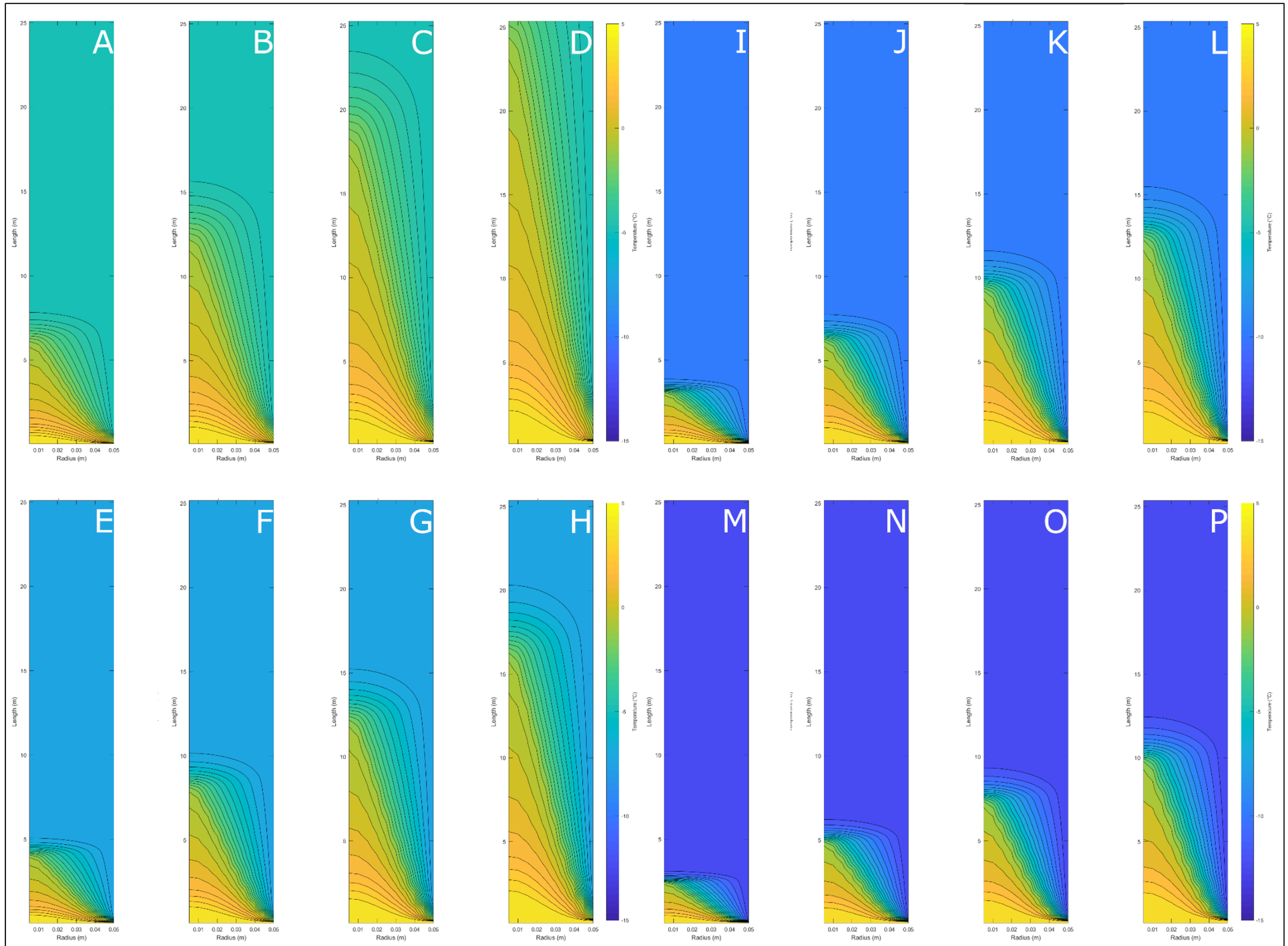

Figure 8-26: Temperature profiles in a freezer with a length of 25m and a diameter of 10mm at steady state, or after 1200s of operation, whichever is shorter. Conditions corresponding to each letter are given in Table 8-3. The colour scale is constant for all runs, ranging from +5°C to -15°C. The image is a 2-dimensional axisymmetric slice with the centre of the modelled region on the left, and the coolant boundary on the left. The fluid inlet is at the base and the product outlet is at the top.

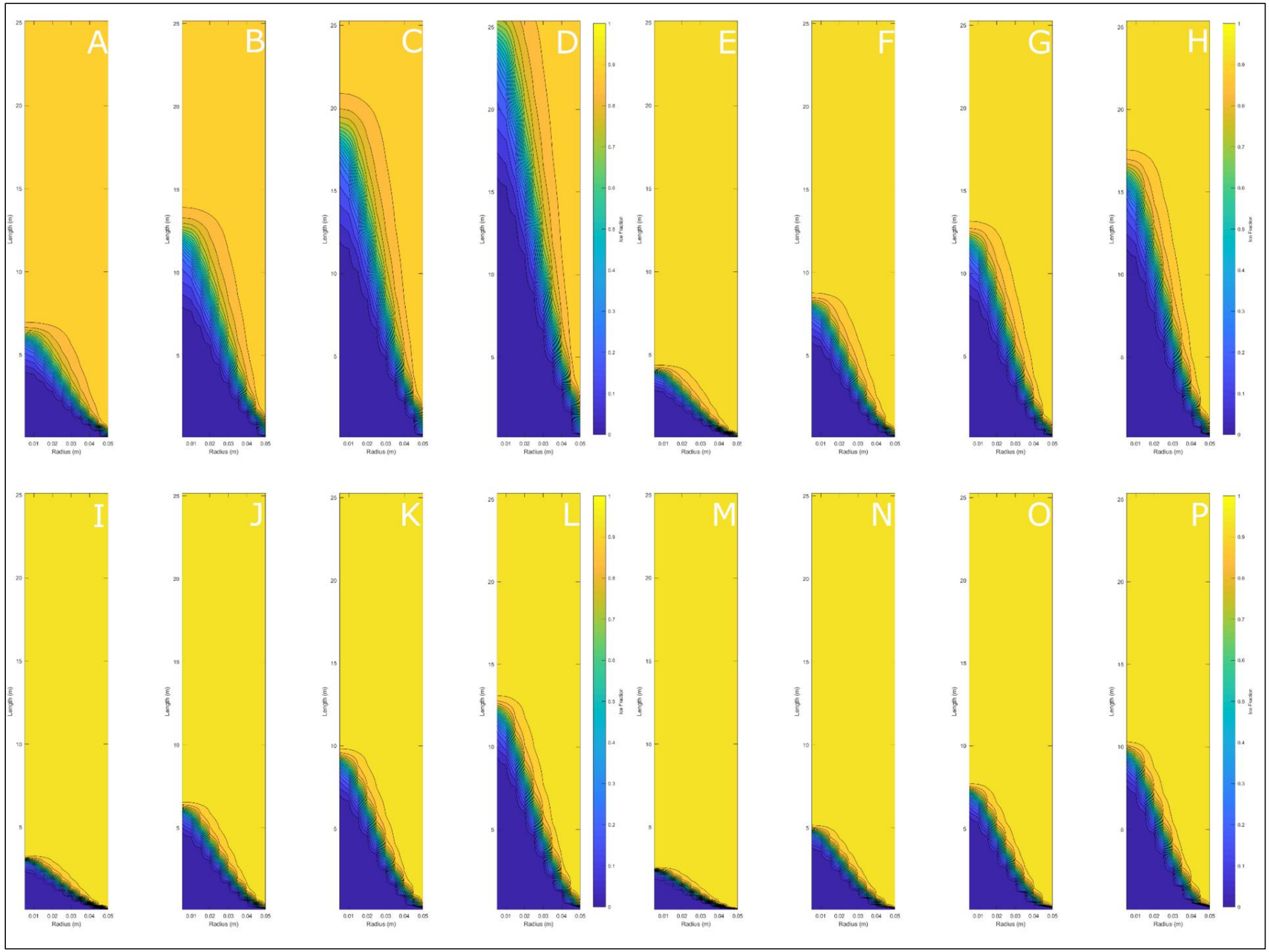

Figure 8-27:Ice Fraction profiles in a freezer with a length of 25m and a diameter of 10mm at steady state, or after 1200s of operation, whichever is shorter. Conditions corresponding to each letter are given in Table 8-3. The colour scale is constant for all runs, ranging from 0 to 1.. The image is a 2-dimensional axisymmetric slice with the centre of the modelled region on the left, and the coolant boundary on the left. The fluid inlet is at the base and the product outlet is at the to

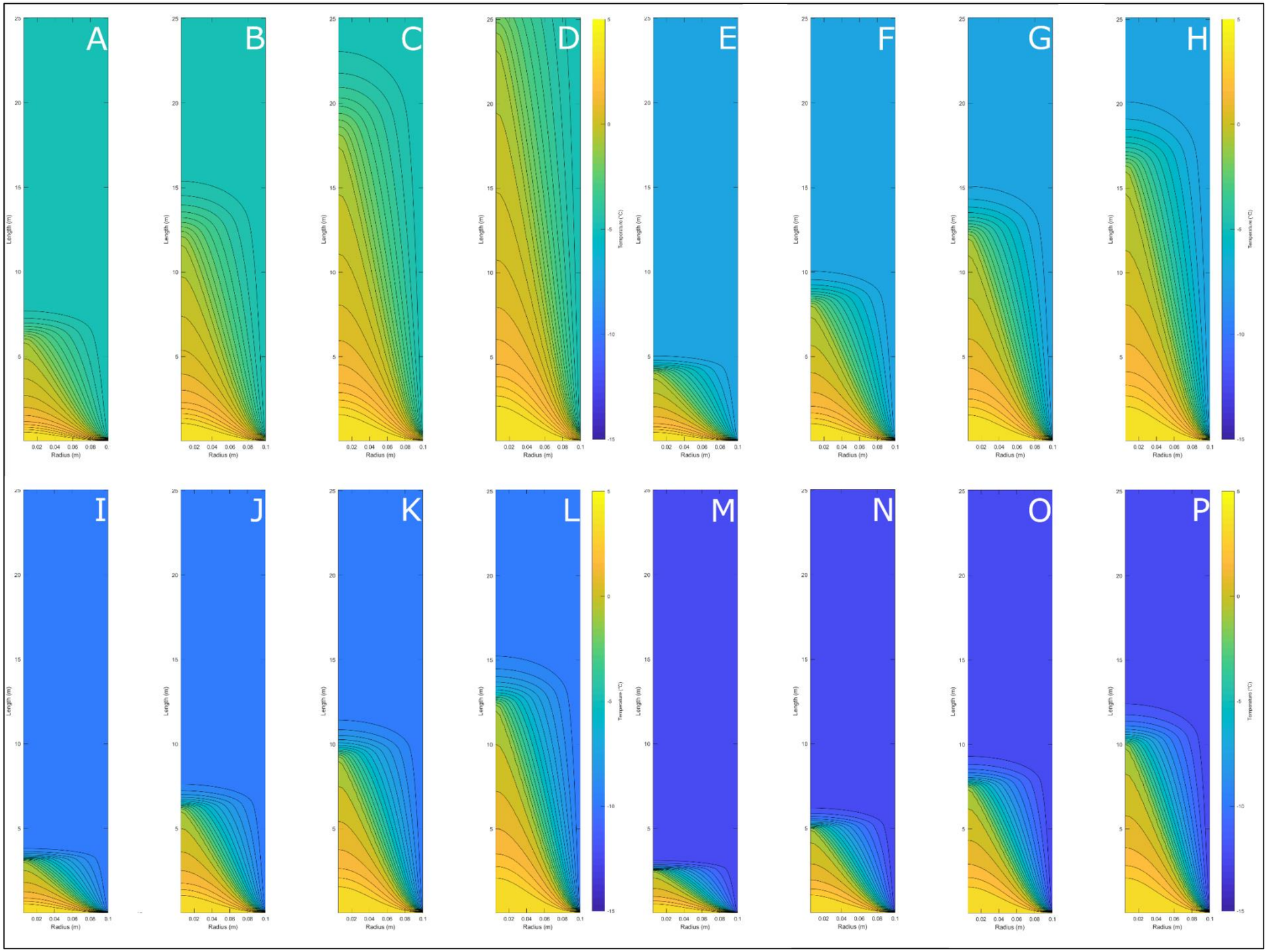

Figure 8-28: Temperature profiles in a freezer with a length of 25m and a diameter of 20mm at steady state, or after 1200s of operation, whichever is shorter. Conditions corresponding to each letter are given in Table 8-4. The colour scale is constant for all runs, ranging from +5°C to -15°C. The image is a 2-dimensional axisymmetric slice with the centre of the modelled region on the left, and the coolant boundary on the left. The fluid inlet is at the base and the product outlet is at the top.

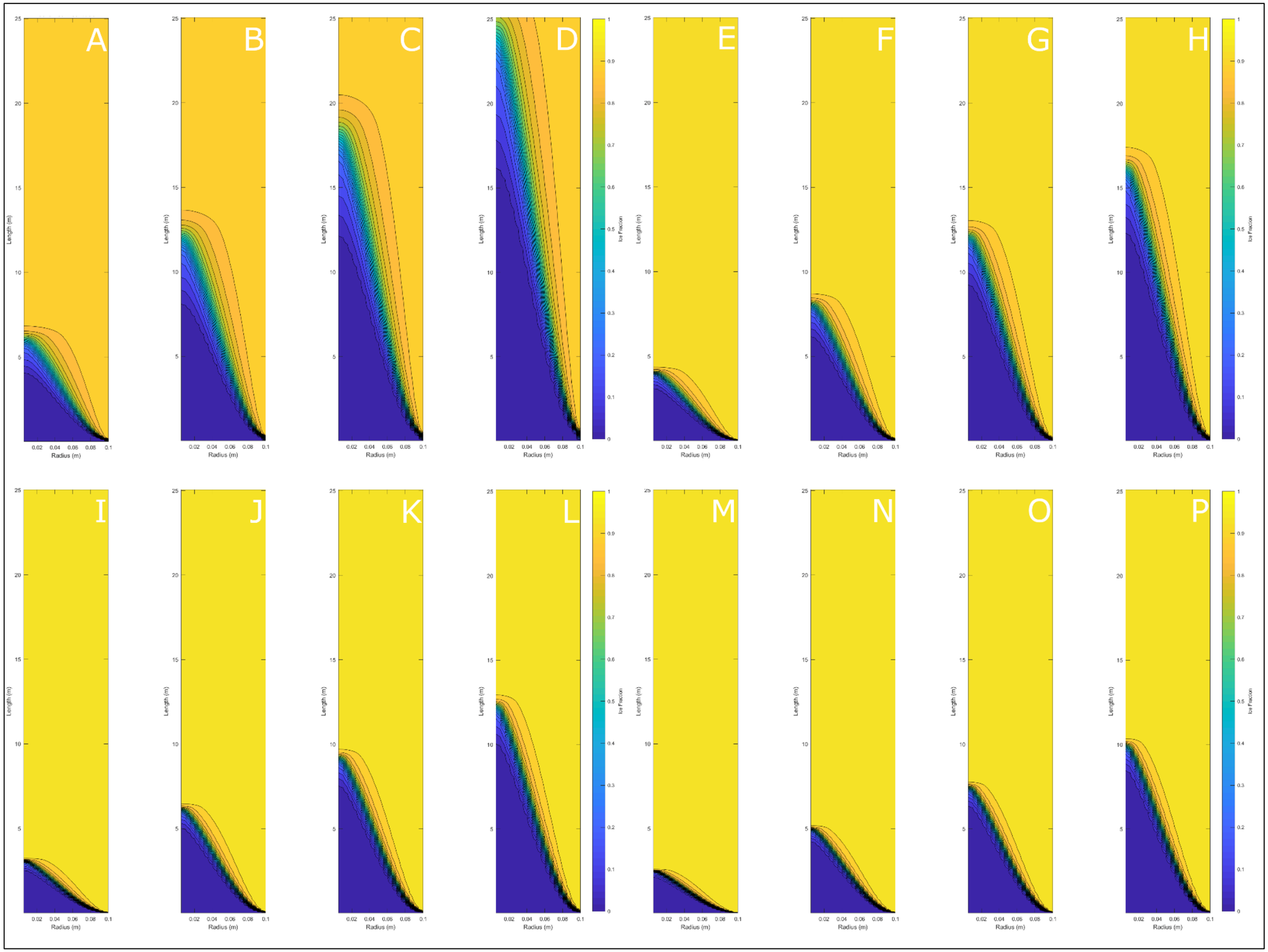

Figure 8-29: Ice fractions profiles in a freezer with a length of 25m and a diameter of 20mm at steady state, or after 1200s of operation, whichever is shorter. Conditions corresponding to each letter are given in Table 8-4. The colour scale is constant for all runs, ranging from 0 to 1.. The image is a 2-dimensional axisymmetric slice with the centre of the modelled region on the left, and the coolant boundary on the left. The fluid inlet is at the base and the product outlet is at the top.

Table 8-4: Results from runs of model with a freezer diameter of 20mm.

Run	Diameter (mm)	Coolant Temperature (°C)	Product Flow ($kghr^{-1}$)	Required Length (m)	Required residence time (s)	V_f average (μms^{-1})
A	20	-5	10	9.07	1026	9.7
B	20	-5	20	18.14	1026	9.7
C	20	-5	30	27.22	1026	9.7
D	20	-5	40	36.29	1026	9.7
E	20	-7.5	10	5.87	664	15.1
F	20	-7.5	20	11.75	664	15.1
G	20	-7.5	30	19.97	664	15.1
H	20	-7.5	40	23.33	660	15.2
I	20	-10	10	4.40	498	20.1
J	20	-10	20	8.80	498	20.1
K	20	-10	30	14.96	564	20.1
L	20	-10	40	17.60	498	20.1
M	20	-12.5	10	3.56	402	24.9
N	20	-12.5	20	7.11	402	24.9
O	20	-12.5	30	12.09	456	21.9
P	20	-12.5	40	14.22	402	24.9

This page intentionally left blank

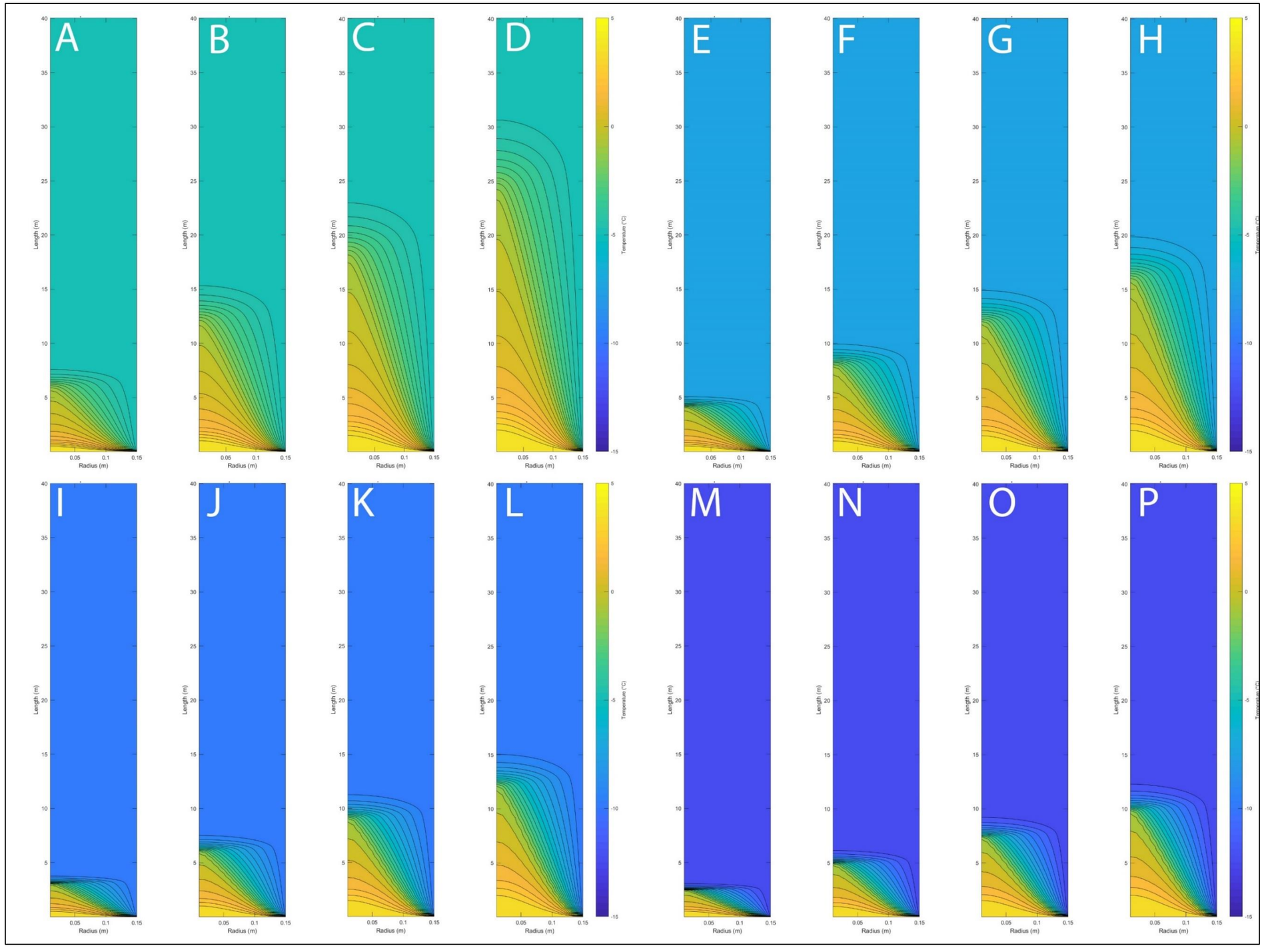

Figure 8-30: Temperature profiles in a freezer with a length of 40m and a diameter of 30mm at steady state, or after 6000s of operation, whichever is shorter. Conditions corresponding to each letter are given in Table 8-5. The colour scale is constant for all runs, ranging from +5°C to -15°C. The image is a 2-dimensional axisymmetric slice with the centre of the modelled region on the left, and the coolant boundary on the right. The fluid inlet is at the base and the product outlet is at the top.

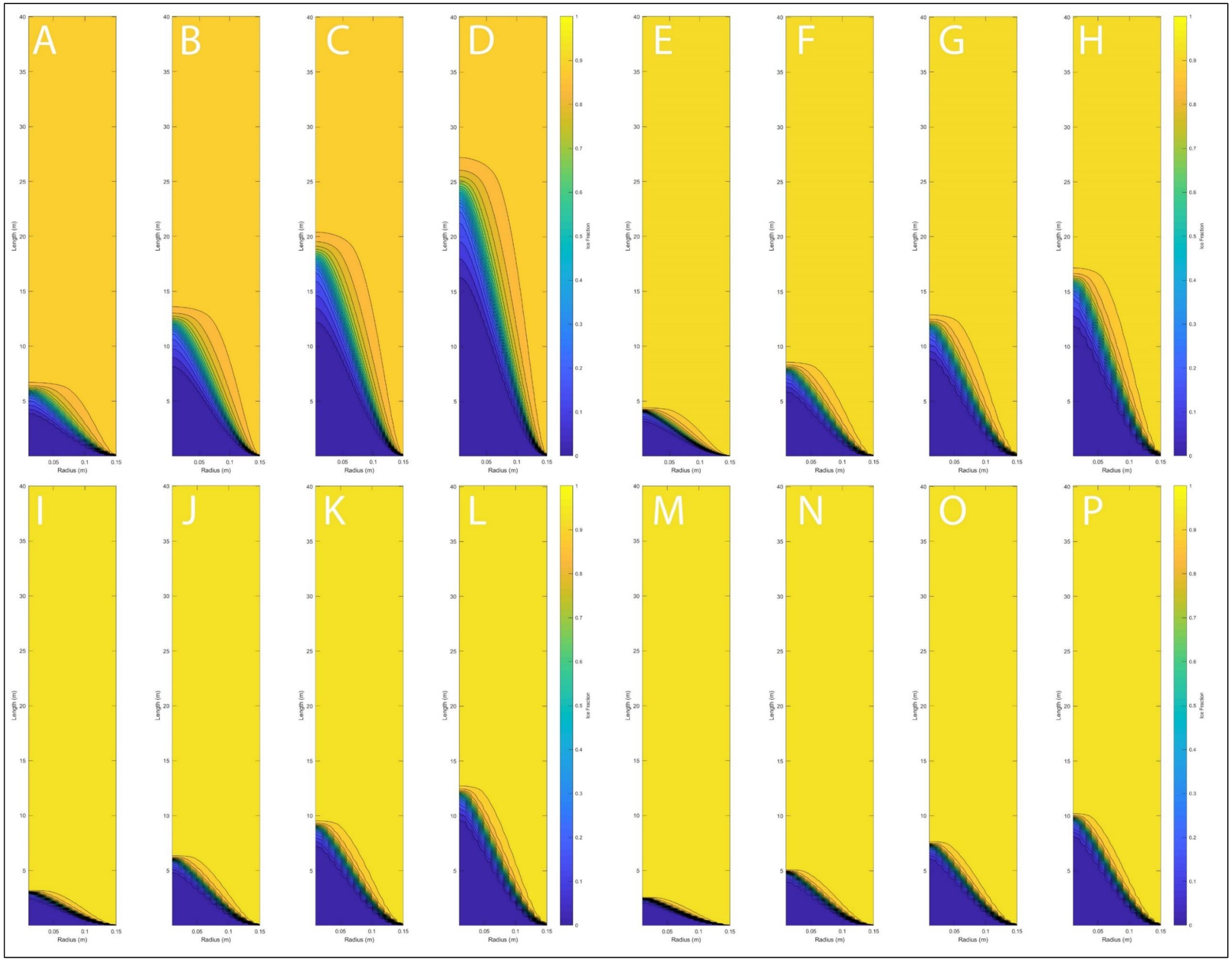

Figure 8-31: Ice fractions profiles in a freezer with a length of 40m and a diameter of 30mm at steady state, or after 6000s of operation, whichever is shorter. Conditions corresponding to each letter are given in Table 8-5. The colour scale is constant for all runs, ranging from 0 to 1. The image is a 2-dimensional axisymmetric slice with the centre of the modelled region on the left, and the coolant boundary on the right. The fluid inlet is at the base and the product outlet is at the top.

Table 8-5: Results from runs of model with a freezer diameter of 30mm.

Run	Diameter (mm)	Coolant Temperature (°C)	Product Flow ($kghr^{-1}$)	Required Length (m)	Required residence time (s)	V_f average (μms^{-1})
A	30	-5	10	16.6	2114	7.1
B	30	-5	20	24.9	2114	7.1
C	30	-5	30	33.2	2114	7.1
D	30	-5	40	5.3	2114	7.1
E	30	-7.5	10	10.7	1356	11.1
F	30	-7.5	20	16.0	1356	11.1
G	30	-7.5	30	21.3	1356	11.1
H	30	-7.5	40	4.0	1356	11.1
I	30	-10	10	8.0	1020	14.7
J	30	-10	20	12.0	1020	14.7
K	30	-10	30	16.0	1020	14.7
L	30	-10	40	3.2	1020	14.7
M	30	-12.5	10	6.5	824	18.2
N	30	-12.5	20	9.7	824	18.2
O	30	-12.5	30	12.9	824	18.2
P	30	-12.5	40	16.6	824	18.2

This page intentionally left blank

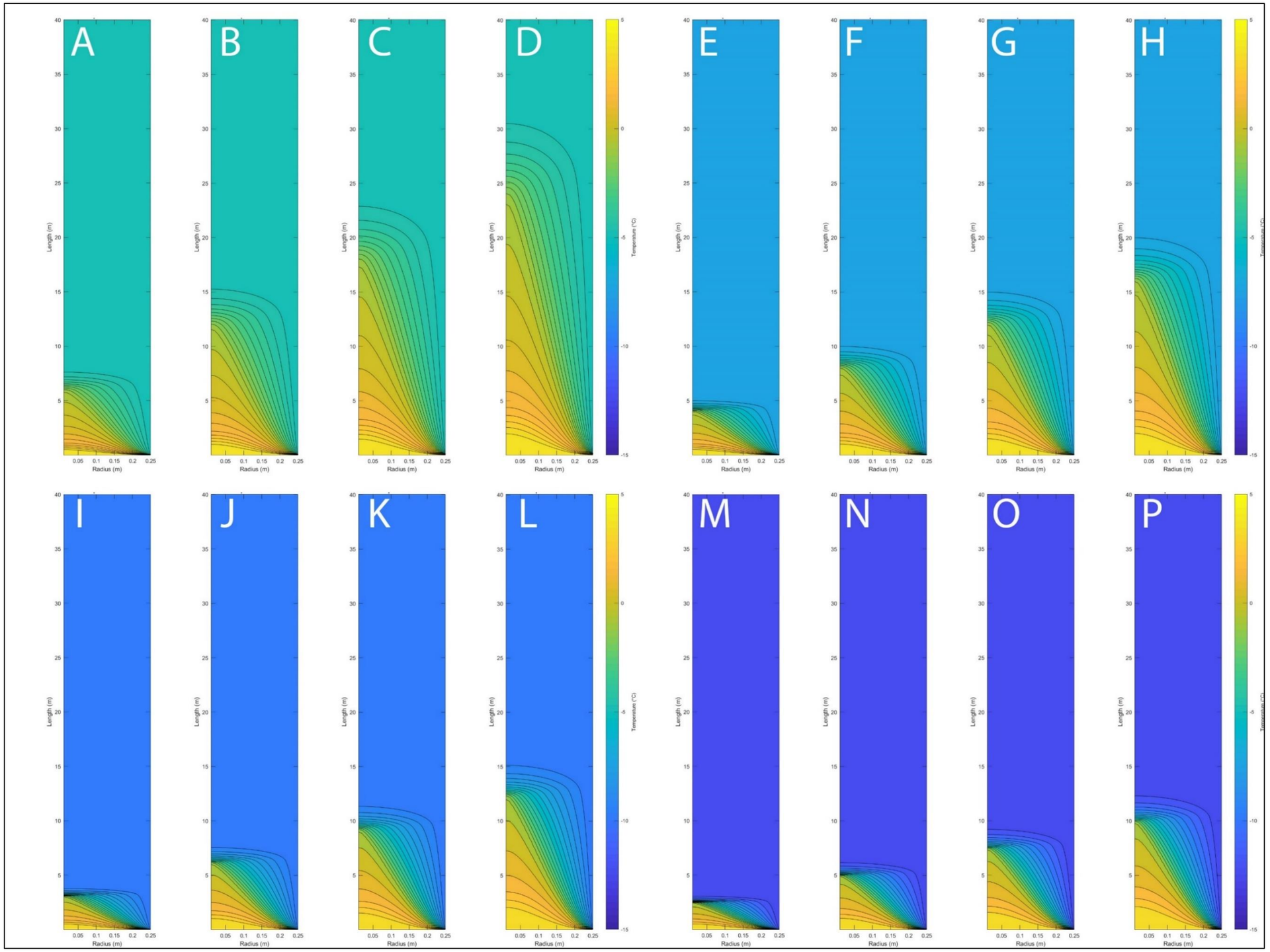

Figure 8-32: Temperature profiles in a freezer with a length of 40m and a diameter of 50mm at steady state, or after 6000s of operation, whichever is shorter. Conditions corresponding to each letter are given in Table 8-6. The colour scale is constant for all runs, ranging from +5°C to -15°C. The image is a 2-dimensional axisymmetric slice with the centre of the modelled region on the left, and the coolant boundary on the right. The fluid inlet is at the base and the product outlet is at the top.

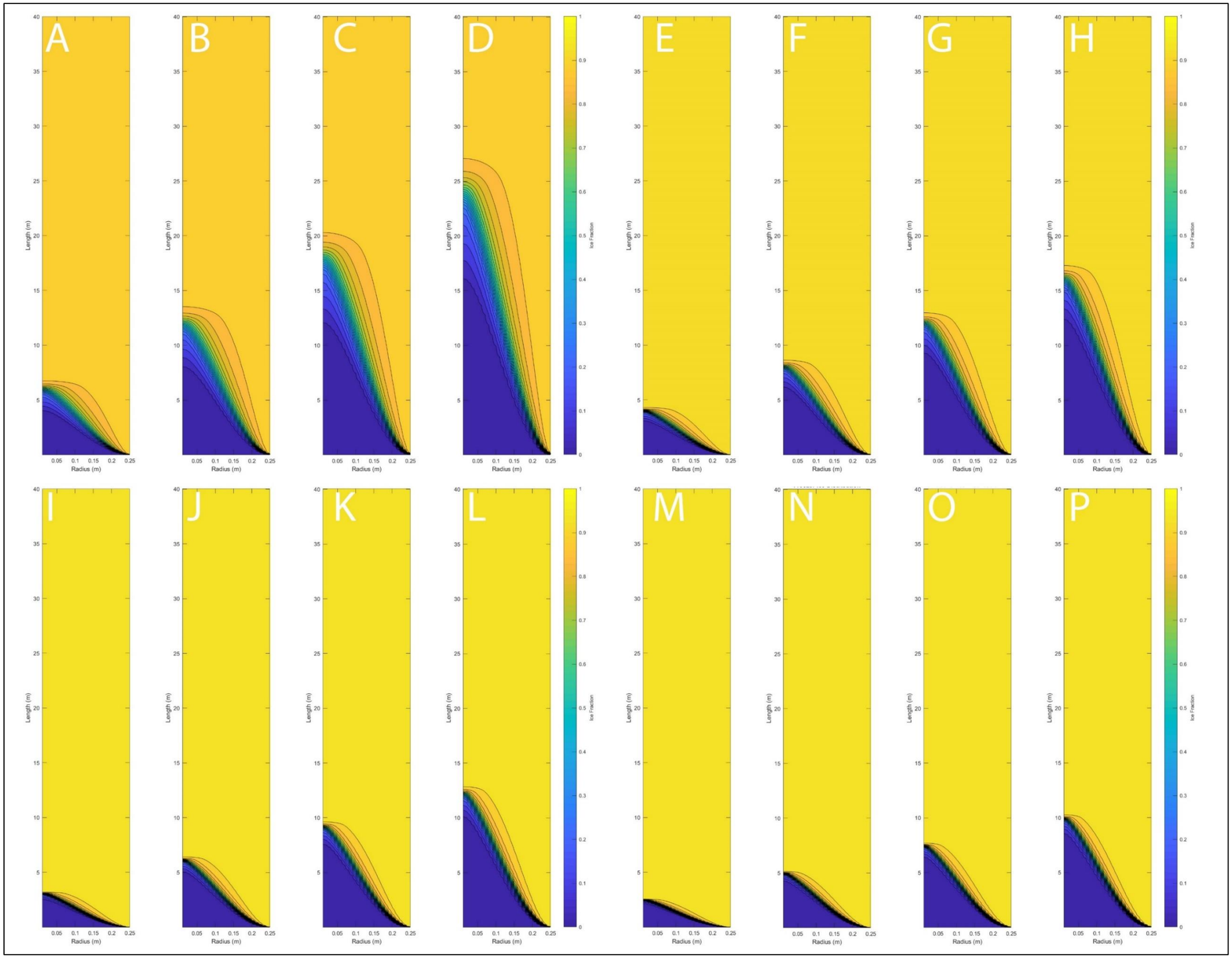

Figure 8-33: Ice fractions profiles in a freezer with a length of 40m and a diameter of 50mm at steady state, or after 6000s of operation, whichever is shorter. Conditions corresponding to each letter are given in Table 8-6. The colour scale is constant for all runs, ranging from 0 to 1. The image is a 2-dimensional axisymmetric slice with the centre of the modelled region on the left, and the coolant boundary on the right. The fluid inlet is at the base and the product outlet is at the top.

Table 8-6: Results from runs of model with a freezer diameter of 50mm.

Run	Diameter (mm)	Coolant Temperature (°C)	Product Flow ($kghr^{-1}$)	Required Length (m)	Required residence time (s)	V_f average (μms^{-1})
A	50	-5	10	7.6	5377	4.6
B	50	-5	20	15.2	5377	4.6
C	50	-5	30	22.8	5377	4.6
D	50	-5	40	30.4	5377	4.6
E	50	-7.5	10	4.9	3464	7.2
F	50	-7.5	20	9.8	3464	7.2
G	50	-7.5	30	14.7	3464	7.2
H	50	-7.5	40	19.6	3464	7.2
I	50	-10	10	3.7	2608	9.6
J	50	-10	20	7.4	2608	9.6
K	50	-10	30	11.1	2608	9.6
L	50	-10	40	14.8	2608	9.6
M	50	-12.5	10	3.0	2114	11.8
N	50	-12.5	20	6.0	2114	11.8
O	50	-12.5	30	9.0	2114	11.8
P	50	-12.5	40	12.0	2114	11.8

Chapter 9: Conclusions and Recommendations

9.1 Project Background and Aims

To grow from its current size, the New Zealand sheep milk industry needs to aggregate the small volumes that individual farms can supply into larger lots, presented in times and places desired by sheep milk processors. Freezing sheep milk into a form easy to transport and to thaw would offer a solution. However, today's slow freezing methods offer a poor solution. They can limit quality[1, 2], and can promote microbial growth due to poor thawing practices [3].

The current project was funded by the New Zealand Ministry of Business, Innovation and Employment (MBIE) through the Food Industry Enabling Technologies (FIET) research programme. The project was aimed at developing sufficient understanding of sheep milk freezing, storage and thawing to provide the basis of a simple, robust, inexpensive and safe on-farm rapid sheep milk freezer suited to farms of up to approximately 500 milking sheep. A solution that was applicable across the wider range of liquid foodstuffs was desirable.

At the outset of this project, an objective was to develop a rolling droplet freezer involving super-hydrophobic surfaces. Freezing of individual rolling droplets of milk into milk hail was shown to be technically possible but technologically and economically challenging. At this point a review of existing methods was conducted.

The decision was made to investigate the well-known technology of flake freezing, which is used for the production of ice[4], and has been evaluated for food-stuffs[5].The final configuration selected was a vertically oriented falling film freezer. The frozen product was to be detached by the application of a brief burst of heat, causing a thin liquid layer to lubricate the surface, and detach the frozen product.

The Research Aims for the overall project were as follows:

1. Investigate the changes in sheep milk during the freezing process, including the energy balances during freezing, the crystallisation behaviour of water, and the changes occurring during frozen storage and thawing. This knowledge would be used to select freezing and storage conditions which minimised quality losses during freezing and storage.
2. Understand the phenomena that occur during the directional freezing of a liquid aqueous foodstuff, specifically ovine milk, and how the heat flux and the speed of the freezing front affects the incorporation of solutes into the frozen ice matrix. This would also involve investigating the effect of freezing conditions on ice morphology
3. Design and optimise a rapid liquid freezer for on-farm use and evaluate this freezer with other feedstocks.

During the testing and modification of the pilot scale falling film, a completely novel freezing method was conceived, deriving from an understanding of the phenomena involved in freezing in liquid foods:

- At high enough freezing front velocities, ice in milk would grow in a columnar or (at higher velocities), dendritic morphologies, trapping regions of unfrozen liquid and milk solids in a matrix of ice.
- Below T_f there is a certain fraction of water which remains unfrozen. The fraction of unfrozen water is temperature dependent.

- If the temperature of the freezer is controlled, a mixed phase of liquid and solid could be maintained. This mixed phase may not have the same adhesion strength to the cooled surfaces of the freezer as a fully-frozen product. Therefore, it was hypothesised that a liquid food product could be frozen in a simple cooled tube, to form a solid matrix with a high liquid content, the proportion of which could be precisely controlled by varying the product outlet temperature.

This hypothesis was evaluated at small scale. The system was found to work successfully, and so was evaluated at a larger diameter, to test basic scaling relationships. The system was then scaled up to a small-scale pilot unit, capable of several $kghr^{-1}$ throughput.

9.2 Frozen Storage of Ovine Milk.

9.2.1 General Observations

When samples of ovine milk were stored at -10°C, for 4 and 8 weeks, significant agglomeration, and separation into a gel and sediment, was observed visually. Milk stored at -18°C for 8 weeks displayed some small flecks of solids which dispersed shortly after thawing. No flecks or gelation was seen in milk stored at or below -28°C. Clearly, the lower the temperature of storage, the more stable the sheep milk system remained. For long term storage, over several months, ovine milk should be stored at or below -28°C.

After centrifugation, milk that was stored at -10°C for 4 weeks and 8 weeks separated into a sediment and a clear serum. There was no cream layer present, indicating that all milk fat globules were trapped in the sediment. No significant sediment or entrapment of fat was observed in samples stored at -18°C or -28°C.

9.2.2 Particle Agglomeration

The particle size distribution was measured after heating and homogenisation in all thawed samples. The particle size distribution after heating in all samples was similar to the original particle size distribution before frozen storage. In a preliminary trial, the particle size distribution of milk was measured after storage for 4 and 8 weeks at -10°C and -28°C. The samples stored at -10°C showed significant increases in particle size after 4 and 8 weeks of storage. This indicates that heating disrupts the particle network that forms during frozen storage at higher temperatures.

The viscosity measured at a shear rate of 230 s^{-1} of samples stored at -18°C and -28°C showed no changes over the storage period. The samples stored at -10°C showed a slight increase in viscosity up to a storage period of 4 weeks. After 8 weeks storage at -10°C, samples showed non-Newtonian shear thinning flow behaviour. The flow behaviour for all other samples was Newtonian. This indicated that aggregation of particles was occurring at -10°C but not at lower storage temperatures.

The changes in the particle size distribution on heating indicates that the gel of agglomerated milk solids observed in samples is disrupted by heat. This is also indicated by the decrease in viscosity in samples heated prior to homogenisation.

9.2.3 Physico-Chemical Changes

There were no long-term trends showing a change of pH of freshly thawed milk after frozen storage.

The level of crude protein in milk serum phase in the-10°C, -18°C and -28°C samples, and in the clear supernatant in -10°C 4 weeks and -10°C 8 weeks samples was constant. This indicates that there is a limited or no solubilisation of casein, including in samples that formed a gel on thawing,

The Ca^{2+} concentration in the serum phase decreased in through the storage period in milk stored at -10°C and -18°C. There was a small decrease at -28°C seen after 2 weeks storage, however the concentration was stable after this. After 8 weeks of storage, the serum Ca^{2+} concentration decreased by 50% in samples storied at -18°C and 34% in samples stored at -10°C. The Ca^{2+} concentration in the sediment or gels formed after storage was approximately twice that of skimmed milk. The total Ca^{2+} concentration in skimmed milk samples was 2.14±0.13 mg/g, and in sediment it was 3.82±0.17 mg/g.

Colorimetric measurements where conducted on samples after frozen storage and after homogenisation treatment on thawed samples.

There was a decrease in whiteness (WI) in all samples, and an increase in the yellowness (YI) of all samples. The response of the WI value of the frozen milk to storage time followed a quadratic relationship. Homogenisation was effective at increasing the WI of sample.

9.2.4 Processing Suitability

Homogenisation at 20 MPa/ 4 MPa at 60°C was effective at reducing particle size and viscosity in all samples. The heating step alone was sufficient to reduce the viscosity (at 20°C) of -10°C 8-week samples, and change the flow behaviour from shear-thinning to Newtonian. The first pass through the homogeniser was responsible for the greatest decrease in viscosity and particle size, and the greatest increase in whiteness, with smaller changes on further recirculation.

The heat stability of ovine milk follows a curve typical of type A milks, with a maximum heat stability at pH 6.8. There was no statistically significant change during frozen storage, despite changes in serum Ca^{2+} levels occurring over frozen storage.

9.2.5 Sintering of Frozen Milk

The increase in unfrozen faction of milk at higher frozen storage temperatures was linked to sintering and agglomeration of particles of frozen milk under simulated storage conditions. Ovine milk pellets stored under simulated storage pressures at -10°C for a period of 4 months had agglomerated and bonded together and were no longer free-flowing. Milk stored at -18°C displayed no agglomeration and was still free-flowing. Concentrated bovine milk was also evaluated for sintering at -18°C and -25°C. After 2.5 months of storage, concentrated bovine milk that was stored at -18°C sintered and deformed significantly. The sample was no longer free-flowing. No sintering or deformation was seen in the sample stored at -25°C. The pellets remained free-flowing. Concentrated frozen milks should be stored below -25°C to prevent deformation and sintering of frozen product.

9.2.6 Further Work

The formation of a gel on frozen storage appears to be reversible. While I suggest that the responsible mechanism is the steric interference between tightly packed casein micelles in the unfrozen phase in a frozen sample, more work should be done to investigate the mechanisms of gel formation.

The pH of frozen ovine milk has not been measured, however it could be measured with pH probes intended for low temperatures [6, 7], or use of a chemical pH probe, as has been done using ^{19}F NMR of 3-fluorobenzoic acid as a pH probe [8].

The gross structure and nano-scale structure of gels formed after frozen storage should be imaged. Confocal Microscopy would be appropriate to show the gross structure of the gel network, and scanning electron cryomicroscopy (Cryo-SEM) would show the structure at a scale of approximately 0.5 µm-500 µm. Transmission electron cryomicroscopy (Cryo-TEM) would allow the nano-scale structure of the gel to be imaged. TEM has been used to image the casein

structure of concentrated skim milk ultrafiltrate[9], casein sub-micelle networks[10],the internal structure of casein micelles[11], and the protein structure of linkages in casein gels [12, 13]. Cryo-EM methods are particularly suited for these studies as the native structure can be imaged without dehydration and fixation steps which may alter the structure of the gel.

To investigate the effect of various bonding mechanisms in gels formed from frozen milk, the response of the gel rheology to the addition of various compounds could be studied:

- Ca^{2+} bridging could be investigated by the addition of Ca^{2+} containing salts or the removal of Ca^{2+} by chelating agents such as EDTA
- Hydrophobic interactions could be investigated by the addition of urea, which affects the hydrophobic interactions in the milk.
- The effect of hydrogen bonding on the gel network could be investigated by the addition of simple sugars which can act as a hydrogen bonding target.

The change in heat stability of ovine milk over a milking season has been measured in European studies[14, 15], but similar data in a New Zealand context is lacking. Gathering this data would be valuable.

9.3 Effect of Freezing Conditions on Ice Morphology

Observation of the morphology of advancing freezing fronts showed a number of different ice morphologies. As the freezing front velocity (v_f) increased, the ice morphology would transition from planar to columnar to dendritic. These transitions are a result of a balance between thermodynamic effects which encourage the formation of a planar interface, and kinetic effects which encourage the growth of perturbations in ice fronts.

As the number of components in fluids increased, the critical v_f for transitions between morphologies decreased. In RO water, a planar ice front existed for v_f< 5 μms^{-1}, and columnar ice growth was observed above this speed. Dendritic growth was not observed in any RO water samples. However, in SSM and WSM columnar growth was observed above 0.5 μms^{-1}, with SSM showing dendritic growth above 20 μms^{-1}, and WSM showing the same growth at 2 μms^{-1}. The increases levels of solutes and particles present in SSM and WSM samples lead to the formation of chemical gradients and alteration of thermal gradients, which encouraged the growth of perturbations and destabilised the interface at lower v_f.

The feature spacing in the freezing front was plotted as a function of v_f. The curve followed a power law relationship. The variation in feature spacing for all samples decreased with increased v_f.

The transition from planar ice fronts to stable columnar ice growth morphology was recorded. At v_f=1 ums^{-1} the columns grew directly out from sinusoidal perturbations on the planar ice front. At v_f=20 μms^{-1}, the ice front subcooled slightly before sinusoidal perturbations grew into dendrites. These dendrites then grew into stable columns, all sharing a parallel orientation.

9.3.1 Cryo-SEM

Samples of whole raw ovine milk were frozen, giving two samples: Directionally frozen (DF) and slow frozen (SF). These samples were imaged by scanning electron cryo-microscopy (Cryo-SEM).

The DF samples had a highly anisotropic frozen morphology. There was a matrix of ice crystals, interspersed with regions of concentrated milk solids. In the DF samples the ice crystals were lamellar, with the long axis of the crystals aligned with the heat flux. The cross sections of the crystals when viewed perpendicular to the heat flux were roughly rectangular. The cross sections

of the ice crystals viewed perpendicular to the heat flux showed a range of different orientations. Some fat globules were engulfed entirely in ice crystals.

The SF samples had large ice crystals, much larger than the FOV of the microscope, with large bands of milk solids between the crystals. Possible clusters of lactose crystals were observed in SF samples. There were no lactose crystals observed in DF samples. This indicated that the longer freezing process experienced by SF samples allowed for the crystallisation of lactose, but this crystallisation was suppressed by the more rapid freezing experience by DF samples.

Milk was also frozen by immersion in LN2 and then imaged with Cryo-SEM. These samples displayed an extremely fine network of ice crystals and bands of concentrated milk solids. This indicates that even with extremely rapid freezing, milk did not form a glassy solid.

The bands of unfrozen solids were significantly larger and displayed larger variability in size in SF samples; The thickness of milk solids bands was 56± 49 µm (standard deviation), compared with 3.2±1.5 µm for DF samples.

9.3.2 Further Work

The temperature gradient imposed on ice fronts in this study was constant. Further work could be conducted to investigate the relationship between temperature gradient and feature spacing for whole milk and skim milk.

Confocal microscopy, coupled with a customised cold stage allowing for controlled freezing rates, and dying of fats and proteins may allow for the distribution of fats and proteins, and their incorporation and rejection from advancing ice fronts to be investigated in greater detail. The distribution of fats and proteins within a frozen sample can also be studied after further processing by freeze-drying, as it has been noted that the surface of freeze dried WMP had significantly higher levels of fats than spray-dried powders [16]and this may be linked to the freezing process.

There is increased interest in freezing concentrated dairy products, so it would be valuable to investigate the effects of concentration on the morphology of the advancing ice fronts, as particle interactions have significant effects on ice front morphology[17-20]. This can be investigated using the methodologies discussed in this thesis, applied to RO/ UF and evaporator concentrated milks, creams and whey products.

The formation of ice, and the morphology of ice in the frozen product is a major determinant of freeze-drying performance and the quality of freeze-dried products [21-28] . Applying the methodologies described above and investigating the links between the morphologies observed and the freeze-drying performance and the quality of freeze-dried milks would be a valuable contribution to knowledge in the dairy processing field.

9.4 Effect of Temperature on Unfrozen Water in Ovine Milk

9.4.1 Freezing Behaviour

The heat flows occurring during the freezing of ovine milk were measured using differential scanning calorimetry (DSC), and this was used to estimate the fraction of liquid that remained unfrozen below the equilibrium freezing temperature (T_f) of ovine whole milk (WSM). The freezing transition was also studied in skim milk (SSM), and a casein and fat free milk serum (SMUC).

There was no significant difference in the nucleation temperature observed, indicating the milk fat globules and casein micelles did not affect the nucleation behaviour of the soluble system. A melting onset transition was observed, T_M which is affected by the presence of casein micelles, but not the presence of fats.T_M occurred at -31±0.7°C in SMUC, -25.3±0.1°C for SSM and -25±0.1°C for WSM.

The amount of freezable water frozen in the range of -40°C to 0°C was estimated in each sample by fitting equations to the system enthalpy above and below the freezing transition, and assigning the unaccounted heat flows to latent heat. The thermal lag directly after the freezing transition was corrected for, and the two-phase heat capacity was estimated by an iterative procedure. The effect of correcting the latent heat of water to account for differences over the freezing temperature range was evaluated and found to make minimal difference.

The concentration of the maximally freeze concentrated solution $X_s(T_m)$ was determined from the latent heat release, $X_s(T_m)$=0.85±0.016, and from the Gordon-Taylor equation using T_m, $X_s(T_m)$=0.875. These two methods agreed well.

A partial phase diagram of ovine milk was plotted from the data derived from the DSC measurements and the Gordon-Taylor equation. The curve of T_f vs C_s determined from DSC measurements agrees well with that determined from the freezing point of reconstituted milks

9.4.2 Further Work

The Cryo-SEM images presented in Chapter 4 indicated that in some freezing conditions lactose could crystallise, but not in others. As the state of lactose in the frozen system has implications for the storage stability and the phase transitions, (e.g. T_g), further study of this is warranted. As this is a dynamic process involving the formation of a crystal it may be suited for investigation by small angle X-ray scattering (SAXS) or X-ray diffraction (XRD) during the cooling and freezing of dairy products at different cooling rates and after annealing at various temperatures and times. The crystallisation of amorphous lactose has been studied with XRD by [29, 30], and ^{1}H-NMR coupled with XRD [31] and the transition from crystalline to amorphous due to milling has also been studied by XRD [32], and by XRD and ^{13}C CP-MAS NMR [33].

The cooling rate has been suggested by several authors to determine storage stability by promoting lactose crystallisation in the unfrozen phase. This could be studied by DSC by cooling at quench rates and very slow rates then holding isothermal at various temperatures for extended periods to detect whether lactose crystallisation occurs. The nucleation rates of supersaturated lactose solutions and supersaturated whey solutions have received considerable interest, but this is more limited in the region below 0°C. Lactose in whole milk becomes supersaturated at approximately -2°C to -3°C[34].

Knowledge of the crystallisation rates of lactose at temperatures below 0°C may also allow the viscosity in the unfrozen phase to be estimated, and models such as the WLF model to be fitted, as crystallisation is partly a function of molecular mobility, which is affected by the viscosity in this phase[35]. The viscosity in this phase is not well studied yet has a strong effect on the rates of various reactions occurring during frozen storage.

A model describing the homogenous nucleation rate, $J_{\mathrm{hom}}(T)$,(or the probability distribution of this[36]) from equations for the degree of supersaturation from the concentration factor and solubility data below 0°C, and the viscosity below 0°C, and integration of this model over the cooling and storage periods may help to determine which conditions will lead to lactose crystallisation, and reduced storage stability.

The diffusion and kinetically limited processes such as crystallisation, hydration of proteins and carbohydrates, and diffusion of calcium phosphates in and out of casein micelles can be investigated by NMR. Crystallisation of water and lactose can also be studied by NMR.

^{1}H-NMR can be used to investigate the movement of water in and out of protein and lactose, as well as the state of what between the solid and liquid phase. NMR has been used to study freezing in model food solutions[37] and the effect of ice-cream formulation of water and ice behaviour during the freezing process, and was able to monitor the behaviour of both liquid and

solid water during the freezing process, and, in addition, detect flocculation of interacting caseins and stabilisers[37].

^{31}P-NMR allows the chemical environment of phosphorous atoms to be investigated. This may allow the movement of colloidal calcium phosphate (CCP) during the freezing process to be investigated, and the effect of freezing speed on this. CCP is critical to the stability of casein micelles, so understanding the behaviour of CCP during the freezing process would increase understand of the freeze-thaw behaviour of milk. ^{31}P-NMR has been applied to study the distribution of phosphorous in UHT milks [38] and in heated milks [39]

9.5 Selection of Freezing Methodology

9.5.1 Methods Evaluated

A number of freezing methods were developed and considered with the aim of choosing one for development for an on-farm ovine milk freezer. Of the methods considered, the rolling droplet freezer was the first selected for development in this project. When developmental issues arose with the rolling droplet freezer, a falling film flake freezer was selected as a promising candidate for development. This was constructed on a pilot scale and development continued until the continuous tubular freezer was developed.

9.5.2 Rolling Droplet

The rolling droplet freezer was selected for development at the start of this project as it promised a system that would rapidly freeze milk, into a form factor that could be easily handled as bulk. Initial trials were mostly promising however the presence of a condensing atmosphere during freezer operation could cause the wetting behaviour of droplets to transition from Cassie-Baxter state to Wenzel state. This transition could lead to the milk adhering to the superhydrophobic surface rather than rolling over it. This phenomenon was observed on the single droplet freezer.

Additionally, the surface geometries required for freezer operation would have been expensive to manufacture and treat with superhydrophobic surfaces. As the aim of the project was to develop a *reliable and low-cost* freezer for on-farm use, this freezing method was abandoned, and development of a falling-film freezer was prioritised instead.

9.5.3 Falling-Film

The falling-film freezer consisted of a tube, cooled by a secondary refrigerant on its interior surface. A falling film of product flowed over the exterior surface and froze to the surface. Once the product reached the desired thickness it was detached. The product was detached by the application of a pulse of heat which would melt a small layer of product at the product/freezer interface, and the remaining frozen product would fall off under gravity.

Once the falling film freezer was designed at constructed initial tests were conducted with water. These tests found that water ice was easily detached by a pulse of heat. Water ice was brittle and would expand and crack as a result of rapid heating and thermal gradients within the solid, on the application of heat, assisting the detachment of ice.

Further tests were conducted with milk. Ovine milk at 20% TS was found to have a partition coefficient ($k = C_s/C_l$) of 0.946±0.127 at an operating temperature of -30°C. At -18°C k=0.926±0.024, and at -15°C k=0.866±0.074. These k values were significantly higher than those encountered in the literature for freeze concentration of milk on falling film freeze concentrators.

Unlike water, milk was not easily detached by a pulse of heat. Frozen milk did not crack during the application of heat and remained attached to the freezer surface. It is suggested that this is

due to frozen milk being less brittle, and therefore more easily deforming under thermal expansions.

As a result, a commercial unit would require a scraper to detach the frozen milk. A scraper was designed and fitted. Frozen milk behaved differently to frozen water during detachment by scraping. Frozen water would detach in large sheets ahead of the scraper, whereas frozen milk would curl away from the scraper.

The development of the falling-film freezer was abandoned due to development of the technically superior continuous tubular freezer

9.6 Development of a Continuous tubular freezer.

9.6.1 Principle of Operation

A novel freezer was envisaged using the following principles:

1. High freezing front velocities would lead to dendritic or columnar ice morphology. The growing dendritic or columnar front would trap concentrated milk solids and unfrozen solutions between ice crystals.
2. This trapped solution would remain in the liquid state due to the progressive freezing behaviour of milk.
3. The total volume fraction of the unfrozen phase could be controlled accurately by controlling the temperature of the product.
4. This fraction of trapped unfrozen solution and milk solids would reduce the adhesion of the ice to a surface, and reduce the increase in volume due to ice formation.

These four principles would allow a frozen milk to be forced through a cooled tube by a high-pressure positive displacement pump, whereas pure water would be unable to be extruded. The pressure required would be significant, but within the capabilities of commercially available pumps.

A 4.2mm internal diameter scale prototype system was constructed. Five different products were trialled on the 4.2mm diameter freezer; Whole Sheep Milk, at a range of solids concentrations; Orange juice; Concentrated coffee extract; Gold kiwifruit pulp; and Smoothie mixes. The pressure required to extrude all frozen products from the freezer increased as the magnitude of $T_{op} - T_f$ increased. The residence time for samples on the 4.2mm diameter freezer varied from 166s to 208s.

The pressure required to extrude the sample, and therefore the adhesion strength between the sample and the tube wall increased as the fraction of freezable water frozen increased. Samples with frozen fractions from 0.8 to 0.98 were extruded.

9.6.2 Scale Up

The freezer was tested at a larger scale with two different setups; a straight tube with an internal diameter of 10 mm, and a length of 1200 mm; and a spiral tube with an internal diameter of 10 mm, and a length of 5000 mm.

The scaled-up systems were tested with ovine milk reconstituted from IWMP, and raw ovine milk. The operating temperature was -5°C, and the maximum operating pressure was 20 MPa. The raw ovine milk was stored frozen for a long-term storage trial, however at the time of writing, the results were unavailable. The residence time for trials on this scale varied from 123s to 184s.

9.6.3 Microstructure

The microstructure of frozen product plugs of ovine milk, and single strength orange juice were observed with optical microscopy, and with Cryo-SEM. The ice structure consisted of predominantly radially aligned ice crystals, with ice crystal size decreasing as towards the exterior of the frozen plug. There was some evidence of centrifugal migration of unfrozen solids, possibly a result of increased pressures at the centre of a plug due to colliding ice crystals. The ice growth was more ordered and more apparently radial in orange juice when compared with the microstructure of ovine milk. This has been linked to the morphology of advancing ice front described in Chapter 4.

9.6.4 Future Work

9.6.4.1 Mechanism of Detachment

It was suggested that the mechanism that reduces the adhesion strength with increasing temperature, is the reduction in ice volume at the interface between the frozen product and the freezer walls (relative to a pure ice layer), due to the combination of progressive freezing and dendritic ice growth at high freezing front velocities. The attachment of frozen milk to stainless steel surfaces has been found to vary with temperature, and milk composition, and some of this variation has been explained by reference to the unfrozen water fraction [40].

Testing the freezer performance with emulsions of low dissolved solids water and a non-freezing component such as hexane, or soft and hard solid particles, at total solids levels equivalent to unfrozen water contents in successfully trailed products would determine whether liquid is needed to reduce the adhesion strength or whether any non-ice entrapped particulate would be sufficient. This would also allow the effects of ice adhesion strength varying as a function of temperature to be separated from the effects of reduced ice volume.

Microscopy was conducted on samples taken from steady-state operation of the tubular freezer. Samples should be taken from unsteady state operation such as start-up and shut-down to allow for imaging and analysis. This will increase understanding of phenomena occurring during start-up and shut-down.

9.6.4.1.1 *Effect of Functionalised Coatings*

Functionalised surfaces to reduce ice adhesion are becoming more common [41]and it is expected that functionalised surfaces that reduce the ice adhesion strength would improve system performance by reducing the pressure required for extrusion.

The roughness of a given material can strongly affect the ice adhesion strength, but there is still active debate about the mechanism of this relationship, and whether increases surface roughness increases or decreases ice adhesion[40].The surface energy of a material also effects the ice adhesion [42], with lower surface energies having lower ice adhesion strengths.

The effects of surface roughness and surface energy on the required pressure for extrusion should be investigated. This could be achieved by constructing a benchtop unit with removable freezer tubes, similar to the 4.2 mm scale unit discussed in this thesis and modifying the surface roughness and surface energy of the internal surface of the tube. The surface roughness can be modified at different scales by methods such as mechanical and electropolishing to reduce roughness, or mechanical or chemical etching to increase roughness. The surface energy can be reduced by coating the freezer surface with fluorinated silane compounds.

9.6.4.2 Parallelisation

The pressure requirement for freezer operation for a given radial heat flux is related to the product flow per tube. In order to scale to larger production volumes, a design with several tubes in parallel should be evaluated, initially at the 4.2 mm scale. A small-scale unit would also

allow the dynamics of a multiple tube system to be evaluated, which would assist in the development of control systems for multiple tube systems.

Other designs that could be evaluated for suitability include an annular arrangement, where there is a cooled core inside the freezer tube leaving an annular flow path for product, and non-circular tube geometries.

9.6.4.3 Control Design

The control system design for the continuous tubular freezer remains unoptimized. There remains a number of open questions about what variables to best monitor, and which factors should be controlled. The basic design of the control system is also an open question: The system may well be controllable with an open-loop control system if a stable operating range is found. This would be simpler and preferable to a closed loop or predictive control system. Further research into the operating principles, and the system's responses to perturbations would allow a control system to be designed and optimised.

9.6.4.4 Heat and Mass Transfer within Tube during Freezing

No attempt was made in this thesis to study or model the mass transfer of solutes within the tube during the freezing process, rather it was assumed that solute concentration was isotropic and invariant on a gross scale. This may not be realistic for all freezer conditions. Qualitative measurements of partition coefficients as a function of freezing front velocity for various milk components will need to be determined, and then this modelling could be used in combination with heat transfer modelling to determine the distribution of solutes within the frozen products.

This modelling could then be validated by freezing samples of simple product solutions and suspensions under controlled conditions, examining the distribution of solutes and particles by μ-CT, and comparing this distribution with the distribution predicted by mathematical modelling.

Further analysis which investigates the effects of localised latent heat release in the region of rapidly growing ice crystals, and the effects of this heat release on other crystals should be conducted. This heat release may affect the heat flows in the freezer and ice morphology of the frozen product.

9.6.4.5 Morphology and Mass Flows during Freeze-drying

As one of the possible uses of this freezer is the production of frozen pellets as a feedstock for freeze-drying, the freeze-drying performance of these frozen pellets should be investigated.

The mass loss rates of these frozen pellets should be evaluated in both vacuum and atmospheric freeze-drying systems, and compared against current commercially used freezing methods. The effect of the smaller characteristic distance should be considered, so both particle scale, and packed bed mass flow characteristics should be measured. The mass loss rate of rapidly frozen particles should also be compared against particles of identical external dimensions, but having undergone differing freezing conditions, such as slow freezing to form a coarser ice structure, or frozen with axial heat flows to form axially aligned ice crystals. This will allow the effects of ice structure and form factor to be studied independently.

As the frozen morphology of the pellets is an important factor governing mass flows during freeze drying [27], detailed measurement of the porosity and tortuosity of the ice matrix should be conducted. Techniques such as μ-CT imaging may prove useful for this[43], and has been used by some authors to conduct time dependent measurements of the freeze-drying process [44, 45]. Two dimensional images give limited information about three-dimensional morphologies. The use of contrast agents with different particle sizes and surface properties will

allow the distribution of solids in the frozen samples to be directly measured. For example, by varying the size of Barium Sulphate contrast agent particles, the effect of particle size of particle spatial distribution could be studied.

9.7 Concluding Remarks

This project aimed to develop a simple, robust and safe system for the on-farm storage of raw sheep milk. To this end, research was conducted to investigate the changes occurring during the frozen storage and thawing process, the phase change behaviour during the freezing process, and the effects of freezing conditions on ice morphology. From the knowledge gained during this research, a novel continuous tubular freezer was conceived, tested, and developed. This continuous tubular freezer exploits the dendritic morphology of rapidly advancing ice fronts and the progressive freezing of whole sheep milk to form a self-lubricating frozen plug. This plug can be extruded continuously from a cooled tube by a high-pressure pump. This freezer meets all the aims laid out at the beginning of the project, and is currently being scaled-up and commercialised for a range of liquid foodstuffs.

9.8 References

[1] M. Ramos and M. Juarez, "Milk | Sheep Milk," in *Encyclopedia of Dairy Sciences*, J. W. Fuquay, Ed. Second Edition ed., 2011.

[2] W. L. Wendorff, "Freezing Qualities of Raw Ovine Milk for Further Processing," *Journal of Dairy Science,* vol. 84, pp. E74-E78, 2001.

[3] A. A. L. Tribst, L. T. P. Falcade, and M. M. de Oliveira, "Strategies for raw sheep milk storage in smallholdings: Effect of freezing or long-term refrigerated storage on microbial growth," *J Dairy Sci,* Apr 3 2019.

[4] J. D. Zhao, N. Liu, and Y. M. Kang, "Optimization of ice making period for ice storage system with flake ice maker," *Energy and Buildings,* vol. 40, no. 9, pp. 1623-1627, 2008.

[5] C. Marizy, A. Le Bail, J. C. Duprat, and Y. Reverdy, "Modelling of a drum freezer. Application to the freezing of mashed broccoli," *Journal of Food Engineering,* vol. 37, no. 3, pp. 305-322,1998.

[6] L. van den Berg, "pH Measurement at Low Temperatures Using Modified Calomel and Glass Electrodes," *Analytical Chemistry,* vol. 32, no. 6, pp. 628-631, 1960.

[7] L. Van Den Berg, "pH changes in buffers and foods during freezing and subsequent storage," *Cryobiology,* vol. 3, no. 3, pp. 236-242, 1966.

[8] C. Robinson, C. S. Boxe, M. I. Guzmán, A. J. Colussi, and M. R. Hoffmann, "Acidity of frozen electrolyte solutions," *Journal of Physical Chemistry B,* Article vol. 110, no. 15, pp. 7613-7616, 2006.

[9] A. O. Karlsson, R. Ipsen, K. Schrader, and Y. Ardo, "Relationship between physical properties of casein micelles and rheology of skim milk concentrate," *Journal of Dairy Science,* vol. 88, no. 11, pp. 3784-3797, 2005.

[10] M. Panouille, D. Durand, T. Nicolai, E. Larquet, and N. Boisset, "Aggregation and gelation of micellar casein particles," *J Colloid Interface Sci,* vol. 287, no. 1, pp. 85-93, 2005.

[11] R. Trejo, T. Dokland, J. Jurat-Fuentes, and F. Harte, "Cryo-transmission electron tomography of native casein micelles from bovine milk," *Journal of Dairy Science,* vol. 94, no. 12, pp. 5770-5775, 2011.

[12] Y. Lu, D. J. McMahon, L. E. Metzger, A. Kommineni, and A. H. Vollmer, "Solubilization of rehydrated frozen highly concentrated micellar casein for use in liquid food applications," *Journal of Dairy Science,* vol. 98, no. 9, pp. 5917-5930, 2015.

[13] Y. Lu, D. J. McMahon, and A. H. Vollmer, "Investigating cold gelation properties of recombined highly concentrated micellar casein concentrate and cream for use in cheese making," *Journal of Dairy Science,* Article vol. 99, no. 7, pp. 5132-5143, 2016.

[14] K. Raynal-Ljutovac, Y. W. Park, F. Gaucheron, and S. Bouhallab, "Heat stability and enzymatic modifications of goat and sheep milk," *Small Ruminant Research,* vol. 68, no. 1, pp. 207-220, 2007.

[15] D. D. Muir, D. S. Horne, A. J. R. Law, and A. W. M. Sweetsur, "Ovine milk. 2. Seasonal changes in indices of stability," *Milchwissenschaft,* vol. 48, no. 8, pp. 442-445, 1993.

[16] K. Fyfe, O. Kravchuk, A. Nguyen, H. Deeth, and B. Bhandari, "Influence of Dryer Type on Surface Characteristics of Milk Powders," *Drying Technology,* Article vol. 29, no. 7, pp. 758-769, 2011.

[17] S. Deville, E. Saiz, and A. P. Tomsia, "Ice-templated porous alumina structures," *Acta Materialia,* vol. 55, no. 6, pp. 1965-1974, 2007.

[18] S. Deville, "Ice-templating, freeze casting: Beyond materials processing," *Journal of Materials Research,* vol. 28, no. 17, pp. 2202-2219, 2013.

[19] J. You *et al.*, "Interfacial undercooling in solidification of colloidal suspensions: analyses with quantitative measurements," *Sci Rep,* vol. 6, p. 28434, 2016.

[20] J. M. H. Schollick *et al.*, "Segregated Ice Growth in a Suspension of Colloidal Particles," *The Journal of Physical Chemistry B,* vol. 120, no. 16, pp. 3941-3949, 2016.

[21] M. Kochs, C. Körber, B. Nunner, and I. Heschel, "The influence of the freezing process on vapour transport during sublimation in vacuum-freeze-drying," *International Journal of Heat and Mass Transfer,* vol. 34, no. 9, pp. 2395-2408, 1991.

[22] M. Kochs, C. Körber, I. Heschel, and B. Nunner, "The influence of the freezing process on vapour transport during sublimation in vacuum-freeze-drying of macroscopic samples," *International Journal of Heat and Mass Transfer,* vol. 36, no. 7, pp. 1727-1738, 1993.

[23] K. Nakagawa, A. Hottot, S. Vessot, and J. Andrieu, "Modeling of freezing step during freeze-drying of drugs in vials," *AIChE Journal,* vol. 53, no. 5, pp. 1362-1372, 2007.

[24] K. Nakagawa, A. Hottot, S. Vessot, and J. Andrieu, "Influence of controlled nucleation by ultrasounds on ice morphology of frozen formulations for pharmaceutical proteins freeze-drying," *Chemical Engineering and Processing: Process Intensification,* vol. 45, no. 9, pp. 783-791, 2006.

[25] J. C. Kasper and W. Friess, "The freezing step in lyophilization: Physico-chemical fundamentals, freezing methods and consequences on process performance and quality attributes of biopharmaceuticals," *European Journal of Pharmaceutics and Biopharmaceutics,* vol. 78, no. 2, pp. 248-263, 2011.

[26] A. Voda *et al.*, "The impact of freeze-drying on microstructure and rehydration properties of carrot," *Food Research International,* vol. 49, no. 2, pp. 687-693, 2012.

[27] P. Foerst *et al.*, "Estimation of mass transfer rate and primary drying times during freeze-drying of frozen maltodextrin solutions based on x-ray μ-computed tomography measurements of pore size distributions," *Journal of Food Engineering,* vol. 260, pp. 50-57, 2019.

[28] R. Geidobler and G. Winter, "Controlled ice nucleation in the field of freeze-drying: Fundamentals and technology review," *European Journal of Pharmaceutics and Biopharmaceutics,* vol. 85, no. 2, pp. 214-222, 2013.

[29] N. Drapier-Beche, J. Fanni, M. Parmentier, and M. Vilasi, "Evaluation of Lactose Crystalline Forms by Nondestructive Analysis," *Journal of Dairy Science,* vol. 80, no. 3, pp. 457-463, 1997.

[30] A. S. Barham and B. K. Hodnett, "In Situ X-ray Diffraction Study of the Crystallization of Spray-Dried Lactose," *Crystal Growth & Design,* vol. 5, no. 5, pp. 1965-1970, 2005.

[31] J. Lefebvre, J. F. Willart, V. Caron, R. Lefort, F. Affouard, and F. Danède, "Structure determination of the 1/1 α/β mixed lactose by X-ray powder diffraction," *Acta Crystallographica Section B: Structural Science,* Review vol. 61, no. 4, pp. 455-463, 2005.

[32] J. F. Willart, V. Caron, R. Lefort, F. Danède, D. Prévost, and M. Descamps, "Athermal character of the solid state amorphization of lactose induced by ball milling," *Solid State Communications,* vol. 132, no. 10, pp. 693-696, 2004.

[33] V. Caron, J.-F. Willart, R. Lefort, P. Derollez, F. Danède, and M. Descamps, "Solid state amorphization kinetic of alpha lactose upon mechanical milling," *Carbohydrate Research,* vol. 346, no. 16, pp. 2622-2628, 2011.

[34] P. Walstra, J. T. M. Wouters, and T. J. Geurts, *Dairy science and technology*. Boca Raton: CRC Taylor & Francis, 2006.

[35] M. Peleg, "On the use of the WLF model in polymers and foods," *Crit Rev Food Sci Nutr,* vol. 32, no. 1, pp. 59-66, 1992.

[36] L. Goh *et al.*, "A Stochastic Model for Nucleation Kinetics Determination in Droplet-Based Microfluidic Systems," *Cryst Growth Des,* vol. 10, no. 6, pp. 2515-2521, 2010.

[37] T. Lucas, M. Wagener, P. Barey, and F. Mariette, "NMR assessment of mix and ice cream. Effect of formulation on liquid water and ice," *International Dairy Journal,* vol. 15, no. 10, pp. 1064-1073, 2005.

[38] M. A. de la Fuente, J. Belloque, and M. Juárez, "Mineral contents and distribution between the soluble and the micellar phases in calcium-enriched UHT milks," *Journal of the Science of Food and Agriculture,* vol. 84, no. 13, pp. 1708-1714, 2004.

[39] N. M. Wahlgren, P. Dejmek, and T. Drakenberg, "A Ca-43 and P-31 nmr-study of the calcium and phosphate equilibria in heated milk solutions," *Journal of Dairy Research,* Article vol. 57, no. 3, pp. 355-364, 1990.

[40] T. Loho *et al.*, "A tensile technique for measuring frozen products adhesion strength: Application to stainless steel/frozen milk interaction," *Journal of Food Engineering,* p. 109772, 2019.

[41] H. Sojoudi, M. Wang, N. D. Boscher, G. H. McKinley, and K. K. Gleason, "Durable and scalable icephobic surfaces: Similarities and distinctions from superhydrophobic surfaces," *Soft Matter,* Review vol. 12, no. 7, pp. 1938-1963, 2016.

[42] T. Bharathidasan, S. V. Kumar, M. S. Bobji, R. P. S. Chakradhar, and B. J. Basu, "Effect of wettability and surface roughness on ice-adhesion strength of hydrophilic, hydrophobic and superhydrophobic surfaces," *Applied Surface Science,* vol. 314, pp. 241-250, 2014.

[43] K.-i. Izutsu, E. Yonemochi, C. Yomota, Y. Goda, and H. Okuda, "Studying the morphology of lyophilized protein solids using X-ray micro-CT: effect of post-freeze annealing and controlled nucleation," *AAPS PharmSciTech,* vol. 15, no. 5, pp. 1181-1188, 2014.

[44] T. Siebert, M. Zuber, E. Hamann, T. Baumbach, H. P. Karbstein, and V. Gaukel, "Micro-CT visualization of structure development during freeze-drying processes," *Drying Technology,* pp. 1-9, 2019.

[45] K. Nakagawa, S. Tamiya, S. Sakamoto, G. Do, and S. Kono, "Observation of Microstructure Formation During Freeze-Drying of Dextrin Solution by in-situ X-ray Computed Tomography," *Frontiers in Chemistry,* Original Research vol. 6, no. 418, 2018.